

**Faculty of Textile Engineering
Technical University of Liberec**

STRUTEX

**Structure and Structural Mechanics of Textile
Fabrics**

Struktura a strukturní mechanika textilií

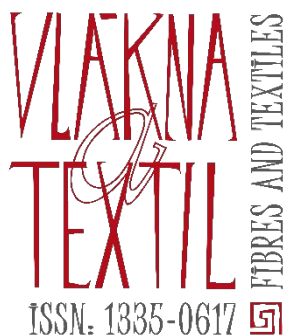
**22nd international conference
22. mezinárodní konference**

2018

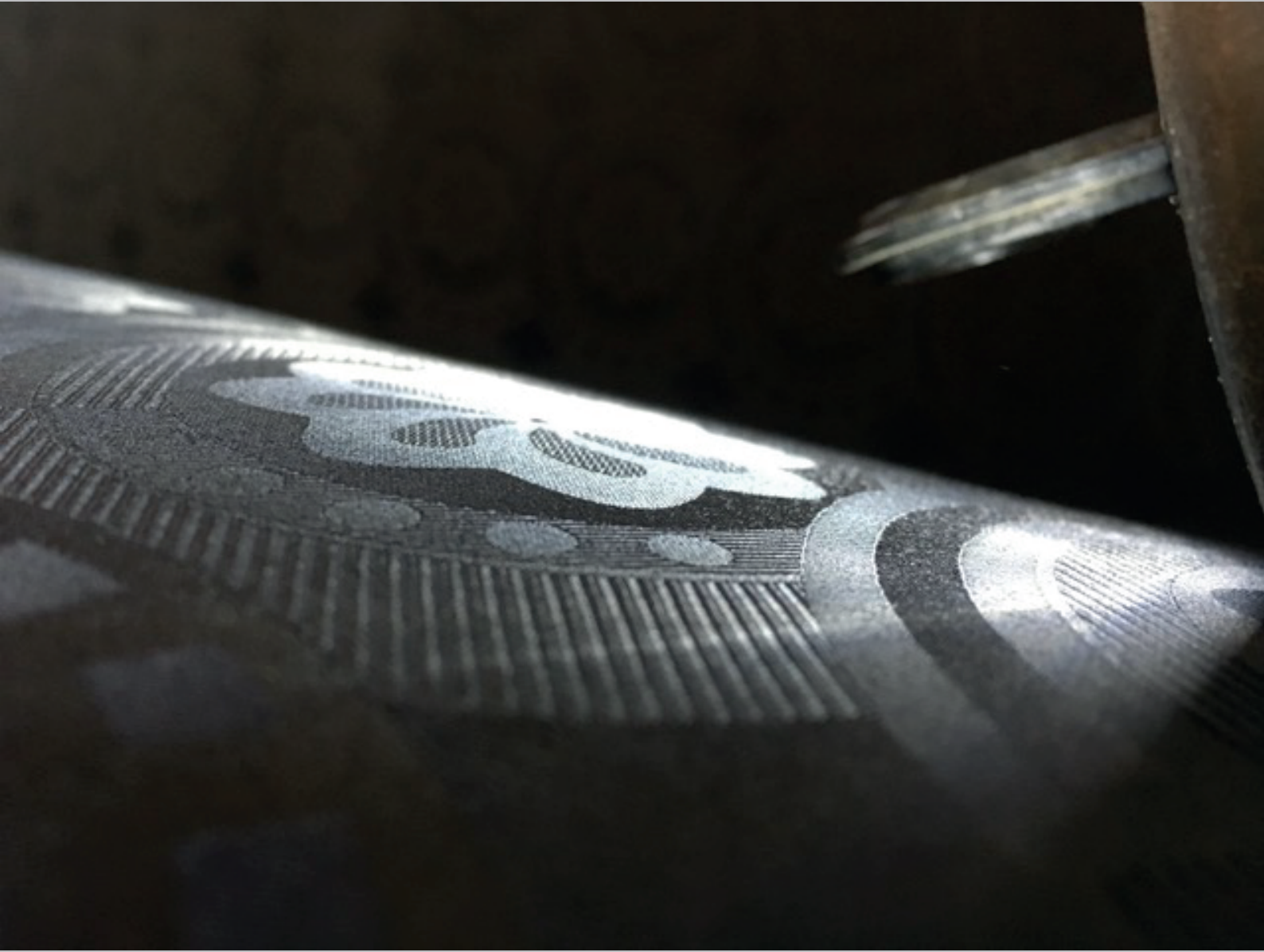
CONFERENCE BOOK

SBORNÍK TEXTŮ

PARTNERS / SPONSORS



We greatly appreciate Technical University of Liberec for education of students in the field of textile. Without next generation textile experts we can not keep working and would be not able to develop new products.

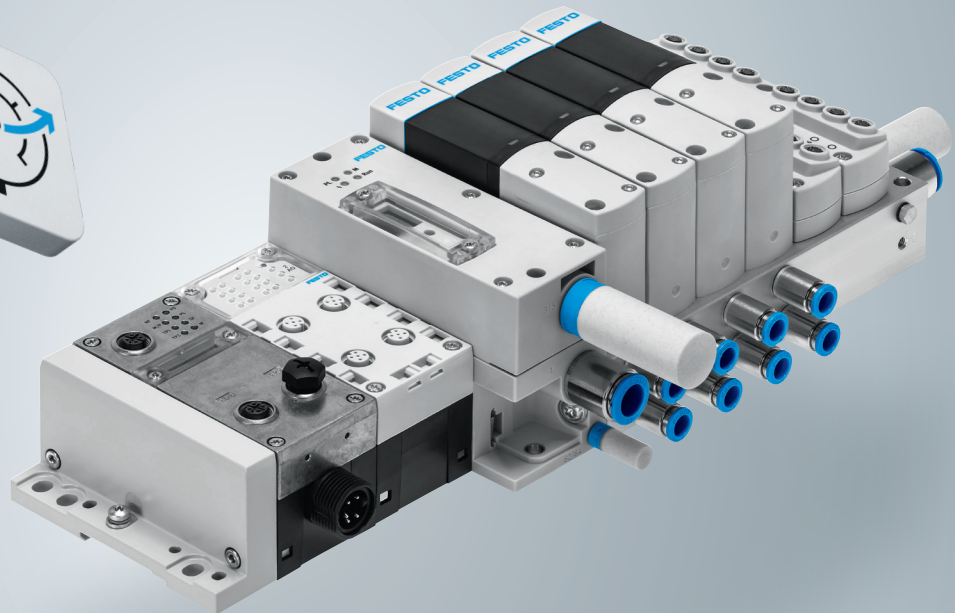


with thanks





FESTO



You rely on maximum flexibility.
You are looking for intelligent and intuitive solutions.
We are making pneumatics go digital.

→ **WE ARE THE ENGINEERS
OF PRODUCTIVITY.**

Pneumatics goes digital: world first Festo Motion Terminal VTEM

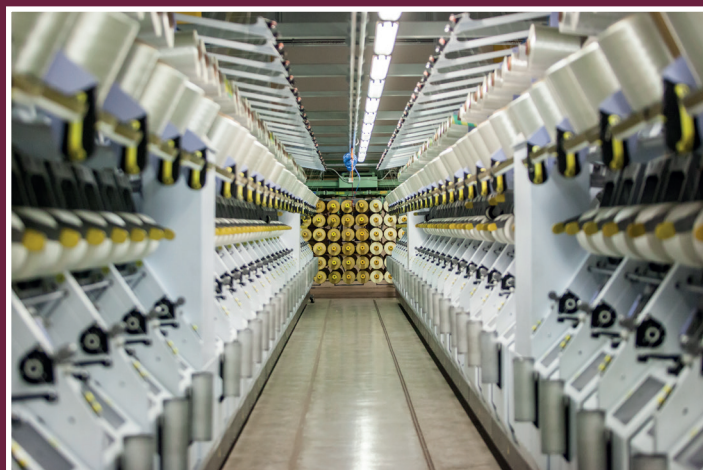
Different functions, always the same hardware! Whether for standard directional control valve functions like for example 4/2, 4/3, 3/2 or for presetting the travel time, you can now control functions using apps. For maximum flexibility and standardisation, reduced complexity and installation times, and many other benefits. Find out more:

www.festo.com/motionterminal



KORDÁRNA
K O R D Á R N A P L U S A . S .

TECHNICAL FABRICS AND YARN MANUFACTURER
INTEGRATED PRODUCTION OF TEXTILE WITH 70 YEARS OF KNOW-HOW



One of the largest manufacturers of technical fabrics in Europe

With seventy years of experience and eight hundred professionally trained employees, we supply fabrics to more than fifteen countries in Europe, North America, South America and Asia.

Supplier of major world's tire manufacturers

Our fabrics serve as tire reinforcements in cars and trucks, motorcycles, buses or even aircraft. Our partners are world-class tire manufacturers such as Continental, Dunlop, Nokian, Good Year or Bridgestone.



Integrated production from fibre to fabric

We integrate the whole manufacturing process from the output of our polyester fibre to the impregnated technical fabric that serves as the backbone of tires and conveyor belts.

Velká nad Veličkou 890
696 74 Czech Republic
+420 518 312 224 | kordarna@kordarna.cz
www.kordarna.cz



KORDÁRNA
K O R D Á R N A P L U S A . S .

The Lohmann & Rauscher Company is an international company with a long history. It has over 160 years of experience in making dressing materials and medical devices and it has always focused on the needs of its customers and patients.



The company is a world-leading supplier of medical devices and hygiene products of the highest quality. It develops individual solutions to the problems of patients and healthcare workers worldwide, from classic dressing materials, to modern therapy systems.



Plant in Nová Paka

Lohmann & Rauscher s.r.o.
Legií 265
509 01 Nová Paka
Czech Republic

Plant in Slavkov

Lohmann & Rauscher s.r.o.
Bučovická 256
684 01 Slavkov u Brna
Czech Republic

Headquarters • General inquiries

Telephone: +420 544 425 601
Fax: +420 544 227 331
E-mail: info.slavkov@cz.LRmed.com
<https://www.lohmann-rauscher.com>





Rieter CZ s.r.o.

Ústí nad Orlicí

Rieter CZ s.r.o. is part of the Swiss Group, Rieter, that is a leading world producer of textile machinery and complete textile systems. Rieter CZ s.r.o. is characterised by a strong emphasis on innovations that are developed in the company development centre. Other features include precision production of textile machines and components for modern technologies and processes.

Rieter – The Comfort of Competence.
<http://www.rieter.cz>, <http://rieter.jobs.cz>

RIETER

ADFORS

People are our strength



2 production plants - in Litomyšl and Hodonice

more than **2000** employees

turnover

7.8
bn CZK

120 k tons of glass fibre per year

6 brands of unique glass fibre production

PEOPLE ARE OUR STRENGTH SO THEY ARE OUR FIRST PRIORITY.

Thanks to this approach, we already have been certified as a Top Employer for the last few years.



We are still growing and investing in both our employees and our technology too.

Working for us is very fulfilling. Come and join us!

CONTACTS

HEADQUARTERS AND LITOMYŠL PLANT

SAINT-GOBAIN
ADFORS CZ s.r.o.
Sokolovská 106
570 01 Litomyšl

+420 461 651 111

HODONICE PLANT

SAINT-GOBAIN
ADFORS CZ s.r.o.
Zahradní 256
671 25 Hodonice

+420 515 207 111

HR department
kariera.adfors@saint-gobain.com
www.adfors.cz



STAP a.s. – Narrow Fabrics Manufacturer from Czech Republic

Our products are tailored to meet exacting specifications established by a number of NATO military forces. STAP a.s. is a major webbing manufacturer of military webbings, bindings and elastics to meet specifications in both IRR webbings and non-IRR webbings.

We are one of the few webbing suppliers who can offer our own in-house dying facilities to colour match to forces exacting shade requirements.

Our Multi Colour Camo printed webbing (up to 5 colours) is widely used on a variety of PLCE (Personal Load Carrying Equipment), MTP Webbing Systems & Pouches, Molle Webbing along our latest IRR Camo printed binding, designed to be used in conjunction with The Multi-Terrain Pattern (MTP) camouflage print.

We can offer bespoke custom printed webbing to match your military camouflage textile pattern.

Special treatments can be applied to the webbing straps including anti-bacterial, rotproof, water-repellent and flame-retardant finishes.

Webbings are cut to length and heat-sealed using our automatic machines and we are also able to offer a cutting and holing service using our ultrasonic facility.



Here we are able to create a wide range of made-up units, sewn webbing straps also with buckles.

We can also offer wide range of commercial products, like webbings, elastics, binding tapes, zippers, woven labels, braids, jacquard ribbons...

www.stap.cz

'TORAY'

Innovation by Chemistry



JOIN OUR TEAM!

THEY WILL FLY
ALSO THANKS
TO YOU.

We seek new members
for our branch in Prostějov.

We offer stability of worldwide
operating company and
many benefits for employees.
You will work in a clean and
modern environment with
advanced technology.

Please contact us:
personalni@ttce.toray.cz

www.toray.cz

Faculty of Textile Engineering
Technical University of Liberec

22nd international conference
22. mezinárodní konference

STRUTEX

**Structure and Structural Mechanics of Textile
Fabrics**

Struktura a strukturní mechanika textilií



CONFERENCE BOOK

SBORNÍK TEXTŮ

**December / Prosinec 2018
Faculty of Textile Engineering
Technical University of Liberec**

President of the conference

prof. Ing.Bohuslav Neckář, DrSc.

Technical University of Liberec

Scientific committee

prof. Luboš HES, Technical University of Liberec, Czech Republic

prof. S. M. ISHTIAQUE, Indian Institute of Technology Delhi, India

prof. Oldřich JIRSÁK, Technical University of Liberec, Czech Republic

prof. Yordan KYOSEV, Hochschule Niederrhein, Germany

prof. Jiří MILITKÝ, Technical University of Liberec, Czech Republic

prof. Bohuslav NECKÁŘ, Technical University of Liberec, Czech Republic

dr. Vincent PLACET, University of Franche-Comté, France

prof. Jakub WIENER, Technical University of Liberec, Czech Republic

assoc. prof. Lukáš ČAPEK , Technical University of Liberec, Czech Republic

© Technical University of Liberec - 2018

ISBN 978-80-7494-430-7

CONTENTS

THE STRUCTURE OF ARCHAEOLOGICAL TEXTILES FROM THE EARLY AND HIGH MIDDLE AGES IN FINDS FROM THE CZECH REPUBLIC	7
Helena Březinová, Milena Bravermanová & Jana Bureš Víchová	
FORMATION OF THE TEXTILE STRUCTURES FOR A SPECIFIED PURPOSE	31
Marcin Barburski	
GEOMETRICAL MODELLING OF WOVEN TEXTILE STRUCTURES	41
Banu Özgen Keleş	
IMPACT OF EXTRACTION PROCESSES ON FIBER PROPERTIES OF LINSEED FLAX FIBERS	49
Pierre Ouagne, Marie Grégoire, Benjamin Barthod-Malat, Philippe Evon, Laurent Labonne, Emmanuel De Luycker & Vincent Placet	
MODELLING THE CROSS-SECTIONAL PROPERTIES OF YARN ALONG THE FABRIC.....	57
R. Befru Büyükbayraktar	
AUTOMATIC ANALYSIS THE BRAIDING ANGLE OF THE BRAIDED FABRICS USING IMAGE PROCESSING.....	65
Yisheng Liu & Yordan Kyosev	
EXPERIMENTAL TESTING AND FINITE ELEMENT SIMULATION OF TH-7 BENDING TEST OF SPORTS BRA TEXTILES.....	73
Michaela Hassmann & Wolfgang Krach	
COMPUTATIONAL METHODOLOGY FOR DETERMINATION OF YARN TWIST AND DIAMETER.....	81
Bohuslav Neckář & Dipayan Das	
METHOD OF GENERATION ZONING AREAS IN PATTERN CONSTRUCTION NET OF SEAMLESS UNDERWEAR	83
Blažena Musilová, Alžbeta Hôrecká & Nareerut Jariyapunya	
THE EFFECT OF RIBS ON COOLING ABILITY OF WETTED SHIRT KNITS AT LOW AIR VELOCITY	91
Lubos Hes & Monika Boguslawska – Baczek	
APPLYING THE ARTIFICIAL NEURAL NETWORK TO PREDICT THE THERMAL PROPERTIES OF KNITTED FABRICS	97
Sinem Güneşoğlu & Binnaz Kaplangiray	
PROBLEMATICS OF LARGE-SIZE BATCH WINDING OF TECHNICAL TEXTILES	103
Josef Žák	
MECHANICAL FIXATION OF TUFTED PILE LOOPS INTO THE PRIMARY BACKING BY USING THE PARAMETERS OF FABRIC WEAVE DESIGN	111
Alexandra Glogowsky, Thomas Brunke, Karin Ratovo, Alexander Büsgen & Bayram Aslan	
THE SET-UP OF A LABORATORY TYPE COATING / LAMINATING UNIT AND THE OPTIMISATION OF LAMINATION PROCESS OF DENIM FABRICS	119
Ayşe Genç, Mehmet Yüceer, Nihan Karakaplan & Cem Güneşoğlu	
COMPOSITE BASED ON GEOPOLYMER MORTAR REINFORCED CHOPPED BASALT FIBER AND CARBON TEXTILE	127
Hiep Le Chi, Petr Louda, Totka Bakalova & Vladimir Kovacic	
OIL-TREATED FIBROUS AIR FILTERS FOR AUTOMOTIVE ENGINE INTAKE APPLICATION	133
Ajay Kumar Maddineni & Dipayan Das	

DEVELOPMENT AND CHARACTERISATION OF NONWOVEN FABRICS FOR APPAREL APPLICATIONS.....	141
M.S. Cheema, T. H. Shah & S. C. Anand	
VARIATION BRAIDING TECHNOLOGY BY THE EXAMPLE OF NOVEL STENT STRUCTURES	151
Marielies Becker, Frank Ficke & Roxana Miksch	
ANALYSIS OF FORMATION OF MASS IRREGULARITY IN DRAFTING DEVICE DURING YARN SPINNING FROM SLIVER	157
Eva Moučková, Petr Ursíny, Petra Jirásková & Martin Janoušek	
AIR-FLOW ANALYSIS OF COMPACT YARN	167
Murat Demir, Musa Kilic, Zeki Kiral, Serdar Sayin, Kıymet Kübra Denge & Furkan Balduk	
EFFECTS OF INTERMINGLING ON PROPERTIES OF FALSE TWIST TEXTURED YARNS... 173	
Musa Kilic, Gonca Balcı Kilic & Buğra Öztürkmen	
CHANGES OF WATER VAPOUR PERMEABILITY AND ABSORPTION BY USING OF BAMBOO MATERIALS IN THREE-LAYERED UPPER FOOTWEAR PACKAGES.....	181
Katarzyna Ławińska, Wioleta Serweta & Nataliia Popovych	
PREDICTIVE MODELLING OF OPEN AREA AND AIR PERMEABILITY OF COTTON PLAIN WOVEN FABRICS.....	189
Julie Abel, Roshan Unmar & Satyadev Rosunee	
THE EFFECT OF YARN LINEAR DENSITY ON STRUCTURE PROPERTIES OF PLATED WEFT KNITTED FABRIC UNDER HOME LAUNDERING PROCESS	197
Irena Lenfeldova & Jana Peckova	
DETERMINATION OF OPTIMAL CONJUGATE STRESS STRAIN PAIRS.....	205
Bohuslav Stříž & Lukáš Čapek	
INVESTIGATION OF THE CAPILLARY KINETIC TRANSPORT OF LIQUID FUELS IN DIFFERENT ROUND BRAIDS.....	211
Peter Philip Glessner	
STRUCTURE ANALYSIS OF CARBONIZED NEEDLE-PUNCHED NONWOVENS BY X-RAY COMPUTED TOMOGRAPHY.....	217
Smita Baheti, Maros Tunak & Daniel Karthik	
FIXATION OF REINFORCING FABRIC FOR ION EXCHANGE MEMBRANE	225
Eliška Stránská & David Neděla	
RE-USE OF PYROLYSED CARBON FIBRES IN SOPHISTICATED COMPOSITES AS INDUSTRIAL VIABLE PROCESS WITH INTEGRATED QUALITY MONITORING: RECYCARB	233
Holger Fischer, Marcel Hofmann, Andrea Miene & Katharina Heilos	
STUDY OF THE TOW BUCKLING DEFECT DURING THE COMPLEX SHAPE FORMING OF SYNTHETIC AND VEGETAL FIBRE REINFORCED STRUCTURAL COMPOSITES	241
M.M. Salem, E. De Luycker, M. Fazzini & P. Ouagne	
INFLUENCE OF THE SEAMS ON THE SUBJECTIVE HAND EVALUATIONS OF TEXTILES . 247	
Vladimír Bajzík & Tereza Zaleská	
EFFECT OF AIR PERMEABILITY ON GRAINLINES, AGED, WASHED AND MOISTED WOVEN FABRIC	255
Frederick T. Fung & Antonin Havelka	
EFFECT OF MOISTURE CONTENT ON THERMOPHYSIOLOGICAL PROPERTIES OF PLAIN KNITTED SOCKS FOLLOWED BY THERMAL RESISTANCE COMPARISON AMONG DIFFERENT SKIN MODELS.....	267
Tariq Mansoor, Lubos Hes, Zenun Skenderi & Muhammad Asif Javed	
A REVIEW ON MULTI-STRAND STAPLE YARN PRODUCTION	279
Murat Demir, Musa Kilic, Zeki Kiral, Kıymet Kübra Denge & Furkan Balduk	
PREDICTION OF PATTERN DIMENSIONS FOR PRESSURE GARMENT	287
Nareerut Jariyapunya, Blažena Musilová & Antonín Havelka	

APPLICATION OF ELECTRIC BASED HEATING IN CLOTHING FOR SENIORS	295
Antonín Havelka, Miroslav Tichý, Radek Soukup, Ladislav Nagy & Michal Martinka	
PROPERTIES OF NANOADDITIVE MASTERBATCHES FOR ANTIMICROBIAL POLYPROPYLENE FIBRES PREPARATION.....	301
Štefan Krivoš, Anna Ujhelyiová & Katarína Holcová	
THE IMPACT OF STORAGE TIME ON THERMAL PROPERTIES OF PP/QA FIBERS.....	309
Mária Gavendová, Vladimíra Krmelová, Tomáš Zatroch, Bibiana Bizubová, Michal Kleščík & Katarína Moricová	
MODIFICATION OF PU- FOAM FOR IMPROVEMENT OF THERMAL COMFORT OF CAR SEAT	317
Funda Buyuk Mazari, Karel Adamek, Jakub Wiener, Adnan Mazari & Antonin Havelka	
IMPACT OF HEAT ON RECOVERY EFFICIENCY OF CAR SEATS FABRICS	327
Viera Glombikova, Petra Komarkova & Kus Zdenek	
HEAT AND HUMIDITY TRANSFER IN SANDWICH TEXTILES FOR AUTOMOTIVE SEATS. 331	
Zuzana Drapáková, Vladimír Bajzík & Luboš Hes	
ABRASION AND ELECTRICAL RESISTANCE OF KEVLAR WITH PVD SURFACE TREATMENT	337
Mário Vančo, Jan Krmela, Vladimíra Krmelová, Ludmila Balogová, Artem Artyukhov & Františka Pešlová	
PRODUCTION OF THERMO-REGULATING CARPET THROUGH PHASE CHANGE MATERIALS (PCMS) TECHNOLOGY.....	343
Azize Ince, Sennur Alay Aksoy, Volkan Balci1, Cem Gunesoglu, Emine Cot, Sebnem Sozcu & M. Sakir Erboz	
A STUDY ON THE PERFORMANCE OF ANTI-MITE & ANTI-BACTERIAL TEXTILES FOR CLIENTS AT NURSING HOMES	351
Adnan Mazari, Antonin Havelka, Marcela Kolinova, Michal Martinka & Renata Nemcokova	
HYDROPHOBIC AND ANTIBACTERIAL TREATMENT OF TEXTILES USING ORGANIC-INORGANIC HYBRID LAYERS PREPARED BY SOL-GEL	355
Vojtěch Miller, Hana Šourková, Irena Lovětinská Šlamborová, Petr Exnar & Jiří Škach	
POLYMERIC NANOFIBERS PRODUCED BY NEEDLELESS ELECTROSPINNING	363
Evren Boyraz & Fatma Yalcinkaya	
OUTPUTS FROM THE PROJECT ERASMUS+ KA107 AT FACULTY OF TEXTILE ENGINEERING	367
Pavla Těšinová	
ESTIMATION OF FOLDING AND LUMINANCE VALUES OF POLYPROPYLENE BCF YARNS USING ARTIFICIAL NEURAL NETWORK TECHNIQUE AND MODELING STUDY	375
Emre Yakut, Cem Güneşoğlu, Emine Çot & Volkan Balci	
MODELLING OF CONSTRUCTION OF WOVEN FABRIC	381
Brigita Kolčavová Sirková & Iva Mertová	



THE STRUCTURE OF ARCHAEOLOGICAL TEXTILES FROM THE EARLY AND HIGH MIDDLE AGES IN FINDS FROM THE CZECH REPUBLIC

Helena Březinová, Milena Bravermanová, Jana Bureš Vichová

Institute of Archaeology of the Czech Academy of Sciences, Prague, Czech Republic

www.arup.cas.cz, +420266009405

brezinova@arup.cas.cz, milena.bravermanova@seznam.cz, JVichova@seznam.cz

Abstract:

Textile production has deep roots in the past, and knowledge of the processing and use of textile fibres can be assumed since the Stone Age. Over the centuries, textile production has constantly improved and a range of raw materials and textile bindings have been used. In archaeological finds we rarely encounter the remains of fragile textile material; however, it is possible to reconstruct the level, maturity and variety of textile structures in the past, above all from small discovered fragments, most often from burial or waste features.

The article provides an overview of weaves, their characteristics and specific examples identified in preserved textiles from archaeological finds in the Czech Republic dating to the period from the Early to the Late Middle Ages.

Keywords:

archaeological textiles, weave, Early Middle Ages, High Middle Ages, Prague Castle

1. Introduction

The investigation and professional processing of textile preserved in archaeological contexts provides an unique opportunity for learning about the method, level and diversity of textile production in the past. Although the Czech Republic lacks ideal conditions for the preservation of organic archaeological material, find units, mainly grave and waste situations, occasionally provide textiles from various time periods.

A major part of the investigation of textiles is the study of weaves and the method of their creation. The following article provides a summary of all weaves documented on textiles obtained from archaeological finds in the Czech Republic in the period between the Early and Late Middle Ages. The work presents basic weaves such as tabby, twill, satin and their extended versions, as well as more intricate and very complicated weaves such as those with floating weft threads, damask, weft-faced compound twill, proto-lampas, lampas and velvet.¹ The selection of specific examples includes both classic variants of individual weaves and variants with certain differences or interesting aspects in their execution. The presented fabrics produced with simple or very complicated weaves are part of the broad spectrum of medieval textile production that achieved, especially in the production of silk fabrics, a high utility, economic and artistic value.

2. Source inventory

The remains of medieval textiles appear in archaeological finds from various environments, with the most frequent being waste pits and features from medieval urban environments where higher moisture and a lack of air create ideal conditions for the preservation of organic material and which generate remnants of common material culture used in medieval households. An important group of textile finds that has been particularly useful for the study of more complicated weaves, period fashion, styles, patterns and trade with luxury fabrics is grave textiles preserved in enclosed graves and tombs connected most frequently with the royal, aristocratic and Church environment, in many

cases with a concrete historical figure. Also offering good conditions for the preservation of textiles are find environments supported by the regular circulation of air, including the backfill of vaults and floors in historical buildings. Another source for studying textiles is small fragments preserved in the corrosion surface layers of metal artefacts; these finds, especially those from the Early Medieval period, provide a unique opportunity for the investigation of textile structures [1].

Specific fabrics representing individual weaves were selected in three types of find environments significant for archaeological textile finds in the Czech Republic. Medieval textiles from waste features and layers make up an assemblage of more than 1,500 textile fragments from the thick waste layers from the 14th and 15th centuries in the centre of Prague [2]. Funeral textiles were chosen from a unique collection from archaeological excavations at Prague Castle, especially from St. Vitus Cathedral, the resting place of the Bohemian rulers, their family members and Church dignitaries [3, 4]. An example of Early Medieval textiles preserved in the corrosion layers of metal artefacts is finds from Great Moravian inhumation graves in Mikulčice [5].

The study of weaves is connected with the development of individual types of looms of various constructions. We focus exclusively on those that were used to make the fabrics documented in Czech territory.

The simplest type was the warp-weighted loom, the use of which appears in prehistoric times and in Europe is regarded as the main weaving device up until the Early Medieval period. The loom was composed of two uprights, a warp beam with tied warp threads and the cloth beam. The warp threads were typically tightened by a set of weights. The shedding device was composed of a certain number of shed rods with heddles that raised the warp threads, and by moving the individual shed rods forwards and backwards, a shed was created for passing the weft through. The weaver operated the loom from the front while standing. The simplest fabrics with tabby and twill weaves were woven on this type of loom.

During the course of the 13rd century, the warp-weighted loom was gradually replaced in the Czech environment by the more technically advanced horizontal treadle loom. The invention of this type of loom is attributed to China in the 2nd century BC. Its use then expanded westward, and by the Early Middle Ages, the horizontal treadle loom could also be found in Europe. The loom was composed of a wooden frame with four uprights and cross beams. Two rollers were attached to the front and back uprights – in the front by the weaver was a cloth roller onto which the finished fabric was wound. In the back was the warp roller to which the warp threads were attached and wound. The most important part of the loom was the shedding mechanism composed of two or more heddle bars, two or more treadles, the heddle harness and the beater. The bottom of each heddle bar was attached by rope to the treadle, which the weaver operated by foot. The shed was created by alternately pushing and releasing the treadles. A two-person horizontal loom operated by two weavers was used to weave exceptionally wide fabrics. This type of loom was used to produce tabby, twill and satin weaves.

The use of the most complicated weaving device in period textile production, the drawloom, began roughly in the 3rd century in the eastern Mediterranean. It was used to produce patterned fabrics, mainly from silk. It developed as a refinement of the horizontal loom and was equipped with a special type of figure harness consisting of lashes controlled by lifting cords. This device was operated by a drawboy sitting opposite the weaver on a raised seat. The drawloom permitted the continual repetition of a pattern in the width and length of the textile. Decorative motifs stood out more because it was possible to work better with the pattern wefts. Drawlooms were used to produce, for example, more complicated weft-faced compound twill, proto-lampas and lampas [6].

Velvet without a pattern was woven on a horizontal loom, and thin metal rods were inserted in the fabric at certain intervals. Loops formed above the ground fabric once the rods were removed. If these rods had a longitudinal channel along which a sharp tool could be run, the loops were cut to create cut velvet. In the case of patterned velvet, pile warps were controlled by a special type of figure harness. If another pattern occurred in the fabric, e.g. woven with metal wefts, a second figure harness was required for work with the warp threads [7].

3. Tabby

Tabby (plain weave) is a weave based on a unit of two ends and two picks in which each end passes over and under one pick, with the points of binding being set over one end on successive picks. It is the simplest and densest weave and has the same appearance on the obverse and reverse sides of the fabric.

The tabby weave is the most commonly documented weave, from the earliest prehistoric textile finds in Europe, including in the Czech Lands [9], up to the studied medieval period, where, in all investigated find units with the exception of assemblages of luxury silk textiles from Prague Castle, it significantly exceeds the occurrence of all other weaves [10].

3.1. *Wool fabric* [11]

Find circumstances: Prague 1 – New Town, waste layer

Storage; inventory number: The City of Prague Museum; 25_A11E_347

Dating: 14th – 15th century

Provenance: Bohemia

Technical analysis (Figure 1)

Weave: tabby

Warp

material: wool, z-twist, light brown colour²

count: 13 threads per cm

Weft

material: wool, s-twist, light brown colour

count: 13 threads per cm

Characteristics of the weave: regular

Pattern: unpatterned

Original use: indeterminable

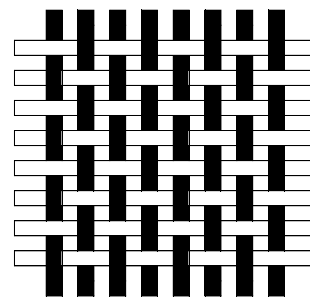


Figure 1. Wool fabric: weave diagram.

3.2. *Crepe fabric* [12]

Find circumstances: Prague Castle, St. Vitus Cathedral, Royal crypt, originally the separate coffin of one of the following queens: Blanka of Valois (†1348), Anne of Bavaria (†1353), Anna of Schweidnitz (†1362), Joanna of Bavaria (†1386), Elizabeth of Pomerania (†1393), as of 1611 a common coffin for all the queens

Storage; inventory number: Prague Castle collection; PHA 4/04, HS 25802

Dating: 14th century

Provenance: Spain (?)

Technical analysis (Figure 2)

Weave: tabby

Warp

material: silk, z-twist, ochre-brown colour

count: c. 60 threads per cm

Weft

material: silk, z-twist, ochre-brown colour

count: c. 60 threads per cm

Characteristics of the weave: warp and weft threads are very wavy (crepe), an effect achieved by means of a relatively high identical z-twist in the warp and weft threads; both edges of the strip of fabric have a decorated waviness, the result of the use of thicker, mostly paired, and weakly spun warp threads in the hem

Pattern: unpatterned

Original use: a typical medieval woman's veil, a so-call 'kruseler'



Figure 2. Crepe fabric: detail of fabric with hem © Prague Castle Administration, photo: J. Gloc.

4. Twill

Twill is a weave based on a unit of three or more ends and three or more picks, in which each end passes over two or more adjacent picks and under the next one or more, or under two or more adjacent picks and over the next one or more. The points of binding are set over by one end, always in the same direction, on successive picks forming diagonal lines. The repetition of a twill may be expressed as a numerical ratio, with the first figure indicating the number of picks over which an end passes, the second the number of picks under which it passes.

Like the tabby weave, the twill weave is documented in finds dating back to prehistoric times. Both weaves appear in great numbers in assemblages connected with the common textile material culture of the medieval population [13].

4.1. *Worsted fabric* [14]

Find circumstances: Prague 1 – New Town, waste layer

Storage; inventory number: The City of Prague Museum; 10_V31_83

Dating: 14th – 15th century

Provenance: western Europe (?), Bohemia (?)

Technical analysis (Figure 3a, b)

Weave: 2.2 twill

Warp

material: worsted wool, z-twist, light brown colour

count: 22 threads per cm

Weft

material: worsted wool, z-twist, light brown colour

count: 16 threads per cm

Characteristics of the weave: regular

Pattern: unpatterned

Original use: indeterminable

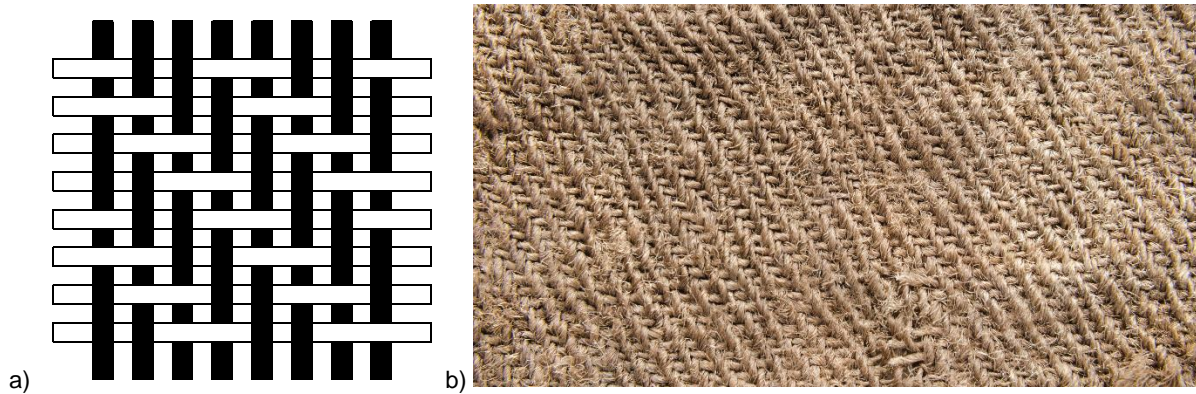


Figure 3. Worsted fabric: a) weave diagram; b) fabric detail © Z. Kačerová.

5. Extended tabby and twill

An extended weave is created from a ground tabby, twill or satin weave by adding or removing certain binding points or through another arrangement of threads, thus producing a new binding of the ground weave.

5.1. Chequered fabric [15]

Find circumstances: Prague Castle, St. Vitus Cathedral, Royal crypt, perhaps the Romanesque chest apparently used to transport the remains of Conrad II Oto, Duke of Bohemia (†1191)

Storage; inventory number: Prague Castle collection; PHA 95/02, HS 25829

Dating: 12th century (?)

Provenance: Spain, southern Europe (?)

Technical analysis (Figure 4a, b)

Weave: 2.2 extended tabby (louisine), 2.2.3. extended tabby (louisine), 3.1.1.1.1.1. weft-faced twill S, 3.1.1.1.1.1.1. weft-faced chevron twill in the warp direction, 3.1.1.1.1.1.1. weft-faced chevron twill in the weft direction, 3.1.1.1.1.1.1. weft-faced lozenge twill

Warp

material: silk, z-twist, ochre-brown colour

count: c. 50-77 threads per cm

Weft *latté*

material: silk, without visible twist, light brown and green colour

count: c. 20-35 threads per cm

Characteristics of the weave: combination of several simple weaves that continually alternate

Pattern: the fabric (*etoffe à carreaux*) is decorated across the entire preserved width with a small geometric pattern of diamonds, zigzags and crosswise and lengthwise stripes achieved with a combination of several simple weaves; the chequered pattern is further enhanced by the use of different colours of weft threads

Pattern rapport: indeterminable

Original use: possible wrap for the relics of Conrad II Oto, Duke of Bohemia

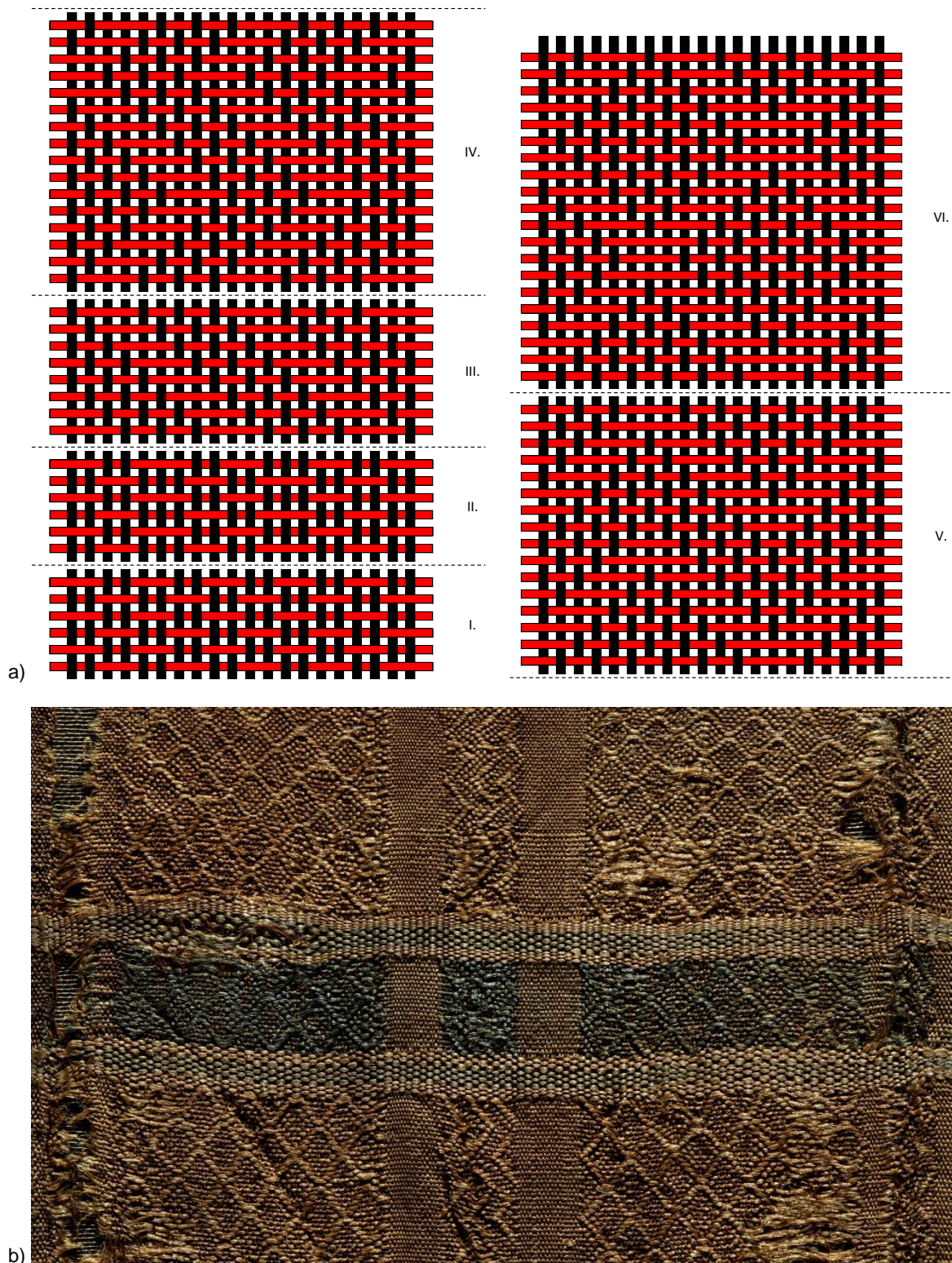


Figure 4. Chequered fabric: a) weave diagram: I. – 2.2 extended tabby; II. – 2.2.3 extended tabby; III. – 3.1.1.1.1.1 weft-faced twill S; IV. – 3.1.1.1.1.1 weft-faced chevron twill in the warp direction; V. – 3.1.1.1.1.1 weft-faced chevron twill in the weft direction; VI. – 3.1.1.1.1.1 weft-faced lozenge twill; b) fabric detail
© Prague Castle Administration, photo: J. Gloc.

5.2. Fabric with stylised diamond mesh [16]

Find circumstances: Prague Castle, St. Vitus Cathedral, Royal crypt, lining of the Romanesque chest apparently used to transport the remains of Conrad II Oto, Duke of Bohemia (†1191)

Storage; inventory number: chest – National Museum; fabric sample – Prague Castle collection; PHA 95/03

Dating: second half of the 12th century (?)

Provenance: Spain (?)

Technical analysis (Figure 5)

Weave: interconnection of 3.1 twill S and 3.1 twill Z

Warp

material: flax, z-twist, brown-red colour

count: 23 threads per cm

Weft

material: cotton, without apparent twist, brown-red colour

count: 13 threads per cm

Characteristics of the weave: patterned twill; several binding points not realised; weave unit 12/12

Pattern: stylised diamond mesh in which stripes falling obliquely from the right to the left are divided by double bars into rectangular fields containing small rectangles

Pattern rapport: height 2 cm, width 2 cm

Original use: lining of Romanesque chest

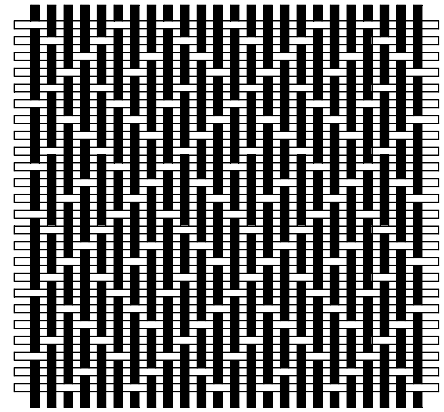


Figure 5. Fabric with stylised diamond mesh: weave diagram.

6. Weaves with floating weft threads

The pattern of this type of fabric is composed of either a floating ground weft or one of the weft threads in a standard weave (double-faced weave; see 6.1.), or a supplementary floating weft is added to the weft thread – pattern or brocading – regularly bound by the warp (see 6.2.).

6.1. Fabric with diamonds [17]

Find circumstances: Prague Castle, St. Vitus Cathedral, graves of the Prague bishops, probably Bishop Nikolaus (†1258)

Storage; inventory number: Church treasury at St. Vitus (held by the Prague Castle Administration); K 434

Dating: first half of 13th century

Provenance: Spain, southern Europe (?)

Technical analysis (Figure 6a, b)

Weave: tabby with floating weft (double-faced weave)

Warp

material: silk, z-twist, light brown colour

count: c. 27-28 threads per cm

Weft

material: silk, without visible twist, light brown colour

count: c. 19-21 threads per cm

Characteristics of the weave: even wefts float on the face, odd wefts on the reverse; floating wefts over 3-13 warps

Pattern: small, constantly repeating diamonds, with each larger diamond containing another smaller diamond

Pattern rapport: height 1.8 cm, width 5.7 cm

Original use: remnant of burial gown, possibly a dalmatic

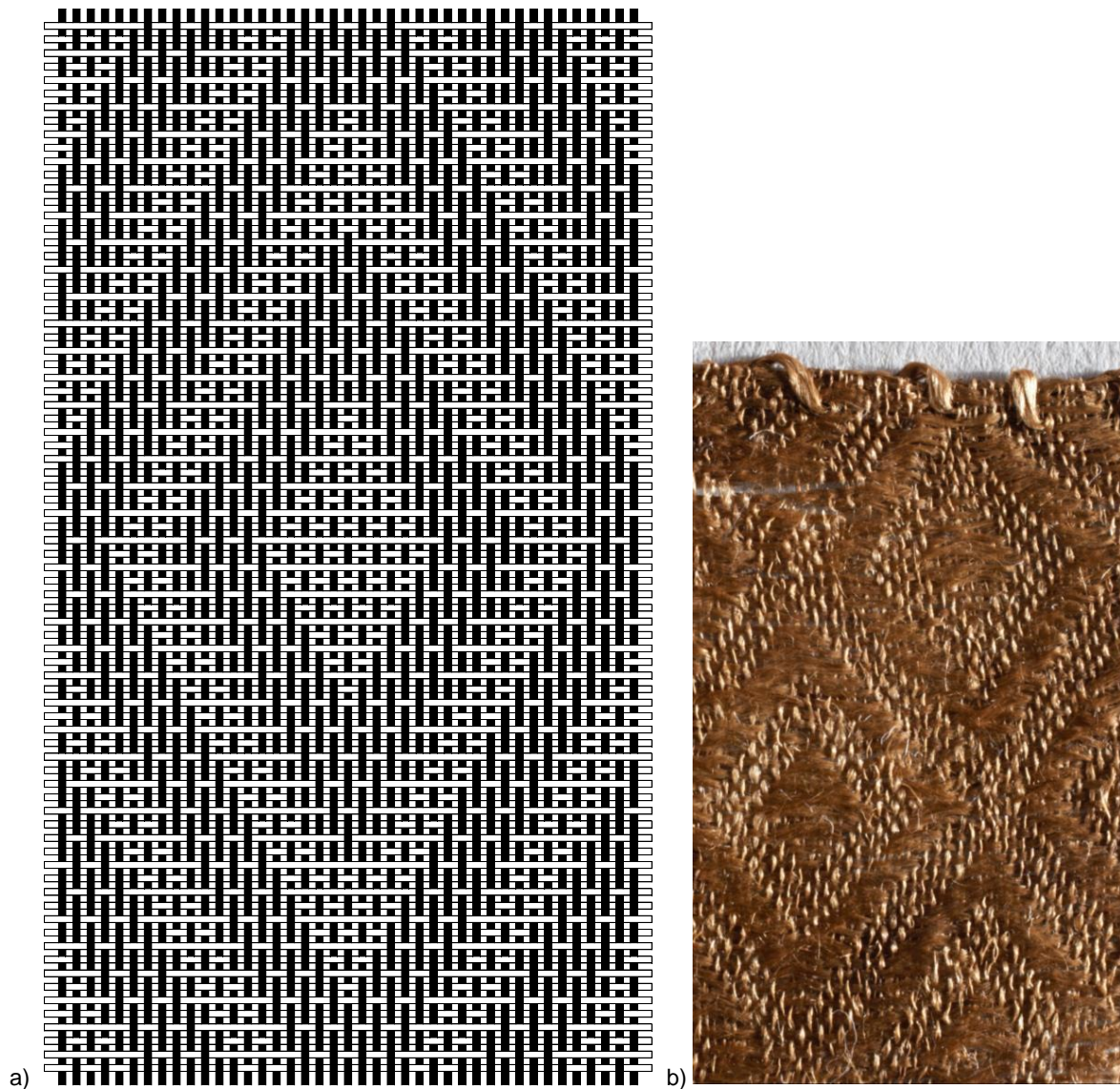


Figure 6. Fabric with diamonds: a) weave diagram; b) fabric detail
 © Prague Castle Administration, photo: J. Gloc.

6.2. Fabric with a supplemental pattern weft [18]

Find circumstances: Mikulčice-Kostelisko, grave no. 2041, small fabric fragments preserved in the corrosion layer of an iron sword in its scabbard

Storage; inventory number: Institute of Archaeology of the Czech Academy of Sciences, Brno; 266/114

Dating: 9th century

Provenance: ?

Technical analysis (Figure 7a, b)

Weave: tabby with a supplemental pattern weft

Warp

material: flax, z-twist, brown colour

count: c. 25 threads per cm

Weft

proportion (pass): 1 ground weft to 1 pattern weft

- ground

material: flax, z-twist, brown colour

- pattern

material: flax, S/2z, brown colour

count: 20 threads per cm (ground weft), 20 threads per cm (pattern weft)

Characteristics of the weave: a tabby weave with one supplementary floating pattern weft whose short floats, always across two warp threads, create a small geometric pattern on the fabric obverse; weave unit 20/16 (8+8)

Pattern: diagonal rows of disarrayed diamonds

Pattern rapport: height 0.4 cm, width 0.8 cm

Original use: part of the inner lining of a wooden sword scabbard

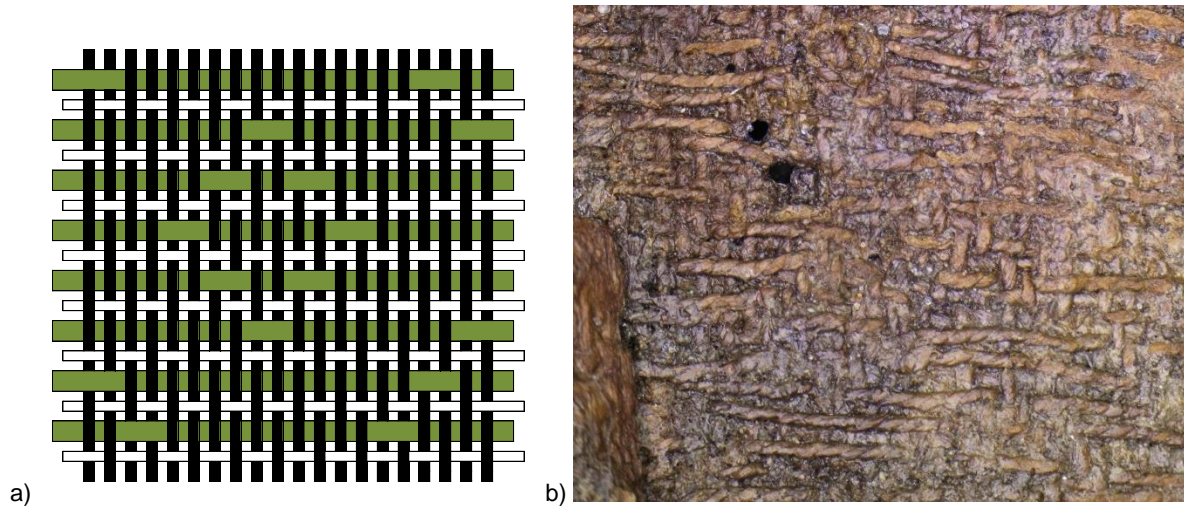


Figure 7. Fabric with supplemental patterning weft: a) weave diagram; b) reverse of mineralised fabric
 © Institute of Archaeology of the Czech Academy of Sciences, Brno

7. Satin

Satin is a weave based on a unit of five or more ends and a number of picks equal to, or a multiple of, the number of ends. Each end either passes over four or more adjacent picks and under the next one, or passes under four or more adjacent picks and over the next one. The points of binding are set over two or more ends on successive picks.

This weave appeared in China in the 9th century and later also gained popularity in central Asia, the Near East and in Egypt, where it was used in the ground of lampas fabrics. It doesn't appear in European silk production until the end of the 13th century, and the use of this weave increases in the following century. Satin's occurrence on wool fabrics in European assemblages from the 14th century is very rare, and it isn't until the 15th century that the weave appears more frequently [19].

7.1. Silk fabric [20]

Find circumstances: Prague 1 – New Town, waste layer

Storage; inventory number: The City of Prague Museum; 40_B5_69

Dating: 14th – 15th century

Provenance: western, southern Europe (?)

Technical analysis (Figure 8a, b)

Weave: 5-end warp-faced satin

Warp

material: silk, z-twist, brown colour

count: 95 threads per cm

Weft

material: silk, without visible twist, brown colour

count: 36 threads per cm

Characteristics of the weave: interruption 2

Pattern: unpatterned

Original use: indeterminable

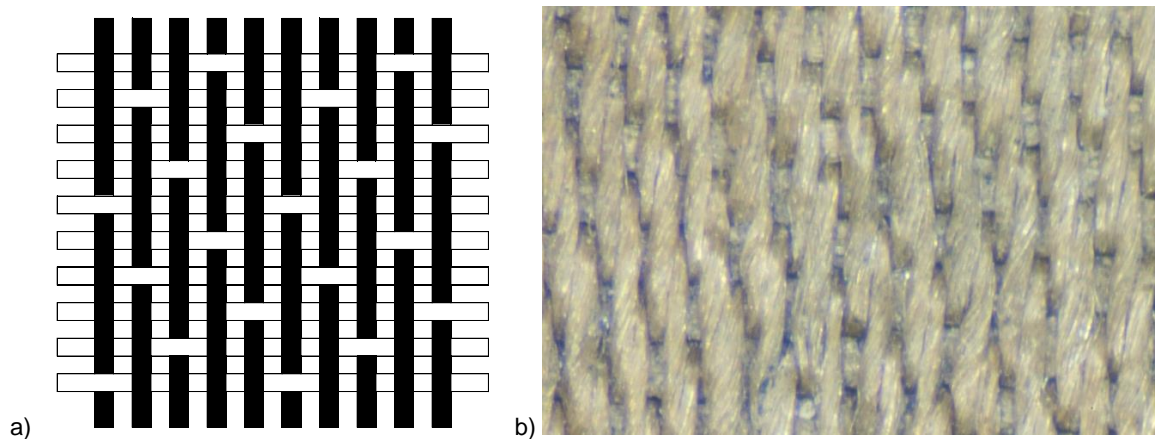


Figure 8. Silk fabric: a) weave diagram; b) fabric detail © Z. Kačerová.

8. Damask

Damask is a figured textile with one warp and one weft in which the pattern is formed by a contrast of binding systems. In its classic form, it is reversible, and the contrast is produced by the use of the warp and weft faces of the same weave.

Damask in twill weaves appeared in the east Mediterranean and the Near East sometime in the 3rd-4th century, in China much earlier. From sometime in the 7th century the production of this type of damask became very important in China, whereas its popularity in the west declined. Thanks to trade on the renewed Silk Road, damask expanded westward again from the end of the 12th century; it was woven primarily in Syria and Egypt. Damask fabric in a satin weave was also produced in China beginning in the 13th century [21, 22].

8.1. Fabric with a plant pattern [23]

Find circumstances: Prague 1 – New Town, waste layer

Storage; inventory number: The City of Prague Museum; 1_V31_82; 1_V31_280; N_R3_58

Dating: 14th century

Provenance: China

Technical analysis (Figure 9a, b)

Textile type: damask

Warp

material: silk, no visible twist, brown colour

découpure: 1 warp

count: 65 threads per cm

Weft

material: silk, no visible twist, brown colour

découpure: 1 weft

count: c. 60 threads per cm

Characteristics of the weave: ground – warp-faced 2.1 twill Z; pattern – weft-faced 1.2 twill S

Pattern: rising in the warp direction are parallel and very wide wavy lines in the form of stylised tendrils with shoots and leaves reminiscent of lotus flowers; the space between the ornamentation is filled with a small geometric pattern

Pattern rapport: height 7 cm, width 4.5 cm

Original use: indeterminable

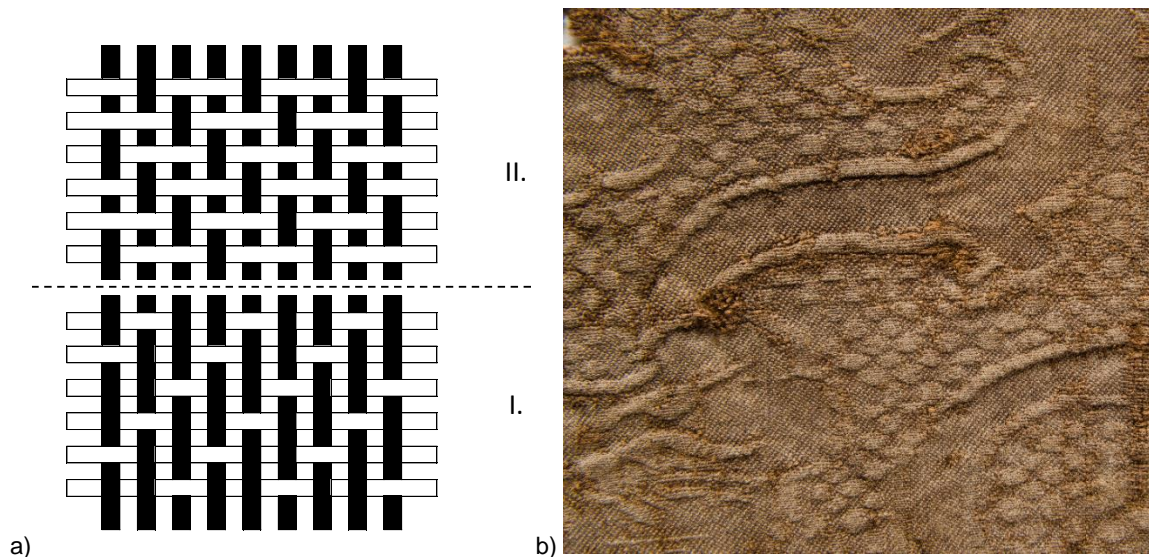


Figure 9. Fabric with plant pattern a) weave diagram: I. – ground; II. – pattern; b) fabric detail © Z. Kačerová.

9. Weft-faced compound twill

Weft-faced compound twill is a weave employing a main warp, a binding warp, and a weft composed of two or more series of threads, usually of different colours. By the action of the main warp ends, only one weft thread appears on the face, while the other or others are kept to the reverse. The ends of the binding warp bind the weft in passes in twill, and the ground and the pattern are formed simultaneously. The entire surface is covered by weft floats that hide the main warp ends.

Weft-faced compound twill first appeared in Persia roughly in the period of 300-500. The oldest fabric woven in this manner has a ratio of one main warp thread to one binding warp thread. In the Near East and the Byzantine Empire, weft-faced compound twill was later made in a ratio of two main warp threads to one binding warp thread, a weave that spread towards Central and Eastern Asia, with Arabs to the west across the Mediterranean to southern Spain. The greatest expansion of weft-faced compound twill dates to around the year 1000; the fabric also occurred in the 12th century before fading from use in the 14th century [24, 25].

9.1. *Fabric with lions* [26]

Find circumstances: Prague 1 – New Town, waste layer

Storage; inventory number: The City of Prague Museum; 1_V31_80

Dating: 13th century

Provenance: Spain

Technical analysis (Figure 10a, b)

Weave: 1.2 weft-faced compound twill

Warp

proportion: 2 main warps to 1 binding warp

- main

material: silk, no visible twist, yellow colour

- binding

material: silk, no visible twist, yellow colour

count: 24 threads per cm (main warp), 12 threads per cm (binding warp)

découpure: 1 main warp

Weft

proportion (pass): 3 wefts

- I. *latté*

material: silk, no visible twist, yellow colour

- II. *interrompu*

material: silk, no visible twist, yellow colour

- III. *interrompu*

material: probably a strip from silver-plated and gold-plated animal substrate wound around a flax core; preserved in minute remnants

count: c. 24 passes per cm

découpure: 1 pass

Characteristics of the weave: weft-faced compound twill with three weft series; binding warp interlaces in 1.2 twill S in passes

Pattern: only part of the pattern with a pair of sitting lions with their backs to one another have been preserved

Pattern rapport: indeterminable

Original use: indeterminable

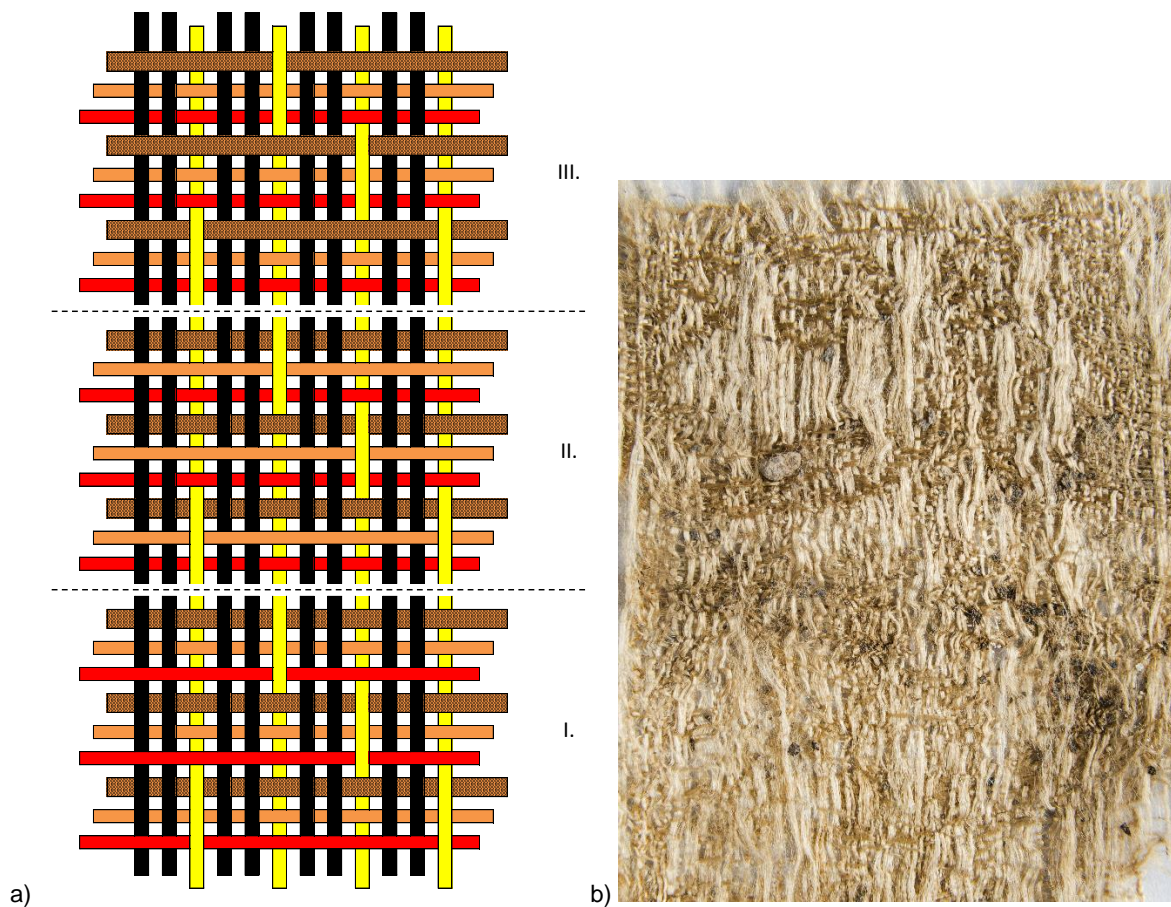


Figure 10. Fabric with lions: a) weave diagram: I. – effect of weft I.; II. – effect of weft II.; III. – effect of weft III.; b) fabric detail © Z. Kačerová.

9.2. *Fabric with birds in medallions* [27]

Find circumstances: Prague Castle, St. Vitus Cathedral, Royal crypt, perhaps the Romanesque chest apparently used to transport the remains of Conrad II Oto, Duke of Bohemia (†1191)

Storage; inventory number: Prague Castle collection; PHA 95/01, HS 12038

Dating: second half of the 12th century

Provenance: Sicily

Technical analysis (Figure 11)

Weave: 1.2 weft-faced compound twill

Warp

proportion: 2 main warps to 1 binding warp

- main

material: silk, z-twist, ochre colour

- binding

material: silk, z-twist, ochre colour

découpure: 2 main warps

count: 40-48 threads per cm (main warp), 20-24 threads per cm (binding warp)

Weft

proportion (pass): 5 wefts

- I.

material: silk, no visible twist, ochre colour

- II.

material: silk, no visible twist, ochre colour

- III. brocading

material: silk, no visible twist, brown-red colour

- IV. brocading

material: silk, no visible twist, red-pink colour

- V. brocading

material: gold-plated animal substrate wound around a silk core (Z twist, ochre colour), assembly Z, *couvert* (?)

count: 26-35 passes per cm

découpure: 1 pass

Characteristics of the weave: weft-faced compound twill with five weft series; binding warp interlaces in 1.2 twill S in passes; weft I. remains on reverse, weft II. on the obverse forms the background of the pattern; the pattern is composed of three brocading wefts

Pattern: the round medallions from two lines are filled with pearl roundel with the Tree of Life with cordate leaves; two birds with their bodies facing away from each other and the heads turned towards one another stand in front of the tree; there are four small stars in the space between individual medallions

Pattern rapport: indeterminable

Original use: possible wrap for the relics of Conrad II Oto, Duke of Bohemia

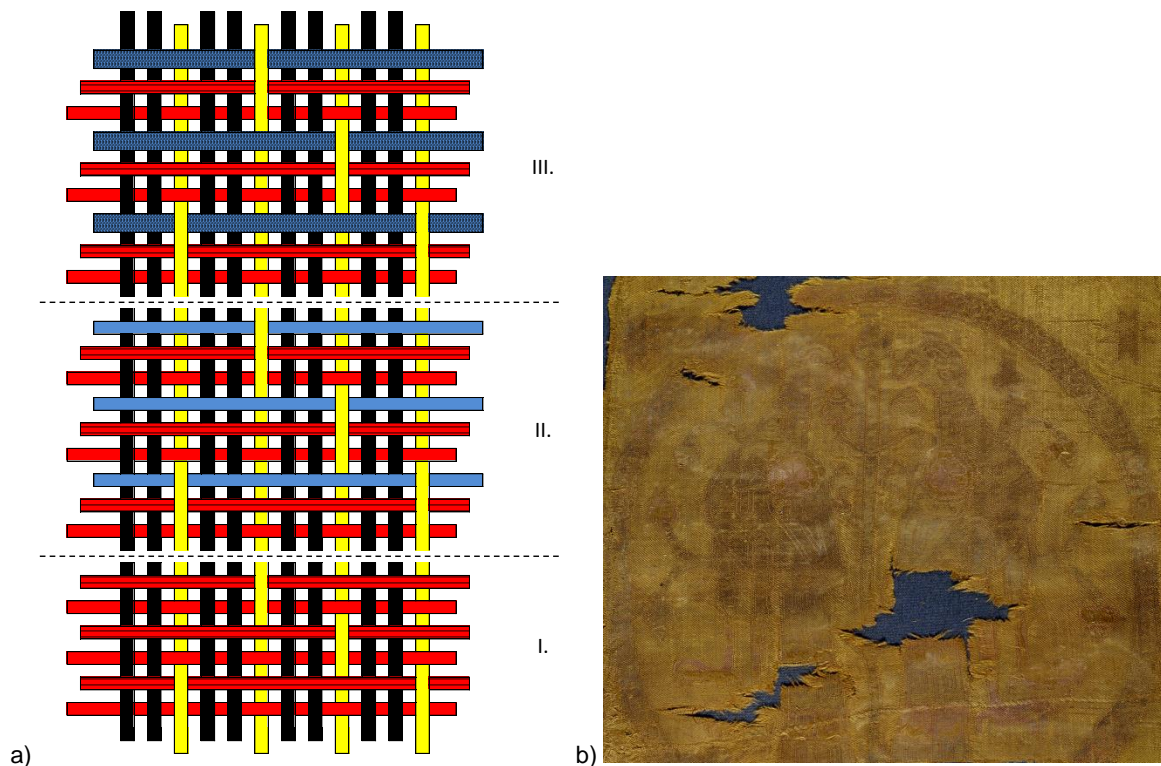


Figure 11. Fabric with birds in medallions: a) weave diagram: I. – effect of weft II.; II. – effect of weft III. or IV.; III. – effect of weft V.; fabric detail © Prague Castle collection, J. Gloc.

10. Proto-lampas

Proto-lampas is a weave composed of a main warp, a binding warp and two weft systems – a ground weft and a pattern weft which, depending on the demands of the pattern, run either on the obverse or reverse of the fabric. The warp threads are often grouped in the ratio of two main warp threads to one binding warp thread. The ground is in an extended tabby weave and is composed of all warp threads and the ground weft, the pattern weft lies beneath the main warp and interlaces with the binding warp in a 1.2 twill S on the face. The pattern is composed of the pattern weft, which lies above the main warp and is connected by a binding warp in a 1.2 twill S on the face; the ground weft is in a tabby weave. The proportion of ground wefts to the pattern wefts in the following order is characteristic: one ground weft, one pattern weft, one ground weft, two pattern wefts (see 10.1.). Other variants also exist (see 10.2.).

Proto-lampas weaves appear at the turn of the 11th century, when in the Byzantine Empire, in a historical region in West Asia situated within the Tigris–Euphrates river system and in Persia, interest in monochrome patterned fabrics grew. Several weaving techniques emerged differentiating the ground and pattern structure, thus making it possible to emphasise the decorative motifs on monochrome fabrics. Proto-lampas was one of these techniques, as the grainy surface of tabby alternates here with the glossy surface of twills [28].

10.1. *Fabric with pointed ovals (?)* [29]

Find circumstances: Prague Castle, St. Vitus Cathedral, graves of the Prague bishops, probably Bishop Cosmas (†1098)

Storage; inventory number: Church treasury at St. Vitus (held by the Prague Castle Administration); K 441

Dating: 11th century (?)

Provenance: Byzantine Empire (?), Syria (?)

Technical analysis (Figure 12)

Textile type: proto-lampas

Warp

proportion: 2 main warps to 1 binding warp

- main

material: silk, z-twist, brown colour

- binding

material: silk, z-twist, brown colour

découpure: 1 main warp

count: 32 threads per cm (main warp), 16 threads per cm (binding warp)

Weft

proportion (pass): 2 ground wefts to 3 pattern wefts (1 ground weft, 1 pattern weft, 1 ground weft, 2 pattern wefts)

- ground

material: silk, no visible twist, brown colour

- pattern

material: silk, no visible twist, brown colour

count: 30 passes per cm

découpure: 4 passes (?)

Characteristics of the weave: ground – extended tabby; pattern – 1.2 twill S; classic proto-lampas

Pattern: indeterminable, it is possible that it was conceived as pointed ovals

Pattern rapport: indeterminable

Original use: burial vestment

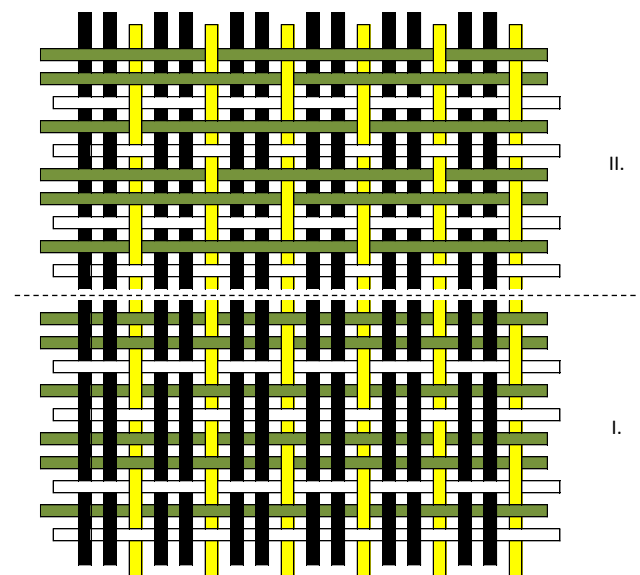


Figure 12. Fabric with pointed ovals (?): weave diagram: I. – ground; II. – pattern.

10.2. Fabric with two patterns – birds in medallions and small connected medallions [30]

Find circumstances: Prague Castle, St. George's Basilica, reliquary tomb of St. Ludmila

Storage; inventory number: Prague Castle collection; PHA 35/03, HS 10999

Dating: about 1000 – first third of the 11th century

Technical analysis (Figure 13a, b)

Textile type: proto-lampas

Provenance: Byzantine Empire (?), Byzantine province in contact with the Islamic countries

Warp

proportion: 1 main warp to 1 binding warp

- main

material: silk, z-twist, natural colour

- binding

material: silk, z-twist, natural colour

découpure: 1 main warp

count: 18-22 threads per cm (main warp), 18-22 threads per cm (binding warp)

Weft

proportion (pass): 1 ground weft to 1 pattern weft

- ground

material: silk, no visible twist, natural colour

- pattern

material: silk, no visible twist, natural colour

count: 50-58 passes per cm

découpure: 3 passes

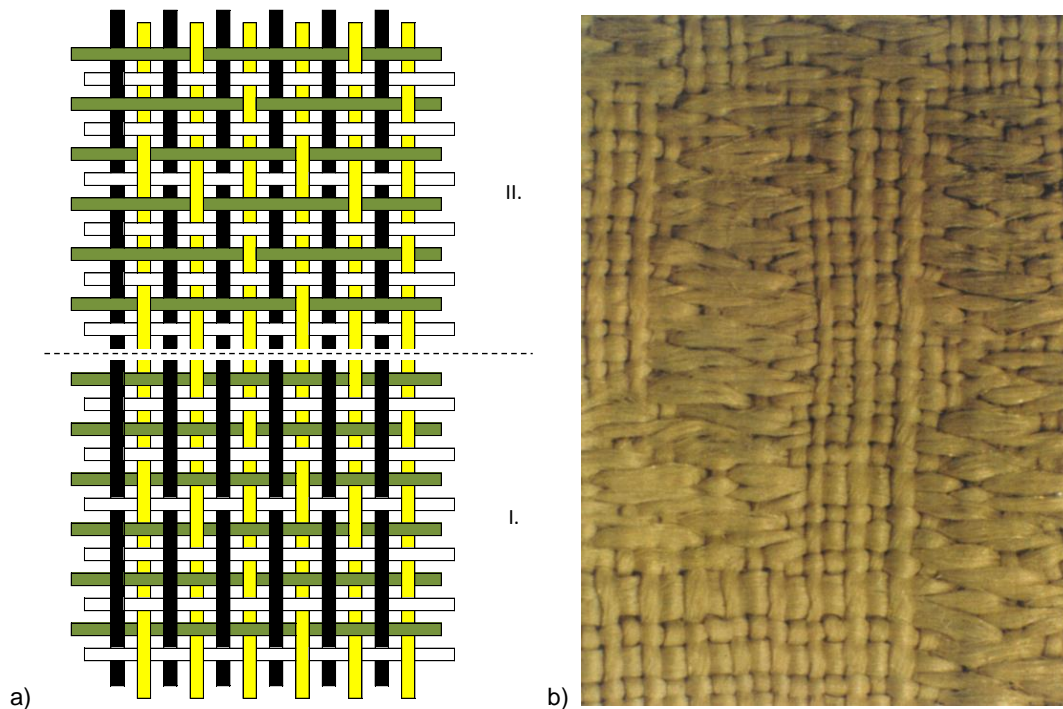


Figure 13. Fabric with two pattern: a) weave diagram: I. – ground; II. – pattern; b) fabric detail
© Prague Castle Administration, photo: J. Gloc.

Characteristics of the weave: ground – extended tabby; pattern – 1.2 twill S; unlike classic proto-lampas, there is a different ratio of warps and wefts in passes; an early variant of proto-lampas

Pattern (large): much of the preserved fabric is decorated with a large pattern with touching medallions formed by double rings; the space between the two lines is filled with tendrils; inside the medallions, birds sit in trees along the sides with their feet touching the pedestal in the shape of leaves; the connecting discs between the medallions form a double circle with pearl roundel; a flower is inside the circle; the spaces between the medallions are filled with flowers

Pattern (small): a smaller pattern in the lower strip of the preserved fabric features one row of medallions made from double circles filled with four small birds standing opposite each other in pairs; the second strip features medallions made from double lines with obliquely placed diamonds with inscribed squares; this octagon is filled with four birds standing opposite one another with flowing ribbons around their neck; in the upper and lower corner of the octagon are small discs; in the side corners are anchored crosses, and the round and octagonal medallions are continuously interconnected by loops

Pattern rapport (large): height 18-24.2 cm, height 24.3-28.2 cm

Pattern rapport (small): the full height is not preserved, the width is half the width of the large pattern

Original use: originally a dalmatic that was one of the wrappings for the relics of St. Ludmila

11. Lampas

Lampas is a term used for figured textiles in which a pattern composed of weft floats bound by a binding warp is added to a ground fabric formed by a main warp and a ground weft. The ground may be tabby, twill, satin, etc. The weft threads forming the pattern may be main, pattern or brocading wefts. They float on the face as required by the pattern and are bound by the ends of the binding warp in a binding ordinarily tabby or twill and which is supplementary to the ground weave.

Lampas was developed sometime in the 11th century, presumably in Iran or Iraq, from where production expanded around the year 1100 to the entire eastern Mediterranean, to Sicily and Islamic Spain. The application of this technique began in northern Italy in the 13th century. Lampas was the predominant weave in the 14th century [31, 32].

11.1. Fabric with a small medallion between larger medallions (?) [33]

Find circumstances: Prague Castle, St. Vitus Cathedral, graves of the Prague bishops, probably Bishop Bernard Kaplíř (†1240)

Storage; inventory number: Church treasury at St. Vitus (held by the Prague Castle Administration); K 435

Dating: 12th century (?)

Provenance: Byzantine Empire, Syria

Technical analysis (Figure 14a, b)

Textile type: lampas

Warp

proportion: 4 main warps to 1 binding warp

- main

material: silk, z-twist, light brown colour

- binding

material: silk, z-twist, light brown colour

découpure: 4 main warps

count: 68 threads per cm (main warp), 17 threads per cm (binding warp)

Weft

proportion (pass): 1 ground weft to 1 pattern weft

- ground

material: silk, no visible twist, light brown colour

- pattern

material: silk, no visible twist, light brown colour

count: 24 passes per cm

découpure: 1 pass

Characteristics of the weave: ground – tabby (main warp and ground weft); pattern – tabby (binding warp and pattern weft in passes)

Pattern: the ground is composed of vertically placed round medallions demarcated by two lines; the space between them is filled with pearl roundel; the centre of the medallions is a flower; two bands made of two lines are always connected to the medallion, again filled with pearl roundel and assembled in an angle who peak always touches the next round medallion

Pattern rapport: indeterminable

Original use: mitre stitched with gold thread

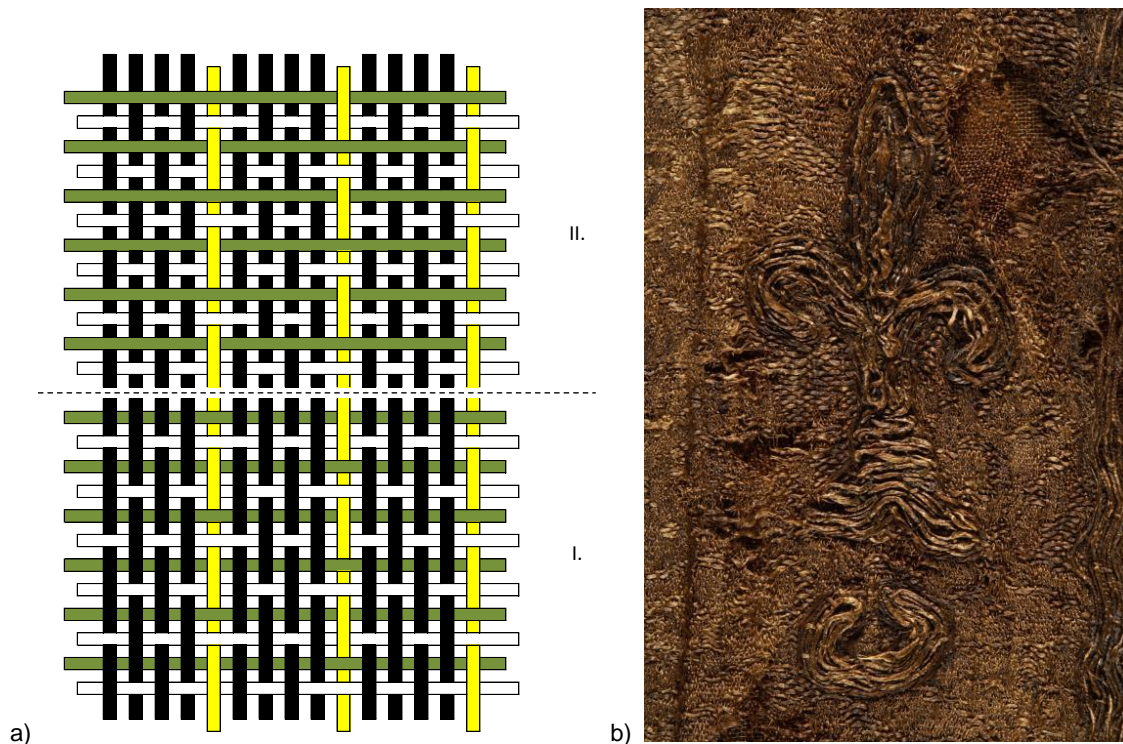


Figure 14. Fabric with small medallion between larger medallions: a) weave diagram: I. – ground; II. – pattern; b) fabric detail © Prague Castle Administration, photo: J. Gloc.

11.2. Fabric with palmettes and a diamond mesh [34]

Find circumstances: Prague Castle, Cathedral of St. Vitus, Royal crypt, possible coffin of Charles IV (†1378)

Storage; inventory number: Prague Castle collection; PHA 41/06, HS 25847

Dating: first half of 14th century

Provenance: Central Asia

Technical analysis (Figure 15a, b)

Textile type: lampas

Warp

proportion: 3 pairs of main warp to 1 binding warp

- main, paired

material: silk, z-twist, blue-green colour

- binding

material: silk, no visible twist, ochre colour

découpure: 3 pairs of main warp

count: 42 pairs thread per cm (main warp), 14 threads per cm (binding warp)

Weft

proportion (pass): 1 ground weft to 1 pattern weft I. to 1 pattern weft II.

- ground

material: silk, no visible twist, blue-green colour

- I. pattern, *interrompu*

material: silk, no visible twist, ochre colour

- II. pattern

material: gold-plated animal substrate; preserved in minute remnants

count: 12 passes per cm

découpure: 1 pass

Characteristics of the weave: ground – warp-faced 5-end satin (interruption 2; main paired warp and ground weft); pattern – tabby (binding warp and 2 pattern wefts in passes)

Pattern: composed of wide horizontal strips filled with grid ornament; the background features rows of two alternating types of palmette blossoms moved by half of their spacing

Pattern rapport: height 12.6 cm, width 25 cm

Original use: perhaps a dalmatic (only one sleeve and several small fragments are preserved)

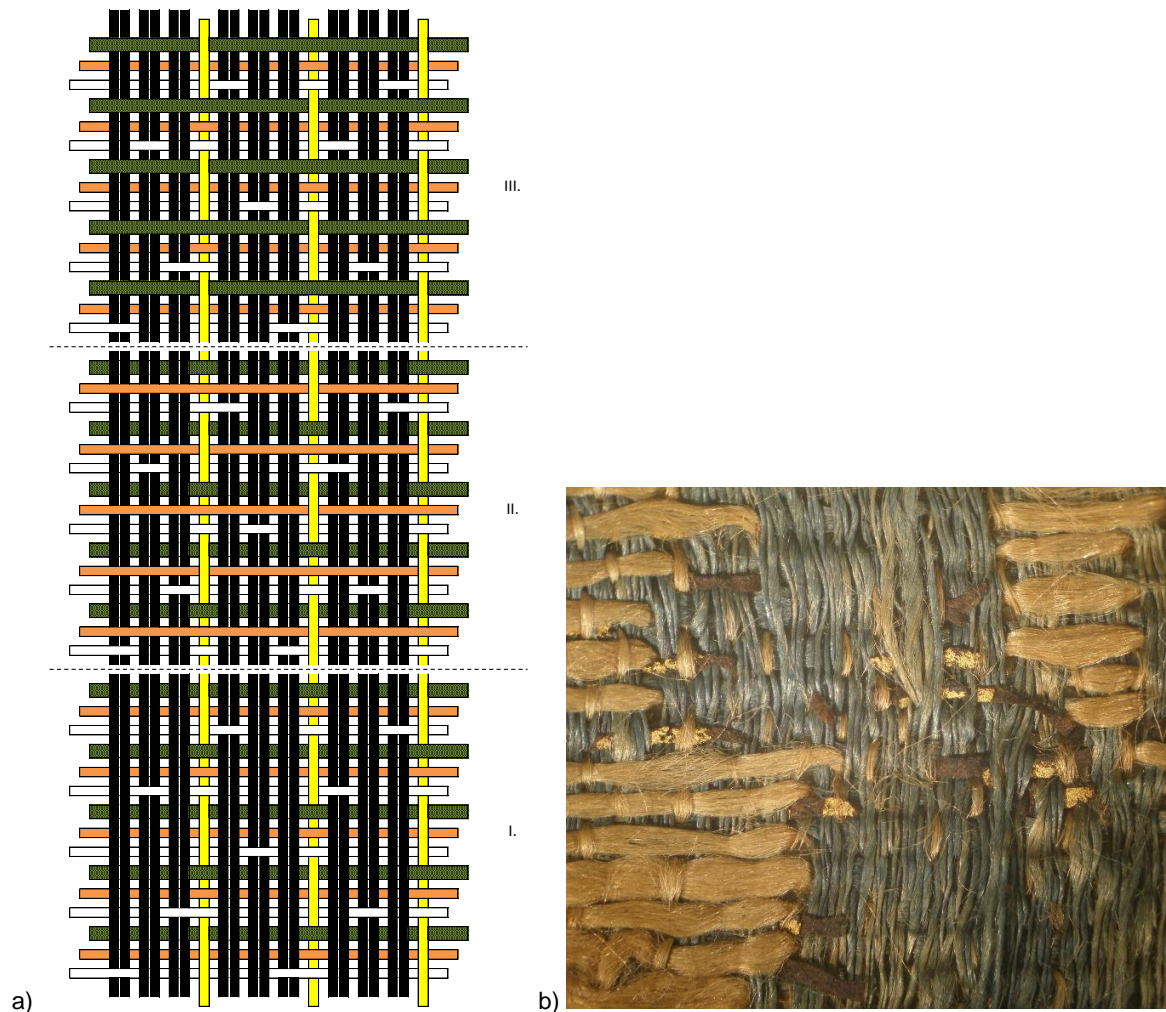


Figure 15. Fabric with palmettes and diamond mesh: a) weave diagram: I. – ground; II. – pattern – effect of weft I.; III. – pattern – effect of weft II.; b) fabric detail Prague Castle Administration, photo: J. Gloc.

11.3. Fabric with pairs of Chinese dogs, birds and a pseudo-Islamic inscription [35]

Find circumstances: Prague Castle, St. Vitus Cathedral, Royal crypt, coffin of Charles IV (†1378) or George of Poděbrady (†1471)

Storage; inventory number: Prague Castle collection; PHA 41/04, HS 21142

Dating: second half of the 14th century

Provenance: Italy

Technical analysis (Figure 16a, b)

Textile type: lampas, double weave

Warp

proportion: 3 pairs of main warp to 1 binding warp

- main, paired

material: silk, z-twist, green colour

- binding

material: silk, no visible twist, ochre colour

découpure: 2 pairs of main warp

count: 45 pairs of thread per cm (main warp), 15 threads per cm (binding warp)

Weft

proportion (pass): 2 ground wefts to 1 pattern weft

- ground

material: silk, weak z-twist, green colour

- pattern

material: gold-plated metal strip wound around a silk core (S twist, ochre colour),

assembly S, couvert

count: 24 passes per cm

découpure: 1 pass

Characteristics of the weave: ground – warp-faced 5-end satin (interruption 2; main paired warp and ground weft); pattern – 1.2 twill S (binding warp and pattern weft); where the pattern weft on the reverse is beneath the ground, it is connected to the binding weft in a tabby weave, but not connected in satin weave; in places with the pattern, the binding warp also runs beneath the ground wefts, thus binding the otherwise separate layers of the fabric

Pattern: a pair of Chinese birds flying towards one another from incomplete lotus palmettes connected below by a band with pseudo-Islamic characters; in their beak, the birds are carrying stalks from which a pair of leaves are growing, and between them is a pair of Chinese dogs

Pattern rapport: height 36.3 cm, width c. 9.2 cm

Original use: dalmatic

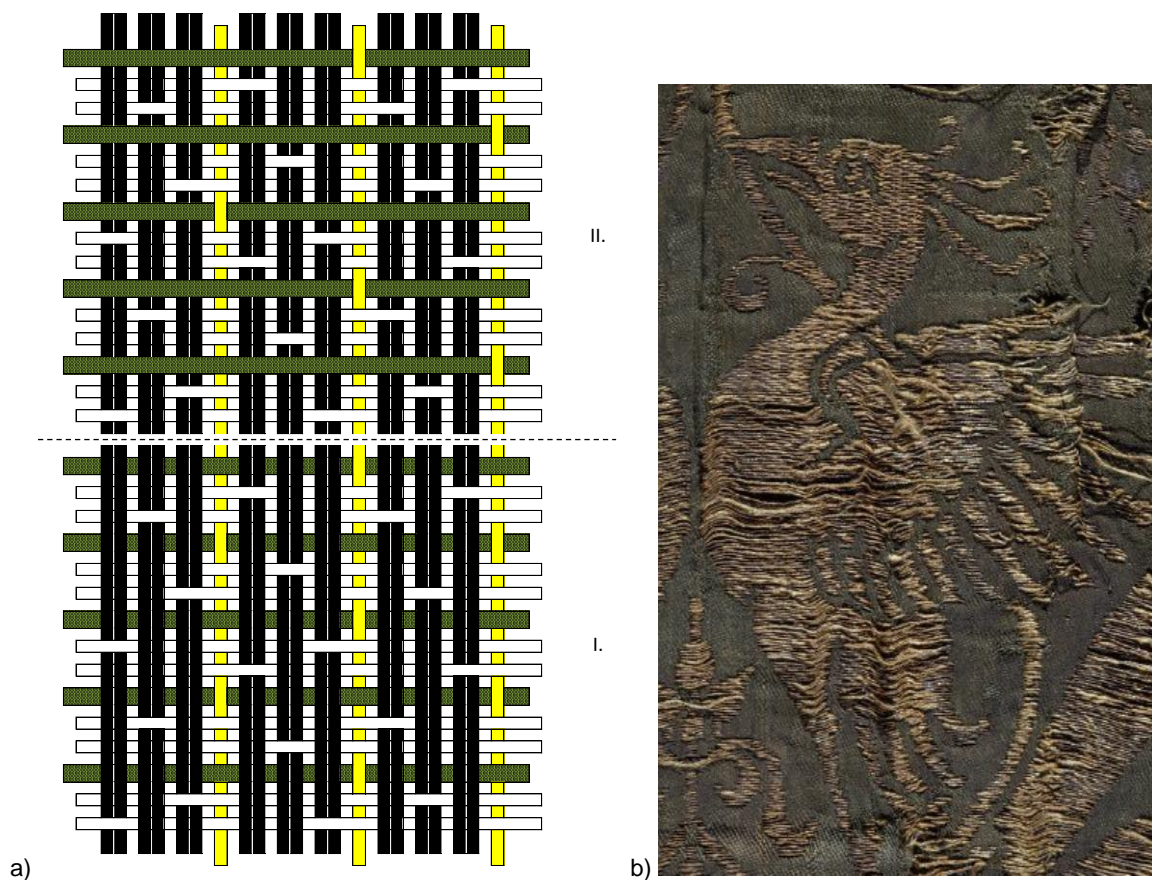


Figure 16. Fabric with a pair of Chinese dogs, birds and pseudo-Islamic inscription: a) weave diagram: I. – ground; II. – pattern; b) fabric detail © Prague Castle Administration, photo: J. Gloc.

12. Velvet

Velvet is a pile weave in which the pile is produced by a pile warp which, by the introduction of thin metal rods during weaving, is raised in loops above a ground weave. Velvets can be classified based on the nature of the pile, e.g. in cut velvet the loops formed by the pile warp are cut, in uncut velvet the loops formed by the pile warp are left uncut.

The real velvet was woven in China and the Near East in the 13th and 14th centuries, despite the fact that knowledge of the loop pile warp technique is much older. The first European town to produce velvet was Lucca, Italy, at the end of the 13th century. Production then spread to other Italian towns, to Spain, France, Germany and England. Velvet was initially monochrome; polychrome velvet and velvet with patterns were introduced later [36, 37, 38].

12.1. *Unpatterned velvet* [39]

Find circumstances: Prague Castle, St. Vitus Cathedral, Royal crypt, coffin of John of Görlitz (†1386)

Storage; inventory number: Prague Castle collection; PHA 53/09, HS 25824

Dating: second half of 14th century

Provenance: Italy

Technical analysis (Figure 17a, b)

Textile type: velvet

Warp

proportion: 3 main warps to 1 pile warp

- main

material: silk, z-twist, brown colour

- pile

material: silk, no visible twist, brown colour

count: 45 threads per cm (main warp), 15 threads per cm (pile warp)

Weft

proportion (pass): 3 wefts to 1 rod

material: silk, no visible twist, brown colour

count: 45 threads per cm

Characteristics of the weave: ground – extended tabby; cut velvet; cut pile warp interlaces with one ground weft identically over one and beneath two weft threads

Pattern: unpatterned; pile covers the entire surface of the fabric

Original use: cloak with a long and free cut composed of trapezoidal segments – 'houppelande'

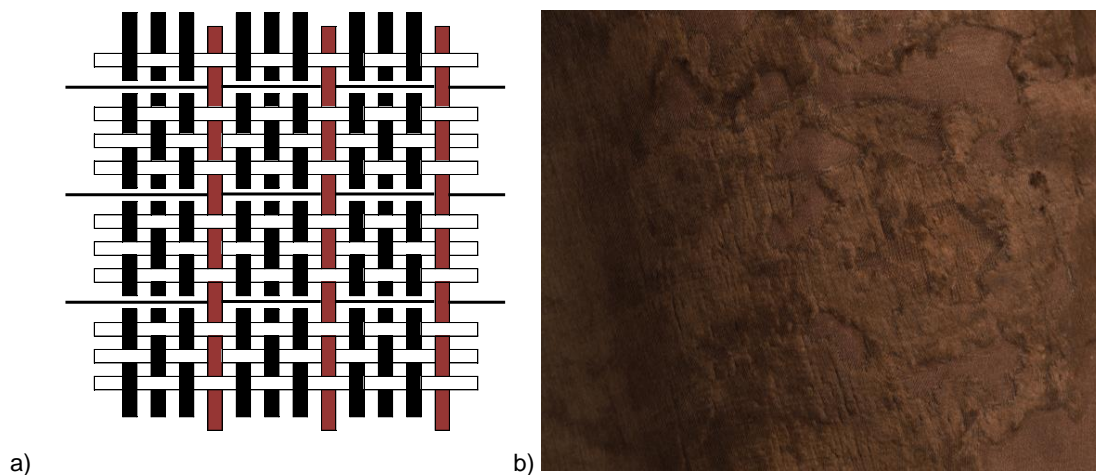


Figure 17. Unpatterned velvet: a) weave diagram; b) fabric detail

© Prague Castle Administration, photo: J. Gloc.

12.2. *Velvet with a grape motif* [40]

Find circumstances: Prague Castle, Cathedral of St. Vitus, Royal crypt, coffin of Charles IV (†1378)

Storage; inventory number: Prague Castle collection; PHA 41/03, HS 21141

Dating: second half of the 14th century

Provenance: Italy

Technical analysis (Figure 18a, b)

Textile type: velvet

Warp

proportion: 6 main warps to 1 pile warp

- main

material: silk, z-twist, brown colour

- pile

material: silk, no visible twist, brown colour

count: 78 threads per cm (main warp), 13 threads per cm (pile warp)

découpure: 1 pile warp (pile warp effect), 1 main warp (brocading weft effect)

Weft

proportion (pass): ground and pile warp effect – 3 ground wefts to 1 rod
ground and brocading weft effect – 3 ground wefts to 2 brocading wefts (2 ground wefts, 1 brocading weft, 1 ground weft, 1 brocading weft)

- ground

material: silk, no visible twist, brown colour

- brocading

material: gold-plated metal strip wound around a silk core (S twist, brown colour), assembly S, *couvert*

count: 39 threads per cm (ground weft), 26 threads per cm (brocading weft)

découpure: 1 brocading weft (brocading weft effect), 1 rod (pile warp effect)

Characteristics of the weave: ground – warp-faced 6-end satin (interruption 3-2-3-2-0-2); pattern – a) cut pile warp interlaces with one ground weft identically over one and beneath two weft threads; b) brocading weft binds in 1.3 weft-faced twill Z with each fifth main warp thread

Pattern: small, S-shaped twigs in oblique rows; each twig has two leaves turned to the opposite side (in cute pile) and one grape-shaped flower from a brocading weft

Pattern rapport: height 15.5 cm, width 15 cm

Original use: semi-circular cloak composed of either horizontally or vertically placed bands

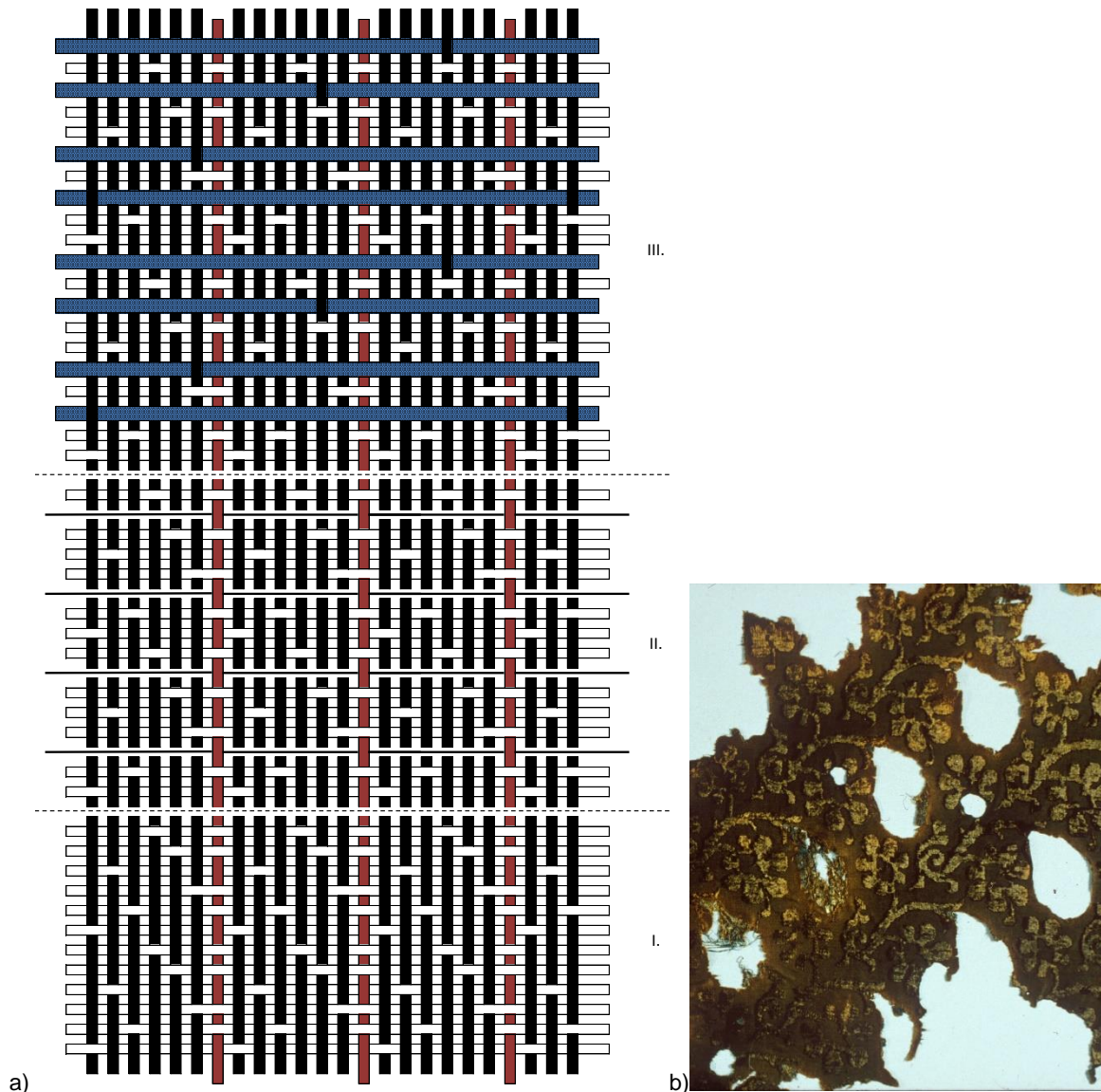


Figure 18. Velvet with a grape motif: a) weave diagram: I. – ground; II. – pattern – pile warp effect); III. – pattern – brocading weft effect; b) fabric detail © Prague Castle Administration.

13. CONCLUSIONS

In the period from the Early to Late Middle Ages, a wide variety of weaves and techniques were used to weave textiles. While only a small number have been preserved in archaeological contexts in the Czech environment, basic weaves, more complicated techniques and their variations testify to the advanced level of medieval textile production. Available finds document common household textile production as well as the ability of ruling dynasties, Church dignitaries and nobles to acquire luxury imported goods.

ACKNOWLEDGEMENTS

This work was accomplished with institutional support RVO:67985912.

For their assistance in producing this article, we thank the Archaeological Institute of the Czech Academy of Science and the Prague Castle Administration.







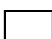







References

1. Bravermanová, M., Březinová, H., Urbanová, K. (2011). *Metodika výzkumu archeologických textilních nálezů. Zprávy památkové péče, 71/2, 97-104.*
2. Březinová, H., Kohout, D., Bravermanová, M., Otavská, V., Selmi Wallisová, M. (2016): *Středověké textilní a barvířské technologie. Soubor textilních fragmentů z odpadních vrstev z Nového Města pražského. Medieval Textiles and Dyeing Technologies. An Assemblage of Textile Fragments from the Waste Layers of Prague's New Town. Institute of Archaeology of the CAS (Praha).*
3. Bravermanová, M., Lutovský, M. (2007): *Hroby a hrobky našich knížat, králů a prezidentů (Praha).*
4. Bravermanová, M. (2016): *Pražský hrad jako pohřebiště lucemburské dynastie. Prague Castle as the burial site of the Luxembourg dynasty. In: Bravermanová, M., Chotěbor, P. (eds.): Koruna království. The Crown of the Kingdom. Katedrála sv. Víta a Karel IV. Charles IV and the Cathedral of St. Vitus (Praha), 78-114.*
5. Březinová, H. (2013): *Finds of textile fragments and evidence of textile production at a major excavation site of the Great Moravia in Mikulčice (South Moravia, Czech Republic). In: Bank-Burges, J., Nübold, C. (eds.). NESAT XI. The North European Symposium for Archaeological Textiles. Verlag Marie Leidorf (Rahden/Westfalen), 193-196.*
6. Broudy, E. (1979): *The Book of Looms (Hanover – London).*
7. Peter, M. (2016). *A Head Start through Technology: Early Oriental Velvets and the West. In: Fircks, J., Schorta, R. (eds.). Oriental Silks in Medieval Europe. Riggisberger Berichte 21. Abegg-Stiftung (Bern), 300-315.*
8. CIETA 1964: *Vocabulary of Technical Terms (Lyon).*
9. e.g. Grömer, K. (2010). *Prähistorische Textilkunst in Mitteleuropa. Geschichte des Handwerks und Kleidung vor den Römern (Wien).*
10. see no. 2, pp. 66-68.
11. see no. 2, p. 318.
12. Bravermanová, M., Leppin, B., Otavská, V. (2011). *Fragment pohřebních šatů a závoj, tzv. kruseler, z rakve českých královen z královské hrobky v katedrále sv. Víta. Das Fragment eines Begräbniskleides und ein Schleir, ein sog. Kruseler, aus dem Sarg böhmischer Königinnen aus der Königsgruft im St. Veitsdom. Archaeologia historica, 36, 593-625.*
13. see no. 2, pp. 66-67.
14. see no. 2, p. 305.

15. Bravermanová, M., Kloudová, R. (2009). Geometricky zdobená tkanina z královské hrobky v katedrále sv. Víta. *Geometrisch verziertes Gewebe aus dem Königsgrab im Veitsdom. Archaeologia historica*, 34, 463-481.
16. Bravermanová, M., Kloudová, R., Sliwka, A. (2007). Pohřební výbava pražského biskupa Mikuláše. *Die Grabausstattung des Prager Bischofs Nikolaus. Archaeologia historica*, 32, 477-489; about the fabric with stylised diamond mesh see pp. 483-486.
17. see no. 15.
18. unpublished.
19. see no. 2, pp. 88, 91.
20. see no. 2, p. 333.
21. Wilckens, L. von (1991). *Die textilen Kunste. Von der Spätantike bis um 1500 (München)*.
22. Kuhn, D. – Zhao Feng eds. (2012). *Chinese Silks. The Culture and Civilization of China. Yale University*, 128-130, 344-346.
23. see no. 2, pp. 294, 347.
24. see no. 21.
25. Geijer, A. (1979). *A History of Textile Art (London)*.
26. see no. 2, p. 294.
27. Bravermanová, M., Otavská, V. (2000). Románská tkanina z královské hrobky na Pražském hradě. *Ein romanisches Gewebe aus der königlichen Gruft. Archaeologia historica*, 25, 405-428.
28. Schorta, R. (2001). *Monochrome Seidengewebe des hohen Mittelalters (Berlin)*, 34-41.
29. Bravermanová, M., Otavská, V., Sliwka, A., Beneš, J., Kopecká, I., Mazura, I. (2001). Nové poznatky o nejstarších textilích z hrobu sv. Ludmily. *Neue Erkenntnisse von den ältesten Textilien aus dem Relikviengrab der Heiligen Ludmila. Archaeologia historica*, 26, 447-486; about the fabric with pointed ovals (?) see pp. 461-462, 479.
30. see no. 29.
31. see no. 21.
32. see no. 25.
33. Bravermanová, M., Foltýn, D., Sliwka, A. (2010). Mitra z hrobu 'ctihodného Bernarda, biskupa pražského'. *The mitre from the grave of 'venerable Bernard, the Prague bishop', Medievalia historica Bohemica*, 13/1, 7-45.
34. Bravermanová, M., Brabcová, T., Odstrčilová, S., Prajzlerová, A., Vrabcová, A. (2017): Nové poznatky o pohřebním rouchu Karla IV. z královské krypty v katedrále sv. Víta. *Neue Erkenntnisse über das Begräbnisgewand Karl IV. aus der königlichen Krypta in der St.-Veits-Kathedrale. In: Nachtmannová, A., Klapetková, O. (eds.): Oděv a textil v životě člověka doby lucemburské (Praha)*, 17-40.
35. Bravermanová, M., Kloudová, R., Otavská, V., Vrabcová, A. (2005). Pohřební roucho Karla IV. z královské krypty v katedrále sv. Víta. *Das Beerdigungsgewand des Karl IV aus der königlichen Krypta in der Kathedrale des Hl. Veit. Archaeologia historica*, 30, 471-496.
36. see no. 25.
37. see no. 21.
38. see no. 22, pp. 399-402.
39. Bravermanová, M., Kloudová, R. (2006). Pohřební oděv Jana Zhořeleckého z královské hrobky v katedrále sv. Víta na Pražském hradě. *Begräbnisgewand von Jan Zhořelecký aus der königlichen Gruft im Sankt – Veits – Dom in der Prager Burg. Archaeologia historica*, 31, 403-412.
40. see no. 35.

Footnotes:

1) Definition of weaves and terms in textile technological studies are taken from professional terminology codified by CIETA [8]. Illustrations of weave diagrams are processed according to the following key:

	main warp		brocading weft
	binding warp		brocading weft - metal thread
	pile warp		weft
	ground weft		weft II.
	ground weft II.		weft <i>interrompu</i>
	pattern weft		weft <i>interrompu</i> - metal thread
	pattern weft - metal thread		rod

2) In all cases, the stated colours are current colours, most of which do not correspond to the original colour.

FORMATION OF THE TEXTILE STRUCTURES FOR A SPECIFIED PURPOSE

Marcin Barburski

Lodz University of Technology, Faculty of Material Technologies and Textile Design,
Institute of Architecture of Textile, 116 Zeromskiego Street, 90-924 Lodz, Poland
Tel: 0048426313333, Fax: 0048426313343, e-mail: marcin.barburski@p.lodz.pl

Abstract:

Woven fabrics are the most common example of flat textile materials used in the manufacturing of clothing, decorative, technical, and special purpose products.

Increasing expectations regarding the variety of fabric uses have prompted researchers to seek the optimal applied properties of fabrics as well as their internal structure. Woven fabric as a complex textile product, with advantages and disadvantages of the fibres and yarns on one side as well as of the way of manufacturing and finishing on the other, is an interesting, however not thoroughly acquainted, study case.

The article presents the possibility of modelling mechanical properties of a dedicated woven product, shaping the bending stiffness of technical woven structures intended for pipe conveyor belts, structures as sound-absorbing barriers and multi-axis woven structures used to reinforce composites. These are a few examples of developed, dedicated woven structures of specific purpose.

Key words:

Textile structures, pipe conveyor belts, sound-absorbing barriers, multi-axis woven structures

1. Introduction

Woven fabrics are the most common example of flat textile materials used in the manufacturing of both clothing and decorative, technical and special purposes products.

Increasing expectations of the variety of fabrics' uses incline to the search of optimal applied properties of fabrics and, following, their internal structure. Woven fabric as a complex textile product consisting of advantages and disadvantages of fibres and yarns on one side, as well as of the way of manufacturing and finishing on the other one, is an interesting, however not thoroughly acquainted, study case.

Parameters of fabric structure are used for its identification, that is, to characterize it so that it can be accurately and precisely reproduced at any time. The more accurate the characteristics of structural parameters of the reference fabric, the more fabric being reproduced is similar to the original. In addition, almost all fabric properties can be shaped as functions of many factors.

In the case of textile design, the endeavour is to make the finished product as similar as possible to the designed one. The designer must be careful in choice of parameters of the fibre, yarn and fabric structure so that the functional properties of the finished product are consistent with the earlier assumptions.

The construction of models of textile products aims at setting the basis for discussion on mechanical and applied properties of these products as well as providing the technologists with the information on the extreme parameters of the products possible to manufacturing from certain materials and on machines available.

2. Modeling of the fabrics

Large number of solutions when it comes to construction of fabrics differing in the raw material used, thickness, structure and filing, weave and finishing, makes it difficult to empirically find the dependence between the product structure parameters and the mechanical properties of its finished form. There are many parameters of the fabric structure, which the designer should choose optimally when modelling the characteristics of the product. This is core for giving fabrics the basic functions that a product should achieve for given needs. Thorough knowledge of rule and structural and utilitarian relations in fabrics is the basis needed in their conscious analysis. For many years, scientists have been introducing mechanical and geometric models for structural analysis of fabrics to characterize their internal geometry.

The textile structure changes under small deforming strengths. There are two consequences of these changes: the first is a significant difference in the barrier of deformed products, and the second - a difference in mechanical properties such as resistance and stiffness.

When considering the properties of fabrics, certain models of their construction can be used [1,2]. There are two basic types of these models:

- mechanical models (eg according to Olofsson, Nosek), based on the analysis of the conditions of fabric creation and the properties of its threads,

- geometrical models (eg Peirce, Kemp), not concentrating on tension of threads, or not taking into account the external forces, but, relatively, most precisely reflecting the actual structure of the fabric.

In the literature on the fabric structure various descriptions are always based on simplified models.

Peirce's geometric model is widely used to describe the structure of fabrics. However, structural changes of fabrics during stretching are characterized using Painter's nomogram.

In order to specify and more accurately describe the structure of fabric subjected to static load, it seems important to look for new methods in this field of research so that they could describe the fabric architecture as precisely as possible, with the possibility of predicting its mechanical properties.

There are many parameters of the fabric structure that the designer should choose optimally when modelling the product features. This is the basis in providing fabrics with the most important functions needed during the use of the finished product. Thorough knowledge of laws and relations between structural and utilitarian features of fabrics makes up the basis for conscious analysis of many aspects of fabrics. This knowledge also serves as an indispensable tool for fabric design.

Experimental and scientific research, as well as fabrics modelling both enable determining the principles of changes in the fabric structure subjected to static forces. By modelling changes in the fabric structure subjected to static forces with the use of new modified nomograms, it is possible to more accurately describe the structure of real fabrics subjected to static strengths, eliminating generalizations of analysis while using Painter's nomogram [9].

All real fabrics can be specified by the deformation of circular cross section of warp and weft threads. The scale of the deformation depends on the kind of thread, material used, the way of weaving, the weave, the weaving strengths and the susceptibility of thread to cross deformation. The shape of cross section of threads in fabric can only be approached by different plane geometric figures, such as: a circle (Peirce) [3, 4, 5, 6], an ellipse, a hippodrome shape (Kemp) [3], a convex lens (Milasius) [7]. The shape of cross section in real fabrics is diverse, which is the result of pressing and bending strengths effecting in the areas of contact of crossing warp and weft threads.

Fabric modelling using Painter's nomogram was compared with three new nomograms created as a result of research carried out at the Institute of Textile Architecture, Lodz University of Technology [8]. The experiment showed that depending on the designer's approach and expectations, various forms of

the internal structure of fabrics may be created. In addition, changes in the internal geometry of the fabric, subjected to static loads, can also be modelled in a different way. Thus, using these nomograms, each designer has the opportunity to achieve whatever they expect as far as the fabric structure is concerned.

Taking the elliptical cross-section of the yarn into account, it is possible to more accurately model the internal structure of fabrics and go through different stages of their changes when subjected to deforming strengths.

3. Conveyor belts design

The knowledge about structure and modelling of woven fabrics was used to shape technical woven products intended for pipe conveyor belts.

Conveyor belts are designed for the technological transport of all kinds of bulk materials and damp which do not cause permanent adherence to the belt and conveyor construction elements. These conveyors are applicable wherever it is necessary to quickly and accurately transport materials on the distance specified by the range of one or more coupled conveyors

The textile conveyor belt is made of fabric-rubber carcass and rubber covers. The carcass may consist of 2 to 6 spacers made of synthetic polyamide-polyester fabrics impregnated with a solution of latex which provides an intermediate layer preventing from delamination of fabric and rubber. Conveyor belt at the point of contact with the drive and reverse drums is flat. Pipe conveyor belt is closed in the work field or return and maintained by a set of four or six rollers on its circuit.

The main problem occurs when the conveyor closes, as previous construction of the pipe conveyor system makes the edges collapse inwards and the conveyor spin, causing unsealing of the belt, which may result in a loss of material transported. In addition, the unsealing causes that the material transported is not sufficiently protected against weather conditions such as rain and wind.

One of the most important elements before designing a new product is to identify and clarify the purpose of the textile product as well as to determine the problem to solve. Precise determination of the characteristics to be fulfilled by a textile product determines the properties of the product through the refinement of the structure of the product.

Formation of bending stiffness of technical woven structures differing in weave and internal geometry allowed designing the innovative pipe conveyor belt that is able to close while eliminating the tendency of collapsing its edges inward and minimizing the stresses generated in the structure during the return of the conveyor belt.

Based on the first test summaries, it was stated that depending on the weave, belts differently press against the rollers, have different stiffness and that the layer of rubber did not largely eliminate the differences in fabric properties. [9,10,11]

The preliminary research opened the way for further research on the optimization of the production process of conveyor belts so that the mechanical properties of the fabric as reinforcement could be used in a controlled manner and as far as possible.

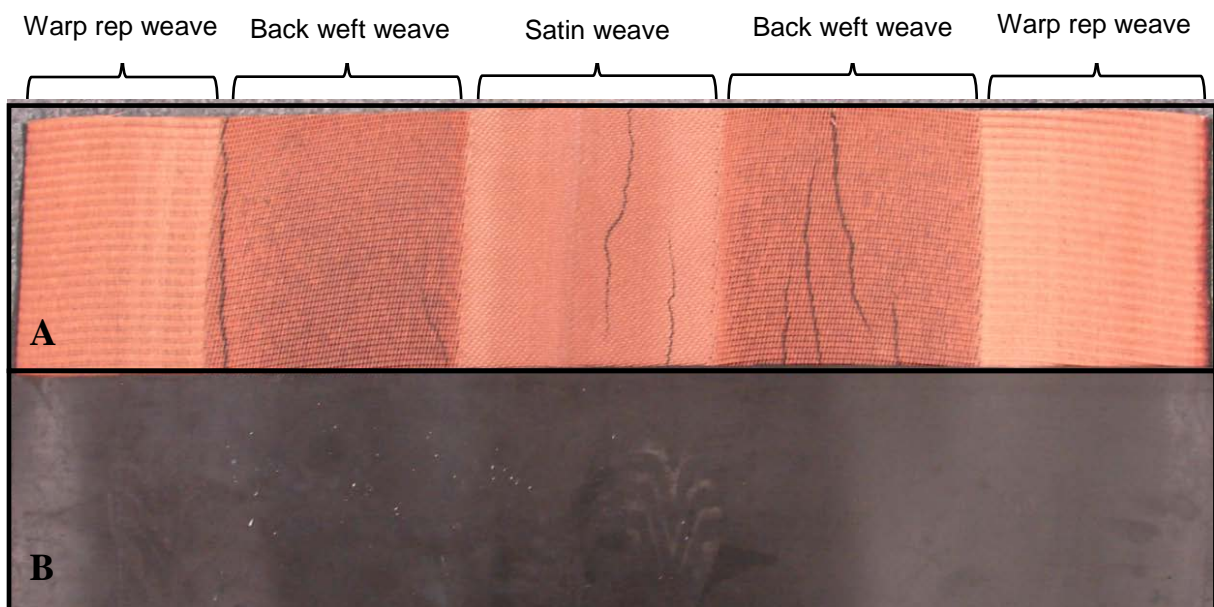
The action was taken to optimize bending stiffness of fabric used in pipe conveyor belt.

The analysis of measurement results enabled designing a new woven structure, symmetric to its longitudinal axis but different in bending stiffness on its width. These differences were possible by using three different weaves paired with each other on the fabric width (Table 1).

Table 1. Weaves applied in a new woven structure [10]

Satin weave	Back weft weave	Warp rep weave
$\frac{1}{7}(3)$	On the basis of twill weaves 1/3 and 3/1	$\frac{1}{1}(0,0,0,1,0,0,0)$

In order to verify the validity of the application of the selected three weaves, a new woven structure was produced and then covered with latex and vulcanized (Figure 1). The measurements were done of structure parameters of the new fabric, as well as of mechanical properties of the belt and its pressure on the set of rollers [9,10].


Figure 1. New woven structure with zones of different weaves symmetrically arranged along the longitudinal axis of the belt. A) covered with latex, B) vulcanized [10]

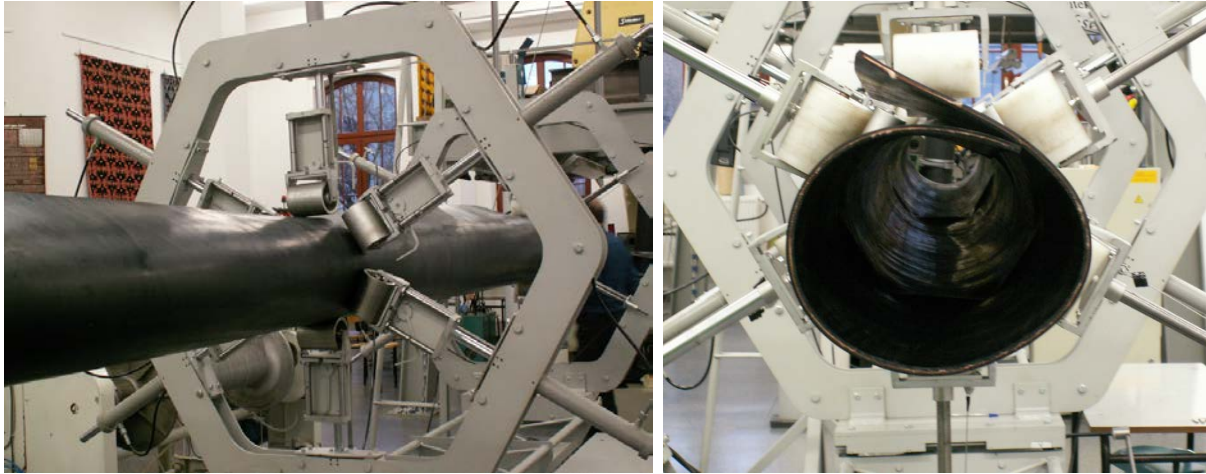


Figure 2. Pipe conveyor belt with the new fabric carcass of different weaves [10]

In line with the project assumptions the fabrics were made as reinforcement of one-spacer conveyor belts. The conveyor belt was made with the possibility of piping and closing but without a tendency of its edges to collapse inward. (Figure 2). The construction of the belt made it possible to minimize the stresses generated in the structure at the stage of the belt return eliminating multiple layers of spacers and gaining high transverse flexibility. One-spacer belt has minimized thickness, which reduces its weight, which in turn minimizes the resistance movement during rewinding the belt through the drums. [12].

This original solution puts a step forward in the conveyor belt industry. The new woven structure will also better protect the carried material from weather conditions such as rain and wind. Implementation of the project allowed the introduction of innovative solutions for the production of conveyor belts produced, inter alia, in the FTT Wolbrom SA.

4. The textile sound absorption barriers

Other dedicated textile structures may be used as acoustic absorption barriers.

The problem of noise is one of the fundamental issues that have a very significant impact on the comfort and safety of people [13]. Currently, noise is a common occurrence in the human environment. It is presented in all types of human environment and has adverse effects on human health, including hindering rest and regeneration. It reduces the efficiency of human work and also increases the likelihood of accidents at work. Long-term exposure to noise on the human body is also accompanied by deterioration of hearing or, in extreme cases, total deafness [14].

Fibrous materials have been widely used in noise reduction due to their porous structures [15]. Researchers are still developing new materials that can absorb sound energy. They comprise experimental studies on acoustic properties improvements of rigid polyurethane closed-cell foams, by incorporating various quantities of textile wastes into the matrix. [16]. Various fibrous materials including inorganic and metallic fibres, synthetic fibres, natural fibres, and nanofibrous membranes for noise reduction are reviewed. The tailored cross-sections of synthetic fibres such as circle, hollow and triangle are beneficial to improve acoustic absorption properties. The use of material wastes, coming from the fibres of fluffs, when manufacturing the sound absorber products, can help to combat two different kinds of problems: the disposal of this kind of waste and the noise control [17].

The main aim of research work was to present the acoustic transmission losses of 10 different structures of woven fabrics and to investigate the influence of weaving on the acoustic attenuation of the fabrics under the presented tests. The patterns of weaves and their structures influence mechanical properties. The internal structures give different effects, for example of abrasion resistance and air permeability,

deformability and complex shape forming including shearing properties. It is interesting how the structures of fabrics influence acoustic attenuation.

10 specimens of 150 cm x 150 cm fabrics of different structures and patterns were used for the study. The raw material for the weaving was the textured Polyester 167 dtex x 2 as the warp material. In eight samples, as the weft, the acrylic yarn 64 tex was used. Cotton and Trevira weft of similar linear density were used in other samples. The fabrics were made on the Picanol Gamma loom with Jacquard machine in the Institute of Architecture of Textiles, Lodz University of Technology. The textiles were especially prepared to specific purposes as acoustic absorption barrier. All fabrics were made on the same loom with constant densities 30 warp/cm but the internal stresses changed it during 24-hour relaxations. The individual fabrics were subjected to sound absorption tests in the aeroacoustic anechoic chamber in the Laboratory of Aeroacoustics of the Institute of Turbomachinery (Lodz University of Technology) to achieve free-field anechoic environment.

As it was expected, all tested fabrics have low sound absorbing properties at low frequencies. The presented studies also showed that all fabrics with honeycomb weaves have much less attenuation than other fabrics. Low attenuation of these fabrics is likely due to their similarity to fabrics with lower number of threads per centimeter, resulting in less dense structures at higher thicknesses. Other woven fabrics are more compact and much thinner, which results in good sound absorbing properties. The research proved that the best absorbing properties were in the cases of satin, double cloth, and back weft weaves. At higher frequencies thickness also had an insignificant effect on sound absorption. It can then be concluded that if there is air space inside and behind a fabric, sound absorption possibilities move through the frequency range. Similar results were obtained by other researchers using different testing method (inside a reverberation room) for cases of coated and uncoated textiles [18].

The proposed honeycomb fabrics can be used in combination with other acoustic adaptations, such as partially blocking and transmitting the sound to a deeper sound damping installations that, due to different reasons, must be otherwise hidden. They can also be used, for example, as covers for voice or loudspeakers systems. The honeycomb fabrics could protect the loudspeaker against the wind or other severe weather conditions without negatively affecting the good quality of the sound. In such cases, modern printing techniques allow creating interesting artistic decorative motifs, for example in concert halls, where acoustic performance is critical, and fabric's job is not only to absorb sound itself, but also to allow other acoustic sound adaptations behind the fabric to absorb sound in more predictive manner. In such cases the main task of a fabric is not to hinder or reflect the sound but to control the hall or room environment and act as additional finishing protective layer. The presented results can also be useful for interior designers and architects as the experiments were performed for the first time on such materials and compared to standard fabrics [19].

5. Textile reinforcement composite

The search for new materials of better properties than those traditionally used in techniques (metal alloys, wood, construction ceramics, etc.) resulted in creating the group of materials referred to as composites. Today, technological progress is inseparable from material engineering which deals with the creation of new materials. Engineers constructing innovative materials base on designing conditioned by the operating conditions and loads they will be subjected. Composite materials can meet these demands. Composites are now a rapidly expanding field linking issues of textiles, metallurgy, mechanics and polymer chemistry as well as plastics processing. [20,21].

The main components of the construction composite are matrix and reinforcement.

The matrix is more or less homogeneous material filling the space between the reinforcing elements. The matrix volume fraction V_m is usually 20-80 %. The reinforcement can be a different material arranged to increase the strength and stiffness of the composite.

Due to the properties of textiles, they are the most common type of reinforcement in the composites. They may be woven, braided or knitted fabrics, non-wovens or parallel-arranged fibres.

The composite resulting from wearing several layers of fabric in a "pile" is not suitable for any application because of its deformability, even under its own weight and the lack of permanent connection of layers. Both of these effects are eliminated in the second stage of producing the composite - lamination step i.e. creating a permanent connection of layers in the stiff construction element. The process involves hardening a sequence of layers arranged complying with the appropriate parameters of temperature, pressure and holding time.

In connection with the development of flat textile structures and the expansion of the area of their applications there is a need to assess the isotropy of their mechanical properties. Classical orthogonally built fabrics (weft threads arranged perpendicular to the warp threads) and less those of the orthogonal structure are one of the types of the sandwich composites reinforcement. They are characterized by isotropic properties only in the directions designated by the systems of threads which may be the same when the threads of both systems have the same mechanical parameters.

In order to provide the layered composite materials with suitable isotropic properties, the fabrics being next layers of the reinforcement are placed at different angles to the main axis of the composite. The number of layers and their layout angles are a result of mechanical requirements for composite construction. In the aeronautics the composites of carbon fibre reinforcement have on average six times higher tensile strength and three times higher modulus of elasticity than steel although they have four times lower weight.

When human safety conditions are not needed to be ensured, glass, aramid or natural fibres are often used as the reinforcement. One of the natural fibres are flax fibres that have mechanical properties similar to glass fibres and significantly better than iron and aluminum.

The flax fibres show the new direction of work of the new quality and new product.

The challenge is to create such composite of natural fibres which would compete with composites of glass reinforcement as well as aluminum and iron [22,23].

During the research work at international cooperation with Politecnico di Milano and KULeuven the research focused on analysing the flax fabric used as a reinforcement of the composite. The fabric was subjected to biaxial tensile, bending and shearing in order to determine formability and mechanical properties of the product. The second part of the experiment focused on the analysis of flax fabric structure deformation at the tetrahedral form. During the formation of complex shaped composites the important parameter characterising the textile product is its drape. Among other things, this parameter determines the mechanical properties of the finished product.

The obtained results of the study are the complete set of data needed to characterize the deformation capacity of this flax product during the formation of the complex shapes of the finished composite product. These results also provide a reference data for numerical modelling. On the basis of the analysis it was found that this type of flax fabric has good deformability at low shear angles when forming on complex moulds and has better quality in this respect than other fabrics used as reinforcement of composites. [24,25].

This is mainly textile isotropy that, together with raw material and finish, decides of the textile product capabilities, hence the necessity for its insightful analysis. Finished products have mostly dimensional structure, which results in that the internal structure of the woven product is not homogeneous. These changes can result in differences in the mechanical, performance and filtration properties and in the finished product manufacturing processes.

Properties of the individual components are different from the properties of the composite but significantly influence it. Hence the need for analysis of the composites components.

Traditional textiles are characterized by, depending on their structure, different degrees of anisotropy of physical and mechanical properties. Meanwhile, the new, non-classical applications of textiles not only require materials with high strength, but also of higher and higher isotropy of its properties. The alternative to classical fabrics having large anisotropy are the multiaxial fabrics. The Institute of Textile Architecture, Lodz University of Technology for many years conducted research on innovative multiaxial

woven structures under the guidance of prof. Marek Snycerski. Among other things, globally innovative technologies producing 3, 4, 5 and even 6- axis textiles were developed [26,27, 28, 29].

Multiaxial woven structure is the name of the flat textile product, formed from at least three sets of threads connected by interlaces. Design of such structure is the formation of a grid where the nodes represent intersections of no more than two threads, and then the introduction of interlaces. The grid only shows the mutual layout of the threads (geometry), presenting them in as straight lines with directions consistent with the directions of the axis structure.

Triaxial fabrics have long been known and described in the literature [30, 31, 32, 33, 34, 35]. There is significantly less information published about fouraxial fabrics and it mainly relates to methods of their production [36,37, 38, 39,40]

The main criterion used to classify the multiaxial structures is the number of thread sets (axes), another is the type of grid and the manner of thread interlacing, i.e. the weave. Theoretically, it is possible to create many types of such fabrics weaves.

Multiaxial fabric structures can actually be oriented to any thread sets. Due to the shed method of producing classical fabrics, it was agreed that multiaxial fabrics will be oriented to the set which can stand for weft (threads arranged horizontally).

Fouraxial fabrics can be created from three warp sets and one weft set. Spans arise between the threads of these sets. Their shape and regularity depend on the weave and the values of thread scales. The sixaxial fabrics are formed by six sets of threads: five warp and one weft [Figure3] Their grids can be modelled by combining respectively mutually rotated classical fabrics [26]. The sixaxial fabric of plain weave was formed in the Institute of Textile Architecture. The fabric has large spans and the largest of them take the dodecagon shape. Structurally the fabric belongs to the group of heterogeneous scale. An alternative to the parallel-arranged fibres or classical fabrics are multiaxial fabrics of increased isotropy.

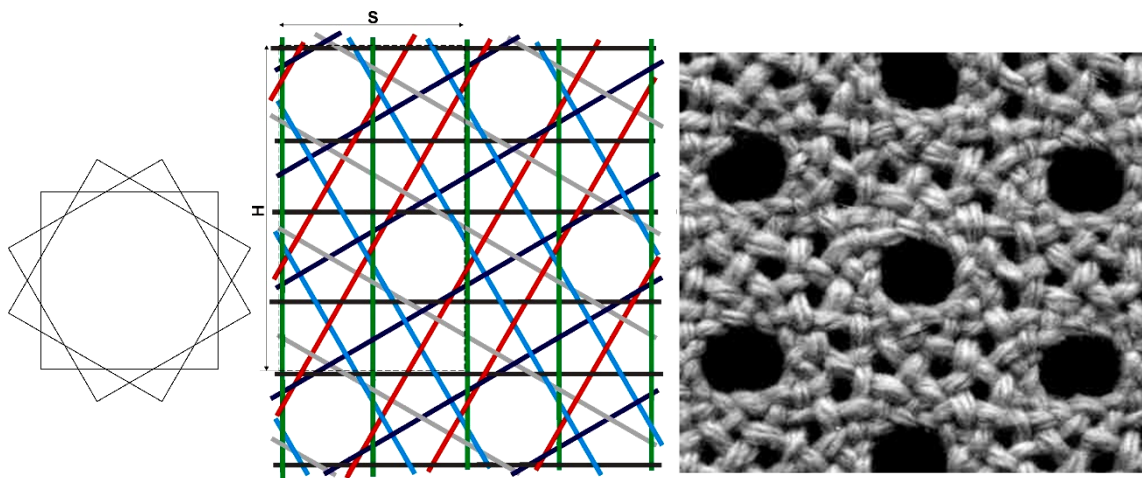


Figure 3. Base for modelling sixaxial grid, report of sixaxial fabric of plain weave and heterogeneous grid, picture of the sixaxial fabric sample [31]

6. Summary

This article presents selected issues regarding designing and formation of woven structures for a specified purpose. Scientific research is focused on formation new woven structures of complex, modified, multi-axial, and spatial, for a specified purpose, which can be used, among others, as textile reinforcements of various composites or acoustic barriers. A wide spectrum of technical application possibilities of textile products has been presented. The manuscript indicates the need for further actions regarding new applications of textile products not yet fully recognized.

References

- 1 J. Masajtis, *Structural analysis of fabrics*, Lodz 1999, (in Polish)
- 2 T. Janusz, *Weaving, part. III*, Warsaw 1963, (in Polish)
- 3 Peirce F.T., *Journal Textiles Institute*, 1937 nr 21(1409), Pages T45-T96
- 4 Szosland J., *Laboratory of the fabric construction and technology*, Lodz 1984, (in Polish)
- 5 Szosland J., *Basics of fabric construction and technology*, Warsaw, 1991, (in Polish)
- 6 Frontczak-Wasiak I., *Laboratory of the basics of mechanical fiber technology - weaving*, Lodz, 1987, (in Polish)
- 7 Milašius V., *Woven Fabric's Cross-Section: Problems, Theory, and Experimental Data*, *Fibres and Textiles in Eastern Europe* 1998, nr 4(23), s. 48-50
- 8 Barburski M., Masajtis J., *Modelling of the change of structure of woven fabric under mechanical loading*, *Fibres and Textiles Easter Europe* 2009, nr 1(72), s. 39-45
- 9 Barburski M., *Analysis of the mechanical properties of conveyor belts on the three main stages of production*, *Journal of Industrial Textiles* 2016, vol. 45(6), s. 1322–1334
- 10 Barburski M., *Analysis of the pipe conveyor belt pressure on the rollers on its circuit* *Journal of Industrial Textiles* 2016, vol. 45(6), s. 1619–1634
- 11 Barburski M., Goralczyk M., Snycerski M., *Analysis of Changes in the Internal Structure of PA6.6/PET Fabrics of Different Weave Patterns under Heat Treatment*, *Fibres and Textiles Easter Europe* 2015, nr 23, 4(112), s. 46-51
- 12 P.404943 Barburski M. Snycerski M., *The method for producing the reinforcing fabrics, particular carcass in pipe conveyors belt and reinforcement fabric, particular carcass in the pipe conveyor belt UPRP 2013-08-01*
- 13 EU Commission: *Directive 2002/49/EC of the European Parliament and of the Council of 25 June 2002 relating to the assessment and management of environmental noise*
- 14 WHO, 2011: *Burden of disease from environmental noise. The WHO European Centre for Environment and Health, Bonn.*
- 15 Tang X., Yan X., 2017: *Acoustic Energy Absorption Properties of Fibrous Materials: A review. Composites. Part A: Applied Science and Manufacturing*, Vol. 101, pp. 360-380.
- 16 Tiuc A., Vermeșan H., Gabor T., Vasile O., 2016: *Improved Sound Absorption Properties of Polyurethane Foam Mixed with Textile Waste*, *Energy Procedia*, Vol. 85, pp. 559-565.
- 17 Maderuelo-Sanz R., Nadal-Gisbert A.V., Crespo-Amorós J. E., Parres-García F., 2012: *A Novel Sound Absorber with Recycled Fibers Coming from End of Life Tires (ELTs)* *Applied Acoustics*, Vol. 73, Issue 4, pp. 402-408.
- 18 Memon H., Wang N, Zhu C, 2015: *Study on Sound Insulation Properties of Different Coated Woven Fabrics*. *J. of Fiber Bioengineering and Informatics* 8:4, pp. 645–656.
- 19 Barburski M, Błaszczak J.R., Pawliczak Z "Influence of Designs of Weaves on Acoustic Attenuation of Fabrics" *Journal of Industrial Textiles*, 2018 DOI: 10.1177/1528083718769945
- 20 German J., *Introduction of basic information about materials*, Kraków 2005, *passim*
- 21 Oczó K.E., *Fiber composites - properties, application, machining*, *Mechanic – Monthly of Scientific and technical* 2008, nr 7, s 1-9
- 22 Wang Wei, Huang Gu, *Characterisation and utilization of natural coconut fibers composites*, *Materials and Design* 2009, nr 30, s. 2741 – 2744
- 23 Boisse P., Buet K., Gasser A. Launay J. , *Meso/macro-mechanical behaviour of textile reinforcements for thin composites*, *Composites Science and Technology* 2001, nr 61, s. 395-401
- 24 Vanleeuw B, Carvelli V, Lomov S.V, Barburski M, Vuure A.W., *Deformability of a flax reinforcement for composite materials*, *Key Engineering Materials* vol. 611-612 (2014) page 257-264; *Trans Tech Publications, Switzerland* doi:10.4028/www.scientific.net/KEM.611-612.257
- 25 Vanleeuw B., Carvelli V., Barburski M., Lomov S.V., Aart W. van Vuure, *Quasi-unidirectional flax composite reinforcement: deformability and complex shape forming*, *Composites Science and Technology* (110), February 2015, s. 76–86, <http://dx.doi.org/10.1016/j.compscitech.2015.01.024>
- 26 Balcerzak M., Frontczak-Wasiak I., Snycerski M., *Four - axis fabric without clearances*, *The patent application P-392601 from 07.10.2010*; Owner: Technical University of Lodz 07.10.2010
- 27 Snycerski M., Cybulska M, Frontczak-Wasiak I., Suszek H. *Patent PL Six axis fabric (in print)*, the application P-383907 from 07.08.2007; Owner: Technical University of Lodz
- 28 Frontczak-Wasiak I., Snycerski M., Stempień Z., Suszek H. *Patent No. 209689, Method and device for evaluating the isotropy of the mechanical properties of flat textile* Owner: Technical University of Lodz
- 29 Frontczak-Wasiak I, Snycerski M., *Characteristics of Multi-axial Woven Structures* *Fibres & Textiles in Eastern Europe* October / December 2005, Vol. 13, No. 4 (52)

- 30 Cybulska M., Frontczak-Wasiak I., *Modeling and Properties of Multiaxial Woven Structures*, 2-nd Autex Conference, 2002.
- 31 Dow N., Tranfield G., *Preliminary Investigations of Flexability of Weaving Triaxial Fabrics*, *Textile Research Journal*. 1969, s.986-998.
- 32 Schwartz P., Fornes R., Mohamed M., *An Analysis of the Mechanical Behavior of Triaxial Fabrics and the Equivalency of Conventional Fabrics*, *Txtile Res. J.* June 1981.
- 33 Schwartz P., Fornes R. E., Mohamed M. H., *Tensile Properties of Triaxially Woven Fabrics Under Biaxial Loading*, *Journal of Engineering for Industry*, November 1980, vol. 102, s. 327 – 332.
- 34 Boisse P., Zouari B., Daniel J.L., *Importance of in-plane shear rigidity in finite element analyses of woven fabric composite performing*, *Composites: Part A* 37 (2006) 2201–2212
- 35 Xue P., Cao J., Chen J., *Integrated micro/macro-mechanical model of woven fabric composites under large deformation*, *Composite Structures* 2005, nr 70, s. 69–80
- 36 Araujo M., Lima M., Costa N., *New Weaving Concept For Multiaxial Fabric*, *TECNITEX 2001, Technical Textiles: "Designing Textiles for Technical Applications" 1st Autex Conference*, 26th to 29th June 2001.
- 37 Iliej M., Jais T., Czu W., *Termouprugij analiz triechaprwlnennych tkanych kompozitow Tkanye konstrukcionnyje kompozity* Izdatielstwo „MIR” 1991 g s.302-314, red. Czu T.W, Ko F.
- 38 Skelton J., *Triaxially Woven Fabrics: Their Structure and Properties*, *Textile Research Journal*, 1971, vol. 41, nr 8, s. 637 – 647
- 39 Trost W. C., *Le tissage triaxial: la machine TW 2000*, *Industrie Textile* 1977, nr 1068, s. 339 – 343; *Chemiefasern/Textil-Industrie* 1977, nr 5, s.444-446.
- 40 Shigenobu I., *Multiaxial Fabric with Triaxial and Quartaxial Portions*, pat. No 5,472,020, Dec. 5, 1995.

GEOMETRICAL MODELLING OF WOVEN TEXTILE STRUCTURES

Banu Özgen Keleş

Ege University, email: banu.ozgen@ege.edu.tr

Abstract:

Textiles are flexible, inhomogeneous, porous materials with distinct visco-elastic properties. These unique characteristics makes textile structures to behave essentially different compared with other engineering materials. In many of their applications, it is important to determine the properties and performance of the textiles. The starting point for the prediction of textile properties and performance is in the realistic representation of the fabric geometry. Geometrical modelling of textile structures has been the subject of investigations starting from the early decades of the 20th century. The introduction of the early basic models paved the way to the mechanical analysis of fabrics – plain weaves in particular – mainly aimed at the production of apparel. Therefore, geometrical model is not only useful in determining the entire structure of a fabric but it also establishes a base for calculating various changes in fabric geometry. This paper focuses on the investigation of the modelling attempts of woven fabrics. The advantages and disadvantages of previously created geometrical models are discussed.

Key words:

Woven fabrics, geometric modelling, yarn cross-section, yarn path

1. Introduction

The structure and properties of a woven fabric are dependent upon the constructional parameters as weave, thread density, crimp and yarn count. The interrelation between these fabric parameters can be obtained by considering a geometrical model of the fabric. Geometrical model is not only useful in determining the entire structure of a fabric from a few values given in technological terms but it also establishes a base for calculating various changes in fabric geometry when the fabric is subjected to known extensions in a given direction or known compressions or complete swelling in aqueous medium. Thus, a geometric model is necessary as an input to many computational models like:

- Modelling the mechanical properties of fabrics for determining forming behaviour, clothing comfort, etc.
- Predicting the permeability of fabrics for processing of composites
- Modelling the damage behaviour for use in engineering applications.

Realistic fabric geometric description is essential for modelling of the mechanical and physical properties of textiles since it determines the accuracy of modelling results. Attempts to model textile geometry were recorded as early as the 1930s [1] and have continued up to the present time. There are many challenging aspects of modelling fabric structures, for example, even the geometry of relatively simple plain-weave fabrics is complicated and requires careful modelling to obtain accurate results [2]. Two things are needed to model a yarn: the first is the path of the yarn through the textile and the second is the cross-section shape, which is not necessarily constant.

2. Yarn Path Representation

The path of a yarn can be considered as a one-dimensional line representing the yarn's centreline in three-dimensional space. In most of the mathematical models, yarns are represented as solid volumes. There are several reasons for this, first of all it is much easier to represent the yarn as a solid volume and secondly this kind of representation is much more useful for computational analysis of textile properties (primarily due to processor speed and memory limitations).

A traditional simplified approach is to use the idealized assumptions on yarn path and cross-sectional shapes in the fabric, such as Peirce's model [1] and its derivatives [3, 4]. Although Peirce's models have been criticised [5, 6] because of their limitations and inapplicability without modification for many modes of fabric deformation, researchers still use his models as the basis of research on fabric structure. Peirce dealt with plain woven fabrics using the "Flexible Thread" model in which no external forces were involved (geometric model) and the "Elastic Thread" model where fabric deformation was due to the forces developed at the intersections. In Flexible Thread model, the yarn path is straight at all points except where it wraps around the crossing yarn that is circular in shape.

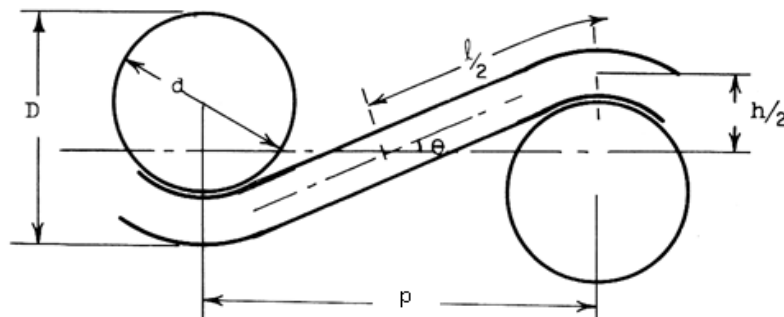


Figure 1. Peirce's flexible thread geometry [1]

Peirce's flexible thread model is acceptable from the geometric point of view, but if we consider the geometric-mechanical interdependence as fundamental, it is quite inadequate. Since the cross-section of the yarn is assumed circular, increased flattening means increased error in the fundamental geometrical relationships. Peirce introduced another model called "Elastic Thread Geometry" in the same study (Figure 2) [1]. He observed that the rigidity and resistance of yarns to bending influenced the form of the yarn in a fabric to some extent and had a big effect on the balance of twist. Thus, he assumed that yarns were elastic and circular cylinders, in which the bending moment was proportional to the curvature of the axis.

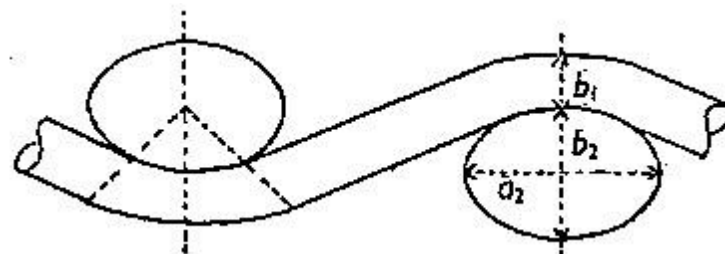


Figure 2. Peirce's elastic thread geometry [7]

Olofsson [6] suggested another model that the waves in the yarns throughout their length were presented by circular arcs as in Figure 2.7.

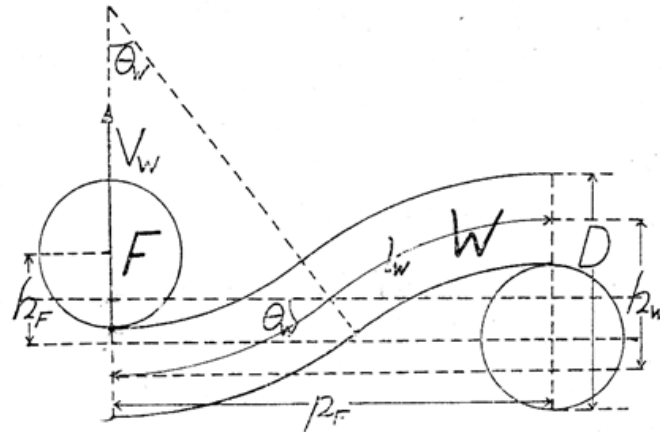


Figure 3. The idealized fabric cross-section (Olofsson) [6]

Olofsson indicated that l_w , l_F , p_w , p_F could be measured with good accuracy from photographs in a given fabric and the quantities θ_w , θ_F and D could be calculated from the equations. According to this model, the yarn shape can be obtained by assuming that the yarn is bent into shape by point loads acting at the intersections. This assumption is in contrast to the yarn shape proposed by Peirce. Peirce proposed that over the region of contact, the yarn conforms to the cross-section of the intersecting yarn and is straight between contact regions since bending resistance is negligible according to his geometry, in which bending stiffness of the yarn and the setting of the yarn crimp in fabric were also considered.

Leaf and Kandil [8] simplified Peirce's elliptic integrals to avoid complex computations, introducing the saw tooth model of the plain woven fabric (Figure 4) in which warp and weft yarns in a unit cell were assumed to be straight piecewise and forming pointed teeth at the crossovers.

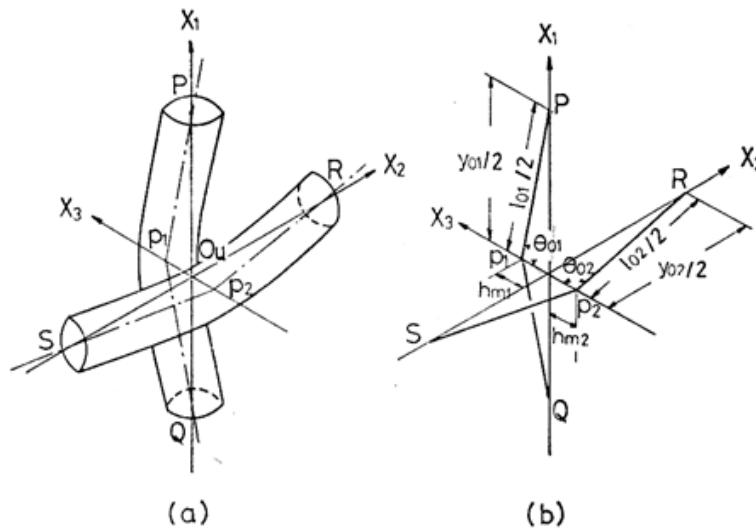


Figure 4. "Straight-line" or "Saw-tooth" model of plain-woven fabric [8]

They assumed that yarns were elastic bodies and straight lines, which bent at points, p_1 and p_2 , on the X_3 -axis.

None of these paths was believed to be the actual path, but all are merely reasonable approximations [9]. The path in real fabrics are complicated and depend on the yarn properties, fabric structure and forces. All these factors affect the yarn arrangement. The most flexible and generic way to describe a yarn path is to specify a number of discrete positions along the yarn length, known as master nodes, and interpolate between these points [10]. Generally, to obtain an accurate yarn path for woven fabrics

it is sufficient to specify one or two master nodes per crossover. There must be no gaps in the yarn path and the yarn path's tangent must vary smoothly. A common solution to this problem is the use of splines that are functions defined piecewise by polynomials.

In its most general form a polynomial spline $S : [a, b] \rightarrow R$ consists of polynomial pieces $S_i : [t_i, t_{i+1}] \rightarrow R$, where

$$a = t_0 < t_1 < \dots < t_{k-2} < t_{k-1} = b \tag{1}$$

That is,

$$S(t) = \begin{cases} S_0(t) & \text{if } t_0 \leq t \leq t_1 \\ S_1(t) & \text{if } t_1 \leq t \leq t_2 \\ \vdots & \\ S_{k-2}(t) & \text{if } t_{k-2} \leq t \leq t_{k-1} \end{cases}$$

The given k values t_i are called knots and each of these subintervals (S) is associated with a polynomial P_i . If the knots are equidistantly distributed in the interval $[a, b]$ the spline is uniform, otherwise it is non-uniform. Several types of splines have been used to create yarn path: B-splines, cubic Bézier splines, natural cubic splines and periodic cubic splines [10].

If basis functions are used for the entire spline, they are named as B-splines meaning that all possible spline functions can be built from a linear combination of B-splines, and there is only one unique combination for each spline function. The B-spline not only keeps functional and aesthetic requirements but also possesses good geometric properties and high flexibility. To define B-spline curves there are some parameters to be known: control points, order of the curve, and knot sequence. Control points are the corner points needed to describe B-spline curves and surfaces. Control polygon is obtained by joining them together. The curve generally follows the shape of control polygon [11]. In accordance with the theory of the B-spline method, to simplify the consideration of the complex forces acting on threads, the control points are generally put at the points where warp threads and weft threads are interlaced and at the mid-points between two neighbouring crossing threads [12].

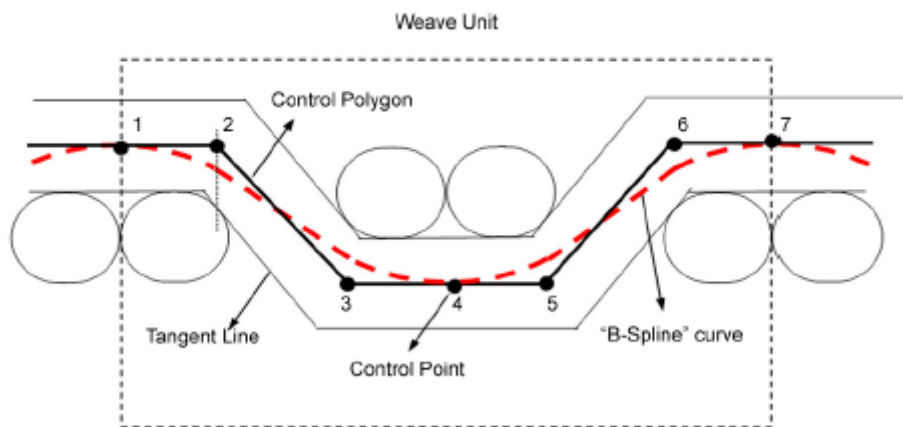


Figure 5. B-spline curve example [11]

The most common form of spline is the cubic spline which is a sequence of piecewise cubic polynomials. Cubic splines allow more complex curves to be represented using fewer spline segments. Cubic splines have polynomial pieces of the form $P_i(x) = a_i + b_i(x - x_i) + c_i(x - x_i)^2 + d_i(x - x_i)^3$.

The most important advantage of spline curves is that they are not global curves. Thus, a change made in any point affects curve only in that region. Local control feature is a desired character in construction design and geometrical model works. It is the most preferred curve in modelling woven and knitted fabrics' geometrical structures [12, 13, 14].

3. Yarn Cross-section Representations

The cross-section is defined as the 2D shape of the yarn when cut by a plane perpendicular to the yarn path tangent. Various shapes have been explored including circular, ellipse, race-track, power ellipse and a modified lenticular shape. In Peirce's Flexible Thread model, the yarns within a fabric were assumed to be incompressible, circular cylinders and there was perfect contact between warp and weft yarns with the cross-sections being constant throughout the fabric. Peirce later considered a model where the yarn was modelled as an elastica and point contact occurs at the crossover between yarns. He also used an elliptical yarn cross-section to represent yarn flattening more accurately induced during the weaving process. However, he concluded that such a geometry would be complex and laborious in application, and instead, adopted an approximate treatment that merely involved replacing the circular thread diameter in his circular thread geometry by the minor diameter of the appropriate elliptic section [7]. The horizontal diameter of the elliptic section was applied only in the calculation of cloth cover. Peirce's approximate treatment of yarn flattening is shown in Figure 6.

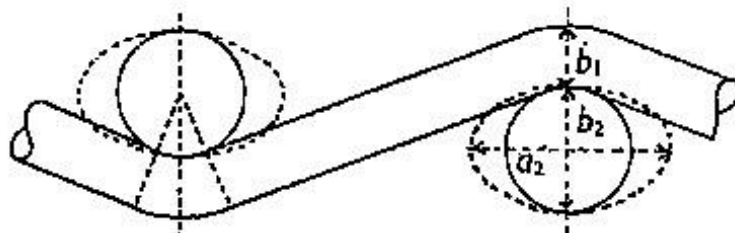


Figure 6. Peirce's approximate treatment of yarn flattening [7]

Kemp [5] reformed the race-track section, which consisted of a rectangle enclosed by two semi-circular ends from the Peirce's circular cross-sectional shape. He used this new shape of the yarn section as the basis for an extension of Peirce's theory to the more general case of non-circular yarns. In a race-track section, the flat portion in the yarn cross-section is equal to $a-b$ and Peirce's formulas are still applicable to calculate the fabric parameters yarn spacing (p), length of yarn between the axis of cross yarns (l), and crimp (c). The yarn flattening coefficient ($e = b / a$) defined by Kemp was used as one of the main factors to compare consecutive yarn cross-sectional shapes. Figure 7 shows Kemp's plain woven fabric geometry based on race-track section.

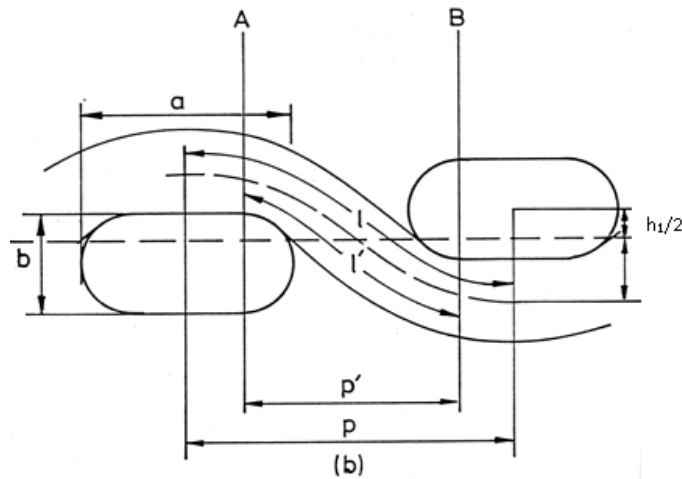


Figure 7. Kemp's race-track geometry

Hamilton [15] expanded the principles of plain-weave geometry established by Peirce [1] and Kemp [5] to weaves other than plain to give a general system that is applicable to all types of woven cloths. He used Kemp's racetrack geometry of plain weave forms as the starting point for non-plain woven fabrics.

Shanahan and Hearle [16] introduced the "Lenticular geometry" in order to avoid the difficulties encountered with Kemp's race-track geometry, while applying their energy method for calculations in fabric mechanics. This geometry was a modification of the Peirce geometry. The lenticular geometry is given in Figure 8.

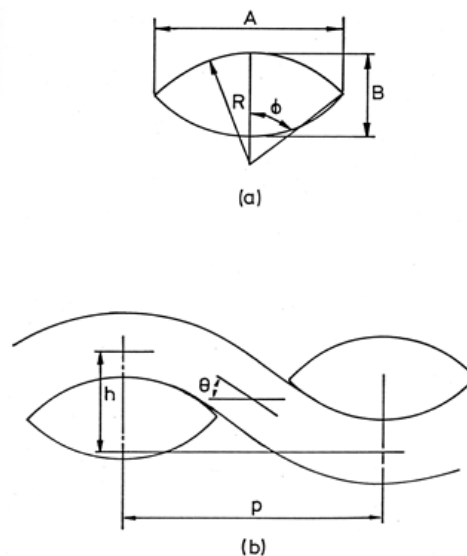


Figure 8. Lenticular geometry [16]

Numerous approaches and models have been developed to represent the woven fabric geometry and for the 3D computer modelling and simulation of yarns in fabrics. Although the inter-yarn forces and yarn flattening due to these forces have been considered in many studies, in all the previous fabric models, yarns were compelled as columns with a uniform regular cross-sectional shape (i.e. circular, lenticular, racetrack, etc.) along its yarn path. However, in most cases, the yarn cross-sections in a fabric take a much more complicated cross-sectional shape and irregular cross-sectional shape is needed in order to represent the yarn flattening and compression along the yarn path more accurately. Jiang and Chen [9] proposed an approach of super ellipse which can design the cross-section in arbitrarily shape represented by combined spline curves. The 2D polar coordinate system is used to construct irregular yarn cross-sections (Figure9).

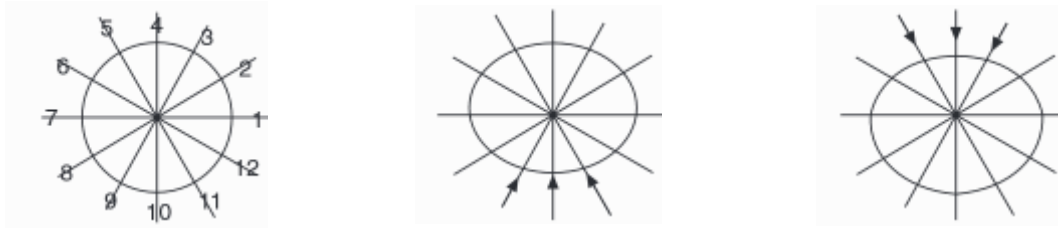


Figure 9. Irregular cross-section [9]

Ozgen and Gong [17] acquired the fabric images through ESRF (European Synchrotron Radiation Facility) without disturbing the yarn and fabric structure. The contours of the yarn in the woven fabrics were accurately measured. They confirmed the non-circular nature of yarn cross-sections and also the flattening of yarns at the warp-weft intersections.

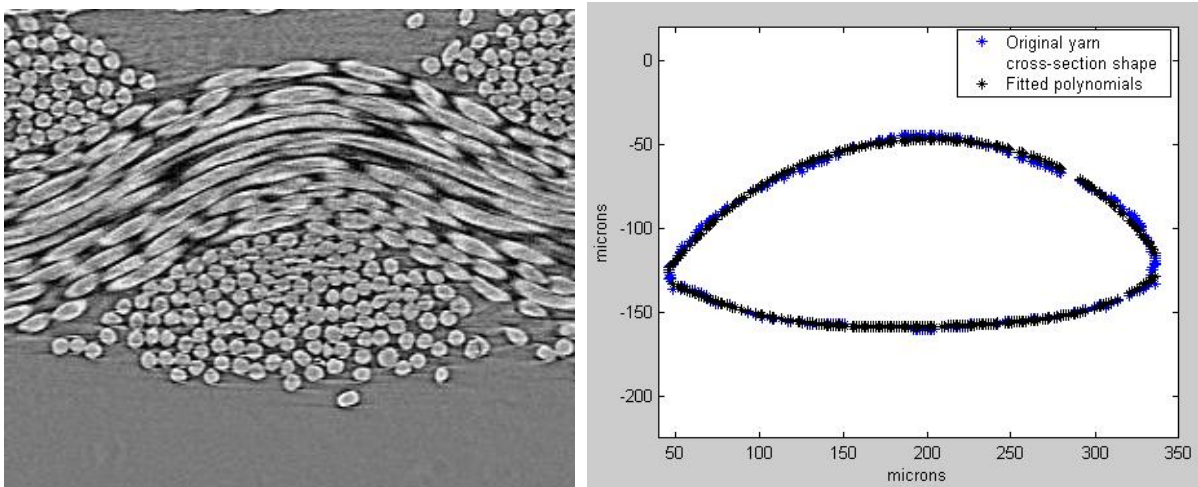


Figure 10. (a) Real Yarn cross-section image (b) Fitted polynomials

Two polynomial functions were used to describe the shape of the varied cross-section. The cross-section shape that was modelled by polynomial curves was variable along the yarn path.

4. CONCLUSION

This paper gives an overview of geometrical modelling of woven textile structures. The geometrical structures of fabrics are mainly determined by the cross-section and the centreline configurations of their constituent yarns, which vary widely and are depend on the weave patterns, the tightness of fabric and the processing parameters. Focusing on the woven fabric, different approaches and models have been developed to represent the woven geometry. This paper describes the fundamental basis of previously created models for the woven fabric geometry and how the representations of these geometries are improved over the years.

References

1. Peirce, F., 1937, *The geometry of cloth structure*, *Journal of Textile Institute*, 28, 45–96.
2. Lin, H., Zeng, X., Sherburn, M., Long, A.C. and Clifford, M.J., 2011, *Automated geometric modelling of textile structures*, *Textile Research Journal*, 82(16), 1689–1702.
3. Kemp, A., 1958, *An extension of Peirce's cloth geometry to the treatment of nonlinear threads*, *Journal Textile Institute*, 49, 44–48.
4. Hearle, J.W.S. and Shanahan, W.J., 1978, *An energy method for calculations in fabric mechanics*. *Journal Textile Institute*, 69, 81–110.
5. Kemp, A., 1958, *An Extension of Peirce Cloth Geometry to the Treatment of Non-circular Threads*, *Journal of The Textile Institute*, 49, T44.
6. Olofsson, B., 1964, *A General Model of a Fabric as a Geometric-Mechanical Structure*, *Journal of the Textile Institute*, 55, T541.
7. Hamilton, J.B., 1959, *A Direct Method for Measuring Yarn Diameters and Bulk Densities Under Conditions of Thread Flattening*, *Journal of the Textile Institute*, 50, T655.
8. Leaf, G.A.V. and Kandil, K.H., 1980, *The Initial Load-extension Behaviour of Plain-woven Fabrics*, *Journal of the Textile Institute*, 1980, 71, 1.
9. Jiang, Y., Chen, X., 2005, 'Geometric and Algebraic Algorithms for Modelling Yarn in Woven Fabrics', *Journal of the Textile Institute*, 96, No 4, 237.
10. Sherburn, M., 2007, *Geometric and Mechanical Modelling of Textiles*, PhD thesis, University of Nottingham.
11. Turan, R.B. and Başer, G., 2010, *Three-dimensional computer simulation of 2/2 twill woven fabric by using B-splines*, *The Journal of The Textile Institute*, 101, 10, 870–881.
12. Lin, H.-Y. and Newton, A., 1999, *Computer Representation of Woven Fabric by Using B-splines*, *Journal of the Textile Institute*, 90, Part I, No 1, 59.
13. Wang, W., Zhu, J., Zhang, R., Li, Y., Ji, F. and Yu, J., 2018, *Numerical characterization and simulation of the three-dimensional tubular woven fabric*, *Journal of Industrial Textiles*, 47(8), 2112–2127.
14. Zheng, T., Wei, J., Shi, Z., Li, T. and Wu, Z., 2015, *An Overview of Modeling Yarn's 3D Geometric Configuration*, *Journal of Textile Science and Technology*, 1, 12-24.
15. Hamilton, J.B., 1964, *A General System of Woven-fabric Geometry*, *Journal of the Textile Institute*, 55, T66.
16. Shanahan, W.J. and Hearle, J.W.S., 1978, *An Energy Method for Calculation in Fabric Mechanics Part II: Examples of Application of the Method to Woven Fabrics*, *Journal of the Textile Institute*, 69, 92.
17. Ozgen, B. and Gong, R.H., 2011, *Modelling of Yarn Flattening in Woven Fabrics*, *Textile Research Journal*, 81, 1523-1531.

IMPACT OF EXTRACTION PROCESSES ON FIBER PROPERTIES OF LINSEED FLAX FIBERS

Pierre Ouagne^{a*}, Marie Grégoire^a, Benjamin Barthod-Malat^{a,b}, Philippe Evon^b, Laurent Labonne^b, Emmanuel De Luycker^a, Vincent Placet^c

^aLaboratoire Génie de Production, (LGP), Université de Toulouse, INP-ENIT, 47 Avenue d'Azereix, Tarbes, France.

^bLaboratoire de Chimie Agro-industrielle (LCA), Université de Toulouse, INRA, INPT, 31030 Toulouse Cedex 4, France

^cUniversité de Bourgogne Franche Comté, FEMTO-ST, CNRS/UFC/ENSMM/UTBM, 25000 Besançon, France

*Corresponding author: pierre.ouagne@enit.fr

Abstract:

This work of a preliminary nature has for goal to investigate the potential of the linseed flax straw for industrial valorization in technical textiles. The impact of two extraction systems ("all fiber" extraction device and a scutching/hackling device) was investigated. In a first part of the paper, it was demonstrated that it is possible to extract the fibers from the other components of the straw such as the shives and vegetal dusts. The fiber yield is of about 38% of the stem mass. This very high fiber yield is particularly interesting and is higher than the one of hemp for example. The fiber properties were also investigated. The fiber length was shown to be in the adequate range of length to be considered for the carded spinning route, and the tensile properties of the individual fibers, even if decreased by about 45% in comparison to carefully manually extracted, are still at a sufficient level of performance for semi-structural composites applications for example. When using a scutching/hackling line, the length of the fibers is preserved and the impact of the fiber extraction was shown to be lower than the all fiber extraction line, particularly for the strength. These fibers could therefore be used for higher load bearing applications. Finally, the amount of fiber that can be extracted from the linseed flax fibers is large and this could certainly be at the origin of an industrial technical textile value chain.

Key words:

Linseed flax, All-fiber extraction, Scutching/hackling, fiber characterization, tensile properties

1. Introduction

To manufacture high performance composite parts, it is necessary to organize and to align the fibers. As a consequence, aligned fibers architectures such as unidirectional sheets, non-crimped fabrics and woven fabrics (bidirectional) are usually used as reinforcement. For numerous applications, it is also important that the fabric may be formed into complex shapes without the appearance of defects such as wrinkles, vacancies, tow buckles etc... [1-4]. These materials are classically constituted from synthetic fibers such as glass, carbon or aramid. However, natural fibers are now considered in Europe as a serious alternative for composite reinforcement from low load up to high load bearing applications. A consequent literature, showing the interest of different fibers extracted from different plant is available. Review papers and even book Chapters summarize the different progresses in the area [5-7]. A recent very complete review on the subject was proposed by Bourmaud *et al.* [8]. This review paper clearly shows the high potential of plant fibers and particularly bast fibers such as flax, hemp or nettles.

If the potential of the natural fibers has widely been demonstrated in numerous publications and review papers, the conversion of this potential to reality is often a problem and this one is not necessarily maximized. The maximization of the high mechanical potential of plant fibers for composite material reinforcement is dependent on several transformation steps, from the plant to the fabric. The fiber extraction step and technology used, depending on the stem arrangement, as it is illustrated by Figure 1 is a crucial key stage. It is particularly important to pay attention to the fiber extraction so that to avoid damaging the fibers to a too large extent.

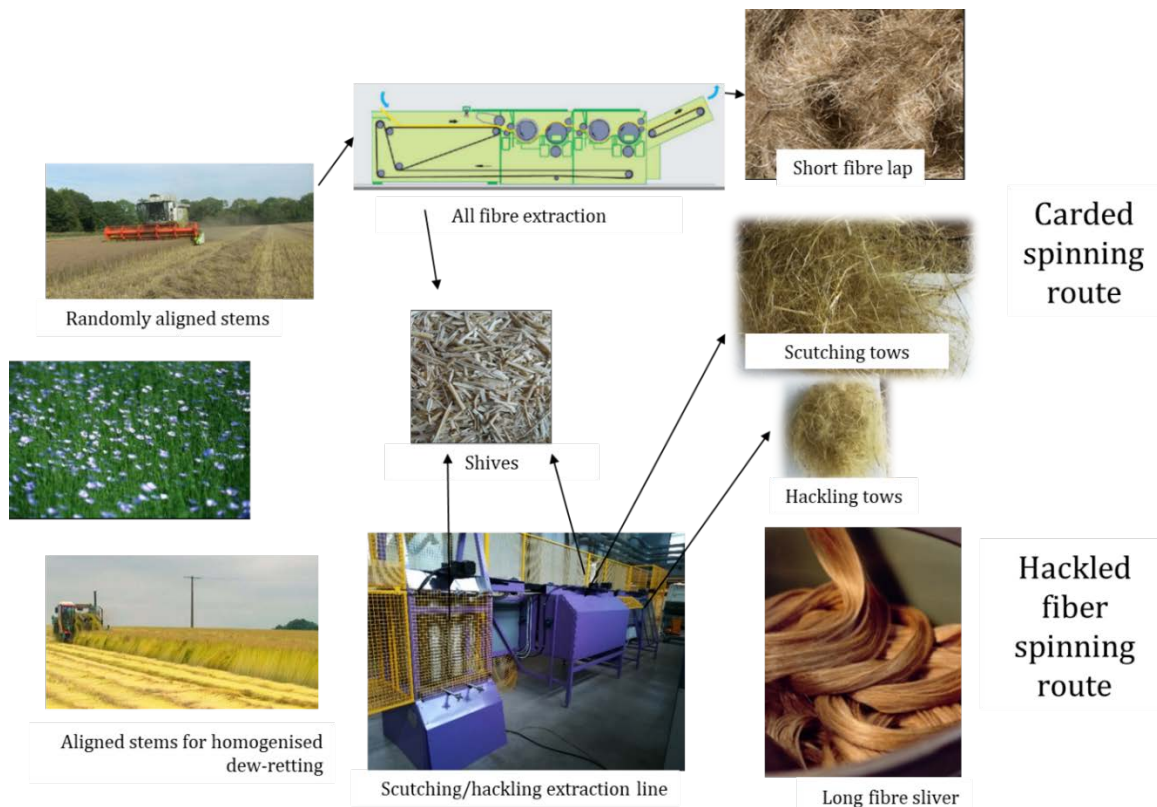


Figure 1. The fiber processing routes

Specific high performance reinforcements are required to manufacture structural or semi-structural biocomposite parts especially for the automotive industry. New flax and comingled flax/bioplastic reinforcements have been elaborated in this goal. If large panels have been realised with a good success, the feasibility to manufacture complex shape parts using a sheet forming process [9] especially with natural fibre based reinforcements without defect is still a challenge. Previous studies [10-11] demonstrated that complex shape parts could be achieved by using specifically prepared fabrics, with particular process parameters.

However, this requires specific care all along the different operations leading to the part manufacture due to the use of finite length natural fibres. It is also necessary when using agro-based material to reduce the impact of the part manufacturing in comparison to synthetic technology. The energy consumption for the production of yarn should be kept low, and the possible fabric treatments should have a minimum impact on the environment. Dissanayake *et al.* [12] indicated that preparing composite reinforcement using natural fibers may have a higher impact on the environment than materials prepared from glass fibers if adequate manufacturing processes are not used. As a consequence, the manufacturing processes need to be adapted and optimized to reach this goal. Moreover, it is also important when considering the manufacturing processes to maximize the mechanical potential of the vegetal fibers. This means that it is important to minimize the length reduction of fibers or the appearance of defects such as dislocations or kink bands during the fiber extraction and the yarn preparation.

This paper therefore focuses on the critical and key fiber extraction stage so that to determine if the linseed flax fibers can be considered for technical textile applications. The linseed flax fibers were extracted by two different techniques and their morphological and mechanical potential characterized before and after extraction so that to determine the impact of the extraction process. Finally, the fiber yield was also studied so that to determine if an industrial value chain can be considered for the valorization of the linseed flax straw.

2. From the plant to the fibers: impact of the extraction processes

Within the plant, the fibers may have different roles. In flax or hemp, the bast fibers have a mechanical structural role. They contribute to the stabilization of the stems so that the plant remains vertical and that with an elongation ratio higher than the one of the highest trees. When extracted with the greatest care, the mechanical properties of the flax or hemp fibers show higher specific properties than glass fibers. However, this is only true in the case the fibers are not damaged during the different processes leading to the manufacture of the reinforcement fabric. Successive extraction and preparation processes take place before the textile architecturation into 1D (yarn) and 2D or 3D reinforcement products.

Depending on the harvesting procedures, the stems may be well ordered (textile flax or hemp in eastern Europe) or randomly aligned (linseed flax or hemp in western Europe). This is at the origin of different routes for the preparation of reinforcement materials. The first one, for randomly aligned stems consists in using a “all fiber” extraction line (textile fiber opener or hammer mills) that is followed by the carded preparation and spinning route. The second one is designed to receive aligned stems. It is based on the traditional well established scutching units classically used in western Europe for flax and in eastern Europe for hemp.

2.1. Impact of the all fiber extraction device on the morphological and mechanical properties of linseed flax fibers coming from un-retted straws.

2.1.1 The all fiber extraction device

In a preliminary study, Ouagne *et al.* [13] studied the potential of using an all fiber semi-industrial extraction line to extract fibers dedicated to technical applications such as semi-structural composites or geotextiles. The Laroche (France) Cadette 1000 “All Fiber” extraction opener from the AGROMAT platform (Tarbes, France), was used to extract the different vegetal fractions from linseed flax straw harvested in the south west of France. A schematic diagram of the device is presented in Fig. 2.

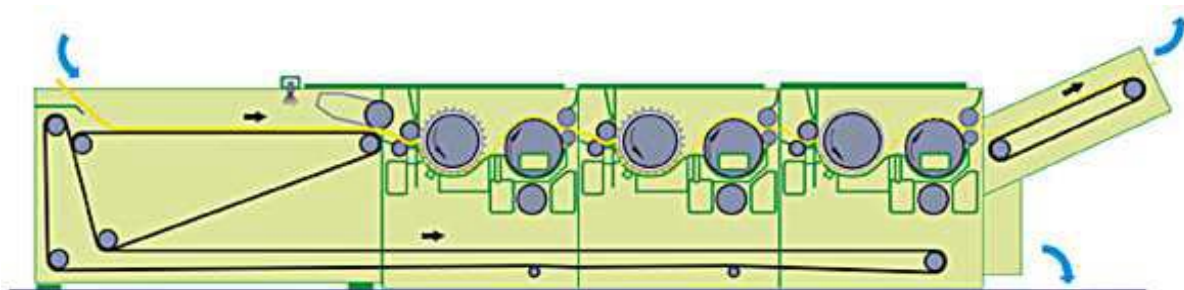


Figure 2. Schematic diagram of the three modules “all fiber” opening device

The all fiber opening device consists of a succession of three extraction and separation modules. In each module a nailed cylinder under a rotation speed that can be up to 1700 rpm performs the

fractionation of the vegetal matter into a fiber lap, shives and vegetal dusts. If the different constituent extraction is performed by the rotating nailed cylinder with the creation of a fiber lap, the shives fall on a rotating belt and are sent by an aspiration system to collecting bags. In each module, a perforated cylinder extracts the fine particles through a suction process so that to separate this matter from the fiber lap. This device has the ability to process up to 175 kg of stems per hour.

2.1.2 Fiber extraction tests

Two sets of experiments were carried out on dry and rewetted by water batches. For each batch of about 25 kg of randomly aligned stem, the different fractions were weighed under similar conditions of humidity (dry state). As the fiber laps contain remaining pieces of shives trapped, these ones are removed after a mechanical sieving step and the last pieces of shives are picked up manually. Figure 3 shows the different vegetal fractions obtained at the end of the extraction process. The goal here is to evaluate the amount of fiber available from the linseed flax straws.



Figure 3. The three vegetal fractions

2.1.3 Reference material

As the goal of the study consisted in studying the impact of the extraction devices on the properties of the fibers, a reference material needs to be tested. Linseed flax fibers were extracted manually with the greatest care so that their initial potential is not decreased and represent as closely as possible the reinforcement performance of these fibers. To do so, pieces of linseed flax straws were soaked in water for 72 h under a temperature of 30°C and the fibers were extracted manually.

2.1.4 Fiber characterization: Impact of the extraction procedure on morphological and mechanical properties of technical and single fibers respectively

In a first extent, the fiber length of the technical fibers (fiber bundles) was characterized. The goal here is to investigate whether or not the technical fibers constituting the fiber lap are appropriate (sufficiently long) for a further transformation into yarns and technical textiles. The measurements were performed on about 600 fibers. To do so, one side of technical fiber was fixed and the other extremity was pulled so that to obtain a straight fiber measured between both its extremities.

In a second extent, the evolution of the single fiber tensile properties was determined. Tensile tests on individual fibers were performed on batches of 40 fibers. The tests were performed at the FEMTO-ST laboratory following the recommendation of the NF T25 – 501 – 2 standard test method [14]. A Bose (USA) Electroforce 3230 tensile testing machine equipped with a 22 N capacity load cell was used to

perform the tests. The fiber apparent diameter diameter was evaluated using an optical microscope (Olympus PMG3-F3, France). The apparent diameters were measured at five different locations so that to calculate both tensile strength and modulus. It is assumed here that the fibers are perfectly cylindrical.

2.1.5 Results

The different vegetal fraction yields were determined after extraction processing and are presented in Table 1 for both dry and re-wetted batches.

Table 1. Fiber, shives and vegetal dust proportions after “all fiber” extraction

	Total fibre content (%)	Total shives content (%)	Total dust content (%)
Re wetted	37.5	57.6	4.9
Dry	37.8	52.4	9.8

Table 1 shows that the amount of fiber (about 38% of the stem masses) is high and much higher than what can be encountered in the literature. Indeed, the amount of linseed flax fibers in the stem is generally much lower [15]. This may be due to the fact that fiber rich stems were considered in this study, or this may be due to a different way of evaluating the fiber yields.

The technical fiber lengths are presented in Table 2:

Table 2. Length of technical fibers

	Fiber bundle length (mm)
Re wetted	53±29
Dry	39±22

Table 2 indicates that the fiber bundle length is of about 40 mm for the fiber extracted from the dry stems. The fibers extracted from the re-wetted batch are longer. This suggests that it is probably interesting to re-wet the fibers before processing. This probably confers some ductility to the fibers and prevents extra breakings.

Table 3 shows the tensile properties of individual fibers manually extracted from un-processed stems and from processed bundles from the re-wetted straws.

Table 3. Tensile properties of individual linseed flax fibers

	Modulus of elasticity (GPa)	Strength (MPa)
Manually extracted	45±27	1080±640
All fiber device extraction	38±17	604±409

Table 3 shows the tensile properties of the single fibers. It particularly compares the evolution of the tensile properties before and after mechanical fiber extraction with the “all fiber” device. The results indicate that the extraction has a clear impact on the tensile properties of the individual fibers. This is particularly visible for the strength with a decrease of about 45%. In the case of modulus, the decrease is more moderate (20%). This decrease in strength is probably due to the introduction of defects such as kink-bands or dislocations in the internal structure of the fibers.

2.2. Impact of a scutching/hackling extraction device on the morphological and mechanical properties of linseed flax fibers coming from un-retted straws.

2.2.1 The scutching/hackling device

A scutching/hackling device is shown in Figure 4. This device is a low scale version of classical industrial scutching/hackling units. It consists of successive breaking, scutching (beating), hackling (combing) units. The scutching and hackling devices are traditionally used when long fibers are expected.



Figure 4. Laboratory scutching/hackling line

In this work, non-retted aligned straws were collected manually to evaluate the potential of the linseed flax fibers and the impact of the scutching/hackling process on the fiber properties.

One of the main interest of using aligned stems in conjunction with scutching/hackling devices is the fact that the technical fiber length is not as much decreased as it is the case for the “all fiber” extraction line. In our case, the bundle length is about equivalent to the length of the collected stems, (about 300 mm). The fibers are therefore much longer than the ones extracted using the “all fiber” line. The hackled technical fibers are about six times longer. Figure 5 shows a sample of hackled linseed flax.



Figure 5. Hackled non-retted linseed flax sliver

If the breaking and scutching steps have an influence on the fiber properties, the most damaging stage is hackling. This stage is particularly important because it finishes the separation of the technical fibers

from the rest of the stem components. It also contributes to the finer separation of the fiber bundles into individual fiber or small clusters of fibers.

The influence of the hackling step on the mechanical properties of individual fibers is given in Table 4 together with a comparison with the impact of the “all fiber” extraction:

Table 4. Tensile Properties of hackled single fibers

	Modulus of elasticity (GPa)	Strength (MPa)
Manually extracted	45±27	1080±640
All fiber device extraction	38±17	604±409
Scutching/hackling	40±10	966±403

Table 4 shows that the modulus does not decrease in a great extent in comparison to the manually extracted fiber. No statistical difference may be observed. The modulus of elasticity is surprisingly equivalent to the one obtained from fibers extracted with the “all fiber” device. The strength of fibers after hackling does not show any significant decrease in comparison to the manually extracted fibers. The result of the tensile strength is however much larger than the strength obtained from fiber extracted from the “all fiber” line. This suggests that the level of defects conferred to the hackled fibers is lower than the number of defects present on fibers extracted by the “all fiber” line.

3. CONCLUSIONS

This work of a preliminary nature has for goal to investigate the potential of the linseed flax straw for industrial valorization in technical textiles. The impact of two extraction systems (“all fiber” extraction device and a scutching/hackling device) was investigated. In a first part of the paper, it was demonstrated that it is possible to extract the fibers from the other components of the straw such as the shives and vegetal dusts. The fiber yield is of about 38%. This very high fiber yield is particularly interesting and is higher than the one of hemp for example [15]. The fiber properties were also investigated. The fiber length was shown to be in the adequate range of length to be considered for the carded spinning route, and the tensile properties of the individual fibers even if decreased by about 45% in comparison to carefully manually extracted are still at a sufficient level of performance for semi-structural composites applications for example. When using a scutching/hackling line, the length of the fibers is preserved and the impact of the fiber extraction was shown to be lower than the all fiber extraction line, particularly for the strength. These fibers could therefore be used for higher load bearing applications. Finally, the amount of fiber that can be extracted from the linseed flax fibers is large and this could certainly be at the origin of an industrial technical textile value chain.

References

1. Potter K, Khan B, Wisnom M, Bell T, Stevens J. "Variability, fibre waviness and misalignment in the determination of the properties of composite materials and structures" *Composites: Part A* 2008; 39: 1343–1354.
2. Ouagne P, Soulat D, Moothoo J, Capelle E, Gueret S. Complex shape forming of a flax woven fabric; Analysis of the tow buckling and misalignment defect. *Composites Part A* 2013; 51: 1-10.
3. Tephany C, Gillibert J, Ouagne P, Hivet G, Allaoui S, Soulat D. Development of an experimental bench to reproduce the tow buckling defect appearing during the complex shape forming of structural flax based woven composite reinforcements. *Composites Part A*, 2016; 81: 22-33.
4. Ouagne P, Soulat D, Tephany C, Gillibert J. Measurement of the Appearance and Growth of Tow Buckling Defect in the Frame of Complex Shape Manufacturing Process by Using Fringe Projection Technique. *Strain*. 2016; 52: 559–569.
5. Dhakal HN, Zhang Z (2015). The use of hemp fibres as reinforcements in composites. In: *Biofiber Reinforcements in Composite Materials*. Woodhead Publishing, pp. 86–103.
6. Mussig J, Haag K (2015). The use of flax fibers as reinforcements in composites. In: *Biofiber Reinforcements in Composite Materials*. Woodhead Publishing, pp. 35–85.
7. Akin D. Flax (2010) Structure, Chemistry, Retting and Processing. In: *Industrial Applications of Natural Fibres; Structure, Properties and Technical Applications*. Wiley publication. 89-108.
8. Bourmaud A, Beaugrand J, Shah DU, Placet V, Baley C. Towards the design of high-performance plant fibre composites. *Prog Mater Sci* 2018;97:347–408. doi:10.1016/j.pmatsci.2018.05.005.
9. Ouagne P, Soulat D, Hivet G, Allaoui S, Duriatti D. Analysis of defects during the preforming of a woven flax reinforcement. *Advanced Composite Letters*, 20 (2011) 105-108.
10. Capelle E, Ouagne P, Soulat D, Duriatti D. Complex shape forming of flax woven fabrics: Design of specific blank-holder shapes to prevent defects. *Composites Part B*, 2014; 62: 29-36.
11. Allaoui S, Hivet G, Soulat D., Wendling A, Ouagne P, Chatel S. Experimental preforming of highly double curved shapes with a case corner using an interlock reinforcement. *International Journal of Materials Forming*. 2014; 7: 155-165.
12. Dissanayake N, Summerscales J, Grove S, Singh M. Life Cycle Impact Assessment of Flax Fibre for the Reinforcement of Composites. *J Biobased Mat and Bioener* 3 (2009) 245-248.
13. Ouagne P, Barthod-Malat B, Evon P, Labonne L, Placet V. Fibre Extraction from Oleaginous Flax for Technical Textile Applications : Influence of Pre-processing Parameters on Fibre Extraction Yields, Size Distribution and Mechanical Properties. *Procedia Engineering*,2017;200:213-220.
14. ASTM D3822 / D3822M – 14. Standard Test Method for Tensile Properties of Single Textile Fibers.
15. MEIRHAEGHE C. ADEME Report: Assessment of natural fibre availability in France. 2011. http://www.ademe.fr/sites/default/files/assets/documents/76290_12_evaluation_dispo_accessibilite_fibres_veg_usages_materiaux.pdf

MODELLING THE CROSS-SECTIONAL PROPERTIES OF YARN ALONG THE FABRIC

R. Befru Büyükbayraktar

Dokuz Eylül University, Textile Engineering Department, Izmir, Turkey, +90 232 3017712, +90 232 3017750, befru.buyukbayraktar@deu.edu.tr

Abstract

Three dimensional (3-D) fabric geometry defines the fabric physical and mechanical properties. For this reason, it is important to obtain realistic fabric models. In this study, the yarn path of the woven fabric was modeled according to structural properties of fabric using Pierce geometry. On the other hand, the cross-sectional properties of the yarn along the weave unit was modeled depending on the movement of the yarn and the interactions between adjacent and perpendicular yarns. The yarn path was divided into regions and the cross-section of the yarn was defined according to region properties. By an experimental study, the variation of the yarn dimension at each region was measurement and the flattening ratio of yarn was determined. These data were used in the cross-section model. The simulations of yarn path and cross-sectional models were obtained by using SolidWorks. These simulations present the variation of yarn cross-section along the weave unit.

Keywords:

Yarn cross-section, yarn path, yarn diameter, woven fabric

1. Introduction

Three dimensional (3-D) fabric geometry was formed according to structural parameters and manufacturing processes. Raw material, yarn properties such as yarn production type, yarn linear density, twist, packing ratio, etc., and construction properties of fabric such as settings and weave type are some of the important structural parameters defined fabric geometry. The fabric geometry affects the physical properties of the fabric, such as mechanical, sensory, permeability and conductivity properties of the fabric. Therefore, the structural parameters of the fabric must be chosen well to design a special product for a defined using area. However, the relationship between structural parameters and fabric geometry and also the performance properties of a fabric is complicated. Thus, modelling studies about the fabric geometry are needed to predict the performance behaviours of product.

Besides, determination of fabric properties at the designing step is important for both designers and manufacturers in terms of time and cost.

Generally, fabrics were idealized into simple geometrical forms. The yarn path along the fabric was described by circular arcs, straight lines, sinus curves, elastic forms, and the yarn cross-section was modeled as circular, elliptical, lenticular, racetrack shapes [4-9]. However, yarn cross-section varies inside the fabric due to inter-yarn compression. In recent years, irregular cross-section shapes of yarns were also studied [1-3,10-12]. The shape of a yarn cross-section shape and size is affected by many factors such as raw material, twist degree, yarn spinning technology, weave type, settings, etc. It is important to provide an efficient modeling technique for creating the yarn cross-sections properties.

In this study, fabric geometry was modeled into two steps. First, the yarn path was defined according to structural parameters and B-spline method was used to get a smooth yarn center line along the weave unit. It is important to define the variation at the cross-sectional shape and size of the yarn into the fabric in order to create more realistic 3-D fabric geometry. In the second step, the cross-sectional properties of yarn were modelled along the yarn path according to the interactions between adjacent and perpendicular yarns. An experimental study was carried out to get data about the variation of yarn size

along the yarn path. Yarn dimensions of different cotton fabrics were measured from different regions of fabric images. The fabric geometry simulations were performed by using SolidWorks 2014.

2. Experimental

2.1. Materials

In this study, both theoretical and experimental studies were carried out. In the experimental part of the study, four different commercial cotton woven fabrics having different structural parameters were used. The structural properties of these fabrics given in Table 1 were analyzed by related standards.

Table 1. Structural properties of measured fabrics

Fabric Code	Weave Type	Unit weight (g/m ²)	Warp Count (tex)	Weft Count (tex)	Warp Setting (cm ⁻¹)	Weft Setting (cm ⁻¹)	Thickness (cm)
P1	Plain	106	11	11	60	35	0.0228
P2	Plain	114	11	11	56	30	0.0226
P3	2/2 Twill	126	10	9	62	56	0.0256
P4	4/1 Twill	215	12	19	90	50	0.0416

2.2. Methods

Sectioning is a more realistic method in order to obtain cross-sectional dimensions of yarn into the fabric. But this is a laborious and time-consuming method. For this reason, in this study measuring of yarn dimensions onto the 2D surface images of fabrics were preferred. The images of various cotton fabrics were observed by a camera system integrated to a microscope. The dimensions of warp and weft yarns were measured from captured images by using the application of the camera system as seen in Figure 1. Measurements were done from the different regions of the weave unit. Regions were defined as the peak point of the intersecting region and the middle point of the interchanging region, for plain weave. For twill weaves, the middle of the floating region was also measured. Ten measurements were done for each region of warp and weft yarns. The results were used to estimate the variation of the yarn dimension along the yarn path. Besides, the possible flattening ratio of different regions was predicted from the measurements.

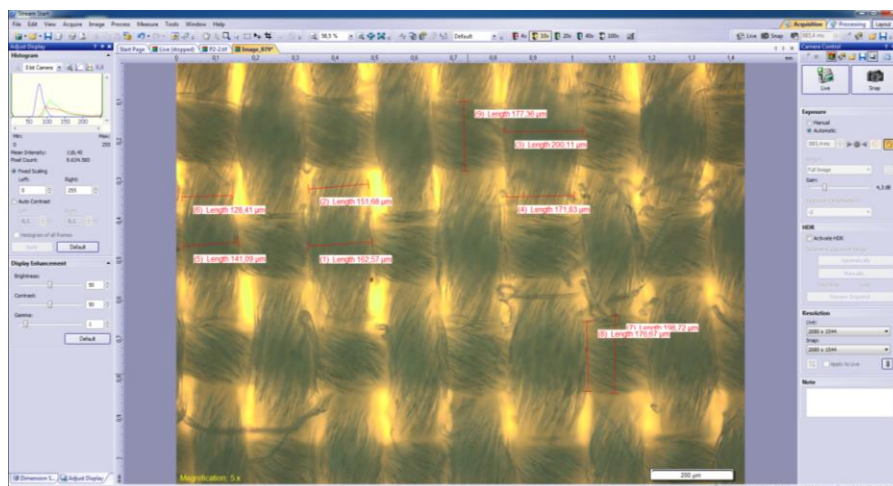


Figure 1. Measurement of yarn diameter at different regions of the yarn path

3. Theoretical

In the theoretical part of the study, the yarn path and yarn cross-section were modeled in order to get realistic fabric simulations. The basic yarn path was defined depending on the structural properties of the fabric according to Peirce geometry [8]. In Peirce geometry, when weaving angle is assumed a small value then the amplitude of yarns (h) can be calculated as in Equation 1. Here, p is yarn spacing, c is crimp factor. Subscripts 1 and 2 were used for warp and weft yarns, respectively. This formula was defined according to plain fabric in Peirce geometry. Some modifications were done and the crimp factor of 2/2 twill and 4/1 twill weaves were calculated in order to use this equation for these weave types, too.

$$h_1 = p_2 \frac{\sqrt{2c_1}}{1-c_1} \quad \text{Equation 1}$$

B-spline curve method was used in order to obtain yarn path as a smooth curve. The open non-uniform cubic B-spline curves with a continuity of the order 2 were used. First, a linear control polygon was defined, for each weave types. The B-spline curve generally follows the shape of control polygon. Seven control points were defined for each weave unit, as seen in Figure 2. The coordinates of these points were calculated by using Peirce geometry. Applying B-spline method, 21 new points confirmed yarn path were calculated. Yarn paths were obtained individually for warp and weft yarns.

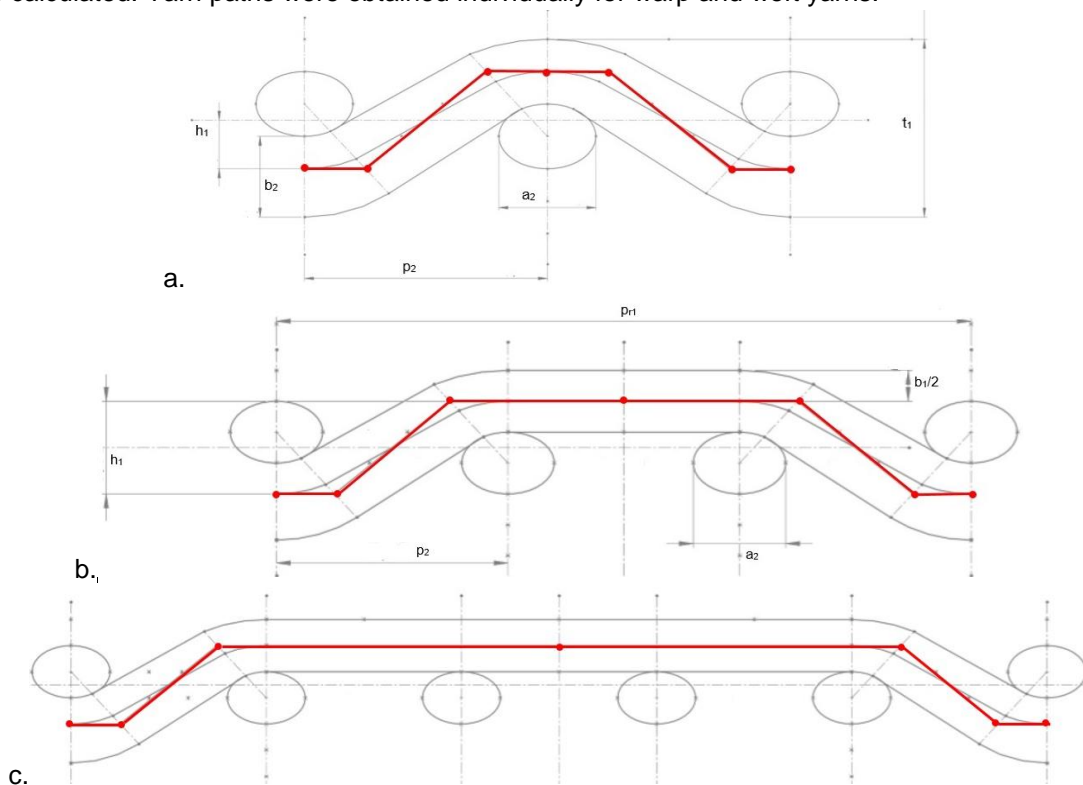


Figure 2. B-Spline control polygon and control points for a. Plain, b. 2/1 Twill, c. 4/1 Twill weave units.

In many studies, the cross-sectional shape of yarn in the woven fabric was modeled as circular. However, it was known that the shape and dimension of yarn changed along the yarn path because of interactions between adjacent and perpendicular yarns. In this study, the dimensions of yarn cross-section were defined by using theoretical calculations and experimental measurements. Theoretical yarn diameter was accepted as the real circular diameter of the yarn before weaving. The theoretical circular yarn diameter depending on yarn count was calculated by Ashenhurst theory (13) given in Equation 2. But, from previous studies and literature, it was known that the cross-sectional shape of the yarn is changed during weaving, and this shape is not constant along the yarn path. Therefore, in this study, it was accepted that this circular yarn shape became elliptical during the weaving. The dimensions of an ellipse having the same perimeter with a circle were calculated by Equation 3. Here a is the major,

b is the minor diameter. Besides, flattening ratio (e) is defined as being the ratio of the minor diameter to the major ($e=b/a$). In the theoretical study, the minor dimension of the ellipse could be calculated by using the relation between fabric thickness (t) and the amplitude of warp yarn (h_1) as given in Equation 4. So, the value of major diameter could be calculated theoretically. In addition, in the experimental study, the dimension of major diameter was measured by using surface pictures of fabrics. Thus, the minor diameter of the yarn was predicted by using the relationship between theoretical circular diameter and major diameter.

$$d = \frac{1}{K\sqrt{N}} \quad \text{Equation 2}$$

$$d = \frac{a+b}{2} \quad \text{Equation 3}$$

$$t = h_1 + b_1 \quad \text{Equation 4}$$

The variation of major diameter was measured along the yarn path, in the experimental study. Flattening ratio of yarn was calculated for different regions. Using these values, the yarn cross-sectional shape and size of yarn along the yarn path were defined for each region. Thus, a realistic yarn geometry which does not accept a constant cross-sectional shape and size was formed.

4. Results and discussions

In Table 2, theoretical circular yarn diameter and mean value of the measured major diameter of elliptical yarn cross sections were summarized. Measurement of yarn dimension was done in different regions of weave unit onto the fabric images. In Table 2, a_{p-m} denotes major diameter at the peak point of intersecting region, a_{i-m} is major diameter at the middle point of the interchanging region, a_{c-m} is major diameter at the middle point of floating region (for twill weaves). It was found that, differences of major diameter between different regions of yarn path is significant according to statistical analysis.

Table 2. Calculated circular yarn diameter and measured major diameters

Fabric Code		d_t (cm)	a_{p-m} (cm)	a_{i-m} (cm)	a_{c-m} (cm)
Warp	P1	0.0129	0,0163	0,0148	x
	P2	0.0126	0,0161	0,0140	x
	P3	0.0118	0,0157	0,0126	0,0142
	P4	0.0131	0,0173	0,0133	0,0144
Weft	P1	0.0129	0,0171	0,0148	x
	P2	0.0129	0,0174	0,0154	x
	P3	0.0116	0,0139	0,0124	0,0128
	P4	0.0167	0,0198	0,0169	0,0211

a_{p-m} : Major diameter at the peak point, a_{i-m} : major diameter at interchanging region, a_{c-m} : major diameter at middle of floating (for twill weaves).

Minor diameter at the peak point of the intersecting region was calculated by using Equation 4, depending on fabric measured fabric thickness (t) and calculated amplitude of warp yarn (h_1). Here, the thickness was accepted forming by warp yarns. In addition, minor diameter at the different regions was calculated by using Equation 3, depending on the relation between theoretically calculated circular diameter and experimentally measured major diameter. In plain fabrics, the minor diameter values at the peak point of the intersecting region were found similar for both calculations. But in twill weaves, especially in 4/1 twill weave, real thickness (measured) was formed differently from the theoretical aspect because of long floating. So the minor dimension value calculated from fabric thickness was

bigger. In order to eliminate this problem, a certain flattening ratio at the peak point of 4/1 twill was used to define yarn dimensions as being 0.6.

Flattening ratio of yarn for different regions are calculated. Maximum flattening was found at the peak of intersecting region in which warp and weft yarns contact each other. The flattening ratio was found nearly 0.5-0.6 at that region. At the interchanging region, the flattening ratio was increased because of the pore region. It was nearly between 0.7-0.85 for different weave types. At the midpoint of the floating region (twill weaves), e was calculated nearly 0,6-0,7.

Table 3. Theoretical calculated yarn dimensions and experimental calculated minor diameter

Fabric Code		a_{p-t}	b_{p-t} (cm)	b_{p-m} (cm)	b_{i-m} (cm)	b_{c-m} (cm)
Warp	P1	0.0164	0.0095	0.0095	0.0110	X
	P2	0.0149	0.0103	0.0092	0.0113	X
	P3	0-0143	0.0093	0.0079	0.0110	0.0094
	P4	0.0084	0.0117	0.0088	0.0128	0.0117

In the theoretical study, the yarn path was defined by using B-spline curve method. The control points of B-spline polygon were calculated depending on structural properties of fabric such as fabric thickness (t), settings, yarn count, crimp ratio. Then the B-spline method was applied by an algorithm written in Visual Basic 2010. Fabric unit weight area (w) and crimp ratios (k) of yarns were calculated as control factors as given in Table 4. This geometrical model is achieved for plain fabrics. But, because of interactions between long floating, the theoretical results of 4/1 twill weave was found different from experimental results.

Table 4. Structural fabric properties calculated by B-spline method

Fabric Code	W	k_1	k_2
P1	121	1.11	1.09
P2	104	1.07	1.11
P3	132	1.2	1.16
P4	246	1.19	1.26

The fabric geometry simulations were performed by using SolidWorks. In Figure 3, some steps of SolidWorks drawing were shown. First, the yarn path was defined as a spline curve using 21 points. Then the planes for cross-sections were defined along the yarn path depending on the region. Five different plain was defined for each weave units. Flattening ratio of different regions was found different and in this study, the cross-sectional dimensions were defined individually for all planes. Then, loft property of SolidWorks was used and different cross-sections at different planes were connected along the yarn path. By this simulations, the variation of the yarn cross-section was reflected, realistically. Both warp and weft yarns were modelled depending on the structural properties of fabrics. In the end, drawn solid yarn simulations were repeated and 3d fabric simulations were acquired as given in Figure 4. In addition, B-spline curve based on control points could be obtained in SolidWorks. Yarn path could be drawn automatically after determined the number and coordinates of control points. This is a faster way to obtain yarn path geometry in SolidWorks. But, the calculation of spline points was chosen in that study in order to define some structural properties of the fabric. Thus, the experimental and the theoretical properties of fabrics could be calculated.

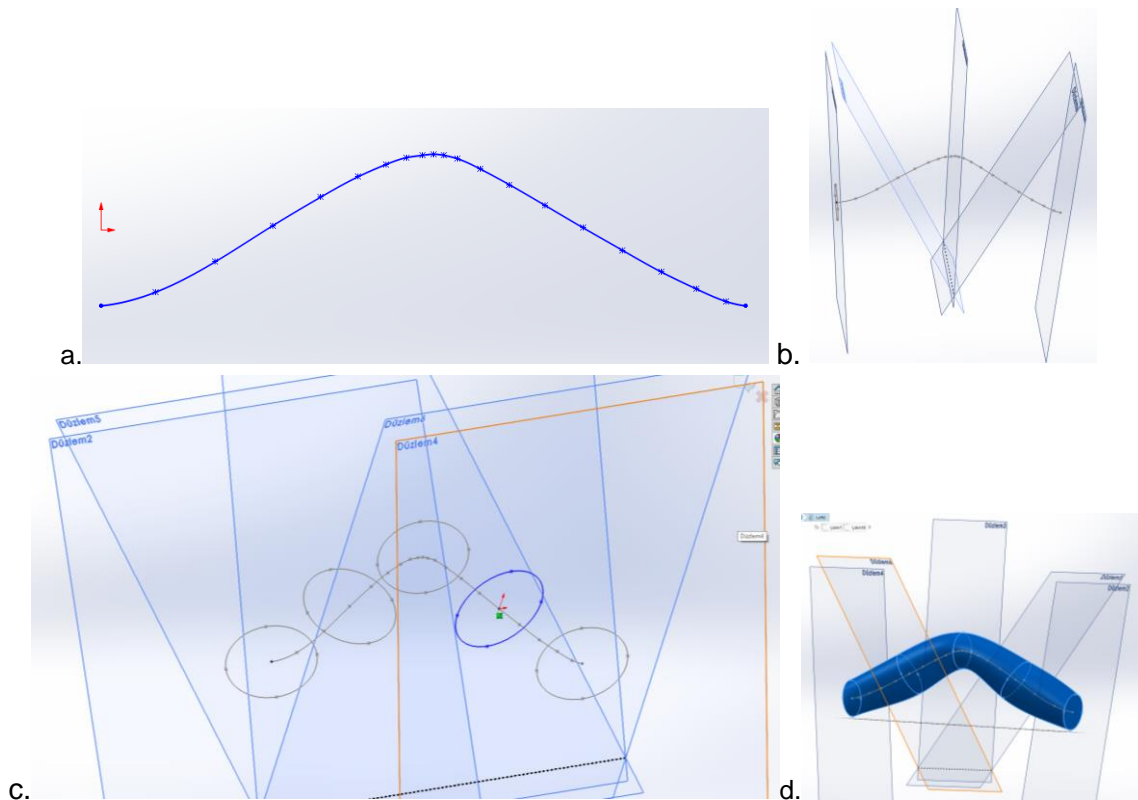


Figure 3. a. The B-spline curve of yarn path, b. Definition of planes for different regions of yarn path, c. Various cross-sections in different planes, d. Simulation of solid yarn model having various cross-section along the yarn path

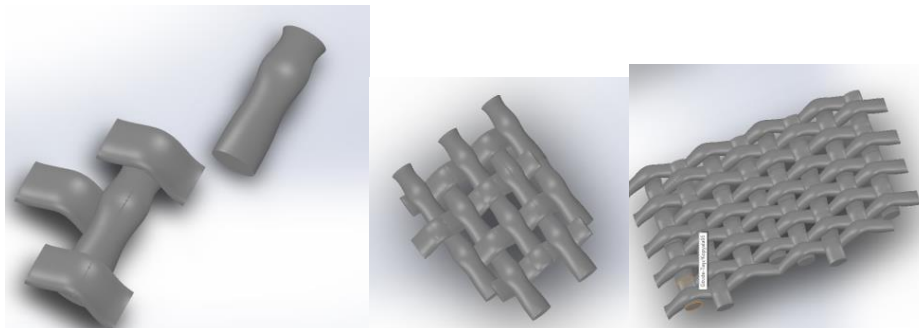


Figure 4. The simulation of fabric (for P1)

5. CONCLUSIONS

In this study, first, yarn path was modeled according to structural parameters of fabric such as weave type, settings, yarn counts, fabric thickness. The B-spline method was used to get a smooth yarn curve. Then, the yarn cross-section was modelled depending on the yarn path. The experimental results were used in order to get the flattening ratio of yarn cross-section at different regions of yarn path. After defining the cross-sectional properties of each region on the yarn path the yarn geometry of fabric weave unit was obtained. The performed fabric simulations were more realistic because of reflecting the variation of yarn cross section along the yarn path. This would help more realistic mechanical models with CAD system. The only disadvantages of using this the program is the material selection. In further studies, it is aimed to generate 3-D fabric geometry with multifilament yarns and to use these fabric models in the prediction of performance properties of fabrics. Besides, an exhaustive experimental study contained different raw materials and structural parameters were planned.

References

1. Alamdar-Yazdi, A., Heppler, G. R. (2011). Cross-sectional shapes of the yarn in cotton gray woven fabric. *Journal of Textile Institute*, 102 (3), 248-262.
2. Gong, R. H, Ozgen B., Soleimani M.(2009). Modeling of yarn cross-section in plain woven fabric. *Textile Res J*; 79: 1014–1020.
3. Jiang, Y., Chen X. (2005). Geometric and algebraic algorithms for modelling yarn in woven fabrics. *J Textile Inst*;96: 237–245.
4. Hamilton, J. B. (1964). A general system of woven-fabric geometry. *J Textile Inst*,; 55: 66–82.
5. Hearle, J. W.S., Shanahan, W. J. (1978). An energy method for calculations in fabric mechanics part I: Principles and methods. *J Textile Inst*,; 69: 81–91.
6. Keefe, M., Edwards, D., Yang, J. (1992). Solid modeling of yarn and fiber assemblies. *J Textile Inst*; 83: 185–196.
7. Kemp, A. (1958). An extension of Pierce's cloth geometry to the treatment of non-circular threads. *J Textile Inst*; 49: 44–48.
8. Peirce, F.T. (1937). The geometry of cloth structure. *J Textile Inst*,; 28-3: T45–T96.
9. Olofsson, B.(1964). A general model of a fabric as a geometric mechanical structure. *J Textile Inst*, 5511: 541–557.
10. Ozgen, B., Gong, H.(2010). Yarn geometry in woven fabrics. *Textile Research Journal*; 81: 738–745.
11. Smith, A. Chen, X. (2008). CAD and constraint-based geometric modelling algorithms for 2D and 3D woven textile structures. *Journal of Information and Computing Science*, 3 (3), 199-214.
12. Turan, R. B., Okur, A. (2012). The Variation of the Yarn Cross-Section in the Fabric., *Textile Research Journal*, 82(7).719-724.
13. Ashenhurst T.R. (1984). *A treatise on textile calculations and the structure of fabrics*, 5th ed. London: J. Broadbent and Co.



AUTOMATIC ANALYSIS THE BRAIDING ANGLE OF THE BRAIDED FABRICS USING IMAGE PROCESSING

Yisheng Liu¹, Yordan Kyosev²

¹Zhejiang Sci-Tech University ,Hangzhou ,China,The Second Street 298,

Xiasha ,310018,Lysleo@zstu.edu.cn

²Hochschule Niederrhein University of Applied Sciences, Moenchengladbach, Germany,

Webschulstrasse 31,D - 41065 Mönchengladbach

Abstract

The braiding angle is one of the most important parameters of the braided structures, because it influences their mechanical properties. For this reason, any way of automatic inspection of the braiding angle can simplify the quality control of such products. Image analysis is one of the feasible non-contact measurement methods to obtain braiding angle. In this paper is presented a new program for image processing and analysis of the braiding angle. Nine different braided structures are analyzed manually and with the help of the program. The comparison of the results demonstrates, that in the most cases the created algorithm produces accurate results, but in few situations it analyses different geometrical properties in the image than those, analyzed by humans.

Key words:

Braiding Angle, automatic detection, Image Analysis, Image Processing, Python, Hough Line Detection

1. Introduction

Braided products are not so popular like the woven and knitted, but are used in large number of applications. In each car are integrated more than 1500 meter of braided products [1]. Large part of the ropes for industrial and marine application are braided and the climbing ropes are as well braided products [2]. In one braided structure there are direct relations between the elasticity, strength, bending stiffness and other parameters and the braiding angle [3, 4]. For this reason its automatical control is important step in the ensuring the quality of the braided products. This paper presents the development of algorithm for automated analysis of the braiding angle, based on the Python libraries.

2. Application of the Image Processing

Python is a high-level language with an open source, high-quality, peer-reviewed code, written by an active community of volunteers [5]. Now Python become one of the most popular program languages in the world. For the image analysis and angle identification, several modules such as Numpy, Scipy, Scikit-image and matplotlib were used and all of these can be found on the web.

Scikit-image [6], Image processing in Python, is a collection of algorithms for image processing. For braiding angle identification, it provides a set of functions for image loading, visualization, manipulation, and analysis. The flow chart of the executive program is Figure.1, it included several steps from loading image to calculation of the braiding angle. The interface of the executive program was shown as Figure.2.

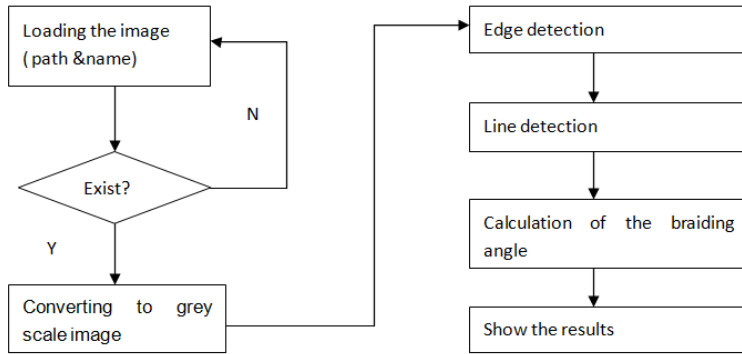


Figure 1. The flow chart of the executive program

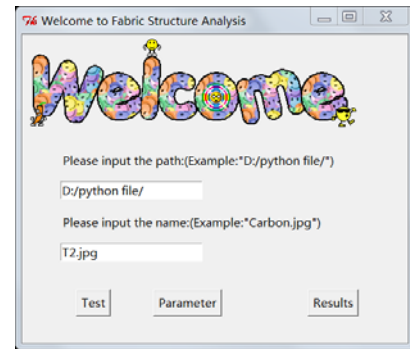


Figure 2. Interface of the executive program

2.1. Loading image

The first step for the analysis is loading image into the executive program. The following code:

```
img2=io.imread(imgpath)
```

opens file with 'imgpath', which can be in different format as jpeg, bmp, png or other and store the information in the variable img2. This variable is now an array, in the current case with size 1077 x 817 x 3 unsigned integers, which means that there are three arrays with the red, green, and blue values of each of the pixels.

2.2 Converting to greyscale image.

In Scikit-image processing, the angle detection and several image processing functions work only with grayscale images, therefore it is necessary to convert the true color image to a grayscale image. In the example, the true color image is represented as an unsigned integers array, it needs to be transferred into floats and then to a grayscale image by using the function 'img_as_float()' and 'rgb2gray()'. The result of this conversion is presented in Figure 3. (right)

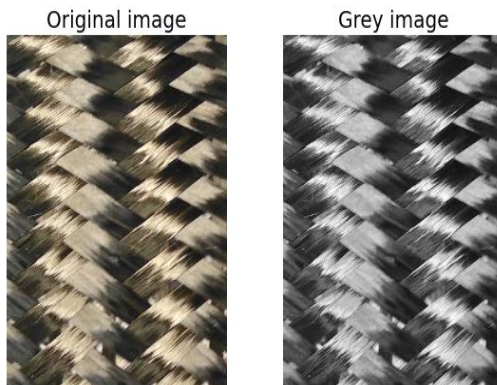


Figure 3. Image of T2.jpg - left original true color image, right after conversion to grayscale.

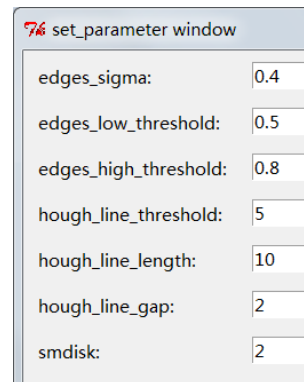


Figure 4. Parameters for the edge detection

2.3 Edge detection

For the image processing several parameters of the algorithms have to be set. As the different samples require different values, a small user interface (Figure 4) was prepared, in order for different configurations to be tested quickly. The seven parameters of the image analysis procedure have to be entered, one for

morphology, three for edges detection and three for hough line detection. After some experience it was found, that the edge detection works better if the image is „homogenized” – some small bright spots are removed and the small dark cracks are connected. This is done by the function ‘Opening’ of the Skimage toolbox.

To find edges in the greyscale image, the ‘canny’ function can be used [7]. This function finds places in the image where the intensity changes rapidly. In the image those places could be the edges of the threads within the braid. The most useful edge-detection method is the ‘canny’ method. This method differs from the other edge-detection methods in that it detects strong and weak edges. As visible in Fig.5(left), the main directions of the yarns can be recognized, The main commands are :

```
import skimage.morphology as sm
from skimage import feature

image=sm.opening(image1, sm.disk(int(sdisk)))
edges = feature.canny(image, sigma=float(pes),
                    low_threshold=float(pelt), high_threshold=float(pelh))
```

2.4 Hough Line detection

To get the braiding angle it is necessary to detect at least one straight line at an edge of a thread. To detect those lines the ‘Hough’ transformation is applied [8]. The Hough transformation creates a dual space where all possible parameters of the to-find point are entered for each point in the image that is located on an edge. After setting the threshold, line length and line gap, The ‘Hough_line’ function will detect the edge line and get a line list, in which the start point and end point of each line is stored as a tuple. As visible in Table 1, the main directions of the edge lines can be recognized. The main command is :

```
import skimage.transform as st
lines = st.probabilistic_hough_line(edges,
                                   threshold=int(pht), line_length=int(phl), line_gap=int(pha))
```

where „edges” is the variable with the result from the application of the canny algorithm over the figure.

3. Results and discussion

The braiding angle is the angle between the product axis and the fibers. Assuming that the image was rotated before the analysis so, that the vertical direction corresponds to the y-axis, the braiding angle can be regarded as the angle between the edge line of yarn and y-axis. Since the start point and end point is detected, the angles of all detected lines can be calculated with the equation


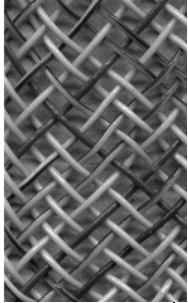
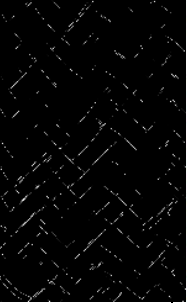
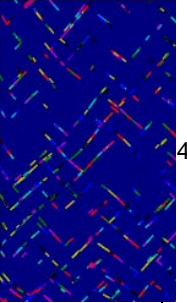


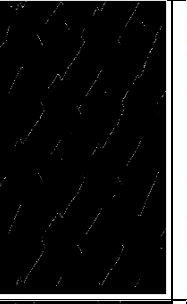
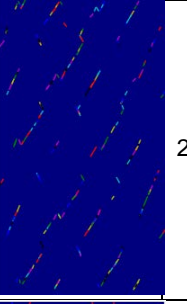

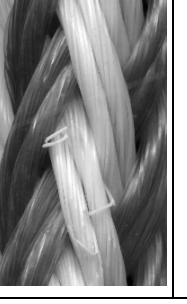

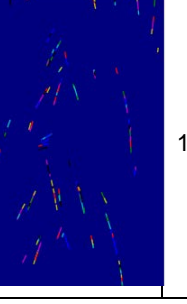
$$\alpha = 90^\circ - \text{abs}\left(\arctan \frac{\Delta y}{\Delta x}\right)$$




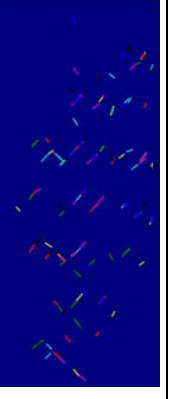
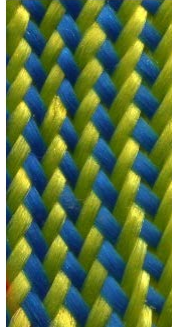
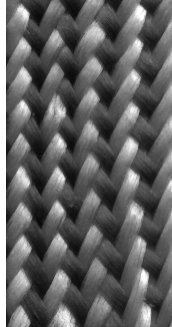

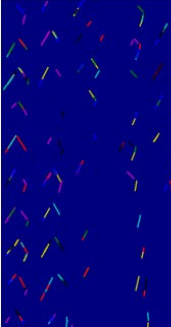


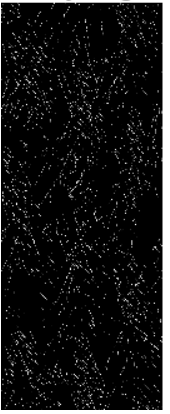
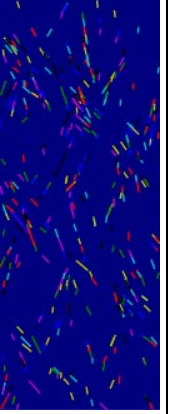

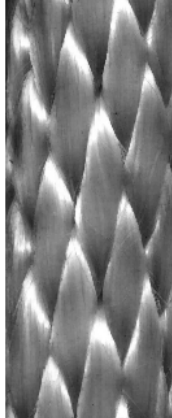

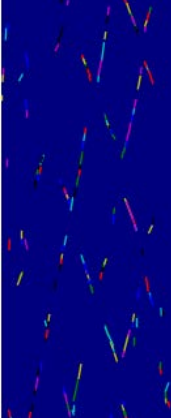
This angle is calculated for each detected line and the histogram of all values is plotted (Table 2). The maximum of the histogram is taken as a braiding angle.

In the current case, nine different samples were selected for testing the algorithm. The samples were selected so, that they cover different application areas and different structures - to have a monofilament braid, ropes and multifilament structures for composites. As demonstrated (Table 2), there are several detected lines from the images, which are not parallel to the fibers. These lines are coming from shadows, different colour appearance or as well the vertical boundaries of image. But the most of the two largest bars shows the actual braiding angle, as the most of the fibers in the braid are detected as lines,

oriented at plus or minus the braiding angle degree. The most difficult step for the application of the algorithm was the detection of the parameters of the edge detection algorithms. During the preparation of the manuscript was found, that the algorithm is sensible against the parameters in the image detection and these has to be re-identified with several trials and errors for for each new sample. The braiding angle was measured as well manually, using the software ImageJ on the same images. The result of the five measurements as arithmetic mean value and the variation coefficients are given in the Table 1. Automated detected angle is presented there too, together with the relative error in % between both measurements.

Table.1 Tested samples and manual and computed results

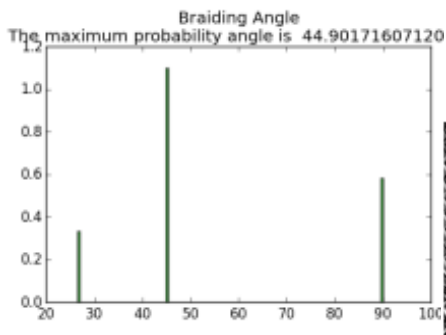
Nr	Original Image	Grey Scale	Canny Edges	Probabilistic Hough	Measured (Mean N=5) °	$V = \frac{\sigma}{\bar{x}}$ %	Detected °	Rel. Error %
1					45,1	1,80	44,9	-0,5
2					28,6	1,7	26,5	-7,3
3					19,3	4,6	18,4	-4,7

4					44,4	2,1	44,5	0,2
5					27,5	4,2	26,5	-3,9
6					25,4	3,5	26,6	4,4
7					15,6	3,9	18,0	15,0

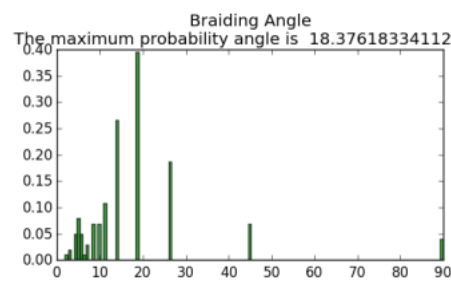
8					40,7	3,8	44,9	10,1
9					56,4	2,1	44,7	-20,7

As it can be seen (Table 1 and Figure 5), in the most cases (1-6) the automatic algorithm determine the braiding angle with less than 10% error. The last three samples have errors up to 20%. The histograms and the images of some typical samples (Table 2) can give explanation of these larger errors. The sample 1 in Table 2 is a structure with monofilament wires. The edges, extracted from this image corresponds to the yarns and the accuracy at this image is very high – it produced 0.5% error. Sample 3 is a braid, produced from slightly twisted yarns. The algorithm detects there a lot of the single filaments, which have different angle than the yarn itself. After playing with the edge detection parameters, still was possible to get the main edges of the yarns and have accurate result with 4,7% error, in the same way as for figure 6 (rope of twisted linen material). In both cases the yarns are still recognizable as objects and produce better visible edges than the single fibers or filaments. Completely different is the behaviour at the braids for composites. In such case the rovings consists of thousands of parallel filaments, which are recognized as lines. These filaments are not always exactly parallel to the roving axis and the edges of the roving are optically not easy to be detected. Because of the large number of the single lines of the filaments there is one very clear maximum in the histogram and all other detected lines remain with significantly lower appearance, almost not visible there. So in this case –the automatically detected angle differs significantly fro the manually detected one, because the operator is able to identify the roving main line and the algorithm detect the orientation at the finer – filament level.

Table 2. Automatically detected braiding angles for some samples



a) Sample 1



b) Sample 3

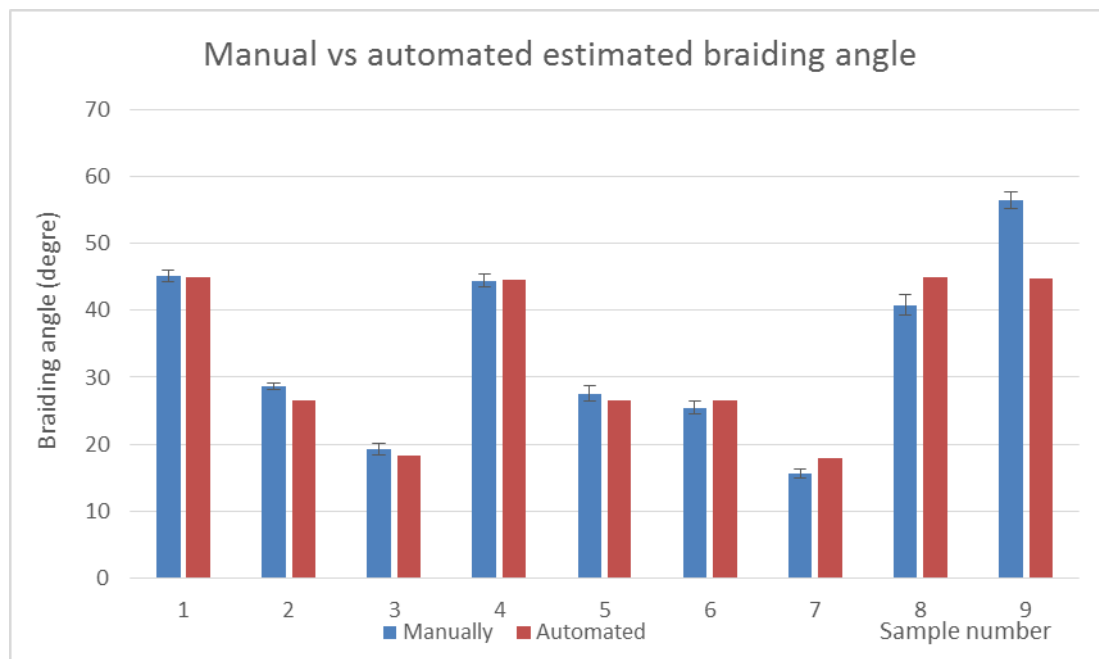
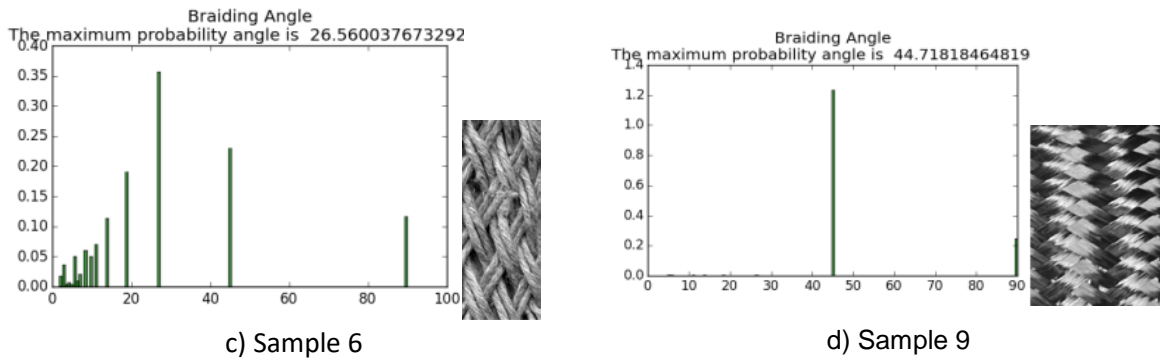


Figure.5 Comparisson between the manually and automated estimated braiding angles of

4. CONCLUSIONS

The automated program for image processing based on Python language was developed and applied for automatic detection of the braiding angle of braided products. It can be used for fast quality control of braided product and allows very good accuracy for the braid, where the yarns can be recognized optically. The algorithm can be applied for structures for composites, too, but in this case it detects the fiber orientation and not always the tow orientation. The main task for using such algorithm in the practical application seems to be the detection of the parameters of the image processing functions. Their values depend on the contrast and the brightness of the image.

References

1. August Herzog, *Product Catalogue*, Oldenburg, 2013
2. Kyosev, Y. (Ed.) *Advanced in the braiding technology*, Elsevier, 2016

3. Brookstein, D.S., Tsiang, T.-H.: *Load-Deformation Behavior of Composite Cylinders with Integrally-Formed Braided and with Machined Circular Holes*. *Journal of Composite Materials* 19(5), 476–487 (1985)
4. Kyosev, Y.K.: *Braiding technology for textiles: Principles, design and processes*. Woodhead Publishing Series in Textiles No. 158, 1st edn. Woodhead Publishing Limited (2014)
5. Python, www.python.org (2018)
6. Scikits Toolbox, <https://www.scipy.org/scikits.html>
7. Canny, J.: *A Computational Approach to Edge Detection*. *IEEE Trans. Pattern Anal. Mach. Intell.* PAMI-8(6), 679–698 (1986). doi: 10.1109/TPAMI.1986.4767851
8. Hough, P.: *Method and means for recognizing complex patterns*. USA Patent U.S. Patent 3,069,654, 18 December 1962

EXPERIMENTAL TESTING AND FINITE ELEMENT SIMULATION OF TH-7 BENDING TEST OF SPORTS BRA TEXTILES

Michaela Hassmann¹, Wolfgang Krach²

¹University of Vienna, Institute of Sport Science, Vienna, Austria, +43-1-4277-48883, michaela.hassmann@univie.ac.at

²CAE Simulation & Solutions GmbH, Vienna, Austria, +43-1-9748991-11

Abstract:

The measurement of mechanical properties of textiles is essential for Finite Element (FE) simulation and virtual garment try-on software. For the determination of bending, the TH-7 device, developed by Technical University of Liberec, Faculty of Textile Engineering, was used. It offers testing of specimens in different shapes. Circular shaped specimens with a diameter $\Phi = 5$ cm were cut from three fabrics used in the Anita momentum sports bra. These specimens were subjected to the bending test in directions from 0° to 360° turned by every 22.5° both up and down. The shape of the specimen during testing was recorded using video. From the measured bending force F_m [mN] the bending rigidity B [Nm²/m] was calculated as described in literature. The value of bending rigidity was verified in FE simulation of TH-7 bending test by comparing resulting specimen shape and bending force. None of the bending tests proposed in literature seems to provide correct values for Young's modulus E , whereas the simulation of non-linear behaviour requires a more complex approach of piecewise linear modelling.

Key words:

bending force, bending rigidity, material properties, knitted fabrics, anisotropy

1. Introduction

Bending rigidity is an important mechanical property of textile fabrics. Therefore, several different procedures and devices for measuring bending behaviour have been proposed in literature. ASTM D1388 proposes the Cantilever test (Option A) and Heart Loop test (Option B) [1] which both subject the specimens to their own weight. They provide limited information about the mechanical behaviour due to the fixed amount of bending and, moreover, they don't include force measurement. The KES-FB (Kawabata Evaluation System) pure bending tester suggests that the fabric is subjected to bending only, which is not thoroughly correct in case of horizontal clamping of fabric. In addition, this device is rather expensive [6]. Yet, the advantage over Cantilever and Loop tests is the ability to detect the non-linear bending behaviour by measuring the relationship between bending momentum and curvature [6]. In the Czech standard ČSN 80 0805 "Testing of stiffness and resiliency of textile fabrics" a similar bending tester is used [6]. The TH-7 bending tester is a much cheaper and more practical device, as it allows the measurement of small specimens in both bending directions (up and down) in one cycle, directly providing bending hysteresis. In addition, good correspondence to the KES-FB was proven [4].

In sports bras, mainly knitted fabrics are used for the construction of cups and wings. The loop structure of knitted fabrics leads to an anisotropic, usually orthotropic, mechanical behaviour, which has to be taken into account when choosing the direction in which the fabrics are sewn. Due to the

assumption of orthotropic behaviour, material properties of knitted fabrics have to be tested in several directions. The idea of using circular shaped specimens was first mentioned by Peirce [7]. Circular shape has the advantage of reducing curl, and moreover the benefit that the stiffness can be measured in any direction using only one specimen. This significantly reduces the amount of required specimens compared to using rectangular ones [4].

2. Experimental

2.1. Specimens

Fabric samples of the required size of the Anita momentum sports bra were available for the wing (5), cup (6) and cup liner (7) fabric (see Figure 1).



Figure 1. Unstitched Anita momentum sports bra, machine direction of samples indicated by arrow

Loop structure was analysed under the microscope to determine the type of knitting for each sample. Wing fabric (5) is a single layered warp knit mesh with fillet, three guide bar structure (one elasthan thread) (see Figure 2a). Cup fabric (6) is double layered, the outer layer is a 2 layer rip structure (weft knit with tuck), the inner layer is standard plush to make the cup more comfortable (see Figure 2b). Cup liner fabric (7) is double layered, with locknit (charmeuse) outer layer and tricot inner layer to provide high strength in machine direction (see Figure 2c and d).

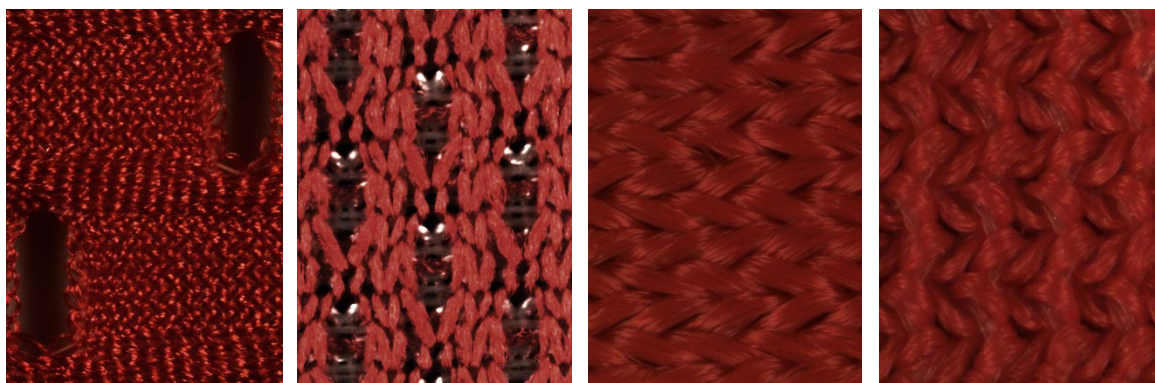


Figure 2. a) Sample 5 (back) b) Sample 6 (face) c) Sample 7 (inner layer, face) d) Sample 7 (outer layer, face); machine direction up

From these three samples, three circular shaped specimens each with a diameter $\Phi = 5$ cm were cut. The specimens were marked with lines at every 22.5° with the machine direction as 0° . Thickness was measured according to EN ISO 5084 [3] and density was calculated as weight per unit area divided by thickness (see Table 1).

Table 1. Specifications of sports bra samples

sample	description	weight per unit area M [g/m ²]	thickness T [mm]	density ρ [t/mm ³]
5	wing	245.8	0.85	$2.892 \cdot 10^{-10}$
6	cup	266.3	1.25	$2.131 \cdot 10^{-10}$
7	cup liner	367.4	1.00	$3.674 \cdot 10^{-10}$

2.2. Experimental TH-7 bending test

The circular shaped specimens were clamped in the TH-7 bending tester (see Figure 3). Measuring range was set to 40 mN. For each direction, 10 cycles of 90° up and down bending were performed and filmed to analyse the deformed shape during the bending test.



Figure 3. Specimen clamped in the TH-7 bending tester, front and side view

The measured bending force F_m [mN] was output as mean value for the 10 cycles and averaged for three specimens per sample, for each direction as well as up and down separately. This bending force can be converted into the bending rigidity B [Nm²/m] (1), where sample width $s = 50$ mm and the constant $\kappa = 0.0334$ [m²] as described in [4]. Instead of bending rigidity of unit width B [Nm²/m], bending rigidity for sample width B_s [Nm²] (2) was used for further calculations.

$$B = \kappa \cdot \frac{F_m}{s} \text{ [Nm}^2\text{/m]} \quad (1)$$

$$B_s = \kappa \cdot F_m \text{ [Nm}^2\text{]} \quad (2)$$

2.3. FE-modelling of TH-7 bending test

FE models were pre-processed in MSC Patran 2016. The fabric was modelled as a semi-circle corresponding to the free bending length of the sample in the test using standard PSHELL shell formulation with linear CQUAD4 and CTRIA3 elements. The sensor jaws were modelled as half cylinders fixed to one node by RBE2 constraints (see Figure 4). Linear elastic material MAT1 for course fitting and stress-dependent MATS1 for piecewise linear fitting were assigned to the fabric. Considering the bending rigidity of a thin structure being the product of Young's modulus E and area moment of inertia I (3,4), Young's modulus E [MPa] can be derived from the bending rigidity for sample width B_s [Nm²] calculated from the experimental TH-7 bending and from the measured thickness T [mm] of the sample (5).

$$B_s = E \cdot I \text{ [Nm}^2\text{]} \quad (3)$$

$$I = \frac{s \cdot T^3}{12} \text{ [mm}^4\text{]} \quad (4)$$

$$E = \frac{12 \cdot \kappa \cdot F_m}{s \cdot T^3} \text{ [N/mm}^2\text{]} = \text{[MPa]} \quad (5)$$

Poisson ratio ν was used from previously performed tensile test. For the Teflon sensor jaw properties were assigned, including a friction coefficient $\mu = 0.05$ in the fabric-jaw contact. The clamped top row of nodes of fabric was rotated by $\pm 90^\circ$ in steps of 2° in accordance with the TH-7 measurement procedure. Inertial load was included to account for the influence of gravity. The solver MSC Nastran Implicit Nonlinear analysis (SOL 400) was used for achieving the numerical results.

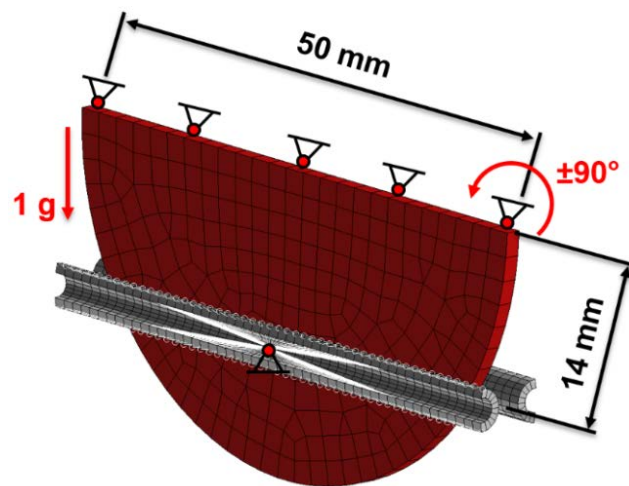


Figure 4. FE model of TH-7 bending test (shell thickness display) with boundary conditions and load case

3. Results and discussion

3.1. Experimental TH-7 bending test

Textiles usually exhibit hysteresis behaviour under bending loading, which can be measured when bending the specimen consequently in both directions. Figure 5 shows exemplarily the hysteresis loop for sample 6 obtained by TH-7 bending test at 0° orientation as the arithmetic mean of 10 cycles averaged for three specimens.

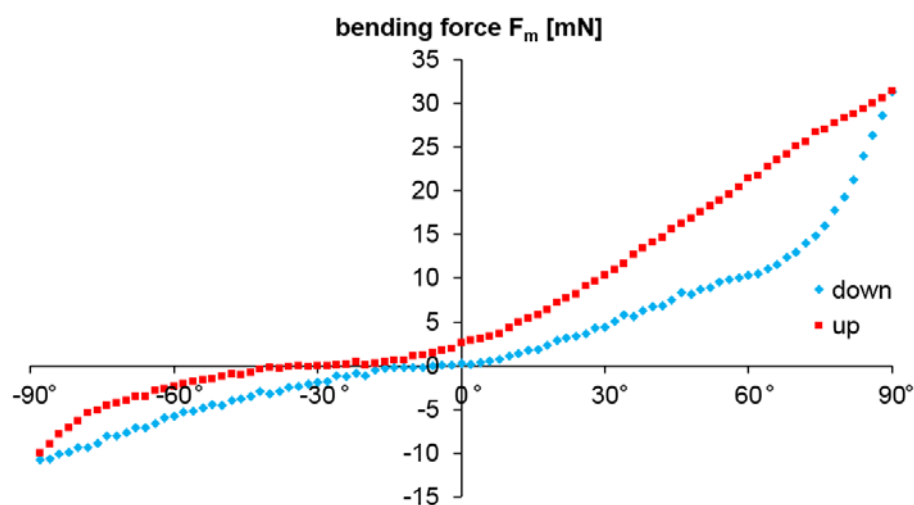


Figure 5. Hysteresis loop obtained by TH-7 bending test (sample 6, degree 0° = machine direction)

The anisotropic mechanical behaviour obtained by subjecting the same specimen to bending in several directions can be evaluated and depicted in a polar diagram. The highest value of bending rigidity B [Nm^2/m] for $+90^\circ$ bending was chosen for comparison of the three samples. Due to symmetry, specimens were measured only for directions from 0° to 157.5° . The data could be copied to the other half of the polar diagram as mentioned in [4] or simply omitted (see Figure 6).

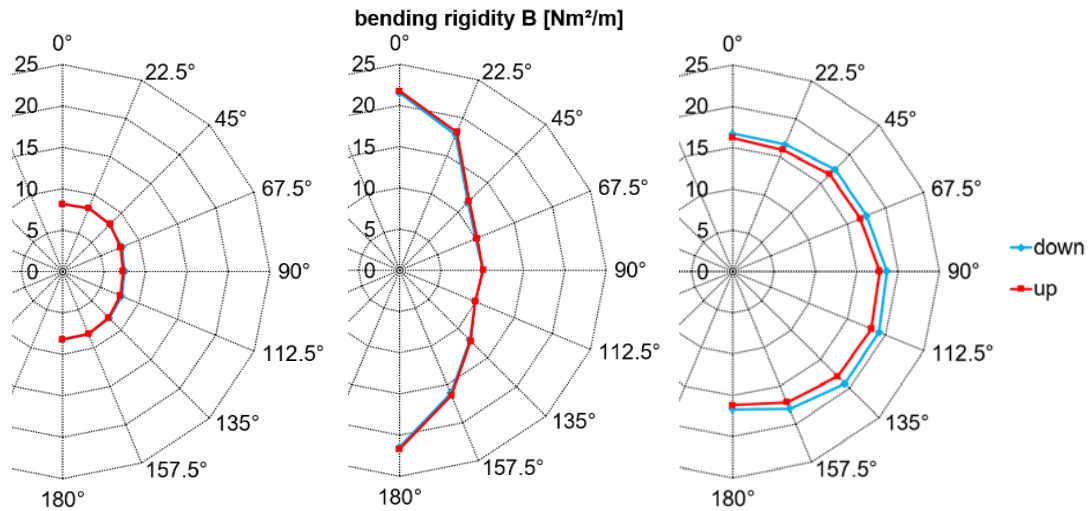


Figure 6. Polar diagram of bending rigidity B [Nm^2/m] at $+90^\circ$ bending **a)** Sample 5 **b)** Sample 6 **c)** Sample 7

Sample 6 shows far more anisotropy than samples 5 and 7, while sample 7 shows the greatest deviation between up and down bending direction. For all three samples, the measurement for directions from 0° to 90° would be sufficient as the first and second quadrant are very similar.

3.2. FE-modelling of TH-7 bending test

Table 2 shows the mechanical properties used for the FE simulation of the TH-7 bending test for the three sports bra samples. Young's modulus E calculated from TH-7 bending test for bending direction 0° , and previously performed tensile test in machine direction are compared. It can be concluded that TH-7 bending test overestimates Young's modulus by a factor of 1000. Therefore, FE simulation had to be performed with values obtained by tensile test to gain comparable bent shape. Based on the resulting values for horizontal bending force F_m , Young's modulus was fitted for 0° to $+90^\circ$ bending, which can be approximated by linear material behaviour.

Table 2. Mechanical properties of sports bra samples for FE simulation

sample	thickness T [mm]	density ρ [t/mm ³]	Young's modulus E [MPa]		Poisson ratio ν [-]
			TH-7 test	tensile test	
5	0.85	$2.892 \cdot 10^{-10}$	158.791	0.165	2.416
6	1.25	$2.131 \cdot 10^{-10}$	421.603	0.409	2.022
7	1.00	$3.674 \cdot 10^{-10}$	321.480	0.332	0.409

The resulting bent shape from experimental TH-7 bending test and FE simulation are compared in Figure 7 exemplarily for sample 6 in machine direction (0°). The shell elements representing the sensor jaws were modelled with offset in order to show the outer surface contacting with the specimen.

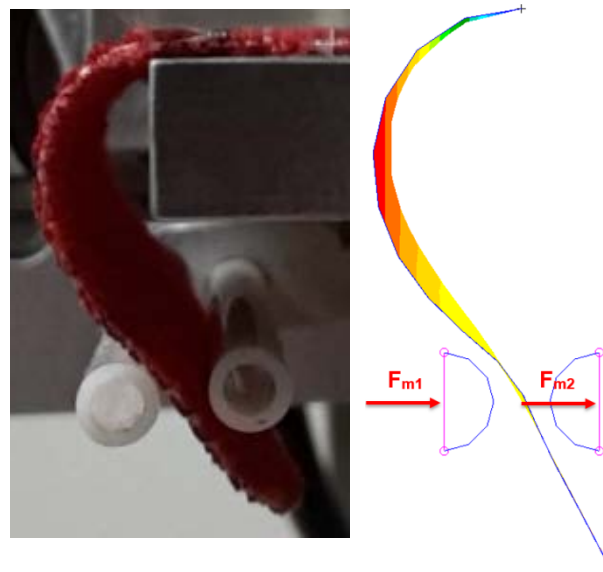


Figure 7. Comparison of bent shape at bending angle $+90^\circ$ of sample 6 **a)** TH-7 test **b)** FE simulation

The nearly linear material behaviour for bending direction up could be coarsely approximated by Young's modulus $E = 0.147$ MPa. The non-linear material behaviour for bending direction down was taken into account by piecewise linear modelling defining stress-dependent MATS1 material. The stress values were calculated from resulting maximum strain for the respective bending angle and adjusted to resulting bending force F_m at the sensor jaw. The sum of horizontal bending forces F_m at both sensor jaws for FE simulation was compared with the measured values for $+90^\circ$ bending (see Figure 8); the procedure for -90° bending was identical. Fluctuations in FE result occur due to stick-slip at the contact of specimen and sensor jaw.

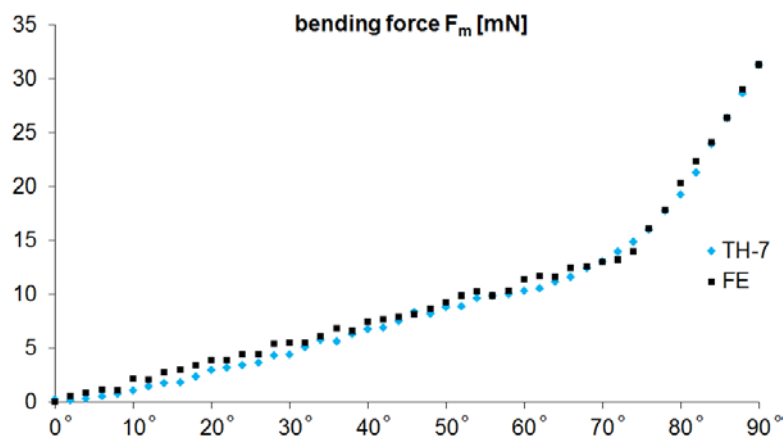


Figure 8. Comparison of horizontal bending force F_m of sample 6 in TH-7 bending test and FE simulation

4. CONCLUSIONS

The TH-7 bending test provides a fast and cheap option to measure the mechanical properties of fabrics. The proposed finite element calculation allows an evaluation of the required Young's modulus for each measured direction. Using this procedure the orthotropic properties of the fabric required for a mechanical analysis of can be derived. Therefore, a numerical procedure has been performed for the verification of Cantilever bending test [5]. None of the bending tests proposed in literature seems to provide correct values for Young's modulus E . The proposed bending rigidity [4] seems to calculate unreasonably high values. The constant $\kappa = 0.0334$ [m²] was calculated by a simple discrete model of continuous bending curve [4] to match TH-7 results with KES-FB results. We suppose that this constant considers using bending force F_m in [mN] rather than in [N] as mentioned in [4]. The

assumption of using bending rigidity as a value for FE simulation should be rejected, only tensile tests are able to provide the necessary material properties for simulation when assuming linear behaviour.

The measured bending force F_m is a function of the bending angle. There is no advice given in [4] on which value at which bending angle to use for the calculation of bending rigidity. Considering the non-linear behaviour of knitted textiles requires piecewise linear fitting defining nonlinear (stress-dependent) material properties adjusted to the resulting bending force F_m at the sensor jaw for the respective bending angle. This procedure is time-consuming, but it allows for realistic bending simulation of sports bra fabrics in one direction. In addition, hysteresis behaviour cannot be taken into account in MSC Nastran solvers.

ACKNOWLEDGEMENTS

The authors would like to thank Prof. Ludmila Fridrichová and Prof. Irena Lenfeldová (Technical University of Liberec, Faculty of Textile Engineering) for their help with the TH-7 device and determination of knitted structures.

References

1. ASTM D1388-14 (2014). *Standard Test Method for Stiffness of Fabrics*.
2. ČSN 80 0858 (1974). *Zkoušení tuhosti a pružnosti plošných textilií [Testing of stiffness and resiliency of textile fabrics]*.
3. EN ISO 5084 (1996). *Textiles – Determination of thickness of textiles and textile products*.
4. Fridrichová, L. (2013). *A new method of measuring the bending rigidity of fabrics and its application to the determination of their anisotropy*. *Textile Research Journal*, 83(9), 883–892.
5. Hassmann, M., Stöger, S., Mentel, N., Krach, W. (2017). *Bending behaviour of sports bra fabrics: Experimental and Finite Element simulation of ASTM D1388 Cantilever test*. *Vlákna a Textil / Fibres and Textiles*, 24(1), 73–77.
6. Naujokaityte, L., Strazdiene, E., Fridrichova, L. (2007). *Comparative Analysis of Fabrics' Bending Behavior Testing Methods*. *Tekstil*, 56(6), 343–349.
7. Peirce, F. T. (1930). 26 – *The "handle" of cloth as a measurable quantity*. *Journal of the Textile Institute Transactions*, 21(9), T377–T416.



COMPUTATIONAL METHODOLOGY FOR DETERMINATION OF YARN TWIST AND DIAMETER

Bohuslav Neckář¹ and Dipayan Das²

¹Technical University of Liberec, Faculty of Textile Engineering, Department of Technologies and Structures, Liberec, The Czech Republic

²Indian Institute of Technology Delhi, Department of Textile Technology, New Delhi, India
E-mail: dipayan@textile.iitd.ac.in

Abstract:

In this work, a set of theoretical relations among yarn count, twist, and diameter is derived. This theory is based on a simplified mechanics of fibre compression. It considers that the fibers present in-between the core and the surface of a yarn are significantly compressed due to twist. It is found that the basic quantity that determines the relations among yarn count, twist, and diameter is the fiber packing density in yarns. The theoretical results are found to be in good agreement with the experimental data. Also, how to use these relations for industrial production of yarns is demonstrated with the help of practical examples. Nevertheless, it is realized that a more precise model of yarn twist and diameter is required to be formulated in future and this can be done by using continuum mechanics. However, it requires to know the law of deformation of fibers in the yarn which, as of now, is not enough precisely known. In order to apply continuum mechanics for solving this problem, an exact knowledge on the stress-strain behavior of fibers and the fibre-to-fibre slippage in yarn is required.

The full text is available as appendix of conference book, page 387.



METHOD OF GENERATION ZONING AREAS IN PATTERN CONSTRUCTION NET OF SEAMLESS UNDERWEAR

Blažena Musilová¹, Alžbeta Hôrecká² and Nareerut Jariyapunya³

^{1,2,3} Technical University of Liberec, Faculty of Textile Engineering, Department of Clothing Technology, Studentská 2, 461 17 Liberec, Czech Republic
Email: blazena.musilova@tul.cz

Abstract:

It is well known that in order to develop tight-fit seamless garment of satisfactory fit it is necessary to use shaping in order to achieve 3D shapes that relate to the shape of the body. This requires a sophisticated approach to create suitable pattern design. In this paper a method of generation zoning areas for 3D shaping has been designed within a 2D pattern construction net of the seamless underwear. To non-contact measure and display a three-dimensional body form the topography technique of the shadow moiré has been applied. To evaluate obtained 2D pictures of digitised zones of moiré fringe pattern the processing system NIS-Elements has been used. The size and location of the editing zoning areas has been compared with the corresponding place positions of zoning areas on the tubular knitted fabric which covers the pelvic part of the female figurine EU size 38. The geometry of the stretch pattern profile has been evaluated through understanding the dynamic effect of the fabric behaviour. Experimental results verify the effectiveness of the moiré topography to determine geometry of a 3D human body surface to achieve information of zoning areas for 3D design of seamless stretch underwear. Measured size and location of the zoning areas have been used as a pattern parameter for generation a 2D construction net of a seamless girdle.

Key words:

Seamless underwear, Constructional net, Non-contact body measurement, Moiré, Zoning area.

1. Introduction

Currently there is a number of specialists knitted garment producers who are using type of seamless circular garments to create highly technical garments, using specific knit structures to map the body surface for comfort. These are mainly types of sportswear, therapy garments and others. In terms of fit, there is evidence to suggest that, although knitwear is stretchy and therefore there is an assumption it will fit a wide variety of body shapes and sizes, there is still need for fit improvements. Thus body mapping can be described as comfort mapping. The specific areas of the garment must map to specific areas of the body. It must be presumed that production technology development should include a sophisticated understanding not just of the functions of the body but also of body size, shape and proportion.

To create knitted garments that fit the body of 3D shape, it is important to have a suitable method of applying body measurement within product development processes. That can be one of non-contact contour mapping technics [1].

Research that is described in this paper has being focused on the development of pattern making method that is associated with seamless garments made by knit technology with the help of circular machinery.

2. Experimental

Experimental steps are concerned with the discovering the suitable way how to measure zoning areas of the female body surface geometry of the pelvic part and with the way how to determinate zoning areas within pattern construction net of seamless underwear.

2.1. Materials and Methods

To target experimental strategy and define a female somatotype, the figurine AlvaForm (Fig.1) made from soft memory foam which simulates a soft human tissue, has been chosen. This AlvaForm of the European size code 38, which is in the half scale form (WAIST = 36cm, HIP = 49cm), is accurately shaped and proportioned physical characteristics derived from relevant consumer data based on Europe female population analysis.



Figure 1. Figurine AlvaForm EU size code 38 (Front, Back and Side View)

For capturing 3D form of body and to found out input pattern construction parameters and position of zoning areas in a tubular knit structure of seamless product, the effective non-contact topography technique of a shadow moiré has been applied. This is a well-known technique, commonly used in analysis of spiral deformities in human body. For clothing application of “Moiré” technique were found in the area of pattern construction of clothing [1]. This is the contour mapping technique, which has been involved positioning a grating close to the surface of figurine and observed its shadow on the figurine through the grating [1, 4].

To measure the size and place position of zoning areas on obtained 2D pictures of digitised moiré fringe pattern the image processing system NIS-Elements AR 40.00.8 has been used.

With regards of the research goal of this paper, to find out method for a design of a suitable seamless underwear shape including specific areas that must map specific areas of the body, a representative type of intimate apparel, an open bottom girdle has been selected. Thus it is necessary to create a suitable construction net. Its parameters should be determined as a dependent variable by computation using the regression equation and corresponding body measurement as an independently variable [5].

The quality of body contouring fit is inextricably linked with the stretch potential of fabric characteristics. Understanding the stretch behavior, visually and mechanically, is an essential part of predicting the pattern profile geometry and the optimum orientation of the pattern placement on the fabric to improve the fit-quality. This is achieved in part by maintaining the stretch extension of fabric within the lower modulus working range. The pattern orientation will affect the garment fit if the stretch fabric extension in the course and wale directions is different [1]. For this research a pattern profile is designed for (course) orientation on the fabric. Pattern grain line is situated in the vertical (wale) orientation.

The starting point of a research of a tight-fit garment pattern development is to use a law whereby the fabric tension, the radius of the part of the body being covered, determine garment pressure.

Therefore a fabric circumference is of a smaller size than the body circumference. The suggested reduction of knitted fabric circumferences by 20%-30% seems to be typical. For this experiment the interlock knitted fabric (54 % PA/46 % EL, 319 g/m²) of a tubular form is been used with the pattern dimensions reduction in weft direction by 26.5% [3].

3. Results and discussion

3.1. Non-contact body measuring method of the shadow moiré

Extensive pre-tests concerning to find out appropriate method to give high quality records of body morphology, and also reliable cross-sectional measurements were carried out. The technique of a shadow moiré has been applied, which enable to map a human body and create picture with a topography effect. The experimental maps of the scanned figurine are given in Figure 2. Those moiré maps were the foundations for creating zoning areas in pattern constructional net of seamless circular garment.

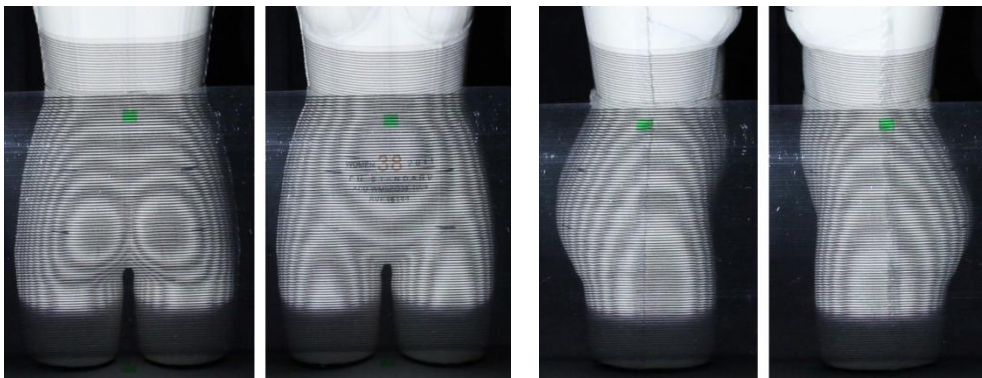


Figure 2. Moiré image of AlvaForm (Back, Front, Right and Left Side View) [3]

For the non-contact shape measurement of the figurine the developed moiré topographic system (Fig. 3) was placed close to the grid, enabling a sharp image of the moiré fringes to be obtained (Fig. 2). For capturing the size of a pelvic part of the figurine, a vertical wooden frame 0.594 m (L) x 0.420 m (W), was designed to mount the plane of grid lines in an exact parallel manner. The plane of the grid lines (1 mm line thickness and pitch size 2 mm) was translated in its own plane in a vertical position. The distance between the figurine surface and the grid (Fig. 3) at a given position $h = 0.08$ m; the distance between the grid and light source $l = 1.8$ m; $d = 0.5$ m represents the distance between the light source and camera.

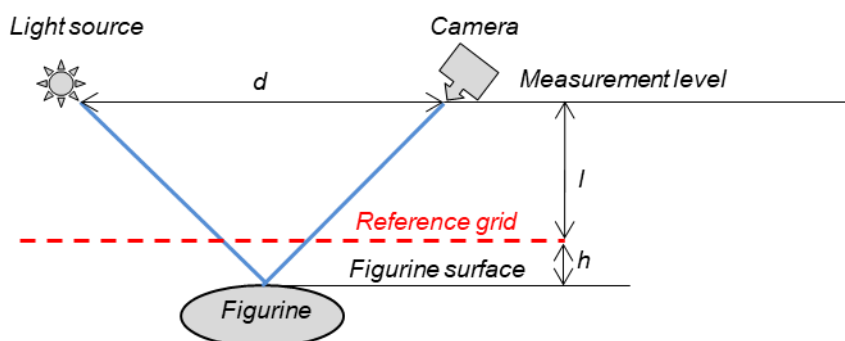


Figure 3. Schematic setup of the moiré system

3.2. Image processing of moiré fringe patterns

The contour map of the moiré fringes generates the required shape information across the pelvic part of the figurine body. A visual interpretation of the fringe pattern is a good means for assessing the shape conformity of a three-dimensional seamless underwear (Fig.4).

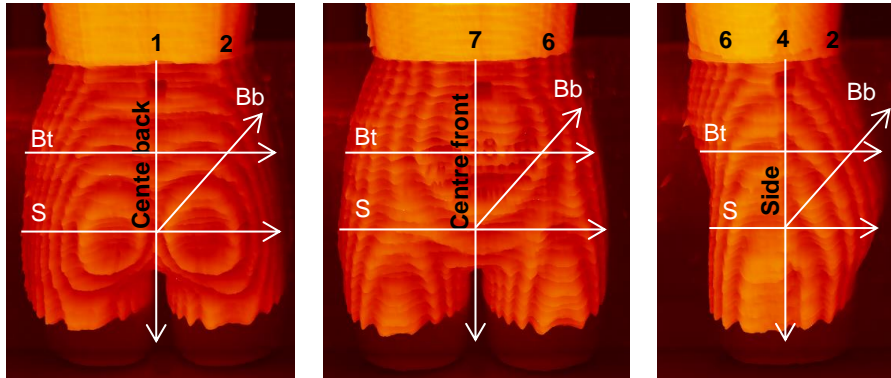


Figure 4. Intensity line profil distribution (back, front and side view)

For the objective measurement of a picture of the pelvic part of the figurine, a digital analysis of different sections of the back, front and side view was performed. The fringe pattern was then measured using tools of NIS-Elements system and a size of topography zones were determined. The shape and size characteristics of fringe zones were derived in the horizontal, vertical and bias direction. The profile of the zones was measured by evaluation of an intensity line profile distribution in Figure 4.

3.3. Evaluation of zoning areas position on the tubular knitted fabric

To evaluate the results of capturing 3D form of body mentioned in paragraph above the size and location of the editing zoning areas has being compared with the corresponding place positions of zoning areas on the tubular knitted fabric which covers the pelvic part of the female figurine. The static width dimension of the tubular has been set according the WAIST = 36 cm. For static length dimensions of the tubular: UPPER HIP DEPTH = 5 cm (From waist to upper hip level); HIP DEPTH = 10 cm (From waist to hip); BODY RISE = 15 cm (From waist to hem edge). The elements of the size 10 mm x 10mm have been marked on the tubular knit (Fig. 5). Then a stretch behaviour of the knit has been tested dressed on a dummy. The dynamic dimensions have been evaluated.

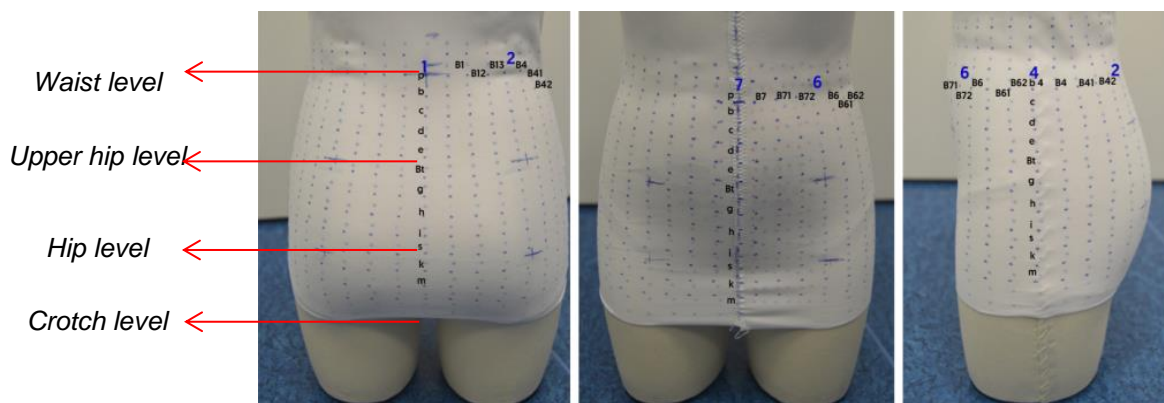


Figure 5. Measured elements on tubular knitted fabric (back, front and side part) [3].

The geometry of the stretch pattern profile has been evaluated through understanding the dynamic form of these elements. Dynamic effect “ Δ ” of the element dimensions was evaluated in horizontal (course) position. A digital calliper was used. The Table 1 lists “ Δ ” value of dynamic effect of the elements of the centre back part of the figurine.

These presented experimental results, highlighted in Table 1, show the similarity of the individual zoning area shape with the comparison with the digitised moiré fringe pattern in Figure 4. The same differences we can see in the intensity line profile of moiré map Figure 2.

Table 1. Dynamic effect of the measured elements

Element	Dynamic effect Δ [mm]				
	1	B1	B12	B13	2
P (Waist level)	$\Delta 1p = 1.00$	$\Delta B1p = 0.60$	$\Delta B12p = 0.68$	$\Delta B13p = 0.80$	$\Delta 2p = 0.80$
b	$\Delta 1b = 1.00$	$\Delta B1b = 1.00$	$\Delta B12b = 0.88$	$\Delta B13b = 0.82$	$\Delta 2b = 0.89$
c	$\Delta 1c = 1.78$	$\Delta B1c = 1.60$	$\Delta B12c = 1.26$	$\Delta B13c = 1.03$	$\Delta 2c = 1.15$
d	$\Delta 1d = 1.97$	$\Delta B1d = 2.05$	$\Delta B12d = 1.82$	$\Delta B13d = 1.72$	$\Delta 2d = 1.98$
e	$\Delta 1e = 2.52$	$\Delta B1e = 2.62$	$\Delta B12e = 2.18$	$\Delta B13e = 2.22$	$\Delta 2e = 2.42$
Bt (Top hip level)	$\Delta 1Bt = 3.09$	$\Delta B1Bt = 3.16$	$\Delta B12Bt = 3.22$	$\Delta B13Bt = 3.62$	$\Delta 2Bt = 4.24$
g	$\Delta 1g = 3.16$	$\Delta B1g = 3.39$	$\Delta B12g = 3.28$	$\Delta B13g = 3.53$	$\Delta 2g = 4.12$
h	$\Delta 1h = 3.15$	$\Delta B1h = 3.45$	$\Delta B12h = 3.37$	$\Delta B13h = 3.53$	$\Delta 2h = 4.47$
i	$\Delta 1i = 3.86$	$\Delta B1i = 4.15$	$\Delta B12i = 3.38$	$\Delta B13i = 3.53$	$\Delta 2i = 4.27$
S (Hip level)	$\Delta 1s = 3.59$	$\Delta B1s = 3.89$	$\Delta B12s = 3.58$	$\Delta B13s = 4.44$	$\Delta 2s = 3.98$
k	$\Delta 1k = 3.59$	$\Delta B1k = 3.89$	$\Delta B12k = 3.58$	$\Delta B13k = 4.30$	$\Delta 2k = 3.90$
l	$\Delta 1l = 3.59$	$\Delta B1l = 3.89$	$\Delta B12l = 3.58$	$\Delta B13l = 4.30$	$\Delta 2l = 3.90$
m	$\Delta 1m = 3.59$	$\Delta B1m = 3.89$	$\Delta B12m = 3.58$	$\Delta B13m = 4.30$	$\Delta B1m = 3.89$

3.4. Seamless girdle construction net development

A close fitting girdle pattern block is constructed to be smaller than the body measurements and to stretch to the body shape. Some adjustments to the horizontal measurements may have made. This should be related to the stretch and relaxation of different fabrics. For this research is used 26.5% hip circumference reduction, which is static width dimension of the tubular knit width.

Experimental results are processed into the construction algorithm for a girdle pattern net design (Fig.6). Individual construction steps are listed in the Table 2.

Table 2. Construction algorithm of seamless girdle pattern net

Step	Definition		Dimension (Formula)
Horizontal lines drafting			
1.	Centre back line	1	
2.	Waist line (w)	$1 \perp w \Rightarrow P1$	
3.	Hip line (h)	$1 \perp h \Rightarrow S1$	$P1S1 = 0.125 \text{ HEIGHT}$
4.	Upper hip line (th)	$1 \perp th \Rightarrow Bt1$	UPPER HIP DEPTH ($0.5 P1S1$)
5.	Hem line (cr)	$1 \perp cr \Rightarrow R1$	$P1R1 = \text{BODY RISE}$
Vertical lines drafting			
6.	Construction net width	Tubular width	$P1P7 = (0.5 \text{ WAIST})$ $P1P7 = 0.5 (73.5\% \text{ HIP})$
7.	Centre front line	$7 \perp w, th, h, cr \Rightarrow P7, Bt7, S7, R7$	
8.	Side line	$4 \perp w \Rightarrow P4, Bt4, S4, R4$	$P1P4 = P4 \quad P7 = 0.5 P1P7$
9.	Back longitudinal line	$2 \perp w \Rightarrow P2, Bt2, S2, R2$	$0.5 P1P4$
10.	Front longitudinal line	$6 \perp w \Rightarrow P6, Bt6, S6, R6$	$0.5 P4P7$

The zoning areas in frame of the pattern constructional net are shown in the (Fig.6). The shape characteristics (in horizontal, vertical and bias direction) are match using the experimental results of image analyses of pelvic part of figurine in Figure 3.

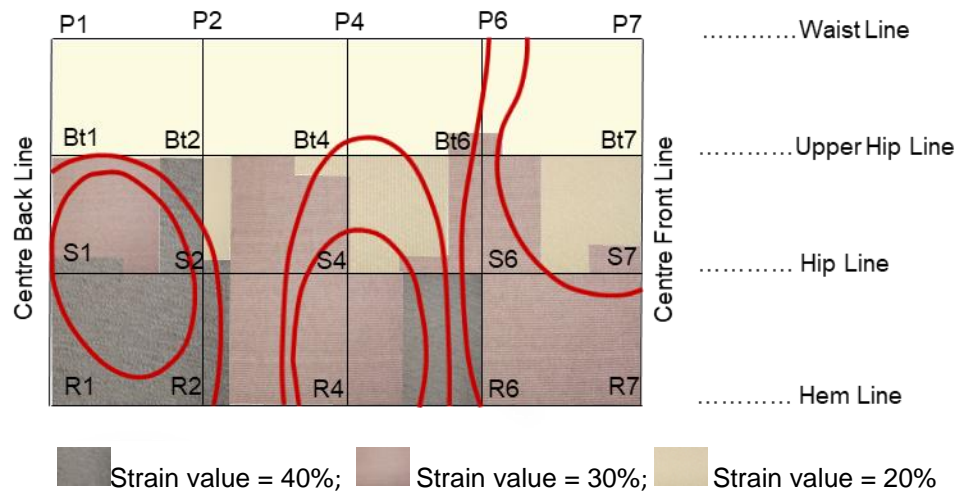


Figure 6. Seamless girdle construction net with zoning areas

4. CONCLUSIONS

Machinery that has the ability to construct garments three dimensionally, such as seamless garment, implies the possibility of creating a product that can conform to the three dimensional shape of the body . Shaping the garment is limited by the number of needles available on which to knit. The zoning areas to map the 3D body shape must commence knitting on specific needles with an exact number of available needles within each zones and between them. There are difficulties associated with knitting tubular stretch garments and its pattern construction definition of a specific zoning area shape. Therefore this presented research is concerned with the development of a construction method for tight-fit seamless garment design that cover a pelvic part of human body.

Extensive experimental pre-tests concerning to find out appropriate method to give high quality records of body morphology, and also reliable cross-sectional measurements were carried out. For experiment of this paper the technique of a shadow moiré has been applied, which is able to map a human body and create picture with a topography effect. The moiré maps were the foundations for creating zoning areas in girdle pattern constructional net of seamless circular garment. Experimental results verify the effectiveness of the moiré topography to determine geometry of a 3D human body surface to achieve information of zoning area size and shape and their location within seamless construction net.

ACKNOWLEDGEMENTS

This work was supported by the Ministry of Industry and Trade of the Czech Republic, Programme Trio - project "Senior Tex - Smart Modular Clothing and Textile Products with Integrated Electronic Microsystems for Improving the Health Care of the Aging Population and Handicapped People", reg. no. FV10111.

References

1. Fan, J., Yu, W., Hunter, L. (2004). *Clothing appearance and fit: Science and technology*. Woodhead Publishing Limited, Cambridge England. ISBN: 1855737450.
2. Hayes, S.G., Venkatraman, P. (2016). *Materials and Technology for Sportswear and Performance Apparel*. CRC Press, Taylor & Francis, Boca Raton. ISBN: 9781138748354.
3. Hôrecká, A. (2017). *Pattern construction of seamless lingerie*. Bakalářská práce. Liberec: TUL.
4. Mandát, D. (2012). *Optické bezkontaktní topografické metody*. UP Olomouc. ISBN 978-80-244-3075-1.
5. Musilová, B. (2012). *Prediction of the corsetry pattern construction parameters*. Ph.D. Thesis. Liberec: TUL.
6. Song, G. (2011). *Improving Comfort in Clothing*. Woodhead Publishing Limited, Cambridge England. ISBN: 9780857090645.
7. Vrba, V. *Střihy prádla: Konstrukce a stupňování*. (1990). Praha: Redakce literatury spotřebního průmyslu. 1990. ISBN: 80-03-00355-5.



THE EFFECT OF RIBS ON COOLING ABILITY OF WETTED SHIRT KNITS AT LOW AIR VELOCITY

Lubos Hes¹, Monika Boguslawska – Baczek²

¹Technical University of Liberec, Faculty of Textiles, Department of textile evaluation, Studentska 2
Czech Republic, lubos.hes@gmail.com

²Katowice School of Technology, Faculty of Architecture, Civil Engineering and Applied Art,
Department of Design, 43 Rolna Street, 40-555 Katowice, Poland

Abstract

In hot-wet countries, a possible way to increase thermophysiological comfort of sweating dressed humans is to wear elastic shirts with larger surface, like rib fabrics. In the paper, cooling ability of 6 various wetted fabrics with surface ribs subject to parallel air flow was investigated. It was found, that at low air velocity, the ribs did not provide the expected enhanced cooling effect. In the last part of the study, the cooling effect of thin wetted woven fabrics was investigated.

Key words:

thermal comfort, rib shirts, wet state, cooling flow

1. Introduction

At high body activity, typical for running sportsman, the body generates up to 1000 W of metabolic power, from which more than 80% should be transferred away from the body in the form of heat. At low outside air temperatures t_A , most of this heat Q [W] is transferred from the human skin of temperature t_{sk} and surface S by simple convection, characterized by the heat transfer coefficient α , as follows:

$$Q_{conv} = \alpha S (t_{sk} - t_{out}) \quad (1)$$

However, when the air temperature exceeds 25° - 30°C, the convection cooling is not sufficient. Then, body starts to generate sweat. In some body parts the partial pressure of the evaporated sweat/water reaches the saturate level p_{sat} . If the partial pressure of the water vapour (wv) in the outside air p_{out} is low enough, then the convection cooling flow generated by water evaporated from the active area $S \cdot w$ (w lies between 0 and 1) is given by the relationship

$$Q_{conv\ evap} = \beta L w S (p_{sat} - p_{out}) \quad (2)$$

Here, L (2 500 000 J/kg) presents the latent heat of evaporation, β is the mass transfer coefficient. The evaporative cooling is extremely efficient, provided the difference of the wv partial pressure is big enough. However, in hot/wet countries the mentioned driving force is too low. The only theoretical way to increase the cooling flow from the body of a moving person is to increase the mass transfer area (surface) of the shirt tightly covering the body of the person exposed to these extreme climatic conditions. The only way to increase this area is the use of relatively large ribs vertically outstanding from the fabric surface.

2. Materials and method

Vertical ribs were prepared by sewing on 8 various single jersey knits made of 100% PES Coolmax and its blends with PES Thermocool, Modacryl and Lycra. Square mass extended from 169 g/m² to 213 g/m². The ribs dimensions were: height 5 and 10 mm, distance between the ribs was 10 and 15 mm.

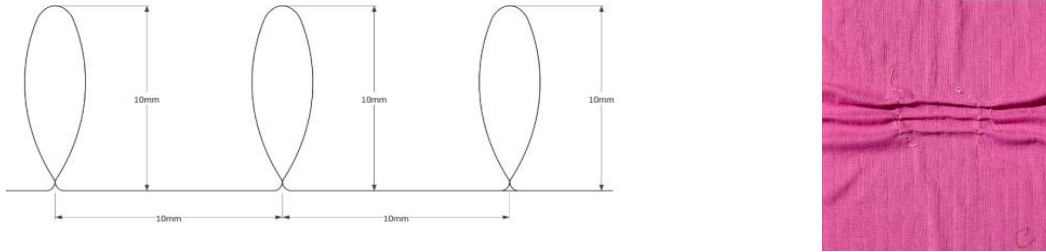


Figure 1. Geometry and appearance of vertical ribs on fabrics

2.1. Calibration of the 100 % cooling flow

The Eq. 2 presents the level of cooling flow, where the parameter β is the convection mass transfer coefficient – see in [2]. This coefficient β can be determined by means of the dimensionless Sherwood Sh and Schmidt Sc numbers defined by the next relations (b is the dimension, ν is the viscosity of the humid air):

$$Sh = \beta b / D_u \quad Sh = 0,664 Re^{1/2} \cdot Sc^{1/3} \text{ (for air flow parallel to a plane)} \quad Re = v \cdot b / \nu \quad (4)$$

Here, the term D_u is the coefficient of water vapour diffusion into air, and for $t = 20^\circ\text{C}$, $p = 0,1013 \text{ MPa}$ reaches the value $1,136 \cdot 10^{-5} \text{ m}^2 \cdot \text{s}$. The term Re is another dimensionless number, reaching here the value of 4970, for the velocity $v = 1 \text{ m/s}$ used in the PERMETEST instrument. Having completed all the calculations, we obtain the level of the Sherwood number:

$$Sh = 0,664 Re^{1/2} \cdot Sc^{1/3} = 39,48 \quad Sc = 0,60 \text{ (for air at room temperature)} \quad (5)$$

As $\beta = Sh D_p / L$ then (for $w = 1$, $S = 1 \text{ m}^2$) from the above theory and Eq. (2) follows

$$Q_{\text{conv evap}} = \beta L [(p_{\text{sat}} - p_{\text{out}})] = L \cdot 0,664 Re^{1/2} \cdot Sc^{1/3} D_p^{2/3} (p_{\text{sat}} - p_{\text{out}}) M_D / RT = L \cdot 1,161 \cdot 10^{-7} (p_{\text{sat}} - p_{\text{out}}) \quad (6)$$

(here the term M_D / RT presents a conversion parameter enabling the use of difference of w_v partial pressure instead of dimensionless w_v concentration drop).

$$Q_{\text{conv evap}} = 2,5 \cdot 10^6 \cdot 1,161 \cdot 10^{-7} \cdot 1250 = 362,8 \text{ W/m}^2 \quad (7)$$

The determined cooling flow presenting in the PERMETEST instrument the 100% cooling effect is quite high. However, in real situations, when a person is wearing a wetted dress under identical climatic conditions, this level of cooling is never achieved, as sweating coefficient w characterising the relative distribution of zones with intensive sweating is mostly lower than 0,4. Thus, the effective cooling flow around 200 W/m^2 already presents a realistic value.

3. Experimental results

Relative water vapour permeability P of the tested samples meaning the relative cooling flow Q_{cool} was determined by means of the Czech commercial PERMETEST instrument, which was in Czech Republic recently certified as satisfying the ISO 11092 standard. During the initial test on dry samples, the samples were (over the semi-permeable membrane) placed on the wetted microporous surface, which

well simulates a human skin with 100% relative cooling flow. The lowest relative cooling effect, 59% exhibited sample No. 4 (modacryl + Thermocool), whereas the higher cooling effect, 72%, offered the sample No. 5 (PES Thermocool). Beside the measurement of cooling flow on dry smooth samples, also the cooling flow from dry rib samples was determined. All these values were determined for the air flowing with the velocity 1m/s along the ribs.

Relative cooling flow [%]

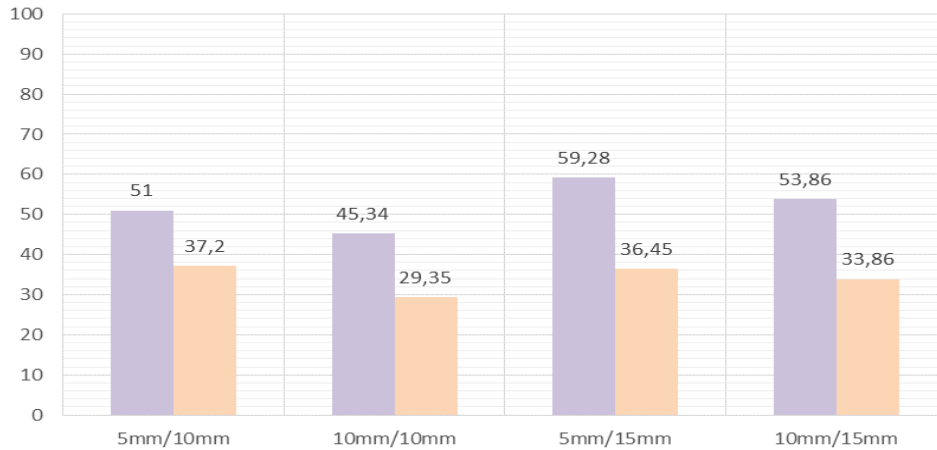


Figure 2. Relative cooling flow / relative water vapour permeability of fabrics in dry state. Higher levels present the results for air flow parallel with the ribs, then in case of the air flow across the ribs. It is evident, that the ribs provide lower wv permeability than smooth fabrics.

Next experiments were focused on the objective of this study: investigation of the influence of the size of the mass (heat) transfer area, executed by forming the surface ribs on the studied fabrics, on the cooling effect given by evaporation of moisture from these rib fabrics enhanced by convection heat transfer from the fabrics.

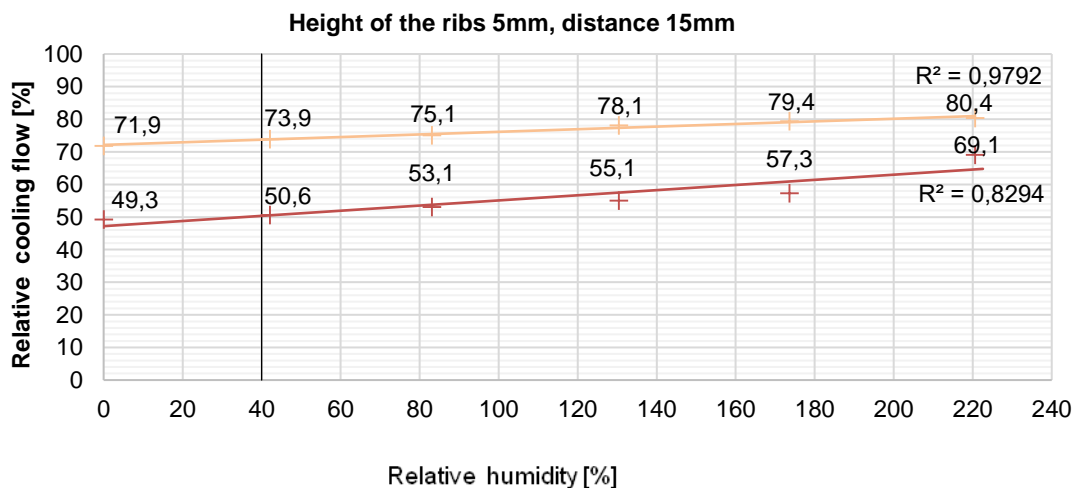
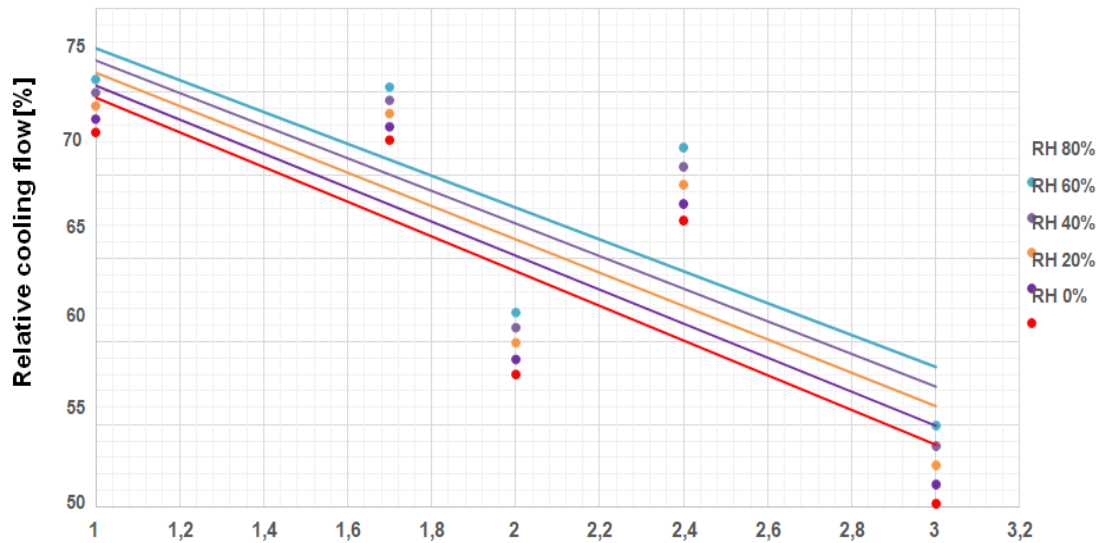


Figure 3. The effect of the sample relative humidity on the relative cooling flow released from the sample No. 5 (PES Thermocool). The higher levels were determined for the air flow parallel with the ribs.



Relative increase of the mass/heat transfer area due to the creation of longitudinal ribs

Figure 4. The effect of fabric relative humidity and heat transfer area on the relative cooling flow of the most efficient fabric No. 5 from the Themocool fibres, when the air passes along the ribs (better case).

From the Fig. 4 follows, that against expectation, the rib fabrics under the applied experimental conditions exhibit lower heat and mass transfer of water vapour than smooth fabrics. Explanation of this observation may depend in the possibility, that at low air velocity, the thermal boundary layer is quite thick, runs above the ribs and does not create thermal contact with the bottom area between the ribs. Second explanation may take into consideration, that cooling effect generated on the upper parts of the ribs is not properly conducted toward the basic level of the fabric, which is in direct contact with the simulated skin.

The amendment of the limited heat conduction along the height of ribs may depend in the use special fibres (carbon fibres) with very high thermal conductivity in the design of the ribs. However, carbon fibres are stiff and do not conduct moisture as well as the COOLMAX fibres used in this research.

As long as the smooth textile surfaces provide the highest cooling effect, it will be important to investigate the effect of the fabric structure and composition. This research should respect the same experimental conditions as in the above study: the wetted fabrics will be placed (over the semi-permeable porous membrane) on the wetted surface which simulates sweating human skin.

3.1. Cooling effect of selected smooth fabrics in wet state

5 thin woven fabrics in a plain structure made of cotton (square mass 163 and 95 g/m²), Lyocel viscose (square mass 175 and 96 g/m²), PES (square mass 92 g/m²) and PAD nanofibre layer (square mass 5,3 g/m²) were stepwise wetted and relative cooling flow generated by evaporation water from their surface in the PERMETEST instrument was registered. The 100% relative cooling flow was caused by evaporation of water from the porous surface which simulates human skin.

The objective of this study was the determination of a fabric with the highest cooling effect in wet state, which should be used for design of a comfortable sport dress. As the reference value of the relative moisture U of the fabric was $U = 40\%$, which presents the moisture level, when the increased friction between a skin and a fabric starts to cause sensorial discomfort.

The highest relative cooling flow, 90% was observed when testing the Lyocel fabric with the square mass 176 g/m². The lowest cooling flow, 63% was registered for the cotton fabric with the square mass 163 g/m². Other fabrics provided the cooling flow in the range of 72 to 79%.

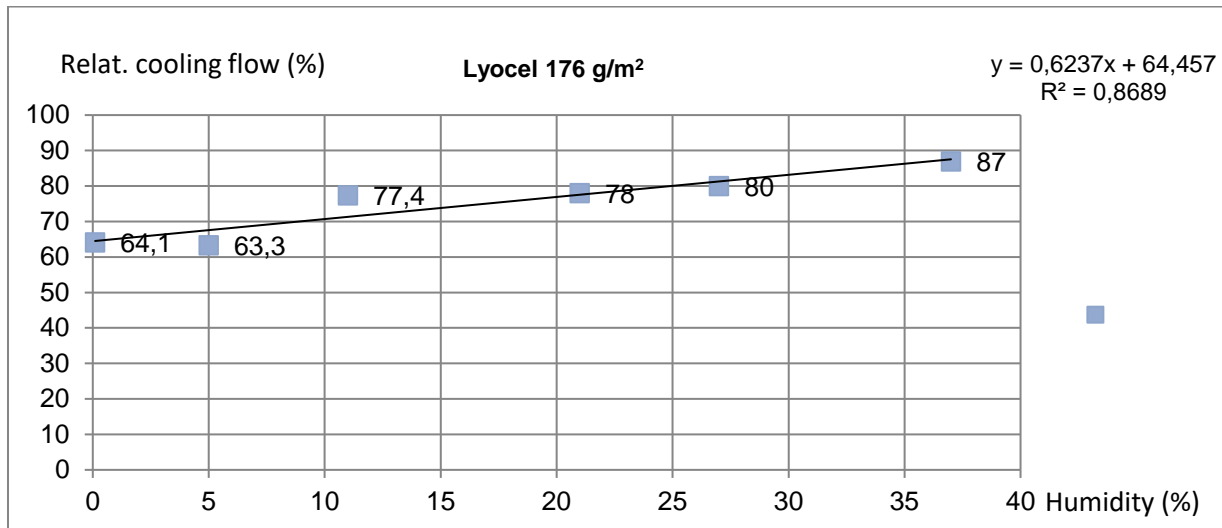


Figure 5. The effect of the fabric relative humidity on the relative cooling flow of the most efficient smooth Lyocel fabric

4. CONCLUSIONS

In the paper, cooling ability of 6 various knitted fabrics with 4 different surface ribs subject to air flow was investigated. The stepwise wetted samples were inserted into the PERMETEST Skin model with ribs oriented parallelly and perpendicularly to the air flow and the relative cooling flow was recorded. This relative heat flow was then converted (calibrated) into the real cooling flow. It was found, that at low air velocity, the ribs did not provide the expected enhanced cooling effect. In the last part of the study, the cooling effect of thin wetted woven fabrics was investigated. The highest level was observed for the relatively thick Lyocel woven fabric.

References

1. Hes, L., Dolezal, I.: *A New Portable Computer-Controlled Skin Model for Fast Determination of Water Vapour and Thermal Resistance of Fabrics*. Asian Textile Conf. (ATC 7), New Delhi 2003.
2. Bogusławska – Bączek M., Hes L.: *The Effective Water Vapour Permeability of Wet Wool Fabric and Blended Fabrics*, *Fibres & Textiles in Eastern Europe*, 2013, Vol 1., 67-17
3. Slancova M.: *Knits with enhanced cooling (in Czech)*. MSc Thesis, TU Liberec 2018
4. Karakoc Y.: *Cooling efficiency of selected fabrics*. Res. Report, TU Liberec 2017.



APPLYING THE ARTIFICIAL NEURAL NETWORK TO PREDICT THE THERMAL PROPERTIES OF KNITTED FABRICS

Sinem Güneşoğlu ¹, Binnaz Kaplangiray ²

¹Gaziantep University, Textile Engineering Department, Gaziantep, Turkey

²Uludag University, Textile Engineering Department, Gaziantep, Turkey

sgunesoglu@uludag.edu.tr

Abstract:

Fabric thermal properties have been of great interest and importance for textile researchers, since they are among the major characteristics that determine wearing comfort. In this study, thermal conductivity and thermal contact properties of a large number of knitted fabrics were measured instrumentally and a learning group was proposed to train the artificial neural network (ANN) algorithm and then prediction was achieved with a strong regression coefficient. Therefore it is concluded that it was possible to predict thermal properties of knitted fabrics by using basic fabric properties as input.

Key words:

Thermal conductivity, warm-cool feeling, ANN

1. Introduction

Traditionally, most measurements of fabric thermal properties were conducted in a state of equilibrium (steady-state), analyzing such easily measured properties as thermal conductivity. Thermal conductivity is a familiar term applied to materials that conduct heat and it is defined as the heat flux divided by the temperature gradient where heat is transferred by conduction. However, the steady-state measurements cannot solely explain the heat-related subjective sensations that determine human comfort, because this approach does not reflect the real wearing situation, since the human body interacts dynamically with clothing. Sudden mechanical contact of textile fabric with human skin causes feeling of warmth or coolness due to the heat flow from human body to the fabric that is at a lower temperature than the skin surface. This dynamic- or transient-state thermal contact property, which is so called thermal absorptivity, is included in the overall assessment of the comfort of textile fabrics. Since both steady and dynamic- state measurements strongly affect the choice of people when buying the clothes or garments, there is an interest in predicting thermal properties of textile fabrics before they are submitted to customers and determining the relations between thermal properties and fabric structural properties [1, 2]. The artificial neural network (ANN) may be an efficient tool for predicting the thermal properties of knitted fabrics.

An ANN is an information processing system that roughly replicates the behavior of a human brain by emulating the operations and connectivity of biological neurons [3]. It performs a human-like reasoning, learns the attitude and stores the relationship of the processes on the basis of a representative data set that already exists. In general, the neural networks do not need much of a detailed description or formulation of the underlying process and thus appeal to practicing engineers who tend to mostly rely on their own data [4 – 7]. Recently, neural networks have been successfully applied to process modelling and control of textile surfaces [8-11].

A typical ANN has feed forward architecture and consists of three or more layers of neurons: one input layer, one output layer and one or more hidden layers (Figure 1). Each of the layers has a set of connections, with a corresponding scalar weight, between itself and each neuron of preceding layer. When the weight of a particular neuron is updated, it is said that neuron is learning and ANN is training. In a feed forward back-propagation ANN, the input data (x_i) is passed to the neurons in input layer as signal. The data is weighted in hidden layers (y_i) by associated weights in each interconnection through non-linear transfer function. In addition, a bias can also be used, which is another parameter that is summed with the neurons weighted inputs. The sum of weighted inputs is converted to outputs (z_i) through activation function (Net_j). The outputs can be defined as:

$$z = f(Net_j) \quad (1)$$

where

$$Net_j = \sum w_i x_i + b \quad (2)$$

and where x_i and w_i are the input data and weightings of neuron. b is the bias, $f(\dots)$ is the activation function.

The most common used activation functions in ANN architectures are linear (*purelin*) and sigmoid (*logsig*) transfer functions. A transfer function determines the relationship between inputs and outputs of a neuron and a network. Selection of transfer function for layers is an important parameter. The best structure of transfer functions is evaluated on the basis of mean square error (MSE) of the training data set. *logsig* function produces outputs in the range of 0 to 1 and it can be defined as:

$$f(Net_j) = \frac{1}{1+e^{-Net_j}} \quad (3)$$

where *purelin* function produces outputs in the range of $-\infty$ and $+\infty$ and can be defined as:

$$(Net_j) = Net_j \quad (4)$$

In this study, the optimum configuration is achieved by using *logsig* transfer function in output and hidden layers.

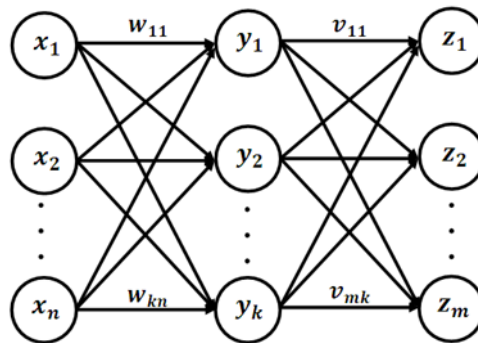


Figure 1. ANN architecture

This study aims to use the ANN with a feed-forward back-propagation learning algorithm for the prediction of thermal conductivity (steady-state) and thermal absorptivity (dynamic-state) properties of knitted fabrics. The results were found to be compatible for prediction of thermal properties of the knitted fabrics by using basic fabric properties as input.

2. Experimental

2.1. Materials

Knitted fabric samples with various constructions in ready to apparel conditions were supplied by various suppliers. The constructional details of the samples are given in Table 1.

Table 1. Some details of the samples

<i>Sample</i>	<i>Weave type</i>	<i>Yarn type and count</i>	<i>Weight (gr/m²)</i>	<i>Thickness (mm)</i>
RL1	RL supreme	%95 Polyamide (78/23 dtex), %5 elastane (33 dtex)	198.4	0.53
RL2	RL supreme	%95 Polyamide (78/23 dtex), %5 elastane (33 dtex)	205.5	0.54
RL3	RL supreme	%95 Polyamide (78/68 dtex), %5 elastane (33 dtex)	210.2	0.47
RL4	RL supreme	%95 Polyamide (78/68 dtex), %5 elastane (33 dtex)	226.6	0.47
RL5	RL supreme	%95 Polyester (100/36 Denier), %5 elastane (40 Denier)	101.2	0.6
RL6	RL supreme	%100 Polyamide (150/136 Denier)	169	0.43
RL7	RL supreme	%95 Polyester (100/136 Denier), %5 elastane (40 Denier)	189.6	0.83
RL8	RL supreme	%100 Polyamide (70/68/2 Denier)	212	0.45
RL9	RL supreme	%30 Polyamide (70/46 Denier) %70 Cotton (Ne 40/1)	185	0.69
RL10	RL supreme	%100 Polyester (70/46/1 Denier)	99	0.56
RL11	RL supreme	%86 Polyamide (110 dtex), %14 elastane (44 dtex)	240	0.72
RL12	RL supreme	%93 Polyamide (156 dtex) %7 elastane (22dtex)	220	0.48
RL13	RL supreme	%84 Polyamide (78 dtex), %16 elastane (44 dtex)	160	0.47
RL14	RL supreme	%100 Cotton (Ne 30/1)	200	0.66
RL15	RL supreme	%95 Cotton (Ne 30/1), %5 elastane (20 Denier)	193.5	0.77
RL16	RL supreme	%95 Viscose (Ne 20/1), %5 elastane (20 Denier)	263.7	0.69
RR1	RR ribana	%95 Polyamide (150/140 Denier), %5 elastane (20 Denier)	269.7	0.76
RR2	RR ribana	%100 Polyester (90/36 Denier)	95.6	0.57
RR3	RR ribana	%95 Cotton (Ne 30/1) %5 elastane (20 Denier)	228.6	1.14
RR4	RR ribana	%100 Cotton (Ne 24/1)	284	0.97
RR5	RR ribana	%100 Viscose (Ne 28/1)	220	0.88
RR6	RR interlock	%100 Polyamide (78/23 dtex)	175.6	0.99
RR7	RR interlock	%100 PA (78/23 dtex)	186.7	1.01
RR8	RR interlock	%50 Polyamide (78/23 dtex), %50 Cotton (Ne 30/1)	186.3	1.14
RR9	RR interlock	%100 Polyamide (78/23 dtex)	173.9	0.87
RR10	RR interlock	%100 Polyester (75/34 Denier)	124.2	0.41
RR11	RR interlock	%96 Polyester (70/46 Denier), %4 elastane (22 dtex)	150	0.81
RR12	RR interlock	%55 Polyamide (70/46 Denier), %45 Cotton (Ne 30/1)	200	1.03
RR13	RR interlock	%100 Cotton (Ne 30/1)	235.9	1.08
RR14	RR interlock	%53 Viscose (120 denier) %47 Polyester (100 Denier)	253	0.71
RR15	RR interlock	%100 Polyester (180 Denier)	324.9	1.0
RR16	RR interlock	%50 Polyester (190 Denier), %50 Viscose (Ne28/1)	217.5	0.98
AS1	RL 2-yarn fleece	%100 Cotton (Ne 20/1) (out), %100 Cotton (Ne 10/1) (in)	302.7	1.25
AS2	RL 2-yarn fleece	%100 Polyester (Ne 20/1) (out), %100 Polyester (Ne 10/1) (in)	313	1.15

AS1R	RL 2-yarn fleece	%100 Cotton (Ne 20/1) (out), %100 Cotton (Ne 10/1) (in – raised)	273.8	1.76
AS2R	RL 2-yarn fleece	%100 Polyester (Ne 20/1) (out), %100 Polyester (Ne 10/1) (in - raised)	295.5	1.37

2.2. Methods

Thermal conductivity and thermal absorptivity of the samples were measured by the ALAMBETA instrument as described before [1]. All the measurements were completed in an uncontrolled laboratory environment of about 24°C and 55% R.H. and repeated for three times. The mean of three measurements was taken as data. The measuring head temperature of the ALAMBETA was approximately 32°C, and the contact pressure was 200 Pa in all cases to simulate the pressure of a finger on a fabric [1].

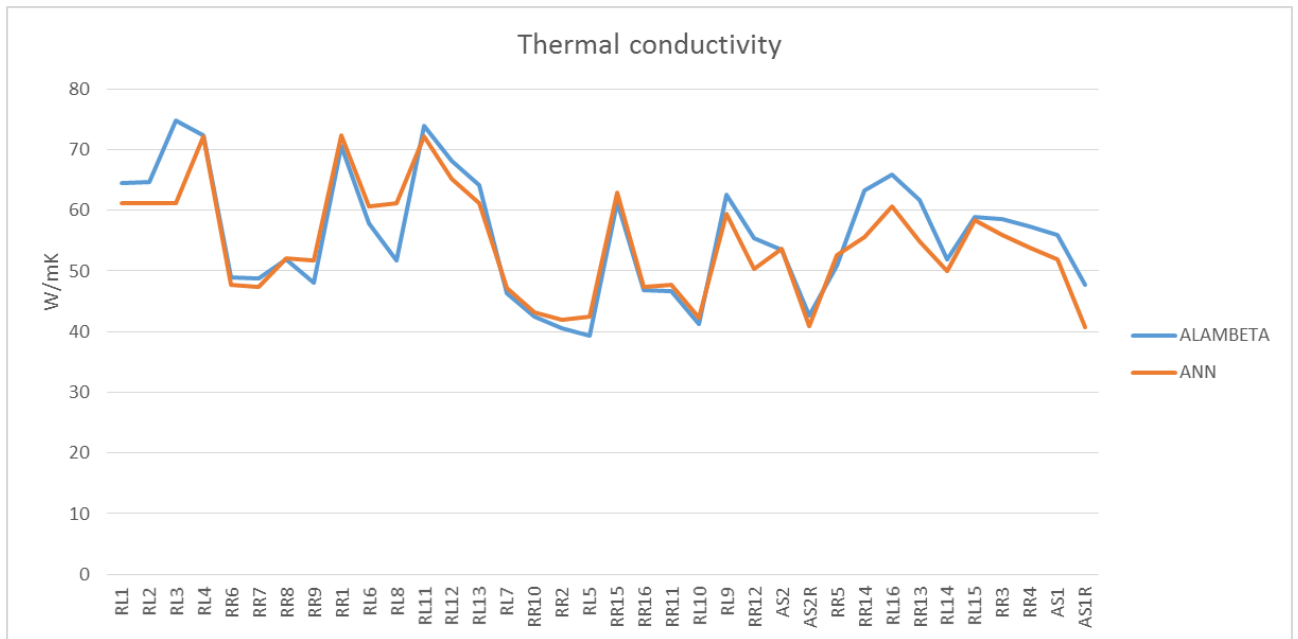
A three-layered (one input, one hidden and one output layer) feed-forward and back-propagation algorithm was chosen for the ANN model. For the development of the ANN model, CORTEX 3.0 was used. The output data for the ANN were thermal conductivity and thermal absorptivity and the input data were selected as fabric weight, fabric thickness, fabric density (determined as fabric mass divided by fabric thickness), fiber density and fiber conductivity as given in [12] and package factor (determined as fabric density divided by fiber density). For the samples which have more than one fiber type, fiber density and fiber conductivity values were calculated by using Equation (5):

$$\text{Property}_{A/B} = (\text{Volume ratio}_A) \times (\text{Property}_A) + (\text{Volume ratio}_B) \times (\text{Property}_B) \quad (5)$$

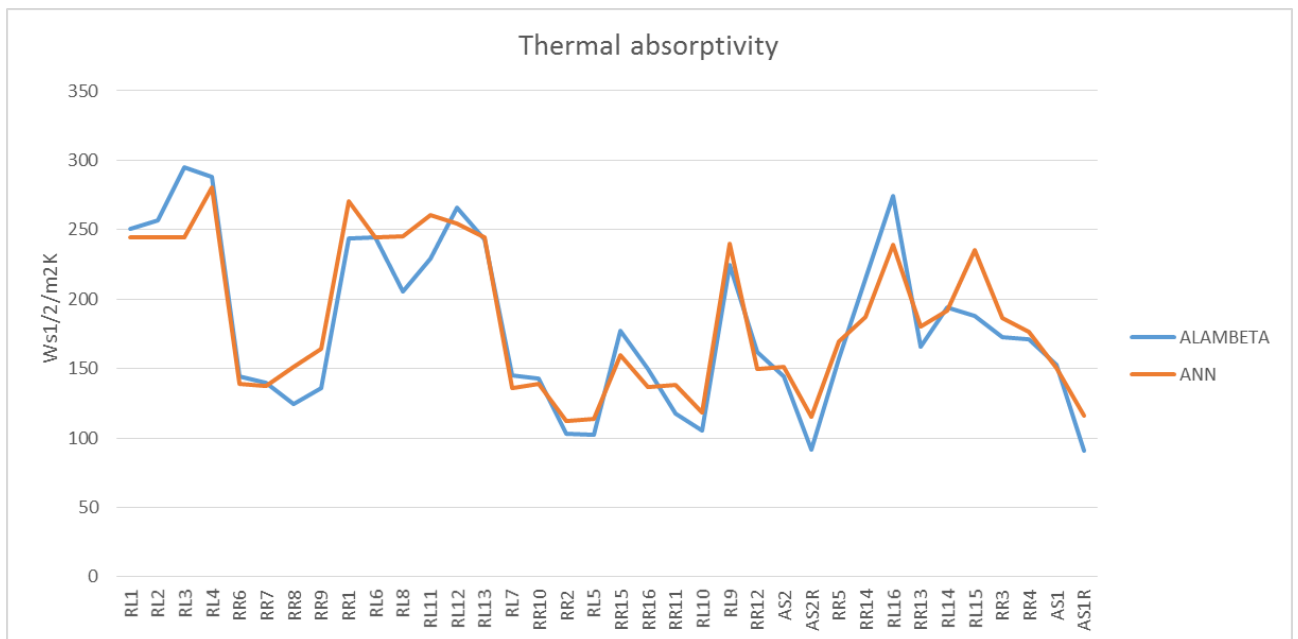
The output data were divided into training and test sets randomly (accomplished by the modelling software) The 16 data was used for training and the rest was used for the test set. In the course of training, which was based on Levenberg– Marquardt method [13], the number of neurons in the layers, training accuracy and number of iterations were determined by using trial and error method; thus the optimum number of neurons obtained in the layers were determined as 6. Mean square error (MSE) value was calculated around 0.01 for 210000 epochs. All data were normalized to be between 0 – 1 using Equation (3) in order to increase accuracy of both models and prevent any parameter from dominating the output. The output data were later de-normalized after the actual application in the models. Finally, the ANN model was applied to all sample inputs.

3. Results and Discussions

The data obtained from both the ALAMBETA and the ANN were given in Figure 2. It is seen that the ANN model gave reliable results in predicting the thermal properties of knitted fabrics. The regression coefficient between ALAMBETA and ANN data were 0,916 and 0,937 for thermal conductivity and thermal absorptivity, respectively.



(a)



(b)

Figure 2. The ALAMBETA and the ANN data for a) thermal conductivity b) thermal absorptivity of the samples

4. CONCLUSIONS

In this paper, thermal conductivity and thermal absorptivity of various knitted fabrics were first measured instrumentally by the ALAMBETA and via using the results as output data, an ANN model was applied to predict the thermal parameters of those fabrics. In this case, basic properties which are easily measured and / or found in the literature were used as input. The study showed that the ANN model would be used to predict thermal properties of knitted fabrics by using basic fabric properties without an instrumental measurement.

References

1. Gunesoglu S., Meric B., Gunesoglu C., (2005), *Thermal contact properties of 2-yarn fleece knitted fabrics*, *Fibers & Textiles in Eastern Europe*, 13 (2), 46 – 50.
2. Güneşoğlu, S., (2005), *An Investigation of Comfort Properties of Sportwear Clothings*, PhD Thesis, Uludag University.
3. Golden, R.M., (1996), *Mathematical Methods for Neural Network Analysis and Design*, MIT Press, USA.
4. Hand, J. W., (2008), *Modelling the Interaction of Electromagnetic Fields (10 Mhz–10 Ghz) With The Human Body: Methods And Applications*, *Physics in Medicine and Biology*. 53, 243–286.
5. Mujtaba, I. M., Aziz, N. and Hussain, M., (2006), *A. Neural Network Based Modelling and Control in Batch Reactor*, *Chemical Engineering Research and Design*. 84, 635–644.
6. Khataee, A. R., Dehghan, G., Zarei, M., Ebadi, E. and Pourhassan, M., (2011), *Neural Network Modeling Of Bio Treatment Of Triphenylmethane Dye Solution By A Green Macro Algae*, *Chemical Engineering Research and Design*. 89, 172–178.
7. Atasoy, I., Yuceer, M., Ulker, E. O. and Berber, R., (2007), *Neural Network Based Control of the Acrylonitrile Polymerization Process*. *Chemical Engineering & Technology*, 30, 1525–1531.
8. Jeong S.H., Kim, J.H., Hong, C.J., (2001), *Selecting optimal interlinings with a neural network*, *Textile Research Journal*, 70 (11), 1005 – 1010.
9. Parki K.C., Kang, T.J., (1997), *Objective Rating of Seam Pucker Using Neural Networks*, *Textile Research Journal*, 67 (7), 494 – 502.
10. Abd Jelil, R., Zeng, X., Koehl, L., Perwuelz, A., (2013), *Modeling Plasma Surface Modification of Textile Fabrics Using Artificial Neural Networks*, *Engineering Applications of Artificial Intelligence*, 26 (8), 1854 – 1864.
11. Matusiak, M., (2015), *Application of Artificial Neural Networks to Predict the Air Permeability of Woven Fabrics*, *Fibers & Textiles in Eastern Europe*, 23 (1), 41-48.
12. Warner, S.B., (1995), *Fiber Science*. Prentice Hall, NJ, USA.
13. Iqbal, J., Iqbal, A., Arif, M., (2015), *Levenberg–Marquardt method for solving systems of absolute value equations*, *Journal of Computational and Applied Mathematics*, 282, 134-138.

PROBLEMATICS OF LARGE-SIZE BATCH WINDING OF TECHNICAL TEXTILES

Josef Žák

VÚTS, a.s. Liberec, Svárovská 619, Liberec, josef.zak@vuts.cz, tel: 485 302 219

Abstract:

When weaving technical textiles we often encounter problems that are not known from weaving ordinary textiles. This is due to the significantly different mechanical properties of the fibers forming the fabrics. At the same time, productivity pressures cause additional complications, especially in the marginal areas of weaving, whether warping or just winding the resulting product. As the resulting batch becomes larger, it becomes corrugated and consequently damages the fabric. This problem has increased in our case when weaving 3D fabric. We were therefore faced with the task of solving this problem.

In the solution, we used the classical mechanics of the continuum. Due to the complexity of the problem, we had to accept some simplifications, such as the assumption of radial isotropy of the wound fabric. It turned out that the resulting relationships are quite complicated, but with the use of computing, the problem is nevertheless solvable.

The result of our work is the design of the wrapping program depending on the fabric being fabricated. We have also shown that there are certain boundaries that cannot be exceeded when packing.

Key words:

Technical textiles, batch winding

1. Introduction

Currently, two different fabric winding systems are commonly used. The first, historically old and essentially original, consists in winding the fabric on a central tube, which is traditionally placed, but not necessarily, directly on the weaving loom. The tube is driven by a single drive that delivers the required tensile force in the withdrawn raw woven. In principle, it is obvious that this force acting on the circumference is transferred from the tube to the towed fabric by already packed woven. This system, therefore, does not allow the creation of large batches, as shown by the experience of generations of weavers.

The second, more modern system consists in separating the fabric from its weaving and removing the woven from the fabric. The tube on which the woven is wound reposes on two rollers that are driven separately. Their circumferential velocities are controlled to produce the desired tension in the cloth withdrawn from the loom. It is clear that the tension in the withdrawn fabric acts on the circumference of the wound fabric and therefore does not affect the already packed cloth. This type of winders can be further divided into two types, namely gravity and controlled pressure. In the first case, the contact force between the valleys and the goods is given by the weight of the packing, in the latter case the compressive force is generated by the auxiliary device and can be controlled.

Following figure gives a schema of such large-size batch winder:

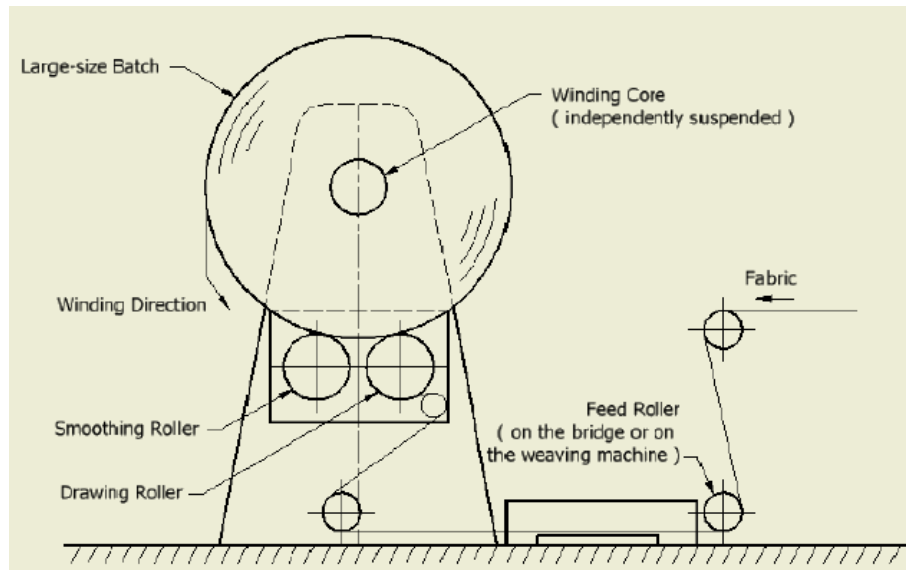


Figure 1. Schema of large-size batch winder; courtesy of CEDIMA

2. Batch geometry description

The first problem encountered in describing a large-size batch is the description of its geometry. The batch can be considered a spiral.

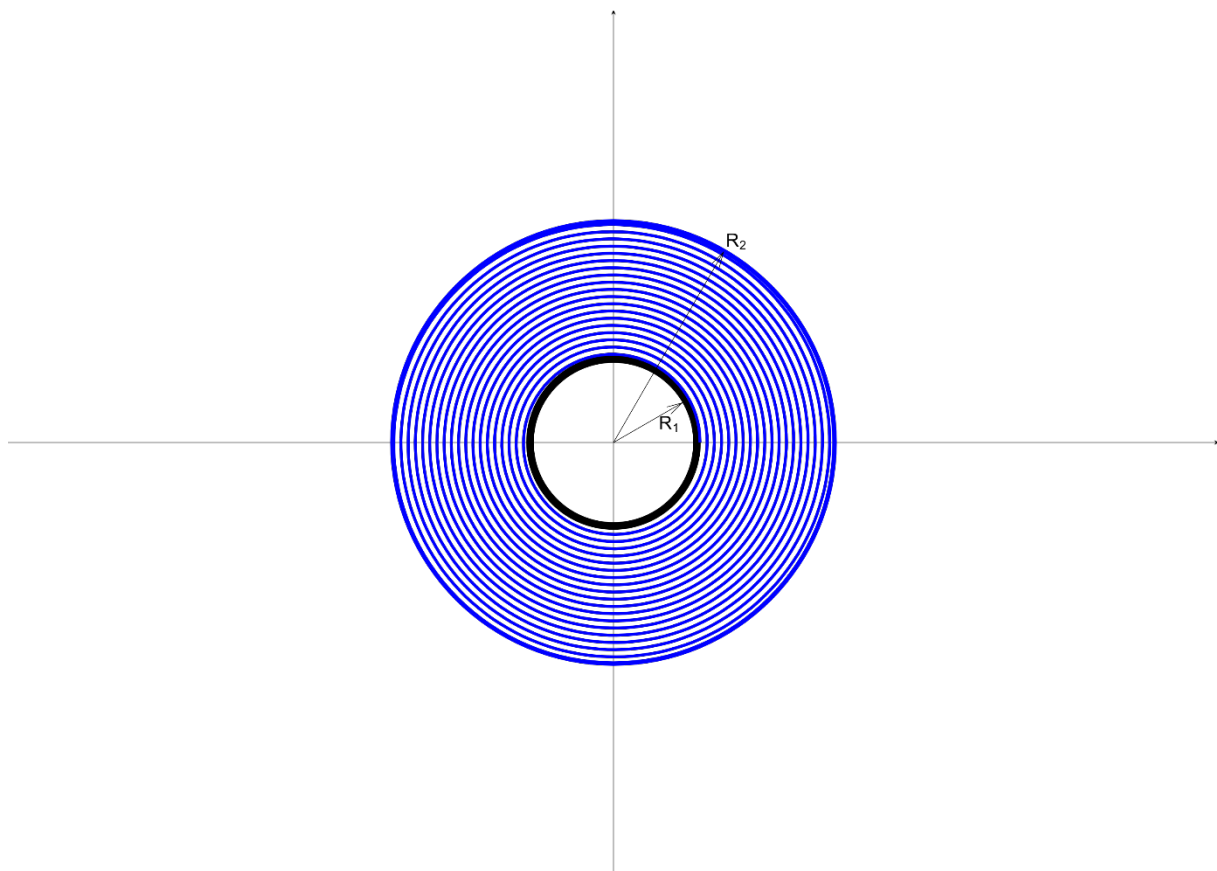


Figure 2. Schema of batch winding

Its length, depending on the outer radius, is expressed as follows:

$$L = \frac{R_2 \cdot \sqrt{t^2 + 4 \cdot \pi^2 \cdot R_2^2}}{2 \cdot t} - \frac{R_1 \cdot \sqrt{t^2 + 4 \cdot \pi^2 \cdot R_1^2}}{2 \cdot t} + \frac{t \cdot \operatorname{arcsinh} h\left(\frac{2 \cdot \pi \cdot R_2}{t}\right)}{4 \cdot \pi} - \frac{t \cdot \operatorname{arcsinh} h\left(\frac{2 \cdot \pi \cdot R_1}{t}\right)}{4 \cdot \pi}$$

Obviously, the relationship in this form is inappropriate for further calculations. An approximate relationship is therefore needed:

$$l = \frac{R_1 + R_2}{2} \cdot 2 \cdot \pi \cdot \frac{R_2 - R_1}{t} = \frac{\pi \cdot (R_2^2 - R_1^2)}{t}$$

Check for $t \rightarrow 0$:

$$\lim_{t \rightarrow 0} (L - l) = \lim_{t \rightarrow 0} \left(\frac{R_2 \cdot \sqrt{t^2 + 4 \cdot \pi^2 \cdot R_2^2}}{2 \cdot t} - \frac{R_1 \cdot \sqrt{t^2 + 4 \cdot \pi^2 \cdot R_1^2}}{2 \cdot t} + \frac{\operatorname{arcsinh}\left(\frac{2 \cdot \pi \cdot R_2}{t}\right) \cdot t}{4 \cdot \pi} - \frac{\operatorname{arcsinh}\left(\frac{2 \cdot \pi \cdot R_1}{t}\right) \cdot t}{4 \cdot \pi} - \frac{\pi \cdot R_2^2 - \pi \cdot R_1^2}{t} \right) = 0$$

Thus, if we know t and l :

$$R_2 = \sqrt{\frac{t \cdot l}{\pi} + R_1^2}$$

If we know R_2 and l :

$$t = \pi \cdot \frac{R_2^2 - R_1^2}{l}$$

It follows from previous relationships that we have a relationship with three variables t , l and R_2 , which are interdependent. To describe the velocity geometry, one of these variables should be defined as independent and the other two parameters. For other purposes and also with respect to the purpose of our work, the variable length of the packing l will be independent, the layer thickness t will be the parameter and the radius of the packing R_2 will be solved from the relations. Otherwise, we would have to continuously measure both the length of the woven fabric and the diameter (the radius) of the wrapper. A key step in the next step will therefore be to determine the thickness t .

3. Fabric thickness estimation

3.1. Plain weave fabrics

To estimate the thickness t , we use the formulation following [3]. Its assumptions are:

- double-sinusoidal cross-section shape of the thread
- 100% fabric filling (close to limit values)

The bulk filling of the cloth in plain weave and with high values of sett then moves around the value $\kappa = \frac{2}{\pi}$. By means of volume filling it is possible to estimate the thickness t in mm of such fabrics by means of their parameters:

$$t = \frac{\gamma}{\rho} \cdot \frac{\pi}{2}$$

Estimating the thickness of a cloth in a non-plain weave binding (e.g. twill or satin) can be done in an analogous manner, but the relevant models have not yet been prepared. Similarly, no analysis has been performed so far and no model of leno binding has been developed. For any measurement as the basis for optimizing the winding of such fabrics, it would be necessary to measure the actual wrapping.

3.2. 3D fabrics

The main motivation of our work is to master 3D fabrics, more accurately the so-called distance fabric. It consists of two fabrics, for example in plain weave, interconnected by a set of threads:

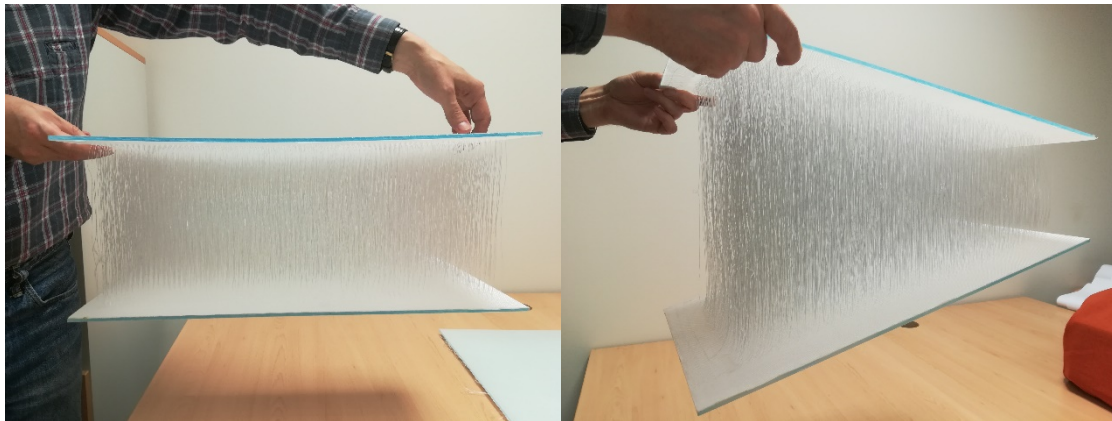


Figure 3. Examples of 3D fabrics

The thickness of the binding yarns layer must also be included in the calculation of the thickness of the 3D fabric. Their number per unit area is given by their warp density and their pitch in the direction of warp. Their weight (weight per unit area in g / m²) is given by:

$$\gamma_3 = n \cdot l_3 \cdot \frac{j_3}{10^6} = \frac{1}{100} \cdot d_3 \cdot j_3 \cdot \frac{l_3}{r}$$

Thickness of layer of binding yarns then is:

$$t_3 = \frac{\gamma_3}{\rho_3} \cdot \frac{1}{\kappa_3}$$

The fill value κ_3 should be determined experimentally, depending, for example, on the twist of the yarns or on the quality of the loop forming. The total weight of the 3D fabric is, of course, the sum of the weights of the surface fabrics and the weight of the staple yarns. The overall thickness is also determined in a similar manner.

4. Theory

The following chapter presents a procedure for calculating the mechanical behavior of the batch.

4.1. Basic concepts

In our work, we came out of the idea of rotational symmetry of the batch. It is then possible to proceed as follows:

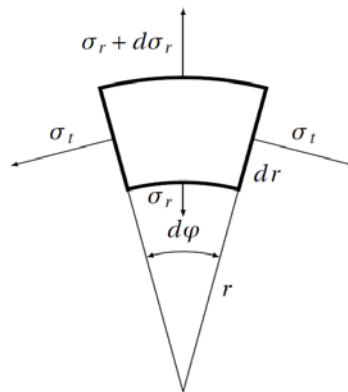


Figure 4. Balance of forces acting on an element

Equilibrium of forces in the radial direction yields as follows:

$$\frac{d}{dr}(r \cdot \sigma_r) - \sigma_t = 0 \quad .$$

Assuming radial isotropy of the batch we get following constitutional laws:

$$\begin{aligned} \sigma_r &= K \cdot (\varepsilon_r + \mu \cdot \varepsilon_t) \\ \sigma_t &= K \cdot (\varepsilon_t + \mu \cdot \varepsilon_r) + f(r) \quad ' \end{aligned}$$

where K is stiffness and μ another Lamé's coefficient (it can be proved that they are meaningless in the case of radial isotropy and assuming state of planar deformations). Then $f(r)$ is the force per width reported on unity of radius.

Using deformation restrictions we obtain for the expression of deformation:

$$\begin{aligned} \varepsilon_t &= \frac{u}{r} \\ \varepsilon_r &= \frac{du}{dr} \end{aligned}$$

By expressing constitutional laws and putting them into the equation of radial equilibrium we get fundamental equation:

$$\frac{d}{dr} \left(\frac{1}{r} \cdot \frac{d}{dr} (r \cdot u) \right) = f(r) \quad .$$

Its solution is easy by double integrating its right side if the $f(r)$ is “reasonably” simple. During this integration we will get 2 unknown constants of integration. In order to obtain their values we must provide two boundary conditions. The first one is obvious:

$$u(R_1) = 0 \quad ,$$

which yields the non-deformability of the central tube.

The second one comes from the fact that the radial stress (or radial pressure) vanishes on the outer radius:

$$\sigma_r(R_2) = 0 \quad .$$

4.2. Practical use of mathematical model

For sake of simplicity of this presentation we will assume the polynomial form of the right side $f(r)$. Even then the resulting formulae are in form of a complex rational function. Figure 3 represents the behavior of the tangential stress in the batch for two standard shapes of tension (in function of r) as used in praxis:

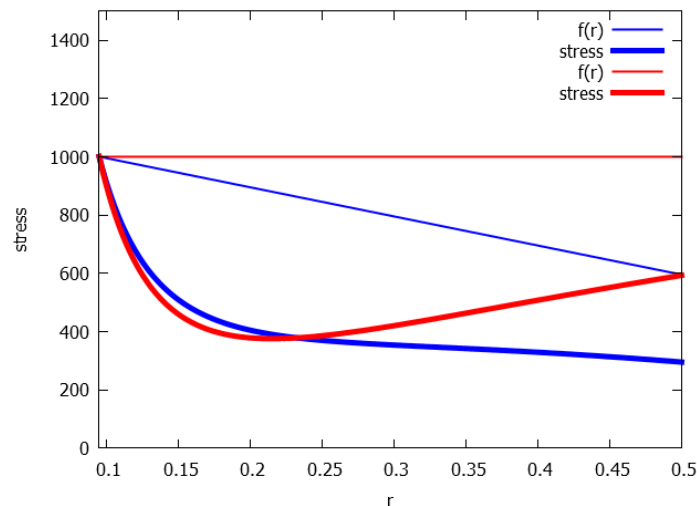


Figure 5. Tension of woven and resulting tangential stress in the batch

It is obvious that such a variation of the cloth tension with the radius of batch has non-negligible effect on the shape of the tangential stress in the wound woven. Variation of the contact press is correspondingly important.

As the control system of winder allows entry of up to 5 point curve along the wound length of woven (not the radius of batch, there no device to measure it), we tried to shape the tension curve using a linear and a quadratic function, as follows:

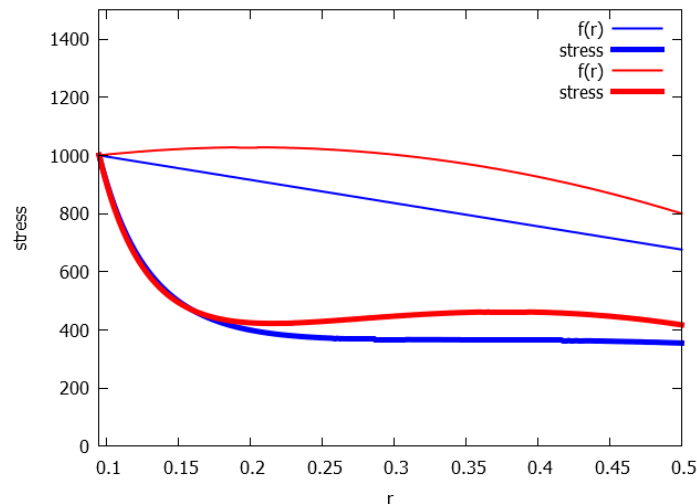


Figure 6. Optimized tension of woven and resulting tangential stress in the batch

It is known that “best” batches are those with little variation of the stress along the length of the woven (this stress is regularly checked in fabric factory using a special device). Evidently there is a function $f(r)$ that allows the creation of large-size batch with a near-constant stress inside, at least along the majority of the wound length of cloth.

5. Experiments

To verify this hypothesis, the following method was chosen:

Several wires are gradually inserted into the batch in the weft direction during wrapping. The force that can be moved by these wires (moving them in the weft direction to one or the other side) is directly proportional to the contact pressure between the layers of the packing between which the wire is inserted. Assuming that the properties of both the fabric and individual wires are constant both in the width direction of the fabric, both the length of the wire and the direction of the warp (i.e., the inserted wires are identical and the fabric sett do not change nor changes lubrication of the fabric, i.e. a constant coefficient of friction between the fabric and the wire can be assumed, it is possible to determine the relation of this force depending on the position of the respective wire, to the radius on which the said wire is located. By this method it is possible to verify the contact pressure distribution along the radius of the packing. The value of the coefficient of friction must be known to determine its absolute values. This can be determined either by a direct measurement by wire tweaking the fabric or by measuring the above-mentioned force immediately after wrapping the respective wire where the contact tension can be determined directly from the fabrics tension when packed. Unfortunately, both methods are burdened by a relatively large measurement error.

Another option would be differential measurement, ie the comparison of the measured values on individual wires, which are gradually located at the same depth below the surface of the packing. So we get sets of pairs $[r_i, T_{iTheor}]$ and $[r_i, T_{iExp}]$, assuming $f = \text{const}$. it will be possible to put through a regression line whose slope will be directly proportional to f . However, this method has not yet been elaborated in more detail.

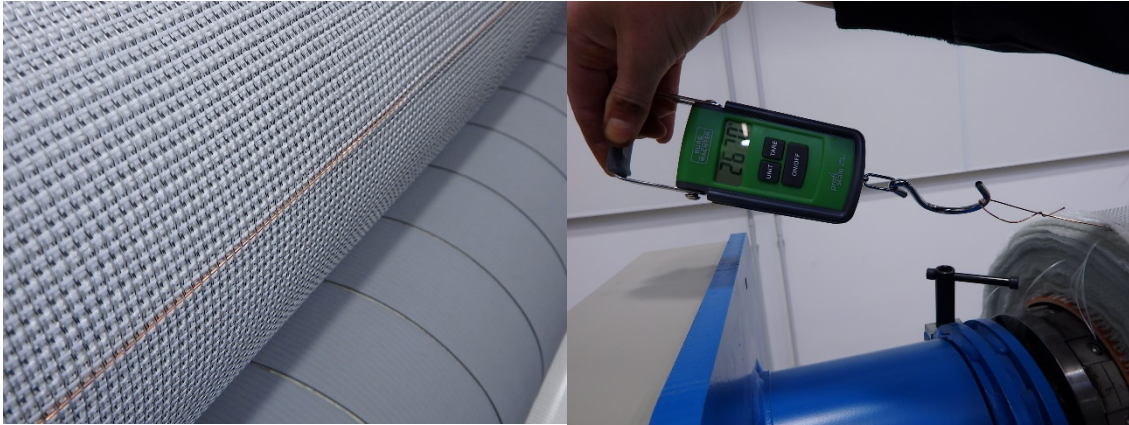


Figure 7. Arrangement of measuring wire and load cell

6. Conclusions

While we have developed a plausible mathematical model its credibility is to be verified. Presently an experimental campaign is prepared in cooperation with a fabric factory. Once this model is verified we should be able to predict behavior of any batch depending on the conditions of the winding.

In future a possible extension of the model for non-isotropic material could be found. Anyway the problems with the determination of the orthotropic moduli of the batch should be solved before.

Another way for a future development leads to find a reverse function $f(\sigma(l) = const.)$ which should allow the loom operator to program in advance the best fitting tension function for any type of batch. Unfortunately the $f(r)$ is rather complex and its reverse function may not exist.

ACKNOWLEDGEMENTS

This work is prepared in cooperation with St.Gobain ADFORS Litomyšl, using CEDIMA large-size batch winder.

References

1. Prof. Ing. Höschl C. (1992): *PRUŽNOST A PEVNOST II (1. vydání)*. Vysoká škola strojní a textilní v Liberci, Fakulta strojní. Liberec
2. CEDIMA Meziměstí s.r.o.: *Basic Installation, Operating and Maintenance Instructions (2006 edition)*, Meziměstí.
3. Josef Dvořák, Petr Karel, Josef Žák (2018): *Study of Interactions between Weaving Process and Weaving Machine Systems*, VÚTS, a.s.

MECHANICAL FIXATION OF TUFTED PILE LOOPS INTO THE PRIMARY BACKING BY USING THE PARAMETERS OF FABRIC WEAVE DESIGN

Application of Newly Developed Yarn Tension Compensation Device for Tufting of Technical Yarns

Alexandra Glogowsky¹, Thomas Brunke², Karin Ratovo¹, Alexander Büsgen¹, Bayram Aslan²

¹Research Institute for Textile and Clothing (FTB), Niederrhein University of Applied Sciences, Mönchengladbach, Germany

Corresponding author: alexandra.glogowsky@hs-niederrhein.de, +49 2161-186 6035

²TFI - Institut für Bodenbeläge an der RWTH-Aachen e.V., Aachen, Germany

Corresponding author: t.brunke@tfi-aachen.de, +49 241-9679 132

Abstract:

Tufting technology is commonly used exclusively for the production of textile floor coverings. With the e-Jerker, the TFI - Institut für Bodenbeläge an der RWTH-Aachen e.V. has developed a yarn storage element that can be parametrised and retrofitted to existing tufting machines, which allows the processing of low-stretch and high-strength pile yarns. In the future, this will enable tufting producers to offer completely new products for innovative applications in the field of technical textiles. A tufted textile is particularly suitable for applications where insulating, shielding or absorbing properties are required due to its three-dimensional pile structure. However, since the latex coatings traditionally used for securing the tufted backing are out of the question for technical applications in which high temperatures have to be considered, heat-resistant alternatives are required. In the current research project "High-Performance Tufting Structures", two alternatives were evaluated with regard to their suitability. On one hand, woven primary backing materials were developed which, in combination with the needled pile yarns, achieve the highest possible pile binding forces. This should allow the omission of coatings entirely, if necessary. On the other hand, temperature-resistant formulations for back coatings based on PU and silicone were also developed. The investigations focused on the use of glass yarns for both the primary backings and the pile yarns. In general, it can be said that both the feasibility of production and the acoustic and thermal properties of a tufted technical textile open up new application possibilities.

Key Words:

Tufting, primary backing, technical textiles, weave design, heat-resistant coating, glass yarn

1 Introduction

Tufting technology is a process for the production of textile surfaces characterized by high productivity. It has been conventionally used for decades to produce textile floor coverings. A tufted product is created by needling pile yarns into a textile base material (non-woven or woven), thus creating a 3-dimensional textile with a pile-surface. In order to produce a stable and usable product, it is necessary to secure the pile to the backing using a back coating. This prevents the pile yarns from coming loose during use. Depending on the machine type and fineness, the tufted 3D structure can be very variable in terms of pile height and ranges from a few millimetres to several centimetres. Correspondingly, the overall density can also be adjusted. 85 % of the yarns used to produce tufted floor coverings are

synthetic bulked continuous filament yarns (possessing inherent elasticity) made from polyamide, polyester or polypropylene [1]. As only elastic pile yarns can be processed, tufting is limited to the product group of floor coverings.

Expanding the range of usable materials for tufted textiles, with their broad range of possible constructions, unlocks potential applications for technical tuftings. Due to its open pile surface, a tufted surface structure is particularly suitable for applications where insulating, shielding or absorbing properties are required. This, in combination with the use of heat-resistant materials for pile yarns and backings, allows manufacturing of tufted structures that have both high acoustic absorption and thermally shielding effects at the same time. However, since the synthetic latex coatings usually used to strengthen tufted floor coverings are thermally unstable, the only option is not to use a coating at all or, alternatively, to use temperature-resistant formulations.

Both options were investigated in the pre-competitive research project "High-Performance Tufting Structures". The absence of a backside coating to firmly bind the needled pile yarns to the primary backing means that the yarns need to be mechanically anchored in the primary backing with sufficient stability to ensure safe product use. In this project, fabrics for the primary backing were structurally optimized to exhibit the best possible pile clamping forces. For possible applications in which the pile clamping forces achievable in this way are not sufficient or a backside coating is desired, corresponding coating tests with temperature-resistant formulations were carried out.

2 Woven Primary Backings

As explained earlier, a core issue within this project is the production of a heat-resistant "primary backing", i.e. a base fabric suitable for the tufting process. Glass fibres are the best option for a high-temperature-resistant base material for this purpose, as well as being a very economical option.

Pre-trials on different weave constructions using polyester-yarn showed that a tight construction (maximum weft density at high warp densities) as well as the use of texturized weft yarns have a major influence on the retention of tufted yarn in the finished product. Furthermore, warp backed weaves and multi-layer construction showed positive effects regarding the resulting tuft withdrawal forces. [2]

The main challenge for the transfer of these results is the production of a stable and relatively tight fabric in warp-backed and double- or multi-layer construction in order to replicate the positive results of the pre-trials.

2.1 Materials and Machinery

All trials were executed on a rapier loom (Dornier HTV8/S20). This machine has two warp beams (for increased flexibility regarding warp densities) and 16 shafts (+2 shafts for selvedge production).

Table 1. Materials used in pre-trials vs. experiments with glass yarn

	Code	PES-trials [2]	Glass-trials
Warp / Weft1	Y1	PES 1100dtex 200f Z60	Vetrotex EC11 204 Z28 T63C H8
Weft 2	Y2	PES 1400dtex bulked	Vetrotex ECO11 T220 T10C (voluminized)
Weft 3	Y3	PES 1400dtex air-texturized	Vetrotex ECT9 T370 T10C (air-jet texturized)
Pile Yarn	YP	HKO Thermo-E-Glass Yarn texturized ET6-300 tex x2 z100 TS	

All yarns were selected for their similarities regarding diameter and structure - however, this proved impossible (s.Y1, Y2, table 1) due to the availability of certain glass yarn grades. All glass-trials were executed at a warp density of 22 ends/cm and utilized only 8 shafts.

2.2 Test Methods

On tufted samples the force needed to draw out one tuft is measured according to ISO 4919.

2.3 Experimental

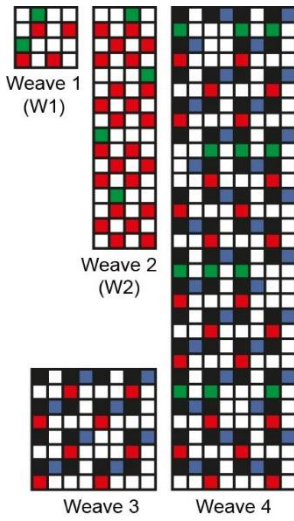


Figure 1. Weaves used in glass-trials

All weaves (s. figure 1) are based on plain fabrics, with weaves 1 and 2 representing weft-backed constructions, weave 3 as a double layer fabric made up of plain weaves and weave 4 as a combination of both (one layer is a regular plain weave and one layer is weft-backed weave 2).

Table 2. List of weave / yarn combinations tested

Code	Max. weft density	
	Glass trials	PES-trials
W2_Y12	8	20
W2_Y13	7	-
W2_Y2	8	16
W2_Y3	6	-
W2_Y23	6	-
W3_Y12	11	14
W3_Y13	10	-
W3_Y2	11	14
W3_Y3	10	14
W3_Y23	10	-
W4_Y12	10	20
W4_Y2	10	20
W4_Y3	9	18

Through intensive experimentation in the pre-trials [2] single layer and warp-backed weave constructions could already be eliminated from the main trials with glass yarn. Furthermore, it was found that one weave construction (weave 1, figure 1) could not be woven with glass yarns, even if the results with PES were hopeful. This is due to the uneven distribution of interlacing points between warp yarns leading to slippage between threads and a high occurrence of warp breaks.

All weaves were woven in various combinations of the threads listed in 2.1. Table 2 shows the full list of finished fabrics.

2.4 Results

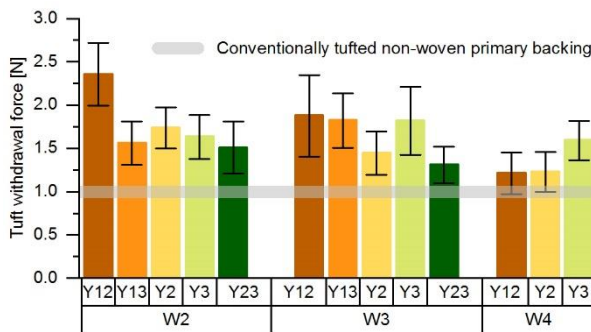


Figure 2. Tuft withdrawal forces of glass trials

tufting of bulked continuous filaments in non-woven primary backings.

Compared to the pre-trials on PES, where weft densities of up to 20 picks/cm were achieved for the same weaves, it can be seen that glass fabrics needed a lower density to be weavable, even if theoretical maximum densities should have been closer (s. table 2). Nevertheless, these glass fabrics have good slippage resistance and were tufted. The respective tuft withdrawal forces are shown in figure 2, with the grey line representing the tuft withdrawal force achieved by conventional

2.5 Discussion

While the pre-trials gave some indication that choice of yarn and weave have a major influence on tuft retention, the glass trials do not follow these trends, as is shown in figure 2. Furthermore, the tuft withdrawal forces do not show any relation to conventional fabric parameters such as thickness, areal weight or air permeability. Weave 4 shows remarkably low tuft withdrawal forces. However, weave W12_Y12 achieved a high tuft withdrawal force of 2.35 N, further confirming the conclusion from the pre-trials that weft-backed weaves result in high tuft withdrawal forces. This fabric will be used in

further experiments. All primary backings surpass the tuft withdrawal force of conventional (raw, uncoated) tufted non-woven primary backings, thereby making it clear, that these textiles are stable enough to be manufactured into finished products.

3 Tufting Process

During tufting, many needles simultaneously stab through the primary backing at tufting cycles of up to 2,000 stitches/min. The primary backing is transported by a set distance (stitch length) between each complete needle stroke. Below the primary backing, the pile yarns pierced by the tufting needles are transferred to hooks and formed into yarn loops. In the production of cut pile fabrics, the yarn loops held on the hooks are additionally cut open by knives arranged on the side of the hooks (s. figure 3) [3].

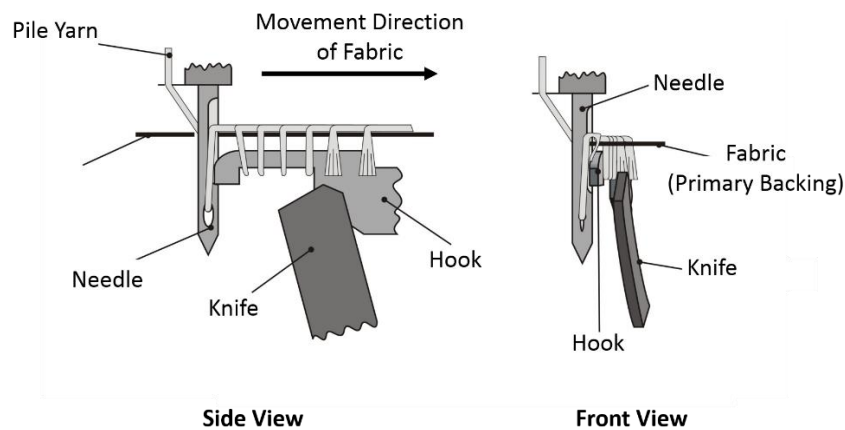


Figure 3. Tufting mechanism for pile fabrics

A tuft cycle corresponds to a complete, vertical stroke of the needles from the top to the bottom dead center and back to the starting position. When the needle passes through the primary backing and the pile yarn is deposited on the hook, temporary deflections of the yarn feeding mechanism cause yarn consumption to vary over time. However, the vertical displacement of a standard jerker bar (horizontal perforated strip for yarn guidance), which is mechanically coupled to the lifting movement of the needles, does not permit any adjustable yarn storage. Instead, the elasticity of the yarns compensates for the difference between yarn demand and yarn supply.

3.1 Use of e-Jerker

In a previous project by the TFI-Institut für Bodensysteme an der RWTH Aachen e.V., a new yarn storage element was developed which, contrary to the method of operation described above, guarantees a programmable lateral yarn displacement and thus an optimized feeding of the pile yarns to the needles at any time during the tuft cycle [4]. The individual displacement of the pile yarns is effected by a servomotor drive of the e-Jerker. This was used in the project described in this paper in order to enable the use of glass fibres, which are non-elastic.

The programming of the e-Jerker is carried out for each new pile yarn individually to customize processing. For this purpose the variation in yarn feed tension during a single tuft is measured over several tufting cycles using a laser sensor that makes it possible to correlate yarn demand at a given point in the tuft cycle with the corresponding position of the needle. The motion profile is logged continuously, producing a typical curve which reflects the yarn requirement of this pile yarn for a tuft cycle (s. figure 4).

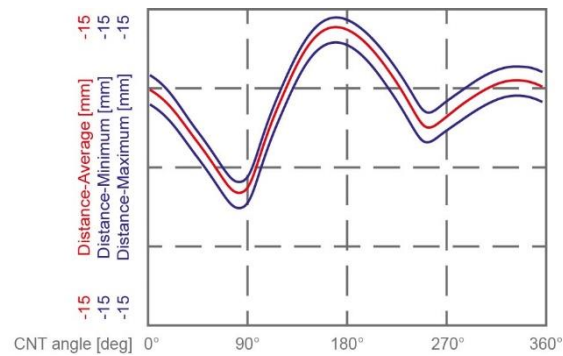


Figure 4. Typical yarn displacement during tufting cycle

The angular positions shown in figure 4 correspond to the following needle positions during a tuft cycle:

- 0° or 360° Needle at top dead center
- 90° Needle eye at the level of the primary backing
- 90° - 180° Needle to bottom dead center
- 180° - 270° Transfer of the loop to hook

The simultaneous video-assisted observation of the tufting tools then allows a precise analysis of any errors or inadequacies during yarn transfer or take-up between needles and hooks. This way it can be decided whether more or less yarn should be delivered from the needles to the hooks at any given time to ensure optimum pile loop formation at all points in the tuft cycle. The adjustment is made by changing splines in the recorded movement curve at those points where errors or inadequacies have been observed in relation to the position of the tufting tools. A motion curve manipulated in this way can then be read into the servomotor control of the e-Jerker as a yarn-specific reference curve.

3.2 Materials and Machinery

In the manner described above, mainly glass yarns were measured and their processability in combination with the developed glass fabrics tested. In addition, further tests have shown that low-stretch pile yarns made of aramide, basalt or steel fibres can also be tufted by programming the yarn storage behaviour using the e-Jerker. In addition to the pile yarns mentioned above and the glass fabrics that were investigated in detail, the feasibility of using high-strength aramid fabrics as primary backings for tuftings could also be confirmed. In order to achieve different material finenesses and surface characteristics, test goods were produced on tufting machines of different designs. Cutting and looping machines with machine gauges of 1/10 inch and 1/8 inch were used.

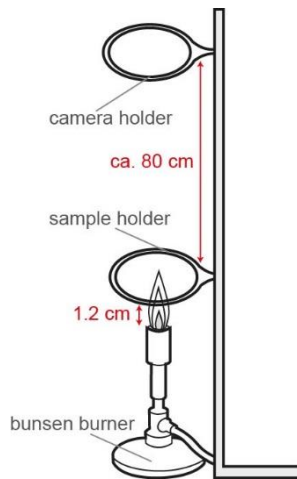
4 Heat-Resistant Coatings

As the goal of a tuft withdrawal force higher than 7N cannot be reached by weave construction alone, a coating with comparable heat resistance is necessary for sufficient tuft retention. The main demands are avoidance of halogenated flame-retardants, improved mechanical stability of the glass fibre fabric after direct contact to flames, limited smoke emission and good coating behavior.

4.1 Materials

In order to achieve different draping behaviors, two different matrix-systems were considered: Polyurethane dispersions for a stiffer fabric and 2K-silicone for a softer drape. The flame retardants tested are shown in table 3.

4.2 Test Method



In order to test the coating resistance against direct contact to flames, testing according to ISO 15025 was considered, but no differences regarding coating performance were observed. Therefore a non-standardized method utilizing a bunsen-burner and an infrared camera was developed (s. figure 5). The main criteria are burning behavior, smoke generation and fibre damage after burning. The infra-red videos can be used supplementally to gain more information on heat dissipation, especially in tufted fabrics. The camera used is a FLIR ONE thermal imaging camera. Figure 4 shows a sketch of the test set-up. The textile is placed coated side down on the sample holder and exposed to the flame for 12 seconds. The time and distance to the flame was set so that an uncoated fabric shows distinct signs of melting and a high degree of fibre damage, making it possible to observe the influence of the coating.

Figure 5. Test set-up for burn tests

4.3 Experimental

The following recipes were tested and evaluated for the criteria listed below:

Table 3. Coating formulations (% of dry weight) using different matrix materials, coating and burning behavior

Sample no.	2a	2b	2c	3a	3b	4a	4b	5a	5b	5c	6a	6b	6c
PU1	x			x		x		x	x	x			
PU2		x			x								
2K-silicone			x				x				x	x	x
Ammonium polyphosphate (APP)	15	15	15	15	15	15	15	15	15	15	15	7.5	7.5
Aluminium-pigment	5	5	5	5	5	2.5	2.5	5	5	2	2.5	2.5	2.5
Dipentaerithriol	5	5	5	5	5	5	5	5	5	5	5	2.5	2.5
Melamine						5	5	5	5	5	5	2.5	2.5
Aluminiumtrihydrate (ATH)								7.5	7.5	7.5	7.5	7.5	7.5
Vermiculite (dispersion)				7	7								
Bentonite									1	1			1
Coating	+/-	+	-	+/-	+/-	+/-	-	--	-	+/-	--	+/-	+/-
Burning	+	+/-	+/-	-	+	+/-	+/-	--	+/-	--	No test	+/-	+/-
Smoke	-	-	-	+/-	+	+/-	-	--	-	--		+/-	+/-
Fabric damage	--	+	++	+	+	+/-	++	+/-	+/-	-		+	++

4.4 Results

It can be seen that in general coating behavior proved a bigger problem for the silicone-based recipes (s. table 3), as for this product it is not possible to influence viscosity. Regarding smoke generation, silicone formulations in general produced smokier outcomes with little influence of the flame retardant combination used. However, while all PU-based samples are stiff, silicone-coatings retain their drapeability.

Formulations 3b, 4a and 6c were further evaluated for their coating behavior on tufted sample W2_Y12. The results of the infra-red camera reading is shown in figure 5. Figure 6 shows the improvement of tuft withdrawal force that can be achieved with each formulation.

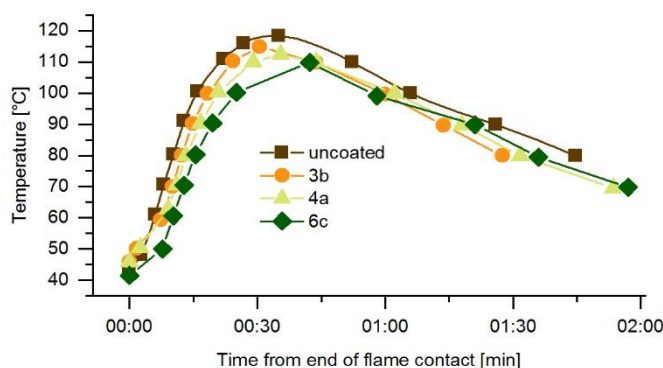


Figure 6. Effect of coating on surface temperature

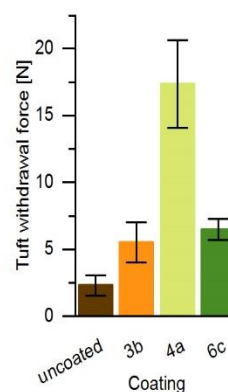


Figure 7. Tuft withdrawal force after coating

4.5 Discussion

Regarding coating performance it was found that certain coating formulas can achieve a good stability against open flames in regard to burning behavior as well as fibre damage. This subjective rating is corroborated by the measurements using an infra-red camera (s. figure 3). It can be seen, that the surface of coated textiles does not get as hot as an uncoated sample, presumably due to the cooling and insulating effect achieved by flame retardants as well as heat reflection from the aluminium-pigment. However, on tufted samples there are big differences between the coatings tested regarding tuft withdrawal force after coating, so that a compromise needs to be made between good drapability and high tuft retention. The goal of a tuft withdrawal force $>7\text{N}$ could only be achieved using a PU-based coating.

5 Acoustic Properties

In order to check the acoustic properties, samples were tested using an impedance tube in accordance with EN ISO 10534-2. The sound absorption coefficient serves as a measure for the improvement of acoustics in a room. Samples tufted with the reference pile yarn (YP) on three different glass fabrics were compared. The coatings, regardless of matrix material, compared to the corresponding uncoated fabrics. All measurements show sound absorption levels similar to or slightly better than those of tufted floor coverings. Since the selected test products are constructions similar to those of tufted floor coverings, it can be concluded that the materials used for primary backings and pile yarns have no significant influence on the sound absorption coefficient. A comparison of the coated variants with the uncoated references does not show a uniform picture or a significant difference. Further tests with constructive modifications (pile height, pile density) for further improvement of acoustic properties are planned.

6 Conclusion and Outlook

It could be shown during this project that it is possible to produce primary backings for tufted textiles from glass yarns. The tuft withdrawal forces achieved using weft-backed weave constructions are higher than those of conventional (uncoated) tufted fabrics, allowing for further processing. Further, it was proven that tufting with glass yarn in the pile is feasible. The benefit of the retrofittable e-Jerker for the production of tuftings from technical yarns is evident in practical use. Furthermore, coatings developed for direct contact with flames improve heat-stability as well as mechanical properties of the tufted fabrics, allowing for a broad spectrum of applications. Lastly, the sound absorbing qualities of a tufted glass fabric were investigated and it could be shown that neither yarn material nor coating change the good acoustic properties known from conventional floor coverings.

In conclusion, both the feasibility of production as well as the acoustic and thermal properties of a tufted technical textile open possibilities for new applications. The fields currently considered for

potential industrialization are lightweight building materials for passive fire safety as well as acoustic insulation for industrial machinery.

ACKNOWLEDGEMENT



Gefördert durch:



aufgrund eines Beschlusses
des Deutschen Bundestages

The IGF project AiF-Nr. 19050N of the research association Forschungskuratorium Textil e. V. was financed by AiF as part of the Industrial Collective Research Programme by the Federal Ministry for Economic Affairs and Energy, based on a decision of the German Bundestag. The final report can be accessed publicly

References

1. Kwoczek, K.: *Die Verarbeitung technischer Garne in der Tuftingtechnik*, Mönchengladbach, Hochschule Niederrhein, Fachbereich Textil- und Bekleidungstechnik, Diplomarbeit am TFI – Institut für Bodensysteme an der RWTH Aachen e.V., 2011.
2. Glogowsky, A., Gsell, E., Brunke, T., and Büsgen, A. 2018. *Glasfasertuftings als eine neue Art technischer Textilien*. In *Technologievorsprung durch Textiltechnik*. Förderverein Cetex Chemnitzer Textilmaschinen e.V., 46–54.
3. Brunke, T.; Lempa, E.; Rabe, M.; Winkler, J.-C.: *Dessinierung multistruktureller Tuftingkonstruktionen mittels eines optimierten Spritzdruckverfahrens (AiF 15954)*, Schriftenreihe des TFI – Deutsches Forschungsinstitut für Bodensysteme e.V. 2011/96, Aachen, 2011
4. Goetz, C.; Hanuschik, D.; Schröder, E.: *Erweiterung des Anwendungsgebietes der Tuftingtechnik durch den Einsatz einer elektronisch gesteuerten Jerkerbarre (AiF 16678)*, TFI-Schriftenreihe 2013/98, Aachen, 2013

THE SET-UP OF A LABORATORY TYPE COATING / LAMINATING UNIT AND THE OPTIMISATION OF LAMINATION PROCESS OF DENIM FABRICS

Ayşe Genç,¹ Mehmet Yüceer², Nihan Karakaplan² and Cem Güneşoğlu³

¹Çalık Denim R & D Centre, The 1st Organized Industrial Zone, Malatya Turkey

²İnönü University, Chemical Engineering Department, Malatya, Turkey

³Gaziantep University, Textile Engineering Department, Gaziantep, Turkey

Ayşe.KorkmazGenc@calikdenim.com

Abstract:

Lamination process is a finishing process applied to bring functionality, physical modification and change at appearance by combining two separate materials (fabric, polymer film layer or membrane). The process increased its popularity at denim industry especially in fabric-fabric lamination form in the last decade. Despite its market interest, lamination has setbacks in R&D studies for optimization to enhance the product performance due to large numbers of parameters and difficulties in producing samples. In this study, an adaptive laboratory type coating / laminating unit was developed as the first time in textile industry and the lamination of denim-denim fabric process has been optimized through statistical analysis and modelling studies by artificial neural network (ANN) and least-square support vector (LS-SVM) machine.

Key words:

Lamination, optimization, Artificial neural network, Least-square support vector machine.

1. Introduction

Coating is a process in which a polymeric layer is applied directly to one or both surfaces of the fabric, on the other hand lamination is defined as finishing process applied to bring functionality, physical modification and change at appearance by combining two separate materials. Conventional laminated textiles normally consist of one or more textile substrates that are combined using a prepared polymer film or membrane by using adhesives or by using heat and pressure [1]. Lamination found increased interest in denim market, especially in fabric-fabric lamination form by adhesive usage. It is clear that adhesive amount (weight) in the process strongly affect laminated product various properties; also it is a matter of cost. In many cases, producers use adhesive amount as recommended by the supplier, however it is needed to examine to determine the optimum adhesive amount for high volume of production. However, experimental study on fabric lamination is limited since there is large number of parameters to examine and the lamination machinery works with whole fabric width which results large amount of sample and adhesive consumption. Best to our knowledge, there is no laboratory type lamination machine available. In this study, we developed an adaptive laboratory type coating / laminating machine with lower than 40 cm working width which has two separate fabric roll feeding, powder scattering head (for particle loadings), hot-melt adhesive tank and adhesive feeding units. The roller pins are adaptive to change the feeding positions, material type and adhesive feeding face also it is possible to control material and adhesive feeding speeds. The scheme and actual view of the laboratory machine is given in Figure 1.

In this study, denim-denim fabric lamination is conducted by the mentioned machine; various properties are measured and lamination process parameters are optimized through statistical analysis (ANOVA and Design Expert) to find the most suitable adhesive weight for industrial scale applications and

modelling studies (ANN and LS-SVM) to assess the predictability of the results and to decide if this study can be applied for industrial scale works as proposed.

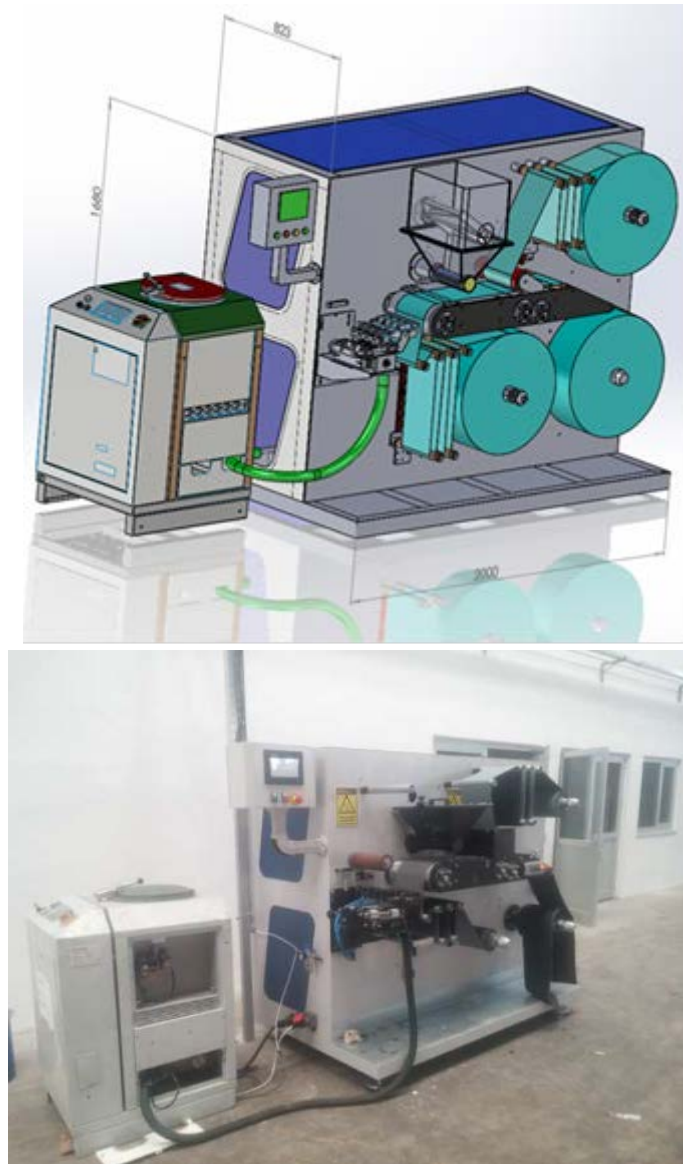


Figure 1. General view of developed coating / laminating machinery

2. Experimental

2.1. Materials

%100 cotton, denim fabric samples used at lamination were supplied by Çalık Denim, Malatya, Turkey. The constructional details of the samples are given in Table 1. The lamination adhesive was polyurethane based (HB Fuller, USA) reactive hot-melt adhesive with low curing temperature and adhesive weight was varied as 25, 50, 75 and 100 g/m² at the trials and 30 m/min fabric feeding speed.

Table 1. Sample details

Sample Code	Weave type	Fabric sett (thread / cm)	Yarn count (Warp x Weft)	Weight (g/m ²)
D1	3/1 Z twill	47 x 25	Ne 24/1 x Ne 30/1	342
D2	3/1 Z twill	42 x 26	Ne 20/1 x Ne 18/1	355

2.2. Methods

After the laminations, the samples were rinsed, dried and tensile strength (ASTM D 5034), tearing strength (ASTM D1424), delamination strength (ASTM D 2724-07), air permeability (ISO 9237), water resistance (ISO 20811) and water vapor permeability (ISO 11092) measurements at the standard laboratory conditions were conducted. All the measurements were repeated for five times and results were recorded as data for optimization studies. All data were subjected to statistical analysis with ANOVA to find out the contribution importance and proposed model strength between adhesive weight and measured property and the optimization study was then applied first with Design Expert V.10. The study is also validated through ANN and LS-SVM modelling as mentioned before.

A typical ANN has feed forward architecture and consists of three or more layers of neurons: one input layer, one output layer and one or more hidden layers (Figure 2). Each of the layers has a set of connections, with a corresponding scalar weight, between itself and each neuron of preceding layer. When the weight of a particular neuron is updated, it is said that neuron is learning and ANN is training. In a feed forward back-propagation ANN, the input data (x_i) is passed to the neurons in input layer as signal. The data is weighted in hidden layers (y_i) by associated weights in each interconnection through non-linear transfer function. The sum of weighted inputs is converted to outputs (z_i) through activation function [2]

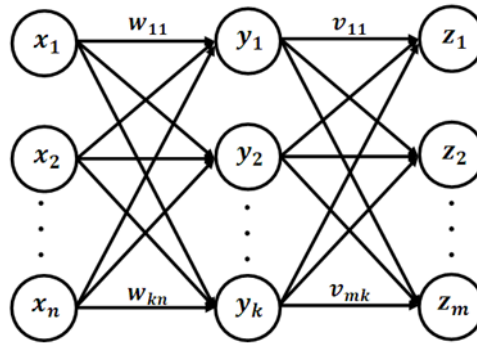


Figure 2. ANN architecture

On the other hand, support vector model (SVM) is a machine learning technique which is based on the statistical learning theory and structural risk minimization principle. The SVM uses a based quadratic programming optimization to identify model parameters, while avoiding local minima, and have an advantage over other regression methods. A modified version of SVM, called the least square support vector model (LS-SVM) results in a set of linear equations instead of quadratic optimization problem [3]. A general LS-SVM architecture is as also given in Figure 3. Detailed information is given elsewhere [4-6]

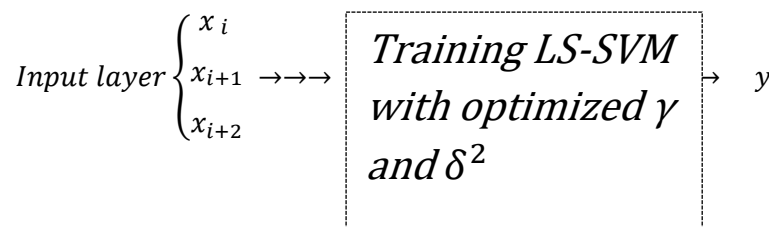


Figure 3. LS-SVM architecture

In the modeling studies, adhesive weights and denim sample mechanical parameters (sett value, yarn count and weight) was selected as input and output was limited to delamination strength, air permeability and water vapour permeability parameters of laminated samples. The random 65% of the measured values were used for the training and the rest for the test. In the course of training of ANN, which was based on Levenberg– Marquardt method [7], the number of neurons in the layers, training accuracy and

number of iterations were determined by using trial and error method; thus the optimum number of neurons obtained in the layers were determined as 9. For the development of the models, Neural Network Toolbox, LS-SVM Lab v1.7 and MATLAB 7.0 were used.

The model performances were then assessed by evaluating the scatter between the experimental and predicted results via statistical parameters, that is correlation coefficient (R), mean absolute percentage error (MAPE %), and root mean square error (RMSE). The statistical values were determined as follows:

$$R = \frac{\sum_{i=1}^N (x_i - \bar{x})(y_i - \bar{y})}{\sqrt{\sum_{i=1}^N (x_i - \bar{x})^2} \sqrt{\sum_{i=1}^N (y_i - \bar{y})^2}} \quad (1)$$

$$RMSE = \sqrt{\frac{\sum_{i=1}^N (y_i - x_i)^2}{N}} \quad (2)$$

$$MAPE (\%) = \frac{1}{N} \sum_{i=1}^N \left(\left| \frac{y_i - x_i}{x_i} \right| \right) \cdot 100 \quad (3)$$

where, x_i is an observed value, y_i is a simulated value, N is the number of data points, \bar{x} is the mean value of observations, and \bar{y} is the mean value of simulations. A higher value of the R and smaller values of MAPE and RMSE would indicate a better performance of the model.

3. Results and Discussions

The average of the measurements are given in Table 2. %CV values of the measurements were lower than %10 in all cases. Table 2 showed that increase in adhesive weight resulted trends in the properties.

Table 2. Measurement results of the samples

Property	Sample Code					
	D1	D2	D1-D2 (25)*	D1-D2 (50)*	D1-D2 (75)*	D1-D2 (100)*
Tensile strength (kgf)	64 (warp) 24 (weft)	67 (warp) 26 (weft)	110 (warp) 59 (weft)	102 (warp) 64 (weft)	110 (warp) 64 (weft)	112 (warp) 69 (weft)
Tearing strength (kgf)	3197 (warp) 1892 (weft)	4567 (warp) 2610 (weft)	6263 (warp) 3262 (weft)	4893 (warp) 3131 (weft)	4175 (warp) 2871 (weft)	3653 (warp) 2022 (weft)
Delamination strength (kgf)	-	-	5,56	11,67	> 20	> 20
Air permeability (mm/s)	139,08	455,65	88,85	49,83	15,20	3,95
Water resistance (mbar)	13,13	6,77	17,10	19,60	19,76	23,20
Water vapour permeability (g/m²/day)	1061,18	956,74	929,66	776,45	570,82	193,35

* The number in brackets is the adhesive weight used to laminate D1 and D2.

The ANOVA tables are given in Table 3 – 10. The proposed models are given at the bottom of ANOVA tables.

Table 3. ANOVA table for tensile strength in warp direction

Source	Sum of Squares	F value	Probability > F
Model	2420,53	15,10	0,0076
A	1922,00	23,97	0,0045
A²	498,53	6,22	0,0549
Residue	400,84		

Tensile strength (warp direction): $68,971 + 1,21 A - 7,075 \times 10^{-3} A^2$ (A : adhesive weight)

Adjusted R² : 0,8011 Standard deviation: 8,95

Table 4. ANOVA table for tensile strength in weft direction

Source	Sum of Squares	F value	Probability > F
Model	2447,03	848,97	< 0,0001
A	0,12	0,13	0,7375
A ²	498,53	518,88	< 0,0001
A ³	128,44	133,69	
Residue	3,84		

Tensile strength (weft direction): $25,137 + 2,054 A - 0,0343A^2 + 1,813 \times 10^{-4} A^3$ (A : adhesive weight)
 Adjusted R² : 0,9973 Standard deviation: 0,98

Table 5. ANOVA table for tearing strength in weft direction

Source	Sum of Squares	F value	Probability > F
Model	5,196xE6	14,97	0,0122
A	2,104xE6	18,18	0,0130
A ²	2,964xE6	25,61	0,0072
A ³	1,731xE6	14,96	
Residue	4,629xE5		

Tearing strength (warp direction): $3929,637 + 157,51A - 3,703 A^2 + 0,02105 A^3$ (A : adhesive weight)
 Adjusted R² : 0,8568 Standard deviation: 340,20

Table 6. ANOVA table for tearing strength in warp direction

Source	Sum of Squares	F value	Probability > F
Model	1,908xE6	62,35	0,0003
A	94902,72	6,20	0,0551
A ²	1,813xE5	118,49	0,0001
Residue	76522,48		

Tearing strength (weft direction): $2296,163 + 39,764 A - 0,427 A^2$ (A : adhesive weight)
 Adjusted R² : 0,9460 Standard deviation: 123,71

Table 7. ANOVA table for delamination strength

Source	Sum of Squares	F value	Probability > F
Model	503,72	107,81	< 0,0001
A	495,50	212,09	< 0,0001
A ²	8,22	3,52	0,1195
Residue	11,68		

Delamination strength: $-0,37371 - 0,30071 A - 9,08455 A^2$ (A : adhesive weight)
 Adjusted R² : 0,9683 Standard deviation: 1,53

Table 8. ANOVA table for air permeability

Source	Sum of Squares	F value	Probability > F
Model	1,056xE5	86,21	0,0001
A	86393,09	141,00	< 0,0001
A ²	19251,07	31,42	0,0025
Residue	3063,49		

Air permeability: $287,39987 - 7,16737 A + 0,043962 A^2$ (A : adhesive weight)
 Adjusted R² : 0,9605 Standard deviation: 24,75

Table 9. ANOVA table for water resistance

Source	Sum of Squares	F value	Probability > F
Model	185,23	64,54	0,0003
A	172,15	119,97	0,0001
A ²	13,07	9,11	0,0295
Residue	7,18		

Water resistance: $10,35763 + 0,23827 A - 1,14562 A^2$ (A : adhesive weight)
 Adjusted R² : 0,9478 Standard deviation: 1,20

Table 10. ANOVA table for water vapour permeability

Source	Sum of Squares	F value	Probability > F
Model	7,955xE5	288,84	< 0,0001
A	7,395xE5	536,99	< 0,0001
A ²	56037,73	40,69	0,0014
Residue	6885,43		

Water vapour permeability: $1008,97129 - 0,60702 A - 0,075005 A^2$ (A : adhesive weight)
 Adjusted R² : 0,9880 Standard deviation: 37,11

“The probability > F” value as recorded as input for optimization with Design Expert when it is smaller than 0,005. Design Expert model was run to consider the highest possible property value with lowest adhesive weight as mentioned before and the result is as given in Table 11. According to Table 11, we concluded that the lowest hot melt adhesive weight in the selected denim fabrics lamination must be 37 g/m² to receive the highest possible property values.

Table 11. Design Expert optimization

Run #	Tensile strength (weft)	Tensile strength (warp)	Tearing strength (weft)	Tearing strength (warp)	Delamination strength	Air permeability	Water vapour permeability	Adhesive weight (g/m ²)
1	100,933	63,4802	5745,19	3185,71	8,29737	60,0566	881,98	37,30
2	101,23	63,5188	5740,43	3186,91	8,34617	59,6796	881,028	37,45
3	100,838	63,4394	5750,07	3184,43	8,24663	60,4527	882,966	37,14

The screening performance of the models are given in Table 12. The results showed that the ANN model produced MAPE values lower than that of the LS-SVM and R values were higher than 0,9 in all of the outputs. The ANN model exhibited better performance in predicting laminated fabric properties but overall evaluation demonstrated that the study performed at the laboratory scale coating / laminating machine could be predicted through the ANN or the LS-SVM modellings; thus it is concluded that the machinery meets industrial requirements of controlling and predicting concerns.

Table 12. Statistical parameters of the models

Output	Training set				Test set		
	Model	RMSE	MAPE (%)	R	RMSE	MAPE (%)	R
Air permeability	ANN	3.053×10^{-6}	7.96×10^{-6}	1.0000	3.7384	4.3420	0.9939
	LS-SVM	24.4744	29.07271	0.9585	29.4573	34.3360	0.9872
Water vapour permeability	ANN	1.50×10^{-9}	2.68×10^{-10}	1.0000	66.5430	3.1370	0.9804
	LS-SVM	28.0534	4.8537	0.9951	33.5706	6.0109	0.9954
Delamination strength	ANN	8.147×10^{-6}	1.33×10^{-7}	1.0000	361.316	2.989	0.9821
	LS-SVM	38.5502	0.8133	0.9998	784.960	14.512	0.8990

4. CONCLUSIONS

In this study, a laboratory type coating / laminating machine was developed as the first time in textile industry and the lamination of denim-denim fabric process has been optimized through statistical analysis and modelling studies by artificial neural network (ANN) and least-square support vector (LS-SVM) machine. We obtained the minimum adhesive weight to be used in the process when considering highest property values of laminated fabrics and the ANN and LS-SVM modelling study revealed that the findings were predictable and reliable. Thus we concluded that findings obtained by using the mentioned machine are applicable for industrial studies.

ACKNOWLEDGEMENTS

This study is supported by TUBITAK under 1505 program with the contract no. 5140065.

References

1. Singha, K., (2012), *A Review on Coating & Lamination in textile: Processes and applications*, *American Journal of Polymer Science*, 2 (3), 39 – 49.
2. Atasoy, I., Yuceer, M., Ulker, E. O., Berber, R., (2007), *Neural Network Based Control of the Acrylonitrile Polymerization Process*, *Chemical Engineering & Technology*, 30, 1525–153
3. Vishesh, S., Manu, S., Vivek, A., Sumit, K.S., Ashwani, K.S., Vyshnav, L., (2017), *Data Mining and Analytics: A Proactive Model*, *International Journal of Advanced Research in Computer and Communication Engineering*, 6, 2, 524 – 526.
4. Vapnik, V., (1998), *Statistical Learning Theory*, John Wiley, NY, USA.
5. Suykens, J. A. K., Vandewalle, J., (1999), *Least Squares Support Vector Machines Classifiers*, *Neural Network Letter*, 9, 293–300.
6. Li, C., Zhu, X., Cao, G., Sui, Sh., Hu, M., (2008), *Identification of the Hammerstein Model of a PEMFC Stack Based on Least Squares Support Vector Machines*, *Journal of Power Sources*, 175, 303–316.
7. Iqbal, J., Iqbal, A., Arif, M., (2015), *Levenberg–Marquardt method for solving systems of absolute value equations*, *Journal of Computational and Applied Mathematics*, 282, 134-138.



Composite Based on Geopolymer Mortar Reinforced Chopped Basalt Fiber and Carbon Textile

Hiep Le Chi, Petr Louda, Totka Bakalova, Vladimir Kovacic

Department of Material Science, Faculty of Mechanical Engineering, Technical University of Liberec,
Studenstká 2, 461 17 Liberec, Czech Republic
hiepletul09@outlook.com

Abstract:

This paper deals with the evaluation of the four-point bending strength of geopolymer composite thin plates, which made of carbon grid embedded in geopolymer mortar containing various contents of chopped basalt fiber. Sodium-based geopolymer binder along with silica sand and chopped basalt fiber (0%, 3%, 5%, 7.5% by weight of geopolymer resin) are mixed together to make fresh geopolymer mortar. Then thin-plate specimens with the dimension 400x100x15 mm³ (length, wide, thickness) are produced by using one-layer of carbon grid embedded in fresh geopolymer mortar. The specimens were tested at a time period of approximately 28 days after casting. The tested results show that the increase in the chopped fiber percentage improves flexural strength (both at first-crack and peak load) of geopolymer composite thin plates.

Key words:

geopolymer, four-point flexural strength, geopolymer mortar, carbon textile, chopped basalt fiber

1. Introduction

Geopolymers are inorganic polymer materials with a chemical composition similar to natural zeolite but containing an amorphous microstructure and possessing ceramic-like in their structures and properties. Geopolymers are formed by reacting an alumino-silicate rich source (metakaolin, fly ash or nature pozzolanic, etc.) with an alkaline solution of the balancing cation of choice. Their amorphous structure composed of cross-linked alumina (AlO₄⁻) and silica (SiO₄) tetrahedra to form polysialates, with an alkali metal ion to balance with the negative charge [1-4]. Geopolymers have recently emerged as novel engineering binder materials with environmentally sustainable properties. The reduced energy consumption and CO₂ emission during manufacture make them attractive alternative over Portland cement [5,6].

Textile-reinforced concrete (TRC) is a new composite material composed of a fine-grained matrix with textile materials such as alkali-glass, carbon, basalt or polymer alternative to usual steel reinforced bars [7]. The major advantages of TRC are its high tensile strength and pseudo-ductile due to its tolerance of multiple cracking. Furthermore, such textile-reinforcement has the ability to withstand corrosion, aggressive environments and therefore does not require a strong covering layer in contrast to steel reinforced concrete, where requires sufficient thickness of the concrete layer to protect the corrosion of steel-reinforcement during the lifetime of the structure [8]. Therefore, it is resulting in thinning and reduction of the mass of the whole structure. Thanks to their excellent material properties, the TRC composite is used in a wide range of application such as thin-walled elements, repairing and/or strengthening in structural elements, façade elements, bridges and also freeform and lightweight structures [9-13]. The textile in composite materials plays an important role in carrying the capacity and stiffness of composite. As compared to other textiles, carbon textile better supported capacities, high tensile strength, high Young's modulus, low weight, high chemical resistance, etc. It is the main reason for the manufacture of Carbon textile as a commercial product for application in TRC composite. This

study is extended to the production of carbon textile reinforced geopolymer composite based on the fine-grain geopolymer mortar matrix containing various contents of chopped basalt fibers. The workflow is carried out by evaluating the four-point flexural strength of geopolymer thin plates at a time period of 28 days after casting.

2. Experimental

2.1. Materials

Baucis LNa aluminosilicate geopolymer binder based on metakaolin was purchased from Ceske Lupkove Zavody, a.s. Czech Republic (in weight percent: SiO₂ – 47.4; Al₂O₃ – 29.7; CaO – 14.5; MgO – 2.6; TiO₂ – 1.8; Fe₂O₃ – 0.5; K₂O – 0.3; Na₂O - 1) along sodium silicate activator of modul 1.73 (in weight percent: SiO₂ – 20.72; Na₂O – 12.33; H₂O – 66.68). The metakaolin geopolymer was synthesized from calcined kaolin and shale clay residues with Si/Al ratio of 2.0. The kaolin was mainly composed of kaolinite with small amounts of quartz, whereas shale clay was composed of kaolinite with low amount of quartz and anatase. Two different types of silica sand were used as the fine aggregates for geopolymer mortar matrix (grain size: 0 – 0.063 mm and 0.6 – 1.25 mm). The chopped Basalt fibers were provided by Kamenny Vek, and the tows were 6.4 mm long with the individual fiber diameters of 13 μm, the density of 2.67 g/cm³. Basalt has a softening and melting point of 1060°C, 1250°C, respectively. It is non-combustible, making it useful for high-temperature applications. The silane coating or sizing helps to protect the brittle fibers from premature fracture and prevents them from binding to each other. In this work, 3%, 5%, and 7.5% of chopped Basalt fiber additions (all by weight of geopolymer resin) were considered.

Carbon meshes of open size 12x16 mm were provided by Frisiverto S.R.O company, Czechina. The carbon mesh was made up of 48000 individual filaments for the yarns in the longitudinal direction and 12000 individual filaments for yarns in the transverse direction, and density of 1.8 g/cm³ (details see in Table 1). In the four-point bending test of geopolymer composite specimens, carbon grids were placed such that the load applied on the specimen was in the longitudinal direction of yarn.

Table 1. Properties of Carbon textile

Form	Carbon fiber grid
Fiber type	Carbon fiber HTC 10/15-40
Binder yarn	PP 110dtex
Fiber construction	Fiber orientation 0/90° (bi-directional)
Tex	800 g/km
Fiber density	1.8 g/cm ³
Number of threads/m	78 (lengthways) and 55 (crossways)
weight	350 g/m ²
Coating	Styro Butadien
Stitch spacing	10 mm x 15 mm (center to center distance)
Tensile strength	2551 N/mm ² (lengthways) and 2847 N/mm ² (crossways)
Elongation lengthways	1.17%
Elongation crossways	1.24%



Figure 1. Textile reinforcement: (a) Carbon grid, (b) chopped Basalt fiber

2.2. Specimen preparation and testing method

Geopolymer mortar matrix was prepared as the following steps. Pure geopolymer resin is the two-component mixture including aluminosilicate source (metakaolin) and alkaline liquid (sodium silicate liquid). This mixture is prepared in a ratio of solid to alkaline liquid (1:0.8) and mixed by mechanically stirring for approximately 5 min to ensure fresh mixture homogenously. After that micro-silica sand added into the prepared mixture and stirring for around 3 min more. Finally, chopped Basalt fiber (with the various percentage contents for each mixture) together with rough sand was added into the prepared mixture followed by stirring for another several minutes to ensure a homogenous mixture. The fresh mortar was cast into 30x30x150 mm³ prismatic molds for the flexural and compressive test to evaluate the mechanical strength of geopolymer matrix. Three samples for each mixture were used for flexural test and then the compressive strength was measured on the far edge of both residual pieces obtained from flexural strength according to EN 196-1 standard [14]. The thin-plate molds with a dimension of 400x100x15 mm³ for four-point bending were prepared. First the fresh mortar was poured in to the molds with a thickness 6 mm. Then one layer of textile is carefully laid over geopolymer mortar followed by filling the rest of the molds. Three thin plate specimens for each mixture were casted. All samples were cured at room temperature until test at a time period of 28 days after casting.

Figure 2 shows four-point bending test with constant bending moment zone (support span 100 mm) was used to determine the bending strength of geopolymer thin plate specimens. The INSTRON testing machine located at Technical University of Liberec Laboratory with the applied load under displacement control at loading rate of 2 mm/min. Three samples from each of the examined were tested. The calculation of the measured data and the evaluation of the test results were made using the following equation (1)

$$\sigma = F.l/(b.h^2) \text{ [MPa]} \quad (1)$$

where σ is the four-point flexural strength in MPa; F is load at a given point on the load-deflection curve in N; b is the width of the tested sample in mm; h is the thickness of tested sample in mm; l is the support span (300 mm).



Figure 2. Four-point bending test of geopolymer composite thin plate

3. Results and discussion

Table 1. Results of mechanical strength of geopolymer mortar matrix at time period of 28 days after casting

Mode	Various contents of chopped basalt fiber [wt.%]			
	0	3	5	7.5
Flexural strength [MPa]	11.23(0.39)	11.95(0.41)	12.77(0.19)	13.05(0.43)
Compressive strength [MPa]	64.36(3.17)	70.05(4.42)	78.52(1.67)	80.50(1.10)

Table 1 shows the compressive and flexural strength results of geopolymer mortar matrix at a maturation period of 28 days. In general, it can be seen that the addition of chopped Basalt fibers and their

increasing percentage improved both of the compressive and flexural strength of geopolymer mortars. The strength of reference mortar is 11.04 MPa (flexural strength), and 64.36 MPa (compressive strength). After that addition of fiber increases the mechanical strength in gradually small value, it reaches a maximum value of 12.52 MPa (flexural strength), and 78.5 MPa (compressive strength) for fiber content of 7.5%.

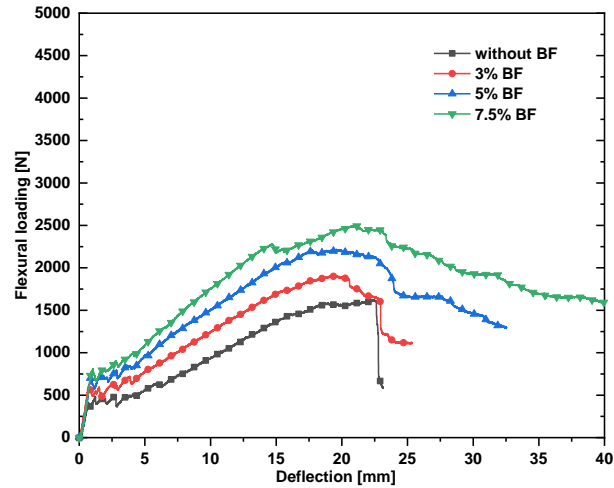


Figure 3. Flexural loading and deflection curves of one textile layer reinforced geopolymer composite thin plates with respect to various contents of BF

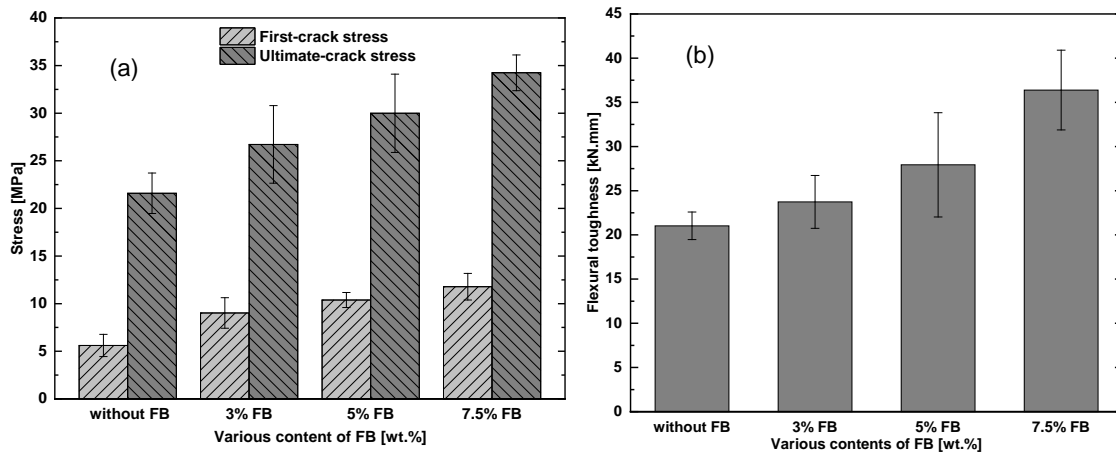


Figure 4. Summary of tested results of one textile layer reinforced geopolymer containing the various content of chopped basalt fiber: (a) flexural strength; (b) flexural toughness

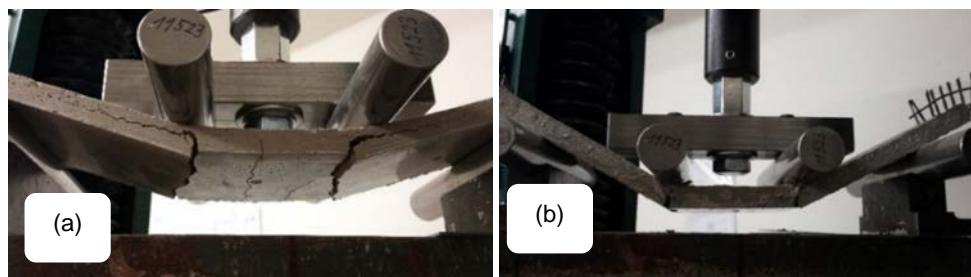


Figure 5. Failure modes of geopolymer composite: (a) geopolymer thin plates with one-layer of textile and without addition of BF; (b) geopolymer thin plates with addition of 7.5% BF and one-layer of textile

Figure 3 shows the average flexural load-deflection curves of all the geopolymer thin plates containing various contents of chopped basalt fiber. In general, the flexural load-deflection curves of all the tested

specimens exposed the similar behavior. It consists of the three parts corresponding to the stages in the flexural test. The three behavior areas are clearly visible. The first stage represents the linear uncrack state where the geopolymer matrix takes the load. Then, as the load increases, the stress transfers from the geopolymer matrix to the textile, which is represented by the multi-crack processing of the matrix. At the point or stage where the first crack takes the place is called transition point. Then, the specimens continue to undergo a multi-cracking process, in which all of the stresses are transferred from matrix to the textile. At this stage, the textile is only carrying the load until it fails by rupturing or slipping. This behavior is similar to textile reinforced cementitious matrix [8]. Figure 4 is presented average values of the first-crack stress, ultimate stresses and flexural toughness of thin plate specimens. It can be seen that the addition of BF reinforced geopolymer mortar is helpful to improve both the first-crack load and the ultimate load of textile reinforced geopolymer specimens. It can be observed by fact that BF contributes to improve the early age performance of the geopolymer mortar, leading to fewer micro-cracks in geopolymer mortar. Moreover, thanks to the bridge effect of basalt fiber at the cracks, the interface bond between yarns of textile and geopolymer matrix is improved, and thus it contributes to improving the efficiency of textile in reinforcing as well. BF reinforced geopolymer composites showed beneficial improvement in terms of flexural strength and the growing fiber content yielded the higher flexural strength when compared to geopolymer composites without addition BF. The bearing capacity of textile reinforced specimens improved gradually with increasing content of BF. The average ultimate strength of specimens without addition BF is 21.59 MPa. The average ultimate strength of specimens with 3%, 5%, and 7.5% of addition BF increased by approximately 23.76%, 38.90%, and 58.59%, respectively, compared to specimens without addition BF (see in **Figure 4a**). Moreover, the flexural toughness of the specimens increases with increasing content of BF (see in **Figure 4b**). The average flexural toughness of specimens without BF addition is 21.03 kN.mm. The average flexural toughness of specimens with 3%, 5%, and 7.5% of addition BF increased by 12.89%, 32.81%, and 73.04%, respectively, compared to specimens without addition BF. Toughness is the ability of a material, which indicates how much energy it can absorb before rupturing. Toughness (energy absorption) is calculated as the area under the respective load-deflection curves up to peak load of each specimen.

Figure 5 displayed the failure modes of several thin plate specimens, which represented for the common failure modes of all the thin plate specimens after finishing bending test. **Figure 5a** showed the failure mode of specimens reinforced with one textile layer and without addition of BF. When these specimens failed, the bottom of specimens was broken and debonding along the matrix-textile interface did occur. As the applied load continue to increase, the interfacial debonding increased followed by collapse of geopolymer matrix. On the contrary, specimens with addition of 7.5% BF, matrix-textile interfacial debonding did not occur, as seen clearly in **Figure 5b**. Failure mode of these specimens resulted in flexural failure by slipping of textile yarn in geopolymer matrix.

4. Conclusions

The flexural behavior of one-layer textile reinforced geopolymer thin plates containing various contents of BF was investigated and tested. The attained results from experiment show that the addition of BF reinforced geopolymer mortar is helpful to improve both the first-crack load, the ultimate load, and flexural toughness of textile reinforced geopolymer specimens. By visual observation of the specimens during the bending test, they indicated the different failure behaviors. The specimens without BF or with low content of BF exhibited the similar failure by debonding along the matrix-textile interface, whereas the specimens with high content of BF resulted in bending failure by slipping of textile yarn in matrix.

ACKNOWLEDGEMENTS

This publication was written at the Technical University of Liberec, Faculty of Mechanical Engineering with the support of the Institutional Endowment for the Long Term Conceptual Development of Research Institutes, as provided by the Ministry of Education, Youth and Sports of the Czech Republic in the year 2018 and by the project „Application of geopolymer composites as fire, AGK“, registration number VI20172019055, were obtained through the financial support of the Ministry of interior in the program "The Safety Research of the Czech Republic" 2015-2020 (BV III/1-VS).

References

1. Subaer, Van Riessen A. Thermo-mechanical and microstructural characterisation of sodium-poly(sialate-siloxo) (Na-PSS) geopolymers. *J Mater Sci.* 2007;42(9):3117-3123. doi:10.1007/s10853-006-0522-9
2. Al Bakri AMM, Kamarudin H, Abdulkareem OAKA, Ruzaidi CM, Rafiza AR, Norazian MN. Optimization of Alkaline Activator/Fly ASH Ratio on the Compressive Strength of Manufacturing Fly ASH-BASED Geopolymer. *Appl Mech Mater.* 2011;110-116(November 2015):734-739. doi:10.4028/www.scientific.net/AMM.110-116.734
3. Saidi N, Samet B, Baklouti S. Effect of Composition on Structure and Mechanical Properties of Metakaolin Based PSS-Geopolymer. *Int J Mater Sci.* 2013;3(4):145. doi:10.14355/ijmsci.2013.0304.03
4. Rickard WDA, Temujin J, Van Riessen A. Thermal analysis of geopolymer pastes synthesised from five fly ashes of variable composition. *J Non Cryst Solids.* 2012;358(15):1830-1839. doi:10.1016/j.jnoncrysol.2012.05.032
5. Alomayri T, Shaikh FUA, Low IM. Mechanical and thermal properties of ambient cured cotton fabric-reinforced fly ash-based geopolymer composites. *Ceram Int.* 2014;40(9 PART A):14019-14028. doi:10.1016/j.ceramint.2014.05.128
6. Rickard WDA, Vickers L, van Riessen A. Performance of fibre reinforced, low density metakaolin geopolymers under simulated fire conditions. *Appl Clay Sci.* 2013;73(1):71-77. doi:10.1016/j.clay.2012.10.006
7. Mechtcherine V. Novel cement-based composites for the strengthening and repair of concrete structures. *Constr Build Mater.* 2013;41:365-373. doi:10.1016/j.conbuildmat.2012.11.117
8. Jabr A, El-Ragaby A, Ghrib F. Effect of the Fiber Type and Axial Stiffness of FRCC on the Flexural Strengthening of RC Beams. *Fibers.* 2017;5(1):2. doi:10.3390/fib5010002
9. Amran YHM, Rashid RSM, Hejazi F, Safiee NA, Ali AAA. Response of precast foamed concrete sandwich panels to flexural loading. *J Build Eng.* 2016;7:143-158. doi:10.1016/j.jobbe.2016.06.006
10. Atahan HN, Pekmezci BY, Tuncel Y. Behavior of PVA Fiber Reinforced Cementitious Composites Under Static and Impact Flexural Effects. *J Mater Civ Eng.* 2012;(October):120922005613009. doi:10.1061/(ASCE)MT.1943-5533.0000691
11. Williams Portal N, Flansbjerg M, Zandi K, Wlasak L, Malaga K. Bending behaviour of novel Textile Reinforced Concrete-foamed concrete (TRC-FC) sandwich elements. *Compos Struct.* 2017;177:104-118. doi:10.1016/j.compstruct.2017.06.051
12. Dey V, Zani G, Colombo M, Di Prisco M, Mobasher B. Flexural impact response of textile-reinforced aerated concrete sandwich panels. *Mater Des.* 2015;86:187-197. doi:10.1016/j.matdes.2015.07.004
13. Colombo IG, Colombo M, Di Prisco M. Bending behaviour of Textile Reinforced Concrete sandwich beams. *Constr Build Mater.* 2015;95:675-685. doi:10.1016/j.conbuildmat.2015.07.169
14. BS EN 196-1:2005. *Methods of testing cement – part 1: Determination of strength*

OIL-TREATED FIBROUS AIR FILTERS FOR AUTOMOTIVE ENGINE INTAKE APPLICATION

Ajay Kumar Maddineni and Dipayan Das*

Dept. of Textile Technology, Indian Institute of Technology Delhi, Hauz Khas, New Delhi-110016

*telephone: +91 11 26591402, E-mail: dipayan@textile.iitd.ac.in

Abstract:

This work deals with development, characterization and performance evaluation of oil-treated fibrous air filters for automotive engine intake application. According to the classical theory of air filtration, an air filter would exhibit higher filtration efficiency when tested at higher face velocity. This is however not found true in the current research work. Here, the filtration efficiency of a cellulosic filter media was found to decrease at higher face velocities for relatively large particles. This happened apparently due to particle bounce and re-entrainment phenomenon. Nevertheless, it poses a major challenge to achieve the futuristic target of filtration efficiency with ever-increasing trend of engine downsizing and less availability of installation space for automotive engine intake air filter media. Here it was demonstrated that the particle bounce could be suppressed by oil treatment to the filter media, as a result, the filtration efficiency of the oil-treated filter media increased at higher face velocities for large particles, unlike the untreated ones. This behavior was explained in the light of theoretical and empirical models of air filtration. In case of less oil loading, the initial pressure drop across the oil-treated filter media was found to be almost the same as that across the untreated one. But, when the oil loading was high, the initial pressure drop increased tremendously. This behavior was discussed with the help of Davies equation by taking into account of the changes in diameter of oil-coated fiber and packing density due to oil treatment. Further, at lower dust loading, the oil-treated filter media exhibited lower pressure drop and lower filtration efficiency at lower face velocities, but, at higher face velocities, the same media displayed higher filtration efficiency but with a similar pressure drop. However, at higher dust loading, the same media exhibited higher filtration efficiency.

Keywords:

Automotive engine intake air filtration, particle bounce and re-entrainment, oil-treated filter media, filtration efficiency, pressure drop, dust loading

1. Introduction

Engine intake air filters in automotive application were primarily used to remove the air borne dust particles to reduce the wear of moving components. Dust particles of 5-10 μm particles causes the major increase in wear over engine life time followed by 10 -20 μm [1]. Therefore, the automotive engine air filters are designed to reliably filter out those fractions of particles. Increasing emission regulations and the evolving requirements associated with engine durability, packaging environment, sophisticated engine technology, etc., are challenging the design of automotive air filter to efficiently capture the dust particles [2]. Wide variety of filter media such as polyurethane based reticulated foam, cellulose based wet laid paper, Polymer based nonwoven were popularly used in automotive industry. Among the said filter media technologies, standard cellulose-based paper filter media is well known in Asia due to its performance, cost and packaging benefits. Particle penetration of such filter media is influenced by various factors such as fiber diameter, packing parameters of the fibers that result in

wide pore sizes, operating conditions. A lot of efforts have been put in the past to optimize these filter media to reduce particle penetration. However, the velocity of the particles to which the media is exposed greatly affects the particle penetration. Reducing installation space in the vehicle for air filters now-a-days increases the flow velocities. It is known that with increasing flow velocity, filtration efficiency increases due to dominance of inertial impaction mechanism [3]. However the same is not true always. Increase in flow velocity increases the energy associated with the particle depending on mass-inertia relation that cause particle to bounce back and re-entrain into the fluid stream to escape through the media. This leads to an elevated risk to the engine components, associated with exposure to dust particles. These limitations are posing a challenge for the futuristic target of filtration efficiency and the air filter system design for automotive engine intake application. These new challenges motivated us to understand the particle penetration behavior of cellulosic filter media. Recently, limited studies showed the improvement of the filtration efficiency by treating the fibrous filter media with oil [4]. The present work made an attempt to investigate the impact of oil treatment on the filtration efficiency and pressure drop of automotive engine intake air filter media for different face velocities at the initial stage of filtration as well as during dust loading.

2. Materials and Methods

2.1. Materials

In this study, a commercially available cellulose based filter media was used. The average fiber diameter of such filter media observed under SEM was found as 23 μm with coefficient of variation of 34%. The thickness of the fabric was measured by a digital fabric thickness tester in accordance with ASTM D5729-97 standard. The average thickness of the fabric was obtained as 0.75 mm. The basis weight of the fabric was measured by using a weighing balance as per ASTM D 6242-98 standard. The average basis weight of the fabric was determined as 181 g/m^2 with a coefficient of variation of 1.73%. Hydraulic oil with density of 0.86 g/cm^3 and viscosity ranging from 25 cSt to 38 cSt at 40 °C temperature was used to treat the cellulose filter media.

2.2. Methods

The cellulosic filter media was treated with Hydraulic oil 32 using the in-house fabricated test setup as shown in Fig.1. The oil will be sprayed in the form of fine droplets onto the filter media, using an oil atomizer. Hydraulic oil is stored in the reservoir tank and is supplied to the spraying gun. The dry filter element is hold by a mounting plate at a distance of 0.45 m from the spray gun. The mounting plate moves in lateral direction of spray gun by means of slider and piston mechanism so as to spray oil onto the filter surface as uniformly as possible. The extra oil is collected in the tray below the fixture. Defined oil quantity on 100 cm^2 of filter area is applied on the raw gas side of the pleated filter media. Iterative measurement of weighting oil element after oil treatment is performed using a weighing balance to maintain proper quantity of oil. SEM image of oil distribution on the fibers of the filter media is shown in figure 3.

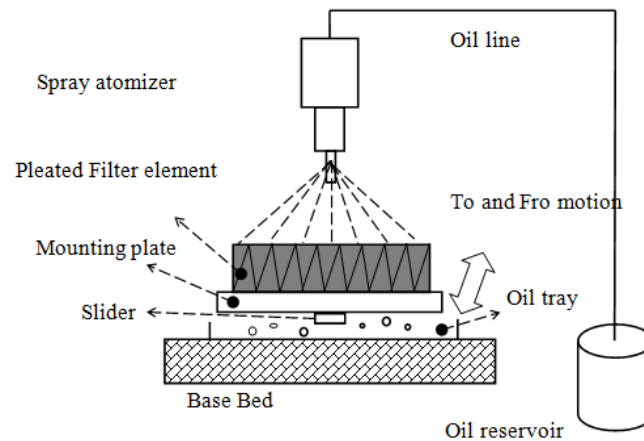


Figure 1. Chemical treatment setup

The oil treated as well as the non-treated filter media is challenged with ISO fine dust aerosol according to ISO 12103-1 was used for filtration efficiency measurements. The experimental setup for measurement of filtration efficiency is displayed in Fig.2. Test dust was dispersed by the powder dispersion generator with brush at a pressure of 2 bar. Aerosol spectrometer of Welas was used to measure particle distribution using light scattering technique. Test dust samples were attached to the particle analyzer using the iso-kinetic probe. Pressure drop was measured using the pressure taps placed across the filter media. Test dust of 0.2 g/m³ concentration was used in the current study. Particle measurements at higher concentration lead to false results. Continuous loading of the circular blank test samples using test dust and simultaneous measurement of pressure drop and particle size downstream was done.

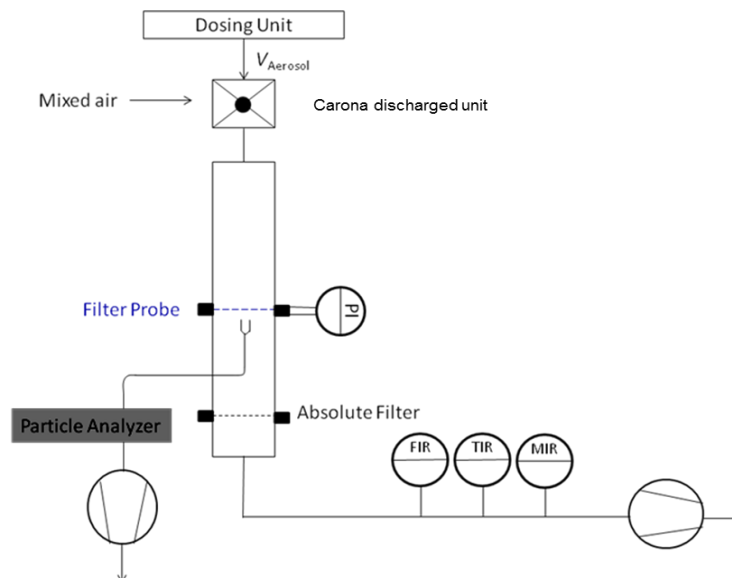


Figure 2. Experimental setup for filtration tests

3. Results and discussion

The effect of face velocity on the initial pressure drop of oil-treated and untreated filter media is displayed in Fig. 3. It can be observed that the untreated and the filter media treated with oil of 80 g/m² exhibited almost similar at all velocities tested. In contrary to this, the filter media treated with 240 g/m² oil displayed an increase of 5 to 9 times pressure drop as compared to the untreated filter media. This might be due to the fact that a higher quantity of oil deposited onto the filter media caused an increase of diameter of oil-coated fiber and a reduction in porosity that in turn resulted in increase of pressure drop across the media. In the following, an attempt was made to explain this scientifically using following expression [3, 5]

$$d_{f,o} = d_f \sqrt{\left(1 + \frac{W_o \rho_f}{W_f \rho_o}\right)} \quad (1)$$

$$\mu_{f,o} = \frac{W_f + W_o}{Z \left(\frac{g_f \rho_f + g_o \rho_o}{g_f + g_o} \right)} \quad (2)$$

$$\Delta P = \frac{64 \mu_{f,o}^{1.5} \left(1 + 56 \mu_{f,o}\right)^3 \nu U Z}{d_{f,o}^2} \quad (3)$$

where $d_{f,o}$ and d_f stand for the diameters of oil-coated and untreated fibers, respectively; W_o and W_f denote the weight of oil per unit area of the filter and weight per unit area of dry filter media, respectively; and ρ_f and ρ_o indicate the densities of fiber and oil, respectively. g_f and g_o are the mass proportions of fiber and oil, respectively, in the filter media and Z is the thickness of filter media. The diameter of oil-coated fiber and the packing density of oil-treated filter media could be substituted in the following Davies equation to determine the pressure-drop across the filter media. where ΔP denotes the pressure drop, ν indicates the viscosity of air, and U refers to the face velocity. It can be seen that the Davies equation using the diameter of oil-coated fiber and the packing density of the oil-treated filter media corresponded satisfactorily with the pressure drop data obtained experimentally.

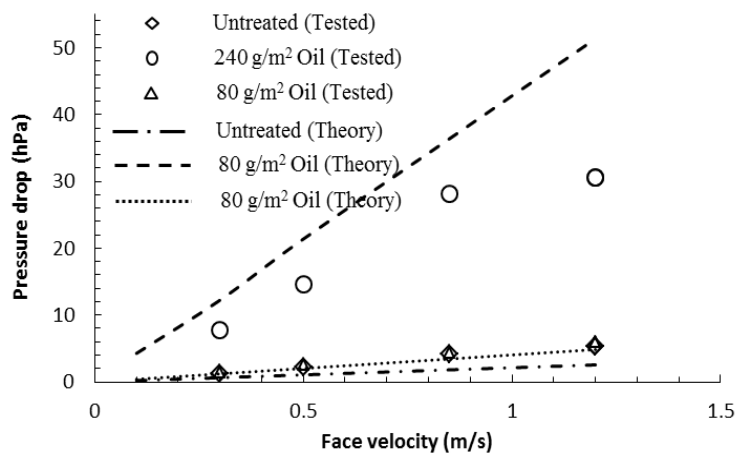


Figure 3. Initial pressure drop as a function of face velocity

Initial filtration efficiency of the untreated and oil-treated filter media at different velocities 0.1 m/s, 0.3 m/s, 0.5 m/s, 0.85 m/s and 1.2 m/s respectively were shown in Fig. 4. Particles beyond 0.5 μ m particle

size, the filtration efficiency increased with the increase of particle diameter as the interception and impaction mechanisms of particle capture were predominating. Filtration efficiency rose to higher than 99 % for larger particles and at the face velocity of 0.1 m/s. A similar trend was observed at a face velocity of 0.3 m/s. However, the efficiency of filtering large particles at a face velocity of 0.3 m/s was less than that at 0.1 m/s. At a face velocity of 0.5 m/s, the filtration efficiency rose to 97 % when the particle size was 4 μm , but decreased afterwards, however. A similar observation was found at a face velocity of 0.85 m/s velocity with significant decrease in filtration efficiency from 95 % to 89 % beyond the particle size of 2 μm . A further reduction in filtration efficiency was observed at 1.2 m/s when the particle size was 2 μm and beyond. It was therefore observed that the filtration efficiency decreased for larger particles at higher velocity. This finding contradicted the classical theory of air filtration. Probably, this unusual behavior was attributed to rebound of particles after colliding the filter surface and followed by subsequent re-entrainment of particles in the air streams at higher velocity. Fig. 4b displays the initial filtration efficiency of the oil-treated filter media with oil loading of 80 g/m². The oil-treated filter media with 80 g/m² oil loading did not show any particle bounce for all particle sizes, regardless of the face velocities chosen. As the oil droplets present on the surface of the filter media caused the particles to adhere to the oil-coated fiber, the oil-treated filter media did not show any reduction in filtration efficiency, especially at higher face velocities and at larger particle sizes. The measured filtration efficiency of the untreated and oil treated filter media was calculated using the theoretical relations of collection efficiency.

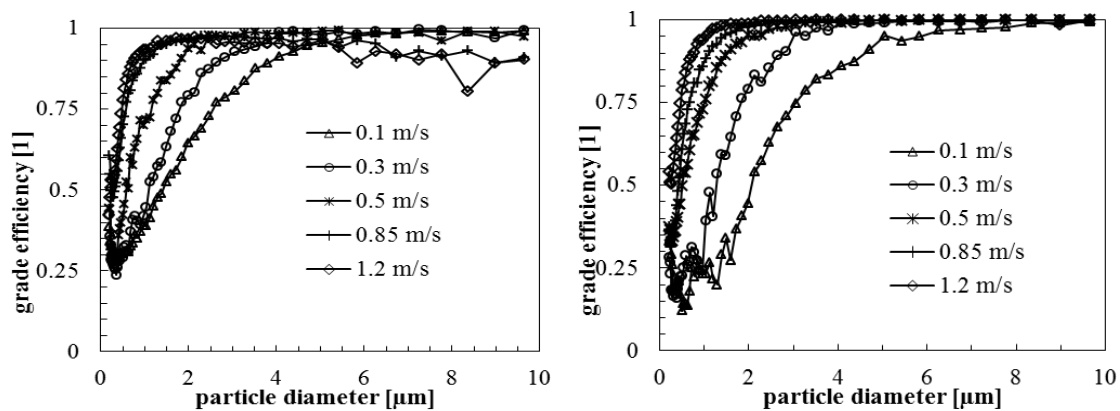


Figure 4. Measured grade efficiency at initial stage for untreated filter media (a) and oil-treated filter media with oil loading of 80 g/m² (b)

The pressure drop curves of untreated and oil-treated filter media during dust loading at face velocities of 0.3 m/s, and 1.2 m/s was shown in Fig.5. At a low level of face velocity, i.e., 0.3 m/s, the untreated media exhibited slow increase of pressure drop till 30 g/m² of dust collection and at the end it accumulated 145 g/m² of dust to reach a pressure drop of 30 mbar. At the same velocity, the oil-treated filter media displayed slow increase of pressure drop till 60 g/m² of dust accumulation, but at the end it accumulated 100 g/m² of dust to reach the pressure drop of 30 mbar. The initial slow increase of pressure drop across the oil-treated filter media was due to the combined effect of depth loading and oil loading. In this stage of dust loading, the pressure curve of oil-treated filter media lay at a significantly lower position than that of the untreated one. In case of oil-treated filter media, the dust particles adhered to the oil and formed dust islands that mobilized around the fiber with the oil, creating more pore space than the untreated one. But, as the oil droplets were saturated with dust particles, surface filtration started that increased the pressure drop suddenly with very little addition of dust particles. At a very high level of face velocity, i.e., 1.2 m/s, the oil-treated and the untreated filter media exhibited similar pressure drop characteristics till the surface filtration started. At higher velocities the aerodynamic drag was dominant due to the fact that the oil droplets were saturated with

the dust particles at a faster rate due to dominant inertial deposition and thus rate of pressure loss increased with dust loading.

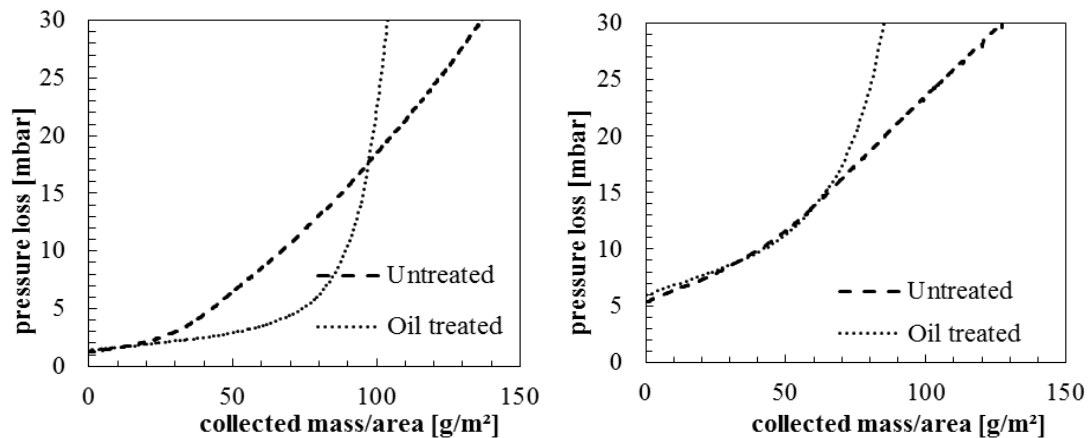


Figure 5. Evolution of pressure drop during dust loading at face velocities of 0.3 m/s (a), and 1.2 m/s (b)

The evolution of gravimetric filtration efficiency of untreated and oil-treated filter media at three different stages of dust loading was displayed at Fig.6. The untreated filter media showed filtration efficiency greater than 99 % at a dust loaded pressure drop of 10 hPa and the same was increased with increasing pressure drop from 10 hPa to 20 hPa at a velocity of 0.3 m/s (Figure 6a). This indicated that a dendritic growth of particles took place at the upstream side [6] and thus the increasing trend of particle capture is observed. The oil-treated filter media also exhibited increasing trend of filtration efficiency with increasing pressure drop from 10 hPa to 20 hPa. However, the oil-treated filter media displayed lower filtration efficiency than the untreated one at pressure drops of 10 hPa and 20 hPa. This behaviour was probably due to the fact that some of the dust particles were captured by the fibres and the rest were adhered to the oil-droplets, hence the dendritic growth was not significant at this stage of filtration. At a further higher level of dust loading (equivalent to 30 hPa pressure loss), the untreated media exhibited a drop in filtration efficiency due to increased local velocities within the filter that caused the particles getting more energy and were able to penetrate the filter media. While the oil-treated media displayed an increase in filtration efficiency with increasing dust loading. Interestingly, the oil-treated filter media showed higher filtration efficiency than the untreated media at a pressure drop of 30 hPa. This might be due to increased adhesion between particles and fibers. At 1.2 m/s face velocity, the oil-treated filter media exhibited an increasing trend of filtration efficiency as the pressure drop increased. The untreated filter media showed a drop in filtration efficiency as dust loading and face velocity increased, whereas the oil-treated media displayed an increase of filtration efficiency with the increase of dust loading and face velocity. The filtration efficiency of the oil-treated filter media was related to the loading of oil by dust particles. As the oil loading was higher the increase of filtration efficiency was lower. Interestingly, the filtration efficiency of the untreated media was higher than the oil-treated media at low levels of dust loading and at lower face velocity.

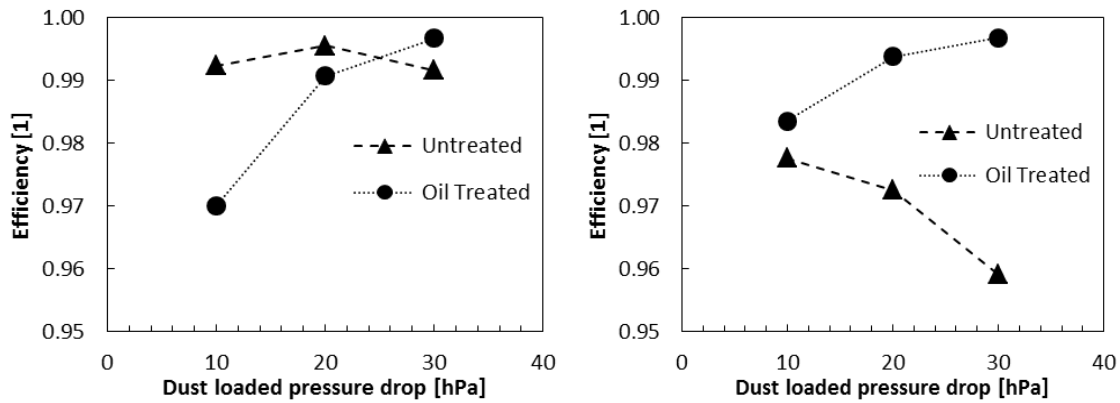


Figure 6. Evolution of filtration efficiency during dust loading at face velocities of 0.3 m/s (a), and 1.2 m/s (b)

4. CONCLUSIONS

Oil-treated and untreated cellulosic filter media were examined for pressure drop and particle filtration behaviors at the initial stage of filtration as well as during dust loading. The initial pressure drop across the oil-treated filter media was found to be almost the same as that of untreated media at a low level (80 g/m²) of oil loading. But, when the oil loading was increased to as high as 240 g/m², the pressure drop was 5 to 9 times higher, depending on the face velocity, than that of the untreated media. This behavior was explained in the light of Davies equation by taking into account of the change in diameter of oil-coated fiber as well as in packing density due to oil treatment. During initial stage of filtration, the untreated filter media displayed higher filtration efficiency at higher velocity for lower particle size, but the filtration efficiency decreased for large particle size as the face velocity increased. This was attributed to particle bounce and re-entrainment phenomenon and its effect was more at higher face velocity. This behavior was explained in the light of theoretical and empirical relations. Inhibition of particle bounce using oil spraying was found to be a suitable technique, as a result, the filtration efficiency of the oil-treated filter media increased at higher face velocities for large particles, unlike the untreated ones. At lower dust loading and lower face velocities, the oil-treated filter media exhibited lower pressure drop and lower filtration efficiency. However, at higher face velocities, the oil-treated filter media displayed higher filtration efficiency but with a similar pressure drop at lower dust loading. Nevertheless, the same media exhibited higher filtration efficiency at higher dust loading.

ACKNOWLEDGEMENTS

The financial support received from Science and Engineering Research Board of Department of Science and Technology, Govt. of India under project number SB/S3/ME/063/2015 for carrying out this work is gratefully acknowledged.

References

1. Mollenhauer, K., Tschoeke, H. (Eds.), *Handbook of Diesel Engines*, Springer, 2010.
2. Maddineni, A. K., Das, D., and Damodaran, R. (2016), *Experimental and Numerical Study on Automotive Pleated Air Filters*, SAE Technical Paper 2016-28-0100.
3. Brown, R. C (1993)., *Air filtration: an integrated approach to the theory and applications of fibrous filters*, Pergoman press, Oxford.
4. Müller, T. K., Meyer, J., Thebault, E., Kasper, G., *Impact of an oil coating on particle deposition and dust holding capacity of fibrous filters*, *Powder Technol.*, 253 (2014) 247-255.
5. Agranovski, I., (ed.) (2010), *Aerosol- Science and Technology*, Wiley (Germany).
6. Oh, Y. W., Jeon, K. J., Jung, A. I., Jung, Y. W. (2002), *A simulation study on the collection of submicron particles in a unipolar charged fibre*, *Aerosol Sci. and Technol.*, 36, 573-582.

DEVELOPMENT AND CHARACTERISATION OF NONWOVEN FABRICS FOR APPAREL APPLICATIONS

M.S. Cheema¹, T. H. Shah², S. C. Anand³

^{1,3}Institute of Materials Research and Innovation (IMRI), University of Bolton, Deane Road, Bolton BL3 5AB, United Kingdom, ²National Textile University, Pakistan
e-mail: chscheema@gmail.com

Abstract:

The cost of making apparel fabrics for garment manufacturing is very high because of their conventional manufacturing processes and new methods/processes are being constantly developed for making fabrics by unconventional methods. With the advancements in technology and the availability of the innovative fibres, durable nonwoven fabrics by using the hydroentanglement process that can compete with the woven fabrics in terms of their aesthetic and tensile properties are being developed. In the work reported here, the hydroentangled nonwoven fabrics were developed through a hybrid nonwoven manufacturing processes by using fibrillated Tencel® and bi-component (sheath/core) polyethylene/polyester (PE/PET) fibres, in which the initial nonwoven fabrics were prepared by the needle-punching method followed by hydroentanglement process carried out at optimal pressures of 50 to 250bars. The prepared fabrics were characterised according to the British Standards (BS 3356:1990, BS 9237:1995, BS 13934-1:1999) and the attained results were compared with those for a standard plain-weave cotton, polyester woven fabric and commercially available nonwoven fabric (Evolon®). The developed hydroentangled fabrics showed better drape properties owing to their flexural rigidity of 252 mg.cm in the MD, while the corresponding commercial hydroentangled fabric displayed a value of 1340 mg.cm in the MD. Tensile strength of the developed hydroentangled fabrics showed an approximately 200% increase than the commercial hydroentangled fabrics. Similarly, the developed hydroentangled fabrics showed higher properties in term of air permeability, such as the developed hydroentangled fabric exhibited 448 mm/sec and Evolon fabric exhibited 69 mm/sec at 100 Pa pressure. Thus for apparel fabrics, the work combining the existing methods of nonwoven production, provides additional benefits in terms of cost, time and also helps in reducing the carbon footprint for the apparel fabric manufacture.

Keywords:

hydroentanglement; nonwoven apparel; durable nonwovens; Tencel®; Evolon®

1. Introduction

Traditionally, it is being assumed that garments are made through woven and knitted fabrics. Because of their acceptable aesthetical and mechanical properties, these conventional methods of making fabrics for garments, captured a big market. From the literature review, it was found that there was very limited penetration of nonwoven fabrics in outerwear owing to their inherent limitations in term of strength, appearance and workability. In 1960, for the first time nonwoven fabric was developed as an outer wear, but could not succeed came as outer fabric but could not success because of its limitations. Nonwoven fabrics are thus being used as supporting materials in garment manufacturing industry, such as garment lining, insulation, and fusing etc. Recently, there has been a great deal of interest in the area of research and innovation activities in nonwoven fabrics for apparel applications, such as Evolon (Evolon.com) and Miratech. Traditionally, it was assumed that nonwoven fabrics can only perform in wipes, scaffolds, geo textiles, filters and disposable articles (Luki, 2004) and only 1 percent of nonwoven fabrics are utilised in apparel sector (Lee, 2006). Now, because of the new

advancements in the nonwoven technologies, especially in the hydroentanglement process, the applications of hydroentangled nonwoven fabrics have diversified into many fields and apparel fabrics application is one of them. The key area of research is to develop the nonwoven fabrics that can withstand the external forces in the use and provide comfort to the wearer in terms of softness, moisture management, appearance and also exhibit enough strength that can withstand the laundry process (Vaibhav, 2012) etc.

Nonwoven fabrics are made directly from the fibres without making any yarn and without the use of weaving or knitting processes. A nonwoven fabric is defined by INDA as follows: "Sheet or web structure bonded together by entangling fibres or filament, by various mechanical, thermal and/or chemical processes. These are made directly from the separate fibres or from molten plastic or plastic film". The unique advantage of the nonwoven fabric manufacture is that it is a continuously linked process, in which at the first stage raw materials (fibres) are converted into webs via the carding process and at the second stage these fibrous webs are bonded into finished products. The first nonwoven apparel fabric was the disposable paper clothing that was launched in early 1966 by an American company Scott Paper, however, the fabric could not capture any significant part of the apparel market because of its ill fit and uncomfortable nature. In the same era, Mars Manufacturing Company invented different types of nonwoven dresses that were used as evening wear and wedding gowns. However, these all-paper-clothing were short-lived and became obsolete in 1968 (Andrew, 2008). The breakthrough in the nonwoven apparel fabrics came in 1970, when DuPont invented the hydroentanglement technique for the nonwoven fabrics, known as spunlace technology (Andrew, 2008). This new technique gave a competitive edge to nonwovens, as the nonwoven fabrics produced by the hydroentanglement process possessed much superior aesthetical properties than the conventional nonwovens. The company also developed the foam bonded spunlaced fabric (polyester spunlaced fabric), wherein 30% soft acrylic latex was used to strengthen the spunlaced fabric that withstood five laundering cycles (Zheng, 2003).

In this study, functional hydroentangled fabrics have been developed through a hybrid process of needling and hydroentanglement, by utilising innovative Tencel and bi-component sheath/core (PE/PET) staple fibres. The resultant fabrics, when compared against the industry standard commercially available Evolon® and woven plain-weave cotton/polyester fabric exhibited acceptable test values related to the aesthetical and mechanical properties of the garments such as flexural rigidity, air permeability and tensile strength etc. The resultant fabrics can be used in different applications such as in the hospital for patients' uniforms. Owing to its comfortability, it can be used in the processing industry as uniforms such as in the meat industry, printing industry and in the chemical industry. Further research work is being carried out in order to enhance the quality of the fabrics especially in relation to laundering and washing.

2. Experimental

2.1. Materials

The fabrics were produced in collaboration with the Nonwovens Research Institute, University of Leeds by utilising two different types of fibres: Tencel® and bi-component sheath/core (PE/PET) staple fibres. Tencel® fibres were 1.4 dtex, 38mm in length with a smooth surface, while the PE/PET bi-component fibres were 2.2 dtex and 40mm in length with a crimped surface. The required amount of each fibre was separately weighed and initially hand blended in preparation of the next process. These hand-mixed fibres were manually opened into small tufts and further mixed in order to obtain a smooth web. After manually opening the fibres, the fibres were then carded through the pilot carding machine and a parallel-laid web produced was used in the next process. Before going into the hydroentanglement process, the carded web was lightly needled by using 8mm penetration and 100 strokes per min, after which the needled substrate was rolled and packed for the next process of hydroentanglement.

2.2. Hydroentanglement process

The needled fibrous webs were uniformly hydroentangled by using pilot hydroentanglement system, as illustrated in Figure 1.

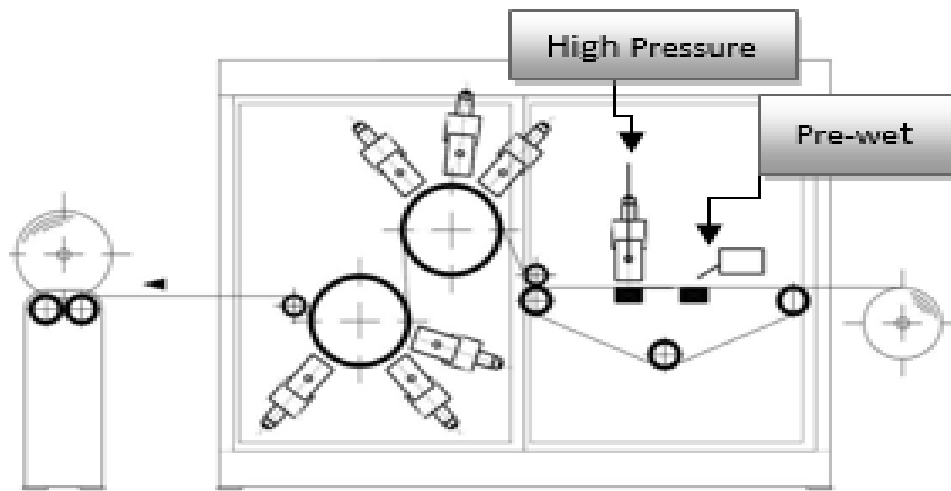


Figure 1. Action View of Hydroentanglement Process

Before going under the high pressure area of the hydroentanglement process, the fibrous web was pre-wetted to minimise the dispersion ratio of the fibres in high pressure zone. After pre-wetting, the material is passed through the high water pressure jet head for bonding of the fibres as shown in Figure 1. The Fabrics were prepared at varying hydroentanglement pressures of 100 and 125 bars with two passes, at the line speed of 3m/min. The orifice of jet strip was 150 μ m and the density of the jet orifice was 5.56/cm. All the fabrics were manufactured from the same web with 120 \pm 5 gm⁻² nominal weight. It was observed that for these specific blends, at lower pressures (50-75 bars), the fibres were not consolidated to the required level, which negatively affected the mechanical properties by reducing the tensile strength of the obtained fabric. On the other hand, at higher pressures (150-250 bars), the fibres were easily dispersed and consequently very limited number of fibres per unit area of the fabric was observed, which reduced the GSM as well as the tensile properties to below the acceptable values. The two hydroentangled nonwoven fabrics denoted as fabric 1 and fabric 2, were prepared at 100 and 125 bars, respectively, at the same constituent levels of 70% Tencel and 30% PE/PET bicomponent fibres. The properties of developed fabrics are shown in Table 1.

Table 1. Details & characteristics of the hydroentangled nonwoven fabrics prepared in this study

Fabric Number	Hydroentanglement Pressure (bars)	Contents	Area Density (gm ⁻²)	Thickness (mm)	Bulk Density (gcm ⁻³)
Fabric 1	100	Tencel (70%) and Sheath core PE/PET (30%)	150 \pm 2.5	0.99 \pm 0.05	0.15 \pm 0.01
Fabric 2	125	Tencel (70%) and Sheath core PE/PET (30%)	145 \pm 2.5	0.88 \pm 0.05	0.17 \pm 0.01

2.3. Mechanical and aesthetical testing

The prepared fabrics were tested according to the British Standards (BS 3356: 1990, BS 9073-6: 2003, BS 13934-1: 1999) in order to determine their mechanical and aesthetical properties. For

flexural rigidity, Shirley flexometer apparatus was used, where a 25 ± 1 mm x 100 ± 1 mm strips were cut and the flexural rigidity values were determined according to the standard procedures. The tensile tests were performed by the Instron apparatus according to the appropriate standard methods. The cross-head speed was $200 \text{ mm} \pm 1 / \text{min}$ and the fabric size was 200 ± 1 x 50 ± 1 mm. Three specimens of each fabric were tested. The wicking test was performed by strip test method and absorption test was carried out by dipping (10 cm x 10 cm) fabric specimens into water for 20 min at 20°C and 65 ± 2 relative humidity.

The results obtained were then compared with the commercially available nonwoven fabric “Evolon” and with the reference fabric of a plain weave of woven fabric to ascertain the suitability of our developed fabrics for use as apparel fabrics.

3. Results and discussion

3.1. Dimensional properties

The results presented in Figure 2 show that fabrics 1 and 2, produced at 100 and 125 bars hydro pressure had thickness values of 0.99 ± 0.05 mm and 0.88 ± 0.05 mm, respectively. This indicates that when the hydroentanglement pressure was increased, a small reduction in the fabric thickness was observed due to a higher compaction and alignment of the fibres, which is expected to influence the tensile properties and bending rigidity of the produced fabric. In a study by Zheng et al (2003), it was shown that by increasing the specific energy (hydro pressure), the fabric area density decreased due to the fabric stretching caused by the impact of the water jets.

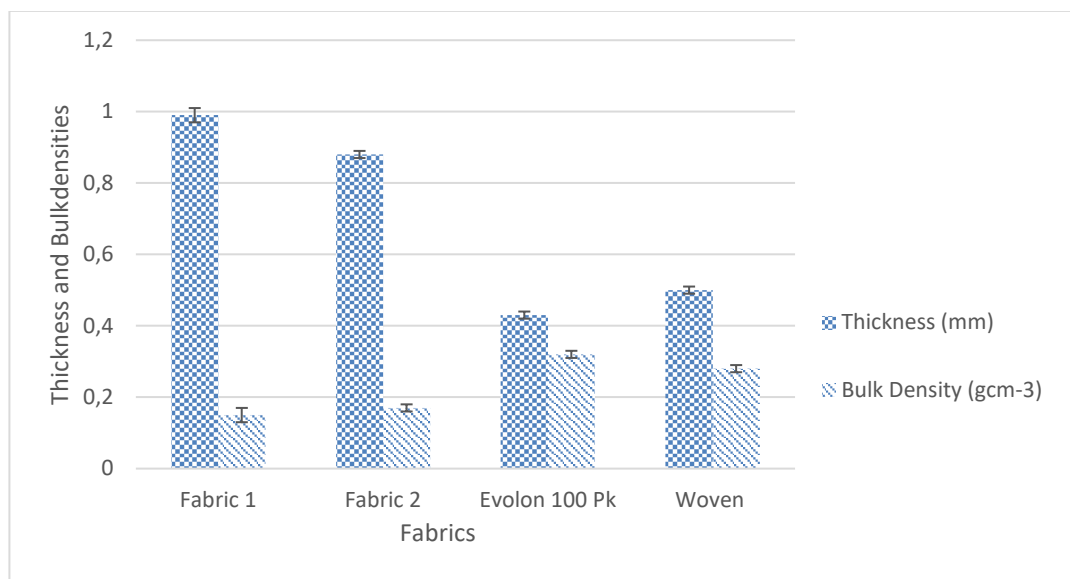


Figure 2. Thickness and Bulk density of developed fabrics 1 (100 bars) and 2 (125 bars)

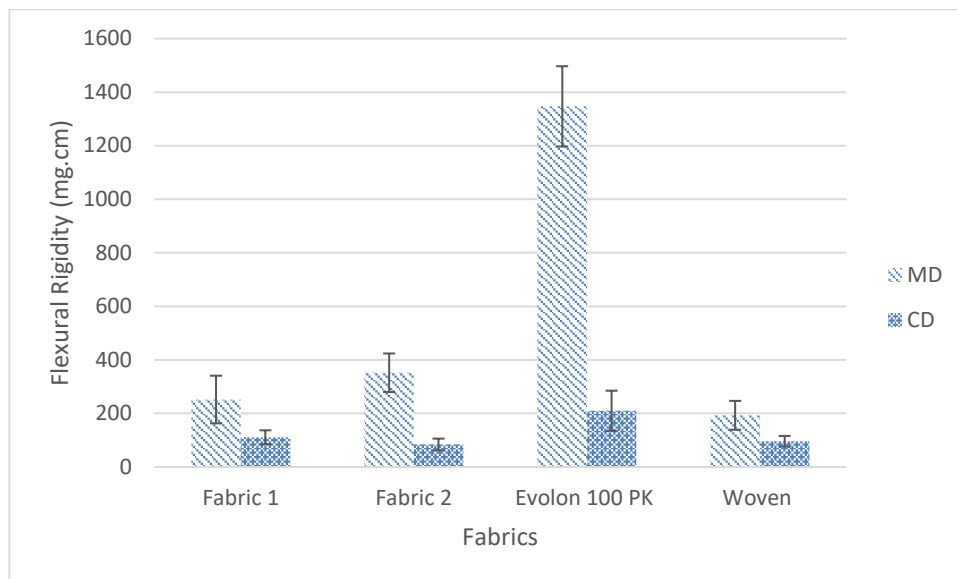
Moreover, it was observed that both the fabrics exhibited almost very similar bulk density values, which is an indication that the number of fibres per unit area in these fabrics were similar to each other. When compared to the values for the commercial nonwoven fabric and a typical woven fabric, these comparative results clearly show that the dimensional properties such as thicknesses of the hydroentangled nonwoven fabrics (1 and 2) were higher, because fabric 1 exhibited 0.99 ± 0.05 mm and fabric 2 exhibited 0.88 ± 0.05 mm thickness and Evolon and woven fabrics showed 0.43 and 0.50 mm thickness values respectively. The bulk densities of both fabrics were lower than Evolon® and woven fabrics. Woven and Evolon fabrics' higher bulk density values were because of their compact structures as shown in table 2.

Table 2. Details of reference fabrics

Fabrics	Processes	Contents	Area Density (gm ⁻²)	Thickness (mm)	Bulk Density (gcm ⁻³)
Evolon®	Hydroentanglement	PET and PA	140	0.43	0.32
Woven	Plain weave	Cotton and PET	144	0.50	0.29

3.2. Flexural rigidity

The flexural rigidity of the fabrics is a pivotal property for apparel applications. The fabric stiffness is related to its inherent properties, such as fibre material and the structure itself of the fabric (Mehmet, 2008). The flexural rigidity results in the machine (MD) and cross (CD) directions for the fabrics produced during this research are presented in Figure 3.


Figure 3. Flexural Rigidity comparison of developed fabrics 1 and 2 with Evolon 100PK and Woven fabric

It was observed that the flexural rigidity values for the nonwoven fabrics prepared in this study were much lower than the commercial nonwoven fabrics (Evolon®) in both the MD and CD. Furthermore, these values were very similar to those observed for the woven fabric (Figure 4). These results clearly show that the flexural behaviour of fabrics 1 and 2 was very similar to that of the woven fabric and it can be further enhanced through the finishing processes.

The bending rigidity of the fabrics depends on the movement of the fibres within the fabric structure. It seems that the Evolon fabrics exhibit higher bending rigidity as the fibres are highly intertwined with its neighbouring fibres due to the nature of the spun-laid process and the inherent fine filaments of the bi-component PA6/PET “island in the sea” filament structure. Additionally, due to the high hydroentanglement pressure, the fine filaments form a tight structure with little or no space for fibre movement to occur within the fabric. On the other hand, the prepared fabrics showed lower flexural rigidity as compared to the commercial nonwoven fabric due to the more open structure of these experimental nonwoven fabrics. In their study, Smith et al (2003) have reported that if the fibres are able to act independently in the fabric structure, a reduction in the flexural rigidity of the fabric is observed. Hence, it is evident that bending rigidity does not depend on the thickness of the fabric and rather is directly proportional to the movement of the fibres within the structure of the fabric. Evolon® exhibited higher flexural rigidity in both the machine and cross directions, even though it had a lower thickness value. On the other hand, the developed hydroentangled nonwoven fabrics exhibited lower flexural rigidity in the machine and cross directions, as compared with the Evolon, while showing

higher thickness values than the Evolon® fabric. Woven fabric had similar thickness as compared with the Evolon® but exhibited much lower values' of flexural rigidity in the machine and cross direction. Ancutiene et al (2010), found in their studies that the fabric structure has a more significant effect on the flexural rigidity of the fabric. Emin et al (2008) too have endorsed this principle that the fabric parameters affect the stiffness of the fabric.

Figure 4 represents the microscopic images of the three different types of fabrics studied during the course of the work.

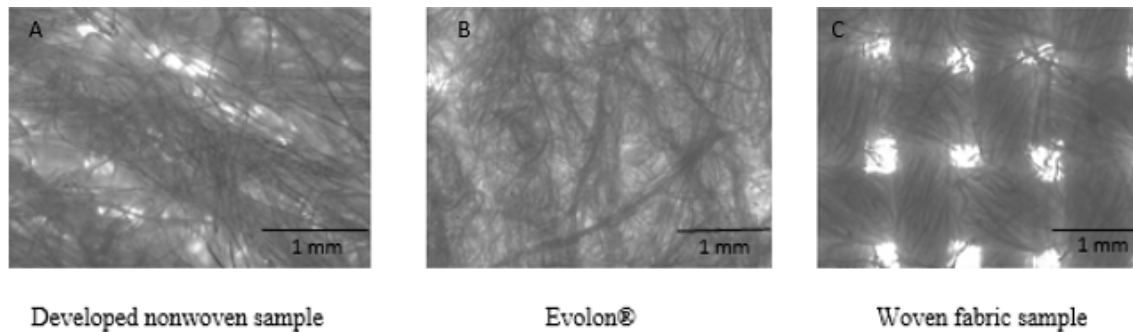


Figure 4. Microscopic Views of (a) developed hydroentangled, (b) Evolon® and (c) woven

These images show that the nonwoven fabrics developed in this study and the woven fabric have similar open structures and the fibres appear to be better aligned than the commercially available Evolon, wherein the fibres appear to be randomly placed. (Komori, 1997) found that the arrangement of the fibres in the fabric structure has a major influence on the mechanical properties of the fabric. Thus, the experimental nonwoven and woven fabrics exhibit similar flexural behaviour and have significantly lower flexural rigidity values as compared to the commercial nonwoven fabric. In the developed hydroentangled fabrics, the fibres are largely aligned in a single direction and the open spaces between the fibres can lead to the lowering of the flexural rigidity. Similar results have been obtained by (Bahari, 2015) and (Smith, 2003), wherein it was observed that the fibre's independent movement within the fabric structure led to a lower fabric flexural rigidity.

3.3. Absorption and wicking tests

The moisture transportation in a fabric determines its cooling effect and thus provides comfort to the wearer. The wear comfort of clothing is continually gaining importance owing to the consumer demand and therefore considerable efforts have been made to study the wicking characteristics of apparel fabrics (Berrfelder, 2013). During exercise or working conditions, the human body produces sweat and if it does not evaporate from the skin to the atmosphere, because of the clothing, then the wearer feels uncomfortable and this may give rise to a loss in working efficiency of the wearer. Therefore moisture management by the fabric is very important in order to optimise the wearer's comfort. The fibre types (natural or synthetic), blending ratio of fibres, the fabric structure and fabric characteristics (densities of yarns, thickness) etc. are the parameters that affect the moisture management and the thermal properties of the fabrics (Hassan, 2012).

The prepared nonwoven and woven fabrics were characterised for their absorption and wicking properties and the results are presented in Table 3 and illustrated in Figure 5.

Table 3. Absorption and wicking properties of nonwoven fabrics

Fabrics	Area Density gm ⁻²	Absorption gg ⁻¹	Wicking (g.cm)	
			MD	CD
Fabric 1	150	6.78	9.61	9.26
Fabric 2	145	4.96	12.44	8.21
Evolon®	140	0.7	1.4	0.6
Woven	144	1.5	1.4	0.6

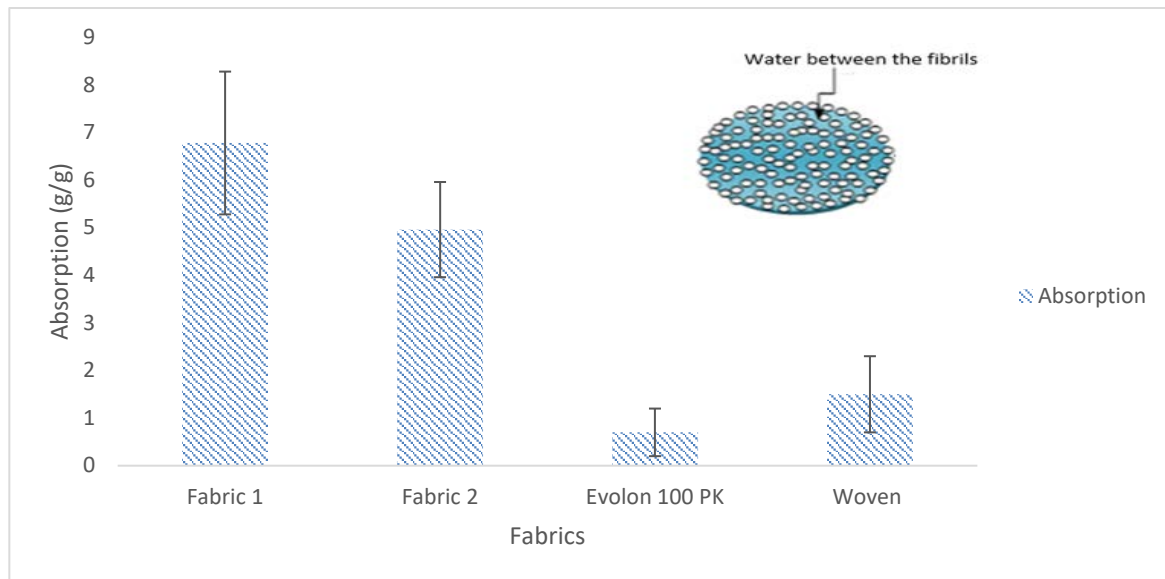


Figure 5. Absorption properties of nonwoven fabrics

The results show that the experimental fabrics 1 and 2 exhibit better absorption and wicking behaviour than Evolon 100PK and the woven fabric. The absorption value of fabric 1 was ~78% higher than the woven fabric and about 90% higher than Evolon® 100PK. Similarly, fabric 2 exhibited 70% and 86% higher absorption values than woven and Evolon® fabrics, respectively. This enhanced absorption is mainly due to the fact that the experimental nonwoven fabrics have a more porous structure and the fibres are well oriented within the fabric structure. Moreover, owing to the Tencel fibres' hygroscopic nature, it absorbs the water molecules readily, thus providing higher absorption values. Furthermore, the Tencel® fibres used have a higher wet and dry strength than the other cellulosic fibres, viscose fibres show 22-26 cN/tex tenacity in dry state and 10-15 cN/tex in wet state and on the other hand Tencel fibres show 34-38 cN/tex and 38-42 cN/tex in dry and wet states respectively and have higher moisture regain properties than the polyamide and polyester fibres used in the commercial nonwoven fabric (Evolon). Additionally, the fibril structure of Tencel fibres provides superior capillary action within the fabric structure (Firgo, 2006). Woven fabric displayed restricted absorption properties owing to its fabric structure, wherein, due to the high number of crimps per unit area, along with the highly twisted yarns, did not allow the fibres to act as capillaries, unlike the exhibited properties of the nonwoven fabrics.

The results presented in Table 3 also show that the wicking values obtained for fabrics 1 and 2 were considerably higher than the woven fabric and Evolon 100PK nonwoven fabrics, both in the MD and CD. The wicking properties mainly depend on the fibre fineness and the fabric structure. Fabric 1 and 2 showed 9.61 and 12.44 g.cm wicking values in MD where as Evolon and woven exhibited wicking values of 1.4 and 1.4 g.cm in MD. The higher wicking values of the developed fabrics were because of the Tencel fibres consist of countless hydrophilic and crystalline nano fibrils which act as tubes and absorb the water through the capillary action between the fibrils (Firgo, 2006). On the other hand, Evolon, composed of polyester and polyamide fibres, show lower absorption, as the synthetic fibres like polyester are hydrophobic in nature. The fibre orientation also contributes in the absorption values of the fabric, Miller, 2000 has studied the pore size effects on the capillary behaviour of the material. For the developed hydroentangled fabrics, the smaller pore size along with the higher capillary action from Tencel fibres led to the enhanced wicking properties, as compared to the other fabrics.

3.4. Tensile properties

The tensile properties of fabrics 1 and 2 in MD and CD are shown in Figure 6 (a, b), respectively.

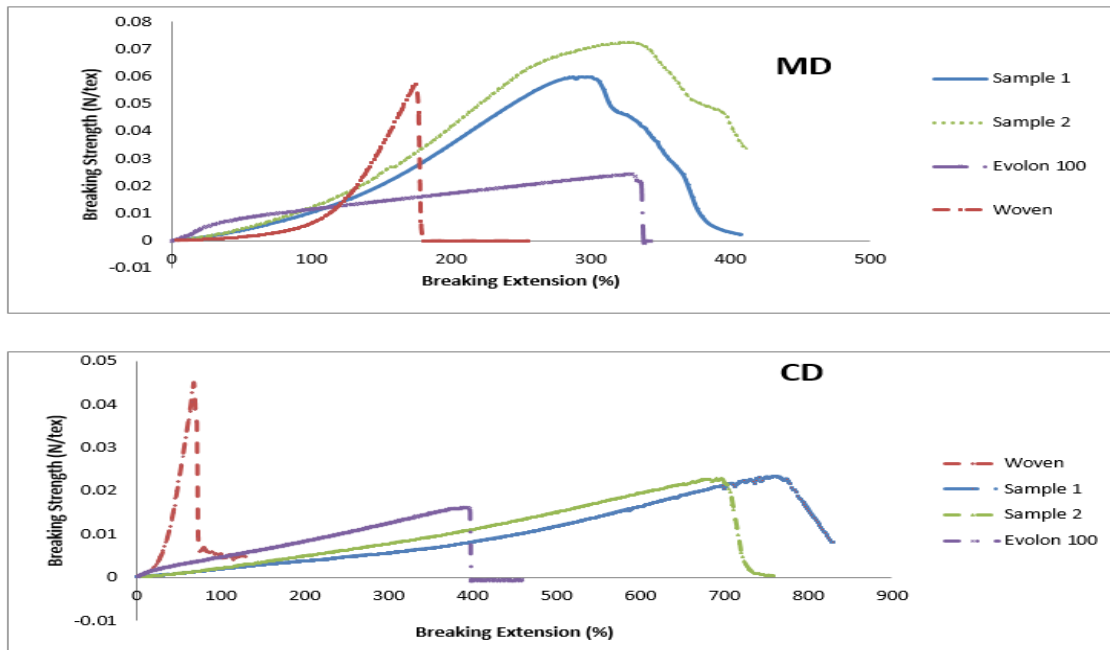


Figure 6. Tensile tests of nonwoven fabrics in MD and CD

The results show that the tensile strength of fabrics 1 and 2 are higher than the Evolon 100 PK and woven fabric in MD (Figure 6a). It also appears that the tensile behaviour of the fabrics 1 and 2 is significantly different from both the woven and the commercial nonwoven fabrics. As mentioned earlier, the developed fabrics were prepared at 100 and 125 bars, respectively. In their study Cannoly, 1993, have observed that an increase in the hydroentanglement pressure results in an increase in the tensile strength due to the higher degree of entanglement of the fibres. The tensile strength also depends on other factors, such as the fibre and web properties. As discussed previously by Ghassemieh, 2001, to prepare a hydroentangled fabric, a sufficient amount of energy is essential to get an optimal product with suitable dispersion and sufficient tensile strength, which itself depends on the web making parameters and fibre properties such as modulus, stiffness, length and friction between the fibres. Mao 2000, found in his research that less stiff fibres consumed less energy for attaining the maximum fibre entanglement within the fabric structure. Moreover, because of the staple fibres in the developed fabrics, during hydroentanglement process, more fibres were twisted around with surrounding fibres, because of the rebound of the water after hitting the plate underneath the web, resulted in intensive entangling behaviour of the fibres that caused the higher tensile strength of the developed fabrics as compared with other fabrics. The experimental nonwoven fabrics have breaking extension values that are similar to the Evolon fabrics, however their failure mechanism is quite different as these fabrics tend to yield before they fail. Due to its rigid structure, the woven fabric exhibited higher modulus and lower breaking extension values as compared to the nonwoven fabrics.

The tensile properties of the various fabrics in CD are illustrated in Figure 6b. The results show that the ultimate strength values of these experimental nonwovens are slightly lower than the woven fabric but higher than Evolon 100PK. The breaking extension values of all the nonwovens are in excess of 80% and these are considerably higher than the woven fabric. The Evolon fabric is composed of continuous filaments of bi-component Island in the sea that can impart higher strength to the fabric, whereas the woven fabric is composed of twisted yarns with a compact weave that give additional strength to the fabric. On the other hand, fabrics 1 and 2 are composed of fine staple fibres and the fibres were aligned in machine direction so because of less number of fibres in the cross direction region, the developed fabric exhibited lower tensile strength in CD. Evolon fabric is also based on synthetic fibres and is produced by using split able bi-component fibres which are finer in diameter than those used for preparation of the experimental fabrics and are therefore able to entangle more

intensely in the fabric structure and also the filaments were in different directions that caused higher tensile strength in CD than the developed fabrics as shown in Figure 7.

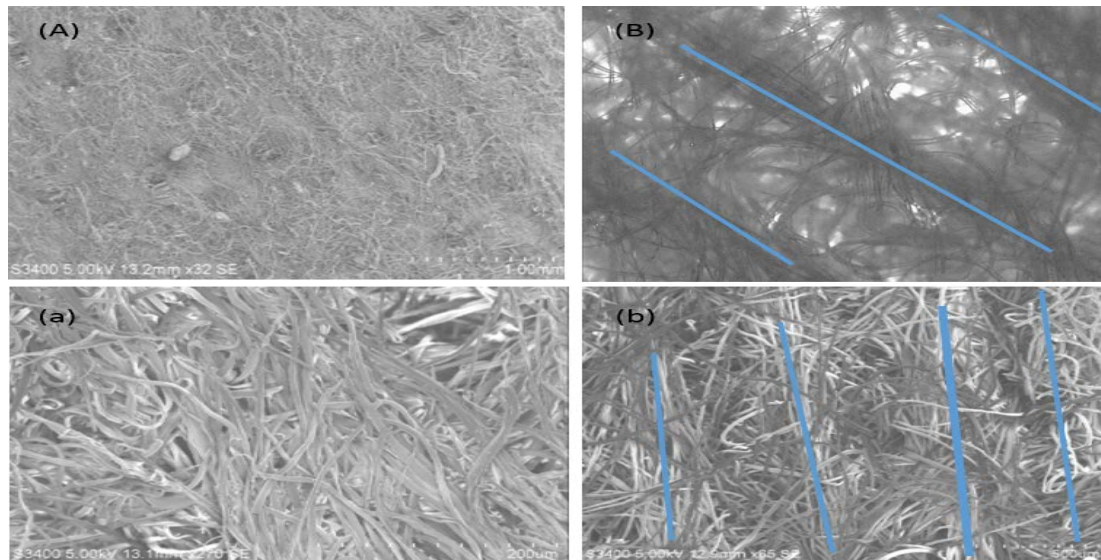


Figure 7. Optical and SEM views of Evolon 100 PK (A,a) and developed hydroentangled fabric (B,b)

4. CONCLUSIONS

In this study, an attempt has been made to develop nonwoven fabrics that are suitable for apparel applications. A hybrid nonwoven approach has been adopted where the fibres are first converted into a parallel-laid web followed by needlepunching of the web. The needlepunched fabric is then subjected to the hydroentanglement process at optimal values of 100 and 125 bars. The results demonstrate that the nonwoven fabrics produced in our study have superior moisture management properties such as developed fabric gave 6.78 g/g values of absorption and Evolon and woven gave 0.7 and 1.5 g/g, respectively. The bending flexural rigidity characteristics of the developed fabrics were also lower than the Evolon fabrics, wherein the developed fabrics exhibited 252 mg.cm in MD while the Evolon fabrics showed a value of 1347 mg.cm in MD. The tensile properties of the experimental nonwoven fabrics are higher than the commercially available nonwoven fabrics, especially the breaking extension values. The developed fabric exhibited a value of 0.07 N/tex in MD and Evolon exhibited value of 0.02 N/tex in MD. The tensile strength of the woven fabric is somewhat higher in CD than the nonwoven fabrics, but the bending rigidity values are very similar to the experimental nonwovens. The absorption and wicking properties of the developed fabrics were higher than the Evolon and woven fabric in both the machine and cross directions because of the hygroscopic and fibril structure of the Tencel fibres. The developed fabric exhibited an absorption value of 6.78 g/g and Evolon fabric exhibited 0.7 g/g absorption value. This prove that the developed fabrics quickly absorb the sweat from the body and because of their strong wicking action, the sweat disperses in the fabric structure that assists in the evaporation into the environment. The wicking values of developed fabric fabrics were 9.61 and 12.44 g.cm and the wicking values of Evolon and woven fabrics were 1.4 and 1.4 g.cm, respectively. It is strongly believed that with further optimisation of the hybrid process parameters and the fabric finishing techniques, nonwoven textile structures can be developed that are suitable for many apparel applications, including patients' uniforms, uniforms for processing industries, outer wear etc.

Acknowledgements

The authors wish to thank Dr S. Rathore at NRI, University of Leeds, for his help with the processing of experimental fabrics.

References

1. <https://store.extension.iastate.edu/Product/pm1663d-pdf>, Accessed on June. 2013.
2. www.Evolon.com
3. Russell S. J. (2007) , *Handbook of Nonwoven*, Woodhead Publishing Limited, Vol. 1, First edition, 286-287
4. Vaibhav K., Webster L., Govekar A., (2012): *Nonwoven in fashion apparel applications*, *International Journal of Fibre and Textile Research*, 2(2), 12-20
5. Shawver S. E., Collier L. W., Estey P.W., Paul S.C., (1997) *Elastic Breathable Barrier Fabric*, US Patent 5,695,849, Dec.
6. www.paperdressvintage.co.uk/livintage-boutique/history
7. Andrew D. H., (2008): *Colouration of Hydroentangled Nonwoven Fabrics*, Phd Theses, University of Leeds, 30
8. Zheng H., Seyam A. M., D. Stiffler, (2003) *The Impact of Input Energy on the Performance of Hydroentangled Nonwoven Fabrics*, INJ
9. Mehmet Y., Thomas H., Sabit A., (2008) *Influence of the fabric properties on fabric stiffness for the industrial fabrics*, *TEKSTIL ve KONFEKSIYON*, 4, 263-267
10. Smith K., Ogale A. A., Maugans R., Walsh L.K., Patel R. M., (2003) *Effect of bond roll pattern and temperature on the micro structure and properties of polyethylene nonwoven*, *Textile Res. J.* 70, 845-853,
11. Kristina A., Eugenija S., Anastasija N., (2010), *The Relationship between Fabrics Bending Rigidity Parameters Defined by KES-F and FAST Equipment*, *Materials Science*, 16, 346-352
12. Emin M., Howard T., Adanur S., (2008) *Influence of the Fabric Properties on Fbaric stiffness for the industrial fabrics*, *TEKSTIL ve KONFEKSIYON*, 4,263-267
13. Komori T., Itoh M., Takaku A., (1997), *Analysising the compressibility of a random fibre mass based on modified theory of fibre contact*, *Textile Res. J.*, 67, 204-210
14. Bahari N., Hasani H., Zarrebini M., Hassanzadeh S., (2015), *Investigating the effects of material and process variables on the mechanical properties of low-density thermally bonded nonwoven produced from estabragh (milkweed) natural fibers*, *Journal of Industrial Textiles*, 1-18
15. Birrfelder P., Dorrestijn, Roth C., (2013), *Effect of fibre count and knit structure on intra and inter-yarn transport of liquid water*, *Textile research Journal*, 83, 1477-1488
16. Hassan M., Qashqary K., Hassan H.A., Shady E., Alansary M., (2012) *Influence of Sportswear Fabric Properties on the Health and Performance of Athletes*, *FIBRES & TEXTILE in Eastern Europe*, 20, 82-88
17. Firgo H., Schustera K. C., Suchomela F., Männera J., Burrowa T., Abu-Rousb M., (2006), *THE FUNCTIONAL PROPERTIES OF TENCEL® - A CURRENT UPDATE*, *Lenzinger Berichte*, 85, 22-30
18. Miller B., (2000), *Critical Evaluation of Upward Wicking Tests*, *International Nonwoven Journal*, 9
19. Connolly T.J., Parent L.R., (1993) *Influence of specific energy on the properties of hydroentangled nonwoven fabrics*, *Tappi Journal*, 76,135-141
20. Ghassemieh E., Acar M., Versteeg K., (2001), *Improvement of the efficiency of energy transfer in the hydroentanglement process*, *Compos. Sci. Technology*, 62, 1681-1694
21. Lee H. J., Cassill N., (2006): *Analysis of World Nonwoven Market*, *Journal of Textile and Apparel, Technology and Management*, 5.10-18
22. Luki S., Jovani P., (2004), *Structural analysis of abrasive composite material with nonwoven textile matrix*. *Material Letters*, 58, 439-443
23. Mao N., (2000) *effect of fabric structure on the liquid transport characteristics of nonwoven wound dressing*, PhD thesis, University of Leeds, UK.

VARIATION BRAIDING TECHNOLOGY BY THE EXAMPLE OF NOVEL STENT STRUCTURES

Marielies Becker¹, Frank Ficker², Roxana Miksch³

¹Fraunhofer Application Center for Textile Fiber Ceramics TFK, Kulmbacher Straße 76, 95213

Münchberg, Germany, 0049 9281 409-8612, marielies.becker@isc.fraunhofer.de

²Institute for Material Sciences at Hof University, Kulmbacher Straße 76, 95213 Münchberg, 0049

9281 409-4540, frank.ficker@hof-university.de

Institute for Material Sciences at Hof University, Kulmbacher Straße 76, 95213 Münchberg, 0049 9281

409-8616, roxana.miksch@hof-university.de

Abstract:

Coronary stents are commercially available in many different types and are already successfully used. In case of a stenosis in a bifurcated coronary region, the otherwise usually uncomplicated and safe treatment still causes some problems.

In the introduced research project different tubular and bifurcated stent structures have been implemented, using a variation braiding machine, which enables the fully automatic production of complex, if required bifurcated braided structures.

Additionally an implanting concept for bifurcated areas has been devised to enable a safe and quick interventional therapy.

Key words:

Braiding, Stents, Bifurcations, Complex tubular structures, Shape memory

1. Introduction

Technical textiles become more and more important in a wide range of medical applications. From well known simple bandaging, and surgical sewing materials to complex high technical textile structures, which are necessary to construct functional artificial ligaments, tendons and cartilages.

A material construction based on textile technique is especially suitable for products, that require a high flexibility and at the same time a suitable amount of stability, such as needed for medical stents.

To re-open a morbid narrowed vessel, for a sufficient blood circulation, an interventional treatment is possible. In this case the vessel gets expanded and is additionally supported by an endoluminal vascular implant, a stent.

Coronary stents are commercially available in many different types and are already successfully used, but in case of a stenosis in a bifurcated coronary region, the otherwise usually uncomplicated and safe treatment still causes some problems.

To enable tailor-made solutions, the novel variation braiding technology has been used to develop new, innovative structures and bifurcations, which have the potential to improve the interventional results.

2. Experimental

2.1. Materials

Stents, especially for the coronary usage require a strong, but at the same time flexible and compressible material.

Nowadays there is a big variety of materials in use, from metal-alloys to bioresorbable polymers that dissolves after a certain time. In the here presented research project metal-alloys have been in the focus. Platinum/chromium alloy is a quite new, but already very important material for coronary stents. Caused by its high amount of platinum it is very tough and enables a delicate, but still stable stent construction, which reduces the occurrence frequency of restenosis, but at the same time requires high pressure while implanting the material into the vessel.

To increase the material flexibility the super elastic nickel/titanium alloy, so called Nitinol, has been selected for the here introduced research project. Nitinol is a popular material for a big number of different stent systems from several manufacturers, especially because of its shape memorizing effect and its super-elastic properties, combined with a good biocompatibility.

While most metallic alloys show a plastic deformation when compressed, Nitinol has the temperature-dependent ability to deform elastic and get back to its original shape, even after a significant deformation. This effect can be explained by different crystal structures in different temperature fields.

2.2. Methods

2.2.1. The variation braider

For the research activities a novel variation braiding machine has been used to develop various complex tubular structures. The braiding machine is constructed with 4x4 horn gears arranged in a square and a maximum of 32 carriers. To enable a high structural braiding flexibility the machine is equipped with 24 selectable pneumatic cross sections, 9 core yarn feeders and 16 filler yarn feeders.

With this technical features a fully automated pattern change and even the production of a bifurcation is possible without an interruption of the braiding process.



Figure 1. Variation braiding machine with selectable cross sections

2.2.2. Braiding of technical materials

The braiding of technical materials like metal or brittle fibers requires a couple of adjustments during the braiding process. The yarn feeding for example has to be as linear as possible to avoid material kinks and the carriers have to be overturned to eliminate material twists and so enable a uniform, intact braid. By using metallic wires in the production, increased abrasion of the corresponding machine parts might accrue. To reduce this effect, all yarn feeding elements have to be sufficiently adapted.

2.2.3. Pattern variations

The used braiding machine has diverse possibilities to create custom structures, which can vary in their pattern, density and overall structure. The technical possibilities enable the production of tubular-square- or flat braids, spiral braids, core/shell braids and combinations of all types. For stent structures different types of tubular braids and interlocking structures can be suitable.

By changing the design of the pattern cycle, carrier movement and the speed of the takedown-wheel, different material densities with varying supporting effects can be achieved. To make the technique even more multifarious, it is possible to bifurcate all types of braids and hereby be able to create stent solutions for complex human vessel architectures.



Figure 2. Multi-branched braids

3. Results and discussion

Based on the research of human anatomic tube structures and in collaboration with different surgeons, several concepts for customized self-expanding stents have been developed.

In a first step a number of braided tubular net structures have been designed. Caused by the different structures and densities, varying strong supportive effects have been achieved, which made it possible to reinforce different sectors in a disparate degree.

Enhancing these results, bifurcated structures as seen in figure 3 have been realized to produce a pattern, which might be suitable for bifurcated vessels. A simple bifurcated braided tube usually shows a varying density and even holes in the transition area. These unwanted effects reduce the supportive force in the affected area and might increase the risk of a re-stenosis. To avoid this problem an adjusted pattern has been developed, which creates a homogeneous structure, even in the transition area.

Beside the customized construction of a bifurcated braid, the possible difficulties during the implantation of such a complex stent system have been investigated. The longer the intervention takes to re-open a stenosed vessel, the higher the risk for the patient gets. This made it necessary to think about a suitable and fast implantation technique.



Figure 3. Example for a bifurcated braid

Following these requirements a Y-shaped bifurcated stent structure with one long main stent and a short side stent has been constructed.

Before implanting the stent, the manufactured short side arm can be pulled into the main arm, similar to a bud. Following, the stent gets compressed and implanted into the stenosed area in the vessel. There the stent expands and re-opens the main vessel. Finally the pulled-in side arm gets inflated, to open and support the crossover to the side vessel. To support the side vessel a second simple tube stent gets implanted through the already opened transition area. (See figure 4)

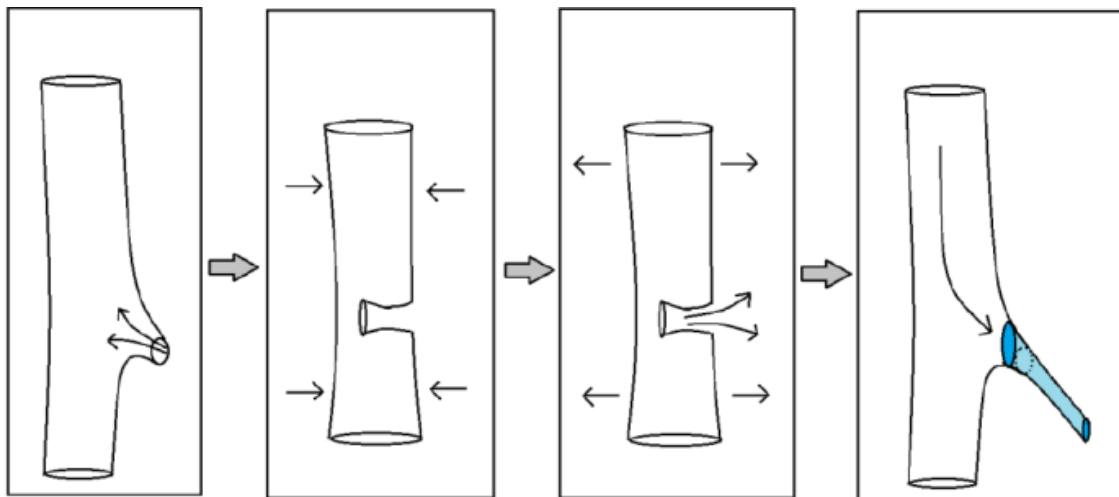


Figure 4. Concept for implantable bifurcated stent

This technique might be an applicable solution for complex stenosis, but has still to be tested conscientiously.

4. CONCLUSIONS

Variation braiding technology is highly innovative when it comes to flexible tubular structures. It offers the technical possibilities to create various different bifurcated forms and is so suitable for the development of complex stent structures. In combination with the use of the super elastic nickel/titanium alloy Nitinol, customizable stent solutions have the potential to generate new features for complex anatomical circumstances and should be followed up in future development projects.

References

1. E. S.-W. H. Wintermantel, *Medizintechnik Life Science Engineering*, 5. Hrsg., Berlin, Heidelberg: Springer-Verlag, 2009.
2. Statistisches Bundesamt, *Statistisches Jahrbuch, Deutschland und Internationales*, 2016 Hrsg., Wiesbaden: Statistisches Bundesamt, 2016.
3. F. v. Buuren, „25. Bericht über die Leistungszahlen der Herzkatheterlabore in der Bundesrepublik Deutschland,“ Springer Verlag, 2010.
4. M. Hoffmann, *Innere Medizin*, Stuttgart: Georg Thieme Verlag KG, 2009.
5. R. e. a. Erbel, *Herzkatheter-Manual, Diagnostik und interventionelle Therapie*, Köln: Deutscher Ärzte-Verlag, 2010.
6. K. Urban, *Materialwissenschaft und Werkstofftechnik, Ein Ritt auf der Rasierklinge*, Berlin, Heidelberg: Springer-verlag, 2015.
7. T. Keller, *Osseointegration einer mit Plasma-Immersionen-Ionen-Implantation behandelten Autokompressionsklammer aus Nitinol*, München: Technischen Universität München, 2004.
8. R. White und T. Fogarty, *Peripheral Endovascular Interventions*, 2 Hrsg., New York: Springer Science + Business Media, 1996.
9. T. Keller, *Osseointegration einer mit Plasma-Immersionen-Ionen-Implantation behandelten Autokompressionsklammer aus Nitinol*, München: Technischen Universität München, 2004. Book, personal author(s): Surname, N. N., Surname, N. (1996). Title of the work. (X ed.). Name of publisher (City).

ANALYSIS OF FORMATION OF MASS IRREGULARITY IN DRAFTING DEVICE DURING YARN SPINNING FROM SLIVER

Eva Moučková¹, Petr Ursíny¹, Petra Jirásková¹, Martin Janoušek²

¹ Technical University of Liberec, Faculty of Textile Engineering, Department of Technologies and Structures, Liberec, The Czech Republic, Studentská 2, 461 17. Phone: 485353274, eva.mouckova@tul.cz

² Rieter CZ s.r.o, Ústí nad Orlicí, The Czech Republic, Moravská 519, 562 01

Abstract:

This work deals with an analysis of formation of mass irregularity of fibrous product in a drafting arrangement of air-jet spinning machine. Sliver is supplied into the machine and attenuated in four-line double-apron drafting arrangements before formation into yarn. There, the total draft is realized within three zones: infeed draft, intermediate draft and main draft. In the work, the components of mass irregularity (limiting, systematic, additional and systematic developed from latent (immeasurable) irregularity), which form the structure of total mass irregularity of fiber strand in the output from the drafting unit, were defined. Transformation of mass irregularity of fibrous assembly by this drafting device was theoretically analyzed. The theoretical analysis of machine irregularity was realized too. Within the experiment, 100% Tencel yarns of count 23 tex were spun from the sliver of three various linear densities using the Rieter air-jet spinning machine J20. Three levels of intermediate draft ratio were also set. Proportionally to it, the level of main draft ratio was changed, while the both infeed draft ratio and other spinning parameters were kept constant. Sliver, and yarn mass irregularity as well as number of yarn faults were measured and analyzed, machine irregularity was calculated. The results showed that the lowest value of yarn mass irregularity is achieved when the sliver with higher linear density in combination with the lowest level of intermediate draft ratio (both from the observed range) is used for air-jet yarn production. It confirmed the theoretical analysis that draft ratios in infeed and intermediate drafting zone has more significant importance for air-jet yarn mass irregularity compared to the level of main draft ratio. Sliver mass irregularity is also very important factor for total yarn mass irregularity. Similar results were also recorded for number of yarn faults (especially for thin places (-40%)).

Key words:

Air-jet spinning, drafting, main draft ratio, intermediate draft ratio, yarn mass irregularity, components of yarn mass irregularity

1. Introduction

In the technology of staple spun yarn production, the draft is used for attenuation of supply fibrous product, fiber straightening and their aligning to a parallel position. The draft occurs usually in the drafting mechanism between pairs of roller, rotating at different speed. The principle of drawing is that fibers move relatively to each other to be distributed over a longer length of the product. It is generally known that drafting processes have significant effect on the yarn mass unevenness. Usually, higher draft ratio leads to higher total yarn irregularity, and number of faults. A lot of research papers deal with analyses of drafting process and with a study of effect of drafting of yarn mass irregularity. Authors predominantly study the movement of fibers in the drafting zone, for example, in works [1], [2], or analyze drafting forces, for example, in works [3] and [4]. The irregularity added by an apron drafting system on the ring spinning frame were studied in work [5]. During spinning from sliver, especially in the case of unconventional spinning systems such as a rotor spinning system, but also in the case of other spinning systems where a high-drafting device is used for given attenuation, it is

necessary to apply a high draft ratio. The air-jet spinning system belongs to them. The process of forming the yarn on the air-jet spinning system comprises attenuation of supply sliver by the draft in the four-roller drafting device equipped with two aprons in the main drafting zone. Consequently, thin fibers strand is transformed into the yarn by means of vortex air in the nozzle houses [6]. Thanks to it, air-jet yarns are featured by a different, specific structure (so called fasciated yarn). The yarn consists of a core where fibers are parallel and without any twist, and of wrapper fibers twisted around the core. Although there are many research works focused on the air-jet yarns, they primarily deal with the influence of technological variables on the properties of air-jet yarns produced on Murata Vortex Spinning Machine (MVS) (for example, [7-10]) or simulation of air flow field in the MVS nozzle chamber (for example, [11]). In the year 2009, Rieter company introduced also their air-jet spinning machine. It differs from the MVS by the machine concept, the nozzle geometry, and fiber guide in the front of spinning tip placed in the nozzle house. Except for several works dealing with prediction of air-jet yarn tenacity [12], properties of plied air-jet yarn [13] or numerical simulation [14], there is a lack of research work about Rieter air-jet spinning system today. The effect of draft ratio on the properties of vortex spun yarn was investigated only in work [10]. Authors measured mass irregularity of yarn (15 tex) made of 100% VS fibres using the Murata Vortex spinning system. They spun set of yarns from slivers of three counts using two levels of intermediate draft ratio (2.3 ; 2.5). During results analysis, the authors limit on a two-way analysis of variance, and statement that yarn samples spun with the lowest main draft ratio with highest used intermediate draft level achieved the worst irregularity. They concluded that it is a reason of out of optimum level of intermediate draft. However, for determination of the conditions ensuring optimal course of drafting process it is important to know the effect of the draft on the structure of mass unevenness. Therefore, the subject of our analysis is a high-drafting device (see Figure 1) used on the air-jet spinning machine. This device is characterized by three drafting zones that ensure the required total draft. Namely, it is a zone of infeed draft P_0 , a zone of intermediate draft P_1 , and a zone of main draft P_2 . The infeed drafting zone and intermediate drafting zone consists in drafting rollers whereas in the main drafting zone also a pair of aprons controls fibers. In our case, the infeed draft ratio is constant for given fibrous material, the intermediate draft as well as the main draft is changed according to the experiment. Because of this, we assume that finally the main drafting zone and intermediate drafting zone form the total yarn mass irregularity. These zones will be a subject of theoretical analysis in the terms of their influence on the total mass unevenness of air-jet yarn. The analysis will be carried out also experimentally. At the same time, more general piece of knowledge about transformation of mass irregularity of linear fibrous product exposed to drafting processes in the given drafting device will be applied.

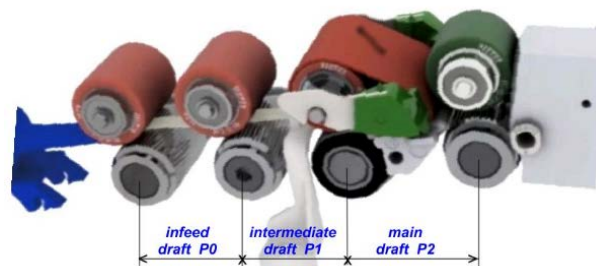


Figure 1. Scheme of drafting device of air-jet spinning machine (adapted and reproduced [17])

2. Theory of changes of mass irregularity due to draft

2.1. General rules

The analysis of mass irregularity formation is performed on the basis of the laws of variation phenomena in random process. The total variation in the mass of short lengths of final product in a

yarn manufacture can be regarded as the sum of the variations of individual components of mass irregularity (see equation (1)).

$$CV^2 = \sum_{i=1}^k CV_i^2 \quad (1)$$

Where CV_i is i -th component of yarn square mass irregularity. We consider following CV_i components [15], [16]:

CV_I - square limiting irregularity. It is determined by a random distribution of number of fibers in the sliver or yarn cross - sections. For better clarity, this component will be further referred as CV_{lim} .

CV_{II} - systematic square mass irregularity. It is caused by negative effects of technological stages before spinning system. For better clarity, this component will be further referred as CV_S . In the case of air jet spinning, CV_S includes also negative effect of infeed draft in the drafting arrangement of the air-jet spinning machine.

CV_{III} - additional square mass irregularity. It is induced only by the given technological stage (in our case by the spinning system). This component will be further referred as CV_P .

CV_{IV} - systematic square mass irregularity which is developed from a latent irregularity (immeasurable on very short lengths) due to drafting in given technological process (spinning). For better clarity, this component will be further referred as CV_{VS} .

We assume that the individual components of mass irregularity are mutually independent. As total variation in the mass of yarn short lengths we can use the parameter CV_m . It is a yarn total square mass irregularity obtained from Uster Tester and it will be further referred as CV_{yam} . In our analysis, we start from above-mentioned components of mass irregularity. We determine the structure of mass irregularity of product in the input to the system, and in the output from the system as well as resulting degree of mass irregularity using the effect of draft ratio and doubling (in general case) on the appropriate components of mass irregularity.

Transformation rules of mass irregularity

Let us consider a general spinning system characterized by a certain draft P and doubling D . Due to different causes of the formation of individual components of total mass irregularity, the following expressions can be made:

$$CV_2^2 = CV_{lim2}^2 + CV_{S2}^2 + CV_P^2 + CV_{VS}^2 \quad (2)$$

and

$$CV_0^2 = CV_{lim0}^2 + CV_{S0}^2 \quad (3)$$

where quantities indexed by 0 express corresponding components of mass irregularity of fibrous product in the input into the spinning system and quantities marked by index 2 express corresponding components of mass irregularity in the output from the system.

Using the general transformation rules for limiting CV_{lim} and systematic CV_S square mass irregularity [15], we can express resulting total square mass irregularity of linear staple-spun product CV_2 :

$$CV_2^2 = CV_{lim0}^2 \left(\frac{P}{D} \right) + \frac{CV_{S0}^2}{D} + CV_P^2 + CV_{VS}^2 \quad (4)$$

We can express the contribution of given drafting system to the total square mass irregularity of output product by so called machine irregularity ($CV_{machine}$):

$$CV_{machine}^2 = (CV_2^2 - CV_{lim2}^2) - (CV_0^2 - CV_{lim0}^2) \quad (5)$$

Using equation (4), we can also express the resulting total square mass irregularity of linear fibrous product on the output from the drafting device CV_2 as:

$$CV_2^2 = CV_{lim0}^2 \cdot P_c + CV_{S0}^2 + CV_P^2 + CV_{VS}^2 \quad (6)$$

where P_c is total draft, CV_p is additional square mass irregularity of fibrous product inducted in the drafting device and CV_{VS} is systematic square mass irregularity of fibrous product developed from latent irregularity by total draft in the drafting arrangements.

Substituting formulas (3) and (6) into the equation (5) we obtain:

$$CV_{machine}^2 = CV_P^2 + CV_{VS}^2 \quad (7)$$

From formula (7) it is evident that not only the additional irregularity, but also the systematic square mass irregularity developed from the latent irregularity of input product influences the level of irregularity which the spinning system inserts into the final product.

Because the draft ratio in the infeed drafting zone is constant for given fibrous material, we will follow up relations in intermediate and main drafting zones of the given drafting device. For the intermediate drafting zone we can write:

$$CV_{PS}^2 = CV_{lim1}^2 \cdot P1 + CV_{S1}^2 + CV_{P1}^2 + CV_{VS1}^2 \quad (8)$$

where CV_{PS} is total square mass irregularity of fibrous product after passing through the intermediate drafting zone; $P1$ means draft ratio in the intermediate drafting zone (intermediate draft ratio); CV_{lim1} is limiting square mass irregularity of fibrous product before entering into the intermediate drafting zone; CV_{S1} is systematic square mass irregularity of fibrous product before the intermediate drafting zone caused by both previous processes and infeed drafting zone; CV_{P1} is additional square mass irregularity caused by the intermediate drafting zone and CV_{VS1} is systematic square mass irregularity of fibrous product developed from the latent mass irregularity in the intermediate drafting zone.

For the main drafting zone we can write:

$$CV_{PH}^2 = CV_{lim2}^2 + CV_{S2}^2 + CV_{P2}^2 + CV_{VS2}^2 \quad (9)$$

where CV_{PH} is total square mass irregularity of fibrous product after passing through the main drafting zone, CV_{lim2} is limiting square mass irregularity of fibrous product after passing through the main drafting zone; CV_{S2} is systematic square mass irregularity of fibrous product before the main drafting zone caused by previous drafting processes; CV_{P2} means additional square mass irregularity of fibrous product inducted in the main drafting zone and finally CV_{VS2} is systematic square mass irregularity of fibrous product developed from the latent irregularity in the main drafting zone.

Because of below mentioned formulas (10a) and (10b) hold:

$$CV_{lim2}^2 = CV_{lim1}^2 \cdot P1 \cdot P2 \quad (10a)$$

$$CV_{S2}^2 = CV_{S1}^2 + CV_{P1}^2 + CV_{VS1}^2 \quad (10b)$$

we can write:

$$CV_{PH}^2 = CV_{lim1}^2 \cdot P1 \cdot P2 + (CV_{S1}^2 + CV_{P1}^2 + CV_{VS1}^2) + CV_{P2}^2 + CV_{VS2}^2 \quad (11)$$

where $P2$ means main draft ratio.

From formulas (10b) and (11) it is obvious that with increasing draft ratio $P1$ in the intermediate drafting zone the component CV_{S2}^2 will have a significant effect on yarn mass irregularity. The component will increase irregularity of final yarn even if the main draft ratio will be reduced.

3. Experiment

Within the experiment, mass irregularity of 100% Tencel air-jet spun yarns as well as number of yarn faults were analyzed in dependence on the intermediate draft ratio as well as the main draft ratio.

3.1. Materials and methods

Tencel staple fibers (38 mm, 1.3 dtex) were used for production of air-jet spun yarns of nominal count 23 tex. Samples of yarns were spun on the Rieter Air-jet spinning machine J20 from a sliver which was processed in 3 passages of doubling and drawing after carding. Three different levels of sliver linear densities (see Table 1) were used for the experiment to analyze influence of main draft ratio on the yarn mass irregularity and yarn faults. Within each level of sliver linear densities, three levels of intermediated draft ratio were set to observe the influence of intermediate draft ratio on the yarn mass irregularity. The infeed draft and other spinning parameters were kept constant and they were set in accordance with the processed raw material and yarn count.

Table 1. Proposal of experiment

Trial Nr.	V1	V2	V3	V4	V5	V6	V7	V8	V9
Sliver linear density [ktex]	3.65	3.65	3.65	4.09	4.09	4.09	4.61	4.61	4.61
Infeed draft $P0$	1.78	1.78	1.78	1.78	1.78	1.78	1.78	1.78	1.78
Intermediate draft $P1$	1.97	2.30	2.64	1.97	2.30	2.64	1.97	2.30	2.64
Main draft $P2$	45.79	38.95	33.93	50.2	43.13	37.39	56.52	48.55	42.41
Total draft	160.6	159.46	159.45	176.06	176.6	175.69	198.19	198.79	199.3
Real average yarn count [tex]	22.72	22.89	22.89	23.23	23.16	23.28	23.26	23.19	23.13
Nozzle air pressure [MPa]	0.6								
Spinning nozzle	Z-1								
Spinning tip type	U1.2mm/A0.8								
Delivery speed [m.min ⁻¹]	400								

For each trial, 5 bobbins were spun. For illustration of fasciated yarn structure, the longitudinal view on the yarn sample and yarn cross-section was made (see Figure 2a and 2b). The Uster Tester IV-SX was used for measuring yarns as well as slivers mass irregularity. Slivers were measured for 5 min with the speed of 25 m/min, whereas yarns were measured for 2.5 min with the speed of 400 m/min. For each yarn sample, 15 measurements were done.

To investigate the effect of main draft ratio on yarn mass irregularity (when the intermediate draft ratio is kept constant), it is necessary to analyze sliver mass irregularity and take it into account. The negative effect of measured sliver mass irregularity can be eliminated by calculating and comparing machine irregularity. Except for draft, all machine process parameters were constant for all tested yarn samples. Based on this, we can assume that square mass irregularity of yarn is the same as square mass irregularity of linear fibrous product in the output from drafting arrangements and thus we can calculate the machine irregularity using formula (5). The limiting mass irregularity is defined by the formula:

$$CV_{lim} = \frac{100}{\sqrt{n}} \quad (12)$$

Where n is mean number of fibers in yarn (sliver) cross-section calculated as ratio of mean yarn (sliver) count and mean fiber fineness.

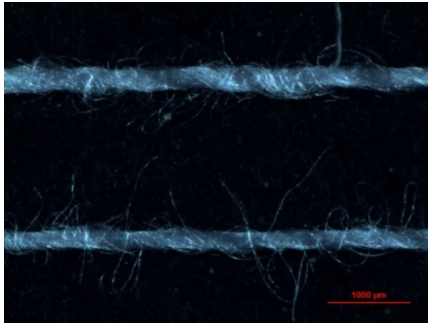


Figure 2a. Longitudinal view on yarn samples (Trial Nr.8)

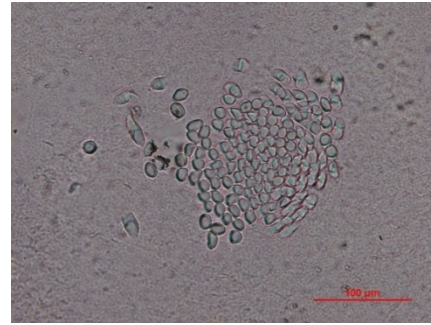


Figure 2b. Cross-sectional view on yarn samples (Trial Nr.8)

4. Results and discussions

4.1. Square mass irregularity

Table 2 shows results of square mass irregularity of sliver on various length sections. From the table, it can be seen that mean value of mass irregularity of sliver in the cross-section (CV_{sliver}) decreases with increasing linear density of slivers. This phenomenon is known. Finer sliver has a lower number of fibers in the cross-section and it expresses in growing of mass variability. Sliver mass irregularity on longer cut length has fluctuating tendency and it is caused by previous technological stages.

Table 2. Results of sliver mass irregularity

Sliver fineness [ktex]	CV_{sliver} [%]	$CV_{sliver(1m)}$ [%]	$CV_{sliver(3m)}$ [%]	$CV_{sliver(5m)}$ [%]
3.65	6.96	1.01	0.63	0.5
4.09	6.28	1.15	0.72	0.6
4.61	5.82	0.96	0.67	0.5

Figure 3a demonstrates spectrogram of sliver. Significant higher harmonic components of mass irregularity at the wavelengths $\lambda = 50$ cm and $\lambda = 1$ m are probably caused by previous technological levels. Figure 3b shows the example of spectrogram of yarn mass irregularity. It can be seen that yarn has not any significant periodical irregularity. Spectrograms of slivers as well as yarns also show that higher periodical irregularity of sliver on long wavelengths does not fully transform into the yarn due to draft on the wavelength corresponding to the value equal to $\lambda * P_c$. The reason can be attributed to the relatively short length of measured yarn for this analysis and less statistical reliability of spectrogram results on the long wavelengths.

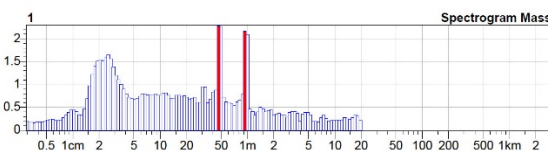


Figure 3a. Spectrogram of sliver mass irregularity (Sliver fineness 4.09 ktex)

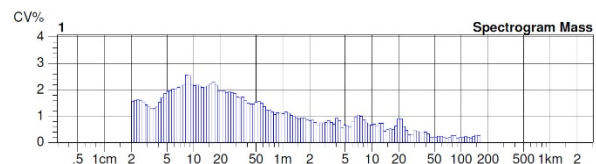


Figure 3b. Spectrogram of yarn mass irregularity (Trial No. V8)

Figure 4 shows dependence of yarn square mass irregularity (CV_{yarn}) on the main draft ratio. Contrary to known theory, it can be seen that when keeping the intermediate draft ratio constant, the yarn mass irregularity decreases with growing the main draft ratio. The yarn mass irregularity also deteriorates with growing the intermediate draft ratio (or we can say with decreasing main draft ratio) when sliver mass density is kept constant. These results confirmed the theory mentioned above. When increasing the intermediate draft ratio, the component CV_{S2}^2 influences total yarn mass irregularity negatively.

At increasing intermediate draft ratio $P1$, this component is affected by increase in components CV_{P1}^2 and CV_{VS1}^2 . It is due to the character of the intermediate drafting zone and resulting friction force field in the longitudinal direction which corresponds to the drafting zone with missing a guiding (controlling) device. Due to its arrangements, the main drafting zone allows to minimize the increase in additional mass unevenness.

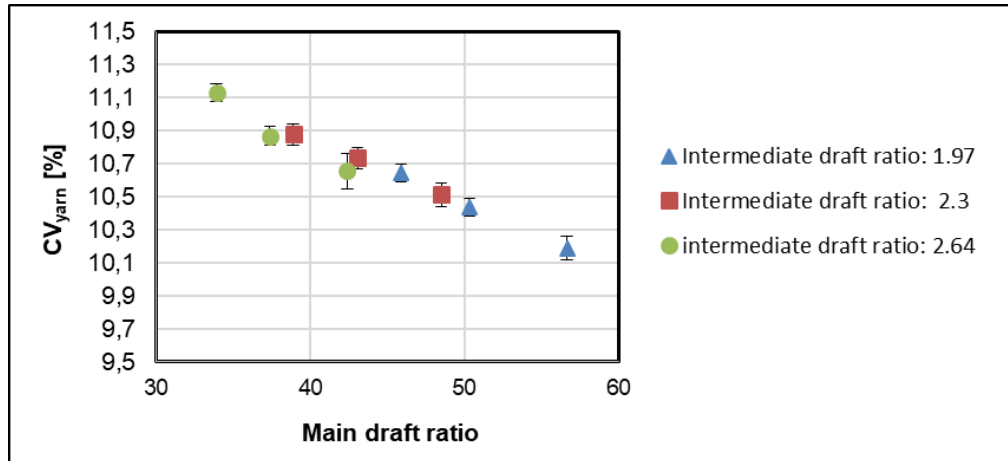


Figure 4. Dependence of yarn mass irregularity on main draft ratio and various intermediate draft ratio

Two-way variance analysis Anova confirmed a statistically significant effect of both intermediate draft ratio and sliver linear density on the yarn mass irregularity at the significance level of 5%. However, the significance of mutual interaction of these two factors was not statistically confirmed (see the results in Table 3).

4.2 Machine irregularity

Figure 5 presents machine irregularity in dependence on the main draft ratio for various intermediate draft ratio. The results showed that:

- When keeping the intermediate draft ratio constant, the main draft ratio is a significant factor which increases machine irregularity. This result is in accordance with theory presented above. Based on the theoretical analysis mentioned above, we can also say that systematic square mass irregularity developed from the latent irregularity by the draft probably contributes to the increase in machine irregularity. Based on this, we can conclude that when the intermediate draft is constant, decreasing values of measured yarn square mass irregularity (CV_{yarn}) with growing main draft ratio (due to higher sliver linear density) was caused by mass irregularity of input sliver which corresponds to the irregularity components CV_{im0} and CV_{s0} . Finer sliver has higher measured valued of mass irregularity compared with course sliver. This irregularity transforms into the yarn and thus influences total square mass irregularity of yarn more than the drafting device itself.
- When sliver linear density is constant, the value of machine irregularity increases with increasing level of intermediate draft ratio (and thus with decreasing main draft). This result is in agreement with the previous one and verifies the higher importance of intermediate draft ratio on total yarn mass irregularity compared with the main draft ratio.

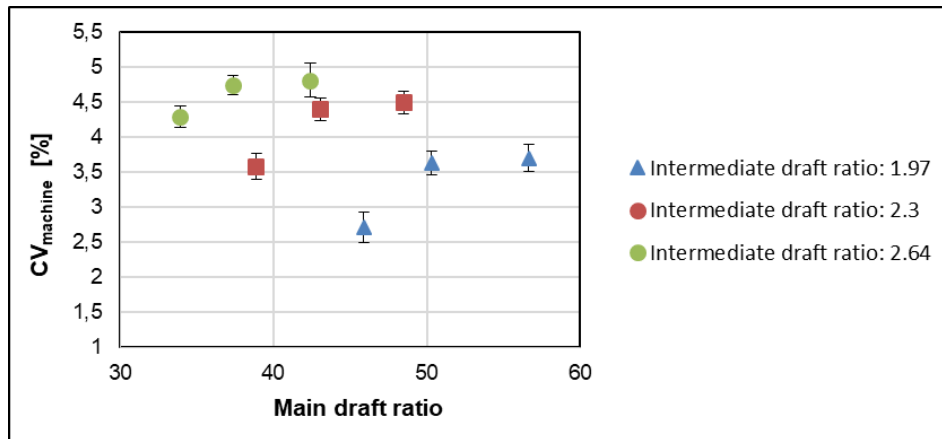
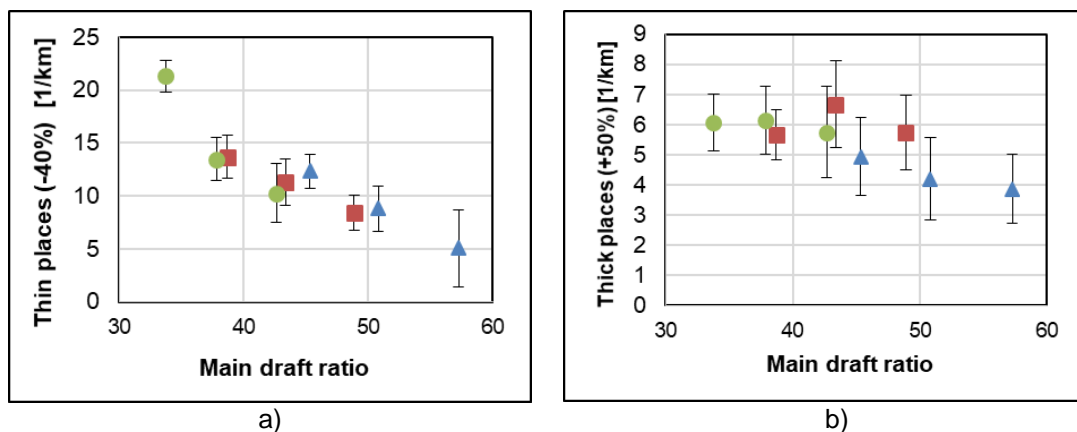
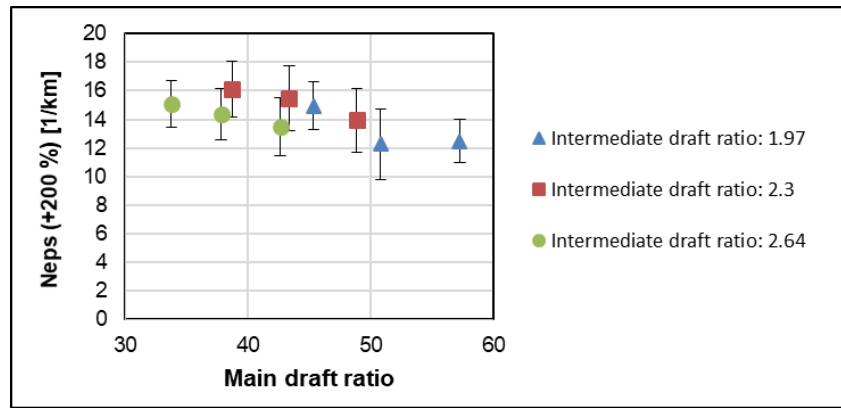


Figure 5. Dependence of machine irregularity on main draft ratio and various intermediate draft ratio

4.3 Yarn faults

Average values and corresponding 95% confidence intervals of yarn faults (thin places (-40%), thick places (+50%) and neps (+200%)) are presented in Figure 6a-6c. Number of thin places (-40%) was observed instead of thin places (-50%) because of zero number of faults in this category. Selected results of two-way analysis of variance are mentioned in Table 3. Results of numbers of thin places have the same trend as results of total mass irregularity of yarns. Number of thin places decreases with decreasing intermediate draft ratio and with increasing linear density of supplied sliver. Results of two-way Anova show that sliver linear density, the intermediate draft ratio as well as interaction of these two factors have a statistically significant effect on number of thin places (-40%). The linear density (and thus the main draft ratio at constant level of intermediate draft ratio) is a factor with a higher significant effect. However, it is clear from the graph in Figure 6a that, in the terms of overlapping confidence intervals, the statistically significant difference is only between the numbers of thin places of yarn sample spun from sliver of linear density 3.65 ktex at intermediate draft ratio of 2.64 and yarn sample made from a sliver of 4.61 ktex at intermediate draft ratio of 1.97. Number of thick places (+50%) shows similar results as in case of thin places, but in this case the effect of interaction of sliver linear density and level of intermediate draft ratio is a statistically insignificant. The results can be attributed to both mass variability of supply sliver, which is higher in the case of finer sliver, and negative effect of the intermediate drafting zone which is stronger with growing intermediate draft ratio. Based on results of two-way Anova, we can state that in the case of number of yarn neps (+200%) the effect of observed factors is statistically insignificant in significance level of 5%. However, we have to note that thanks to the specific yarn structure, the Uster Tester can also records as a nep the place where the ends of the wrapping fibers are not tightly twisted around the yarn core due to the air flow in the nozzle.





c)

Figure 6. Dependence of yarn faults on main draft ratio and various intermediate draft ratio

Table 3. Results of two-way Anova

Property	Source of variance	F-ratio	Critical quantile	Results	p-value
CV _{yarn} (CV _m)	Intermediate draft ratio	172.68	3.07	Significant	$3.55 \cdot 10^{-36}$
	Sliver linear density	146.93	3.07	Significant	$4.22 \cdot 10^{-33}$
	Interaction	1.30	2.45	Non-significant	0.27
Thin places (-40%)	Intermediate draft ratio	27.28	3.07	Significant	$1.61 \cdot 10^{-10}$
	Sliver linear density	42.42	3.07	Significant	$1.03 \cdot 10^{-14}$
	Interaction	2.62	2.46	Significant	0.04
Thick places (+50%)	Intermediate draft ratio	8.50	3.07	Significant	$3.48 \cdot 10^{-4}$
	Sliver linear density	0.77	3.07	Non-significant	0.46
	Interaction	0.61	2.46	Non-significant	0.66
Neps (+200%)	Intermediate draft ratio	2.49	3.07	Non-significant	0.09
	Sliver linear density	1.25	3.07	Non-significant	0.29
	Interaction	0.95	2.46	Non-significant	0.43

5. CONCLUSIONS

In this work, the analysis of draft in the four-roller two-apron drafting device of air jet spinning machine was done together with theoretical analysis of transformation of mass irregularity of fibrous product by this drafting unit. The effect of intermediate and main drafting zones were observed. Within the experiment, mass irregularity of air-jet yarns of the same count, produced with various setting of intermediate and main draft ratio, was evaluated together with sliver mass irregularity and yarn faults. Based on theory, the mass irregularity of fibrous product is deepened by the draft mostly. Despite the fact that the main draft ratio is much higher compared with the intermediated draft ratio, this study shows that the intermediate draft ratio has more significant influence on the yarn mass irregularity than the main draft. It can be explained by the fact that fibers move in the intermediate drafting zone without aprons. The aprons are a part of the main drafting zone, and they control the fibers movement in the zone. Thus, in this zone, they minimize the creation of the additional irregularity, which is one of a component of total yarn mass irregularity. The additional irregularity is probably highly deepened in the

intermediate drafting zone due to the fact that various drafting force is applied on each fiber in the zone and change of speed of fiber movement does not occur at the same place. Also the irregularity of supplied sliver (limiting and so called systematic) has negative influence on the total yarn mass irregularity. The experiment shows that for achieving the lowest value of total mass irregularity of tested yarn samples it is suitable to use the lowest value of intermediate draft ratio ($P1 = 1.94$) in combination with coarser supply sliver (4.61 ktex). Compared with finer sliver, the sliver with higher linear density (from the observed range) seems to be suitable because it has lower irregularity thanks to higher number of fibers in the sliver cross-section and due to lower draft ratios used in previous spinning processes. When observing number of yarn faults, the same trends were achieved. But the statistically significant differences were recorded only in the case of thin places (-40%). Finally, based on Uster Statistics, we have to note that tested samples of air jet yarns have lower irregularity. Also the differences between minimum and maximum Cvm values were in the range up to 5%. For verification of results it is necessary to extend the experiment in terms of both wider draft range and raw material and to observe impact of yarn mass irregularity on various yarn properties.

References

- [1] Grishin, P. A. (1954). *Theory of drafting and its practical applications. Journal of the Textile Institute Transaction.* 45 (3). T167-T266.
- [2] McVitie, J., De Barr, A. E. (1960). *Fiber motion on roller and apron drafting system. Journal of the Textile Institute Transaction.* 51 (4). T147-T156.
- [3] Lin, Q., Oxenham, W., Yu, C. *A study of the drafting force in roller drafting and its influence on sliver irregularity, Journal of the Textile Institute.* 102(11). 994-1001.
- [4] Audivert, R., Viilaronga, M., Coscolla, R. (1967). *Drafting force in the front zone of a double apron drafting system. Textile Research Journal.* 37(1). 1-10.
- [5] Balasubramanian, N. (1969). *A study of the irregularities added in apron drafting. The Textile Research Journal.* 39(2). 155-165.
- [6] Stalder, H. (2014). *The Rieter Manual of Spinning. Volume 6 – Alternative Spinning Systems. Wintherthur: Rieter Machine Works Ltd.. ISBN 10 3-9523173-6-5.*
- [7] Basal, G., Oxenham, W. (2006). *Effects of some process parameters on the structure and properties of Vortex spun yarn. Textile Research Journal,* 76 (6), 492-499.
- [8] Kuthalam, S. E., Senthilkumar, P. (2013). *Effect of Fibre Fineness and Spinning Speed on Polyester Vortex Spun Yarn Properties. FIBRES & TEXTILES in Eastern Europe,* 21, 5(101), 35-39.
- [9] Erdumlu, N. (2012). *The structure and properties of carded cotton vortex yarns. Textile Research Journal,* 82(7), 708-718.
- [10] Erdumlu, N., Ozipek, B. (2010). *Effect of the Draft Ratio on the Properties of Vortex Spun yarn. Fibres and Textile in Eastern Europe ,* 18 (3), 38-42.
- [11] Zeng, Y., C. (2003). *Numerical Simulation of Air Flow in the Nozzle of an Air-Jet Spinning Machine. Textile Research Journal ,* 73(4), 350-356.
- [12] Eldeeb, M., Demir, A. (2018). *Optimizing the production process of rieter airjet spun yarns and model form prediction of their strength. Fibres and Textiles in Eastern Europe,* 26(1), 36-41.
- [13] Eldeeb, M., Moučková, E., Ursíny, P. (2017). *Properties of viscose air-jet spun plied yarns. Indian Journal of Fibre and Textile Research,* 42(4), 386-390.
- [14] Eldeeb, M., Moučková, E. (2017). *Numerical simulation of the yarn formation process in Rieter air-jet spinning. Journal of the Textile Institute,* 108(7), 1219-1226.
- [15] Ursíny, P. (2003). *Mass irregularity changes in spinning technology. Vlákna a textil (Fibres and Textiles),* 10 (2), 62-65.
- [16] Bowles, A. H., Davies, L. (1978). *The influence of drawing and doubling proces on the evenness of spun yarn I. The Textile Institute and Industry,* 11, 371-374.
- [17] *Rieter J 20 Air-Jet Spinning Machine Com4jet, Yarn Formation original animations, animation made by Rieter, downloaded from: <https://www.youtube.com/watch?v=rMYCb9ea11g>, 10.3.2017.*

AIR-FLOW ANALYSIS OF COMPACT YARN

Murat Demir¹, Musa Kilic¹, Zeki Kiral², Serdar Sayin³, Kıymet Kübra Denge⁴, Furkan Balduk⁴

¹ Dokuz Eylül University, Dept. of Textile Engineering, 35397, İzmir, Turkey, tel: +902323017730

² Dokuz Eylül University, Dept. of Mechanical Engineering, 35397, İzmir, Turkey, tel: +902323019232

³ Dokuz Eylül University, The Graduate School of Natural and Applied Sciences, Dept. of Mechatronics Engineering, 35397, İzmir, Turkey tel: +902323019232

⁴ KİPAŞ Mensucat R&D Center, Kahramanmaraş, Turkey tel: +903442363800

murat.demir@deu.edu.tr

Abstract:

Despite the ring spinning is one of the oldest and most widely used spinning technology, alternative spinning technologies have also been developed for better yarn quality and production processes. Compact spinning is one of the alternative spinning technologies that developed from conventional system for producing yarn in better quality. For compact spinning, small modifications were made on conventional system to condense fiber bundle with the help of air-flow to reduce spinning triangle between drafting unit and yarn formation point. In this study, air-flow analysis for Rieter's compact spinning technology was studied. The CAD models of the relevant section of the Rieter's compact spinning machine were created and the air-flow analyses were performed in SolidWorks Flow Simulation environment in order to calculate the variations in pressure and velocity of the air-flow around the fiber bundle. The condensing performance and yarn hairiness were discussed using the resultant force and friction force values calculated for the fiber bundle.

Key words:

Compact spinning, air-flow analysis, pressure distribution, resultant force.

1. Introduction

Compact spinning technology can be counted amongst modern spinning technologies which was developed from conventional system and it was introduced by Dr. Ernest Fehrer in 1992 [1]. Despite the advantages of ring spinning technologies, ideal performance for yarn quality has not been achieved yet. In ring spinning technology, fiber bundles are delivered from drafting area larger than spinning triangle and as a result of this situation some fibers are not join into yarn structure properly. The aim of compact spinning is to minimize spinning triangle between drafting unit and yarn formation unit with the help of aerodynamic forces and to provide joining of all fibers into yarn structure. For this purpose, some modifications were made on conventional system. In order to get benefit of aerodynamic forces, perforated cylinder, suction insert and air guide elements are placed for compact spinning.

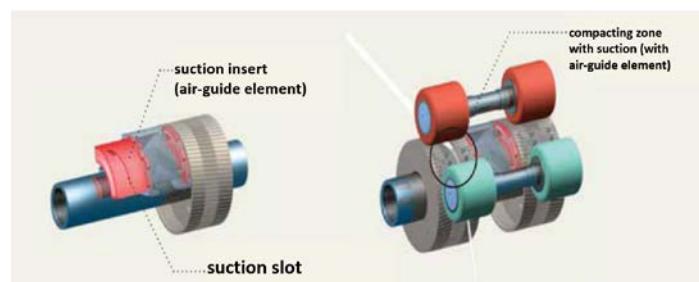


Figure 1. Rieter's compact spinning technology [2]

In Figure 1, fibers are supported and delivered by perforated drum which has also suction unit inside. Air guide element is also placed on perforated drum to provide aerodynamic forces to both side of yarn. Comparing properties of compact and ring yarns are showed that visually better and superior yarns are produced by compact spinning [2].

In the literature, it is seen that many researchers have studied compact spinning and its comparison with other alternative spinning technologies. Unal and Omeroglu [3] compared different compact siro-spun yarns and bursting strength of fabrics that produced from these yarns. Salhotora [4] and Soltani and Johari [5] compared compact yarns with conventional, siro-spun and solo-spun yarn properties. Besides, some researchers studied pneumatic system of different compact spinning technologies. Liu et. al. [6] compared different compact technologies which are Rieter COM4 and complete condensing spinning (CCS), Sussen's three-line compact spinning (TLCS) and Toyata's four-line compact spinning. Between these compact technologies Rieter COM4 and complete condensing spinning (CCS) are counted as compact spinning with perforated drum while Sussen's three-line compact spinning (TLCS) and Toyata's four-line compact spinning are counted as compact spinning with lattice apron. Producing and comparing yarn with different linear densities on these four systems showed that the evenness and breaking strength of yarns were decreased on compact spinning with perforated drum. Moreover, hairiness values of yarns were higher for compact spinning with perforated drums. Yinghui et. al. [7] studied air-flow distribution of complete compact spinning (CCS) and four-lines compact spinning (FRCS) with finite element method. Results showed that the negative velocity component on Y axis gives better S1+2 values. CCS have more negative velocity on Y axis than FRCS. Negative velocity of X axis has direct relation with evenness. For the same linear density of CCS and FRCS, greater negative velocity component on X axis result better yarn evenness. The velocity component of Z axis has relation with breaking strength. FRCS have greater velocity component of Z axis than CCS and better breaking strength. Yilmaz et al. [8] investigated packing densities of compact yarn and they concluded that compact yarns have roughly 30% higher packing densities than conventional ring spun yarn. Besides comparing packing densities of yarns that produced in four different compact spinning technologies showed that there are no significant differences between those yarns. Krifa and Etheridge [9] investigated the effect of interactions between compact spinning and fiber characteristics on cotton yarns. They pointed out that compact spinning gained maximum yarn hairiness reduction for short fibers. However, for longer staples and higher uniformity level of fibers, yarn hairiness reduction is not significant.

2. Airflow Analyses

In this study, the airflow analyses of compact yarn spinning mechanism are performed using SolidWorks Flow Simulation software. This CAE software is beneficial for both designing parts and analyzing them in the same platform. To simulate the fluid flow considering the real boundaries, the software uses the Navier-Stokes Equations which are the formulations of mass, momentum and energy conservation laws [10]:

$$\frac{\partial \rho}{\partial t} + \frac{\partial}{\partial x_i}(\rho u_i) = 0 \quad (1)$$

$$\frac{\partial \rho u_i}{\partial t} + \frac{\partial}{\partial x_j}(\rho u_i u_j) + \frac{\partial p}{\partial x_i} = \frac{\partial}{\partial x_j}(\tau_{ij} + \tau_{ij}^R) + S_i \quad i = 1,2,3 \quad (2)$$

$$\frac{\partial \rho H}{\partial t} + \frac{\partial \rho u_i H}{\partial x_i} = \frac{\partial}{\partial x_i}(u_j(\tau_{ij} + \tau_{ij}^R) + q_i) + \frac{\partial p}{\partial t} - \tau_{ij}^R \frac{\partial u_i}{\partial x_j} + \rho \epsilon + S_i u_i + Q_H \quad (3)$$

$$H = h + \frac{u^2}{2} \quad (4)$$

where u is the fluid velocity, ρ is the fluid density, S_i is the mass-distributed external force per unit mass due to a porous media resistance, h is the thermal enthalpy, Q_H is a heat source or sink per unit volume,

τ_{ik} is the viscous shear stress tensor, q_i is the diffusive heat flux. The subscripts are used to denote summations over three coordinate directions.

To perform the flow analysis, the assembly model of the Rieter's compact spinning mechanism was created with suction insert and perforated drum as seen in Figure 3.

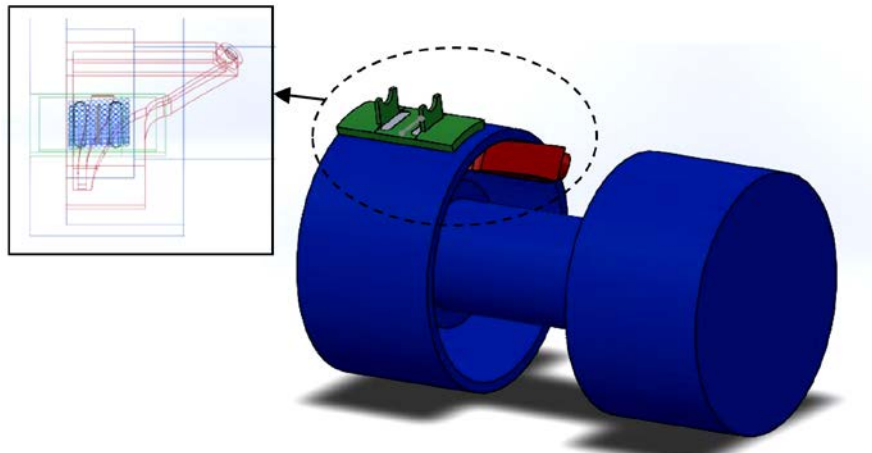


Figure 3. Assembly model of Rieter's compact spinning mechanism

The fiber bundle subjected to the air flow is modeled as a cylindrical tube with diameter 0.4 mm to calculate the normal forces acting from left and right sides of the compacting bundle. The model and boundary conditions are given in Figure 4.

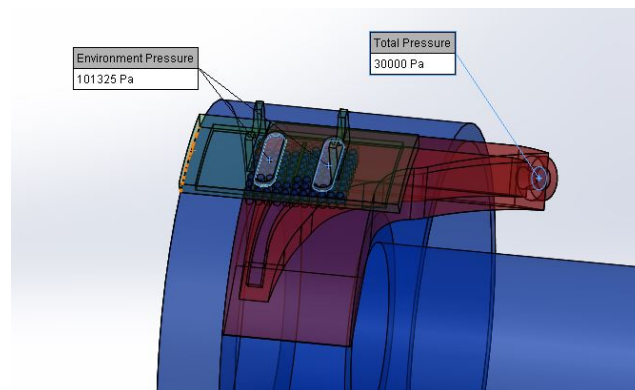


Figure 4. Pressure definitions for the suction insert.

The air suction effect is created by defining negative pressure, which is approximately 0.3 atm at the inlet of the suction insert as shown in Figure 4. The other end of the suction insert is exposed to atmospheric pressure. The computational domain used in flow analyses is shown in Figure 5.

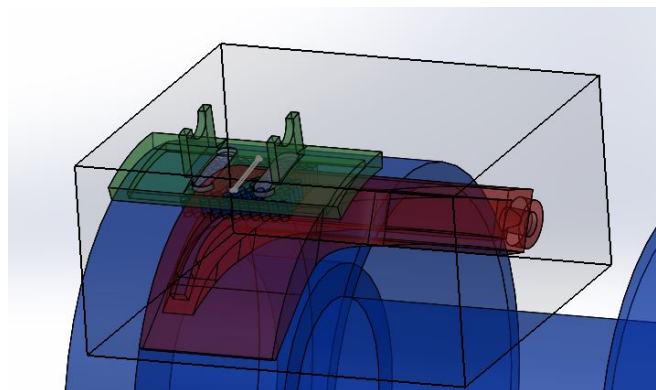


Figure 5. Computational Domain for the Analyze

3. Results and Discussions

The transient airflow analysis was performed by using the computational domain including the all components of the Rieter's compact spinning mechanism and the predefined boundary conditions. As a result of the flow analyses the pressure and the velocity distribution calculated on the yarn center plane for steady-state case are given in Figure 6 and Figure 7.

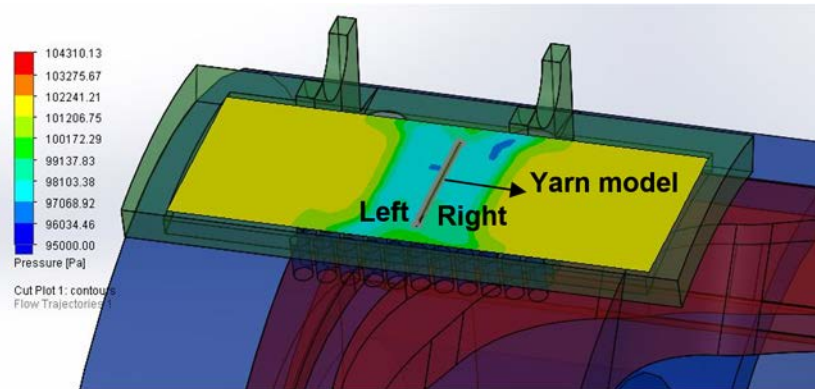


Figure 6. Pressure distribution on the yarn center plane.

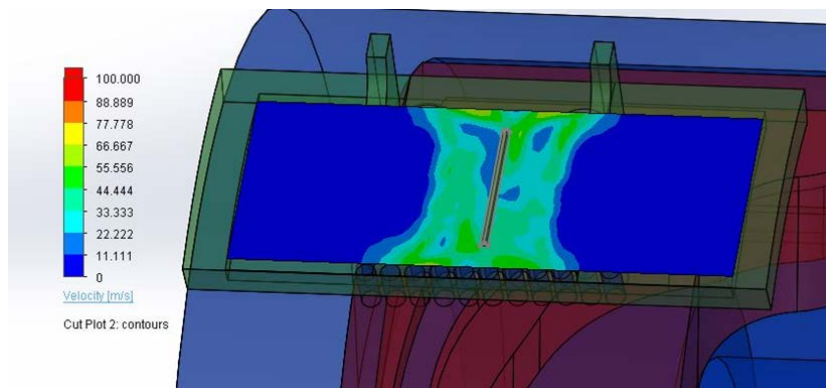


Figure 7. Velocity Distribution on the yarn center plane

After performing the flow analysis, the resultant force acting on the left half and right half cylindrical surfaces of the yarn model were calculated to show the basic effect, which condenses the fiber bundle. Figure 8a shows the change in the resultant force on the left half cylindrical surface of the simple yarn model. The steady-state value of the resultant force is calculated as 0.0105 N. Figure 8b shows the change in the resultant force on the right half cylindrical surface of the simple yarn model. The steady-state value of the resultant force is about 0.009 N. The difference between these force values explains the condensing mechanism of the fiber bundle from outside to inside. Flow analysis allows the calculation of friction forces on the exposed surfaces. Figure 9 shows the change in the resultant friction forces on both left and right half cylindrical surfaces of the simple yarn model. The level and variation of the frictional forces can be used to interpret the yarn hairiness.

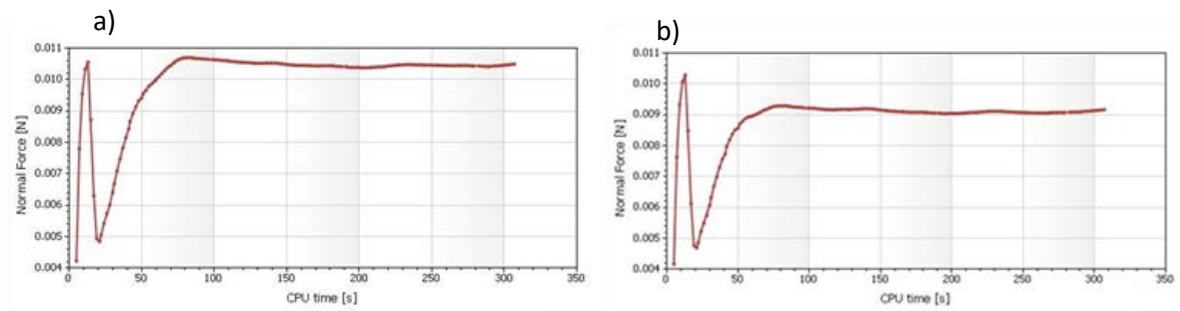


Figure 8. Calculated resultant force a) on the left half surface b) on the right half surface.

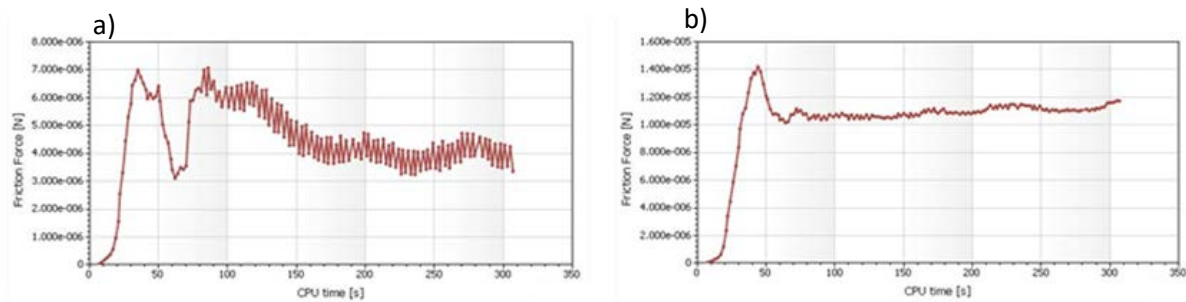


Figure 9. Calculated resultant frictional force a) on the left half surface b) on the right half surface.

4. CONCLUSIONS

In this study, initial results of a flow analysis conducted for compact spinning were presented. The air pressure distribution on the yarn center plane and the change in the normal and frictional forces acting on the simple yarn model were analyzed to form the basis for further developments in future studies. The simulation results showed that the condensing effect of the air suction can be observed by interpreting the numerical results and the form of the components in the suction zone can be improved to obtain better performance for condensing the fiber bundle.

ACKNOWLEDGEMENTS

This study is supported by TÜBİTAK - TEYDEB 1505 University-Industry Collaboration Grant Programme with the project number 5160091.

References

1. Fehrer, E. (1992). *Process and Apparatus for Feeding at Least Two Drawn Rovings to Respective Ring Spinning Stations*. US Patent 5,085,046.
2. Klein, W. and Stalder, H. (2008). *The Rieter Manual of Spinning vol. 4- Ring Spinning*. pp. 56-58.
3. Salhotra, K. (1987). *Some Quality Aspects of Ply-Spun Yarn*. *Indian Journal of Textile Research*, Issue 12, pp. 197-200.
4. Soltani, P. and Johari, M. (2012). *A Study on Siro, Solo, Compact, and Conventional Ring-Spun Yarns. Part I: Structural and Migratory Properties of the Yarns*. *The Journal of the Textile Institute*, 6(103), pp. 622-628.
5. Ünal, S. and Ömeroğlu, S. (2013). *Effects of Properties of Two-Ply Spun Yarns Produced Directly by Different Systems on Knitted Fabric Properties*, *Journal of Textiles and Engineer*, 20:91, pp.9-15.
6. Liu, X., Zhang, H. and Su, X. (2016). *Comparative analysis on pneumatic compact spinning systems*, *International Journal of Clothing Science and Technology*, vol. 28 issue: 4, pp.400-419, <https://doi.org/10.1108/IJCST-09-2015-0104>.
7. Yinghui, L., Xie, C. and Liu, X. (2017). *Comparative analysis of two kinds of pneumatic compact spinning using finite element method*. *International Journal of Clothing Science and Technology*, vol.29 issue: 4, pp.514-524, <https://doi.org/10.1108/IJCST-09-2016-0108>.
8. Yılmaz, D.; Göktepe, F. and Göktepe, Ö. (2007). *Packing densities of compact yarns*. *Textile Research Journal Vol 77 (9)*: 661-667.
9. Krifa, M. and Ethridge, M.D. (2006). *Compact spinning effect on cotton yarn quality: interactions with fiber characteristics*. *Textile Research Journal Vol 76 (5)*: 388-399.
10. *SolidWorks Flow Simulation 2017 Technical Reference*, Dassault Systemes.

EFFECTS OF INTERMINGLING ON PROPERTIES OF FALSE TWIST TEXTURED YARNS

Musa Kilic¹, Gonca Balci Kilic¹, Buğra Öztürkmen¹

¹Dokuz Eylül University, Department of Textile Engineering, İzmir, Turkey, tel: +90 232 301 77

01 musa.kilic@deu.edu.tr

Abstract:

Texturing is a process to give bulk and extra stretch to the flat continuous filament yarns. Texturing is a way to feature natural fibre properties to synthetic fibres. In this study, 100% polyester melange POY was textured by the help of false twist friction discs and intermingled at different pressure levels. To evaluate the effects of intermingling pressure level on yarn properties, linear density, tenacity, elongation, yarn-to-yarn, yarn-to-metal and yarn-to-ceramic friction coefficients were measured. Results showed that intermingling process decreases the tenacity and elongation of textured yarn. However, increasing level of pressure increases the values of tenacity and elongation until 0.8 bar. Additionally, effect of intermingling pressure was investigated in terms of number and stability of interlaces and amount of spin finish oil. Maximum number of interlaces and the highest stability were measured at 0.8 bar pressure level. Within the study, knitted fabrics were also produced by textured yarns. Visual assessment of the fabrics showed that intermingling pressure level has an important role on appearance of the fabrics.

Key words:

intermingling, textured yarn, false twist, friction discs, POY, tenacity, elongation

1. Introduction

In recent years, synthetic fibers have gained great importance due to the rapid consumption of natural fibers. The most important characteristic expected from products produced from synthetic fibers is to carry similar properties with products they are substituted for. Texturing imparts desirable textile properties to continuous filament yarns without destroying their continuity. Textured yarns have suitable volume, stretch and recovery, and air porosity for everyday use [1]. Texturing of continuous-filament yarns became established as a commercial success in the 1950s. False twist process is one the basic yarn texturing methods. The false-twist process can be broken down into three fundamental elements: tension, twist and temperature. By controlling these three fundamental variables a wide variety of different textured-yarn types can be made from one POY feedstock [2].

Intermingling is an optional facility used to combine the filaments in yarn structure. Textured yarns are basically intermingled for imparting the essential interfilament cohesion to multifilament yarn using an air-jet which is positioned in the path of the yarn. This creates intermittent, knot-like entangled nodes along the yarn [3]. Intermingling and intermingling process parameters have significant effects on yarn properties and many studies have been dealt to investigate these effects [4-14]. Intermingling has also a discernible effect on denier. The increase is small and is proportionate to the number of intermingled points inserted due to yarn compaction [1].

2. Experimental

2.1. Materials

In this study, 150 denier 288 filaments melange 100% polyester POY was used as raw material. POY was consisted of 144 ecru and 144 black filaments. The texturing process was performed using false twist friction discs (Figure 1). Intermingling device was replaced after the second drawing roller and four types of textured yarns were produced under 0.2 bar, 0.5 bar, 0.8 bar and 1.0 bar intermingling pressure levels. For better comparison, textured yarn without intermingling was also produced.

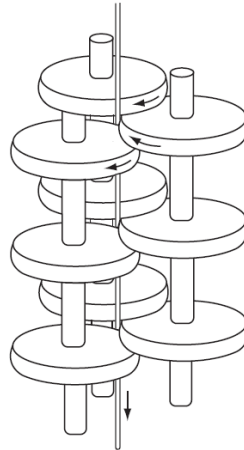


Figure 1. False twist friction discs [2]

2.2. Methods

Linear densities of textured yarns were measured by conventional cut and weigh method using yarn creel. Mechanical properties were measured by Textechno Statimat ME+ with 500 mm gauge length and 20 seconds test duration. Total number and stability of interlaces were measured by Textechno Iteamat+TSI testing instrument. Amount of spin finish oil was determined using Alfa NMR test instrument based on the technique of Time Domain NMR (Nuclear Magnetic Resonance) (Figure 2). To determine frictional properties of textured yarns, yarn-to-yarn, yarn-to-metal and yarn-to-ceramic friction tests were performed by using Lawson Hemphill CTT at 100 m/minute test speed and 18 cN input tension.



Figure 2. Lenzing-instruments Alfa NMR testing instrument for spin finish level

In the experimental part of the study, knitted fabrics were also produced by using five types of textured melange yarns. Appearances of the fabrics were evaluated visually to check out whether intermingling has any effect.

3. Results and discussion

In this study, effects of intermingling pressure level on the properties of textured polyester yarns were evaluated by statistical methods. For this purpose, analysis of variance (ANOVA) at $\alpha = 0.05$ importance level was performed. Additionally, bar charts and 95% confidence interval graphs were used to visualize the results.

3.1. Yarn Linear Density

Table 1 shows the linear densities (dtex) of textured yarns.

Table 1. Linear densities (dtex) of textured yarns

Intermingling Pressure Level	Yarn Linear Density (dtex)
Not intermingled	177
0.2 bar	181
0.5 bar	182
0.8 bar	182
1.0 bar	182

3.2. Mechanical Properties

Table 2 shows the mechanical properties of yarns intermingled at different pressure levels. Moreover, Figure 3 illustrates the 95% confidence interval graphs for tenacity and elongation values, respectively. As it can be seen from Table 2 and Figure 3, all the mechanical properties are the highest for the yarns with no intermingling. However, while intermingling has an overall negative effect on mechanical properties, increasing pressure level leads to increasing mechanical properties until 0.8 bar.

Table 2. Mechanical properties of the yarns

Intermingling Pressure Level	Elongation (%)	Breaking Strength (cN)	Tenacity (cN/dtex)	Work at Break (cN.cm)
Not intermingled	21.70	617.05	3.49	4399.2
0.2 bar	12.46	469.75	2.60	1823.8
0.5 bar	13.95	517.94	2.85	2208.4
0.8 bar	15.12	532.84	2.93	2509.8
1.0 bar	13.35	492.12	2.70	1987.6

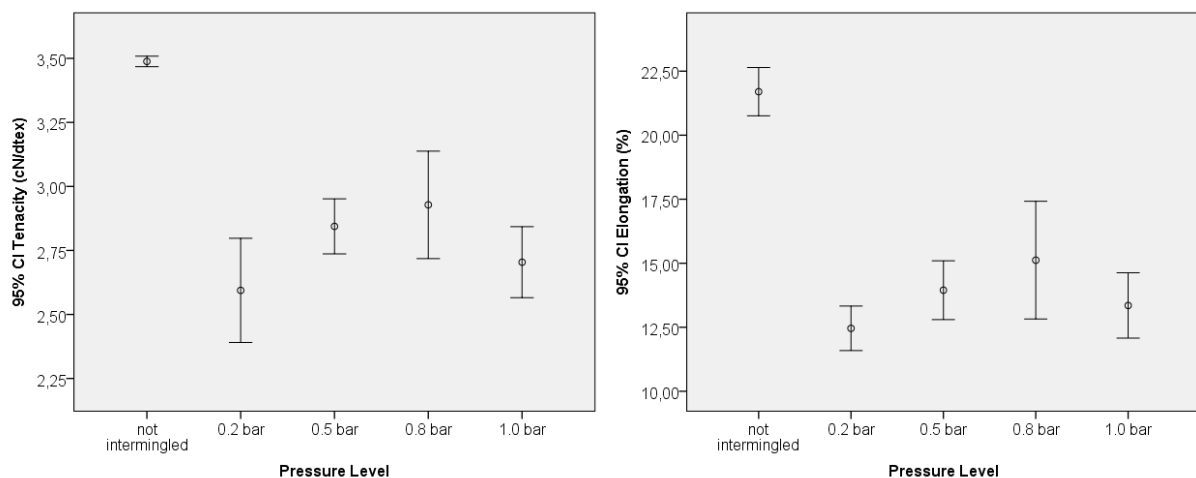


Figure 3. 95% confidence intervals for tenacity (cN/tex) and elongation (%)

ANOVA results for tenacity values are given in Table 3. As it can be concluded from Table 3, effect of intermingling pressure level is statistically significant on yarn tenacity ($p=0.000$) just like elongation ($p=0.000$), breaking strength ($p=0.000$) and work at break ($p=0.000$).

Table 3. ANOVA results for tenacity (cN/dtex) values

Source	Sum of Squares	Degree of Freedom (df)	Mean Squares	F	Sig. (p)
Corrected Model	2.405	4	0.601	39.753	0.000
Intersect	211.935	1	211.935	14011.329	0.000
Pressure Level	2.405	4	0.601	39.753	0.000
Error	0.303	20	0.015		
Total	214.643	25			
Corrected Total	2.708	24			

3.3. Yarn Surface Properties

Figure 4 illustrates the 95% confidence interval graphs for yarn-to-yarn, yarn-to-metal and yarn-to-ceramic friction coefficients, respectively. It is seen that intermingling has a statistically significant effect on yarn surface properties. Yarns with no intermingling have the highest friction coefficients for yarn-to-yarn, yarn-to-metal and yarn-to-ceramic friction. Increasing intermingling pressure leads to get decreasing friction coefficients until some level. Friction coefficients for yarn-to-yarn and yarn-to-ceramic tests are the lowest at 0.5 bar pressure level, while for yarn-to-metal test it is the lowest at 0.8 bar.

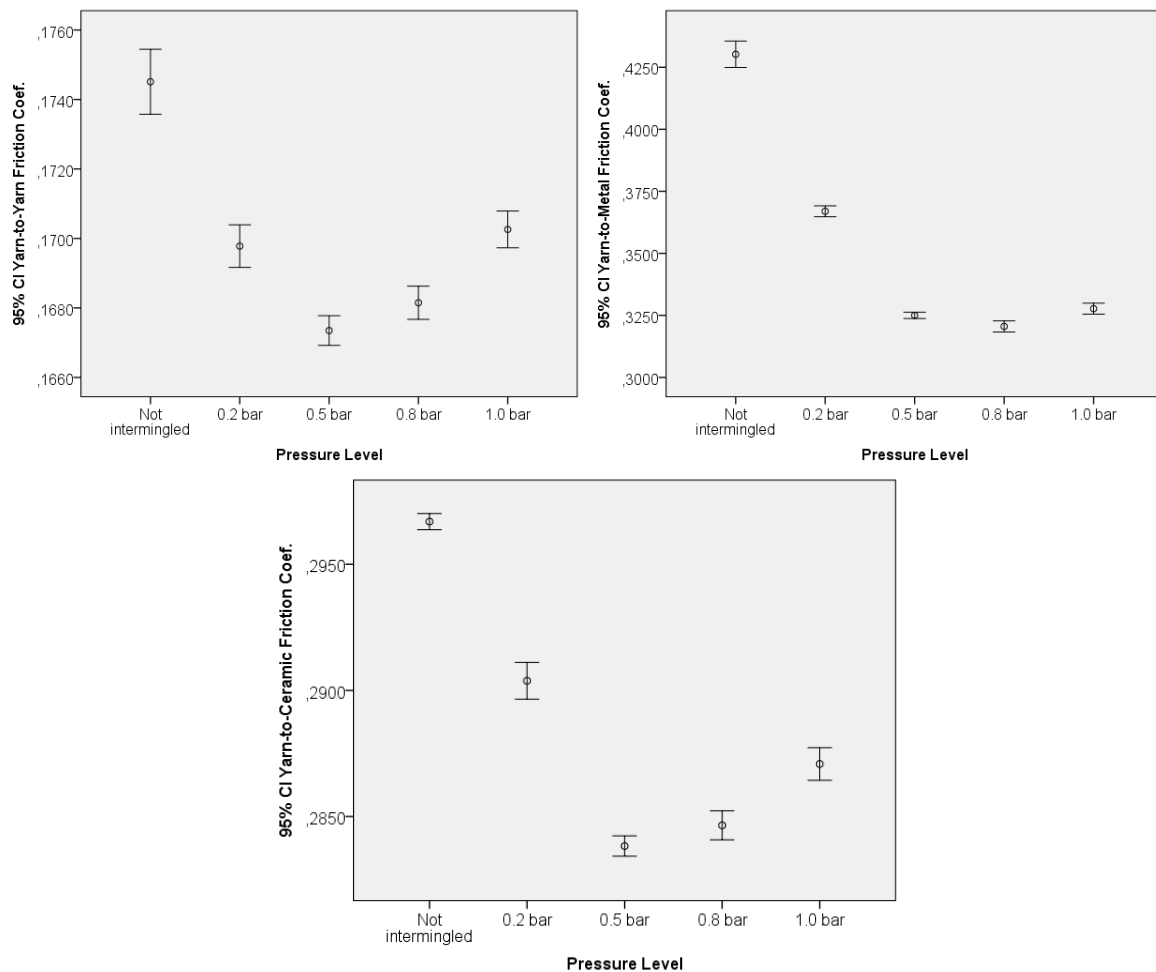


Figure 4. 95% confidence intervals for yarn-to-yarn, yarn-to-metal and yarn-to-ceramic friction coefficients

3.4. Total Number and Stability of Interlaces

Table 4 and Figure 5 illustrates the total number and stability of interlaces for the yarns intermingled at different pressure levels. Results showed that optimum values are obtained at 0.8 bar pressure level in terms of number of interlaces and stability.

Table 2. Total number and stability of interlaces

Intermingling Pressure Level	No. of Interlaces /m <i>Under no Tension</i>	No. of Interlaces /m <i>Under 4% Elongation</i>	Stability (%)
Not intermingled	0	0	
0.2 bar	62	20	32,2
0.5 bar	87	79	90,1
0.8 bar	93	88	94,6
1.0 bar	88	77	87,5

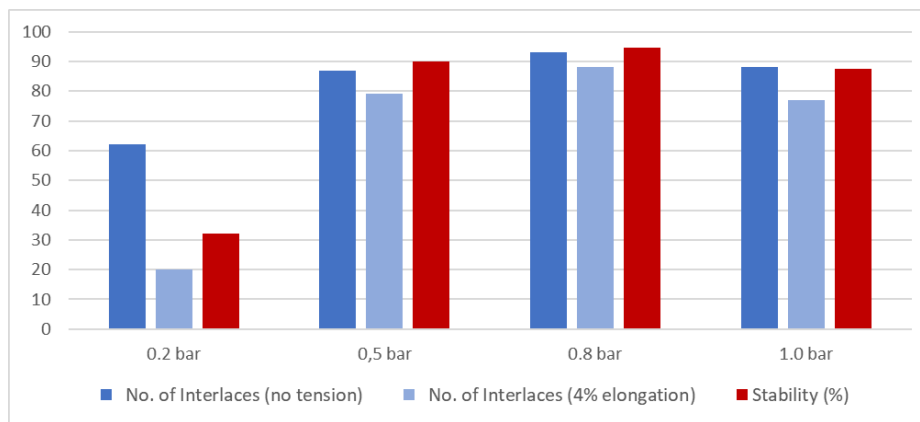


Figure 5. Total number and stability of interlaces

3.5. Amount of Spin Finish Oil

Figure 6 shows the amount of spin finish oil for the yarns intermingled at different pressure levels. It can be concluded that increasing level of pressure level leads to increasing amount of spin finish oil until 0.5 bar pressure level. After this optimal pressure level, increasing pressure level have negative effect in terms of oil content.

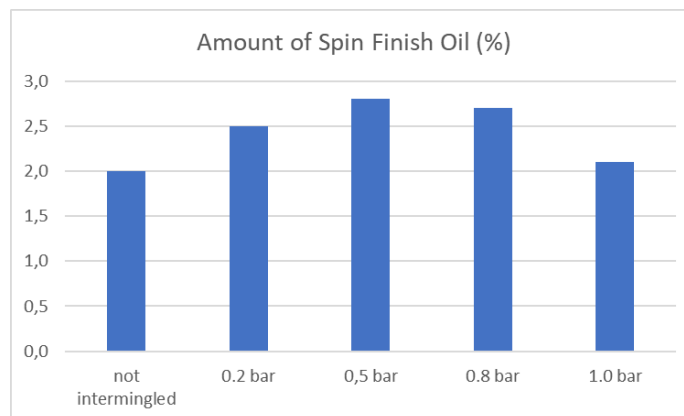


Figure 6. Amount of spin finish oil

3.6. Fabric Visual Evaluation

In the study, melange textured yarns were knitted on sample knitting machine to evaluate the effect of intermingling on appearance of the fabrics. Figure 4 illustrates the images of knitted fabrics produced by textured yarns intermingled at different pressure levels.

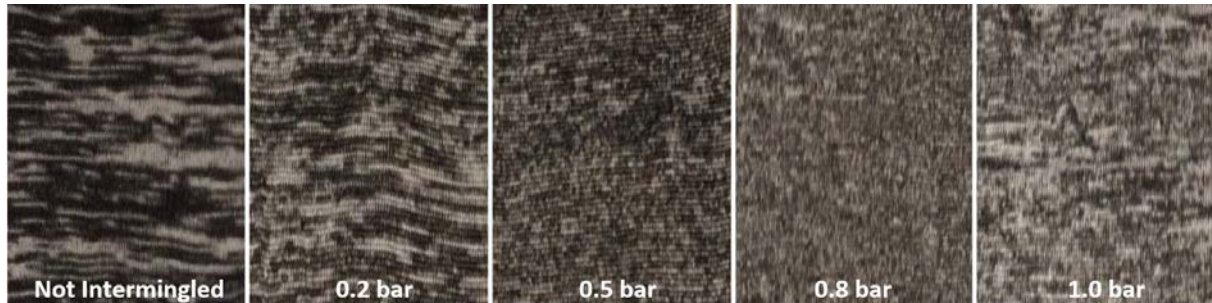


Figure 4. Images of knitted fabrics produced by melange textured yarns

4. CONCLUSIONS

In this study, effects of intermingling pressure level on properties of 100% polyester textured yarns were evaluated. Basically, it can be concluded that intermingling has negative effect on mechanical properties of yarns. Nevertheless, results showed that 0.8 bar intermingling pressure gives the optimum results amongst the intermingled yarns. Additionally, total number and stability of interlaces achieved the maximum values at 0.8 bar pressure level. To determine the effects of intermingling pressure level on frictional properties of textured yarns, yarn-to-yarn, yarn-to-metal and yarn-to-ceramic friction coefficients were measured. Friction coefficients were the highest for textured yarns without intermingling. Within the context of study, knitted fabrics were produced from melange textured yarns and it was observed that the most homogenous fabric surface appearance were obtained by use of yarns intermingled at 0.8 bar.

ACKNOWLEDGEMENTS

Thanks to Işıksöy Tekstil for their support about materials and laboratory tests.

References

1. Atkinson, C. (2012). *False twist textured yarns - Principles processes and applications*. Woodhead Publishing Limited (Cambridge, UK).
2. Hearle, J.W.S., Hollick, L., Wilson, D.K. (2001). *Yarn texturing technology*. Woodhead Publishing Limited (Cambridge, UK).
3. Duru Baykal P., Özkan, İ., (2013). *The effects of intermingling process parameters and number of filaments on intermingled yarn properties*. *Journal of the Textile Institute*. 104(12). 1292-1302.
4. Özkan, İ., Duru Baykal, P. (2012). *The effect of the production parameters of intermingling and filament properties on the stability of yarn nips*. *Journal of Textiles and Engineer*, 19, 1–6.
5. Acar, M., Wray, G.R. (1986). *An analysis of the air-jet yarn-texturing process. Part vii: The effects of processing parameters on yarn properties*. *Journal of The Textile Institute*, 77, 377–385.
6. Bilişik, A., Demiryürek, O. (2010). *Analysis and off-axis tensile characterization of air-entangled textured polyester woven fabrics depending on unit cell interlacing frequency*. *Fibers and Polymers*, 11, 805–811.

7. Chau, S., Liao, W. (2008). Determination of yarn interlacing frequency of triangular interlacing nozzles through a compressible flow simulation. *Textile Research Journal*, 78, 699–709.
8. Marengo, E., Robotti, E., Bobba, M., Liparota, M.C. (2005). Optimization of the setting parameters of a probe analyzer used for quality assessment of the interlace level and variation of textile polyester fibers. *Journal of The Textile Institute*, 96, 371–379.
9. Miao, M., Soong, M. (1995). Air interlaced yarn structure and properties. *Textile Research Journal*, 65, 433–440.
10. Versteeg, H.K., Acar, M., Bilgin, S. (1999). Effect of geometry on the performance of intermingling nozzles. *Textile Research Journal*, 69, 545-551.
11. Kothari, V.K., Mukhopadyay, A., Kaushik, R.C.D. (2001). Effect of process variables on textured yarn instability. *Textile Research Journal*, 71, 657-660.
12. Alagirusamy, R., Ogale, V., Vaidya, A., Subbarao, P.M.V. (2005). Effect of jet design on commingling of glass/nylon filaments. *Journal of Thermoplastic Composite Materials*, 18, 255-268.
13. Golzar, M., Brunig, H., Mader, E. (2007). Commingled hybrid yarn diameter ratio in continuous fiber-reinforced thermoplastic composites. *Journal of Thermoplastic Composite Materials*, 20, 17-26.
14. Miao, M., Soong, M.C. (1995). Air interlaced yarn structure and properties. *Textile Research Journal*, 65, 433-440.

CHANGES OF WATER VAPOUR PERMEABILITY AND ABSORPTION BY USING OF BAMBOO MATERIALS IN THREE-LAYERED UPPER FOOTWEAR PACKAGES

Katarzyna Ławińska¹, Wioleta Serweta¹, Natalia Popowych²

¹Institute of Leather Industry, Lodz, Poland, w.serweta@ips.lodz.pl, phone: +48422536108, fax: +48426576275

² Lviv University of Trade and Economics, Lviv, Ukraine, popovich.n@i.ua, phone: +380322756550
corresponding author: k.lawinska@ips.lodz.pl

Abstract

The aim of this work is to analyse of water vapour transport mechanism through the upper footwear material packages. These packages were made up of three layers: inner layer in the foot skin neighbourhood, outer layer – which have contact with surrounding environment. As an integrating layer, the polyurethane foam was used. Experimental results of changes in water vapour permeability and absorption values of material packages by using of bamboo textiles in comparison with standard cotton materials used as linings. In the next step, the coefficient of vapour transfer was measured in order to point optimal configuration of layers.

Key words:

bamboo textile, footwear, upper, material packages

1. Introduction

The aim of this work is objective evaluation of some textile properties connected with water vapour transport, which are important from the user's point of view. In final product – footwear in this case – the water vapour transport properties are one of basis parameters, which describe the footwear physiology in a field of temperature, moisture and air circulation [2]. Water vapour permeability indicates breathability of textiles and measures of the passage of water vapour through material or material packages. The result of the low permeability property is in extreme case wet feet. But high permeability is not a guarantee of high comfort properties. It must be connected with high absorption, because the perspiration process is important to keep the foot dry [3]. For example natural fibres like flax, cotton or their mixtures give higher ability to absorb of water or water vapour. However some polymer materials possess good permeability but in the field of absorption are weaker. So the polymer materials are very often combined with absorbent lining in the neighbourhood of skin surface.

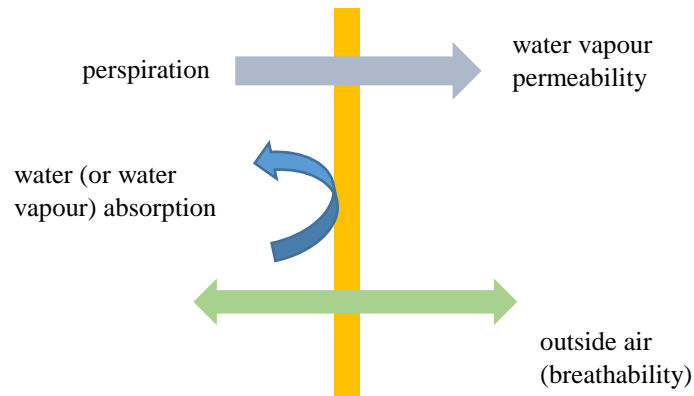


Figure 1. Movement of water vapour or water as liquid through the upper

Abovementioned properties lies very close to the textile composition. A lot of papers describe effects such material properties as weave or knit structure [6, 11], fibre type and level of blend [1, 6, 11, 14], porosity of material [14] or tightness factor [1, 11]. Ozdil and coauthors [9] gave a proposal of regression equation between water vapour permeability and fabric parameters as twist coefficient (α_e), loop length (L) and fabric thickness (T). This relation is given as follows:

$$WVP = 39.6 + 2.10 \cdot \alpha_e + 7.28 \cdot L - 12.2 \cdot T \quad (1)$$

In paper [5] by using linear regression, several linear models were developed. The models involved some factors as: fibre volume, weft density, air permeability, warp density, picks, weight, ends and weight.

Making a two (or multi) layered materials: with conductive and diffusive functions give a possibility of improve a hygienic properties of material packages and it plays a significant role in comfort sensation for users [12, 13]. This concept was also inspiration of research described in this work. There was created two – layered upper combinations of textiles with bamboo fibres with use of a polyurethane foam as an adhesive medium. It process was important in order to examine properties of bamboo packages in comparison with standard materials used today – especially cotton.

2. Experimental

2.1. Materials

In order to examine hygienic properties of material packages, the two layered materials based on bamboo textiles were moulded with use a perforated polyurethane foam of thickness 1.2 mm as an adhesive medium. The set of textiles, which were used is listed in Tab. 1. In such prepared material packages (Tab. 2) the water vapour absorption and permeability were measured and compared with the same properties of single materials.

Table 1. Characteristics of the tested materials

Sample	Material type	Mass per square meter, [g/m ²]	Thickness, [mm]	Bulk density, [kg/m ³]
M1	Woven	170	0.40	425
M2	Woven	500	1.74	287
M3	Woven	300	0.61	492

M4	Woven	170	0.35	486
B1	Woven	230	0.58	397
B2	Woven	145	0.37	392
M5	Knitwear	290	1.20	242
M6	Knitwear	220	0.38	579
M7	Knitwear	320	0.86	372

Table 2. Characteristics of the tested packed materials

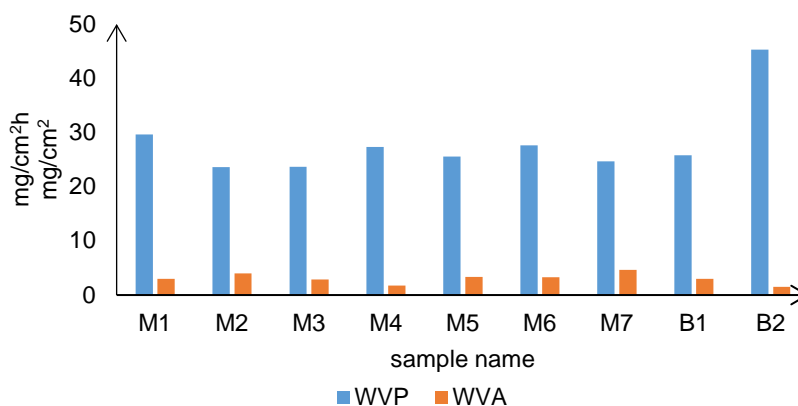
Sample	Mass per square meter, [g/m ²]	Thickness, [mm]	Composition, [%]
B1/B2	375	2.15	cotton 100%/PU/cotton 100%
B1/M1	400	2.18	cotton 100%/PU/bamboo 100%
B1/M2	730	3.52	cotton 100%/PU/bamboo 100%
B1/M3	530	2.39	cotton 100%/PU/95% bamboo+5% polyester
B1/M4	400	2.13	cotton 100%/PU/50% bamboo+50% flax
B1/M5	520	2.98	cotton 100%/PU/85% bamboo+15% polyester
B1/M6	450	2.16	cotton 100%/PU/95% bamboo+5% elastane
B1/M7	550	2.64	cotton 100%/PU/97% bamboo+3% elastane

2.2. Methods

In order to measure the hygienic properties of listed in Table 1 material packages, the water vapour permeability (W_{VP}) and water vapour absorption (W_{VA}) were measured due to methodology described in ISO standard [10].

3. Results and discussion

In order to create optimal material packages, the single textiles were measured in a field of basic hygienic properties. Figure 2 shows, that in the group of bamboo materials M1 – M7, the coefficient of variation of results reached low level – 9% for WVP and 28% for WVA. The obtained results were not drastically different than each other and ranged from 23.61 mg/cm²·h for M2 to 29.62 mg/cm²·h for M1. Absorption property was described by values ranged from 1.72 mg/cm² for M4 to 4.62 mg/cm² for M7.


Figure 2. Results of hygienic properties of tested materials

In order to create material packages based on bamboo textiles, as outer layer was used B1, which is standard material for children footwear. As a lining were used bamboo materials M1 – M7 in order to improve hygienic parameters. Experimental results for material packages are shown on a Fig. 3.

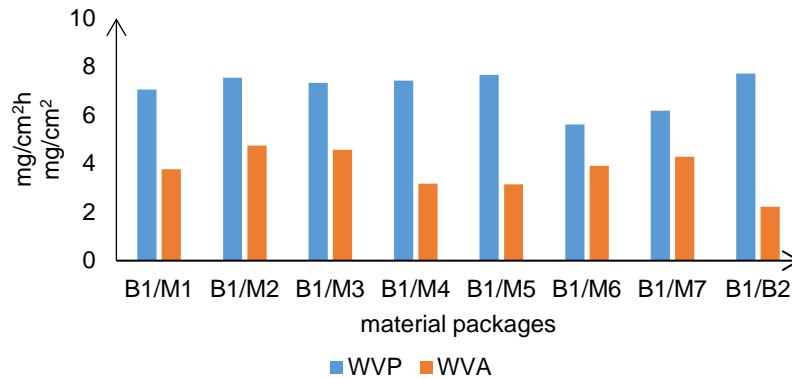


Figure 3. Results of hygienic properties of tested material packages

It can be seen, that the maximum value of water vapour permeability occurred for B1/M5 package and was equal to 7.7 mg/cm²h in contrast to B1/M6 package, where the WVP reached 5.6 mg/cm²h. According to absorption property, the values ranged from 4.8 mg/cm² for B1/M2 to 3.2 mg/cm² for B1/M5. It was observed (Fig. 3), that through conducted moulding of materials, the values of water vapour absorption increased rapidly. When the standard cotton lining material B2 was used, the control sample was characterised by the weakest water vapour absorption value – 2.2 mg/cm². On the Figure 4 are described the differences between values of absorption of material packages with use of bamboo textiles compared with control sample B1/B2. This situation could be transposed into the comfort properties of the final product. Literature sources give a lot of examples, when properly combined material packages could improve the breathability or other properties of products. For example in paper [8] it was shown, that relationship between the thermal – insulation properties of single materials and multi-layered packages is very strong. In [13] authors showed that reduction of the total thermal resistance in warm – cool feeling fabrics is possible by spot bonding the outer fabric interlining and lining together.

In case of indoor children footwear, very important aspect is connected with breathable properties rather than for example liquid water penetration. Modification of upper combination by use of bamboo textiles gave good results in order to improve hygienic property and functionality.

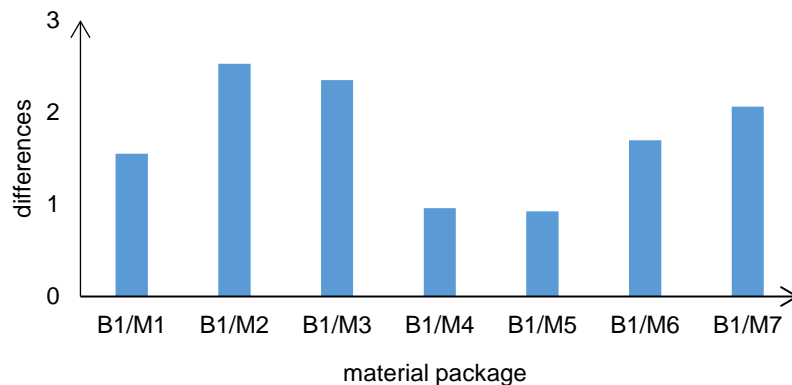


Figure 4. Differences between values of absorption of bamboo packages and B1/B2 (control sample)

The maximum differences were observed for B1/M2 and B1/M3. This means that M2 and M3 were qualitative better materials for linings than B2. Cotton material is popular material used for linings and uppers for footwear. Experimental results done in his paper prove, that cotton material can be substituted by textile bamboo materials and it change improve hygienic properties of whole materials package. It is worth noting (Fig. 5), that the water vapour absorption for material packages is close to the sum of particular absorptions. In contrast – the water vapour permeability is lower for packages.

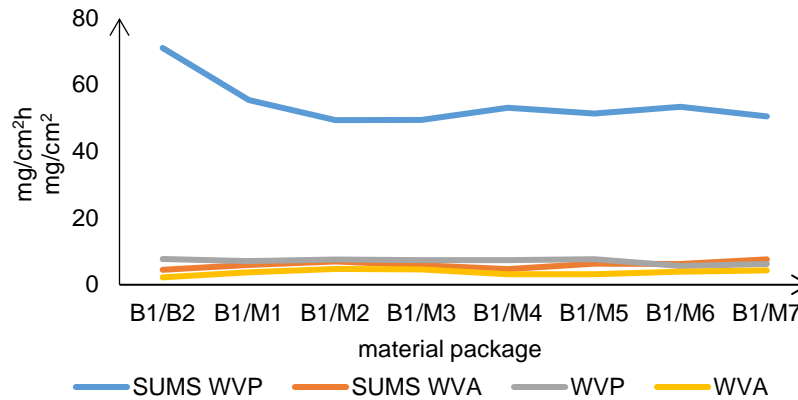


Figure 5. Relation between hygienic properties for single materials in contrast to packages

The same tendency is transposed to water vapour coefficient, which is equal to:

$$W_{VC} = 8 \cdot W_{VP} + W_{VA}. \quad (2)$$

It is a linear dependency between water vapour permeability and absorption. For these materials the water vapour coefficient demonstrates strong non – additive property (Fig. 6).

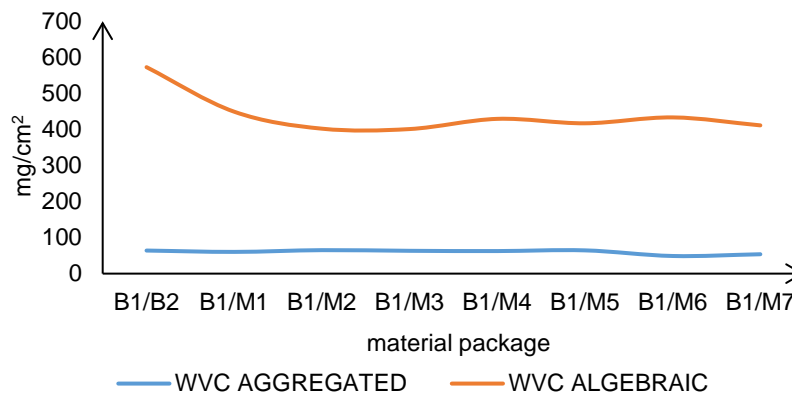


Figure 6. Aggregated water vapour coefficient versus algebraic sums of coefficients for examined packages

In the next part of this paper, authors tried to find at least one statistically significant dependence between material characteristics and hygienic properties. Thickness of packages was taken into account. In packages B1/M1 – B1/M7, B1/B2, only the thickness of single materials: M1 – M7 and B2 were treated as variables. On the other hand thickness of B1 and polyurethane adhesive foam were constant and equal to 0.58 and 1.2 mm, respectively. So in order to find relationship between predictor variable (water vapour coefficient, water vapour absorption and permeability) and criterion variable (thickness of material) the multiple regression was done. This method gave a linear dependence between water vapour coefficient and thickness of material. This relationship is described by following equation:

$$\overline{W_{VC}} = 8.423 \cdot Thickness + 6.755, \quad (3)$$

where \overline{W}_{vc} is estimated water vapour coefficient. The rest of parameters as effects of multiple regression procedure are given in the following tables (3) - (5).

Table 3. Summary regression model (superscript a means predictor - W_{vc})

Model	R	R Square	Adjusted R Square	Std. Error of the Estimate
1	0.985 ^a	0.971	0.966	0.79242

Table 4. ANOVA^b table for regression model (superscript b means dependent variable – thickness)

Model	Sum of squares	df	Mean Square	F	Significance
Regression	126.064	1	126.064	200.762	0.000 ^a
Residual	3.768	6	0.628		
Total	129.832	7			

Table 5. Table of standardized and unstandardized coefficients

Model	Unstandardized Coefficients		Standardized Coefficients	t	Significance
	B	Std. Error	Beta		
1 Constant	6.755	0.521	0.985	12.969	0.000
Thickness	8.423	0.594		14.169	0.000

The F-test value equal to 200.762 determines the good fit of this model for the data on the satisfactory significance level (less than confidence: $\alpha = 0.05$). Also R – value near to 1 describes a strong dependence between water vapour coefficient and thickness of given material.

4. CONCLUSIONS

Studies performed in this paper, showed, that bamboo textiles can be used for footwear elements in order to effective improvement of their hygienic properties. Although water vapour permeability decreases with the increase of mass per unit area, there are possibilities to improve other parameters, like absorptivity of inner layer, which can reduce precipitation of shoe materials. It is important aspect in creating an optimal comfort conditions inside a shoe volume during footwear using. A lot of literature sources show, that bamboo textiles have a lot of incredible properties. These materials are breathable, cool, extremely soft, which is very big advantages, with regard to footwear. Moreover, they are good water absorbers and have antimicrobial properties. They are more hydroscopic than conventional fibres like cotton or polyester. Results showed in this paper are fragmentary research, which were carried out in this field [7]. The experimental tests of bamboo materials will be continued in the wider spectrum of parameters and configurations in order to confirm a possibility of use the bamboo textiles to improve the hygienic and mechanical properties of children footwear. The second aim of this research is to find a specific material package, which will be optimal from the comfort use and health point of view.

ACKNOWLEDGMENT

The research work has been carried out within project: "Use of bamboo extract and fibres in the elements of leather, textile and combined leather and textile children's footwear" financed by the National Centre for Research and Development (Agreement No. LIDER/16/0091/L-8/16/NCBR/2017).

References

1. Cil, M.G., Nergis, U.B., Canndan, C. 2009. An experimental study of come comfort – related properties of cotton – acrylic knitted fabrics, *Textile Research Journal*, 79(1), 917- 923.
2. Das, S., Kothari, V.K. 2012. Moisture vapour transmission behaviour of cotton fabrics. *Indian Journal of Fibre and Textile Research*, 37, 151-156.
3. Gulbiniene, A., Jankauskaite, V., Saceviciene, V., Mickus, K.V. 2007. Investigation of water vapour resorption – desorption of textile laminates. *Materials Science*, 13(3), 255- 261.
4. Hes, L., De Araujo, M., Djulay, V.V. 1996. Effect of mutual bonding of textile layers on thermal insulation and thermal contact properties of fabric assemblies, *Textile Research Journal*, 4 (66), 245.
5. Irandoukt, S., Irandoukt, A. 2011. Development of the predictive models for the fabric water vapour resistance. *Journal of Engineered Fibers and Fabrics*, 6(2), 40-49.
6. Knight, B.A., Hersh, S. P., Brown, P. 1970. Moisture characteristics of some knit fabric made from blend yarns. *Textile Research Journal*, 1, 843- 851.
7. Ławińska, K., Serweta, W., Gendaszewska, D. 2018. Applications of bamboo textiles in individualised children's footwear. *Fibres and Textiles in Eastern Europe*, 5(131), 87-92.
8. Matusiak, M., Kowalczyk, S. 2014. Thermal – insulation properties of multilayer textile packages. *AUTEX Research Journal*, 14(4), 299-307.
9. Ozdil, N., Marmarali, A., Kretzchmar, S.D. 2007. Effect of yarn properties on thermal comfort of knitted fabrics. *International Journal of Thermal Science*, 46(12), 1318- 1322.
10. PN-EN ISO 20344: 2012 Personal protective equipment – Test methods for footwear
11. Prahsarn, C., Barker, R.L., Gupta, B. S. 2005. Moisture vapour transfer behaviour of polyester knit fabrics. *Textile Research Journal*, 75(4), 346- 351.
12. Serweta, W., Olejniczak, Z., Woźniak, B. 2017. Influence of the thermal and humidity properties of multi – layered lining fabrics on microclimate of leather footwear. In: Frydrych I, Bartkowiak G, Pawłowa M, editors. *Innovations in Protective and E-textiles in Balance with Comfort and Ecology*. Lodz: Lodz University of Technology.
13. Serweta, W., Olejniczak, Z., Woźniak, B. 2018. Analysis of insole material impact on comfort during physical exertion. *Fibres and Textiles in Eastern Europe*, 26, 2(128): 100-103.
14. Yoon, H.N., Buckley, A. 1984. Improved comfort polyester, part I: transport properties and thermal comfort of polyester/cotton blend fabrics. *Textile Research Journal*, 54(3), 259-298.

PREDICTIVE MODELLING OF OPEN AREA AND AIR PERMEABILITY OF COTTON PLAIN WOVEN FABRICS

Julie Abel¹, Roshan Unmar² & Satyadev Rosunee²

^{1,2}Department of Applied Sustainability and Enterprise Development, University of Mauritius, Reduit (Mauritius), ¹p.julie.abel@gmail.com, +23059155068
²unmarr@uom.ac.mu & s.rosunee@uom.ac.mu

Abstract:

The pore properties of fabrics have been found to affect to a large extent its permeability and thermal properties. The open area of 100% cotton plain woven fabrics was evaluated considering the inherent randomness of its structure using image processing and image analysis techniques. Most of the existing open area models are based on idealistic assumptions such as uniform cylindrical yarn and uniformly distributed rectangular inter-yarn pores. However, it is known that the pores in real fabrics have different dimensions and shapes throughout the fabric area and hence the pore distribution deviates significantly from such idealistic assumptions. In this work multiple linear regression (MLR) and artificial neural network (ANN) methodologies were investigated for the prediction of the open area. Warp sett, weft sett, warp linear density and weft linear density were the structural parameters used as inputs to the open area model. Both methods were found to give acceptable predictive errors, much lower than those obtained with theoretical model that assumes uniform circular cross-section of yarn and regular spacing between adjacent yarns. Corresponding values of air permeability were then obtained using FX3300 air permeability tester to produce an empirical equation relating air permeability to open area. For comparison purposes another empirical equation was developed to relate air permeability to average values of warp and weft linear density and warp and weft setts. Validation of both empirical models revealed much better prediction of air permeability when using open area as input instead of the warp and weft parameters. This may be due to the ability of the image analysis technique to capture variations in the pore structure of the fabric which have a significant effect on its air permeability.

Key words:

Woven fabrics, open area, image analysis, multiple linear regression, artificial neural network, air permeability.

1. Introduction

Open area is defined as the ratio of the total void area to the total area of a fabric [13]. It contributes to the porosity of a fabric which is defined as a fraction of the total volume spaces over the total fabric volume. The porosity is characterised as the air trapped inside the voids formed by the yarn interlacement of a cloth in dry state [6]. Porosity can be classified as inter-yarn, intra-yarn and intra-fibre; these are spaces in-between the yarns, in-between fibres in yarn and in fibre substances respectively. The importance of the type of porosity depends on the fabric purposes. The inter-yarn porosity is of great significance in the case of air permeability, transmission of UV rays, screen printing, etc. For the absorption of humidity and capillary phenomenon, the intra-yarn porosity, also known as micro porosity [15] and inter-fibre porosity [13], is essential. It was reported that the inter-yarn porosity is influenced by the fabric structural parameters: yarn sett, yarn diameter, yarn twist, weave type, fabric thickness [1, 10], yarn density [7], as well as the fibre characteristics [13].

In theoretical open area model, yarns are represented as impermeable monofilament structures [13]. The fabric open area is determined as the complement to the cover factor, equations 1 and 2, where CF and OA are the cover factor and open area, in percentage, respectively [4,7,15]. Figure 1 shows one inter-yarn pore and its characteristics. The cover factor of a fabric is defined as the ratio of the area covered by its yarns to the total area of the web [11].

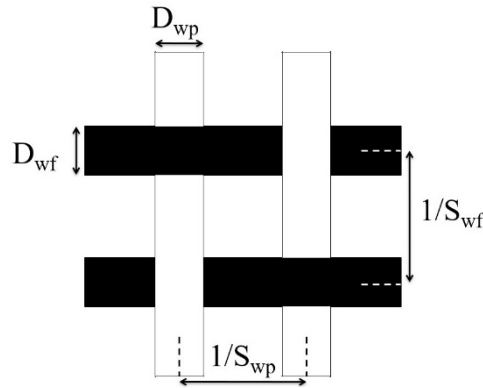


Figure 1. One inter-yarn pore dimensional characteristics scheme

D_{wp} : warp diameter (m); D_{wf} : weft diameter (m); S_{wp} : warp sett (1/m); S_{wf} : weft sett (1/m)

$$CF = (S_{wp}D_{wp} + S_{wf}D_{wf} - S_{wp}D_{wp}S_{wf}D_{wf}) \times 100 \quad (1)$$

$$OA = 100 - CF \quad (2)$$

The model is based on idealistic assumptions, such as the uniform cylindrical yarn and uniformly distributed rectangular inter-yarn pores. However, during the weaving process yarn flattening and yarn cross-section deformation occur due to normal forces applied between the yarn systems [9]. In this work the open area of woven fabrics was evaluated considering the inherent randomness of its structure, namely, the pore non-uniform cross-sectional shape and dimension of yarn throughout its length. Consequently, predictive models of the fabric open area were developed from the experimental data obtained. Multiple linear regression technique and artificial neural network methodology were used for modelling. Artificial neural network (ANN) which is one tool of AI is a simplified representation of the biological neurons and their functioning. It is mainly related to statistical estimation, optimisation and control theory. ANN which is mostly used in machine learning has shown great success in the field of speech recognition, image analysis and adaptive control mechanisms through software agents [8]. Nowadays ANN is applied more and more to textile engineering; in the prediction of fibre properties [5], yarn properties [3, 14] and fabric properties [2,9,12] The influence of the fabric structural parameters, namely, warp sett, weft sett, warp linear density and weft linear density was studied.

2. Experimental

2.1. Materials

For this study seventy 100% cotton plain woven fabrics with varied structural parameters were selected to develop (60) and validate (10) the open area predictive models. Sixty-four samples were used for the development of the air permeability models and the testing of the effect of the open area values on the air permeability. For the air permeability model validation ten fabric samples were used.

2.2. Methods

2.2.1 Open Area Measurement

The methodology is composed of the open area measurement and model development respectively and the air permeability model development. The open area, yarn linear density, yarn sett and air permeability of the fabric samples were measured. All fabric samples were conditioned at 65±4% relative

humidity and at a temperature of $20 \pm 2^\circ\text{C}$ for a minimum of 6 hours before all tests. The optical fabric open area measurement consisted of two parts, image capture and analysis respectively. Magnified representation (4X) of the fabric samples were taken using Motic digital microscope (model BA310) which includes built-in 3.0 mega pixel digital camera and its integrated Motic Images software (Plus 2.0ML version). The fabric samples were placed under the microscope with the light source found underneath. Forty-five images of resolution 2048×1536 corresponding to $3.28\text{mm} \times 2.45\text{mm}$ were taken on three A4 fabric samples. Image processing techniques were developed to measure the open area of fabrics using Microsoft Visual C++ and OpenCV library. The fabric microscopic images were processed through the following steps (see Figure 2).

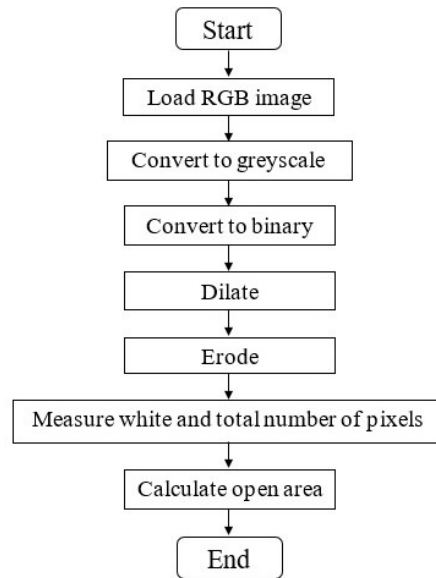


Figure 2. Open area measurement algorithm flowchart

The digital image, in JPEG format, which is loaded in RGB colour image, is converted first in greyscale, and then to binary in order to segment the pore (white) and the yarn (black) regions. To eliminate the hairs inside the pore area, dilation and erosion operations which aim at enlarging and reducing the object (pore) pixel borders, respectively, were applied (see Figure 3). A rectangular structuring element of size 37×37 were used for dilation and erosion, respectively.

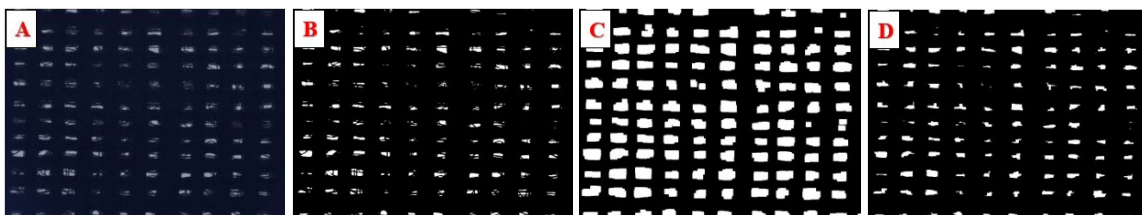


Figure 3. Image processing of fabric (a) RGB image, (b) binary image, (c) dilated image, (d) eroded image

The fabric open area was calculated based on equation 3. The sum of the pore area and the fabric area were measured by counting the white pixels and the total number of pixels in the image respectively. The number of warps and wefts per centimeter was measured according to ASTM D3775-03a. The yarn linear density was measured using a Shirley crimp tester, according to ASTM D3883-99.

$$Open\ Area = \frac{\sum Open\ Area}{Fabric\ Area} \times 100\% \quad (3)$$

2.2.1 Open Area (OA) Modelling

Multiple linear regression with fabric structural parameters as input: warp sett (WPS), weft sett (WFS), warp linear density (WPLD) and weft linear density (WFLD) were developed using IBM SPSS statistics. The details of the dataset variables are given in table 1. The adjusted coefficient of determination (Adjusted R^2) was used to analyse the regression model. The coefficient of determination (R^2) of simple linear regression model reveals the degree to which the variance in the dependent variable can be predicted from the independent variable. In the case of the multiple linear regression the adjusted coefficient of determination better explains the prediction capability of the model. With the addition of predictors, the coefficient of determination increases automatically, even if the independent variables do not significantly improve the model predictability. This can lead to the overfitting of the data. On the other hand, the adjusted coefficient of determination will increase only if the new term added enhances the model more than what would be expected by probability. The adjusted R^2 can be calculated based on the coefficient of determination of the sample, the number of predictors (p) and the total sample size (N), equation 4.

Table 1. Open area modelling dataset details

Fabric Structural Parameters	OA (%)	WPS (per cm)	WFS (per cm)	WPLD (tex)	WFLD (tex)
Mean	4.79	37.92	27.21	14.94	15.29
Std. Deviation	4.03	8.79	4.77	5.23	5.52

$$\text{Adjusted } R^2 = 1 - \frac{(1-R^2)(N-1)}{N-p-1} \quad (4)$$

Artificial intelligence, namely back-propagation feed-forward neural network (ANN) was also used to model the fabric open area. ANN consists of numerous simple and highly interconnected neurons joined by weights which decide how the data is transferred from one neuron to another. A set of input and its corresponding output data allow the whole system to learn from examples. It is known as supervised learning. During the training process the weights are adjusted iteratively to match the two sets of data [3]. The weighted neuron is passed through some activation function which needs to be defined to generate its output. In this work several ANN were developed with 4-element input comprising of warp sett, weft sett, warp linear density and weft linear density, and one output, open area. The Levenberg-Marquardt algorithm which is used to update the weights and biases was chosen because of its fast convergence and good performance for training small and medium-sized networks. Twenty-eight networks comprising of only one hidden layer were tested. Every two networks consisted of varying number of neurons, from 2 to 15, respectively, with alternate transfer functions: log-sigmoidal and tan-sigmoidal. Each network has an output layer of linear neurons. The network architecture is shown in figure 3.

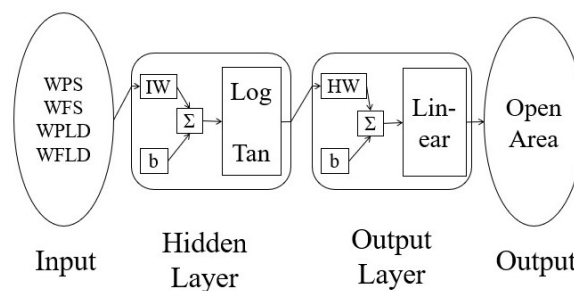


Figure 3. Neural Network Architecture (IW: input weight; HW: output weight; b: bias; WPS: warp sett; WFS: weft sett; WPLD: warp linear density; WFLD: weft linear density)

The most appropriate combination network with highest coefficient of correlation (R) and lowest mean squared error (MSE), equation 5, was chosen.

$$MSE = \frac{1}{n} \sum_{i=0}^{n-1} (t_i - o_i)^2 \quad (3)$$

Where t_i and o_i are, in general, the target and output values of i th trial presentation, respectively. In this work the target and output values correspond to the open area values obtained experimentally and from the neural network model, respectively.

2.2.1 Air Permeability (AP) Modelling

The open area values obtained from image analysis and processing were tested in air permeability linear regression models. It was considered as one of the independent variables. The fabric thickness (Th), warp sett, weft sett, warp linear density and weft linear density were also investigated as predictors. Table 2 shows the details of the variables. The air permeability of the fabric samples were measured according to BS EN ISO 9237. FX3300 air permeability tester was used. The fabric thickness was measured according to ASTM D1777.

Table 2. Air permeability modelling dataset details

Fabric Structural Parameters	AP (mm/s)	OA (%)	Th (mm)	WPS (per cm)	WFS (per cm)	WPLD (tex)	WFLD (tex)
Mean	728.32	5.09	0.29	35.80	26.04	17.58	18.89
Std. Deviation	568.38	4.60	0.10	9.89	5.71	11.14	12.79

3. Results and discussion

3.1. Open Area Multiple Linear Regression Model

The results obtained revealed a highly moderate linear relationship between open area and the fabric structural parameters, with an R²-value of 0.64. The regression equation is given below:

$$OA = 39.45 - 0.40WPS - 0.33WFS - 0.11WPLD - 0.59WFLD \quad (4)$$

Where WPS and WFS are warp and weft sett, per centimetre, respectively, and WPLD and WFLD are warp and weft linear density, in tex, respectively. An average error of 2.47% were obtained when new samples data were fed to the model which shows good generalization of the model.

3.2. Open Area Artificial Neural Network Model

Several back-propagation feed-forward neural networks with different architectures were developed to predict the fabric open area. The results obtained from the twenty-eight architectures tested are shown in figure 4. The best network was obtained from an architecture made up of one hidden layer with 11 neurons having a log-sigmoidal transfer function with an MSE of 17.35%.

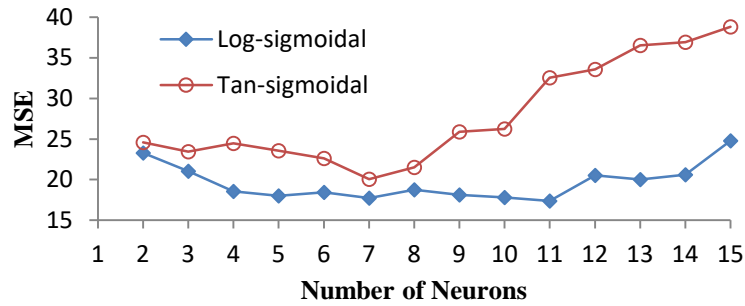


Figure 4. MSE of ANN architectures

The selected network was fed with fresh data (testing dataset) and simulation was performed to test its degree of generalisation. A percentage average error of 1.05 was obtained. The results obtained were compared with those of multiple linear regression model (see Figure 5). It is observed that the open area predicted by ANN gives more accurate results with very low percentage errors. Thus, the predicted values from the ANN prove that the network is a successful tool in reasonably predicting the open area of 100% cotton plain woven fabrics.

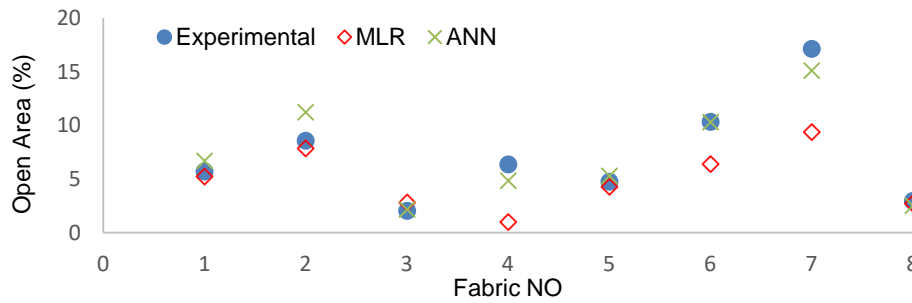


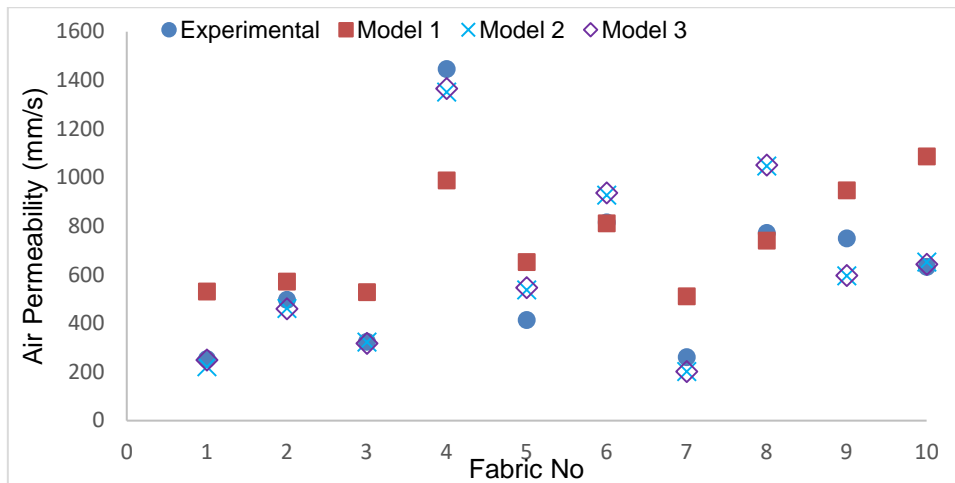
Figure 5. Predicted and experimental open area values of testing samples

3.3 Air Permeability Linear Regression Model

Three air permeability linear regression models were developed to investigate the effect of the open area, fabric thickness, yarn sett and yarn linear density as predictors. The models developed and their results are found in table 3. The fabric open area and thickness are observed to give the best results with a high coefficient of determination (0.93) and low average error when tested on new samples (14%). However, the fabric thickness was found to be insignificant (p -value=0.49). According to the literature review, the volume of the openness plays an important role in the air permeability prediction [15]. The high p -value of the fabric thickness may be due to the thin fabric samples used for the model development with an average of 0.3 millimetres. Therefore, the openness of the sheet-like fabric samples has a greater effect on the air passing through compared to the pore channels since the fabric thickness is so small that it is negligible. The air permeability model validates the pore area models developed which consider the randomness of the pore dimensions. Figure 6 shows the values obtained from the different air permeability models when ten fabric samples were used to test the models. It is observed that when the four parameters: yarn sett and yarn linear density, are used as predictors, the air permeability values deviate more compared to the other models. This is due to the fact that the variation in these parameters from which random pore sizes arises are not considered. However, the other models with the fabric open area values obtained from the image analysis and processing as independent variable consider the variation in the pore sizes throughout a fabric and hence gives better air permeability results.

Table 3. Air permeability regression models results

Model No	Predictors	R ² /Adjusted R ²	Average error (%)
1	WPS, WFS, WPLD, WFLD	0.57	48
2	OA	0.93	15
3	OA, Th	0.93	14


Figure 6. Predicted and experimental air permeability values of testing samples

4. CONCLUSIONS

A multiple linear regression model and an artificial neural network model for comparison were developed to predict the open area of 100% cotton plain woven fabrics. It was assumed that the yarn was free of any hairiness. In addition, the inherent randomness of the textile structure, namely the variable pore dimensions, was considered. Warp sett, weft sett, warp linear density and weft linear density were the structural parameters used as inputs. The work performed demonstrates a good predictability of the MLR model with adjusted R² value of 0.64. The model was tested on ten samples and an average error of 2.47% which highly validates the model were obtained. However, the back-propagation feedforward neural network model when tested with the same samples give better average error of 1.05% which validates ANN as a good tool in predicting the fabric open area. Air permeability models were developed considering the fabric open area obtained from image analysis and processing, fabric thickness, yarn sett and yarn linear density as predictors. It was found that the fabric open area as input in the model gives results close to the values obtained experimentally with an R² value of 0.93. An average error of 15% were obtained when ten new fabric samples data were input into the model. The results obtained validates the open area model considering the random pore sizes and it shows that it has an impact on the fabric air permeability prediction. However, the open area model could further be improved, with the inclusion of hairiness.

ACKNOWLEDGEMENTS

The authors gratefully acknowledge the sponsorship of Tertiary Education Commission, Mauritius for the research.

References

1. Backer, S. (1951). *The relationship between the structural geometry of a textile fabric and its physical properties: part IV: Interstice geometry and air permeability*. *Text. Res. J.*, 21(10), 703-714.
2. Bhattacharjee D and Kothari VK. (2007) *A neural network system for prediction of thermal resistance of textile fabrics*. *Text. Res. J.*, 77(1), 4-12.
3. Chattopadhyay R. (ED.). (2011). *Artificial neural networks in yarn property modeling*. (1st ed.). In: Majumdar A (ed) *Soft computing in textile engineering*. Woodhead Publishing Limited (UK), pp.105-125.
4. Havlova M. (2013) *Air permeability and constructional parameters of woven fabrics*. *Fibres Text. East. Eur*, 2(98), 84-89.
5. Kuo CFJ, Hsiao KI and Wu YS. (2004) *Using neural network theory to predict the properties of melt spun fibers*. *Text. Res. J.*, 74(9), 840-843.
6. Mangat MM, Hes L and Bajzik V. (2015) *Thermal resistance models of selected fabrics in wet state and their experimental verification*. *Text. Res. J.*, 85(2), 200-210.
7. Matusiak M. (2015) *Application of artificial neural networks to predict the air permeability of woven fabrics*. *Fibres Text. East. Eur*, 1(109), 41-48.
8. Muruganath M. (Ed.) (2011). *Artificial neural networks in materials modelling*. In: Majumdar A (ed) *Soft computing in textile engineering*. (1st ed). Woodhead Publishing Limited (UK). pp.25-44.
9. Pattanayak AK, Luximon A and Khandual A. (2011) *Prediction of drape profile of cotton woven fabrics using artificial neural network and multiple linear regression*. *Text. Res. J.*, 81(6), 559-566.
10. Robertson AF. (1950). *Air porosity of open-weave fabrics: Part I: Metallic meshes*. *Text. Res. J.*, 20(12), 838-844.
11. Tapias M, Rallo M and Escofet J. (2011). *Automatic measurements of partial cover factors and yarn diameters in fabrics using image processing*. *Text. Res. J.*, 81(2), 173-186.
12. Tokarska M. (2004). *Neural model of the permeability features of woven fabrics*. *Text. Res. J.*, 74(12), 1045-1048.
13. Turan RB, Okur A, Deveci R, et al. (2011). *Predicting the intra-yarn porosity by image analysis method*. *Text. Res. J.*, 82(16), 1720-1728.
14. Turhan Y and Toprakci O. (2013) *Comparison of high-volume instrument and advanced fiber information systems based on prediction performance of yarn properties using radial basis function neural network*. *Text. Res. J.*, 83(2), 130-147.
15. Urbas, R, Kostanjsek K and Dimitrovski K. (2011). *Impact of structure and yarn colour on UV properties and air permeability of multilayer cotton woven fabrics*. *Text. Res. J.*, 81(18), 1916-1925.
16. ASTM 3775-03a. *Standard Test Method for Fabric count of Woven Fabric*.
17. ASTM D3883-99. *Standard Test Method for Yarn Crimp or Yarn Take-up in Woven Fabrics*.

THE EFFECT OF YARN LINEAR DENSITY ON STRUCTURE PROPERTIES OF PLATED WEFT KNITTED FABRIC UNDER HOME LAUNDERING PROCESS

Irena Lenfeldova, Jana Peckova

Technical University of Liberec, Department of Textile Technologies, Studentská 2, 460 17, Liberec, Czech Republic, irena.lenfeldova@tul.cz, +420 48 535 3328, +420 48 535 3542

Abstract

The nature of the single jersey plating fabric produced by a circular weft knitting machine depends on the length of the yarn for technical face and back that enters the knitting point. According manufacturing experience the knitted structures are produced without holes and pores, i.e. if the length is very short, there are existed possibility to design the structural model. Although the fabrics are stretched during knitting, after relaxation processes the state without stress and friction are achieved and the changes of plated knitted fabrics structural parameters after laundering and drying are discussed. Fabric shrinkage in both direction in comparison of the different yarn linear density of back thread are explained.

Key words:

Plated weft knitted structure, geometry model, loop length, prediction

1. Introduction

A plated structure contains loops composed of two (or more) yarns, usually with differing physical properties. Each has been separately supplied through its own guide or guide hole to the needle hook, in order to influence its respective position relative to the surface (technical face and technical back of the fabric). Plating may be used to produce surface interest, coloured patterns, open-work lace or (especially in that case) to modify the wearing properties, abrasion resistance and hardness of the knitted structure [1].

Although a machine may be set to knit a specific stitch length, fluctuations in yarn or machine variables can affect yarn surface friction or yarn tension and ultimately influence yarn input tension at the knitting point. As a result, the ration of “robbed back” to newly-drawn yarn changes and this alters the size of the knitted loop [1, 2].

Knapton and Munden [2].suggested the phenomenon of “robbing back” to be the reason why the measured loop length in a knitted structure is smaller than the theoretical loop length when calculated from the depth of the stitch cam setting, as well as the reason for fluctuations in input tension producing large variations in loop length.

The optimal value of the ratio w/c is not observed during manufacture of the fabric under the different gauge and linear density of the yarn. According to Chamberlain model for single jersey structure that ratio is given by the value 1,155 (dependence on the yarn diameter only). Analogous the authors looked for the ratio l/d as expression of the fullness. Chamberlain's value reaches 16,64, Peirce's 16,66 and Daniel's 17,56, etc. All values or model are based on the input parameter – yarn diameter [1, 3, 4].

2. Theory and method

Although the achievement to make more closely – compact knit structures (the higher loop density of fabrics and structure with minimum of pores) with modern electronic control knitted machine, the yarn diameter still differs in the each part of the loop. Together with the spirality of the single-faced structure from the large diameter knitting machine, which influences the inclination of the columns, the yarn diameter varies in left and right parts of the loop legs. In the Figure 1 there is shown the plated knitted structure (technical face and back) with two different count of material, i.e. yarn and multifilament.

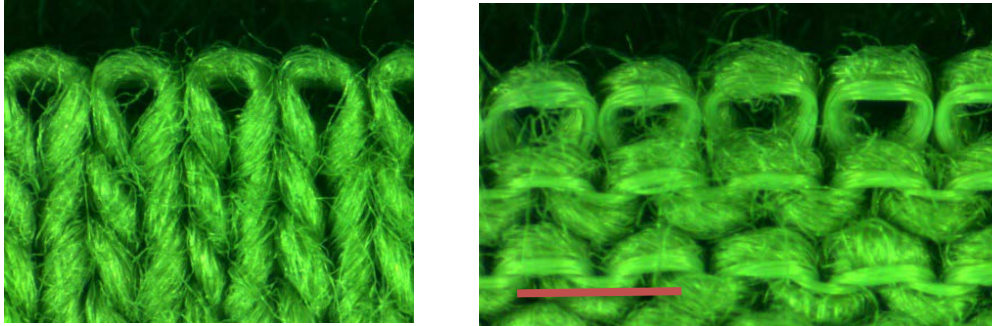


Figure 1. Technical back of produced plated weft knitted fabrics (1 mm scale)

The idea of the Chamberlain model for plain weft knitted structure [2]. was used for construction of the plated model of single jersey fabric (Figure 2). The structure of plated knitted fabric is reduced to a simple form in which the yarn axis follows a path composed of circular arcs and straight lines. This element – knitted stitch consists of two threads, back loop length l_I and face loop length l_{II} .

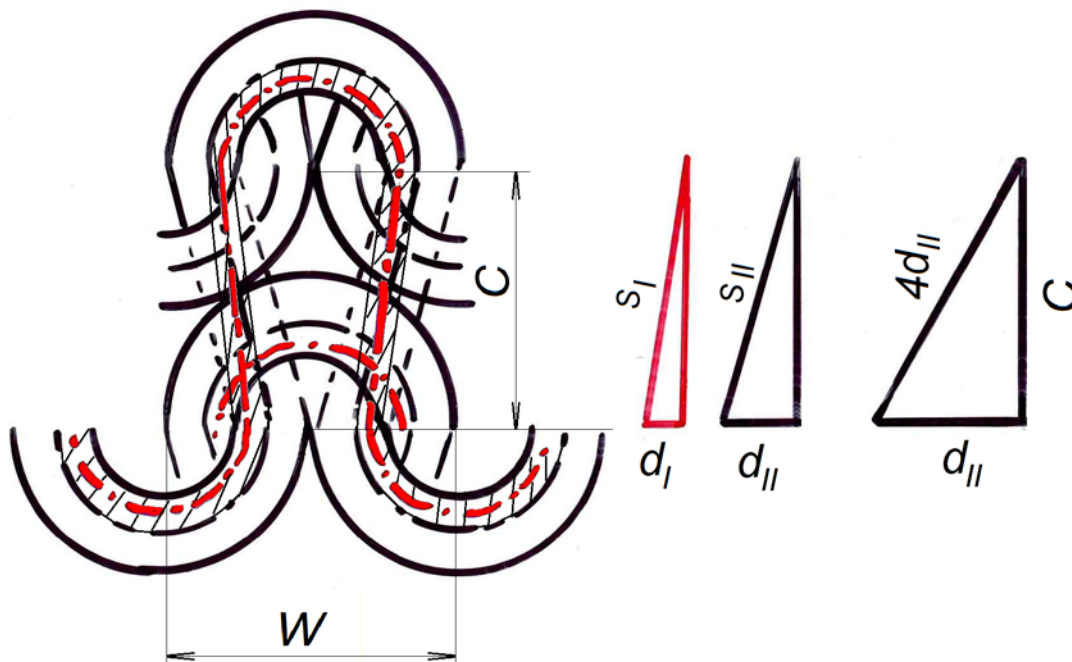


Figure 2. The model of the plated knitted structure

Firstly, consider what we may call the “closed structure” in which the yarn touches itself in each loop of course and one course just touches the next, as is presented in Figure 2. The formulas derived for flat plain plated knitting are given with the length of the yarn which includes the needle loop and half the sinker loop on either side of it, plus two legs (the length of the face loop l_{II}):

$$l_{II} = \frac{\pi}{2} (D_{jII} + D_{pII}) + 2s_{II}. \quad (1)$$

Where the needle loop diameter is given by $D_{II} = 3 d_{II}$ and the wale spacing is defined as $w = 4 d_{II}$ (Figure 2). The legs are given by the equation from modelled length (triangles)

$$s_{II}^2 = c^2 + d_{II}^2 \quad (2),$$

Where the d_{II} is thread diameter for the face yarn, c is the course spacing, s is the length of the leg.

So that for leg length is evident that

$$s_{II} = d_{II}\sqrt{13} \quad (3).$$

For the whole loop length for face thread is valid equations with using the equation (1) and (2)

$$l_{II} = \pi 3 d_{II} + 2 \sqrt{c^2 + d_{II}^2} \quad (4).$$

After model condition (3) the formulas derived for plated weft knitted loop knitting are

$$l_{II} = d_{II} (3\pi + 2 \sqrt{13}) \quad (5).$$

$$c = 2 d_{II}\sqrt{3}$$

The loop length for back thread is expressed with the similar condition for the thread geometry. The needle loop diameter is given by the formulas according construction in Figure 2

$$D_I = (2 d_{II} + d_I) \quad (6)$$

Whence d_I is the diameter for back thread (thinner one). The length of the leg is expressed with same analogy from the triangles geometry conditions: $s_I^2 = c^2 + d_I^2$ and is given by equation

$$s_I = 2 \sqrt{12 d_{II}^2 + d_I^2} \quad (7).$$

The final formula for loop length of back thread for plated weft knitted structure is:

$$l_I = \pi (2 d_{II} + d_I) + 2 \sqrt{12 d_{II}^2 + d_I^2} \quad (8).$$

2.1. Geometry of the plated knitted structures

Experimental data of input material for four plated weft knitted fabrics which can be produced with large diameter knitting machine (28 E, 30", No. of feeders 96) are given in Table 1.

To find the experimental yarn diameter it was used the same methodology. Different type of materials, structure of the comb yarn, bent of the yarn, and on top of it all the process of knitting causes that the yarn (multifilament) diameters will be varied in each part of the loop structure (leg, arc, foot) but in different way (see Figure 1). Yarn and multifilament diameter which are not measured in knitted samples, but before knitting are used for calculation of plated loop length. The real value of diameter for polyester multifilament in knitted structure will be smaller than comb cotton yarn owing to the phenomena of knocking off and creating loop in the case of different yarn structure (number of filament, twist, etc.).

Table 1: Experimental value of yarn parameters for knitted samples (count of yarn and multifilament, diameter) and some geometrical parameters of the knitted samples (wale w and course c spacing, weight per 1m^2 , thickness t)

	Yarn ($Z = 695\text{ m}^{-1}$)		Multifilament		Weft knitted fabrics – plated			
	T [tex]	d [μm]	T [dtex]	d [μm]	w [mm]	c [mm]	t [mm]	m [$\text{g}\cdot\text{m}^{-2}$]
CO	20	174			0,70	0,54	0,59	153,3
CO/PA	20	174	22 f 6	63,2	0,71	0,58	0,525	151,6
COPA	20	174	44 f 12	93,4	0,69	0,55	0,585	176,2
CO/PES	20	174	75 f 34	192,4	0,70	0,51	0,62	178,2

The input parameters for calculation of the loop length of the face and back thread are diameters of the used material therefore the structure is designed as compact. In Table 2 there were result (loop length) which are based only on the thread diameters (Face and Back threads), the Dalidovič, Model 1 and Model 2 [5]. used data are based on the thread diameters and course spacing and extra parameter – wale spacing are used as input parameter for the Model 3 [5].

Table 2: Theoretical value of calculated loop length for four plated knitted structure

Loop length	CO	CO	PA 22dtex	CO	PA 44dtex	CO	PES 75dtex	PES *
Experiment [mm]	2,53	2,78	2,5	2,75	2,61	2,38	2,07	2,07
IS	0,0334	0,0334	0,303636	0,0668	0,151818	0,0334	0,089067	
Face thread [mm]	2,90	2,90	-	2,90	-	2,90	-	-
Back thread [mm]	-	-	2,50	-	2,61	-	2,96	2,68
Dalidovič [mm]	0,55	0,55	0,20	0,55	0,29	0,55	0,60	0,35
Model 1 [mm]	1,99	1,99	2,85	1,99	2,80	1,99	2,72	1,99
Model 2 [mm]	2,78	2,85	1,42	2,80	1,57	2,72	2,08	1,67
Model 3 [mm]	1,59	1,59	1,02	1,59	1,18	1,59	1,69	1,28

For result from the material CO/PES 75 dtex the experimental value of the thread diameter was not used therefore the chosen method for measuring was not so suitable. The data of last column were calculated with the condition $\mu = 0,55$.

2.2. Crosswise and lengthwise shrinkage in laundering upon the knitted fabric geometry

Four 500 mm X 500 mm. specimens of each fabric were used for measuring dimensional change in laundering according the standard method ČSN EN 26330 (methods C and E). All samples were took away and tested according the standard method ČSN EN ISO 3759.

After describing the knitted samples with structural parameters, the process of 10 cycles of laundering was started. All samples were carry out with the same process of laundering and with two methods of drying:

- One group of samples has got the dried state with air only at horizontal sample direction,
- Another group of samples has got the dried state with handle drum dryer.

Lengths of yarns and multifilaments unravel from all plated knitted fabric before and after ten cycles of laundering / drying were measured. The shrinkages of the input material of each materials were not so significant, they were shown in Figure 3 and 4.

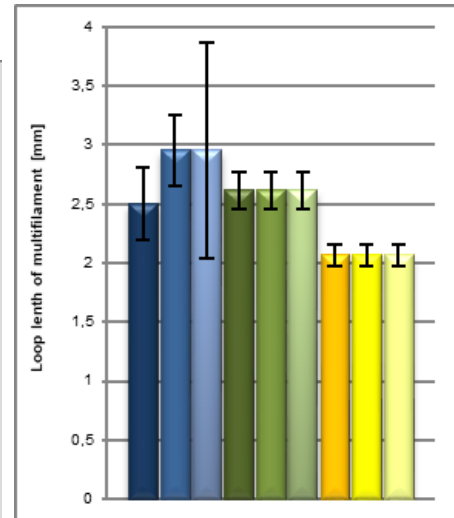
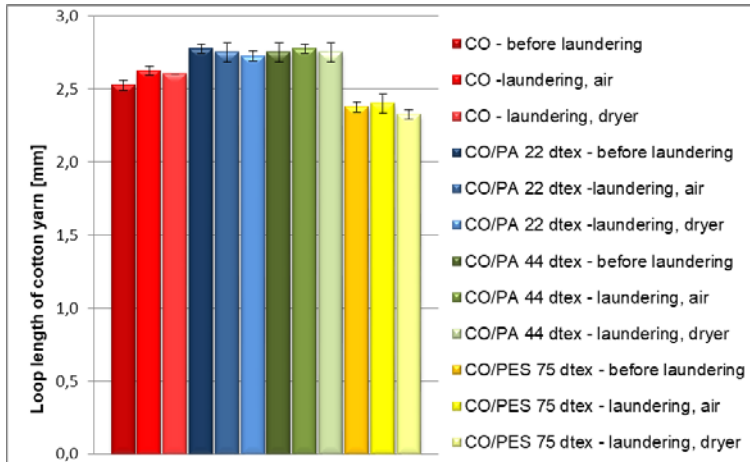

Figure 3. Experimental data of loop length of yarn

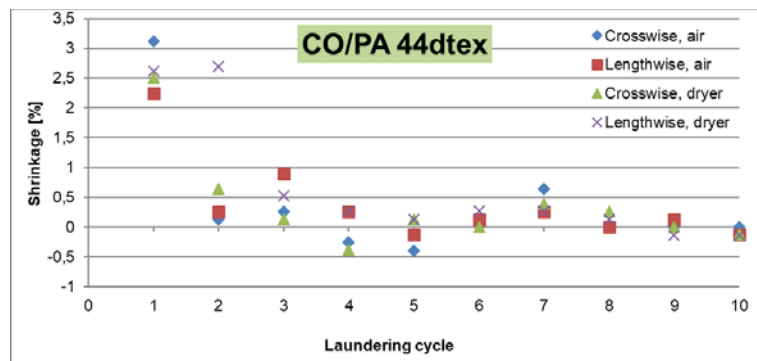
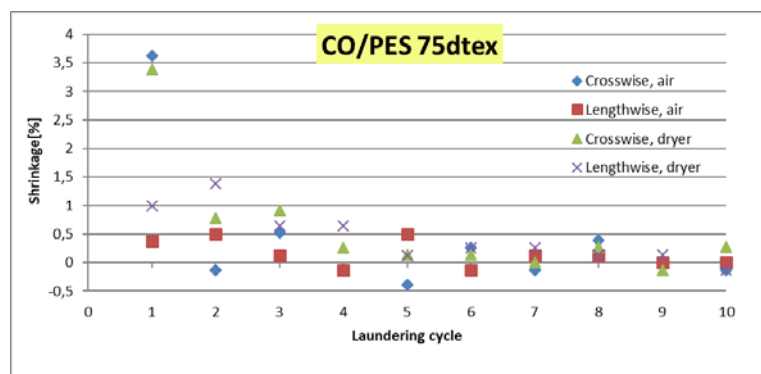
Figure 4. Experimental data of loop length of multifilament

In Figure 5 and 6 we can see the example of shrinkage results for CO/PA 44 dtex and CO/PES 75 dtex. After three or four cycles the spacing changes began lower and shrinkage of whole samples nearly stopped. The parameters of crosswise shrinkage for all materials are plotted in the Figure 7. The formulas for shrinkage is given by:

$$s_{(w,c)} = \frac{l_n - l_{n+1}}{l_n} \cdot 100 \text{ [%]} \quad (9)$$

Where: l_n dimension before laundering [mm]

l_{n+1} dimension after laundering [mm].


Figure 5. Individually value of the shrinkage of one knitted single jersey fabric in both direction with or without drum dryer for sample CO/PA 44 dtex

Figure 6. Individually value of the shrinkage of one knitted single jersey fabric in both direction with or without drum dryer for sample CO/PES 75 dtex

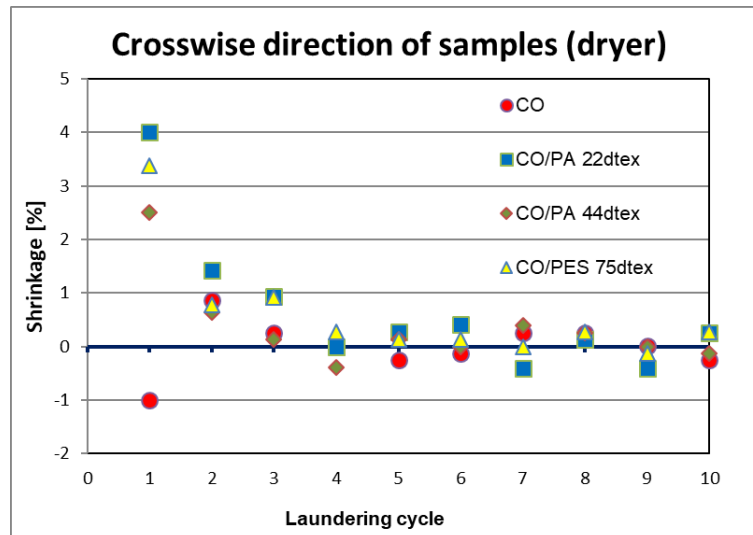


Figure 7. Individually value of the shrinkage in crosswise direction of all tested samples with the using of the drum dryer

On the other hand, marked changes in the relationship of wale to course spacing occurred during laundering (Figure 8). The loop construction was changed, the fabric thickness increased (6 -25 %) in all cases and the rectangularity of the rows and columns (if there are existed before) got lost and spirality of the column and row made deeper. A study of the data for the laundered knits revealed that wale spacing plotted against course spacing follow nonlinear curves and both parameters were declined.

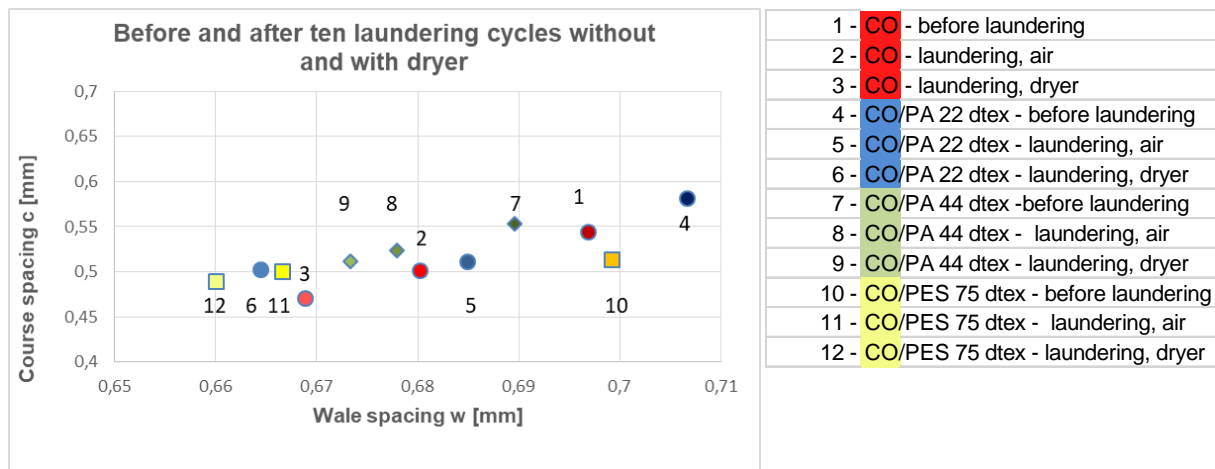


Figure 8. The relationship of wale spacing to course spacing before and after laundering of knitted plated fabric

The other structural parameter which was be obtained according the standard ČSN EN ISO 5084 (1 kPa) from the knitted material before and after laundering was thickness, is shown in the Figure 9. The expected increase of that parameters followed the prediction. Differences between the methods of drying were very huge in all causes. That phenomena of extensively growth thickness loop construction and behaviour of that plated weft knitted structure is same as single plain structure. The influence of the different multifilament count to that thickness are not performed.

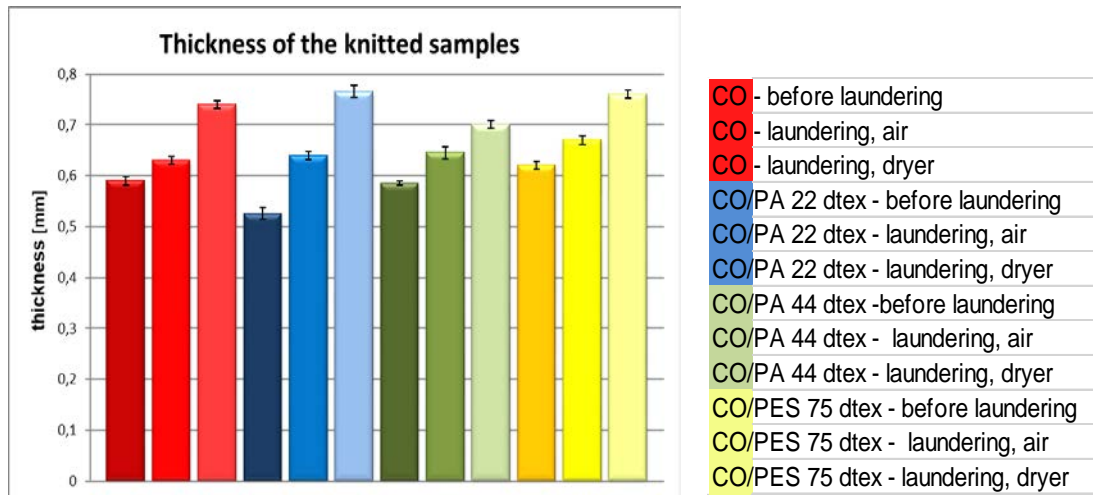


Figure 9 Thickness of the plated weft knitted fabric before and after laundering (ten cycles)

3. Results and discussion

In this study of the geometry of plated single jersey knit cotton fabrics, it was found that:

- The dependence on the method of the yarn diameter determination for simple geometry model of plated knitted structure is important. That designed model and calculated result of loop length for based multifilament with the different count are similar and with the good agreement in case of the smaller value of multifilament count (PA 22dtex, PA 44dtex). In case of the PES 75dtex, i.e. multifilament with higher count it is necessary to carry out the obtaining diameter from cross section.
- The yarn/multifilament in the finished fabrics shrank a negligible amount in laundering. The relatively small shrinkage of the yarn (the yarns were unravel and measured) and increasing the fabric thickness after laundering and drying contributed little to the dimensional change.
- Those finished fabrics from cotton and plated fabrics with smaller linear density of multifilament exhibited the large change in specimen length and width.
- In both cases (drying with or without drum dryer) the shrinkages in crosswise direction were higher than in lengthwise direction and it is significant, not negligible. The reason is that behaviour is the change the yarn geometry – construction of the loops, changing the wale and course spacing and especially thickness of the fabrics. The area of the laundered fabric exceeded that of the original specimen.

4. CONCLUSIONS

Experimental data on dimensional change in laundering /drying were obtained for each knitted material. In the case of smaller multifilament count, the dimensional stability after laundering cycles was smaller and dimensional changes of samples were higher than in case of higher values of multifilament count. It is well known that laundering consolidated the loop construction of knitted goods [5, 7].and dimensional changes in crosswise direction were smaller (to 5 %) than in the lengthwise direction (from 5 % for CO/PES to 15 % for CO or CO/PA 44dtex).

With using different back yarn in depth descent needle zone the changing of the crossing yarn cross section can change the variation and different condition which can modify the structure construction of all produced fabrics. In that case the “robbed back” can be affected by the yarn count of the back thread.

Owing to the enormous increase of the fabric thickness after ten cycles of laundering and drying, the other study will be focus to the possibility to evaluation, measuring of the yarn diameter, changing the yarn structure into the knitted structure.

ACKNOWLEDGEMENTS

Grateful acknowledgement is made to Jana Peckova for assistance with laboratory determinations and preparation of data reported in this paper.

References

1. Spencer, D. (2001). *Knitting technology a comprehensive handbook and practical guide. Third edition 2001. Woodhead Publishing Limited and Technomic Publishing Company Inc. (Cambridge). ISBN 1855733331.*
2. Koci, V. (1980), *Vlastnosti osnovních jednolícniých pletenin, in Vazby pletenin, SNTL, Praha, (In Czech) ISBN: 04-825-8*
3. Peirce, F.T. (1947) *Geometrical Principles Applicable to the Design of Functional Fabrics, Textile Research Journal, Vol. 17, 123 - 147.*
4. Fletcher, H.M., Roberts, S. H.(1952) *Geometry of Plain and Rib Knit Cotton Fabrics and Its Relation to Shrinkage in Laundering, Textile Research Journal, Vol 22 , 84-8 (1952).*
5. Pecková, J. (2018). *Plated single-face fabric – knitted structure. Diplomal thesis, Technical University of Liberec, Faculty of Textile Engineering, 2018.*
6. Fletcher, H.M., Roberts, S. H.(1954) *The Relationship of the Geometry of Plain Knit Cotton Fabric to Its Dimensional Change and Elastic Properties, Textile Research Journal, 729- 737 (1954).*
7. Pavko-Cuden, A., Hladnik, A. and Sluga, F (2013). *Loop Length of Plain Single Weft Knitted Structure with Elastane. Journal of Engineered Fibres and Fabrics, Vol. 8,2 – 2013, pp. 110 -120.*

DETERMINATION OF OPTIMAL CONJUGATE STRESS STRAIN PAIRS

Bohuslav Stríž, Lukáš Čapek

Technical University of Liberec, Faculty of Textile Engineering, Department of Technologies and Structures, Liberec, The Czech Republic, Studentská 2, 461 17. Email: bohuslav.striz@tul.cz, lukas.capek@tul.cz

Abstract:

The aim of this paper was to show a new methodology for determining an optimal conjugated pair for Cauchy stress tensor. Methodology demonstrated in this work can be used for various materials loaded by uniaxial tension, e.g. for textiles, soft tissues etc.

Key words:

Stress tensor, Strain tensor, Conjugated pair

1. Introduction

In engineering practice, the mechanical parameters are usually identified in a simplified form as engineering stress and deformation. These material parameters are used worldwide since 19th century for linear tasks. When large deformation presents, as in composite materials or others, this simplified approach cannot be used any more. It is necessary to define these deformations and stress as second order tensors that are energetically conjugated. It means that their double-dot product express strain energy in the system.

When expressing derivative quantity, e.g. Young moduli, according to different conjugated pairs, different values will be obtained [1,2]. In view of the fact that the true stress tensor is not conjugated with any known strain tensor, it is difficult to decide about suitable conjugated pair. It will be shown, that for uniaxial loading of the specimen it is possible to determine to Cauchy stress tensor a suitable conjugated strain tensor.

2. Materials and methods

Let us have a specimen of an anisotropic material, loaded by a force F_1 . Cartesian coordinates of points 1-4 were determined by an optical method.

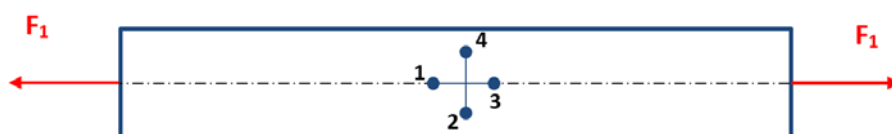


Figure 1. Testing sample

From Cartesian coordinates of points 1-4 it is possible to calculate displacements as:

$$\begin{aligned}
 (1 + u_{11})(x_1^{01} - x_1^{03}) + u_{12}(x_2^{01} - x_2^{03}) &= x_1^2 - x_1^3 \\
 (1 + u_{11})(x_1^{02} - x_1^{04}) + u_{12}(x_2^{02} - x_2^{04}) &= x_1^2 - x_1^4 \\
 u_{21}(x_1^{01} - x_1^{03}) + (1 + u_{22})(x_2^{01} - x_2^{03}) &= x_2^1 - x_2^3 \\
 u_{21}(x_1^{02} - x_1^{04}) + (1 + u_{22})(x_2^{02} - x_2^{04}) &= x_2^1 - x_2^4
 \end{aligned} \tag{1}$$

where the Lagrangian coordinate system is noticed as x_i^{0j} and Euler's coordinate system is x_i^j . For uniaxial type of loading (symmetrical sample) the equations (1) can be simplified. Displacements u_{12} and u_{21} are zero. Thus

$$\begin{aligned}
 (1 + u_{11})(x_1^{01} - x_1^{03}) &= x_1^1 - x_1^3 \\
 (1 + u_{22})(x_1^{02} - x_1^{04}) &= x_2^1 - x_2^4
 \end{aligned} \tag{2}$$

If we assume the lines 13 and 24 perpendicular than only two equations can be used. For lower values of parameter x the higher scatter of coordinates x_i^j is. So that the scatter of displacement u_{11} and u_{22} is also higher.

Regarding the fact that the sample is slightly pre-stress at the beginning of the measurement so that the displacement u_{11} , u_{22} will not be zero at the beginning of measurement too. Let's suppose that displacement evaluates linearly with some constant k_1 and k_2 . We can write it down as:

$$\begin{aligned}
 u_{11} &= u_{11}^0 + k_1 x \\
 u_{22} &= u_{22}^0 + k_2 x
 \end{aligned} \tag{3}$$

It is clear that $u_{11}^0 > 0$, $k_1 > 0$, $u_{22}^0 < 0$, $k_2 < 0$, because the sample is lengthen along line 13 and shorten along the line 24.

Suppose we have a variable h as an actual thickness of the sample and h_0 as an initial thickness. We can write the transversal displacement as:

$$\frac{h}{h_0} - 1 = u_{33} \tag{4}$$

where $u_{33} \leq 0$ due the thinning of the sample. The deformation gradient F is then

$$F = \begin{pmatrix} 1 + u_{11} & 0 & 0 \\ 0 & 1 + u_{22} & 0 \\ 0 & 0 & 1 + u_{33} \end{pmatrix} \tag{5}$$

If we assume initial length of sample l_0 , the Cauchy stress can be expressed by

$$S_{11} = \frac{F_1}{l_0 h_0 (1 + u_{22})(1 + u_{33})} \tag{6}$$

which forms the first member of Cauchy stress tensor

$$\Sigma = \begin{pmatrix} S_{11} & 0 & 0 \\ 0 & 0 & 0 \\ 0 & 0 & 0 \end{pmatrix} \tag{7}$$

Further we can write Biot's stress tensor

$$S_B = \frac{J}{2} \left[F^{-1} \Sigma + \Sigma^T F^{-1} \right] \tag{8}$$

Where R is a rotational matrix, J is a Jacobian and F a deformation gradient.

In case of uniaxial loading, we simply write an inversion of deformation gradient as inversion of diagonal matrix:

$$F^{-1} = \begin{pmatrix} \frac{1}{1+u_{11}} & 0 & 0 \\ 0 & \frac{1}{1+u_{22}} & 0 \\ 0 & 0 & \frac{1}{1+u_{33}} \end{pmatrix} = F^{T-1}$$

After some manipulating with expressions, we finally get a formulation of Biot's stress tensor for uniaxial loading:

$$\begin{aligned} S_B &= \frac{(1+u_{11})(1+u_{22})(1+u_{33})}{2} \left[\frac{F_1}{l_0 h_0 (1+u_{11})(1+u_{22})(1+u_{33})} \right]^2 \\ &= \frac{F_1}{l_0 h_0} = C_{11} \\ S_B &= \begin{pmatrix} C_{11} & 0 & 0 \\ 0 & 0 & 0 \\ 0 & 0 & 0 \end{pmatrix} \end{aligned}$$

Stress tensor for conjugated pairs

In order to get a conjugated pair of stress-strain tensors, we define a exponent-generalization of different stress tensors as:

- $m = 2$ – Piola-Kirchov
- $m = 1$ – Biott
- $m = 0$ – logarithmic
- $m = -1$ – Cernych
- $m = -2$ – Hill, Almansi

$$S(m) = \frac{1}{2} [S_B U^{1-m} + U^{1-m} S_B] \quad (9)$$

Since we know all members of above equation we can simply write down a formulation for uniaxial stress tensor in a generalized form:

$$S(m) = \begin{pmatrix} C_{11}(1+u_{11})^{1-m} & 0 & 0 \\ 0 & 0 & 0 \\ 0 & 0 & 0 \end{pmatrix} \quad (10)$$

this expression is valid for Cauchy stress tensor, but with unknown parameter m . The strain tensor that fulfill the term of conjugation is defined by

$$\varepsilon_{ij}(m) = \frac{1}{m} [U^m - I] \quad (11)$$

For above mentioned parameters m , it's necessary to find out power of strain tensor U , except of $m=0$. In this case numerator and denominator is zero (11). Calculating limit following equation is obtained

$$\varepsilon_{ij}(0) = \ln U \quad (12)$$

Equation (12) is valid only in the case when augmenting deformation the main axes of the tensor U is not rotated. When using different values of parameter m we obtained following strain tensors

$$\begin{aligned} \varepsilon_{ij}(2) &= \frac{1}{2} \left[\begin{pmatrix} (1+u_{11})^2 & 0 & 0 \\ 0 & (1+u_{22})^2 & 0 \\ 0 & 0 & (1+u_{33})^2 \end{pmatrix} - \begin{pmatrix} 1 & 0 & 0 \\ 0 & 1 & 0 \\ 0 & 0 & 1 \end{pmatrix} \right] \\ &= \begin{pmatrix} u_{11} + \frac{1}{2}u_{11}^2 & 0 & 0 \\ 0 & u_{22} + \frac{1}{2}u_{22}^2 & 0 \\ 0 & 0 & u_{33} + \frac{1}{2}u_{33}^2 \end{pmatrix} \\ \varepsilon_{ij}(1) &= \frac{1}{2} \left[\begin{pmatrix} 1+u_{11} & 0 & 0 \\ 0 & 1+u_{22} & 0 \\ 0 & 0 & 1+u_{33} \end{pmatrix} - \begin{pmatrix} 1 & 0 & 0 \\ 0 & 1 & 0 \\ 0 & 0 & 1 \end{pmatrix} \right] \\ &= \begin{pmatrix} u_{11} & 0 & 0 \\ 0 & u_{22} & 0 \\ 0 & 0 & u_{33} \end{pmatrix} \\ \varepsilon_{ij}(0) &= \begin{pmatrix} \ln(1+u_{11}) & 0 & 0 \\ 0 & \ln(1+u_{22}) & 0 \\ 0 & 0 & \ln(1+u_{33}) \end{pmatrix} \\ \varepsilon_{ij}(-2) &= \frac{1}{2} \left[\begin{pmatrix} 1 & 0 & 0 \\ 0 & 1 & 0 \\ 0 & 0 & 1 \end{pmatrix} - \begin{pmatrix} \frac{1}{(1+u_{11})^2} & 0 & 0 \\ 0 & \frac{1}{(1+u_{22})^2} & 0 \\ 0 & 0 & \frac{1}{(1+u_{33})^2} \end{pmatrix} \right] \\ &= \begin{pmatrix} \frac{u_{11} + \frac{1}{2}u_{11}^2}{(1+u_{11})^2} & 0 & 0 \\ 0 & \frac{u_{22} + \frac{1}{2}u_{22}^2}{(1+u_{22})^2} & 0 \\ 0 & 0 & \frac{u_{33} + \frac{1}{2}u_{33}^2}{(1+u_{33})^2} \end{pmatrix} \end{aligned}$$

Similarly, stress tensor $S(m)$ might be determined.

$$\begin{aligned} S(2) &= \frac{C_{11}}{1+u_{11}} \\ S(1) &= C_{11} \\ S(0) &= C_{11}(1+u_{11}) \\ S(-1) &= C_{11}(1+u_{11})^2 \\ S(-2) &= C_{11}(1+u_{11})^3 \end{aligned}$$

For Cauchy stress tensor following equations is obtained

$$S(m) = C_{11}(1+u_{11})^{1-m} \quad (13)$$

$$\varepsilon_{ij}(m) = \frac{1}{m} \left[\begin{pmatrix} (1+u_{11})^m - 1 & 0 & 0 \\ 0 & (1+u_{22})^m - 1 & 0 \\ 0 & 0 & (1+u_{33})^m - 1 \end{pmatrix} \right] \quad (14)$$

Comparing relation (6) and (13) following equation is obtained

$$\frac{1}{(1+u_{22})(1+u_{33})} = (1+u_{11})^{1-m} \quad (15)$$

$$m = 1 + \frac{\ln(1+u_{22}) + \ln(1+u_{33})}{\ln(1+u_{11})}$$

Parameter m is a function of thickness defined by (4). By substituting u_{11} , u_{22} , u_{33} by terms (3) and (4) a functional dependency of parameter m on displacement x and k_3 is received

$$m = 1 + \frac{\ln(1+u_{22}^0+k_2x) + \ln(1+k_3x)}{\ln(1+u_{11}^0+k_1x)} \quad (16)$$

Equation (16) describes formally Cauchy conjugated pair for uniaxial type of loading. It's clear that the result is strongly influence by parameter k_3 .

The requirement of dot product for equations (13) and (14) will be shown

$$A = \int_0^{x_{max}} S(m) \frac{d\varepsilon_{11}(m)}{dx} dx = \int_0^{x_{max}} C_{11} (1+u_{11})^{1-m} (1+u_{11})^{m-1} \frac{du_{11}}{dx} dx \quad (17)$$

$$= \int_0^{x_{max}} \frac{F_1}{l_0 h_0} k_1 dx$$

Theoretically the parameter "m" can reaches any value, but there is only one corresponds to Cauchy stress tensor. According to Hook law

$$\begin{aligned} \overline{E}_{11}\varepsilon_{11}(m) + \overline{E}_{12}\varepsilon_{22}(m) - J C_{11} (1+u_{11})^{1-m} &= 0 \\ \overline{E}_{12}\varepsilon_{11}(m) + \overline{E}_{22}\varepsilon_{22}(m) &= 0 \\ \overline{E}_{11}\overline{E}_{22} - \overline{E}_{12}^2 - \overline{E}_4(\overline{E}_{11} + \overline{E}_{22} - 2\overline{E}_{12}) &= 0, \end{aligned} \quad (18)$$

where:

$$\overline{E}_{12} = \nu(m) \sqrt{\overline{E}_{11}\overline{E}_{22}}, \quad \nu(m) = -\frac{\varepsilon_{22}(m)}{\varepsilon_{11}(m)} \quad (19)$$

Modules \overline{E}_{11} , \overline{E}_{22} and \overline{E}_4 can be found. Poisson ratio $\nu(m)$ depends on choice of conjugated pair.

An invariant shear modulus $\overline{E}_4(m)$ is given

$$\overline{E}_4(m) = \frac{1}{2} \left[\frac{1}{4} (\overline{E}_{11} + \overline{E}_{22} - 2\overline{E}_{12}) + \overline{E}_4 \right] \quad (20)$$

In engineering practice following expression is often used

$$G = \frac{\tau_i}{\gamma_i}$$

Where

$$G = \frac{E}{2(1+\nu)}$$

$$\tau_i = \frac{1}{\sqrt{6}} \sqrt{(S_{11} - S_{22})^2 + S_{11}^2 + S_{22}^2 + 6S_{12}^2},$$

$$Y_i = \sqrt{\frac{2}{3}} \sqrt{(\varepsilon_{11} - \varepsilon_{22})^2 + (\varepsilon_{22} - \varepsilon_{33})^2 + (\varepsilon_{33} - \varepsilon_{11})^2 + 6S_{12}^2}$$

In our case can be found

$$\bar{\bar{E}}_4 = \frac{\frac{1}{\sqrt{3}} S_{11}}{\sqrt{\frac{2}{3}} \sqrt{(\varepsilon_{11} - \varepsilon_{22})^2 + (\varepsilon_{22} - \varepsilon_{33})^2 + (\varepsilon_{33} - \varepsilon_{11})^2}} \quad (21)$$

This makes a system of equations that enables to find out values of “m” and u33.

3. CONCLUSION

When evaluating the experimental data of a material, usually it is performed as a uniaxial tension test. What is actually measured is a force versus displacement curve, but in order to make these results independent of specimen size, the results are usually presented as stress versus strain. It is interesting that most, perhaps even all, stress definitions can be paired with a corresponding strain tensor. They come in pairs such that the product of the two will give strain energy. This does not mean that the corresponding pairs must be used together when performing structural analyses. But they must be when computing strain energy density. In view of the fact that the trues stress tensor is not conjugated with any known strain tensor, it is difficult to decide about suitable conjugated pair. It was shown, that for uniaxial loading of the specimen it is possible to determine to Cauchy stress tensor a suitable conjugated strain tensor. Methodology demonstrated in this work can be used for various materials loaded by uniaxial tension, e.g. for textiles, soft tissues etc.

4. References

1. G. A. Holzapfel. *Nonlinear Solid Mechanics: A Continuum Approach for Engineering*. Wiley, 2000.
2. R.W Ogden. *Non-Linear Elastic Deformations*. Dover, 1997.

INVESTIGATION OF THE CAPILLARY KINETIC TRANSPORT OF LIQUID FUELS IN DIFFERENT ROUND BRAIDS

Peter Philip Glessner

Hovener Straße 202, 41066 Mönchengladbach, Nordrhein-Westfalen, glessner.peter@gmail.com, Mobil: 015170113966

Abstract:

This Paper shows experiments of transport from liquid fuels in round braids due to capillary forces. The capillary effect of textiles is used for a lot of applications such as candles where the wick provides melted fuel for a constant and clean burning process. Candlewicks are mainly made from cotton yarn, however in special candle applications like oil lamps there are technical fibres necessary. In this case, the wick must transport the liquid on the whole length to the flame without shorten itself until the oil bin is empty. To prevent the burning of the wick, more heat resistant fibres are used which also need to deliver the right amount of fuel by a defined time.

Another challenge in oil lamps is the variation of the liquid fuel. The fuel as well as the wick properties influence the capillary function. For monetary reasons fuels sometimes are diluted which requires an adjustment of the wick properties to ensure the given burning time and flame height. Depending on the composition of the dispersion, the wick can become clogged and loses its function.

In this work the capillary transport of two different methyl esters with different braid constructions is presented with low cost measurements.

Key words:

Braids, capillary forces, candle, wick, transport

1. Introduction

The liquid transport in textiles is used for many applications and discussed in earlier publications. Based on the well-investigated capillary currents in cylindrical tubes, there are adapted mathematic models for textile structures as yarns [1], weaved fabrics [2] or knitted fabrics [3]. The liquid transport in knitted fabrics is also shown in [4] as well as an extension of the Washburn equation [5]:

$$\frac{m(t)}{(S-S_f) \cdot \rho} = \sqrt{\frac{r \cdot \gamma \cdot \cos \theta}{2 \cdot \eta}} \cdot t = K \cdot \sqrt{t} \quad (1)$$

where S is the area of sample cross section, S_f is the area of fibres in the cross section, r is the radius of pores, γ is the surface tension of distilled water, ρ and η are the density and viscosity of distilled water, respectively and θ denotes contact angle.

Furthermore, research projects developed the possibility to predict the capillary rise height in textiles by a mathematic calculation as well as an extension of the standard practical measurement [6]. There are also investigations aimed on candlewicks, which show the liquid transport [7], but the influence of wax or fuel materials as well as braiding construction is not mentioned.

This study concentrates on classical round braids and their well-known and documented properties [8], however there are more complex profiles possible with the braiding technology [9] where the phenomenon of capillary rises can differ.

The need of a deeper investigation of capillary forces in this special application is the changing candle industry. Like in other industries, the candle producers try to use more sustainable and environmentally friendly raw materials. Concerning this trend, the candlewick manufactures must adapt their products for a steady quality and a forward-thinking business.

In the special case of oil lamps, the raw material of liquid fuel changes to more clean compounds like vegetable oil or methyl ester, which is also used in biodiesel. However, as in most other things, the crucial factor is the price. There are differences in methyl esters like the carbon chain length, which influences the price but also the capillary effect. In this context, every methyl ester needs the development of an own wick. The distinctions of the capillary rises are shown in the following experiments.

2. Experimental

To show the influence of raw materials, this paper shows experiments concerning the capillary rise of various braids in different methyl esters.

2.1. Materials

All braids have the same amount of carriers and the same braiding density. There is cotton such as fibre glass used but the braids have a different construction. Braid No. 015 and 003 have a different count of core yarns, No. 001 has fibre glass included as braided yarn and No. 004 has no core yarns but four inlay yarns.

Table 1. Different braids used for the investigation of the capillary rise

Braid-No.	015	001	003	004
Carriers	16	16	16	16
Material	CO: Nm 34/2 Fibre glass: 68 tex	CO: Nm 34/2 Fibre glass: 68 tex	CO: Nm 34/2 Fibre glass: 68 tex	CO: Nm 34/2 Fibre glass: 68 tex
Braiding yarns	8 x 1 CO 8 x 2 CO	8 x 1 CO 8 x 1 CO 1 fibre glass	8 x 1 CO 8 x 2 CO	8 x 1 CO 8 x 2 CO
Core yarns	2 x 6 fibre glass	2 x 6 fibre glass	1 x 6 fibre glass	-
Inlay yarns	-	-	-	4 x 1 fibre glass
Braiding density	36 [picks/5 cm]	36 [picks/5 cm]	36 [picks/5 cm]	36 [picks/5 cm]
Diameter	3 [mm]	2 [mm]	2,5 [mm]	2,5 [mm]

The two types of methyl ester differ in their carbon chain length. One of them has a chain length of 10-12, the other 12-14 carbon atoms.

2.2. Methods

The method for testing the capillary forces is leant to the german standard DIN 53924. This standard describes the implementation for testing capillary rises of textile structures, however it is meant for wider surfaces like weaved or knitted fabrics and only for the transport of water.

In this case, the textile structure is thin and the liquid is methyl ester with two different carbon chain lengths.

To stay close to the german standard, the braids are fixed on a bracket including a ruler to see the exact height of the rising liquid and weighted with small 4g rings that keep the braids straight without elongation. The methyl ester is colored with a special candle dye called RED 345-0001 in a 0,5 % concentration to see the rising height. Figure 1 shows the schema of the test.

The experiment starts with diving the braids in the liquid with a length of 5 cm. From that point the time and rising height is noted.

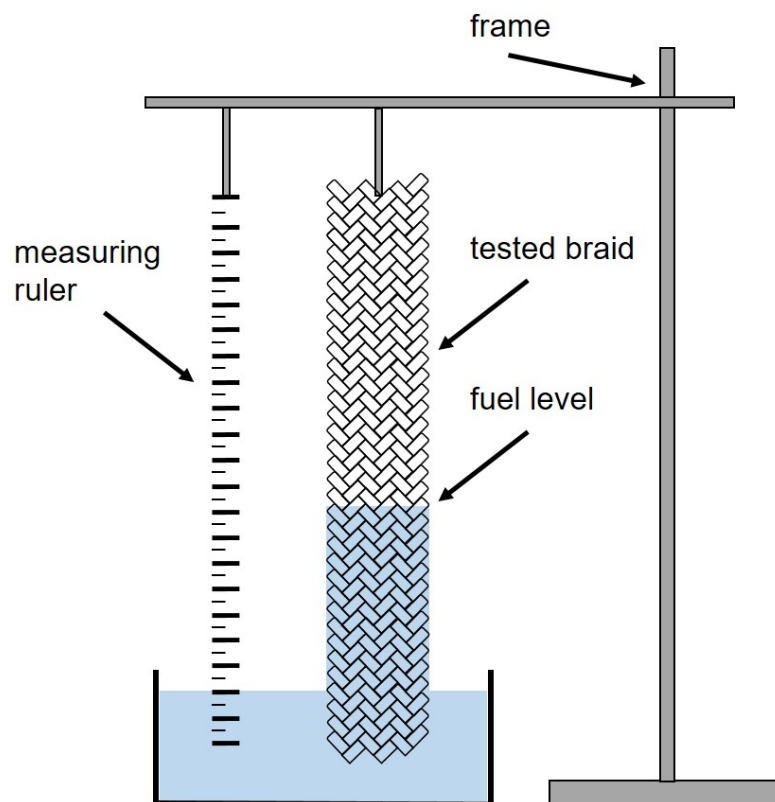


Figure 1. Schema of the experimental arrangement

3. Results and discussion

The results of the capillary rise height of different braids in two methyl esters are shown in table 2.

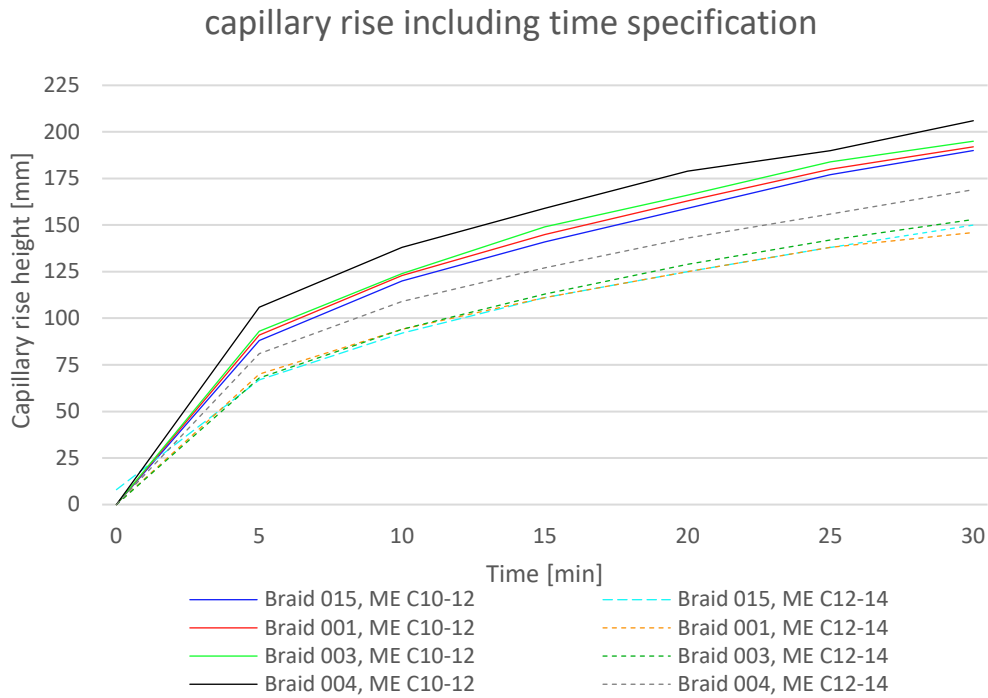


Table 2. Influence of the liquid fuel and braid constructions on the capillary rise height.

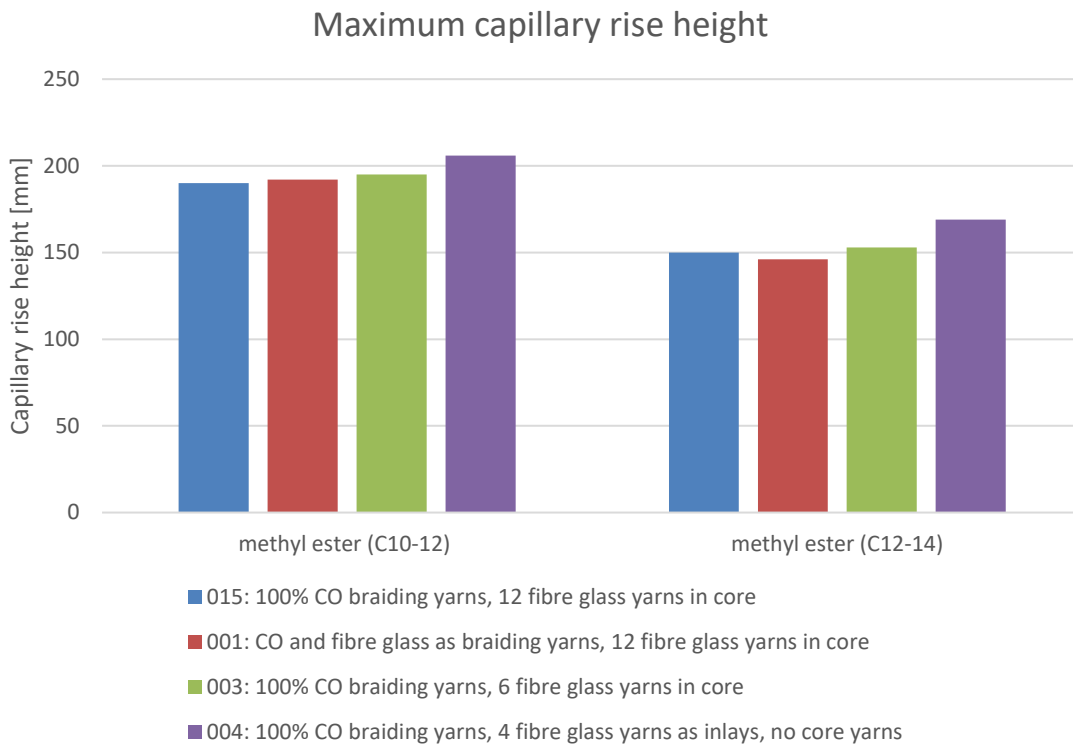


Table 3. Maximum capillary rise height with different liquid fuels and braid constructions after 30 minutes.



Figure 2. Results of the capillary rise height after 30 minutes in methyl ester with C₁₀₋₁₂ (left) and C₁₂₋₁₄ (right).

4. CONCLUSIONS

The results in table 2, 3 and figure 2 show an obvious influence in both variables, the fuel as well as the braid construction.

All braids achieve a higher capillary rise with the methyl ester with a short carbon chain length of C₁₀₋₁₂. Compared to the knowledge in classic candles, this is a logical effect. A candle made of a clean paraffin burns much easier as a compound with dye or scents because of the more complicated chemical structures. For this reason, it is not uncommon that candle wicks become clogged during the burning process.

When you have a longer carbon chain length in methyl ester, the capillary forces have to be stronger to get the same rise height like the shorter chain length. All braid constructions get a height about 20% less with the longer carbon chain length.

Moreover, the braid construction has an influence to the capillary rise height as well. Braid type 004 shows the highest rise in both groups. This type is the only braid without core yarns, but with four inlay yarns.

In braiding technology, core yarns are placed in the middle of every braiding yarn in a 0° direction. Inlay yarns also have a 0° direction, however they are not placed in the central middle of the braid but between two crossing yarns by getting led through the middle of a horn gear.

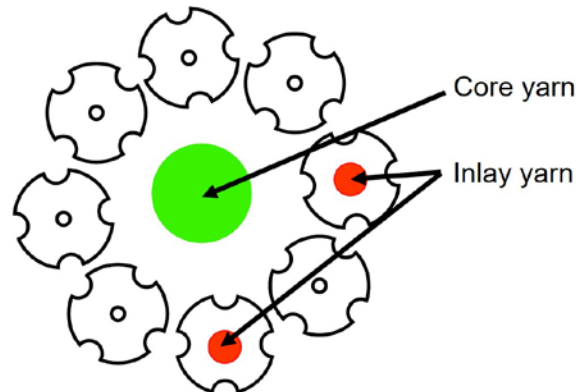


Figure 3. Core and inlay yarns in braiding technology

When you compare the other braid types, you can see no big differences in the capillary rise height. The used fibre glass as braiding yarns shows no positive effect on the fuel transport. One interesting point is the comparison of type 015 with 12 and type 003 with 6 core yarns. Type 003 with less core yarns shows a 2% higher rise height than type 015. That result comes to the conclusion that more core yarns can aggravate the liquid transport.

Summarized the chemical composition of the liquid fuel has a big influence on the mass transport. This requires a development of wicks for every liquid fuel to get a perfect burning process and flame height.

References

1. Benltoufa S. "Capillary Rise in Macro and Micro Pores of Jersey Knitting Structure", *Journal of Engineered Fibres and Fabrics*, 2008. S.47-54.
2. DasB., et al. "Moisture Transmission through textiles", *Autex Research Journal*, Vol. 7, 2007. S.194-216.
3. Glessner P.,Kyosev, Y. "Pattern design with the vaiation braider VF of company Herzog GmbH". Kyosev Y. *Narrow and Smart Textiles*. 2018, S.149-158.
4. Kyosev Y. "Braiding Technology for textiles". 2015.
5. Kyosev Y.,Tomas, S. "Experimental study over porosity and liquid transport in viscose knitted fabric", 2003
6. Maschler T.,Stegmaier, T., Dinkelmann, A., Finckh, H. "Entwicklung einer selbstlernenden Methode zur Prognose der kapillaren Steigkinetik von Fluiden in textilen Fasergebilden", 31. Hofer Vliesstofftage, 2016.
7. Maschler T.,Stegmaier, T., Finckh, H., Tilebein, M. "Eine methode zur charakterisierung und Prognose der Kapillarkinetik textiler Fasergebilde". 2016.
8. Rajagopalan D.,Aneja, A.P., & Marchal, J.M. "Modeling capillary flow in complex geometries", *Research Journal*, 2001.
9. Washburn E. "The dynamics of capillary flow, the physical review". 1921, S.273-283.

STRUCTURE ANALYSIS OF CARBONIZED NEEDLE-PUNCHED NONWOVENS BY X-RAY COMPUTED TOMOGRAPHY

Smita Baheti, Maros Tunak, Daniel Karthik

Department of Textile Evaluation, Faculty of Textile Engineering, Technical University of Liberec,
Studentska 2, Liberec 46117, Czech Republic

Department of Material Engineering, Faculty of Textile Engineering, Technical University of Liberec,
Studentska 2, Liberec 46117, Czech Republic

smita.baheti@hotmail.com

Abstract:

This paper aims to fabricate activated carbon nonwoven mat from acrylic fibrous wastes with enhanced porosity and electrical conductivity. For this purpose, the structural changes of acrylic fiber needle-punched nonwovens were evaluated when exposed to different stages of carbonization using micro X-ray computed tomography. The change in fiber diameter, fiber volume fraction, fiber orientation, fabric porosity and fiber-fiber contact efficiency of original acrylic fiber needle punched mat was examined after the stabilization and carbonization temperatures. Furthermore, the change in electrical conductivity of acrylic nonwovens was also examined at the different carbonization temperatures.

Key words:

Acrylic fibrous wastes; Needle-punched nonwoven web; X-ray computed tomography; Fiber diameter; Fiber-volume fraction; Fiber orientation; Porosity

1. Introduction

Nonwoven mats are manufactured by mechanically, thermally, or chemically entangling short fibers into randomly oriented fiber assemblies (Jeon, Yu, Kim, Lee, & Kim, 2014). The properties of nonwoven mats depend on the properties of their constituent fibers, the relative orientations of those fibers, and the bonding process used to fabricate the mat. In particular, the internal structure of nonwoven mats, which is characterized by fiber orientation and distribution, fiber entanglement, and/or interlocking features, has a great impact on the mechanical properties of the mat. Therefore, considerable effort has focused on predicting the mechanical properties of nonwoven mats by defining and characterizing internal structure (Jeon, Na, et al., 2014). An image analysis method was developed using optical microscopy to characterize the micro-structure of nonwoven mats. In a given image, fibers were separated from the background by setting an appropriate image threshold, creating binary, black and-white images. From these, fiber orientation and distribution were calculated using a Fourier transform of the image. Many efforts have also focused on measuring the degree of fiber entanglement as a way to explain the relationship between internal structure and the properties of a nonwoven material (Jeon, Na, et al., 2014).

Due to three-dimensional complex structure of needle-punched nonwoven fabrics, the investigation of overall 3D structure analysis gained significant importance. However, as an indirect method, image analysis is limited in its ability to provide definitive information on the inner structure of nonwoven mats. In contrast, X-ray computerized tomography has been considered as an effective means of investigating the microstructural factors of materials such as porosity and micro cracks; the meso-structures of composites; and the self-locking or coherent structures in nonwovens. X-ray computed tomography (XCT) has started to be used for the 3D structure analysis of materials including needle-punched nonwoven fabrics (Ishikawa, Kim, & Ohkoshi, 2017). It enables nondestructive 3D study of

the internal structure, minimizing fiber disturbance and involves the collection of shadow images by rotating a sample at discrete angular increments before reconstructing each individual cross-section (Nguyen Thi et al., 2015). Gilmore et al. first applied XCT to observe the 3D structure of nonwoven fabrics. Following their research, several research groups have analyzed the structure of nonwoven fabrics by XCT, and some have attempted to reveal the relationship between the structure and properties (Bernasconi, Cosmi, & Hine, 2012). For example, Manickam and McCutcheon focused on the void structure (i.e. pore diameter and porosity) of nonwoven fabrics. Soltani et al. investigated the influence of fiber orientation on the permeability of nonwoven fabrics. Jeon et al. evaluated the in-plane fiber orientation, fiber volume fraction, and contact level between fibers of needle-punched nonwoven fabrics, and analyzed the change in these structure parameters during tensile deformation (Ishikawa, Ishii, Nakasone, Ohkoshi, & Kyoung Hou, 2017). Surprisingly, the effect of carbonization temperature on the structure properties of fibrous nonwovens has not been studied by XCT. The present work analyzed the microstructure of acrylic fiber needle punched nonwoven fabrics after exposure to different stages of carbonization. The change in fiber diameter, fiber volume fraction, fiber orientation, fabric porosity and fiber-fiber contact efficiency of original acrylic fiber needle punched web was examined after the stabilization and carbonization temperatures. Furthermore, the change in electrical conductivity of acrylic nonwovens was also examined at the different carbonization temperatures. In this way, the findings of this work could be beneficial for fabrication of porous and electrically conductive activated carbon nonwoven web from acrylic fibrous wastes.

2. Experimental

The acrylic fibrous waste was obtained from Grund Industries, Czech Republic in form of short lengths generated during mechanical processing of bath mats. The acrylic fibers are anionic copolymers containing 85-89 % of acrylonitrile. Table 1 shows the physical properties of acrylic fibrous wastes.

Table 1. Physical properties of acrylic short fiber wastes

Fineness (Denier)	13
Tenacity (GPD)	2.7
Elongation (%)	45
Shrinkage (%)	2.5

The compact dense structure of nonwoven web having thickness 11.6 mm and density 2.78 g/cm³ was prepared by opening of short acrylic fibers on Carding Machine (Laboratory Roller Card, Befama, Poland) with subsequent action of Needle Punching Machine (Hansa, Germany). The predetermined size of acrylic nonwoven web was cut and transferred to high temperature furnace (Elektrické Pece Svoboda, Czech Republic) for carbonization in two stages. The sample was initially stabilized at 250 °C with heating rate of 35 °C h⁻¹ and under predetermined tension. Further, the stabilized web was carbonized at 1000 °C with heating rate of 300 °C h⁻¹ and without any holding time. The structural changes in the nonwoven mats during carbonization stages were investigated using a micro X-ray CT instrument (SkyScan 1272, high-resolution micro-CT from BRUKER). Scanning was performed at a resolution of 3.50 μm/voxel. The voltage, current, and irradiation time were optimized to obtain good contrast and were 50 kV, 200 μA, and 456 ms, respectively. The angle increment for scanning samples was 0.20° per step for 360°, providing 1507 cross-sections for reconstruction. The scanned images were reconstructed using NRecon into three dimensional object, which was further analyzed for structural properties using CTan. The CTvox and Data Viewer tools were utilized for visualization and measurement of image database. The physical properties of acrylic fibrous and activated carbon nonwoven web were also determined in terms of shrinkage, flexibility and dusting tendency. The shrinkage measurement was performed as per ASTM D 2259 standard available for testing textile fibers. The shrinkage was evaluated from change in length of acrylic fiber web before and after carbonization. The flexibility or stiffness was evaluated from bending length by employing the principle of cantilever bending of the web under its own weight as per ASTM D 1388 standard. The dusting tendency was evaluated from amount of generated dust particles after rubbing the surface of web on

Taber wear and abrasion tester as per ASTM D 3884 standard. The rotary rubbing action was performed for 30 cycles under controlled conditions of pressure and abrasive action. Finally, Hewlett Packard 4339 B high resistance meter was used to measure the electrical resistivity of activated carbon web samples according to ASTM D257-14 at temperature 22 °C and relative humidity 40 %. The specific voltage potential of 100 ± 5 V using direct current was applied across opposite ends of activated carbon web and resultant current flowing across the sample was measured after 15 ± 1 s.

3. Results and discussion

The three dimensional morphology of original acrylic fiber nonwoven, stabilized acrylic fiber nonwoven and carbonized acrylic fiber nonwoven can be seen from Figure 1(a), Figure 1(b) and Figure 1(c) respectively. The number of smaller diameter fibers in activated carbon web was found in higher quantity than the acrylic fibrous web.

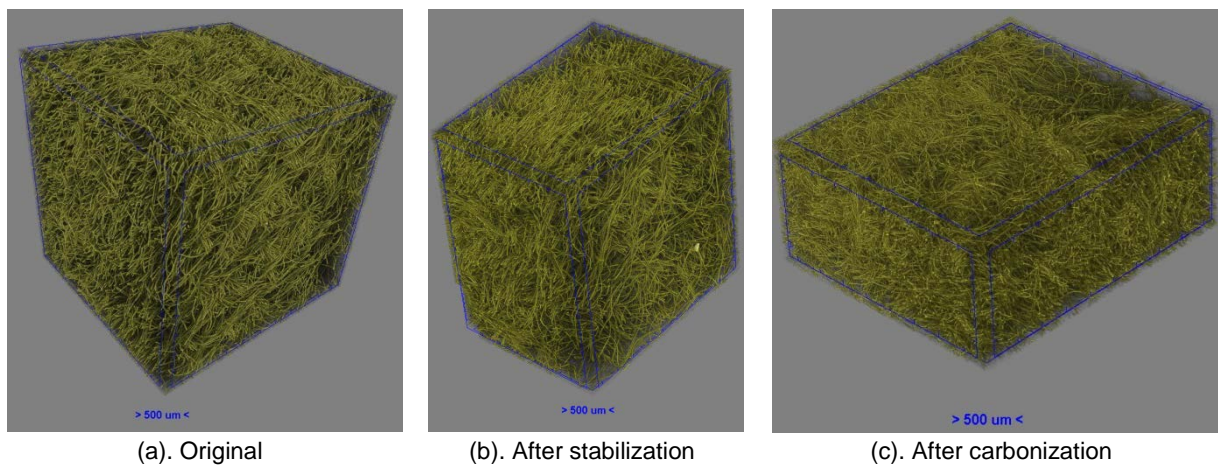


Figure 1. 3D view of acrylic fiber nonwoven mat

To measure the fiber diameter, fiber orientation, fiber volume fraction and fiber-fiber contact efficiency, the cross-sections of nonwoven mats were scanned in the thickness direction to obtain a total of 1500 images. Figure 2 shows a typical 2D X-ray CT image of the nonwoven mats obtained parallel to the fabric surface at the half thickness of the fabric. Two distinct shapes can be observed: small solid ellipses and long white lines. Each represents constituent fibers in different orientations. The circular shape represents the cross-section of short fibers oriented perfectly perpendicular to the plane (cross-section), while the lines indicate fibers oriented parallel to the plane. We focused on objects inside a region of interest (ROI) with a 10-mm diameter. The major (a) and minor (b) diameters of the objects were obtained by image analysis. Fiber orientation angles were measured using a simple equation shown in Figure 3 (Jeon, Na, et al., 2014). Fiber volume fractions were obtained by taking the reciprocal value of porosity, which was calculated from the vacant area surrounding the fibers in the 2D X-ray images.

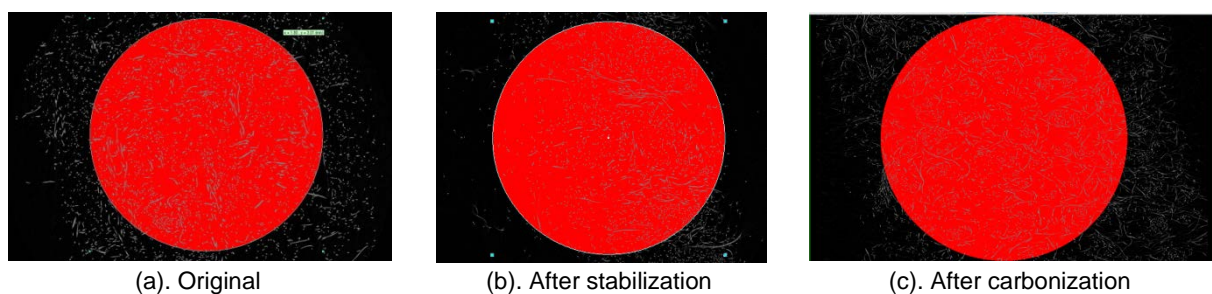


Figure 2. Tomographic 2D image obtained at half thickness of acrylic fiber nonwoven mat

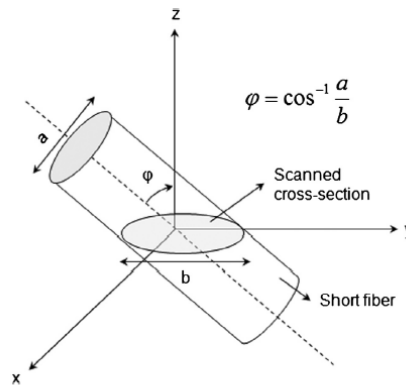


Figure 3. Measurement of fiber orientation angle

Table 2, Table 3 and Table 4 show the different microstructure parameters of acrylic fiber needle punched nonwoven mats at different stages of carbonization. The fiber diameter and fiber volume fraction was found to decrease with exposure to higher temperature, whereas the porosity and fiber-fiber contact efficiency was found to increase. Further, these microstructure parameters were found to be different in the middle layer of the fabric than in the surface layer.

Table 2. Results of original acrylic fiber nonwoven structure at different cross-sections

Slice number	Number fraction of correctly detected objects (%)	Average minor diameter of selected objects (μm)	Average major diameter of selected objects (μm)	Fiber volume fraction (%)	Orientation (degree)	Porosity (%)	Fiber-fiber contact efficiency
1	1910	20	173	8.54	32.81	91.45	0.024
300	1772	24	186	8.18	50.95	91.81	0.027
600	1892	19	154	8.45	79.97	91.54	0.024
900	1917	23	169	9.17	54.31	90.82	0.025
1200	1918	22	180	9.26	41.32	90.73	0.025
1500	1818	21	181	8.58	66.32	91.41	0.026
Average	1871.16	21	173	8.69	54.28	91.29	0.025

Table 3. Results of acrylic fiber nonwoven structure after 250 °C stabilization at different cross-sections

Slice number	Number fraction of correctly detected objects (%)	Average minor diameter of selected objects (μm)	Average major diameter of selected objects (μm)	Fiber volume fraction (%)	Orientation (degree)	Porosity (%)	Fiber-fiber contact (%)
1	1463	13	91	5.46	92.77	94.53	0.029
300	1618	14	84	5.78	90.96	94.21	0.026
600	1757	12	157	6.44	110.62	93.55	0.024
900	1464	14	60	4.84	100.57	95.15	0.027
1200	1454	16	102	5.35	112.71	94.64	0.029
1500	1253	14	74	4.31	118.65	95.68	0.033
Average	1501.5	14	95	5.36	104.38	94.62	0.028

Table 4. Results of acrylic fiber nonwoven structure after 1000 °C carbonization at different cross-sections

Slice number	Number fraction of correctly detected objects (%)	Average minor diameter of selected objects (μm)	Average major diameter of selected objects (μm)	Fiber volume fraction (%)	Orientation (degree)	Porosity (%)	Fiber-fiber contact (%)
1	216	8	62	0.46	29.72	99.53	0.15
300	2892	9	72	7.54	8.92	92.45	0.012
600	2863	8	63	7.97	159.53	92.02	0.013
900	1479	10	115	4.38	119.47	95.61	0.026
1200	517	9	124	1.91	37.05	98.08	0.083
1500	20	9	68	0.065	68.85	99.94	1.86
Average	1331.16	9	84	3.72	70.59	96.27	0.35

The physical characteristics of activated carbon webs prepared at 800 °C, 1000 °C and 1200 °C of temperature, under 300 °C h⁻¹ heating rate and without any holding time are shown in Table 5.

Table 5. Effect of carbonization temperature on physical properties of activated carbon web

Temperature (°C)	Yield (%)	Shrinkage	Flexibility	Dusting
800	61.7	Good	Good	Good
1000	57.12	Good	Average	Average
1200	45	Average	Poor	Poor

Figure 4 shows the average values in 95 % confidence interval for electrical resistivity of activated carbon web samples. The electrical resistivity was found to decrease with increase in carbonization temperature. The linear regression model was applied and 76.15 % coefficient of determination was found between carbonization temperatures and achieved electrical resistivity. The 1200 °C activated carbon sample exhibited 1000 times reduction in electrical resistivity over 800 °C activated carbon sample. The higher electrical conductivity of 1200 °C activated carbon sample was attributed to more graphitization.

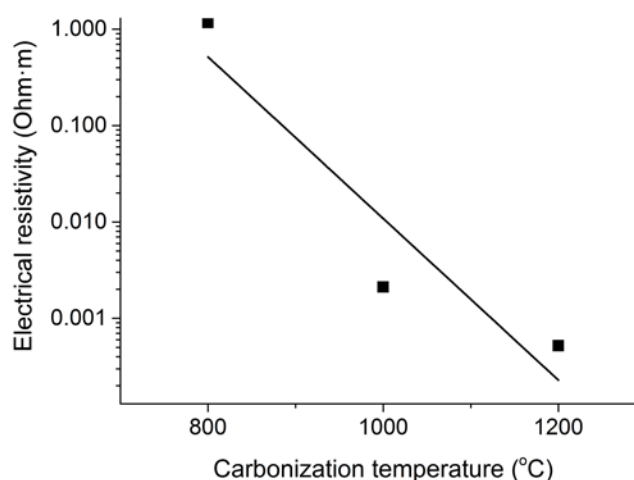

Figure 4. Electrical conductivity of carbonized acrylic nonwovens

Figure 5 show the two possible modes of electron transport (i.e., migration and hopping) in the activated carbon web produced at 800, 1000 and 1200 °C, respectively. The development of electrical conductivity can be explained from the migration of electrons in one graphite layer or their jumping across the defects/interfaces between disordered graphite layers (Cao, Song, Hou, Wen, & Yuan,

2010; Song et al., 2009; Wen et al., 2013). The higher electrical conductivity indicated relatively easier migration and hopping of electrons in case of 1200 °C activated carbon than 800 and 1000 °C activated carbon samples. This behavior can be attributed to their higher graphite content, uniform distribution of graphite layers, reduced fiber diameter, etc shown in Figure 5, which ultimately resulted into the formation of dense micro-current network in 1200 °C activated carbon structure (Arjmand, Chizari, Krause, Pötschke, & Sundararaj, 2016; Arjmand & Sundararaj, 2015).

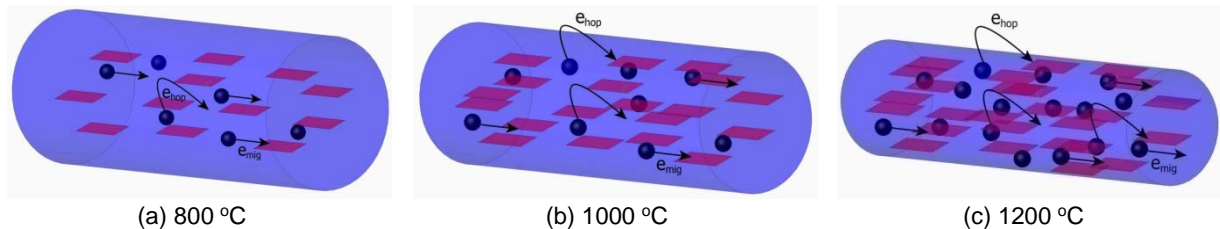


Figure 5. Mechanism of charge transport in activated carbon fabric

4. CONCLUSIONS

We analyzed the structure of acrylic fiber needle-punched nonwoven fabrics by X-ray computed tomography. The relationships between the carbonization temperature and structural parameters were investigated. The fiber diameter and fiber volume fraction was found to decrease with exposure to higher temperature, whereas the porosity and fiber-fiber contact efficiency was found to increase. Further, these microstructure parameters were found to be different in the middle layer of the fabric than in the surface layer. These results demonstrated that XCT image analysis is effective to evaluate the structure of needle-punched nonwoven fabrics and thus to design the properties of activated carbon nonwoven fabrics.

ACKNOWLEDGEMENTS

This work was supported by the research project of Student grant competition of Technical University of Liberec no. 21251 granted by Ministry of Education, Youth and Sports of Czech Republic.

References

1. Arjmand, M., Chizari, K., Krause, B., Pötschke, P., & Sundararaj, U. (2016). Effect of synthesis catalyst on structure of nitrogen-doped carbon nanotubes and electrical conductivity and electromagnetic interference shielding of their polymeric nanocomposites. *Carbon*, 98, 358–372. <http://doi.org/10.1016/j.carbon.2015.11.024>
2. Arjmand, M., & Sundararaj, U. (2015). Electromagnetic interference shielding of Nitrogen-doped and Undoped carbon nanotube/polyvinylidene fluoride nanocomposites: A comparative study. *Composites Science and Technology*, 118, 257–263. <http://doi.org/10.1016/j.compscitech.2015.09.012>
3. Bernasconi, A., Cosmi, F., & Hine, P. J. (2012). Analysis of fibre orientation distribution in short fibre reinforced polymers: A comparison between optical and tomographic methods. *Composites Science and Technology*, 72(16), 2002–2008. <http://doi.org/10.1016/j.compscitech.2012.08.018>
4. Cao, M. S., Song, W. L., Hou, Z. L., Wen, B., & Yuan, J. (2010). The effects of temperature and frequency on the dielectric properties, electromagnetic interference shielding and microwave-absorption of short carbon fiber/silica composites. *Carbon*, 48(3), 788–796. <http://doi.org/10.1016/j.carbon.2009.10.028>
5. Ishikawa, T., Ishii, Y., Nakasone, K., Ohkoshi, Y., & Kyoung Hou, K. (2017). Structure analysis of needle-punched nonwoven fabrics by X-ray computed tomography. *Textile Research Journal*. <http://doi.org/10.1177/0040517517736470>

6. Ishikawa, T., Kim, K. H., & Ohkoshi, Y. (2017). Visualization of a pillar-shaped fiber bundle in a model needle-punched nonwoven fabric using X-ray micro-computed tomography. *Textile Research Journal*, 87(11), 1387–1393. <http://doi.org/10.1177/0040517516652351>
7. Jeon, S. Y., Na, W. J., Choi, Y. O., Lee, M. G., Kim, H. E., & Yu, W. R. (2014). In situ monitoring of structural changes in nonwoven mats under tensile loading using X-ray computer tomography. *Composites Part A: Applied Science and Manufacturing*, 63, 1–9. <http://doi.org/10.1016/j.compositesa.2014.03.019>
8. Jeon, S. Y., Yu, W. R., Kim, M. S., Lee, J. S., & Kim, J. W. (2014). Predicting the tensile strength of needle-punched nonwoven mats using X-ray computed tomography and a statistical model. *Fibers and Polymers*, 15(6), 1202–1210. <http://doi.org/10.1007/s12221-014-1202-z>
9. Nguyen Thi, T. B., Morioka, M., Yokoyama, A., Hamanaka, S., Yamashita, K., & Nonomura, C. (2015). Measurement of fiber orientation distribution in injection-molded short-glass-fiber composites using X-ray computed tomography. *Journal of Materials Processing Technology*, 219, 1–9. <http://doi.org/10.1016/j.jmatprotec.2014.11.048>
10. Song, W. L., Cao, M. S., Hou, Z. L., Fang, X. Y., Shi, X. L., & Yuan, J. (2009). High dielectric loss and its monotonic dependence of conducting-dominated multiwalled carbon nanotubes/silica nanocomposite on temperature ranging from 373 to 873 K in X-band. *Applied Physics Letters*, 94(23), 1–4. <http://doi.org/10.1063/1.3152764>
11. Wen, B., Cao, M. S., Hou, Z. L., Song, W. L., Zhang, L., Lu, M. M., ... Yuan, J. (2013). Temperature dependent microwave attenuation behavior for carbon-nanotube/silica composites. *Carbon*, 65, 124–139. <http://doi.org/10.1016/j.carbon.2013.07.110>

FIXATION OF REINFORCING FABRIC FOR ION EXCHANGE MEMBRANE

Eliška Stránská, David Neděla

MemBrain s.r.o., Pod Vinicí 87, Stráž pod Ralskem, 471 27, Czech Republic,
Eliska.Stranska@membrain.cz, tel. +420 725 358 422

Abstract:

A reinforcing fabric is an integral part of heterogeneous ion exchange membranes (IEMs). It guarantees the mechanical resistance of IEMs. Thermal fixation of the fabric is one of the most important refining operations, which is also reflected in the production of IEMs during lamination on heated cylinders.

The influence of the fixation temperature (grey variant, 120, 160 and 215 °C) of the Ulester 31HDA polyester fabric with a twill weave on the production of IEMs was studied. DSC, iodine sorption value measurement, or dimensional stability during the additional heat load were studied for commercially supplied fabrics Ulester 31HDA. The values were compared with the model series of fabrics prepared in laboratory drying under precisely defined conditions (temperature and time). The principle of fixation is the rearrangement of the internal fiber structure associated with the change of the crystalline phase. The reinforcing fabric is dimensionally stable up to the fixation temperature.

Iodine sorption value decreased with the increasing temperature of fixation. Any changes were not seen from SEM images or density measurements. DSC analysis did not show the predicted dependence for the model series of fabric. Dimensional changes after temperature loading increased with temperature.

Key words:

heterogeneous ion exchange membrane, preparation of membrane, reinforcing fabric, iodine sorption value, differential scanning calorimetry, shrinkage of reinforcing fabric

1. Introduction

Heterogeneous ion exchange membranes (IEMs), which are used in electroseparation processes, consist of a polymeric matrix and an ion exchange resin. It contributes to the transport of ions through the ion exchange membrane during the process. An inseparable part is also a reinforcing fabric that guarantees good mechanical properties of IEMs [2 - 4]. Heterogeneous IEMs can be prepared by extrusion, polymer and ion exchange resin mixture, with the simultaneous incorporation of a reinforcing fabric on heated rollers [3, 4]. In this manufacturing process, it is important to have a properly fixed fabric in terms of temperature. If the reinforcing fabric is insufficiently fixed, additional shrinkage is occurred during lamination of IEMs, which affects the quality of the IEM production, decreases the free area of the reinforcing fabric and thus also increases the electrical resistance of the manufactured IEMs [9]. Production is more demanding - extending the runway time, adjusting the entire production line, quality of the fabric is transferred to the manufactured IEMs quality. It is also necessary to buy a larger width of fabric to keep the required width of the manufactured IEMs. These factors increase the entry price of the reinforcing fabric.

For synthetic fiber fabrics, fixation is one of the most important refining operation. The desired touch and shape stability is resulted by heat-fixation with simultaneous stretching of the fabric. The main changes in synthetic fibers during fixation is the increase of the content of the crystalline fraction [11]. The fabric should be dimensionally stable up to the fixation temperature. The degree of fixation can be determined by several procedures, for example, by measuring DSC (different scanning calorimetry), ISV (iodine sorption value), fiber density, critical time measurement, temperature, concentration, or measurement of dimensional changes before and after thermal loading in a laboratory press.

The aim of the work was to characterize the commercially supplied grey reinforcing fabric and fixed fabrics at 120, 160 and 215 °C and then to test them in the process of manufacturing IEMs. First, it was necessary to create a model line of fixed fabrics at different temperature and time, which was characterized by DSC and ISV. The commercially available reinforcing fabrics Ulester 31HDA were compared with the model series and additionally the dimensional changes at 120, 140 and 160 °C, mechanical properties and density were determined. These temperatures are normally used on cylinders in the IEMs manufacturing process lamination.

2. Experimental

2.1. Materials

The reinforcing woven fabric Ulester 31HDA (Silk & Progress, Czech Republic) in 4 variants was used to test the degree of fixation and quality of IEMs preparation. The basic measurement parameters of fabrics are shown in Table 1. Ulester 31HDA was a polyester woven fabric with a twill (2:2) weave, consisting of a monofilament of 150 µm in warp and 100 µm in weft direction. Ulester 31HDA grey was not washed and fixed. Other fabrics (Ulester 31HDA 120, 160 and 215) were already washed and fixed at 120, 160 and 215 °C at Alligard (Czech Republic). The fabrics were stretched to the frame during the fixation, the duration of the heat was 2 minutes.

Ulester 31HDA grey was used to prepare the model fabric series that were fixed at 120 - 215 °C for 1 or 2 minutes in the laboratory drying oven.

Table 1. Properties of used reinforcing fabrics

Reinforcing fabric	Temperature of fixation °C	Thickness µm	Warp/weft 1 cm ⁻¹	Free (open) area %
Ulester 31HDA grey	-	263	27,7 / 30,5	40,6
Ulester 31HDA 120	120	249	28,5 / 30,5	39,8
Ulester 31HDA 160	160	260	29,8 / 30,2	39,2
Ulester 31HDA 215	215	242	29,2 / 30,4	39,1

2.2. Methods

Model reinforcing fabrics were characterized by DSC, ISV. Commercially supplied reinforcing fabrics (Ulester 31HDA grey, 120, 160 and 215) were characterized using SEM (scanning electron microscopy), and DSC. The measurement of the dimensional changes before and after the thermal loading in the laboratory press, the ultimate force and strain, ISV, and the density by pycnometry was determined. All commercial reinforcing fabrics were subsequently tested in the production of IEMs on the continuous lamination line in MemBrain s.r.o. and the influence of the degree of fixation on the production and quality of IEMs was evaluated.

2.2.1. DSC – differential scanning calorimetry

The purified sample was placed in a DSC PT 10 (Linseis) pan. DSC analysis was performed during heating and cooling. Two cycles of heating and cooling were measured in the Ar atmosphere. The heating rate was 15 °C min⁻¹, the cooling rate was 2 °C min⁻¹. The maximum temperature was 305 °C. The melting point and melting enthalpy were evaluated from DSC curves. Crystallinity (%) was calculated using the enthalpy melting ΔH_m from the 1st cycle according to the equation:

$$\text{Crystallinity} = \frac{\Delta H_m}{\Delta H_m^0} 100 \%$$

where ΔH_m^0 is enthalpy melting for 100 % crystallinity of polyester from 2nd cycle.

2.2.2. ISV – iodine sorption value

Sorption of I₂ [5, 6, 10, 11] into the amorphous regions of the fabric was determined by the iodine sorption value (ISV - mg I₂ g⁻¹). First the solution of 40 g KI + 5 g I₂ + 50 ml of water was prepared. The samples were degreased and dried. 1.2 ml of the prepared solution was added to the 0.2 g reinforcing fabric. After 5 minutes, 100 ml of water was added. After 1 hour, 75 ml of the solution was taken and titrated with 0.02 M sodium thiosulphate of the exact concentration. Starch was used as an indicator. ISV was calculated according to the equation:

$$ISV \left(\frac{\text{mg I}_2}{\text{g}} \right) = \frac{\left(V_{\text{blind sample}} - \frac{V(101,2 \text{ ml})}{V(75 \text{ ml})} V_{\text{titre with sample}} \right) c(\text{Na}_2\text{S}_2\text{O}_3) M(\text{I}_2)}{m}$$

where V is the volume, $c(\text{Na}_2\text{S}_2\text{O}_3)$ is the concentration of sodium thiosulfate, $M(\text{I}_2)$ is molar weight of iodine.

2.2.3. SEM – scanning electron microscopy

The structure of the reinforcing fabrics was investigated using a FEI Quanta 250 FEG scanning electron microscope. The conditions for measurement on SEM were 10 kV voltage, in low vacuum (80 Pa) with LFD (large field detector) for secondary electrons.

2.2.4. Dimensional changes during temperature loading

Shrinkage in the warp and weft direction was determined at 120, 140 and 160 °C for all fabrics according to EN ISO 80 0823 in the laboratory press. Testing was only to dry conditions; the reinforcing fabrics were placed between cold metal sheets.

2.2.5. Mechanical properties

The mechanical properties of the reinforcing fabric were measured with samples of dimensions of 50 mm × 200 mm (clamping length) according to the EN ISO 13934-1 using an H5KT (Tinius Olsen) tensile testing machine with a speed of 100 mm min⁻¹. The direction stress was in the warp and weft direction.

2.2.6. Density

Density was measured using the Pycnomatic ATC automatic helium pycnometer (ThermoFisher Scientific).

2.2.7. Preparation of IEMs

IEMs were prepared from an anion exchange resin and polyethylene. The mixture was extruded through a flat head between the rollers, into which the Ulester 31HDA (grey, 120, 160 and 215 °C) commercially available fabric was introduced. The rollers temperature for all fabrics was 140 °C, the temperature of the extruded mixture was 136 °C. The continuous lamination line speed was 1 m min⁻¹. IEMs were laminated on both sides. IEMs were rolled up after cooling [7].

3. Results and discussion

The dimensional changes (length – warp direction, width – weft direction, thickness) of commercial Ulester 31HDA after additional heating at 120, 140 and 160 °C was tested by the laboratory press. The reinforcing fabric was fixed by cold metal sheets and was inserted into the heated press to the desired temperature. Sample sizes were determined before and after exposure. The results for the warp and for the weft are shown in Figure 1. The thickness of the samples increased in all cases due to the shrinkage of the fibers in the cross fabric. During the IEMs lamination, additional shrinkage occurred only in the weft direction. The warp is stretched by the roll from which it is unwound. Dimensional changes increased with higher temperature in the warp and weft directions. Dimensional changes in the warp direction were much lower than in the weft direction. This is due to the process of fixation and weaving, where the anisotropy of the reinforcing fabric properties occurs [8]. Ulester 31HDA grey had the highest shrinkage. The shrinkage decreased with the increasing Ulester 31HDA fixation temperature, which was assumed.

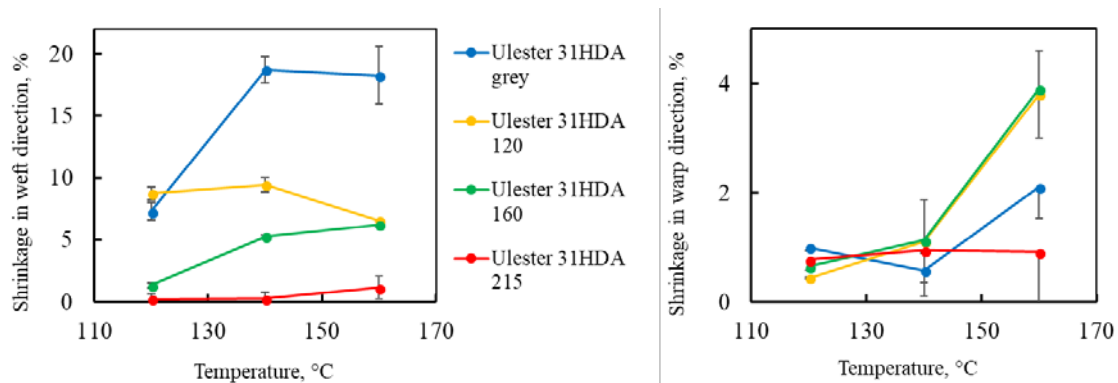


Figure 1. Shrinkage of reinforcing fabrics Ulester 31HDA in the warp and weft direction

Significant changes were not observed on the results of fabric density and mechanical properties. Mean values for ultimate force had the increasing tendency, but they are within the measurement error. The ultimate strain in the weft direction also showed a slight increase (Table 2). The anisotropy of mechanical properties in the weft/warp direction was already published by many authors [1, 8, 12]. The impact of stress on mechanical properties is enormous. The anisotropy of fabric properties is given by the fabric structure based on the perpendicular threads in the warp and weft. It can also affect the relative shifts of individual threads and the interaction of the threads at the bonding points.

During the fixation, the internal structure is rearranged, increasing the content of the crystalline fraction. From the thermodynamic point of view, it is the establishment of new conformational equilibria of the polymer chains in the threads deformed during the refining operation. Sorption I₂ is the basic method for determining the degree of fixation of synthetic fibers. I₂ is absorbed only into the amorphous regions of the threads at polar sites (NH, CO). The proportion of crystalline regions in the fiber increases with the increasing degree of fixation and the sorption of I₂ decreases [5, 6, 10, 11]. From the model series and commercially available fabric Ulester 31HDA, it is seen that ISV decreased with the increasing fixation temperature. The decreasing dependence is well evident in Figure 2. The

ISV is determined with a relatively high error. For more accurate measurement of the fabric with an unknown fixation temperature, the method should be adjusted.

Table 2. Density, ultimate force and strain for commercial reinforcing fabrics

Reinforcing fabric	Density - pycnometry g cm ⁻³	Ultimate force – warp/weft N/ 5 cm	Ultimate strain – warp/weft %
Ulester 31HDA grey	1,380	1260 ± 25 / 543 ± 12	46 ± 3 / 28 ± 2
Ulester 31HDA 120	1,393	1240 ± 35 / 571 ± 13	46 ± 3 / 28 ± 1
Ulester 31HDA 160	1,380	1330 ± 16 / 621 ± 9	44 ± 1 / 34 ± 3
Ulester 31HDA 215	1,385	1290 ± 65 / 635 ± 6	42 ± 4 / 36 ± 1

From DSC analysis, it was possible to calculate the crystallinity of the material, which varied according to the temperature history of the sample. There was a melting peak in the DSC curve, which did not change with the temperature of the fixation of the reinforcing fabric. Crystallinity was calculated from the 1st cycle (heating and cooling) when the sample still had a temperature history given by the fixation temperature. The problem with DSC measurement for fabrics was the small sample weight at the detection limit and poor heat transfer from the pan to the sample. The heat transfer was improved in the 2nd cycle (fabric is in the sheet form), but the temperature history of the sample was not visible on the DSC curve. An increasing proportion of the crystalline phase to temperature was only apparent for commercially available Ulester 31HDA samples (Figure 2). For a model series of samples, the increasing proportion of the crystalline phase was not confirmed. This was probably due to insufficient heat transfer from the pan to the sample, or a low sensitivity of the DSC.

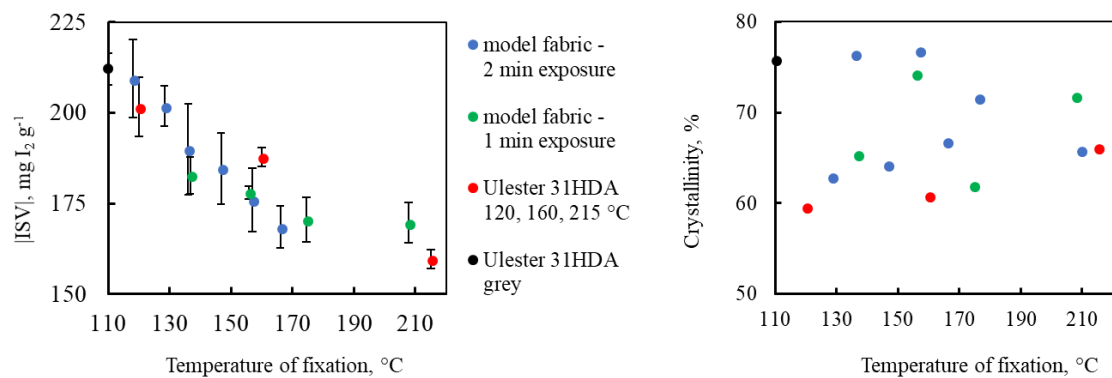


Figure 2. ISV and crystallinity of model fabric and commercially supplied Ulester 31HDA

SEM scans of commercially supplied Ulester 31HDA are shown in Figure 3. No significant changes during fixation were visible on the threads. The increasing fixation temperature occurred only with a slight decrease of the free (open) area of the reinforcing fabrics (Table 1) in the order of percentages.

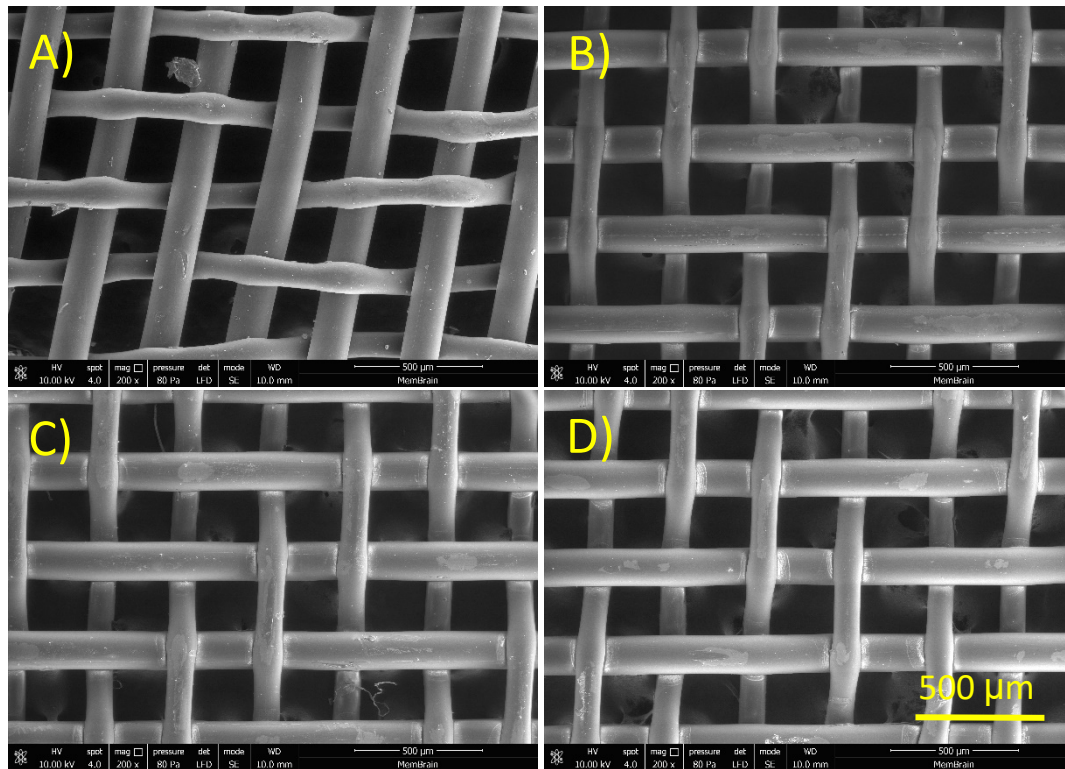


Figure 3. SEM scan A) Ulster 31HDA grey, B) Ulster 31HDA 120, C) Ulster 31HDA 160 and D) Ulster 31HDA 215

The production of IEMs with Ulster 31HDA 215 and 160 took place without any significant problems. The Ulster 31HDA 215 and Ulster 31 HDA 160 had shrinkage on 140 °C warm rollers by 0.4 %, respectively, by 2.6 % in the weft direction. Values correspond to the measured data from the laboratory press at 140 °C. Production of IEMs took place at temperatures lower (140 °C) than the temperature of the fixation of the reinforcing fabric (160 and 215 °C). Textiles were stable at this temperature.

IEMs production with Ulster 31 HDA grey and 120 was more problematic. Greater parameters change and setting of pressures on rollers had to be done. The Ulster 31HDA grey and Ulster 31 HDA 120 had shrinkage on 140 °C warm rollers by 16.7 %, respectively 10.2 % in the weft direction. These values also correlate with the measured data presented in Figure 1. The formation of wrinkles and fabric duplication occurred with high shrinkage of the reinforcing fabrics on the rollers, where there is uneven tension and material distribution. The defects are visible at Figure 4. In some places, the reinforcing fabrics were folded and rolled into IEM in two layers. Another problem was the formation of surface wrinkles formed by the imprinting of PET foil which is used to separate IEM on heated rollers. The reinforcing fabric rumbled the PET foil during the high shrinkage and wrinkles from PES foil was imprinted on the IEM surface. These IEMs were then marked as unsatisfactory. Despite the difficulties, it was possible to set production with this type of reinforcing fabric after a long time, so all variants would be used in the production of IEMs.

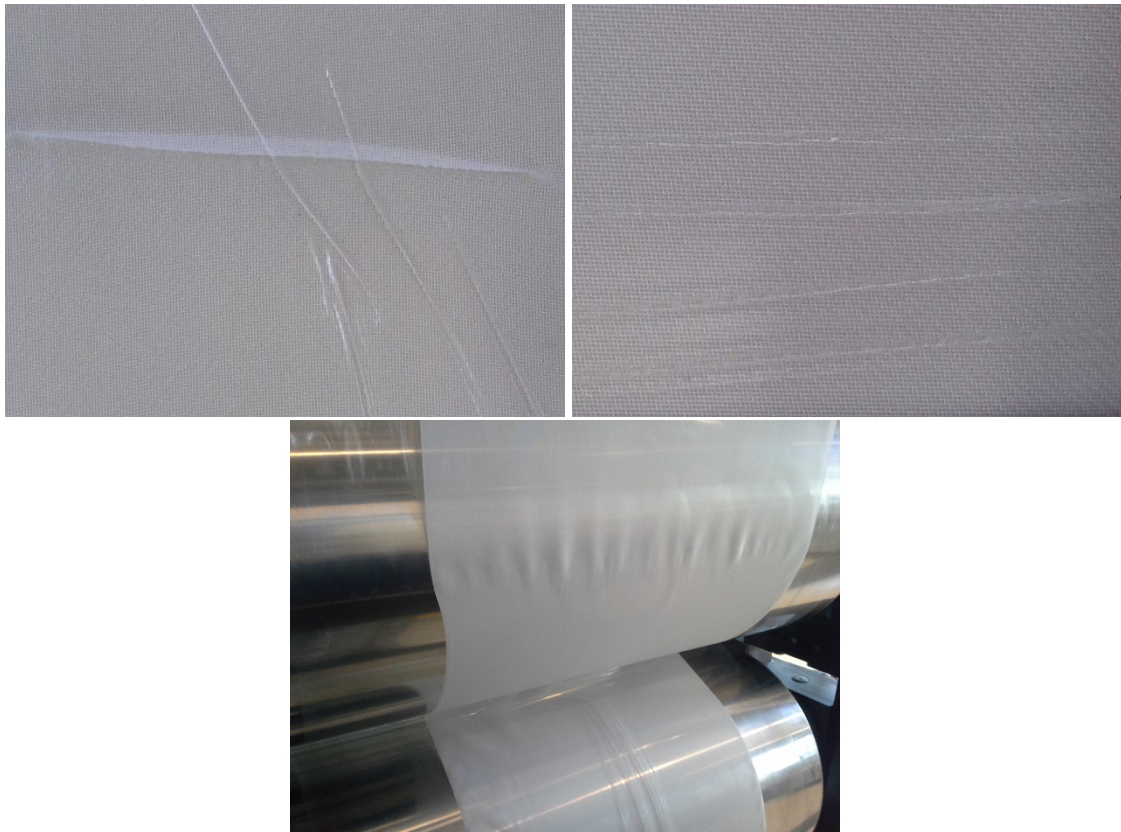


Figure 4. Images of unsatisfactory production of IEMs; wrinkles caused by high shrinkage of the fabric on the warm rollers

4. CONCLUSIONS

The effect of the fixation temperature of reinforcing fabric Ulester 31HDA on IEMs production and their characterization was investigated using basic methods such as DSC, ISV measurements or dimensional changes before and after the temperature exposure.

It was found that

- ISV decreased with the fixation temperature due to lower sorption of iodine to the crystalline regions. However, the method is not sensitive enough to determine the precise fixation temperature of reinforcing fabrics.
- Dimensional changes at temperatures below the fixation temperature of the fabric were within 5%. Shrinkage increased with increasing temperature. Below the fixing temperature, the fabric is still thermally stable.
- The crystallinity was determined from DSC analysis. An increasing trend was only demonstrated in commercial samples Ulester 31HDA.
- From SEM, density, or ultimate force and strain images, there was not visible difference between reinforcing fabrics treated at different temperatures.
- All types of Ulester 31HDA textiles can be used in the manufacture of IEM by lamination. In some cases, it is necessary to increase the correction of the individual parameters of the continuous lamination line.

ACKNOWLEDGEMENTS

The work was carried out within the framework of the project No. LO1418 "Progressive development of Membrane Innovation Centre" supported by the program NPU I Ministry of Education Youth and Sports of the Czech Republic, using the infrastructure Membrane Innovation Centre.

References

- [1] Adomaitienė, A., Kumpikaitė, E. (2011). Analysis of mechanical properties of fabrics of different raw materials. *Mater. Sci.*, 17(2), 168-173.
- [2] Ariono, D., Khoiruddin, Subagjo, Wenten, I. G. (2017). Heterogeneous structure and its effect on properties and electrochemical behavior of ion-exchange membrane. *Mater. Res. Express*, 4, 024006.
- [3] Kariduraganavar, M. Y., Nagarale, R. K., Kittur, A. A., Kulkarni, S. S. (2006). Ion-exchange membranes: preparative methods for electrodialysis and fuel cell applications. *Desalination*, 197, 225-246.
- [4] Nagarale, R. K., Gohil, G. S., Shahi, V. K. (2006). Recent developments on ion-exchange membranes and electro-membrane processes. *Adv. Colloid Interface Sci.*, 119, 97-130.
- [5] Nelson, M. L., et al. (1970). The Iodine Sorption Test. Factors Affecting Reproducibility and a Semimicro Adaptation. *Text. Res. J.*, 40(10), 872-880.
- [6] Pušić, T., et al. (2014). Istraživanje jednog broja pamučne tkanine nakon pranja. *Tekstil*, 63(1-2), 41-48.
- [7] Stránská, E. (2015). Relationship between transport and physical-mechanical properties of ion exchange membranes. *Desalin. Water Treat.*, 56(12), 3220-3227.
- [8] Stránská, E., Zárybnická, L., Weinertová, K., Neděle, D., Křivčík, J. (2016). Anisotropy of mechanical properties of heterogeneous ion exchange membrane. *Chem. Listy*, 110, 498-503.
- [9] Stránská, E., Neděle, D. (2017). Reinforcing fabrics as the mechanical support of ion exchange membranes. *J. Ind. Text.*, 1-16.
- [10] Weaver, J. V. (Ed.). (1984). *Analytical Methods for a Textile Laboratory*.
- [11] Weiner, J., Průšová, M., Kryštůfek, J. (2008). *Chemicko-textilní rozbor*, Technická univerzita v Liberci.
- [12] Zouari, R., Amar, S. B., Dogui, A. (2016). Experimental characterization of anisotropic mechanical properties of textile woven fabric. *Int. Scholarly Sci. Res. Innovation*, 10(2), 409-415.

RE-USE OF PYROLYSED CARBON FIBRES IN SOPHISTICATED COMPOSITES AS INDUSTRIAL VIABLE PROCESS WITH INTEGRATED QUALITY MONITORING: RECYCARB

Holger Fischer¹, Marcel Hofmann², Andrea Miene¹, Katharina Heilos²

¹Faserinstitut Bremen e.V. FIBRE, Bremen (DE), fischer@faserinstitut.de

²Sächsisches Textilforschungsinstitut e.V. STFI, Chemnitz (DE)

Abstract

Within the frame of the research project RecyCarb a team of four industrial partners and two research institutes has established the basis for a qualified value-added chain for recycled carbon fibres (rCF). This enables the high-quality and sustainable re-use of rCF in sophisticated fibre-reinforced plastics, e.g. in sports equipment, medical technology or transportation. The progress in processing technology was accompanied by setting up a reliable scheme of quality assurance. The research project RecyCarb is finishing in late 2018. This article focuses on (1) definition of relevant quality parameters over the entire process from waste recovery to the high-quality re-use of rCF in suitable parts, accompanied by definition of the sampling positions for off-line sampling and on-line monitoring, and (2) the use of different web formation and bonding technologies to produce nonwovens, ranging from highly-oriented to quasi-isotropic nonwoven structures, in order to match different application markets. Results of on-line fibre orientation analysis are compared to mechanical properties of composites produced from rCF nonwovens

Key words:

recycled carbon fibres (rCF); quality monitoring; nonwoven; lightweight construction

1. Introduction

The markets for carbon fibre-reinforced plastics (CFRP) are growing since years. Consequently, there are increasing amounts of materials reaching the 'end-of-life'. Actually these wastes can be recycled by milling or shredding and subsequent pyrolysis. The resulting products are entering the markets for recycled carbon fibres (rCF), although they are inhomogeneous in their morphology. These mixtures comprise roving residues & filaments in wide fibre length distribution. The only established industrial market is use of short fibres or milled material for injection moulding — a cheap product, more for improving the antistatic properties than the mechanical properties of plastics. In addition, in the beginning of the project there were no definitions for long rCF (>10 mm) and final products concerning:

- Necessary qualities (length distribution, minimum tenacity, homogeneity, ...)
- Sampling in process (sampling locations, modality of sampling, reproducibility, ...)
- Quality of the final products compared to virgin fibres.

For these reasons the commercialisation of rCF as semi-finished product for sophisticated composite applications was hindered or impossible. In preliminary studies the project partners developed the basic knowledge which was a base for the project work reported here. In the successful German project ZIM VP2444804VT0 a first process for production of carded nonwovens from rCF was developed [1]. Basic principles for characterisation of rCF were defined. These enabled the quality

classification for several types of rCF [2]. Successful attempts have been made in fibre processing to process different CF waste / cutting scraps or CF from pyrolysis using modified cutting and tearing machines. The resulting average fibre length was 60 mm, i.e. 85% of the pre-cut. This work was combined with technical and technological developments for transfer to the industrial scale.

Result of this preliminary work was first-time processing of long, but not endless carbon fibres by means of the carding principle, using either 100 % carbon fibres or blends with natural fibres and / or synthetic fibres [3]. The results depicted clearly, that web formation is possible not only from 100% primary carbon fibres, but as well from 100% recycled carbon fibres via mechanical carding [1, 3]. These carbon fibre nonwovens displayed high formability and sufficient strength, making them suitable as semi-finished products for CFRP-structures.

Consequently, in 2016 the research project RecyCarb had been initiated with special focus on:

- Process scale-up for waste recovery and nonwoven production into industrial and economical relevant scale with respect to the quality requirement
- Set-up of a process-integrated monitoring of quality parameters, starting with waste recovery and reaching to the high-quality re-use of rCF in suitable parts
- Evaluation of the effects of different nonwoven technologies, first-time application of a combined nonwoven process for generating quasi-isotropic nonwoven structures
- Specific application-oriented adaption of technology and products to the different requirements of the target applications and potential end-users.

The project team consisted of two research institutes and four industrial partners, covering the desired value-added chain. Aim of the project work has been setting up a qualified value-added chain for recycled carbon fibres (rCF) by closing the technological gap between rCF and functional high-value re-use. The work comprises the definition of necessary initial quality & standards for consistent sampling in the process, process-attached monitoring in terms of Industry 4.0, reproducible intermediate quality by optimisation of the carding process and finally upcycling by re-use of rCF in high-value parts.

2. Experimental

2.1. Materials & processing line

Recycled carbon fibres have been supplied by the industrial partners in the project consortium from own factory offcuts as well as pyrolysed rCF from carboNXT, Stade, DE. These rCF lots were processed in the new 'Centre for Textile Lightweight Engineering' at STFI, Chemnitz, DE. The processing line for converting carbon fibre waste into nonwovens comprises:

- Cutting und tearing technology to convert dry rCF to applicable fibres for further textile processing, followed by
- Either carding technology for processing rCF to webs: carding machine & cross-lapper (working width 100 cm),
- Or alternatively random web technology for processing rCF to mechanically bonded nonwovens: airlay random carding machine,
- Followed by needle loom and/or stitch-bonding machine (working width 100 cm)

The line setup is displayed in figure 1.



Figure 1. rCF nonwovens line, (a) tearing unit, (b) roller card supply and (c) roller card [4].

2.2. Sampling Scheme & positions

Due to lack of standards for rCF, a new scheme for sampling had to be developed for the entire process, comprising off-line quality control as well as definition of the positions at the processing line for on-line control.

To ensure constant product qualities, the incoming rCF lots have to be characterised preceding to processing as described above. For the processing line a sampling scheme has been developed covering the possibility of taking samples for intensive off-line analysis on one hand (enabling further improvement of the process itself) and defining positions for on-line control by image analysis on the other hand, enabling direct control of parameters like fibre orientation and homogeneity of the nonwoven [4]. A scheme of the different sampling positions is displayed in figure 2.

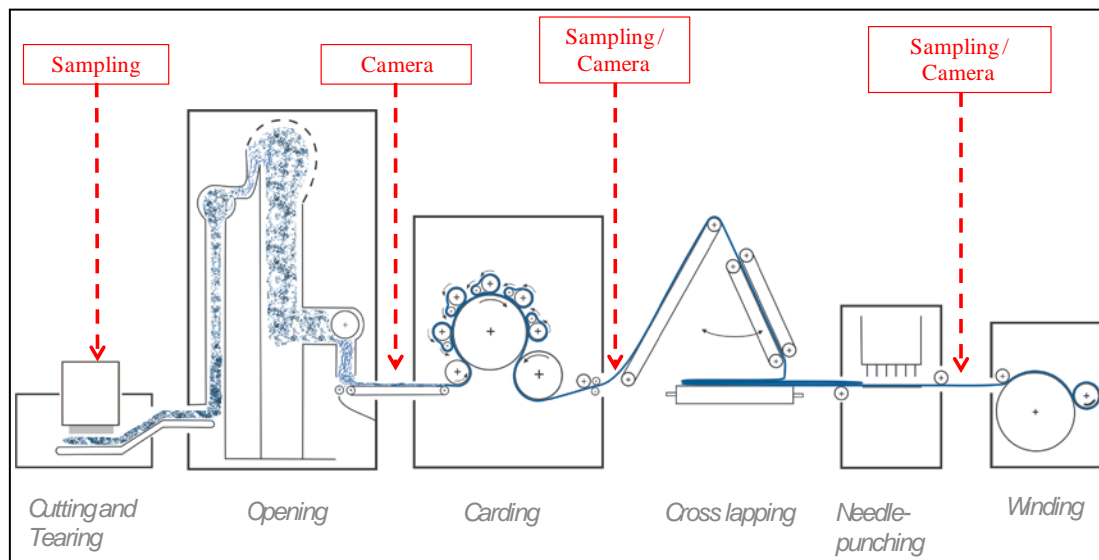


Figure 2. Monitoring positions in nonwoven production and bonding process [4].

The sampling scheme comprises each three positions or off-line sampling and on-line control:

- Off-line samples are taken for the incoming lots (initial quality control, enabling rejection of insufficient qualities), after carding (or airlay, resp.) to control the quality of web formation, and finally after needling as product quality control.
- On-line control will be performed at the card (or airlay) supply belt (controlling the feed homogeneity and to identify contaminations), after carding (or airlay, resp.) to control the web and finally after needling to control fibre orientation as well as needling & nonwoven homogeneity.

In the beginning of the project it became clear, that established sampling methods, e.g. for natural fibres, cannot be adapted 1:1 to the sampling of rCF. Thus, for the rCF lots supplied as raw material, a sampling scheme has been developed, which is roughly similar to DIN EN 12751:1999 (*'Textiles — Sampling of fibres, yarns and fabrics for testing'*). The method was derived from the sampling scheme for cotton bales: up to ten sub-samples from up to ten layers of equal height. If there are visibly different zones in the lot, a sub-sample has to be taken from each of these zones (similar to the procedure of sampling wool sacks).

If possible, the sub-samples shall be mixed and the resulting sample has to be analysed as specified in the subsequent section. Otherwise, each of the sub-samples has to be analysed as described below and the results have to be summed up to an average value.

2.3. Methods

Incoming fibre lots have been characterised using Dia-Stron single-element analysis (Dia-Stron Ltd., Andover, UK) to assess fibre tenacity and Young's modulus based on DIN EN ISO 5079 (1996), clamping length 3.2 mm. Preceding the tensile tests the cross-section of each single specimen was measured via laser beam. Up to 45 specimens were measured to ensure statistically firm results as described in [5]. A part of the lots has been examined by SEM (Cam Scan CS24, EO Elektronen-Optik-Service GmbH, Dortmund, DE with Software analySIS 3.2, SIS Soft Imaging System GmbH, Münster, DE) to identify contaminations, dust, and/or fibre damages. Fibre length distribution of rCF lots shorter than 100 mm is analysed by image analysis FibreShape V6.1.2f with add-on FiVer (IST AG, Vilters, CH), based on 2500 – >6,000 fibres, depending on sample homogeneity. The adaptation of the sample preparation and measurement parameters has been described in [6].

3. Results and discussion

Different lots of rCF have been processed on the line specified in section 2.1. It was possible to produce nonwovens by roller-carding as well as by airlay processing. Both process variants are exemplarily shown in figure 3.



Figure 3. Production of nonwovens from rCF by airlay and roller-carding process.

In addition, experiments have been performed to examine the influence of repeated processing: produced nonwovens from rCF have been supplied again to the process in order to produce 're-recycled carbon fibre' nonwovens 'rrCF'. The fibre (bundle) length during these process steps was reduced from initially 119 ± 8 mm (supplied rCF) via 104 ± 16 mm (first tearing process) to finally 69 ± 26 mm ('rrCF' after tearing the rCF nonwoven). In the carding process, the areal weight of resulting needle felts was 300 g/m^2 for the rCF nonwoven, but had to be reduced to 100 g/m^2 for the rrCF nonwoven in order to produce homogeneous material. This was realised by increasing the haul-off speed in the cross-lapper. As discussed later, this leads to different fibre orientations in the nonwovens. The same process has been performed using the airlay, leading to a quasi-isotropic nonwoven. The fibre orientation has been analysed by image analysis, using a NOS 200 system. The results for rCF airlay, rCF and rrCF after carding compared to a standard carbon nonwoven are displayed in figure 4.

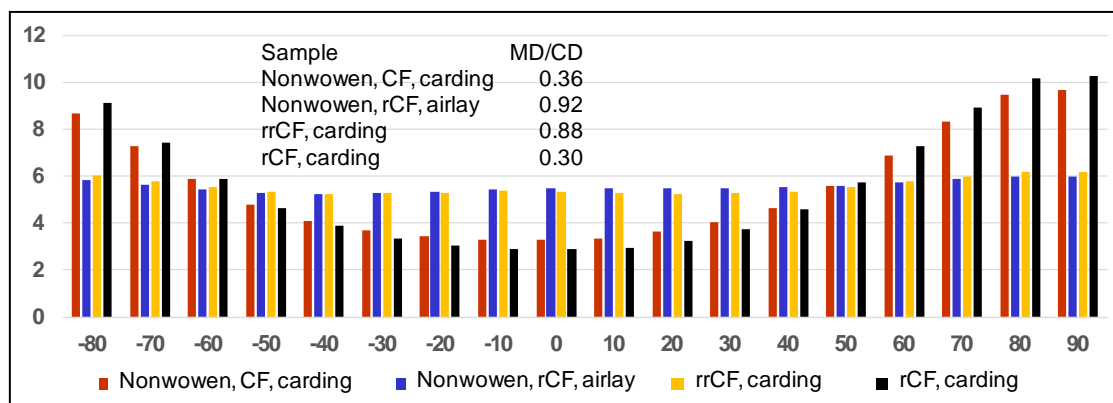


Figure 4. Distribution of fibre orientation after airlay and carding process.

Composites have been produced from both nonwovens, using either six layers rCF or 18 layers rrCF nonwoven (both summing up to 1800 g/m²) in epoxy resin. The mechanical properties of these composites have been analysed according to DIN EN ISO 14125. The results of the tenacity analysis are compared to the results of fibre orientation analysis in table 1.

Table 1. Parameters, MD/CD ratio and mechanical properties of the rCF and rrCF samples.

Sample	rCF, airlay	rrCF, airlay	rCF, carding	rrCF, carding
Nonwoven, areal weight in g/m ²	300	250	300	100
Number of layers in composite / total areal weight in g/m ²	6 / 1800	7 / 1750	6 / 1800	18 / 1800
Composite tenacity (MD) in MPa	290	262	279	318 ^a
Composite tenacity (CD) in MPa	351	323	532	344 ^a
MD/CD ratio from image analysis	0.92		0.32	0.88

^aAdditional value for 45°: 304 MPa.

The results for the composites made from airlay nonwoven are as expected: nearly isotropic, and a small but significant loss of tenacity in the second tearing process. This conforms to the MD/CD ratio of 0.92 found for the rCF airlay. The results for the carded rCF nonwoven were as expected: the composite displays a much higher tenacity in CD than in MD. This is the regular effect of cross-lapping, where the main fibre direction MD from carding is converted into a main orientation in CD. This is reflected by the MD/CD ratio of 0.32 found for this nonwoven. The results for the composites made from carded rrCF nonwoven were unexpectedly different: the tenacity values for MD and CD were 318 MPa and 344 MPa. An additional value measured in angle of 45° (304 MPa) indicated as well, that this sample is nearly isotropic. This could be confirmed by the result of the image analysis: the fibre orientation of this sample is nearly isotropic as well (cf. fig. 4) with MD/CD ratio of 0.88. This is caused by the higher haul-off speed in the cross-lapper and leads to a fibre orientation similar to that of airlay nonwovens.

4. CONCLUSIONS

Within the frame of the research project RecyCarb a process line has been set-up enabling the processing of recycled carbon fibres into high-quality nonwovens. In parallel a quality control system has been defined to ensure constant product qualities. Alternatively this offers the possibility to operate with varying rCF qualities. The quality control system comprises the definition of sampling positions along the line for off-line analysis and on-line control. The on-line analysis can be used potentially as input for process control in the future. Various lots of rCF, ranging from production wastes to pyrolysed fibres from 'end of life' parts, have been processed successfully to carded and airlay nonwovens. A high variability of the fibre orientation after carding process has been demonstrated and validated by results of the on-line measurement system. Actually final measurements are going on to demonstrate the on-line analysis of fibre orientation directly in the carded web, using a modified camera / illumination unit.

The carbon fibre nonwovens generated on the line are very suitable as semi-finished products for CFRP-structures. Due to their high formability sufficient strength, and adjustable MD/CD ratio they are ideal candidates for sophisticated composites.

ACKNOWLEDGEMENTS

Financial support by the German Ministry of Education and Research (BMBF) within the framework Entrepreneurial Regions, project futureTex, grant no. 03ZZ0608A-I is gratefully acknowledged.



References

1. Hofmann, M. & Fischer, H. (2016): RecyCarb: Process Optimisation and On-Line Monitoring in the Recycling of Carbon Fibre Waste for the Re-Use in High-Grade Fibre-Reinforced Plastics. In Borgmann, H. (Ed.): ITHEC 2016 — 3rd International Conference and Exhibition on Thermoplastic Composites, 11 – 12 October 2016, Congress Center Bremen, Germany. Conference Proceedings. WFB Wirtschaftsförderung Bremen GmbH, Bremen, Germany, pp. 60 – 63. ISBN 978-3-933339-29-4.
2. Fischer, H. & Schmid, H. (2013): Quality control for recycled carbon fibres. *Kunststoffe International* 103,11, pp. 68 – 71. ISSN 0945-0084.
3. Hofmann, M. & Gulich, B. (2015): Nonwovens for composites — recycling carbon waste in the form of long fibres. *JEC Composites Magazine* No. 98, pp. 50 – 51. ISSN 1639-965X.
4. Hofmann, M., Fischer, H., Yuan, Q. & Miene, A. (2017): RecyCarb: process optimisation and on-line monitoring in the recycling of carbon fibre waste for the re-use in high-grade fibre-reinforced plastics. In DITF, DWI & ITM (Eds.): *Proceedings Aachen-Dresden-Denkendorf International Textile Conference*, Stuttgart, November 30 – December 1, 2017. CD-ROM Proceedings, Paper lecture_hofmann.pdf. Deutsche Institute für Textil- und Faserforschung DITF, Denkendorf, DE. ISSN 1867-6405.
5. Müssig, J.; Fischer, H.; Graupner, N. & Drieling, A. (2010): Testing Methods for Measuring Physical and Mechanical Fibre Properties (Plant and Animal Fibres). Chapter 13 in Müssig, J. (Ed.): *Industrial Applications of Natural Fibres — Structure, Properties and Technical Applications*. Wiley-VCH, Weinheim, DE, pp. 269 – 309. ISBN 978-0-470-69508-1.
6. Fischer, H., Hofmann, M., Miene, A. & Heilos, K. (2017): RecyCarb — Aufbau einer qualifizierten Wertschöpfungskette für rezyklierte Carbonfasern (rCF) zum Wiedereinsatz in anspruchsvollen Bauteilen. In Sächsisches Textilforschungsinstitut e.V. (Organiser. & Ed.): *Proceedings 13. STFI-Kolloquium „recycling for textiles“*, 6. und 7. Dezember 2017 im Günnewig Hotel "Chemnitzer Hof". Sächsisches Textilforschungsinstitut, Chemnitz, DE.

STUDY OF THE TOW BUCKLING DEFECT DURING THE COMPLEX SHAPE FORMING OF SYNTHETIC AND VEGETAL FIBRE REINFORCED STRUCTURAL COMPOSITES

M.M. Salem¹, E. De Luycker¹, M. Fazzini¹, and P. Ouagne¹

¹Laboratoire Génie de Production (LGP), INP-ENIT, Univ. de Toulouse, Tarbes, France.

Abstract:

Fibrous reinforcements for structural composites manufacturing need to undergo in certain cases a complex shape forming process during which multiple defects could appear. These defects, such as tow buckling and tow sliding may reduce the integrity of the final part. The onset of these defects depends on the initial loading conditions, the shape of the preform and the characteristics of the textile material. While mechanisms behind the formation and development of both defects are yet to be fully understood. We focused, in this work, on investigating the buckling defect. In order to do so, we used optical field measurement techniques to monitor the kinematics of the defect appearance and predict it via an adapted analytical model. of the defect appearance.

Key words:

Composite manufacturing, Preforming defects, Textile reinforcement, Tow buckling, Full field strain measurement.

1. Introduction

Fibre reinforced composites receive an ever growing interest, because of their interesting mechanical properties, low cost and progressively mastered manufacturing techniques [1]. The complex shape forming of fibre reinforced composites might be done using techniques such as Resin Transfer Molding or Thermoplastic-Matrix Composites Stamping to produce seamless materials [2] but it can be less productive than regular laminates and susceptible to produce defects that alter the mechanical properties of the composite [3].

Thus, it is essential to fully understand and anticipate the appearance of defects such as the tow buckling which will be the focus of this paper. In the literature, the buckling defect appears on woven reinforcements and seems to be the result of the in-plane bending of the tows coupled with initial loads and reinforcement properties. Thus a buckling device, presented in Figure 1, was designed and manufactured to reproduce those conditions in a controlled environment [4].

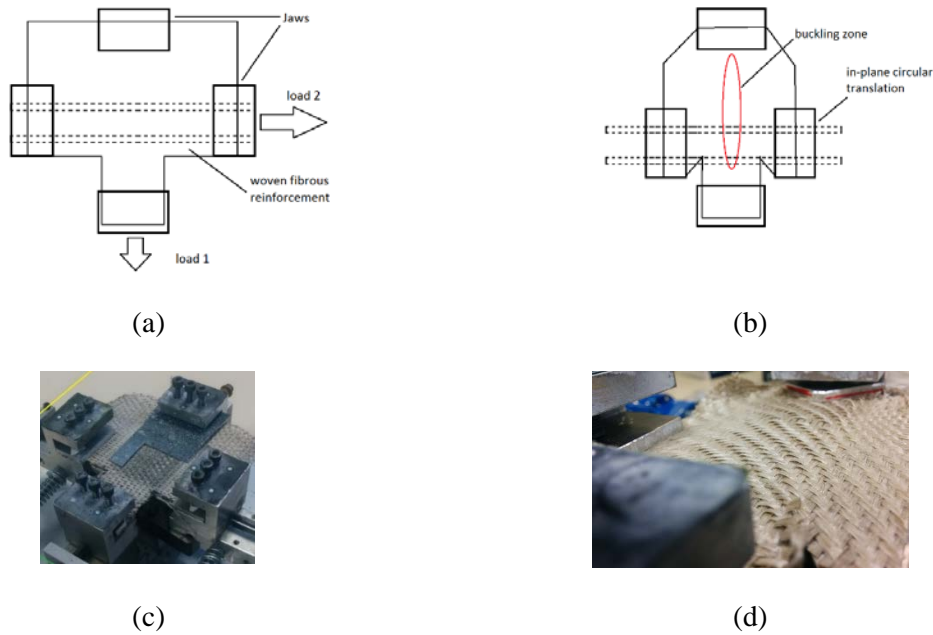


Figure 1. (a), (b) Buckling device principle (c), (d) Appearance of the buckles on the bent reinforcement surface

2. Experimental study

2.1. Description of the buckling device

The buckling device is instrumented with two load cells, one in each direction of the weave in order to monitor the applied load. The buckling device was also equipped with a digital image correlation camera in order to record the bending angle between the tow's initial position and the bent state at any given moment. T shape samples were loaded in the device. This allowed the in-plane bending of one network (the transverse one) up to a 40° bending angle from the initial tow position (Figure 1b).

Furthermore, three full field optical systems: Various-focus microscopy (Figure 2 (a)), Fringe projection (Figure 2 (b)) and Stereo-Digital Image Correlation (Figure 2 (c)), were considered and tested to assess the formation of the buckle. Three tests were performed in similar conditions as it is impossible to combine the optical systems equipments. The reconstructed surfaces of the tows from each technique are presented in Figure 2.

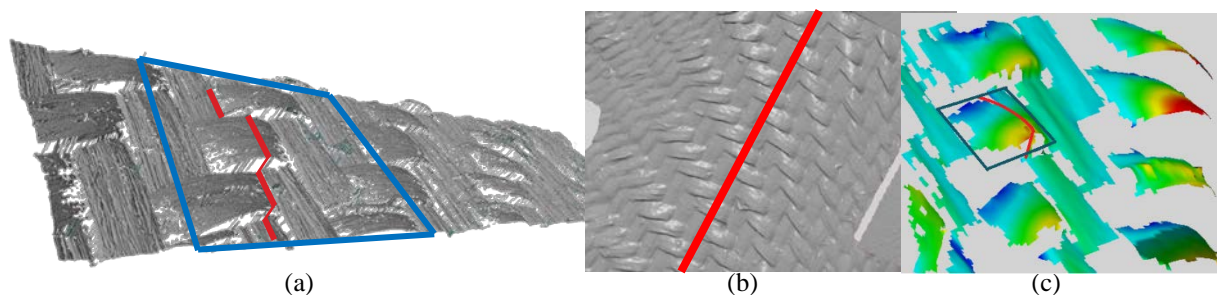


Figure 2. Reconstructed surface and profile of the tows (red line) obtained by (a) focus-variation microscopy, (b) fringe projection, (c) Stereo-digital image correlation (S-DIC).

The profiles of the tow buckle (red lines in figure 2) at the initial state 0° and after an in-plane bending angle of 25° are given in Figure 3 for the three reinforcements tested with the three full field optical systems. One can globally see that the three techniques indicate relatively similar profiles and thus results from each technique can be considered valid. The S-DIC was finally chosen as it allows both fast and accurate enough results plus native displacement data.

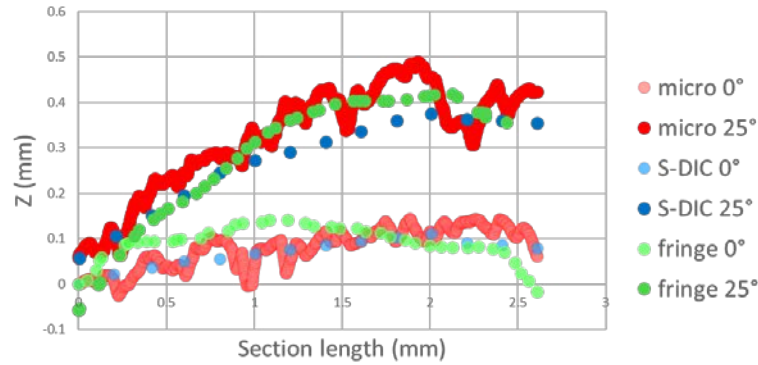


Figure 3. Buckles profiles comparison using stereo-DIC, Fringe projection and Various-focus microscopy at tow bending angles of 0° and 25°

2.2. Buckling tests

Three different reinforcements, listed in Table 1, were tested. Some of their geometrical characteristics are also given in Table 1. The influence of multiple parameters, such as initial loading in both weave directions as well as the reinforcement mechanical and geometrical properties are considered. In the following, the bending rigidity and tow's geometries were investigated. The reinforcements were subjected to a 300N load in the fixed tows network and 20N in the bending tows network and bent up to 40° angle. Figure 4 shows the evolution of the maximum tow elevation as a function of the in-plane bending angle.

One can observe in Figure 4 that the buckles appear for lower in-plane bending angles for the carbon twill weave. For the carbon reinforcement we notice the onset of the buckle at a bending angle of 5° , followed by the sized-up linen reinforcement at an angle of 10° and finally by the desized-up linen reinforcement at an angle of 13° . As the bending rigidity (measured independently on an adapted system) decreases the onset of the buckle is much more delayed and the size of the final buckle is smaller. Since the tows are under displacements constraints, the load repartition for the same bending angle are different depending on the material. More rigid tows achieve a critical buckling load for lower values of bending angles which explains the earlier buckling. Consequently, the bending rigidity of the tow for relatively similar contextures and tow geometries is therefore a key parameter that controls the appearance and the evolution of the tow buckling defect.

Table 1. Characteristics of reinforcement used for tow buckling

Weave	Material	Area density (g/m ²)	Warp density (m ⁻¹)	Weft density (m ⁻¹)	Unsupported length (mm)	Unsupported width (mm)	Tow bending rigidity (N.mm)
Twill 2x2	Sized up linen	476	380	385	6.1	2.5	1.18
Twill 2x2	De-sized up linen	465	380	430	5.7	2.4	0.72
Twill 2x2	Carbon fiber	600	380	380	6.4	2.3	7.55

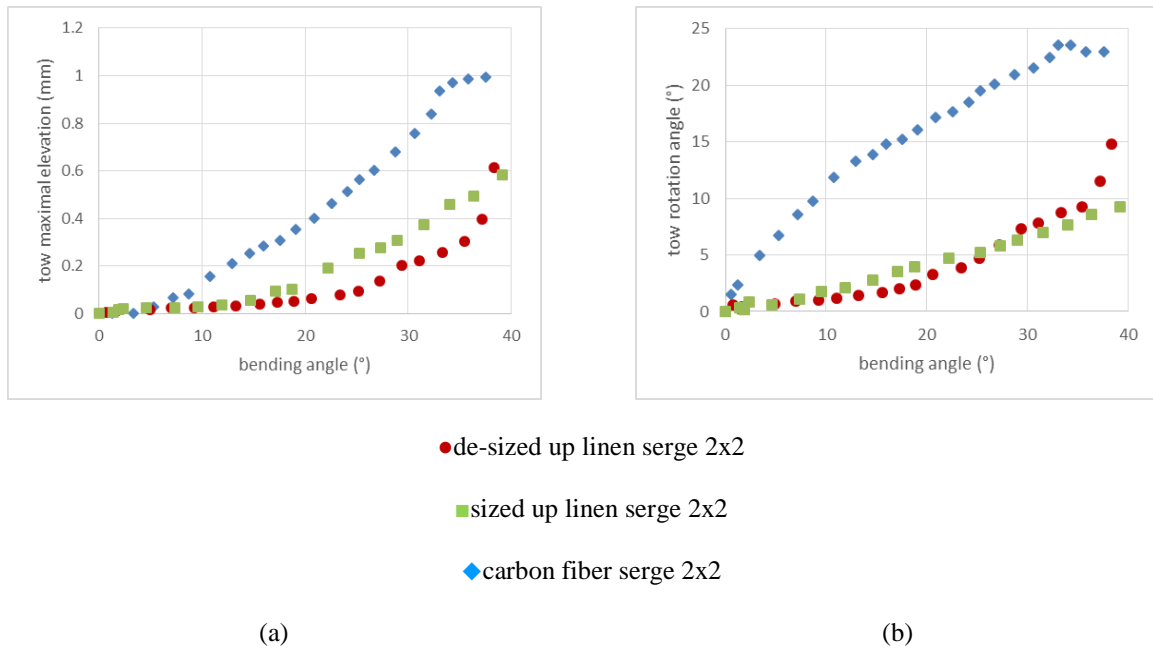


Figure 4. Maximum elevation (a) and rotation angle of the tow (b) as a function of the bending angle.

As for the effect of tows geometry, taking into account the variation of the unsupported length and width of the tows and using the same experimental conditions as before, we compared for a de-sized up linen based reinforcements the impact of the unsupported tow length (the length for a given architecture between two weft perpendicular tows) and the unsupported tow width (the width of the tow showing the in-plane bending (the warp tow) in figure 5. As the unsupported length grows in figure 5(a), so does the tow deflection and rotation. This is explained by the added freedom for the buckle to rise and develop. But as the unsupported width grows in figure 5(b), the deflection grows while the rotation diminishes. This could be explained by smaller size buckles compared to the tow width, which means even if they deflect higher, the deflection compared to the tow width seems to be declining.

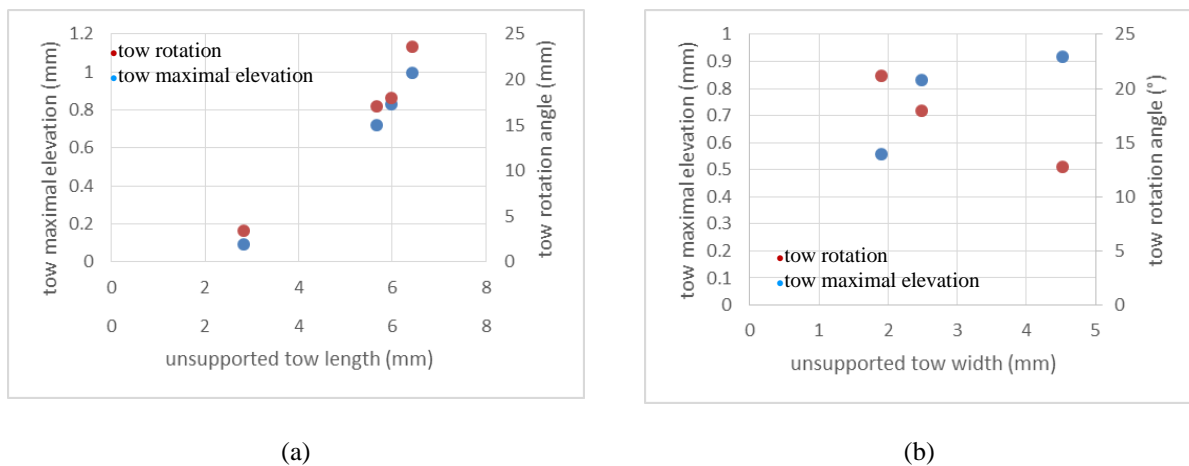


Figure 5. Maximum elevation and rotation angle of the tow (a) as a function of the unsupported tow length and (b) as a function of the unsupported tow width.

3. Analytical model

An analytical framework based on the buckling of orthotropic homogenous plate is proposed to predict the buckling of tows inspired from a work made for tape on an elastic foundation for the buckling of steered tows in automated dry fibre placement [5]. Considering the tow as an orthotropic thin plate [6], the differential equation for plate bending, was solved by using the Rayleigh-Ritz approach. This approach allows us to determine the critical buckling load P_{cr} , for which the tow starts to deflect:

$$P_{cr} = \frac{\frac{24D_{11}m^2\pi^2}{L^2} + \frac{90D_{22}L^2}{b^4m^2\pi^2} + \frac{160D_{66}}{b^2} - \frac{40D_{12}}{b^2}}{6 - \alpha} \quad (1)$$

With D_{11} being the bending stiffness in the longitudinal direction, D_{22} the bending stiffness in the transversal direction, D_{12} is the Poisson-action bending stiffness, D_{66} is the torsional stiffness, L is the tow length, b is the tow width, m is the buckling mode and α is the non-uniformity load coefficient which characterize the bending - tension combination (2 for pure bending and 0 for pure compression) as illustrated in figure 6.

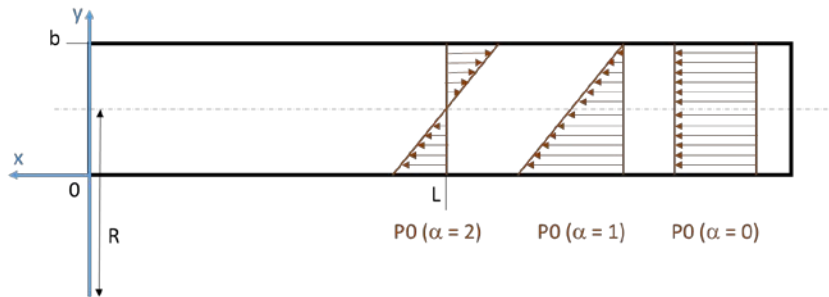


Figure 6. Tow representation from above as an orthotropic plate with compressive load P_0 ; representation for different values of the non-uniformity coefficient α .

By equating P_{cr} to the minimal buckling load on the inner edge of the tow, P_0 defined geometrically in equation 2, the critical curvature radius for buckling, R_{cr} , was identified in equation 3.

$$P_0 = \frac{E1 h b}{\alpha R} \quad (2)$$

$$R_{cr} = \frac{E1(6 - \alpha)bh}{\alpha \left(\frac{24D_{11}m^2\pi^2}{L^2} + \frac{90D_{22}L^2}{b^4m^2\pi^2} + \frac{160D_{66}}{b^2} - \frac{40D_{12}}{b^2} \right)} \quad (3)$$

With $E1$ is the longitudinal tensile modulus and h is the thickness of the tow. As stipulated in [5], D_{12} and D_{22} are orders of magnitude lower than D_{11} and D_{22} and thus can be neglected with close to no impact on the critical radius, thus, the expression of R_{cr} becomes:

$$R_{cr} = \frac{E1(6 - \alpha)b^3hL^2}{\alpha(160 D_{66} L^2 + 24 D_{11} \pi^2 b^2 m^2)} \quad (4)$$

The bending stiffness D_{11} was then evaluated using a Peirce cantilever test and the torsional stiffness was evaluated using a torsion test. α was also estimated using digital image correlation. This finally allowed us to calculate the critical buckling radius and compare it to the experimental buckling radius that were measured experimentally using ImageJ® on the previously mentioned digital image correlation pictures. $E1$ was retrieved from the literature as the used tows resemble those used by Bassoumi [7] in her work. All the results are compiled in Table 2.

Table 2. Parametric results, analytical and experimental critical radii.

Reinforcement	Serge 2x2 sized up	Serge 2x2 de-sized up
E1 (N/mm ²)	19800	7800
L (mm)	6.1	5.7
b (mm)	2.5	2.4
h (mm)	0.4	0.4
α	2	2
m	1	1
D11 (N.mm)	1.18	0.72
D66 (N.mm)	0.44	0.17
Rcr (mm)	2082.9	1482.2
Rcr(exp) (mm)	2255	1627
Δ (%)	7.63	8.90

The analytical and experimental results seem to be in agreement with only 8.2% difference so we can assume that the model can safely predict the critical buckling radius. Yet, more reinforcement needs to be studied in order to confirm the results.

4. Conclusion

The tow buckling defect was investigated using a specifically made device and some parameters were studied. The effect of tows dimensions and tow rigidities was experimentally studied and related to the buckling. An analytical framework was adapted from the literature and was found to be able to predict the critical buckling radius so far with a need for further tests on different reinforcements to fully validate it.

References

1. K. L. Pickering, M. G. A. Efendy, and T. M. Le, "A review of recent developments in natural fibre composites and their mechanical performance," *Composites Part A: Applied Science and Manufacturing*, vol. 83, pp. 98–112, 2016.
2. P. Boisse. "Mise en forme des renforts fibreux de composites". *Techniques de l'ingénieur*, am3734, pp. 1–10, 2004.
3. K. Potter, B. Khan, M. Wisnom, T. Bell, and J. Stevens, "Variability, fibre waviness and misalignment in the determination of the properties of composite materials and structures," *Compos. Part A Appl. Sci. Manuf.*, vol. 39, no. 9, pp. 1343–1354, 2008.
4. C. Tephany, "Analyse de la formabilité de renforts composites à base de fibres naturelles," PhD thesis, Université d'Orléans, 2014.
5. M. Y. Matveev, P. J. Schubel, A. C. et al., I. A. et al., *Understanding the buckling behaviour of steered tows in Automated Dry Fibre Placement (ADFP)*. *Composites Part A: Applied Science and Manufacturing*, 90, pp.451–456, 2016.
6. C. Florimond, "Contributions à la modélisation mécanique du comportement de mèches de renforts tissés à l'aide d'un schéma éléments finis implicite," INSA-Lyon, 2013.
7. A. Bassoumi, "Analyse et modélisation du choix des renforts pour optimiser la mise en forme de matériaux composites à base de fibres végétales," PhD thesis Université d'Orléans, 2016.

INFLUENCE OF THE SEAMS ON THE SUBJECTIVE HAND EVALUATIONS OF TEXTILES

Vladimír Bajzík, Tereza Zaleská

Technical University of Liberec, Department of Textile Evaluation, Liberec, Czech Republic,
Studentska 2, 46117 Liberec, Czech republic, tel: +420485353298, fax: +420485353542,
vladimir.bajzik@tul.cz

Abstract:

The hand of textiles is understood as one of the first properties with which a consumer is met when he or she is considering getting closer to the fabric properties, for example, besides its own handle of textile with stiffness, smoothness etc. In the field of the understanding of sensory analysis or subjective hand evaluation of textiles was published a lot of research papers. In order the knowledge about the evaluation of the subjective hand was recognized the key aspects for the course of the evaluations were defined. These aspects plays important role when the objective hand evaluation can be reached as the hand belongs among the complex properties consisted of so called primary ones and in addition belongs among to psycho physiological properties and so its prediction is complicated.

When the clothing is created the single parts are connected by means of seams. Inappropriate use of seams can lead, for example, to seam puckering or the higher stiffness in the area of connection and so the subjective feeling of hand of textile may be different (worse) in this area. In present paper five types of sewing seams is compared from the point of view of subjective hand evaluation. The experiment was realized using three different fabrics which were connected by polyester and polyamide threads with the similar fineness. Theoretically the number of combination was 30, however practically only 15 types of samples were productive.

At first, the evaluation was realized by means of the panel of 40 respondents. The degree of agreement among the panelists was calculated and reached value about 0.4. Also difference of single respondents was investigated. The influence of seam types on the subjective hand evaluation was compared by means of five degree ordinal scale and the median of the ordinal scale. The results show that type of seam leads to distinguishable evaluation of hand of seams.

Key words:

ordinal scale, seam, subjective hand evaluation, thread

1. Introduction

When the consumer thinks about buying new garment in addition to the suitability for given use he must solves set of other aspects, eg. fashion (including appearance), hand, price and other relevant aspects. The appearance and hand belongs to the properties with which the consumer is met at first when he decides to purchase new cloth. Both these properties belong to the properties called organoleptic. Their evaluation is difficult as besides their "inner" properties flowing generally from the construction of a textile the psychological state of evaluator plays the important role during the subjective evaluation. Kawabata [1] in his study pointed out that when the hand is evaluate by experts each of

them at first classifies the primary components of the hand and then they make a final decision about the hand. Therefore the hand of textiles is understood as complex psychophysical property.

When the hand of textiles is realized by means of panel of respondents the set initial problems is necessary to solve when the repeatability and reproducibility is required. These ones are needed for model building when the prediction of subjective hand evaluation is realized. Repeatability and reproducibility then leads to better stability of the prediction model. Based on the research of the last several decades of many researches and also his own, Bishop [2] presented and discussed 6 basic elements connected with the preparation and the course of the subjective hand evaluation experiment:

- 1) the judges,
- 2) the criteria of judgement,
- 3) the assessment conditions,
- 4) the assessment technique,
- 5) the method of ranking or scaling the assessment,
- 6) the analysis of results.

When the clothing is created the single parts are connected by means of seams. Inappropriate use of seams can lead, for example, to seam puckering or the higher stiffness in the area of connection and so the subjective feeling of hand of textile may be different (worse) in this area. Therefore in this paper research and results in the field of subjective hand evaluation of sewing seams is presented.

The experiment was realized using three different fabrics which were connected by polyester and polyamide threads with the similar fineness. The chosen fabrics are used for production of clothing for outdoor activities in winter. Theoretically the number of combination was 30, however practically only 15 types of samples were produced.

2. Experimental

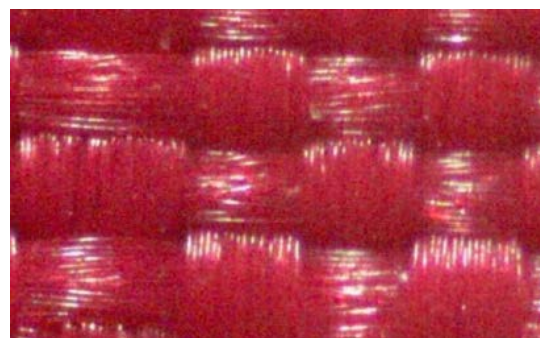
2.1. Materials

Three types of material were chosen. The first is used as a surface material, the second one as an insulation which is put among outer and inner layer of textiles and the third fabric is used as a inner layer. All textiles are from industrial production.

- material 1 (marked as M1) – plain weavel (Fig. 1a,b) – made from nylon fibers, plain weave, warp sett 40 threads/1 cm, weft sett 60 threads/cm, areal weight 37g/m², with permanent waterproof finish,
- material 2 (marked as M2) – insulation material (softshel) (Fig.1c) – three layered textile material – outer layer, membrane, suction layer, areal weight is 312 g/m². Characterization of the single layer: outer layer – 94/6 polyester/polyamide, plain weave, warp sett 40 threads/1 cm, weft sett 40 threads/cm, membrane – polyurethane, suction layer – fleece, polyester fibres, double jersey, 12 columns/cm, 14 rows/cm, knit is raised from one side.
- material 3 (marked as M3) – fleece (Fig. 1d) – fleece, polyester fibres, areal weight is 225 g/m², double jersey, 15 columns/cm, 19 rows/cm, knit is raised from the one side.



a)



b)

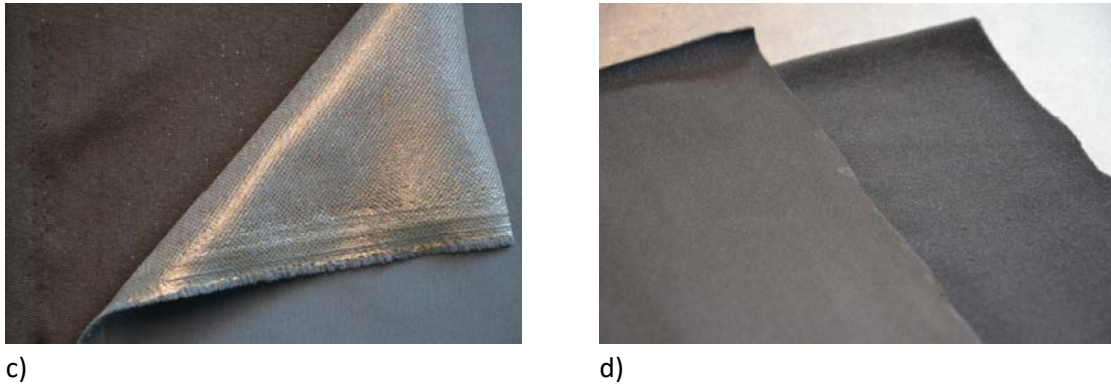


Figure 1. Used textiles: a) material M1, b) detail of material M1, c) layers of material M2, d) material M3.

As the aim of the paper the subjective evaluation of hand of seams is the textiles were sewn by two types of threads which were made from different fibres. The first one is made from polyester staple fibres (in the experiment marked as PES) and the yarn fineness is 74 tex and the second one is made from polyamide multifil (in the experiment marked as PAD) with the yarn fineness 75 tex. The polyester threads were chosen as they belongs to the most used threads in the sewing process. The used polyamide threads are characterized by the high strength and surface smoothness. Five the most used stitches in the production of clothing for outdoor activities were chosen. The schemes of the single stitches are shown in the Table 1.

Table 1. Used stitches

Stitch marking in the experiment	Scheme
S1	
S2	
S3	
S4	
S5	

2.2. Methods

Two types of the scales were used for evaluation. For evaluation of the influence of type of stitch the comparative method was used (T1). This method is based on sorting of textiles according to subjective criterion of evaluation (e.g., ordering from textiles with the most pleasant hand to textiles with the worst hand and vice versa). The obtained data belongs to the ordinal scale and therefore median of ordinal scale (x_R) can be applied:

$$x_R = Me + 0.5 - \frac{F_{Me-0.5}}{f_{Me}} \quad (1)$$

where Me is a median category which is defined by inequalities

$$F_{Me-1} < 0.5, F_{Me} \geq 0.5 \quad (2).$$

where F_{Me} is cumulative relative frequency of median category and f_{Me} is relative frequency of median category.

The second method (T2) was used for comparison of the influence of type of threads. This method is based on the comparison with standard. In the experiment the stitch prepared from polyamide threads was considered as a standard and the same stitch made from polyester threads was compared with it. It was evaluated if the second stitch (stitch from PES fibres) has better or worse hand than standard. The used scale is shown in the Table 2

Table 2. The ordinal scale for sign and preferential data

Sign description	Numerical description	Preferential description
++	2	much better than standard
+	1	better than standard
0	0	the same as standard
-	-1	worse than standard
--	-2	much worse than standard

Obtained data were processed by means of asymmetry in respects to limits A and its confidence interval. The confidence interval was calculated the level of the significance $\alpha=0.05$. If the confidence interval covers zero it means that no difference exists in the evaluation. Asymmetry A was calculated using formula (3):

$$A = \frac{-2f_{--}-f_{-}+f_{+}+2f_{++}}{2f_{--}+f_{-}+f_{+}+2f_{++}} \quad (3)$$

where f represents given relative frequencies according to the sign description (see Table 2). In all cases panel of 40 respondents was used. All respondents had textile education and sure experiences with the evaluation of textiles. Before and during the experiments the rules used for the sensory analysis was kept. More details is possible to find in [3].

The same two materials were used for preparation of experiments. It means M1 and M1, M2 and M2, M3 and M3 were sewn together. Three types of materials, two types of threads and five types of stitches with the same length of stitch so enabled 30 combinations for sample preparation (see Table 3). From technical point of view 50% of combination was not possible to prepare (Table 3).

Table 3. Possible combinations and prepared samples

stitch	material	thread	marking	produced	stitch	material	thread	marking	produced
S1	M3	PES	S1M3PES	yes	S3	M3	PAD	S3M3PAD	no
S1	M2	PES	S1M2PES	yes	S3	M2	PAD	S3M2PAD	no
S1	M1	PES	S1M1PES	yes	S3	M1	PAD	S3M1PAD	no
S1	M3	PAD	S1M3PAD	yes	S4	M3	PES	S4M3PES	yes
S1	M2	PAD	S1M2PAD	yes	S4	M2	PES	S4M2PES	yes
S1	M1	PAD	S1M1PAD	yes	S4	M1	PES	S4M1PES	no
S2	M3	PES	S2M3PES	yes	S4	M3	PAD	S4M3PAD	no
S2	M2	PES	S2M2PES	no	S4	M2	PAD	S4M2PAD	yes
S2	M1	PES	S2M1PES	no	S4	M1	PAD	S4M1PAD	no
S2	M3	PAD	S2M3PAD	no	S5	M3	PES	S5M3PES	yes
S2	M2	PAD	S2M2PAD	no	S5	M2	PES	S5M2PES	yes
S2	M1	PAD	S2M1PAD	no	S5	M1	PES	S5M1PES	no
S3	M3	PES	S3M3PES	yes	S5	M3	PAD	S5M3PAD	no
S3	M2	PES	S3M2PES	yes	S5	M2	PAD	S5M2PAD	yes
S3	M1	PES	S3M1PES	no	S5	M1	PAD	S5M1PAD	no

As it was possible under given condition to prepare only 15 (it means 50%) combinations only some experiments could be realized. Experiment setting for subjective hand evaluation is shown in Table 4. As it flows from Table 4 nine groups of textiles was prepared for testing. The groups G1 – G3 were used for comparison of the influence of stitch type on the subjective hand evaluation using test T1. This test was also used for observing of influence of combination thread type and used material on the subjective hand evaluation (group G4). Last 5 groups (groups G5 – G9) were used for testing of the influence of the thread types on the subjective hand evaluation. In this cases test T2 was used.

Table 4. The groups used in testing

	G1	G2	G3	G4	G5	G6	G7	G8	G9
	testing method T1				testing method T2				
S1M3PES	X			X		X			
S1M2PES		X		X	X				
S1M1PES				X			X		
S1M3PAD				X		X			
S1M2PAD			X	X	X				
S1M1PAD				X			X		
S2M3PES	X								
S3M3PES	X								
S3M2PES		X							
S4M3PES	X								
S4M2PES		X							X
S4M2PAD			X						X
S5M3PES	X								
S5M2PES		X						X	
S5M2PAD			X					X	

3. Results and discussion

As it flows from Table 4 the groups G1, G2 and G3 were used for determination in the type of stitch has influence on the subjective hand evaluation. The group G1 was consisted of 5 type of stitches the group G2 from 4 type of stitches and group G3 was consisted of 3 type of stitches. As the comparative method was used the size of group has influence on the results of the median of ordinal scale. For group G1 it can reach values from 1 to 5, for G2 from 1 to 4 and from G3 from 1 to 3. Results are presented in Figure 2.

The results (see Fig. 2a-c) shows the same trend. The type of stitch has the influence on its subjective hand evaluation. As the worse the stitch S1 was evaluated at all types of textiles and the best evaluation was reached at S5. The stitch S1 is more spread and during the evaluation is so more perceived than stitch S1 and also influence of the textile on hand evaluation is more suppressed by comparison with stitch S1. The results of subjective hand evaluation of the group G4 indicate that used thread plays important role. At all cases the more pleasant evaluation of hand were reached when the polyester threads were used in the same types of textiles. The application stitches on the material M3 shows the results. It this case the fleece was used and it has very soft and pleasant hand.

In the second experiment pairs of samples were compared. In all cases the pairs were differed in the used thread (see Table 5). To avoid some influence of systematic evaluation as a standard both type of threads were randomly determined. Material used as a standard is on the first place in the Table 5. It means that at groups G5, G8 and G9 polyamide threads were used as a standard and at groups G6 and G7 as a standard polyester threads were chosen.

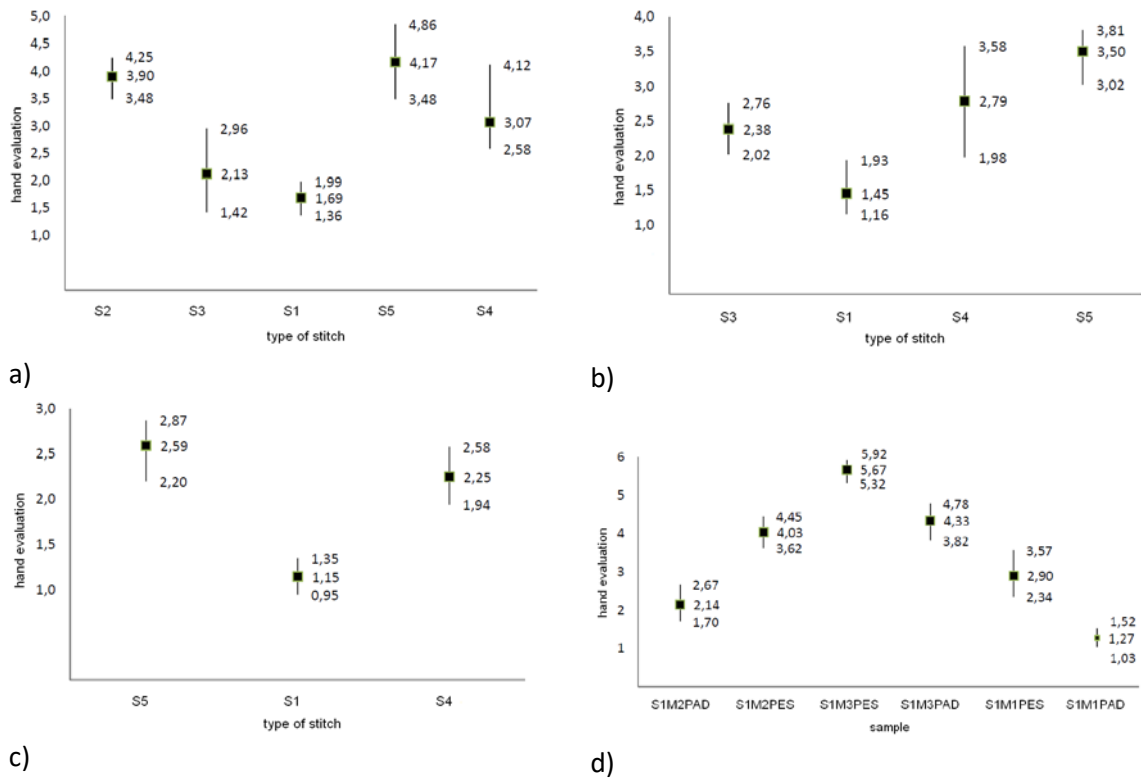


Figure 2. The results of the subjective hand evaluation a) group G1, b) group G2, c) group G3, d) group G4.

Table 5. The paired samples for evaluation of asymmetry

group	samples	parameter A	confidence interval
G5	S1M2PAD - S1M2PES	0.97	0.78 - 0.99
G6	S1M3PES - S1M3PAD	-0.94	-0.99 - -0.64
G7	S1M1PES - S1M1PAD	-0.97	-0.99 - -0.78
G8	S5M2PAD - S5M2PES	0.47	-0.07 - 0.80
G9	S4M2PAD - S4M2PES	0.90	0.44 - 0.99

Notice: the first sample was taken as standard

The parameter of asymmetry A for evaluated groups G5, G8 and G9 reached positive values and at groups G6 and G7 negative ones. It means that at groups G5, G8 and G9 the compared stitches produced from polyester threads were evaluated as with better hand than standard and at groups G6 and G7 the compared threads were evaluated with worse hand in comparison with standard. However here as a standard the stitches made from polyester threads were used. It means that in all cases all stitches made from polyester threads were evaluated better on hand. Except the group G8 all results are statistically significant for significance level $\alpha=0.05$. The better evaluation of stitches can be explained by using polyester staple fibres in comparison with threads produced from polyamide multifil.

4. CONCLUSIONS

In present paper influence of type of stitches on the subjective hand evaluation was shown. Three types of materials used for production of clothing for production of outdoor activities were used as basic materials for preparing of five types of stitches. The reached results indicate that type of stitch has influence on subjective hand evaluation. Also two types of threads were used. The stitches made from polyester threads reached better results in the subjective hand evaluation in comparison with polyamide ones. On other hand polyester thread was produced from staple fibres but polyamide from multifil and it could play also big role during evaluation of the hand.

References

1. Kawabata, S. (1980). *The Standardisation and Analysis of Hand Evaluation*. (2nd ed.). The Textile Machinery Society of Japan (Osaka).
2. Bishop D. P. (1996). *Fabric: Sensory and Mechanical Properties*. *Textile Progress*, 26, 1-62.
3. Bajzik, V. (2013). *Influence of Visual Stimuli on Subjective Hand Evaluation of Fabrics and Its Reproducibility and Repeatability*. *Tekstil*, 62(7/8), 311-318.

EFFECT OF AIR PERMEABILITY ON GRAINLINES, AGED, WASHED AND MOISTED WOVEN FABRIC

Frederick T. Fung, Antonin Havelka

Technical University of Liberec, Faculty of Textile Engineering, Department of Clothing, Czech Republic, e-mail: tassfashion@gmail.com, e-mail: antonin.havelka@tul.cz

Abstract:

This paper is a study of the effect of air permeability on aged, washed, moisted and grainlines of woven fabric. It is part of a series of research focusing on how clothing pattern of a men's shirt for woven fabric relates to different parameters: clothing insulation, evaporation resistance, body movements and breathability/air permeability. Results from all these different experiments will be analyzed and will be used to create the ideal clothing pattern for a men's shirt theoretically. In this research, three woven materials were used; which are popular fabric for long sleeve men's shirt in tropical condition. They were including: 1) 100% cotton, 139g/m², thickness 0.43mm, warp 26/cm, weft 24/cm; 2) 50% cotton 50% polyester, 153g/m², thickness 0.44mm, warp 26/cm, weft 24/cm; 3) 98% cotton 2% elastin, 110g/m², thickness 0.27mm, warp 42/cm, weft 34/cm. 25 x 25cm samples were cut from the materials for grainline tests, washed fabric tests and moisted fabric tests. Samples for the aged fabric tests were cut bigger; 31 x 31cm for storage and easier to be found. All fabric were plain woven and had been pre-washed, pre-shrunk and ironed flat before experiments. Fabric Breathability Test Machine was used for part 1, 2 and 3. The air pressure was maintained at 100 Pascal, testing head ring diameter was 50.5mm and the tested surface area was 20cm². For part 4, FX 3300 Air Permeability Tester III was used and the air pressure was set to 100 Pascal for apparel materials. Results would be analyzed in the conclusion.

Key words:

clothing pattern, air permeability, woven fabric, grainline, breathability

1. Introduction

In garment industry, fabric is being cut either manually by using paper printout clothing pattern set in different sizes or by computer with laser cutting machine^[1]. Pattern pieces are arranged according to their grainline, number of pieces needed as well as material saving (space between pattern pieces)^[2-3]. Pattern pieces are usually line up parallel to the fabric grainline. Sometimes pattern pieces are put on cross grain and on bias which depends on the purpose of the finished look. Good clothing patterns will produce a good fit to customers and increase business sales. Hence, clothing pattern is a key point for clothing comfort and better sales. In fact, there are a lot of articles related to improvement of clothing patterns and different parameters researches for clothing comfort. For examples, Hes talked about thermal absorptivity $b = (\lambda\rho c)1/2$ which was the warm-cool feeling when human skin first touched the fabric^[4-6]. Ogulata, Fatahi, Haleen and Zupin investigated separately in air permeability of woven fabric and its mechanical properties in dry state^[7-10] while Hes searched for the answer for water vapor permeability of woven fabric in wet state^[11]. For clothing pattern improvement, Musilova et al. compared the East and West pattern making methods and evaluated Czech male body proportion in order to find out a better men's shirt patterns^[12-14]. And Chan et al. found that artificial neural network (Ann) was better in predicting pattern sizes and MLR multiple linear regression worked better in predicting shirt pattern^[15-17]. However, all of their researches are based on the traditional pattern shapes and regular men's shirt materials properties. The traditional men's shirt pattern set (including sleeve, front, back and yoke pieces) has been used for over a hundred years^[18]. No article has ever challenged the shapes of the pattern pieces, only investigated on improving the fit and the properties of shirt materials. Are these traditional pattern shapes the best for the fit and comfort? Will there be

any shapes that will work better? My research is based on this curiosity to find out whether there are pattern shapes which will fit better and will feel more comfortable for woven men's shirt. My approach is through different parameters: clothing insulation, evaporation resistance, movements and breathability to determine the new shapes of the men's shirt patterns. In this part, in order to fully understand how air permeability will affect the chosen three woven fabrics (mentioned in the Abstract), different conditions are set up for the test: grainlines test, aged fabric test, washing cycle test and moistened fabric test. All materials are pre-washed, pre-shrunk and ironed flat before experiments. Then each material will be divided into 4 groups.

Group 1-- grainlines test, this test serves two purposes: a) To show the air permeability influences on straight grain, cross grain and bias. b) To act as a reference/standard for other tests.

Group 2-- aged test, to find out any different from grainline test after materials are put in an open environment for a period of 6 months.

Group 3— washing cycle test, to find out any different from grainline test after materials are gone through 3 times of washing, hang drying and iron flat cycle.

Group 4—moistened fabric test, to stimulate fabric with sweat and find out the air permeability influences.

2. Method and Experiment

2.1. Air Permeability on Grainlines (Part 1)

Materials used and samples condition have already mentioned in the Abstract. The Fabric Breathability Machine was used according to the Standard of CSN EN ISO 9237. Air pressure was set to 100 Pascal. Sample squares were marked on straight grain in Black, cross grain in Blue and bias in Red (Figure 1). Spots for testing were randomly chosen and circled. Each spot went through 3 tests: straight grain, cross grain and bias. Three successfully tested spots were marked that would number 1, 2 and 3. Some circled spots were not numbered because it may only be tested on straight grain but not the other grain lines due to unstable reading (weaving pattern uneven, see Appendix 3) et cetera.

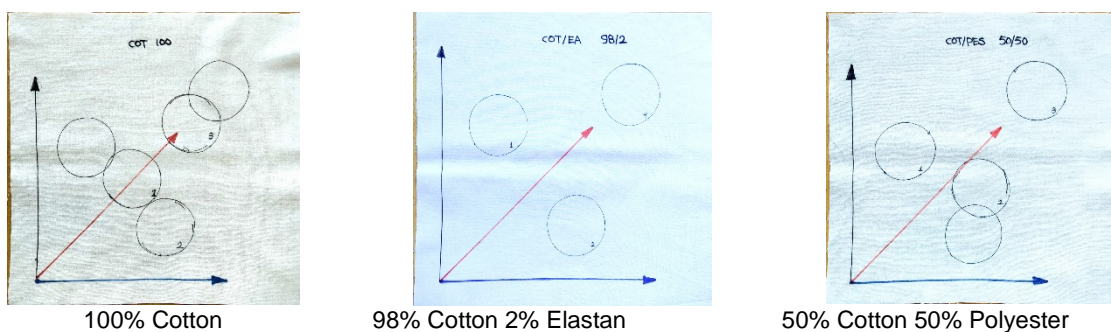


Figure 1. Shows different grainlines on each fabric and those chosen spots for tests

(see Table 1 to Table 4, Figure 2 to Figure 4. for the results) Results were in unit liter per minute. According to the following formula, L/min will be converted into Standard Unit (mm/s).

$R = qv/A \times 167$ qv is the result in L/min from the conversion chart, A is the tested surface area 20cm^2 , 167 is an constant and the result unit is in Standard mm/s.

From each of the table, the result of the same fabric tested spot is highly similar and some results are exactly the same through straight, cross and bias grainline of the fabric; for examples, Test 1 of 100% cotton, Test 3 of cotton/polyester blend and Test 3 of cotton/elastan blend. When comparing the mean value of straight grain, cross grain and bias of the same fabric, they are almost identical. From this analysis, I believe that whether on straight grain, cross grain or bias, air permeability does not have any significant influence to the directions of grainline.

Table 1. Numbers are the results from the Fabric Breathability Testing machine. Appendix 2 shows the conversion from these numbers to liter per minute (l/min).

	Straight Grain			Cross Grain			Bias		
100% Cotton	75	82	74	75	83	75	75	82	75
50% Cotton 50% Polyester	70	78	74	72	77	74	70	77	74
98% Cotton 2% Elastan	93	106	104	94	105	104	94	105	104

Table 2. Results of air permeability of 100% cotton on straight grainline, cross grainline and bias (mm/s)

	Straight Grain	Cross Grain	Bias Grain	Mean	SD
Sample 1	249.00	249.00	249.00	249.00	0.00
Sample 2	274.00	278.00	274.00	275.33	2.31
Sample 3	245.00	249.00	249.00	247.67	2.31

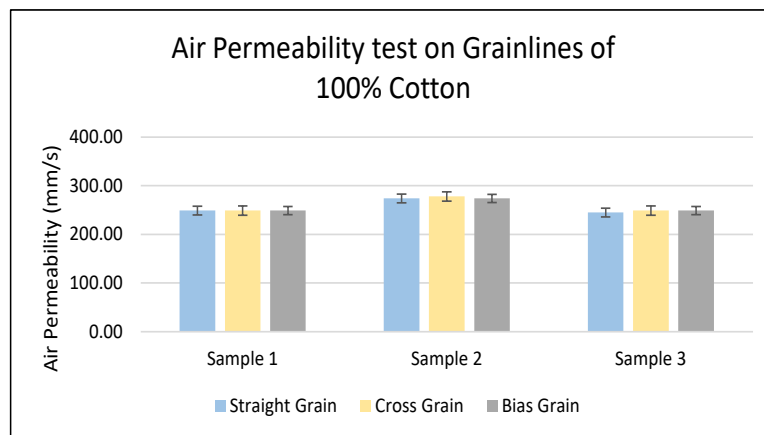


Figure 2. Grainline tests on 100% Cotton

Table 3. Results of air permeability of 50% cotton 50% polyester on straight grainline, cross grainline and bias (mm/s)

	Straight Grain	Cross Grain	Bias Grain	Mean	SD
Sample 1	231.00	238.00	231.00	233.33	4.04
Sample 2	260.00	256.00	256.00	257.33	2.31
Sample 3	245.00	245.00	245.00	245.00	0.00

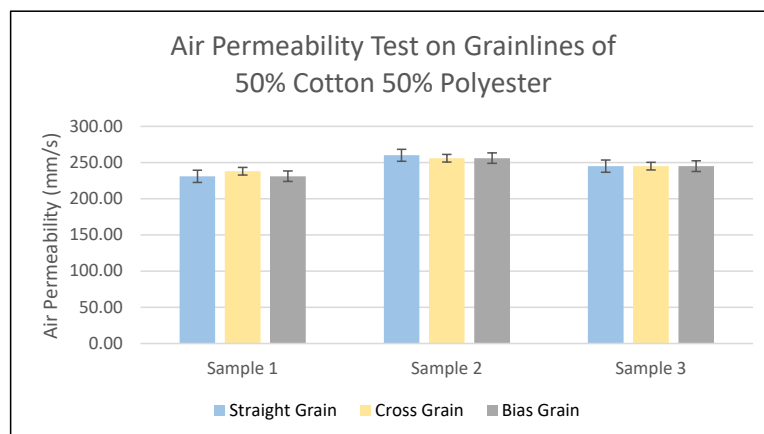


Figure 3. Grainline tests on 50% Cotton 50% Polyester

Table 4. Results of air permeability of 98% cotton 2% elastan on straight grainline, cross grainline and bias (mm/s)

	Straight Grain	Cross Grain	Bias Grain	Mean	SD
Sample 1	316.00	320.00	320.00	318.67	2.31
Sample 2	365.00	361.00	357.00	361.00	4.00
Sample 3	357.00	357.00	357.00	357.00	0.00

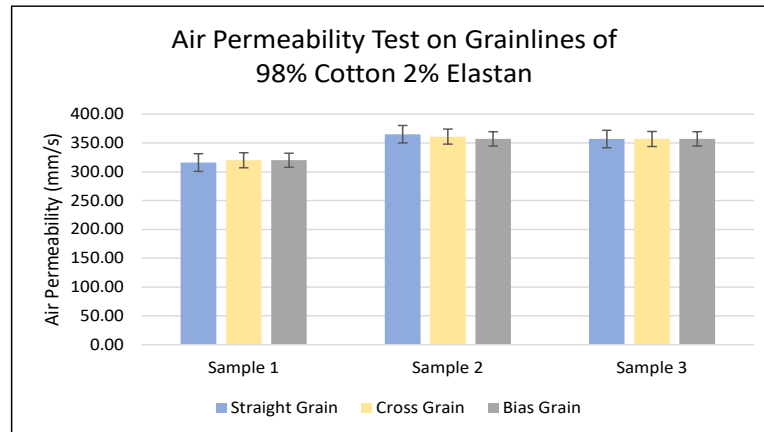


Figure 4. Grainline tests on 98% Cotton 2% Elastan

2.2. Air Permeability on Aged Fabric (Part 2)

Three 31 x 31cm samples were cut from each material (100% cotton, 50% cotton 50% polyester, 98% cotton 2% elastan) and put aside in the open area in the laboratory with no restrictions on any condition for 6 months, from 09/2017 to 02/2018. Weather, wind speed, humidity, heat and other unexpected conditions were changing every moment. After that, two spots were chosen randomly from each sample of the same material. Total six results were recorded from one material (see Table 5 and Figure 5 for the result).

	Sample 1		Sample 2		Sample 3		Mean	SD
	Test 1	Test 2	Test 1	Test 2	Test 1	Test 2		
100% Cotton	427.00	372.00	278.00	293.00	293.00	293.00	326.00	59.81
50% Cotton 50% Polyester	267.00	286.00	286.00	286.00	260.00	249.00	272.00	16.03
98% Cotton 2% Elastan	353.00	316.00	500.00	507.00	525.00	398.00	433.00	89.15

Table 5. Results of air permeability of fabrics aged for 6 months

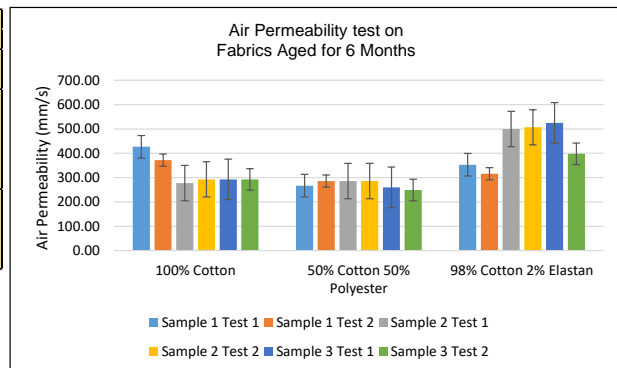


Figure 5. Aged fabric tests results for air permeability

From the aged fabric test results, the mean value of air permeability of each material was higher than the same material when it compared to the previous test (Part 1) where materials were not aged (see Table 6 and Figure 6 for the comparison). This may be caused by the expansion of the pores (spaces between wefts and warps) in the fabric due to the exposure in the open environment, temperature and humidity constantly changing all the time. Bigger pores, higher air permeability rate.

Table 6. Table of comparison of the mean value of air permeability from grainline test, aged fabric test and the washed fabric test

	Mean Value of Grainlines	Mean Value of Washed Fabric	Mean Value of Aged Fabric
100% Cotton	257	275	326
50% Cotton 50% Polyester	245	242	272
98% Cotton 2% Elastan	346	463	433

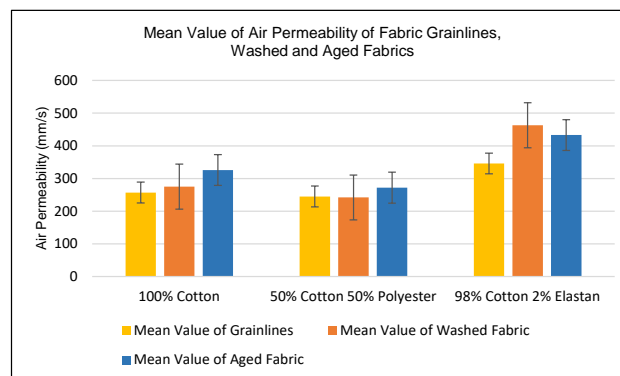


Figure 6. Chart of comparison of the mean value of air permeability from grainline, aged and washed fabric tests

2.3. Air Permeability on Washed Fabric (Part 3)

Three 25 x 25cm samples were cut from each material as in Part 1. Nine samples were in total. Each sample would be tested twice so that eighteen tests were in total. All samples went through 3 times of washing and drying process. Washing condition: 40+/- oC in gentle cycle with mild detergent and tumble dry. Drying condition: Hang to dry naturally then ironed flat (this is 1 cycle). Fabric Breathability Test Machine with 50.5mm testing head ring, 20cm² testing surface area were applied. The Standard of CSN EN ISO 9237 for apparel was followed and the condition of the machine was maintained at 100 Pascal air pressure. Results are in Table 7 and Figure 7.

Table 7. Results from 3 cycles of washed and dried samples

	Test 1	Test 2	Test 3	Test 4	Test 5	Test 6	Mean	SD
100% Cotton	278	271	301	260	278	260	275	15.22717
50% Cotton 50% Polyester	242	252	252	249	256	242	242	5.741661
98% Cotton 2% Elastan	489	449	471	456	427	489	463	24.31255

When compared the 3 cycles of washed and dried fabric test results to Part 1, the mean value of the washed fabric showed a small increase in air permeability (see Table 6, Figure 6). It showed that after 3 cycles of washing and drying, air permeability increased slightly and continued to increase in time

when it was aging, except the 98% cotton 2% elastan blend increased a lot after the washed/dried cycles. This increase may cause by error or fabric damaging during the process. Overall, the air permeability was still increasing with time when the fabrics were aging.

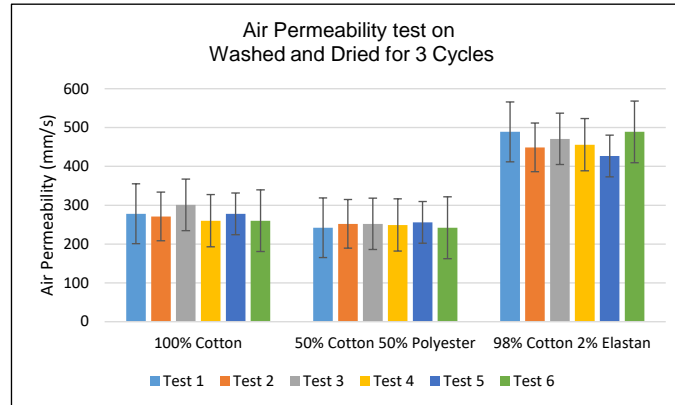


Figure 7. Air permeability results from washed and dried fabrics for 3 cycles

2.4. Air Permeability on Moistened Fabric (Part 4)

FX 3300 Air Permeability Tester III was used for this Part 4 research. Test area was 20cm², EN ISO 9237 Standard for apparel fabrics test was applied and the air pressure was set to 100 Pascal. One 25 x 25 cm sample from each material was used. Steps as follow:

- 1-- Dry mass of samples were weighted separately.
- 2-- Samples were soaked in water (stimulation of sweat) and towel dried. Noted: moisture percentage were different because of difficulty of water content control.
- 3-- Wet mass of samples were weighted separately. The value of moisture percentage was calculated by:

$$\text{Moisture\%} = \frac{\text{Wet mass} - \text{Dry mass}}{\text{Dry mass}} \times 100$$

- 4-- Each wet sample went through a pattern of test direction (Figure 8. showing the patterns of test direction) to minimize error. The reason for this was because samples were drying during the process when the air was blown out from the testing machine. All samples were kept inside a plastic container to keep the moisture. Only the sample for the test would be used to follow the pattern of test direction.
- 5-- Repeat step 2, 3 and 4 three more times. Each time the pattern of test direction would change to minimize errors. Results as follow in Table 8,9,10 and Figure 9, 10, 11.

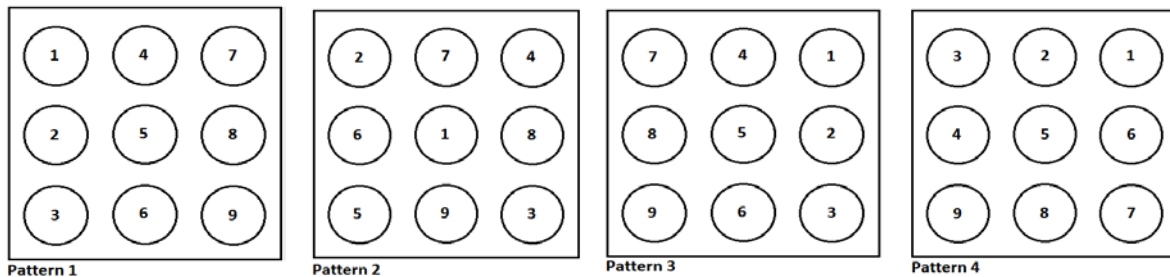


Figure 8. Four patterns of testing direction

Table 8. Air permeability tests on moisted 100% cotton in different moisture content

	Test 1	Test 2	Test 3	Test 4	Test 5	Test 6	Test 7	Test 8	Test 9	Mean	SD
Pattern 1 -- 53.36% moisture	132	198	187	149	155	205	147	148	184	167	26.33
Pattern 2 -- 71.37% moisture	87	101	166	139	110	71	168	136	204	131	43.14
Pattern 3 -- 69.86% moisture	137	148	146	109	126	140	147	165	162	142	17.25
Pattern 4 -- 72.44% moisture	143	97	155	159	113	150	133	136	153	138	20.79

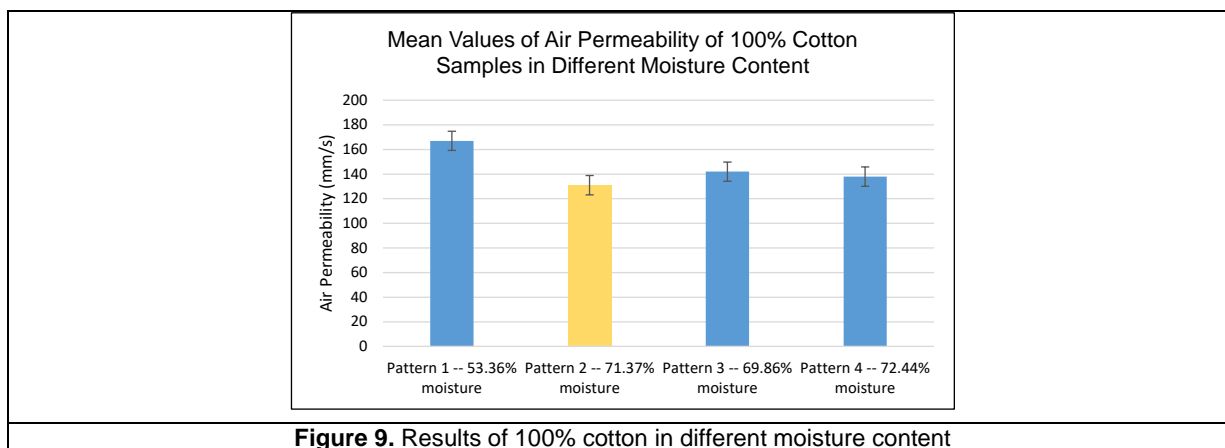


Figure 9. Results of 100% cotton in different moisture content

Table 9. Air permeability tests on moisted 98% cotton 2% elastan in different moisture content

	Test 1	Test 2	Test 3	Test 4	Test 5	Test 6	Test 7	Test 8	Test 9	Mean	SD
Pattern 1 -- 48.24% moisture	395	394	387	406	392	356	408	441	422	400	23.70
Pattern 2 -- 47.78% moisture	398	407	373	392	422	435	380	394	366	396	22.43
Pattern 3 -- 54.82% moisture	366	370	337	376	374	343	406	434	394	378	30.23
Pattern 4 -- 54.10% moisture	370	377	397	412	376	375	369	348	392	380	18.54

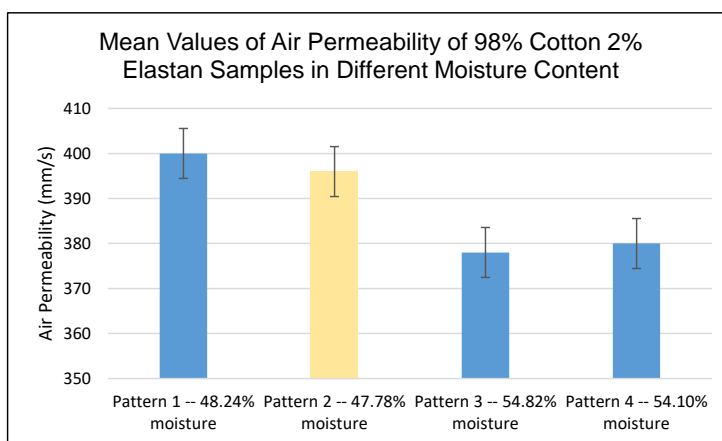


Figure 10. Results of air permeability of 98% cotton 2% elastan in different moisture content

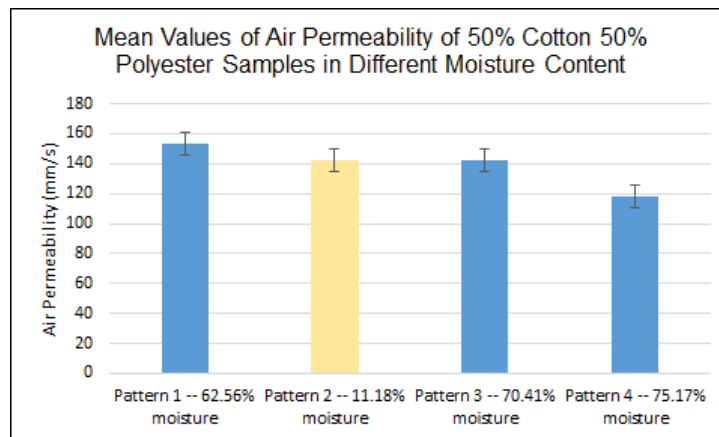
The experiment results showed that whether it was cotton, cotton/polyester or cotton/elastan; they all had the similar influence by the air permeability. That was when the moisture content was high, the air permeability was low. When the moisture content decreased, the air permeability increased. These results were from experiments of all three materials from Test Pattern 1, 3 and 4 which results were inversely proportional. Only when using the Test Pattern 2, the dynamic of proportion disrupted which

might be caused by taking longer time to finish the Pattern 2. The irregular results from Test Pattern 2 might also cause by human errors.

Table 10. Air permeability tests on 50% cotton 50% polyester in different moisture content

	Test 1	Test 2	Test 3	Test 4	Test 5	Test 6	Test 7	Test 8	Test 9	Mean	SD
Pattern 1 -- 62.56% moisture	179	177	138	154	128	116	152	166	164	153	21.685
Pattern 2 -- 11.18% moisture	143	138	144	140	119	168	114	155	158	142	17.460
Pattern 3 -- 70.41% moisture	141	161	175	111	131	119	139	167	131	142	21.840
Pattern 4 -- 75.17% moisture	106	87	131	156	136	135	118	81	110	118	24.402

Figure 11. Results of air permeability of 50% cotton 50% polyester in different moisture content



3. Conclusion

3.1. Air Permeability on Grainlines (Part 1)

Air permeability does not have any influence on straight grainline, cross grain nor bias grainline. Hence, it will not affect the clothing patterns that are being positioned for cutting fabric. However, the grainlines still have a certain effect on wearing comfort; for example, bias cut clothing have more drapability than cut on straight grainline even for woven fabrics.

3.2. Air Permeability on Aged and Washed/Dried Fabrics (Part 2 and 3)

When fabrics are getting exposed, used and washed for a while, air permeability tends to rise up. This influence may be due to the deterioration or damaged of the materials, the pores of the materials enlarged and become more porous. Please see Appendix 1.

3.3. Air Permeability on Moistened Fabrics (Part 4)

Air permeability is inversely proportional to the moisture content of the fabric. When the moisture content is high, air permeability will be low. When the moisture content is low, the air permeability will become high. It is because when moisture content is high, pores of the woven fabric are blocked by water, allowing less air to go through the fabric and vice versa. Also from the result of comparing the mean value of Part 1, 2 and 3 (Table 6, Figure 6), cotton/elastan has the highest air permeability value than cotton and cotton/polyester blend (COT/PES is the lowest among three)

From the about conclusion, only Part 1 and 4 are related to clothing pattern directly. However, in Part 1 air permeability has no influence on any grainlines and in Part 4, suitable wearing ease (air gap) in clothing pattern can minimize sweating rate and maintain a good air flow between skin and clothing.

ACKNOWLEDGEMENTS

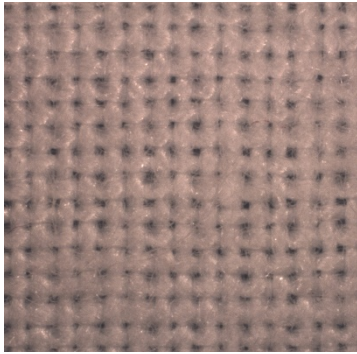
This work was supported by the research project of student grant competition of Technical University of Liberec no. 21246 granted by Ministry of education, youth and sports of Czech Republic.

References

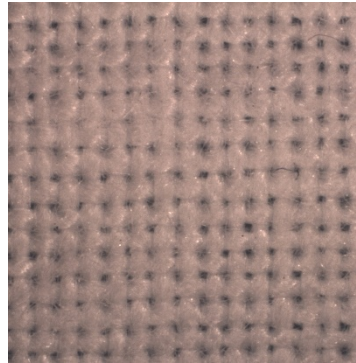
1. Gradišar, Miro, Jože Jesenko, and Gortan Resinovič. "Optimization of Roll Cutting in Clothing Industry." *Computers & Operations Research* 24, no. 10 (October 1, 1997): 945–53. [https://doi.org/10.1016/S0305-0548\(97\)00005-1](https://doi.org/10.1016/S0305-0548(97)00005-1).
2. "Marker Making in Small Clothing Companies - Part 1." Cathy Hands, Helmut H.A. Hergeth, and Peyton Hudson. *International Journal of Clothing Science and Technology* 9, no. 2 (May 1, 1997): 154–65. <https://doi.org/10.1108/09556229710168289>.
3. Aldrich, Winifred. *Metric Pattern Cutting for Menswear*. John Wiley & Sons, 2011.
4. Hes, Luboš. "An Indirect Method for Fast Evaluation of Surface Moisture Absorptivity of Shirt and Underwear Fabrics." *J-Scopus*, 2000. <https://dspace.tul.cz/handle/15240/16686>.
5. Hes, Lubos, and Mario de Araujo. "Simulation of the Effect of Air Gaps between the Skin and a Wet Fabric on Resulting Cooling Flow." *Textile Research Journal* 80, no. 14 (September 1, 2010): 1488–97. <https://doi.org/10.1177/0040517510361797>.
6. Hes, Lubos. "Optimisation of Shirt Fabrics' Composition from the Point of View of their Appearance and Thermal Comfort." *International Journal of Clothing, Science and Technology* Vol. 11, Issue. 2/3, pp.105-119, (1999). <https://doi.org/10.1108/09556229910276250>
7. Ogulata, R. Tugrul, and Serin (Mavruz) Mezarciöz. "Total Porosity, Theoretical Analysis, and Prediction of the Air Permeability of Woven Fabrics." *The Journal of The Textile Institute* 103, no. 6 (June 1, 2012): 654–61. <https://doi.org/10.1080/00405000.2011.597567>.
8. Haleem, Noman, Zulfiqar Ali Malik, Mumtaz Hassan Malik, Tanveer Hussain, Qummer Gillani, and Aisha Rehman. "Predicting the Air Permeability of Polyester/Cotton Blended Woven Fabrics." *Fibers and Polymers* 14, no. 7 (July 1, 2013): 1172–78. <https://doi.org/10.1007/s12221-013-1172-6>.
9. Zupin, Živa, Aleš Hladnik, and Krste Dimitrovski. "Prediction of One-Layer Woven Fabrics Air Permeability Using Porosity Parameters." *Textile Research Journal* 82, no. 2 (January 1, 2012): 117–28. <https://doi.org/10.1177/0040517511424529>.
10. Iman Fatahi, A. Alamdar Yazdia. "Assessment of the Relationship between Air Permeability of Woven Fabrics and its Mechanical Properties." *Fibres and Textiles in Eastern Europe*, Vol 18, no. 6 (2010). imanfatan@gmail.com
11. Hes, Lubos. "Analysis and Experimental Determination of Effective Water Vapor Permeability of Wet Woven Fabrics." *Journal of Textile and Apparel, Technology and Management* 8, no. 4 (May 29, 2014). <http://ojs.cnr.ncsu.edu/index.php/JTATM/article/view/5317>.
12. "EBSCOhost | 108920686 | STUDY OF CZECH MALE BODY PROPORTIONS AND EVALUATION OF MEN'S SHIRT PATTERN MAKING METHODS." Accessed July 26, 2017. <http://eds.a.ebscohost.com/abstract?site=eds&scope=site&jrnl=13003356&AN=108920686&h=amKFb7tmCF939nF5pnzJYMdbgC%2fkWRwRU24j6q9lvMevJyGDenfefpuY9uq9CrF4iFiGAPpjVXH1UE8kC6a%2bKw%3d%3d&crl=c&resultLocal=ErrCrlNoResults&resultNs=Ehost&crlhashurl=login.aspx%3fdirect%3dtrue%26profile%3dehost%26scope%3dsite%26authtype%3dcrawler%26jrl%3d13003356%26AN%3d108920686>.

13. Blazena Musilova, Renata Nemcokova, Petra Komarkova. "Computerized Made-To-Measure System for Customisation." *7th International Conference – TEXSCI 2010* (September 6-8, 2010): blazena.musilova@tul.cz
14. Blazena Musilova, Petra Komarkova, Kus Z.. "Project on Assessment Methods of Constructional Allowances for Looseness of Clothing." *Vlakna a Textil, Vol 10, no. 2* (2003): blazena.musilova@tul.cz
15. A.P. Chan, J. Fan, and W.M. Yu. "Prediction of Men's Shirt Pattern Based on 3D Body Measurements." *International Journal of Clothing Science and Technology* 17, no. 2 (April 1, 2005): 100–108. <https://doi.org/10.1108/09556220510581245>.
16. Chan, A. P., J. Fan, and W. Yu. "Men's Shirt Pattern Design Part I: An Experimental Evaluation of Shirt Pattern Drafting Methods." *Sen'i Gakkaishi* 59, no. 8 (2003): 319–27. <https://doi.org/10.2115/fiber.59.319>.
17. Chan, A. P., J. Fan, and W. Yu. "Men's Shirt Pattern Design Part II: Prediction of Pattern Parameters from 3D Body Measurements." *Sen'i Gakkaishi* 59, no. 8 (2003): 328–33. <https://doi.org/10.2115/fiber.59.328>.
18. Cunnington, Cecil Willett, and Phillis Cunnington. *The History of Underclothes*. Courier Corporation, 1992.

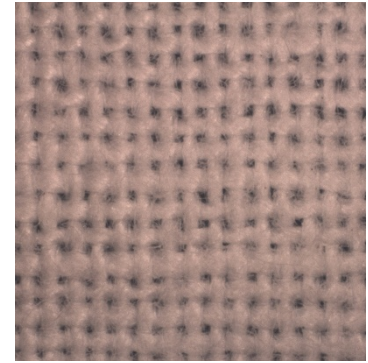
Appendix 1



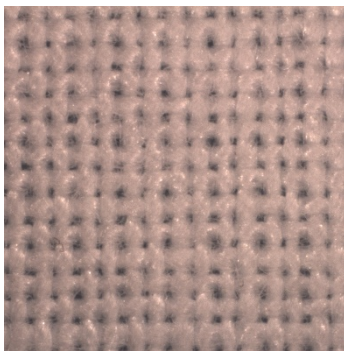
100% Cotton Washed/Dried 3 cycles



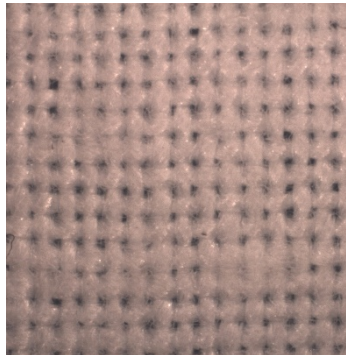
100% Cotton



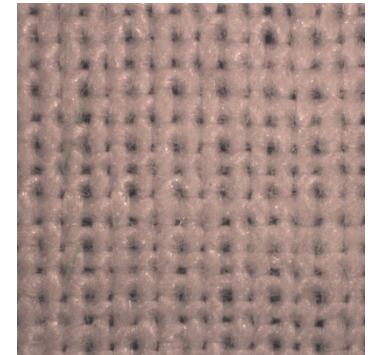
100% Cotton Aged 6 months



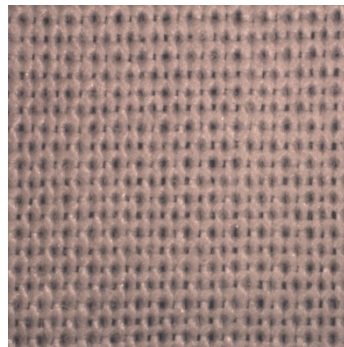
50% Cotton 50% Polyester Washed/Dried 3 cycles



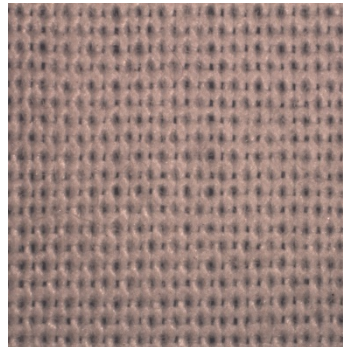
50% Cotton 50% Polyester



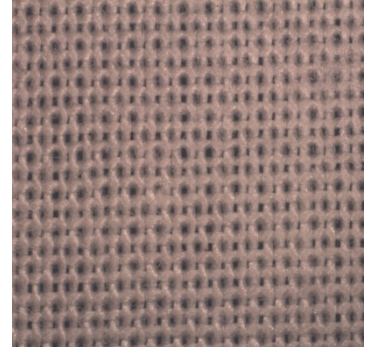
50% Cotton 50% Polyester Aged 6 months



98% Cotton 2% Elastan Washed/Dried 3 cycles



98% Cotton 2% Elastan



98% Cotton 2% Elastan Aged 6 months

Left column are the samples which have been washed and dried for 3 cycles, middle column are the regulars for reference and the right column are samples that have been aged for 6 months. When compare the empty spaces (pores) between weft and warp threads, noticed that pores are getting bigger and wider in Aged samples than the regulars. Especially in Cotton/Elastan blend shows more spacing than the regular sample. The regular Cotton sample has a lot of blocked spaces by its own fiber when it compares to the Aged cotton sample. Photographies are taken by Navitar microcamera Zoom 12X

Appendix 2

hodnota na průtokoměru	průtok vzduchu	hodnota na průtokoměru	průtok vzduchu	hodnota na průtokoměru	průtok vzduchu
5	1,713	53	20,296	101	41,463
6	2,056	54	20,728	102	41,903
7	2,399	55	21,160	103	42,343
8	2,742	56	21,592	104	42,783
9	3,084	57	22,024	105	43,223
10	3,427	58	22,457	106	43,663
11	3,770	59	22,889	107	44,103
12	4,113	60	23,321	108	44,543
13	4,455	61	23,753	109	44,983
14	4,798	62	24,185	110	45,423
15	5,141	63	24,617	111	45,863
16	5,484	64	25,049	112	46,303
17	5,827	65	25,481	113	46,743
18	6,169	66	25,914	114	47,183
19	6,512	67	26,346	115	47,623
20	6,855	68	26,778	116	48,063
21	7,198	69	27,210	117	48,503
22	7,540	70	27,642	118	48,943
23	7,883	71	28,074	119	49,383
24	8,226	72	28,506	120	49,823
25	8,568	73	28,939	121	50,263
26	8,911	74	29,371	122	50,703
27	9,254	75	29,803	123	51,143
28	9,597	76	30,235	124	51,583
29	9,939	77	30,667	125	52,023
30	10,282	78	31,100	126	52,463
31	10,718	79	31,532	127	52,903
32	11,154	80	31,964	128	53,343
33	11,589	81	32,417	129	53,783
34	12,025	82	32,870	130	54,222
35	12,461	83	33,323	131	54,656
36	12,897	84	33,776	132	55,091
37	13,333	85	34,228	133	55,525
38	13,768	86	34,681	134	55,959
39	14,204	87	35,134	135	56,393
40	14,640	88	35,587	136	56,828
41	15,076	89	36,040	137	57,262
42	15,512	90	36,493	138	57,696
43	15,948	91	36,946	139	58,131
44	16,384	92	37,399	140	58,565
45	16,819	93	37,852	141	58,999
46	17,255	94	38,305	142	59,434
47	17,691	95	38,758	143	59,868
48	18,127	96	39,211	144	60,302
49	18,563	97	39,664	145	60,736
50	18,999	98	40,117	146	61,171
51	19,431	99	40,570	147	61,605
52	19,863	100	41,023	148	62,039
				149	62,474
				150	62,908

Conversion Chart from the index (result from the machine) to liter per minute (L/min)
 Bold numbers are the indexes, regular numbers are the L/min

EFFECT OF MOISTURE CONTENT ON THERMOPHYSIOLOGICAL PROPERTIES OF PLAIN KNITTED SOCKS FOLLOWED BY THERMAL RESISTANCE COMPARISON AMONG DIFFERENT SKIN MODELS

Tariq Mansoor¹, Lubos Hes², Zenun Skenderi³ & Muhammad Asif Javed⁴

Faculty of Textile Engineering, Technical University of Liberec, Czech Republic^{1, 2, 4}

Faculty of Textile Technology, University of Zagreb, Croatia³

Corresponding Author email: tariq.mansoor@tul.cz

Abstract:

Socks comfort has great significance in our daily life. This significance even increased when we have undergone a work of low or high activity. It causes the sweating of our body with different rates. One human can produce 27.5g/hour sweat averagely with 23g per hour in low activity and 32g/h in higher activity of work. In this study, plain socks with differential fibre composition were produced on the same knitting machine with homogeneous yarn linear densities and wetted to a saturated level. Then after successive intervals of conditioning, these socks are characterized by thermal resistance, thermal absorbtivity, relative cooling effect and moisture loss rate in dry and wet states. Hydrophobic have best results followed by semi hydrophilic and hydrophilic. In a comparison of FM Rct in a dry state, a correlation of 0.7335 and 0.55 is observed with permetest and alambeta respectively.

Keywords:

Thermal resistance, thermal absorbtivity, plain socks, moisture loss rate, relative cooling effect

1. Introduction

Consumers consider comfort as one of the most important attributes in their purchase of apparel products, therefore companies tend to focus on the comfort of apparel products. Comfort is a pleasant state of physiological, psychological and physical harmony between a human being and the environment [1]. Clothing comfort has two main aspects that combine to create a subjective perception of satisfactory performance: thermo-physiological and sensorial. The first relates to the way clothing safeguards and dissipates metabolic heat and moisture [2][3], whereas the latter relates to the interaction of clothing with the senses of the wearer [4][5]. Thermal-wet comfort being the strongest among tactile and pressure comfort perceived by subjects during exercise [6].

Dry heat transfer occurs through conduction, radiation, convection and ventilation, whereas wet heat transfer when sweating includes several additional complex processes including evaporation, wicking, sorption and desorption, wet conduction (additional conductive heat transfer due to the clothing being wet) and condensation of moisture [7][8].

Thermal-wet comfort is mainly determined by the heat and moisture transport of fabric, which is related to fibre characteristics as well as yarn, fabric construction and fabric finish, recognizing that the extent of their relationship to comfort perception in clothing is also influenced by garment design, cut and fit. The basic thermal comfort properties are just two: thermal resistance (or insulation), and water vapor resistance (or permeability)[8]. Hes and Dolezal proved that as the moisture content of the fabrics increases, their water vapor permeability decreases, but the total RWVP (cooling effect) due to

water evaporation from the fabric surface increases [10]. Hes & Araujo simulated the effect of air gaps between the skin and a wet fabric on resulting cooling flow and found that when layers of 2mm and 4mm thickness were introduced between the skin and the fabric, the relative water vapor permeability or relative cooling heat flow was smaller than the fabric when it was in direct contact with the skin, and in this case it did not depend significantly on the fabric moisture content [9]. In another study increasing moisture content in fabrics significantly worsens their ability to transport water vapour. For wool fabrics and wool/viscose blended fabric the value decreases by over 70 - 80%. However, in the case of the addition of polyester fibres, the effective permeability of water vapour almost disappears, which is caused by substituting the air in pores by water with higher thermal conductivity. This means also that the physiological properties of the fabric, which is becoming increasingly wet as a result of use, are subject to sudden changes, which significantly affects the quality of the apparel [11]. Oğlakcioğlu and Marmarali measured the thermal resistance of cotton knitted fabric in wet state. Coolmax wetted fabric was used to simulate wetted skin. 0.5 ml of water (containing detergent) was injected onto its surface and waited for 1 minute for the liquid had been uniformly distributed within a circle of 45-50mm. When this interface fabric wetted, it was turned down and inserted into the space between the measured sample and the centre of the measuring head of the instrument. It was found that the wetted fabrics indicate lower thermal insulation and cooler feeling [12]. Clothing thermal insulation decreases during perspiration, and the amount of reduction varies from 2 to 8%, as related to water accumulation within clothing ensembles [13]. Another study on footwear reported about 19-25% (30-37% in toes) reduction of thermal insulation during sweating [14]. Kalev Kuklane et al. measured the effect of different sweat rates on thermal insulation and found a strong negative correlation. Furthermore he found that 30% of the total moisture can be stayed in socks [15]. Thermal manikin results of dry and wet heat loss are presented from different laboratories for a range of 2-layer clothing with similar dry insulations but different water vapour permeabilities and absorptive properties. For each climate, total wet heat loss is predominately dependent on the permeability of the outer layer. At 10 °C, the apparent evaporative heat loss is markedly higher than expected from evaporation alone (measured at 34 °C), which is attributed to condensation within the clothing and to increased conductivity of the wet clothing layers [16]. Although there is enough research available on footwear comfort during perspiration but the area "wet comfort of socks" with differential raw materials and construction need more exploration. Because many researchers used different shoes with same sock even though they have accepted the consequences of socks composition on foot comfort. Some studies on socks with different fibre compositions found but those are lacking the measurement in wet state. So this study is planned to fulfill this deficiency.

2. Material & Methods

2.1. Socks

All the socks samples have been knitted on same machine settings by just varying the main yarns to get the homogeneous samples with respect to specs and stretches for contrast comparison. After knitting, all the samples were processed for washing in the same machine bath followed by tumble drying and boarding.

Table 1.

Fibre Composition (%)		Sock Codes
Plaiting Yarn	Main Yarn	
Polyester Air Covered Elastane	100% Cotton	P1
	100% Viscose	P2
	100% Spun Polyester	P3
	100% Nylon Filament	P4
	100% Polypropylene	P5
	100% Wool	P6
	100% Acrylic	P7
	100% Coolmax*	P8
	100% Micro Nylon*	P9

* Coolmax and micro nylon used only for thermal resistance comparison

2.2 Alambeta

Thermal resistance (R_{ct}) and thermal absorptivity (b) were assessed by means of the Alambeta tester [17], which enables fast measurement of both steady-state and transient-state thermal properties. This instrument simulates, to some extent, the heat flow q (Wm⁻²) from the human skin to a fabric during a short initial contact in the absence of body movement and external wind flow. Thermal resistance (R_{ct}) [m².KW] is used to express the heat insulation properties of a fabric. R_{ct} of textiles is affected by fibre conductivity, fabric porosity, and fabric structure. It is also a function of fabric thickness, as shown by the following expression:

$$R_{ct} = \frac{h}{\lambda} \text{ --- (1)}$$

Thermal absorptivity (b) [W. s^{1/2} / m².K] has below equation;

$$b = \sqrt{\lambda \rho c} \text{ --- (2)}$$

2.3 Permetest

Relative cooling effect and R_{ct} [m².K/W] were measured by using Permetest. The Permetest [18][19][9] instrument is the so-called skin model, which simulates dry and wet human skin in terms of its thermal feeling and serves for determination of water vapor and thermal resistance of fabrics. Results of measurement are expressed in units defined in the ISO Standard 11092. Thermal resistance R_{ct} follows the following equation:

$$R_{ct} = K(t_H - t_0) \times \left(\frac{1}{U_1} - \frac{1}{U_0} \right) \text{ --- (3)}$$

Where U_s and U₀ represent the steady state electrical voltages shown on the digital display, for the case of measurement with and without sample. The sensitivity constant K is determined by the calibration. Relative water vapor permeability (P) is a non-standardized but practical parameter (P = 100% indicates the permeability of free measuring surface). It is given by the following relationship:

$$P (\%) = 100 \left(\frac{q_s}{q_0} \right) \text{ --- (4)}$$

2.4 Thermal Foot Model

Thermal resistance also measured by Thermal Foot Manikin (FM) is part of “Thermal Sweating Foot Manikin System”. The FM component is a 1:1 scale foot model. It consists of 13 silver alloy surface segments, stainless steel supporting structure, shock absorbers, heating subsystem and sweating subsystem. The FM is intended to test the thermal resistance and evaporation resistance of the footwear. The FM geometrically resembles a human foot with several geometrical modifications. The size of the FM has been tuned as to fit into the footwear of standard 42 EU size. The heating subsystem is connected by highly flexible cables to Thermal Manikin Controller (TMC). The sweating subsystem is connected to water Dispensing Unit (DU). At the moment, water dispensing is functional as per gravimetric method. Both TMC and DU are controlled programmatically by means of MANICON computer program on a standard PC. Figure 1a depicts an assembled FM, attached to Gait Simulator. Figure 1b is a general layout of individually controlled surface segments.



Figure 1a. Assembled foot manikin

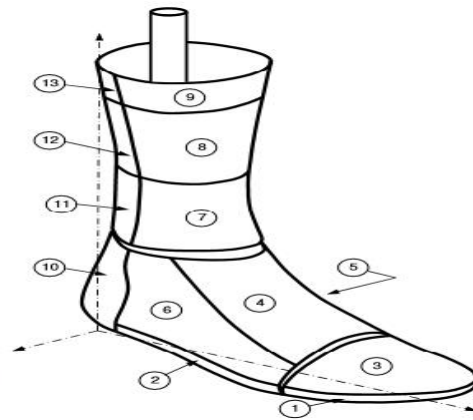


Figure 1b. The layout of surface segments

Thermal resistance of the sock is measured as per below equations;

Bare Foot Resistance $R_{ct0} = \frac{(tb-ta) \times A}{p}$ ----- (5)

Bare Foot + Sock Resistance $R_{ctn} = \frac{(ts-ta) \times A}{p}$ ----- (6)

Sock Resistance $sock R_{ct} = R_{ctn} - R_{ct0}$ ----- (7)

Where;

tb = Bare foot temperature (°C)

ta = Ambient temperature (°C)

ts = Bare foot temperature with sock (°C)

A = Area of the foot model (m²)

P = Power transmitted (W)

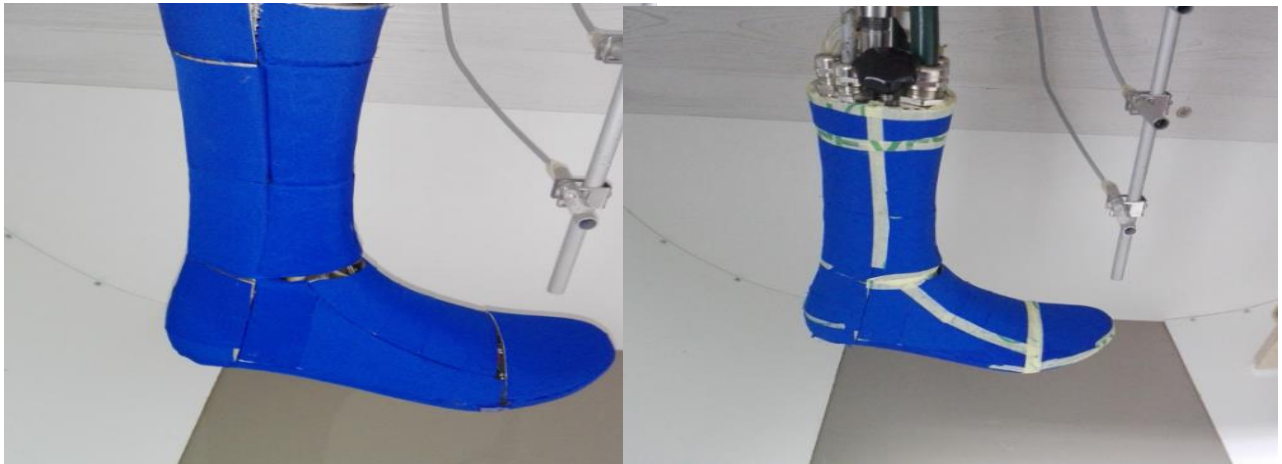


Figure 2a. A semi-permeable membrane of $2.9 \text{ m}^2 \cdot \text{pa/w}$ glued

Figure 2b. Open spaces between segments are covered with paper tape

Table 2. Thermal FM Vs Permetest Vs Alambeta parameters

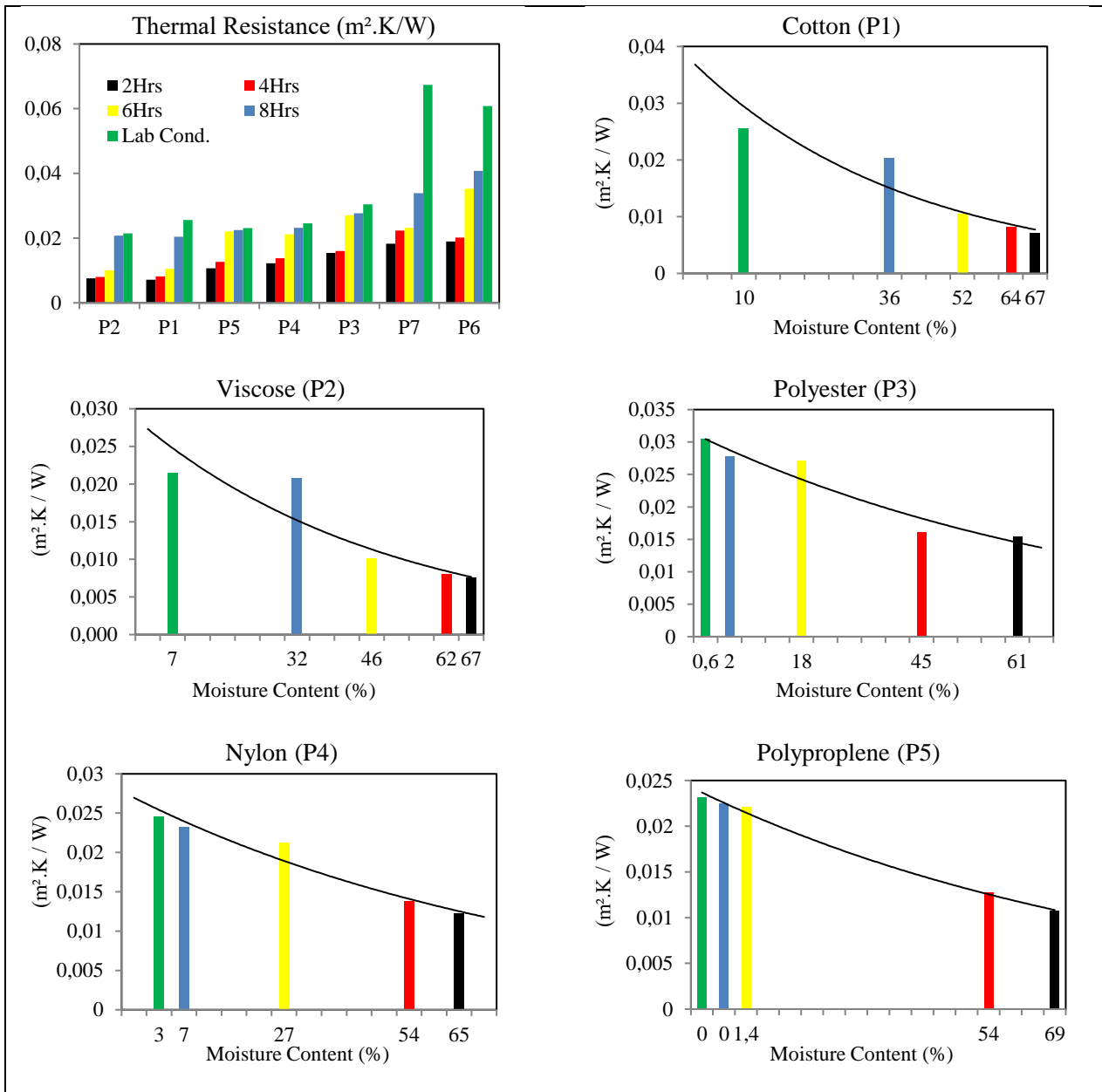
Parameter	Foot Model	Permetest	Alambeta
Convection	1m/Sec	1m/Sec	No free convection
Relative Humidity	65 ± 5 (%)	65 ± 5 (%)	65 ± 5 (%)
Ambient Temperature	17 ~ 20 (° C)	23 ~ 25 (° C)	23 ~25(° C)
Foot Model/ skin Temperature	35 (° C)	35 (° C)	35 (° C)
Chamber Door	Open	Closed	Not Applicable
Membrane	FM glued with a semi-permeable membrane as shown in figure 2a and 2b.	Permetest already has GORE-TEX membrane. A polythene sheet used to block the moisture permeation.	Not Applicable
Isothermal conditions	Not Applicable	Not Applicable	Measuring head is covered by an isothermal ring

3. Results & Discussion

Oven dry weights and lab conditions weights were recorded for each sock. Then samples were wet and squeezed manually. Before testing them for relative cooling effect, thermal resistance & thermal absorptivity samples were weighted after every 2hours of conditioning consecutively in laboratory standard environmental conditions for moisture loss rate and eventually evaporation rate for different socks.

3.1. Effect of Moisture on Thermal Resistance ($m^2.K/W$)

As mentioned earlier, dry and wet socks with differential moisture content were checked on alambeta. Figures 3 clearly demonstrated that as the moisture (%) increased thermal resistance decreased and vice versa irrespective of sock fibre composition or structure. Only P3, P4, and P5 socks have resumed their dry (lab conditions) Rct after 6 hours of conditioning. P2, P6 & P7 couldn't resume their thermal resistance even after 8 hours. P5 (polypropylene) has the highest moisture loss or evaporation rate followed by P6 (wool) and P3 (polyester). P1 (cotton) and P2 (viscose) are the worst one. P4 (nylon) and P7 (acrylic) fall in the middle.



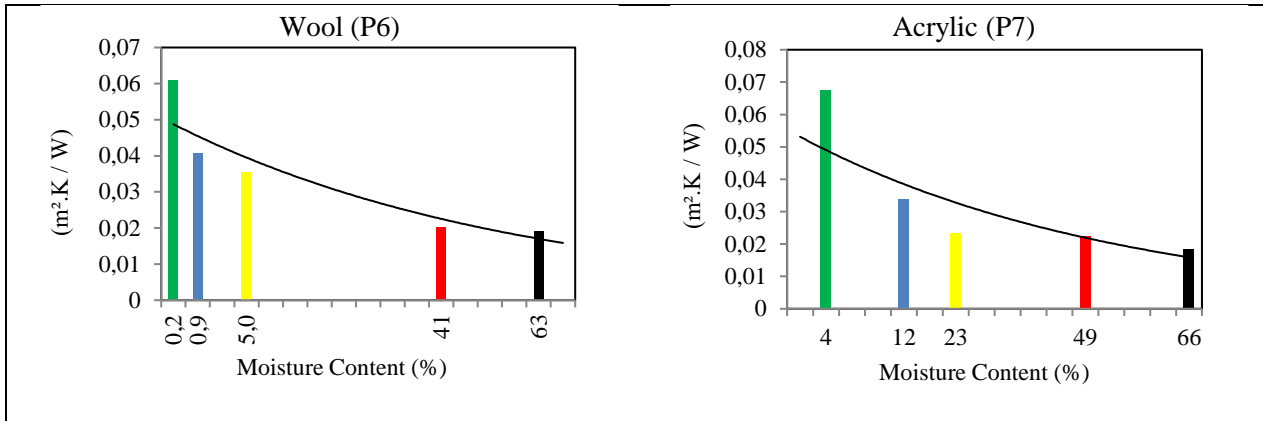
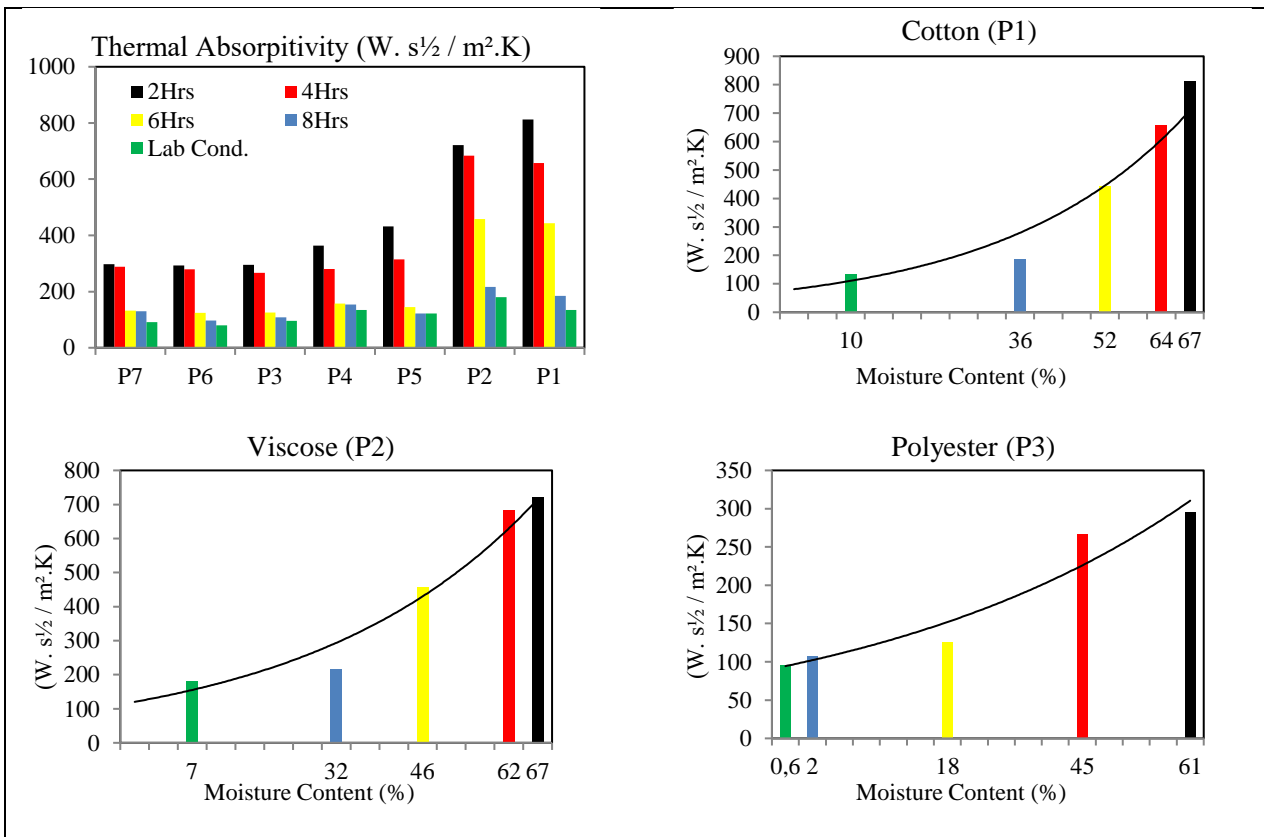


Figure 3. Effect of moisture content on thermal resistance

3.2. Effect of Moisture on Thermal Absorptivity ($W \cdot s^{1/2} / m^2 \cdot K$)

Figure 4 has verified that thermal absorptivity increases by increasing the moisture (%). In case of plain socks, only P5 could resume its dry Rct (lab conditions) after 8 hours of conditioning. P3, P4, P5, P6 & P7 having highest resumption after 6 hours and these socks attained $<160 W \cdot s^{1/2} / m^2 \cdot K$. At this limit the wearer is comfortable with dry feeling. P1 (cotton) and P2 (Viscose) has the highest thermal absorptivity with lowest evaporation rate. It means that these are the coolest socks.



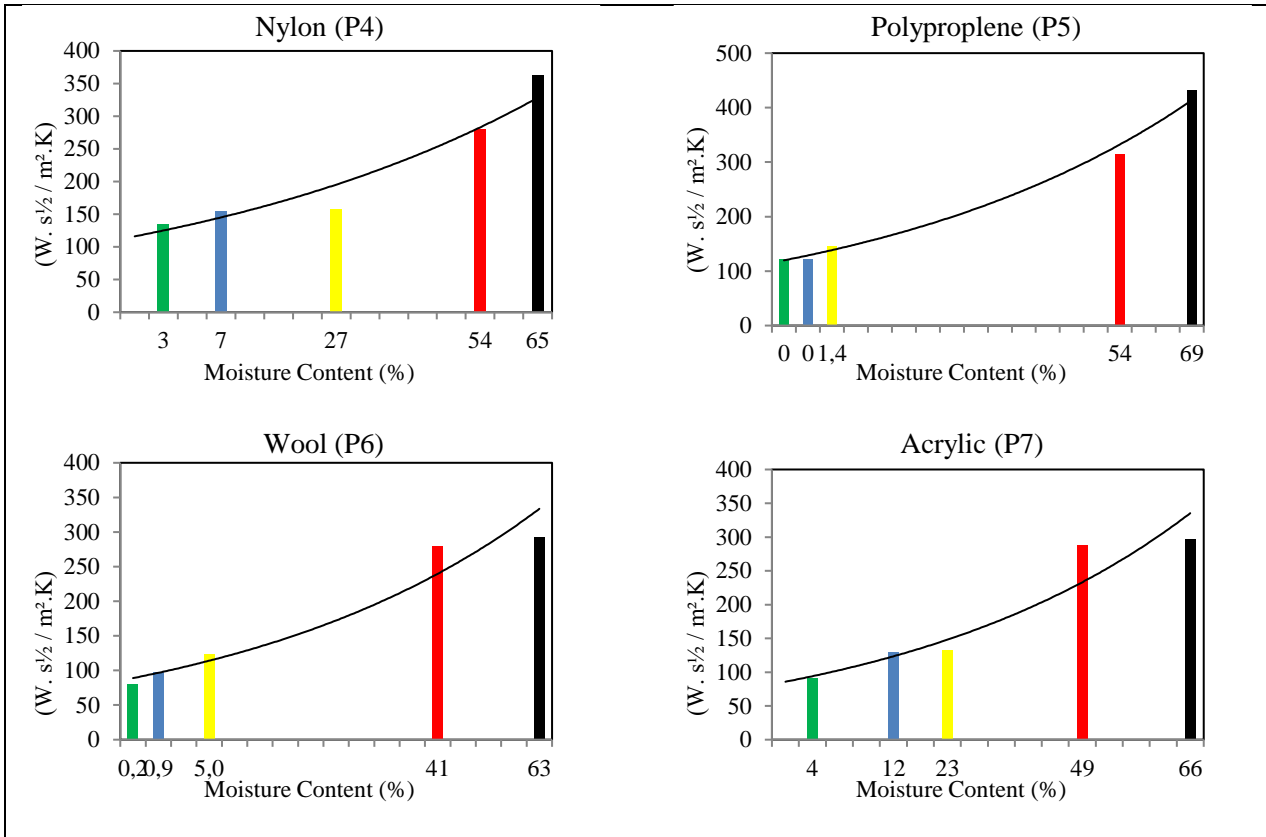
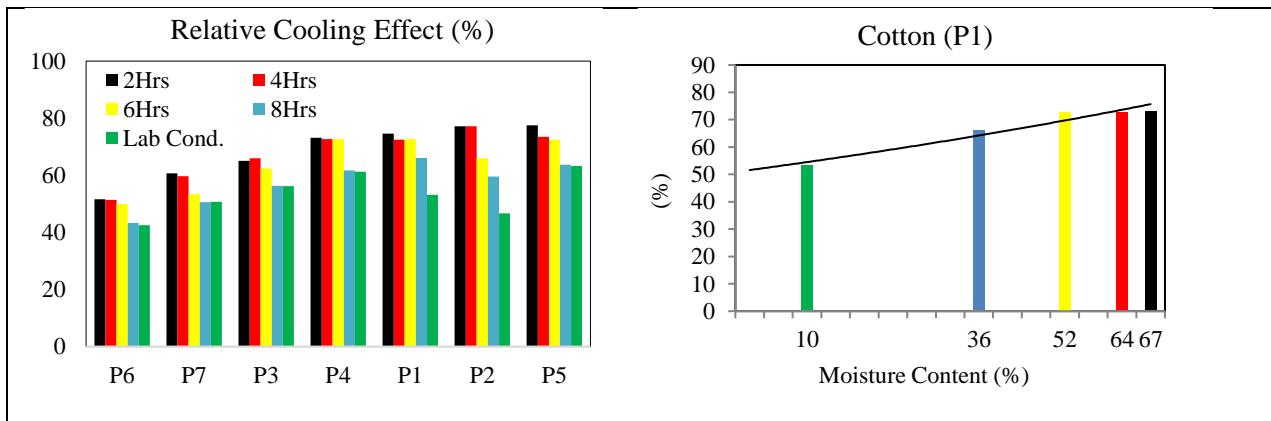


Figure 4. Effect of moisture content on thermal absorptivity (W. s^½ / m².K)

3.3. Effect of Moisture on Relative Cooling Effect (RWVP %)

Figure 5 shows that highest the RWVP (%) leads to higher cooling effect. P3, P6, P7, T3, T6 & T7 will be the warmest socks with lower RWVP (%). All the samples have achieved their dry conditions (lab conditions) RWVP (%) except P1 (cotton), P2 (viscose).



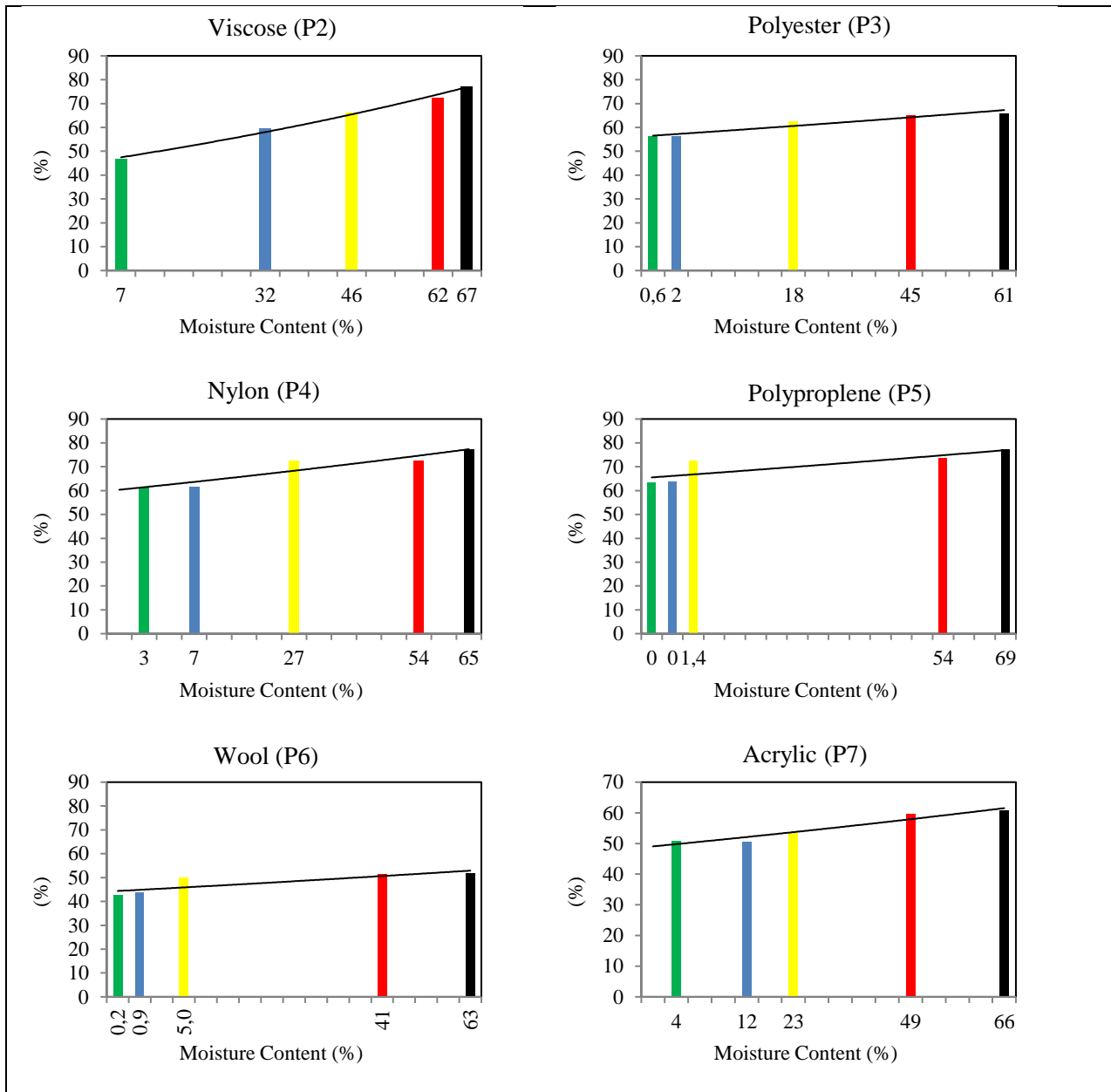


Figure 5. Effect of moisture content on Relative Cooling Effect

3.4. Thermal Resistance Comparison with Different Skin Models

Before discussing the comparison of R_{ct} between alambeta, thermal FM, and permetest, it is very important to understand the difference of measuring conditions as given above in table 2. R_{ct} measured on FM is always lower than permetest and alambeta's measurement irrespective of sock composition as shown in figure 7. The previous experiments on alambeta, dry and wet socks were tested in a relaxed state without any extension. For real simulation of extension like thermal FM, socks were loaded on a dummy leg and marked a circle of 12cm diameter on the foot and calf with the help of a paper card (figure 6). Then socks were slashed and extended on an embroidery hoop to the marked circle (figure 8). Finally, these samples were tested on alambeta and permetest for R_{ct} together.



Figure 6. Preparation of sample for measurement in extended stated

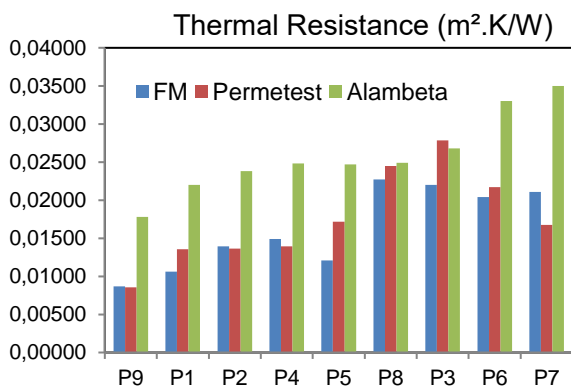


Figure 7. Thermal Resistance Comparison

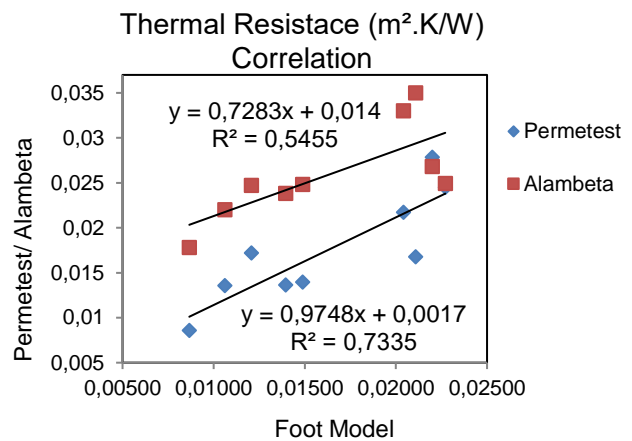


Figure 8. Thermal Resistance Correlation (R^2)

4. CONCLUSION

A higher value of moisture leads to increase the relative cooling effect to a large extent.

Although thermal resistance and absorptivity greatly affected by moisture this could be prevented by correct selection of fibre composition sock structure with respect to the end use.

Thermal resistance is inversely proportional to the amount of moisture content. Sock samples P3, P4 and P5 socks have resumed their dry (lab conditions) Rct after 6 hours of conditioning. P1, P6, and P7 couldn't resume their insulation even after 8HRS of conditioning.

Higher is thermal absorptivity leads from dry to cool and cold effect. The results of this study show that the thermal absorptivity values of dry fabrics range from 79.7 to 180 ($Ws^{1/2} / m^2 \cdot K$). When the fabrics get wet, since the thermal conductivity of water is much higher than those of fibers and there is entrapped air in the textile structure, these values increased. In case of plain socks, only P5 could resume its dry Rct (lab conditions) after 8 hours of conditioning. P3, P4, P5, P6 & P7 having highest resumption after 6hours and these socks attained $<160 W \cdot s^{1/2} / m^2 \cdot K$. At this limit the wearer is comfortable with dry feeling. P1 (cotton) and P2 (Viscose) has the highest thermal absorptivity with lowest evaporation rate.

All the samples have achieved their dry conditions (lab conditions) RWVP (%) except P1 (cotton), P2 (viscose).

Thermal resistance measured in an extended state by alambeta and permetest is comparable with R_{ct} measured by thermal Foot Model with the correlation (R²) of 0.55 and 0.7335 respectively.

References

- [1] K. Slater, "Discussion paper the assessment of comfort," *J. Text. Inst.*, vol. 77, no. 3, pp. 157–171, 1986.
- [2] M. M. Adler and W. K. Walsh, "Mechanisms of transient moisture transport between fabrics," *Text. Res. J.*, vol. 54, no. 5, pp. 334–343, 1984.
- [2] Adler, M.M., Walsh, W.K., (1984). Mechanisms of transient moisture transport between fabrics. *Text. Res. J.*, vol. 54, no. 5, pp. 334–343.
- [3] A. H. Woodcock, "Moisture transfer in textile systems, Part I," *Text. Res. J.*, vol. 32, no. 8, pp. 628–633, 1962.
- [4] A. P. Gagge and R. R. Gonzalez, "Physiological and physical factors associated with warm discomfort in sedentary man," *Environ. Res.*, vol. 7, no. 2, pp. 230–242, 1974.
- [5] A. M. Plante, B. V. Holcombe, and L. G. Stephens, "Fiber hygroscopicity and perceptions of dampness part I: subjective trials," *Text. Res. J.*, vol. 65, no. 5, pp. 293–298, 1995.
- [6] A. S. W. Wong and Y. Li, "Psychological requirement of professional athlete on active sportswear," in *The 5th Asian Textile Conference*, Kyoto, Japan, 1999.
- [7] G. Havenith et al., "Assessment of thermal properties of protective clothing and their use," *EU Final Rep.*, 2006.
- [8] W. A. Lotens, "Heat transfer from humans wearing clothing." TNO, 1993.
- [9] L. Hes and M. de Araujo, "Simulation of the effect of air gaps between the skin and a wet fabric on resulting cooling flow," *Text. Res. J.*, vol. 80, no. 14, pp. 1488–1497, 2010.
- [10] L. Hes and I. Dolezal, "Precise measurement of water vapour permeability of wet fabrics," in *Proceedings of the Autex International Textile Conference*, Tampere, 2007.
- [11] M. Bogusławska-Bączek and L. Hes, "Effective water vapour permeability of wet wool fabric and blended fabrics," *Fibres Text. East. Eur.*, 2013.
- [12] K. V. E. I. D. P. ÖRME, "THERMAL COMFORT PROPERTIES OF COTTON KNITTED FABRICS IN DRY AND WET STATES."
- [13] Y. S. Chen, J. Fan, and W. Zhang, "Clothing thermal insulation during sweating," *Text. Res. J.*, vol. 73, no. 2, pp. 152–157, 2003.
- [14] K. Kuklane and I. Holmér, "Effect of sweating on insulation of footwear," *Int. J. Occup. Saf. Ergon.*, vol. 4, no. 2, pp. 123–136, 1998.
- [15] K. Kuklane, I. Holmer, and G. Giesbrecht, "Change of footwear insulation at various sweating rates," *Appl. Hum. Sci.*, vol. 18, no. 5, pp. 161–168, 1999.
- [16] M. G. M. Richards et al., "Dry and wet heat transfer through clothing dependent on the clothing properties under cold conditions," *Int. J. Occup. Saf. Ergon.*, vol. 14, no. 1, pp. 69–76, 2008.
- [17] L. Hes and I. Dolezal, "New method and equipment for measuring thermal properties of textiles," *Sen'i Kikai Gakkaishi (Journal Text. Mach. Soc. Japan)*, vol. 42, no. 8, pp. T124–T128, 1989.
- [18] L. Hes and I. Dolezal, "A new computer-controlled skin model for fast determination of water vapour and thermal resistance of fabrics," in *7th Asian Textile Conference*, New Delhi, 2003.
- [19] L. Hes, "Non-destructive determination of comfort parameters during marketing of functional garments and clothing," 2008.

A REVIEW ON MULTI-STRAND STAPLE YARN PRODUCTION

Murat Demir¹, Musa Kilic¹, Zeki Kiral², Kıymet Kübra Denge³, Furkan Balduk³

¹Dokuz Eylül University, Department of Textile Engineering, İzmir, Turkey, tel: +902323017701

²Dokuz Eylül University, Department of Mechanical Engineering, İzmir, Turkey, tel: +902323019232

³KİPAŞ Mensucat R&D Center, Kahramanmaraş, Turkey, tel: +903442363800

musa.kilic@deu.edu.tr

Abstract:

Ring spinning is one of the oldest and most widely used spinning technology. Recently, many alternative spinning technologies have been introduced. Some of these technologies work on completely different working principle while some of them were developed from conventional system with some modifications. Siro-spun technology is one of the systems that developed from conventional ring spinning. In siro-spun technology, two strands are fed into drafting zone simultaneously and composite yarn is produced in single process. Benefits of siro-spun technology encouraged researchers to investigate multi-strand yarn production. For multi-strand yarn production, strands are also fed into drafting zone simultaneously and multi-layered composite yarn is produced in single process. Controlling strands in drafting area and yarn convergence point are two critical parameters that affect yarn quality for multi-layered staple yarn production. Multi-strand staple yarns can be used either for substitution of plied yarns or specific purpose using by different strands in single yarn.

Key words:

ring spinning, twist spinning, siro-spun spinning, multi-strand staple yarn

1. Introduction

Ring spinning machine was investigated in 19th century and part from small developments; it still keeps the main working principle. With the advantage of spinnability of any kind of raw material, the widest yarn count range and producing the optimum quality yarn ensures the conventional ring spinning technology is the most commonly used spinning technology. However, limitations on ring spinning technology such as production speed or necessities for better yarn quality, many alternative spinning technologies have been introduced. Some of these technologies work on completely different system while some of them were improved from conventional system with small developments (Table 1). Nevertheless, there has not been developed a system that can be alternative to the conventional method yet.

Table 1. Classification of spinning technologies based on working principle

Different Working Principle Spinning Technologies	Developed from Existing Technologies
OE Spinning (Rotor, Electrostatic, Friction, Disc, Air-vortex)	Siro-Spun Spinning
Air-jet Spinning	Siro-Fil Spinning
Hollow Spindle Spinning	Core-Spun Spinning
Self-Twist Spinning	Compact Spinning

2. Two Strand Spinning

Twist spinning or mostly known as siro-spun spinning was introduced in 1970s by Dieter Plate [1]. In this spinning technology, two separate staple strands are fed into drafting zone simultaneously with the help of small modifications that made on conventional system. Each strand is twisted for single yarn and

each yarn is also twisted to produce composite yarn in single process. Elimination of two main production process from two-ply yarn, siro-spun has become the rival of two-ply yarn.

Since the introduction of siro-spun yarn, many researchers have been focused to analyze siro-spun yarns and production technology. In the process of twisting two single strand for single yarn production, yarn formation zone is important to know tenacity of each strand. Emmanuel and Plate introduced yarn formation zone after front cylinder for siro-spun yarn in Figure 1 [2]. In Figure 1, F , is tension and M is elastic torque in the two-strand yarn below the convergence point, f is tension and m is elastic torque in two-strand yarn above the convergence point, 2α is convergence angle and R is radius of strand. Equations of twist variables are given as;

$$f = F / (2 \cos \alpha) \quad 1.1$$

$$m = (M - F \cdot R \tan \alpha) / (2 \cos \alpha) \quad 1.2$$

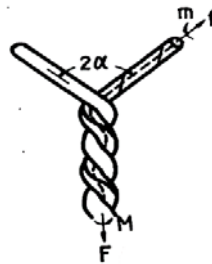


Figure 1. Siro-spun yarn production [2]

Some of researches were also focused to compare the effect of production process on yarn qualities and it was noted that strand space is one of the main production parameters that directly effects of properties of the siro-spun yarns [3-7] Tenacity of each strand is related with the length of each strand in yarn formation zone. Larger strand space means larger convergence angle (α) and which means longer strand length [8]. Relation between strand length (l), strand space (s) and convergence angle (α) is given as;

$$l = s / (2 \sin \alpha / 2) \quad 1.3$$

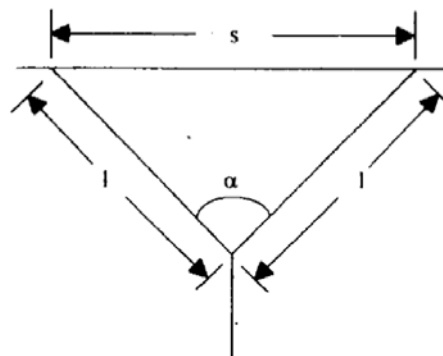


Figure 2. Yarn convergence point in siro-spun yarn [8]

He and Zhang [9] claimed that convergence point of two strand yarn spinning is not determined by force balance and it is the reason why Emanuel and Plate [2] equations are not solvable for fluid system. They claimed that convergence point of yarn can be expressed with flow equations. In the other study, Zhang and He [10] discussed how optimally control unsteady process by geometry constrains for siro-spun yarns. They concluded geometry condition for optimal control of the unsteady yarn spinning in equations 1.4 where H is the distance between front cylinder and yarn convergence point, L is the half of the strand space and D is the distance between front cylinder and yarn guide. Geometric model of two-strand yarn spinning is given in Figure 3. He et al. [11] also claimed that dynamic character of siro-sun yarn has strong relationship with convergence angle.

$$H^2 + \frac{8L^2}{D}H - 4L^2$$

1.4

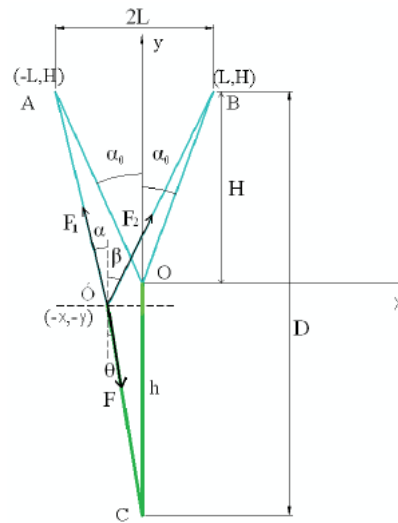


Figure 3. Dynamical analysis of the strand convergence point at equilibrium

As an alternative of two-plyed yarns, there are also some researches that compare the properties of siro-spun and conventional spun yarns. Siro-spun have better hairiness, elongation, abrasion resistance and strength when it compared with single plyed yarns [12]. Siro-spun yarns also have better hairiness values than two-plyed yarns and have similar results for breaking force and elongation values [13].

Guo et al. [14] designed double-channel spinning system that inspired from siro-spun spinning. In this system; two strands are fed into drafting zone likewise siro-spun system but with different drafting ratio. To provide different drafting ratio for each strand, two back rollers are driven by two different motors and strands are fed in to drafting zone with different tension (Figure 4). Feeding into two separate strands into drafting zone with different drafting ratio cause differences on yarn appearances and relation between back roller speed and yarn appearances on two-colored yarn was showed in Figure 5. As it can be seen from Figure 5 increasing back roller speed result lower drafting ratio and strand that go through faster cylinder have more appearances on yarn surface.

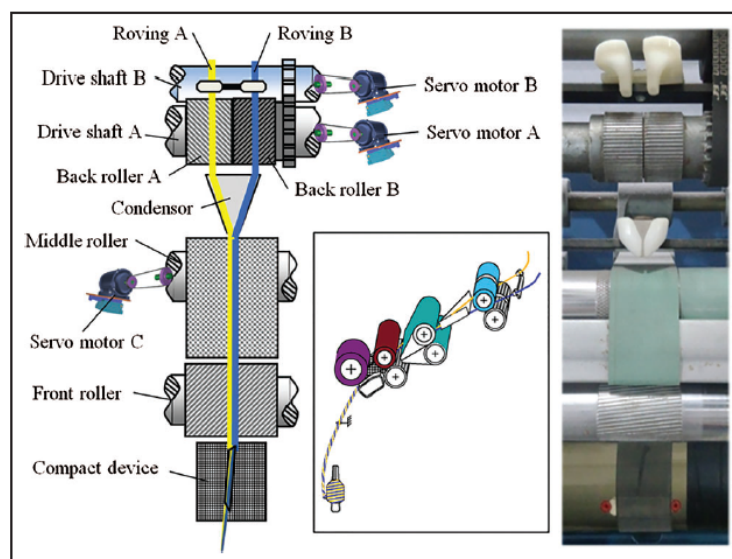


Figure 4. Schematic diagram and the real image of the double-channel compact spinning machine

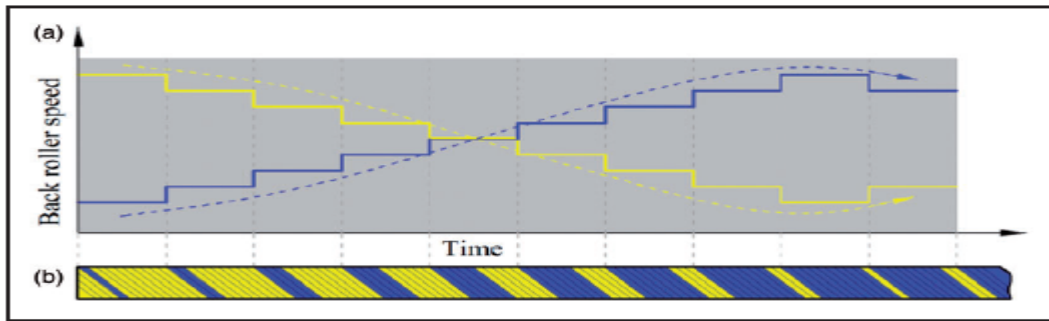


Figure 5. Relationship between yarn appearances and back roller speeds

3. Three-Strand Spinning

Three-strand staple yarn production is one of the system that aim to produce three-strand as a substitution of three-ply yarn or produce yarn from three different strands for special purpose. He [15] claimed that three strand yarns can be used for intelligent textile and multi-functional materials. However, there are limited study on the production of three-strand staple yarns.

Matsumoto et. al. [16] were investigated the production of three strand yarn but part from optimizing production process they mainly focused on fiber formation in yarn structure or strand tension during production. Matsumoto claimed that fiber distribution is affected by strand position in spinning triangle and different yarn cross section was proposed according to different spinning triangle (Figure 6). For the equal strand space (S), three strand has equal tensions ($T_A=T_B=T_C$) and it was expected to have equal fiber distribution in yarn structure. Since the strand spaces are not equal differences also occur on strand tension ($S_1 < S_2 = S_3$; $T_A < T_B = T_C$). As a result of this situation two yarn convergence points appear and two close strands are placed in yarn structure while the other strand cover them.

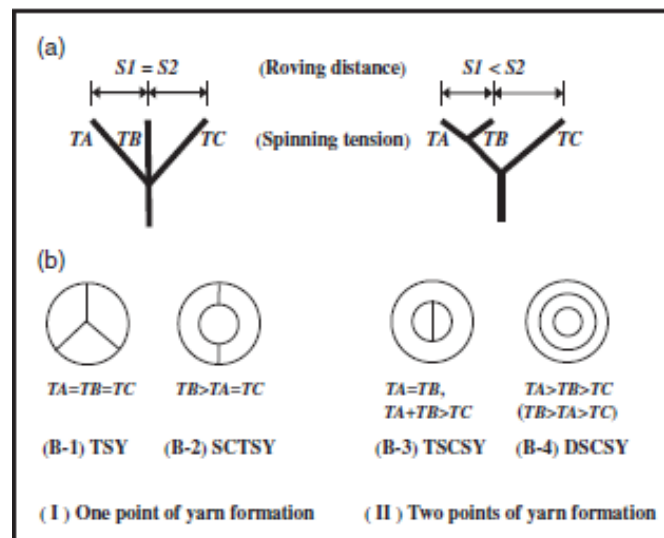


Figure 6. Different structure yarn convergence point and different yarn cross sections [16]

Since the tension on each strand is directly related with strand length between front cylinder and yarn convergence point, each strand length is important for multi-strand yarn production. In the case of production example in Figure 7, strand space between strand A and B is smaller than strand space strand B and C and eventually, strand length of strand C between yarn formation point and front cylinder nip is greater than strand length of strand A and B.

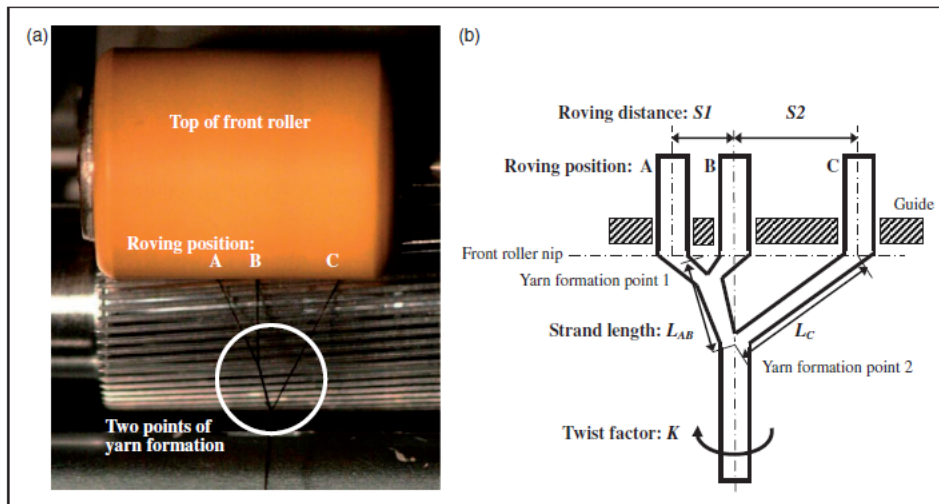


Figure 7. Three-strand yarn production with different strand space [16]

Assuming fibers distribution within the yarn structure depends only on the strand position; it was expected that strand A and strand B creates yarn core while strand C totally wrapped around them. However, fiber position in yarn structure is also related with fiber length and while long, thin fibers are located in yarn center, and shorter and coarser fibers cover around them. Cross sections of yarns that produce with same strand space and different fiber length are given in Figure 8. To produce each yarn, strand space S_1 was 3 mm and strand space S_2 was 6 mm. For Figure 8i, fiber length of three strands were 38 mm and for Figure 8ii, strand A and strand B had 51 mm fiber length while strand C had 38 mm fiber length. As it can be seen from Figure 8; strand space as well as the fiber length is important for fiber distribution of multi strand staple yarn.

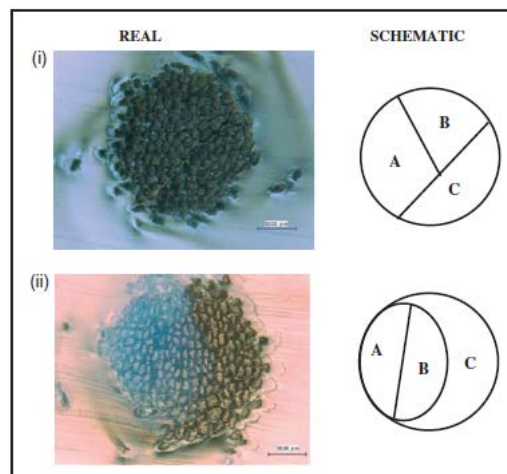


Figure 8. i. Cross section of yarn with different strand space and same fiber length, **ii.** Cross section of yarn with different strand space and different fiber length [16]

In another study of Matsumoto et. al [17], effects of fiber length and fiber linear density were investigated for three strand yarn production. For the study, length and linear density of center strand were changed and core-sheath ratio were investigated. For the first example fiber length of strands were chosen 38 mm-51 mm-38 mm respectively and fiber linear densities were 0.9 dtex for all strands (Figure 9a). For the second example linear densities of strands remained same and length of fibers in strands were changed with 51mm-38mm-51mm, respectively (Figure 9b). Results showed that using center strand with greater fiber length provide better core-sheath ratio (Figure 9).

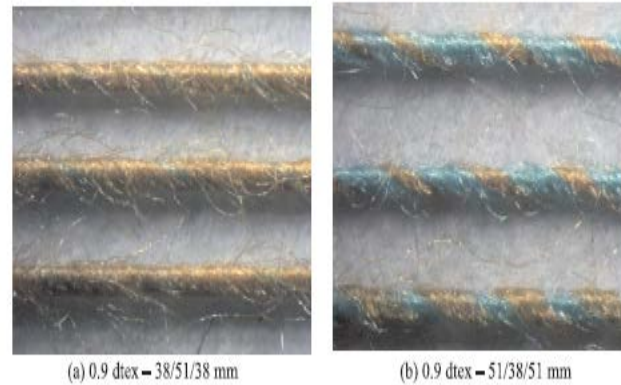


Figure 9; **a.** Longitudinal view of three-strand yarn with 0.9 dtex linear density and 38mm-51mm-38mm fiber length, respectively **b.** Longitudinal view of three-strand yarn with 0.9 dtex linear density and 51mm-38mm-51mm fiber length, respectively [17].

Demir and Kilic [18] were investigated three-strand yarn production and they concluded that it is possible to produce three-strand yarn in conventional system. To production of three-strand staple yarn, additional strand funnel was placed on siro-spun technology to guide third strand into the drafting zone (Figure 10). Properties of three-strand staple yarns were compared with conventional three-ply yarns.

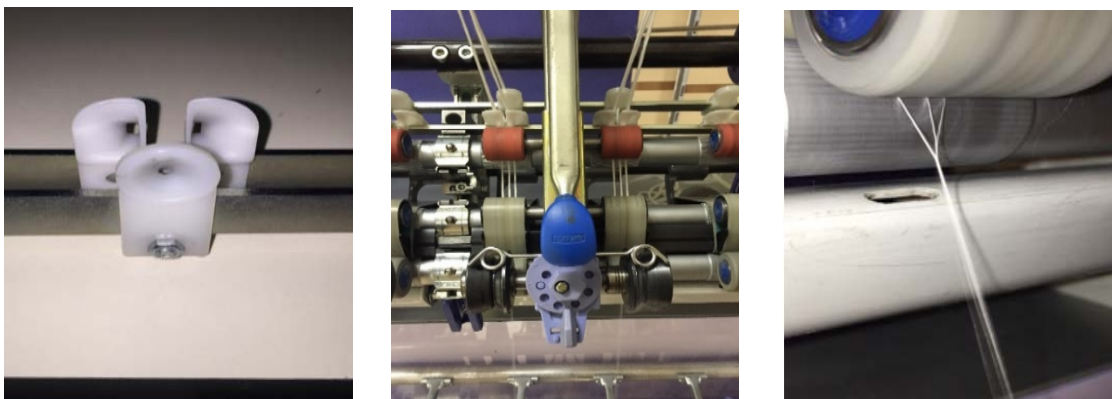


Figure 10. Three-strand funnel for three-strand and yarn convergence point in three-strand yarn production [18]

When the strand spaces are not equal in drafting zone, strand length as well as strand tenacity are not also equal in yarn formation zone. In the later study of Demir and Kilic [19], three-grooved delivery cylinder was also placed in drafting zone to control strand space in drafting area. Results were also compared with three-ply yarn and three-strand staple yarn without delivery cylinder (Figure 11).

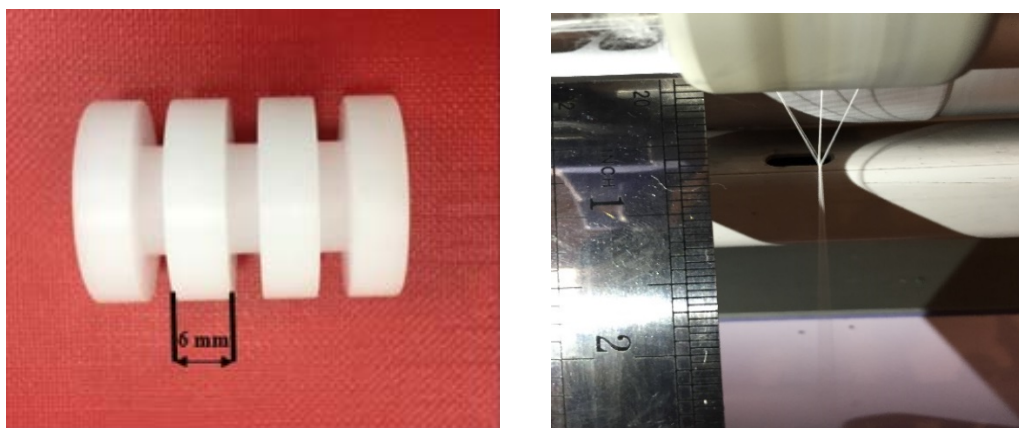


Figure 11. Three-grooved delivery cylinder and yarn convergence point in three strand yarn production with three-grooved delivery cylinder [19]

4. CONCLUSIONS

Conventional ring spinning system is the oldest spinning technology and has been using since the 19th century. Comparison of ring spinning and modern spinning technology showed that ring spinning is superior than modern technologies in terms of yarn count, optimum yarn quality and etc. On the other hand, modern technologies are also superior in terms of production speed and certain yarn quality parameters, such as hairiness and unevenness. Modern spinning technologies can be grouped under two main sections, as different principle spinning technologies and improved from existing technologies. Siro-spun technology is one of the system that developed from conventional technology. In siro-spun technology, two strands are fed into drafting zone simultaneously to produce single yarn. With the economic benefit of eliminating twisting and doubling machine and similar properties with two-ply yarns, siro-spun yarns become rival for two-ply yarns. Recently, inspiring from siro-spun technology, production of three-strand staple yarns has also gained importance. In this new method, three staple strands are fed into drafting zone to produce single yarn. By this method, it is possible to produce yarn from same raw material as an alternative for three-ply yarns or produce yarn from different raw material for specific purposes.

ACKNOWLEDGEMENTS

This study is supported by TÜBİTAK - TEYDEB 1505 University - Industry Collaboration Grant Programme with the project number 5160091.

References

1. CSIROpedia, (2009). Sirospun. <https://csiropedia.csiro.au/sirospun/>.
2. Emanuel A., Plate, D. (1982). *Alternative Approach to Two-Fold Weaving Yarn, Part II. The Theoretical Model*, *Text Inst*, 73 108-116..
3. Üte, T. ve Kadoğlu, H. (2014). *Regression estimation of cotton sirospun yarn properties from fiber properties*. *AUTEX Research Journal*, 3 (14), 161-167
4. Tyagi, G.K., Rajdev, A., Mehta, M., Jain, S. ve Jindal, B.M. (1987). *Contribution of fiber length, fiber linear density and strand spacing to physical and mechanical characteristics of siro-spun viscose yarns*. *Indian Journal of Textile Research*, 12, 63-67.
5. Gokarneshan, N., Anbumani, N. ve Subramaniam, V. (2006). *Influence of strand spacing on the interfiber cohesion in siro yarns*. *The Journal of The Textile Institute*, 3 (98), 289-292.
6. Subramaniam, V., Srinivasamoorthi, V.R. ve Mohammed, M.R. (1989). *Effect of processing parameters on the properties of double rove-spun yarn produced on short staple spinning system*. *Textile Research Journal*, 59, 762-767.
7. Gowda, R., Sivakumar, M. and Kannan, M. (2004). *Influence of process variables on characteristics of modal siro-spun yarns using box-bohen response surface design*. *Indian Journal of Fiber & Textile Research*, 29, 412-418.
8. Cheng, K.P.S. and Sun, M.N. (1998). *Effect of Strand Spacing and Twist Multiplier on Cotton Siro-Spun Yarn*. *Text Res J* 68 (520).
9. He, J. and Zhang, L. (2008). *On convergence point of the two-strand yarn spinning*. *Textile Research Journal Vol 78(11)*, 1022-1024.
10. Zhang, L. and He, J. (2009). *Geometry condition for optimal two-strand yarn spinning part I: Siro-spun*. *Textile Research Journal Vol 79(3)*, 243-246.
11. He, J., Yu, Y., Yu, J., Li, W., Wang, S. (2005). *A linear dynamic model for two-strand yarn spinning*. *Textile Research Journal Vol 75(1)*, 87-90.
12. Salhotra, K. (1987). *Some quality aspects of ply-spun yarn*. *Indian Journal of Textile Research*, 12, 197-200.

13. Yıldız, B.S. and Kilic, M. (2017). *An investigation on Properties of Siro-spun Yarns. Annals of University Orades Fascicles of Textile and Leatherwork. Vol . 18. Pp. 131-136.*
14. Guo, M., Sun, F., Wang, L., Xue, R.Y. and Gao, W. (2018). *Analysis of the appearance of two-color cotton yarn by the double-channel spinning system. Textile Research Journal 0(00) 1-13.*
15. He, J. (2007). *Variational Approach to Nonlinear Coupled Oscillators Arising in Sirospun Yarn Spinning. FIBERS & TEXTILES in Eastern Europe Vol 15. No (1) 60.*
16. Matsumoto, M., Matsumoto, Y., Kanai, H., Wakako, L., Fukushima, K. (2014), *Construction of twin staple-core spun yarn with two points of yarn formation in one twisting process. Text Res J, Vol. 84(17) 1858–1866.*
17. Matsumoto, Y., Kanai, H., Wakako, L., Morooka, H., Kimura, H., Fukushima, K. (2010). *Exploratory Work on the Spinning Condition of the Structure of Staple-core Twin-spun Yarns. Text Res J Vol 80(11): 1056–1064 DOI: 10.1177/0040517509352521*
18. Demir, M. and Kilic, M (2017). *Investigating Possibilities of Three-Strand Yarn Production. Fibers and Textiles, vol 24(1) pp.30-35.*
19. Demir, M. (2017). *An Investigation on Production Possibilities Of Three-Roving Sewing Threads, Master Thesis, Dokuz Eylul University.*

PREDICTION OF PATTERN DIMENSIONS FOR PRESSURE GARMENT

¹Nareerut Jariyapunya, ²Blažena Musilová and ³Antonín Havelka

^{1,2,3}Technical University of Liberec, Faculty of Textile Engineering, Department of Clothing Technology, Liberec, Czech Republic, Studentská 1402/2, email: nareerut.jariyapunya@tul.cz

Abstract

The paper presents the garment pattern dimensions method for stretch fabrics by using the mathematic modelling to predict the strain values. The tensile properties according to standard EN ISO 14704-1 was used for calculating the relationship between stress-strain to apply the mathematical modelling based on theory of circumferential stress in a thin-walled cylindrical pressure vessel. For the body measurement experiment, used sense™2 3D scanner was applied to find out the values of body circumferences and diameters with different parts. Besides, strain value has been predicted for estimating the initial circumference of pattern dimensions with optimum for pressure garment; additionally, this research used the PDS Tailor XQ software for developing the pattern dimensions. This method will help navigate garment industries to predict the precise pattern dimensions for pressure garment.

Key words

Elastic fabric, Pressure, Compression garments, Circumferential stress, Patternmaking, Laplace's Law

1. Introduction

Patternmaking is considered to be an important functional factor for clothing pressure with the purpose of producing tight-fitting garment [1, 2, 3] which is generally applied to develop patterns and reduction size of patterns and to optimize from the perspective of the stretch ability of elastomeric fabrics [4, 5]. Clothing pressure are the fabrics devices made of natural or synthetic yarns in combination with the elastomeric yarn with help to apply certain pressure on the surface of the body to compress and stabilize the body tissues [6]. While simple body movement usually causes skin expansion around 10% to 50% [7] and thus, fabric stretch ability is by some means higher than expansion ability of human skin. Furthermore the elastic recovery is considered to be equally as important as stretching [8, 9, 10] especially when it has a capability in keeping the pressure value of clothing stability.

When considering at theory to help predict human body pressure value of clothing, countless numbers of researchers commonly choose and apply Laplace's Law as a way to determine pressure of clothing on the human body. In those studies, moreover, the basic geometric form of the cylinder is used to represent human figure [11, 12, 13, 14]. Nevertheless, the Laplace's law does not consider the fabric thickness since Khaburi, J A and et al [15] who used the interface pressure model of thin and thick wall cylinder theories to derive the mathematical model used to describe the interface pressure applied by single-layer bandage. They reported that the result model of thick wall cylinder theory was more accurate than the other model in terms of pressure estimation when compared which was approximately 1.8% at the limb radius of 35 mm due to the ratio of the fabric thickness and size of radius. Consequently, when making consideration on the upper part of the body, the ratio of fabric

thickness and body radius were lesser and therefore the results of pressures estimated were very close.

The pressure estimation based on energy principle, Chattopadhyay, R., and Bera, M., [16] used the Instron tensile tester to find out the energy principle of the relationship between force-elongation and further predicted the mathematical modelling. The results of predicted pressures by fabric on the rigid cylinder were found to be more accurate and considerably closer to actual measured values. Thus energy principle approach could be used for predicting pressure on human by clothing pressure.

This research reports on the work that will be carried out using the mathematical model based on energy principle of elastic fabric and theory of circumferential stress thin wall cylinder to predict the strain value. Through experiment the strain value results will be calculated to find out the initial size of pattern construction.

2. Experimental

2.1. Materials

The materials used in this experimental study were constant fiber composition and knitting machine. In case of producing constant, 4 track single jersey machine of GOANG LIH, model GLF/s-3F-4T, CYL.DIA 32", GAUGE N.P.I. 28 G, Feeders 96F was run at a constant speed of 22 rpm. As can be seen from Table 1, characteristics of elastic knitted fabrics in the study are presented.

Table 1. Elastic knitted fabrics characteristics

Parameters	Single jersey knitted fabrics		
	Sample A	Sample B	Sample C
Polyamide (dtex/ply)	78x2	78x2	78x2
Elastane (dtex)	22	33	78
Weight (g/m ²)	271	305	318
Thickness (mm)	0.60	0.61	0.57
Polyamide (PA) %	94.38	92.94	83.46
Elastane (E)%	5.62	7.06	16.54

2.2. Methods

The aim of this experiment is to find out the relationship between force-elongation according the standard EN ISO 14704-1 [17] and this force-elongation curve of fabric from Instron tensile tester was assumed that the curve remains same energy principle state during fabric stretching on the human body. Regarding to the energy principle of force-elongation, calculation of the relationship between stress-strain of elastic fabrics was done.

In order to determine the specimens for testing EN ISO 14704-1 by Instron tensile tester, fabrics were cut into 50 x 200 mm (width x length), gauge length at 100 mm and they were tested for their loading set Constant-rate-extension (CRE) rate at 100 mm/min and thus the extension from 0% - 50% until 5th cycle of loading-unloading of fabrics was determined.

According to the interface pressure model using thin wall cylinder theory, there are three types of stresses namely circumferential, longitudinal and radial stresses [18, 19]. When the ratio of fabric thickness of the cylinder wall to its inside radius is less than 1:10, then it can be assumed that the radius stress is very small and thus it can be neglected. It could be assumed from this research that

the pressure during fabric stretching on the body was caused by the circumferential stress while longitudinal stress did not have any influences on fabric stretching.

Based on the above assumptions, circumferential stress (σ) can be expressed [15, 20] as follow:

$$\sigma = \frac{DP}{2d} \quad (1)$$

Where σ is fabric stress (N/m^2 or Pa), D is diameter of the cylindrical model or the body (m) and d is fabric thickness (m).

A polynomial fitting-line is accurate to predict the mechanical characteristics stretch fabric between the predicted strain (ε) at the magnitude of the fabric stress (σ). The stress-strain equation can be applied to described with the following the model for prediction equation (2).

$$\varepsilon = a_1\sigma^3 + a_2\sigma^2 + a_3\sigma \quad (2)$$

Substituting dependence (1) of fabric stress in to the function equation (2) then it obtains equation (3) of the strain value as function prediction model of its diameter of the cylindrical model or diameter of body, pressure, fabric thickness and mechanical characteristics of stretch fabric (leading coefficients a_1 , a_2 and a_3).

$$\varepsilon = a_1 \left(\frac{DP}{2d}\right)^3 + a_2 \left(\frac{DP}{2d}\right)^2 + a_3 \left(\frac{DP}{2d}\right) \quad (3)$$

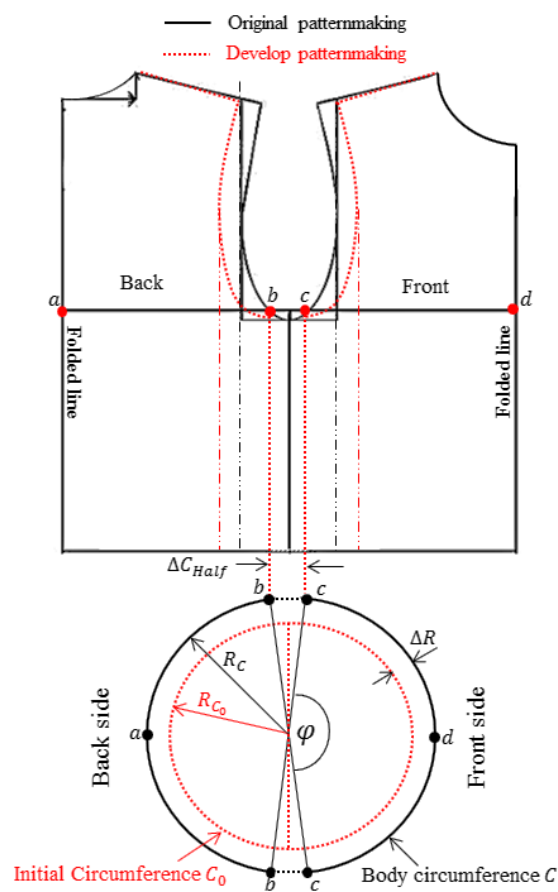


Figure 1. Patternmaking relate to a circle shape

Concerning the basic of patternmaking method, the original size of patternmaking creates from the actual size of body measurement while patternmaking for tight-fitting garment was reduced to the original size of patternmaking as shown in the Figure1. The bodice pattern illustrates the patternmaking in which related to a circle shape for estimating the initial circumference at the bust part.

To develop pattern for tight-fitting garment, the shape of human body was assumed to be similar to cylindrical model and thus the strain values from prediction could be used to calculate the initial circumference (C_0) as given in the following equation:

$$C_0 = \frac{C}{\varepsilon+1} \quad (4)$$

Where C_0 is initial circumference (m), C is body circumference (m) and ε is fabric strain (-).

An initial half T-shirt can be described when $\overline{ab} = \overline{cd}$ and the equation can be re-written as follows:

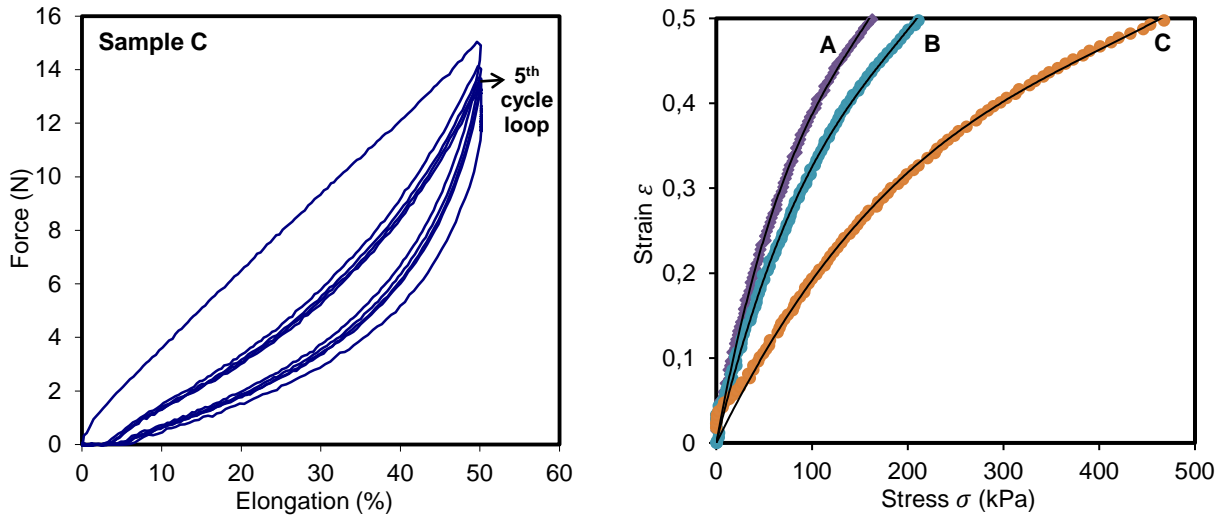
$$(\overline{ab} + \overline{cd}) = \frac{C}{2(\varepsilon+1)} \quad (5)$$

$$\overline{ab} = \overline{cd} = \frac{C}{4(\varepsilon+1)} \quad (6)$$

3. Results and discussion

Mechanical tensile properties

The mechanical characteristic of stretch fabrics presented the relationship between force-elongation until loading at 5th cycle in the Figure 2(a) that the force-elongation curve at the 1st cycle obtained the highest curve of force-elongation then drastically dropped down at the 2nd cycle. Subsequently, the loading curves from 2nd to 5th cycle dropped lightly. Due to this reason, the prediction stress-strain curve will use the data from tensile loading at 5th cycle to predict strains at the magnitude of the fabric stress. As shown in the Figure 2(b), the stress-strain curve of the three fabrics samples were shown, whereas, Table 2 described the equations of how the coefficients values of the 3rd order polynomial fitting-lines of the strain-stress curves 50% elongation the samples used in experiment.



(a) Graph force-elongation curve 5th cycle of sample C (b) The graph characteristics between stress-strain

Figure 2. The mechanical characteristics of elastic knitted fabrics

Table 2. The coefficients of the 3rd order polynomial fitting-lines

Sample	Value				Statistics R-Square
	Intercept	a_1	a_2	a_3	
A	0	6.10E-06	-2.86E-11	6.27162E-17	0.99912
B	0	4.66E-06	-1.71E-11	2.97727E-17	0.99913
C	0	2.30E-06	-4.26E-12	3.46716E-18	0.99908

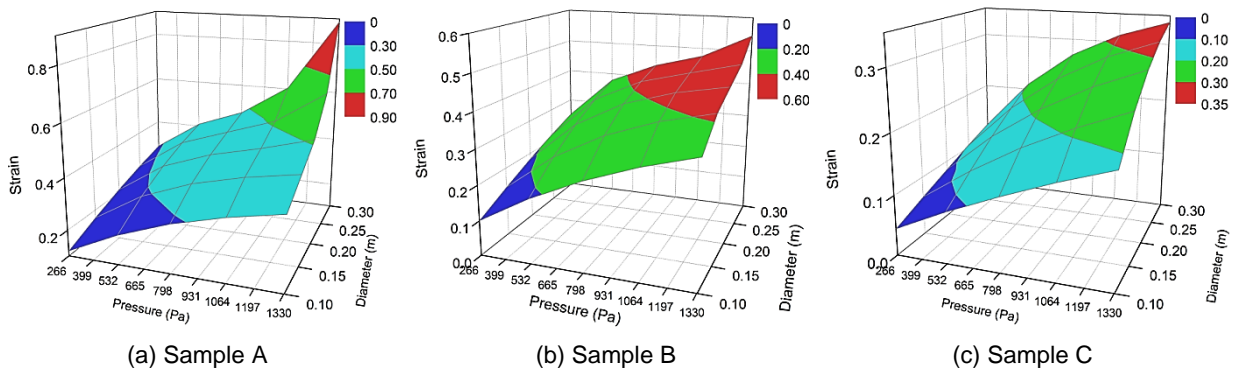
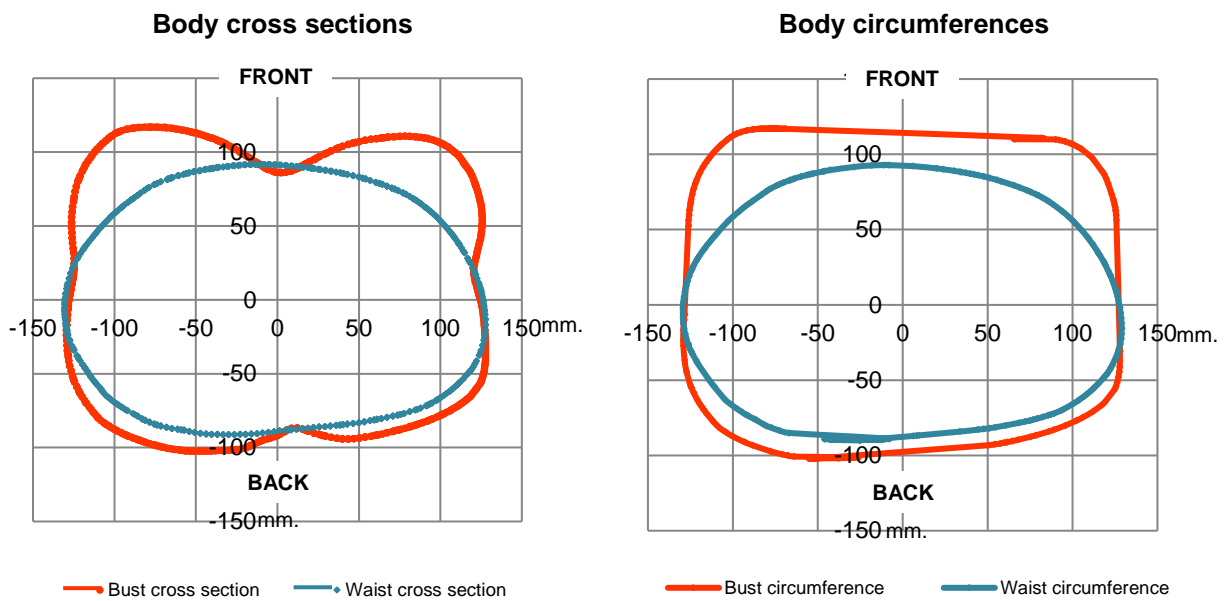


Figure 3. The stretch fabric effect of pressure and diameter of the body on the strain

The analysis of modelling results of the strain value of stretch fabric would be depending on their pressure and diameter of the principle energy by equation (3). The graphs represented the analysis of the strain values which were difference in accordance to their tensile properties and could be found that when making estimation the strain values of the sample C were lowest when compared to other samples under the same condition.

Development for patternmaking method for stretch fabrics

This part of experiment, female mannequin according to European standard sizing system 38 was chosen to perform a 3D body scanning using sense™2 3D scanner for capturing the body measurement. Furthermore, measurement of body circumference using the girth of the convex hall was selected instead of the body cross sections as shown in the Figure 4(a). In the Figure 4(b), circumference line from the contact measuring of the body was processed and simulated by the software was similar to the one using tape measuring method.



(a) Body cross section with different parts

(b) Body circumference with different parts

Figure 4. The graphs of cross sections and circumferences of the body

Results of body circumferences calculation from different part of the body were shown in the figure 4(b). These results could eventually be used for conducting patternmaking while strain values varied from characteristics of stretch fabric and body circumference should be determined initially. In this particular experiment, pressure values applied on the body at 1.15 kPa was used to make prediction of strain values. In table 3, the stress was calculated by applying pressure value, diameter and thickness of the fabric on the modelling equation as shown on the Table 2 in an attempt to predict strain value ranging in different parts of the body.

Table 3. The predicted strain values on the bust and waist parts of the female body

Body part	Circumference C (m)	Diameter D (m)	Pressure P (kPa)	Predicted strain: $\epsilon = a_1 \left(\frac{DP}{2d}\right)^3 + a_2 \left(\frac{DP}{2d}\right)^2 + a_3 \left(\frac{DP}{2d}\right)$		
				$d = 0.00060$ (m)	$d = 0.00061$ (m)	$d = 0.00057$ (m)
				Sample A	Sample B	Sample C
Bust	0.866	0.276	1.15	0.60	0.48	0.31
Waist	0.715	0.228	1.15	0.50	0.45	0.28

It could be found from the results of the strain values that under the same pressure condition at 1.15 kPa, the sample C obtained the lowest strain value at bust 0.31 and waist 0.28, whereas sample A

and B were close to one another in terms of their strain values. In Table 4, strain values were calculated to determine the initial circumference of fabric (C_0) by applying the equation (4). In last column of Table 4, the half width of pattern was calculated by applying equation (6).

Table 4. The prediction the pattern dimensions with different parts of the body under the pressure at 1.15 kPa

Body part	Circumference C (cm)	Initial circumference (cm)			Half width of pattern (cm)		
		$C_0 = \frac{C}{\varepsilon + 1}$			$\overline{ab} = \overline{cd} = \frac{C}{\varepsilon + 1} \times \frac{1}{4} ; (cm)$		
		Sample A	Sample B	Sample C	Sample A	Sample B	Sample C
Bust	86.6	54.18	58.70	66.03	13.54	14.67	16.51
Waist	71.5	47.52	49.36	55.65	11.88	12.34	13.91

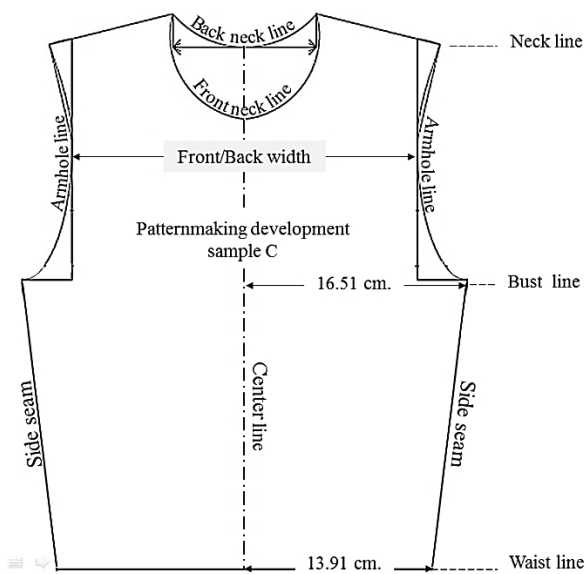


Figure 5. Bodice pattern development of the sample C

According to the results of predicted strain values they were used for calculating the initial size of bodice pattern by the PDS tailor XQ software in which based on Computer-aided Design (CAD) system. This software product was manufactured by a Czech company and it contains a powerful function of patternmaking for elastic fabric. Moreover, it obtain a anthropometric database in order to compute the pattern design parameters and use the regression analysis for generation well-fitting patternmaking of clothing as described by Musilová [21, 22]

The process to producing bodice pattern in this experiment was conduced by applying value of elastic coefficient from the predicted strain and determining pressure at 1.15 kPa. Later on, elastic coefficient parameter was being input into the software and manually selected the data of body measurement. The software would then automatically conducted and processed and led into digital patternmaking as show in the Figure 5.

4. CONCLUSIONS

Through this research work, patternmaking development method based on the induvial of elastic material and the principle energy of three samples with difference of force-elongation curves were introduced. The mathematical model was then used to predict the strain value in order to find out the initial circumference of patternmaking on the body. This research will put its emphasis on the patternmaking development at bust to waist area. In fact, the mentioned area of pattern construction was being related to the cylindrical model and it could be assumed that when applying the theory of interface pressure of thin wall cylinder, the pressure from fabric stretched on the human body would be determined. However, pattern on the upper parts of bust did not relate as the cylindrical model and the fabric would not be able to stretch itself and therefore it was complicated to estimate the strain values. From the mentioned reason, the pattern should be adjusted in relation to the magnitude of the pattern reduction, the proportion and shape of the body measurement. We hope that this method would be guiding and helpful for the patterner in industries to produce the patternmaking under pressure for tight-fitting garment.

ACKNOWLEDGEMENTS

The authors would like to extend sincere appreciation to the department of Clothing Technology, faculty of Textile Engineering, Technical University of Liberec and this work was supported by the Ministry of Education of the Czech Republic within the SGS project no. 21246 on the Technical University of Liberec.

References

1. Kilinc, F., Balci in. (2011). *Improving Comfort in Clothing*. Cambridge,: Woodhead Publishing
2. Liu, Y., Dongsheng, C. (2015). An analysis on EEG power spectrum under pressure of girdle. *International Journal of Clothing Science and Technology*, 27(4), 495-505, .
3. Jariyapunya, N., Musilová, B., Geršák, J., Baheti, S. (2017). The influence of stretch fabric mechanical properties on clothing pressure. *Vlákna a Textil*, 24(2), 43–48.
4. Ziegert, B., Keil, G. (1998). Stretch fabric interaction with action wearables: defining a body contour pattern system. *Clothing and Textile Research Journal*, 6, 55-64.
5. Watkins, P. (2011). Designing with stretch fabrics. *Indian Journal of Fibre & Textile Research*, 36, 366-379.
6. MacRae, B. A., Cotter, J. D., Laing, R. M. (2011). Compression Garments and Exercise:Garment Considerations, *Physiology and Performance*. *Sports Medicine*, 41(10), 815-843.
7. Geršák, J. (2013). *Design of clothing manufacturing processes*. Cambridge, UK: Woodhead publishing series in textile.
8. Voyce, J., Dafiniotis, P., Towlson, S. (2005). *Elastic textile*. In *Textile in sport*. Cambridge, UK: Wood head publications.
9. Gulillaume, M., Stephane, P., Caroline, D., Matthieu, F. (2006). The role of engineering in fatigue reduction during human locomotion - a review. *Sports engineering*, 9, 209-220.
10. Senthilkumar, M., Anbumani, N. (2014). *Dynamics of elastic knitted fabrics for tight fit sportswear*. Germany: LAP LAMBERT Academic Publishing.
11. Lim, N.-Y., NG, S-P., YU, W., Fan, J. (2006). *Innovation and technology of women's intimate apparel*. In *Pressure evaluation of body shapers*. Cambridge, UK: Woodhead publishing limited.
12. Zhao, L., Li, X., Yu, J., Li, C., Li, G. (2017). Compression sleeves design based on Laplace Laws. *J Textile Engineering & Fashion Technology*, 2(2).
13. Kowalski, K., Mielicka, E., Jasinska, I. (2012). Modelling a analysis of the circumferential force and susceptibility of vascular prostheses to internal pressure changes. *Fibres & Textile in Eastern Europe*, 20(3(92)), 87-91.
14. Kowalski, K., Mielicka, E., Kowalski, T. M. (2012). Modelling and designing compression garments with unit pressure assumed for body circumferences of a variable curvature radius. *Fibres & Textile in Eastern Europe*, 20(6A(95)), 98-102.
15. Khaburi, J. A., Dehghani-Sanij, A. A., Nelson, E. A., Hutchinson, J. (2012). Effect of bandage thickness on interface pressure applied by compression bandages. *Medical Engineering & Physics*, 34, 378–385.
16. Chattopadhyay, R., Bera, M. (2017). Prediction of Pressure due to Elastic fabric Tube Following Energy Principle. *Journal of Textile Engineering & Fashion Technology*, 2(5).
17. BS EN 14704-1: Determination of the elasticity of fabrics part 1: Strip tests (2005).
18. Plummer, J. (2013, Jan 21). jeffplummer. Retrieved April 8, 2018, from <http://www.jeffplummer.net/2013/01/introduction-to-math-behind-similarity.html>
19. Hearn, E. (1997). *Mechanics of materials volum1: an introduction to the mechanics of elastic and plastic deformation of solids and structural materials*. Oxford: Butterworth-Heinemann.
20. Bansal, R. (2010). *Strength of Materials*. New Delhi: LAXMI PUBLICATION (P) LTD.
21. Musilová, B., Nemčoková, R. (2013). Implementing Mass Customization into Clothing Production. *Vlákna a textil*, 20(4), 12-19.
22. Musilová, B., Nemčoková, R. (2014). Study of Czech male body proportions and evaluation of men's shirt pattern making methods. *Tekstil ve Konfeksiyon*, 24(4), 399-404.

APPLICATION OF ELECTRIC BASED HEATING IN CLOTHING FOR SENIORS

Antonín Havelka¹, Miroslav Tichý², Radek Soukup³, Ladislav Nagy¹, Michal Martinka¹

¹ Technical university of Liberec, Faculty of Textile Engineering, Department of Clothing Technology, Studentska 2, Liberec, Czech Republic, e-mail: antonin.havelka@tul.cz

² VUB A.S., Na Ostrove 1165, Usti nad Orlici, Czech Republic, e-mail: tichy@vubas.cz

³ University of West Bohemia, Faculty of Electrical Engineering, Department of Technologies and Measurement, Univerzitni 8, Pilsen, Czech Republic, e-mail: rsoukup@ket.zcu.cz

Abstract:

Active integral electronic elements in smart clothes can increase the utility value of the garment and the user's comfort. This article is primarily focuses on the comfort of clothing designed especially for the elderly, or people with impaired thermoregulatory capabilities. The research part is focuses on the possibilities of increasing clothing comfort of application a smart electronic textile element into garments. It deals especially with the possibilities of application of electric heating built directly into clothing for seniors, especially for clothes designed for cold environment. The proposed heating system based on embroidery with using hybrid threads can be use especially in winter clothing, but can also be used for home-use clothing or everywhere it is disadvantageous or inappropriately to increase the ambient temperature. The main goal is to improve physiological comfort and ensure thermal comfort in the winter months. From the textile point of view, it is important to ensure that the integration of the heating structure into the garment in order to fulfil its function as best as possible and allow the normal maintenance of the garment by the user and have no impair to the physiological comfort and other utility properties which are also important for the garment. In the case of seniors, the electronics must contain safety features to prevent tampering and avoid the risk of injury to the user. The textile part must therefore comply with both the textile and maintenance requirements as well as the electrical properties. When using active elements in clothing, we need to address the issue of safety, routine clothing maintenance, battery placement, electronics interconnection, durability and other aspects of textile and electronic character. This paper describes the possibilities of creating heating elements using an embroidery machine and the possibility of their integration into selected types of clothing. A practical example then demonstrates the use of hybrid threads that are applied by embroidering the heating structure directly onto a suitable textile backing, demonstrating their potential for increasing the utility properties of the garment.

Keywords:

Thermoregulation, clothing, comfort, heating, smart textiles.

1. Introduction

With an influence of various factors on the human organism, it is a crucial ensures that a human body should be in a thermal optimum, called thermal comfort [1]. The determination of thermal comfort and its optimization is given considerable attention form a researchers, sellers and companies especially for the younger and middle generation, which is more active than older population. Research is also focused on the relaxing athletes and especially to the top athletes. Scientific research is focuses than mainly on a medical, military and sports. Interest of a clothing manufacturers and their research has

less focusing an older population at this area, because the older people are not for them their typically customers. This group of people is enough big but has a different clothing requirements and also expectation from a clothing comfort.

2. Subject of research

The research part described in this article focuses on the area of a comfort of clothing designed especially for the elderly with the possibility to increasing of garment comfort by using a hybrid textile structure integrated into garment.

2.1. Comfort of clothing for seniors

Thermal comfort, or a thermal well-being, it is the achievement of such thermal ratios, when is a person in balance without any unpleasant feelings as cold, or warm feelings [1-2]. The properties of clothing significantly affect heat transfer and feelings of user. We can conclude that for a good thermal comfort is the most important characteristic the thermal resistance of the garment. The heat resistance of the garment is based on the layering of the material and the air layers between them.

Other properties important for clothing include air permeability, water-vapor permeability, type of a textile structure, resistance to water penetration, resistance to surface wetting, sweating management, etc. and they has to be also consider in a design of clothes [3].

2.2. Specifics of clothing comfort in the age group of seniors - utility of clothing

Elderly and consumers with diseases prefer to buy clothes with high levels of comfort that can meet their physiological, hygienic and health needs. Clothing requirements for seniors are based on physico-mechanical values of garment comfort. Utility value is a set of utility features that meet the demands of clothing in terms of appearance, durability, easy maintenance and user-friendliness. The process of aging affects every living creature. It affects all the tissues of the organism and is characterized by a different speed. This also applies to human skin, which is an extremely important organ that provides contact with the external environment and represents a mirror, respectively is a monitor of both physiological and pathological phenomena outside and within the body. Therefore, it is important to keep the skin at optimum temperature.

3. Experiment – preparing of samples embroidered by using a special hybrid threads for heating

Next text is describing simplified procedure of preparing and embroidering of samples and their basic characteristics.

3.1. A simplified procedure for a creating a draft of embroidery

On the beginning it was necessary to design embroidery pattern suitable for their purpose of use. Proposed embroidery topology was after that transferred to a vector by using SW AutoCAD. Subsequently, these vectors were imported into Tajima program. In this program was carried out their optimization and was prepared program for an automatic embroidery machine TEJT-C1501, on which specimens were have been made.

For embroidering we have used two types of conductive hybrid threads, which were made for this purpose in company VÚB a.s. First hybrid thread contains a Cu/Ag wires a second contains a brass wires (Msx), see table 1 for detailed specification of hybrid thread. Hybrid thread for embroidering was used on the top and on the bottom of embroidery.

Table 1. Basic characteristics of hybrid threads used for embroidering

Type	Yarn fineness [tex]	Composition	Resistance [Ω/m]
Hybrid thread no. 53	50	47 % PESH / 53 % Cu/Ag wire	6.50
Hybrid thread no. 25A	72	31 % PESH / 69 % Msx brass wire	8.90

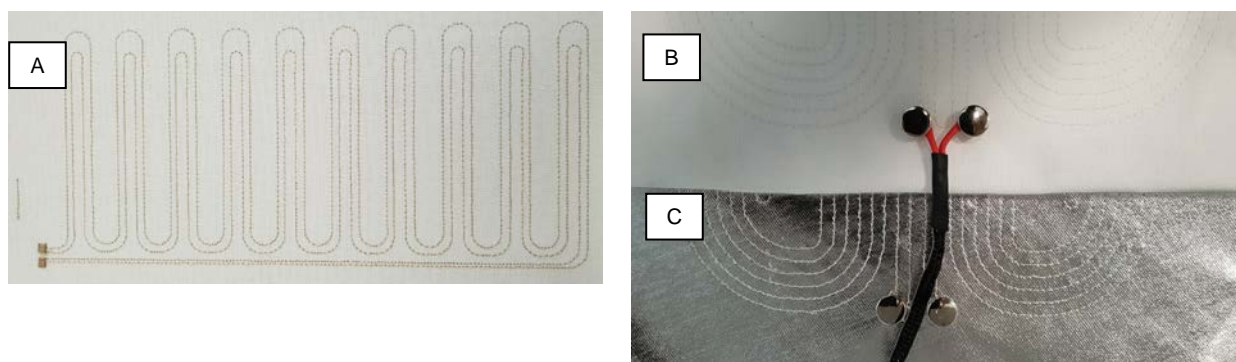
3.2. Preparing, modification and embroidering textile hybrid heating structures

For a real testing were prepare four different type of textile hybrid heating pad. Differences and their basic properties are in the table 2. As a underlying fabric for embroidering was used a canvas and for a special embroidery sample model with knitted fabric with a reflecting coating which should be able to reflect a heat flow to a human body.

Table 2. Realized embroidered textile heating samples and their basic characteristics

Sample (type)	Dimensions of embroidery [mm]	Thread consumption - top + bottom [m]	Electrical resistance of embroideries R [Ω]	Type of used hybrid thread	Underlying material
A1 (Meander)	125 x 283	9.2 + 3.1	5.36	Hybrid thread no. 53	Canvas (PES/Co)
A2 (Meander)	125 x 283	9.2 + 3.1	6.53	Hybrid thread no. 25A	Canvas (PES/Co)
B (Kidney)	190 x 186	12.2 + 4.1	23.56	Hybrid thread no. 53	Canvas (PES/Co)
C (Kidney)	190 x 186	12.2 + 4.1	20.86	Hybrid thread no. 53	Special knitted fabric with a reflecting coating

As is it evident from the table 2 a different type of hybrid thread and different length and shapes of embroidery lead to a variety electrical resistance of embroideries. All these changes lead to on the basis of that to the different heating performance of pads. It has to be consider before next step a proposal of power supply and electronic parts and conductive textile wires which have to be able to manage lead an electric current till 2 amperes. Samples of embroidery A, B, C are showing on the figures 1. Sample A is at the end of the embroidery terminated by a sewing spots, which are ready to application a metal connectors or textile poppers. Samples B, C are connected with metal poppers and wired via textile conductive wire called "Ribbon". It is a conductive textile ribbon, which combines thin metal wires (30 strands) made from Cu with Ag coating with a textile braiding with resistance 0.30 [Ω/m]."


Figure 1. Textile hybrid heating pads, samples B, C are connected with metal poppers and wired via textile conductive wire called "Ribbon"

One of the most important and a difficult part of preparing hybrid textile heating pads was made an improving of automatic embroidery machine which consist with several steps. Basic machine for embroidering is not ready for using a hybrid threads with metal components. List of adaptations which have to be done to reach reasonable quality of embroidery: right size of a needle with titanium or ceramic surface finishing with bigger eye, reduction and normalization friction of a sewing thread, removing the jump change of friction in the sewing thread, adjustment of leading the sewing thread in the machine (reduction of bends), using removable oil to improving a friction.

Inappropriate machine settings or using a wrong type of needle leads to a poor quality of the embroidery, or to violation of sewing thread see figure 2. This leads to a malfunction of the electrical circuit and it is necessary to repeat the process of embroidering.



Figure 2. Violation of sewing hybrid thread in the middle of embroidering process

4. Theory – electrical power in resistive circuits

In physics, power is the rate of doing work, the amount of energy transferred per unit time. The SI unit of power is the watt [W], which is equal to one joule per second [J/s].

In the case of resistive (linear) loads as our textile heating structure, Joule's law can be combined with Ohm's law (see equation 1) to produce alternative expressions for the amount of power that is dissipated and can be expressed by equation 2:

$$U [V] = I [A] \cdot R [\Omega] \quad (1)$$

$$P = dW/dt = U \cdot I = R \cdot I^2 = U^2/R [W] \quad (2)$$

For each type of textile heating structure (heating pad A1, A2, B, C) was according equation 2 calculated theoretical electrical power P^* in watt from known resistance and expectation of voltage on input to circuit. Changes in the internal energy of the wires caused by the passage of the current lead to an increase of their temperature and exchange heat flow between the wires and the surroundings [4].

4.1. Experiment – measuring electrical power in closed resistive circuits based on textile heating structures

Methodology

All types of samples were placed into climate room with standards textile condition where is a temperature 21 ± 1 [°C], relative humidity 60 ± 10 [%]. After acclimatization a heating pad was connected via textiles metal poppers with the laboratory power supply EA-PS 3016-10 B, which is able to precisely set and measure current and voltage at the power source output. Voltage was set step by step (5V, 10V, 12V, 16V) and after 5 minute of stabilization for every step was taken a thermogram and data of a current in the electrical circuit.

4.2. Results

Results with theoretical calculated power and based on the measurement of electrical power from experiment are shown in the table 3.

Table 3. Measured electrical properties and calculated electrical power P in a comparison with theoretical electrical power P*

Sample (type)	Power P [W] (measured value)	Electric current I [A]	Electrical voltage U [V]	Power P* [W] (calculated value)
A1 (Meander)	4.0	0.8	5.0	4.7
A1 (Meander)	16.0	1.6	10.0	18.7
A1 (Meander)	22.8	1.9	12.0	26.9
A2 (Meander)	3.5	0.7	5.0	3.8
A2 (Meander)	15.0	1.5	10.0	15.3
A2 (Meander)	21.6	1.8	12.0	22.1
B (Kidney)	3.0	0.3	10.0	4.2
B (Kidney)	4.8	0.4	12.0	6.1
B (Kidney)	9.6	0.6	16.0	10.9
C (Kidney)	4.0	0.4	10.0	4.8
C (Kidney)	6.0	0.5	12.0	6.9
C (Kidney)	9.6	0.6	16.0	12.3

4.3. Evaluation of an embroidered heating pads made by using a hybrid threads

For a qualitatively evaluation of embroidering process is a good to use a thermography. The following thermograms were taking by using a thermocamera system Flir S60 in a room with climate control where is a temperature 21 +1 [°C], relative humidity 60 +10 [%], wind circulate 1 [m/s]. Pads were set to a maximum heating power see a table 3. On the thermogram see figure 3 is easily to recognize o spot where is a temperature extreme, which can lead in o long time to make circuit breaks and a dysfunction of heating pad.

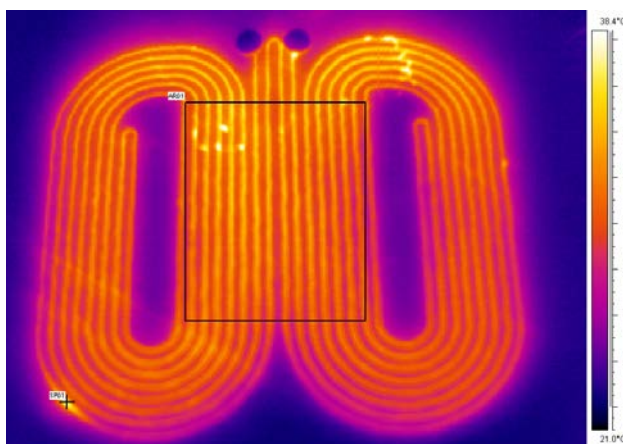


Figure 3. Thermogram of a sample C with an analysis of temperature: Area - AR01: Min. 27.5 °C, Max. 40.3 °C, Avg. 31.1 °C, Spot - SP01: 38.1 °C

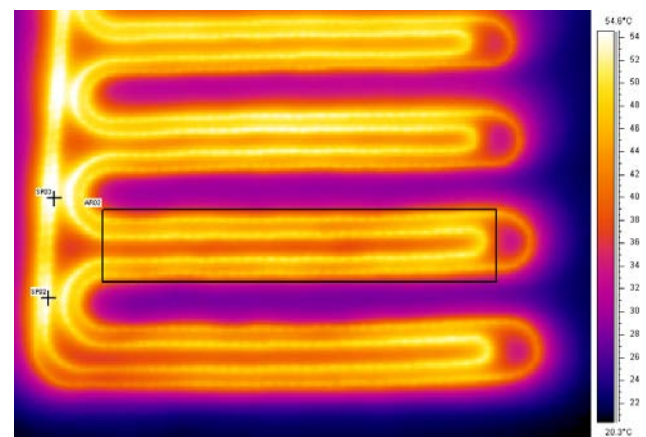


Figure 4. Thermogram of a sample A1 in detail with an analysis of temperature: Area - AR02: Min. 34.0 °C, Max. 52.2 °C, Avg. 45.1 °C, Spots - SP02: 55.0 °C, SP03: 57.1 °C. ($\epsilon = 0.95$ [-], Temp. refl. = 20 [°C])

Thermograms can be also used for a detailed analysis of linking stitch and analysis of flowing of heat direction and spreading in a background material and to the other layers of clothing see figure 4. The heating pad should to be near to the human skin, but also we need to be ensuring that the temperature in contact points does not to exceed 40°C.

Whit this technique we can also visualization of the most critical spots for each part of embroider which are place for connectors to join a power supply or other electronics like a logic board. In this case we used textile poppers for a connection to power supply. This article is not focused on other important parts as electronic parts and power wires or durability.

5. Discussion and Conclusion

Improving of thermal comfort of garment and ensuring a good thermal comfort is important for the older people and for people with an impaired thermoregulation. This can be achieved by using a textile hybrid structure like is a heating pad made by embroidering directly on the surface of a clothing, or as a separated par of textile, which can be inserted into a clothing. This article describes in two parts the procedure for the preparing of embroideries with a special hybrid threads and the evaluation of embroidered heating pads. For a using special hybrid threads with a metal parts to embroidering it is important to make some changes in setting of automatic sewing machine to achieve a good quality of embroidery. Also is important to use a thermography for an analysis to discover problematic spots and improve a technology of sewing means change a needle, lubricate, improve of friction of a thread and so on, or also improve a topology of embroidery. Results from experimental part are promising and mainly hybrid thread with Cu/Ag wires which have better sewing properties than hybrid thread with brass wires is suitable for next research and application as a heating textile structure in smart clothing. The use a technology of embroidering of a heating structure in the garment allows us to make a design of an optimal shape according to the location and type of clothing where will be used.

ACKNOWLEDGEMENT

This work was supported by the Ministry of Industry and Trade of the Czech Republic, Programme Trio - project "Senior Tex - Smart Modular Clothing and Textile Products with Integrated Electronic Microsystems for Improving the Health Care of the Aging Population and Handicap People", reg. no. FV10111.

References

- [1] Hes, L. and Sluka, P. *Introduction to the comfort of textiles (Úvod do komfortu textilií)*. Skriptum. Liberec: Technical university of Liberec, 2005.
- [2] Apurba, D. and Alagirusamy, R. *Science in clothing comfort*. 1st pub. New Delhi : New Delhi Cambridge Oxford: Woodhead Publishing India, 2010. str. 175. ISBN 978-18-456-9789-1.
- [3] TAO, Xiaoming, ed. *Handbook of smart textiles: with 565 figures and 66 tables*. Singapore: SpringerReference, [2015]. ISBN 978-981-4451-44-4.
- [4] Wagner, J. 1989. *Physics: Summary for Textile Faculty (Přehled pro textilní fakultu)*. Liberec: Technical university of Liberec,

PROPERTIES OF NANOADDITIVE MASTERBATCHES FOR ANTIMICROBIAL POLYPROPYLENE FIBRES PREPARATION

Štefan Krivoš¹, Anna Ujhelyiová², Katarína Holcová¹

¹Research Institute for Man-Made Fibres, a. s., Štúrova 2, 05921 Svit, Slovak Republic, tel. 00421 52 7842 184, fax 00421 52 7755 663, krivos@vuchv.sk
Technology in Bratislava, Faculty of Chemical and Food Technology, Institute of Natural and Synthetic Polymers, Radlinského 9, 81237 Bratislava, Slovak Republic, tel. 00421 2 59325578, anna.ujhelyiova@stuba.sk

Abstract:

In the production of standard chemical fibres and textile products, modification of the weight or surface of materials by nanotechnologies is one of the most prospective ways how to ensure special mono and multi-functionally modified fibre properties of clothing and technical textiles. Permanent antimicrobial treatment of the fibre mass of synthetic polymers belongs to the most desired functional modifications of chemical fibres. It involves the use of additional premix with appropriate rheological, colour and processing properties necessary for the preparation of antimicrobial modified PP fibres. This article presents the results of our study on the influence of two types of nanoadditives (calcium carbonate (A) and calcium carbonate modified with antimicrobial active ingredient (AMB-A) in combination with various dispersing systems) on rheological and processing properties of PP polypropylene nanoadditive masterbatches. The obtained experimental results are evaluated according to suitability of the properties of prepared nanoadditive premixes for the preparation of antimicrobial nanocomposite PP fibres, in which the impact of additivation on their coloristic properties and antimicrobial activity was studied.

Key words:

antimicrobial nanoadditive, PP masterbatch, rheology, color, processing and antimicrobial properties

1. Introduction

The global production of textile fibres increased by 1.7% in 2016 to 95.3 million tonnes, with an increase in chemical fibres production by 2.8% to 70.4 million tonnes and a decrease in natural fibres production by 1.4% to 24.9 million tonnes. The production of polypropylene (PP) fibres increased by 3.0% in 2016 to 5.5 million tonnes (excluding spunbonds, meltblowns and tapes) [1]. The textile market is expected in the future to reach 106 million tonnes in 2020 and almost 139 million tonnes in 2030. This translates to a further increase in the volume of the global production of man-made fibres to 75 million tonnes in 2020, at an average annual increase of 4% [2, 3].

Asia holds a dominant position in the global production of standard man-made fibres, having held an 88.5% share of production in 2016 [1]. This dictates the need to sophisticate of European fibre and textile products in today's highly competitive environment. It particularly concerns the development of special, modified, mono- and multi-functional active fibres and textiles necessarily characterized by their high functionality, diversification, flexibility and highly effective and environmentally acceptable production [4, 5]. The most promising way to ensure sophisticated properties of textiles is modify their mass or surface using nanotechnologies. The most important nanotechnological procedures in the area of textiles include nano-treatment of their surface and the addition of nanoparticles to fibres during their extrusion (nanocomposite fibres). Using such procedures, mono- or multi-functional properties of fibres

can be achieved even at low concentrations of nanoadditives, which is also very beneficial in economic terms [5, 6].

Permanent functional modifications of chemical fibres are mainly achieved by adding a functional additive masterbatch to the basic polymer during the spinning process. The incorporation of an additive into the PP fibre mass is thus always preceded by the preparation of a functional additive masterbatch with PP carrier and an appropriate dispersing system, which ensures a high degree of dispersion of the modifier in the fibre mass. In addition, the masterbatch must have appropriate rheological and processing properties (i.e. it should not reduce the technological stability of fibre preparation processes) and should not significantly affect the colour properties of fibres. A masterbatch is added to main PP stream in a pre-defined volume during the spinning process. The mixture is then melted, homogenized and spun into the form of modified PP fibres.

Functional modifications of chemical fibres ensuring the protective, hygienic and comfort properties of textiles are the most desired in the textile industry. This group mainly includes the permanent antimicrobial (AMB) modification of fibres [7-16]. Today's market offers AMB additives with an average particle size in the micro range ($d_{50} = 2-4 \mu\text{m}$), or polymer dispersions of those additives [17-21]. Of AMB nanoadditives only metal Ag nanoparticles are known, and their applications recently encounter environmental obstacles. It is assumed that using nanoadditive as a carrier of an AMB active ingredient with a much higher specific surface than current microadditives will result in the more even spread of AMB active ingredient on the surface of the inorganic carrier. At the same time, AMB efficiency will be achieved at even proportionally lower concentrations compared with microadditives, with positive impact on technical as well as economic aspects of production of AMB fibres modified in the mass. This article presents the results of the study of the influence of two types of nanoadditives (nanocalcium carbonate and nanocalcium carbonate modified by an AMB active ingredient) and various dispersing systems on rheological, colour and processing properties and antimicrobial activity of PP nanoadditive masterbatches. The obtained experimental results are evaluated in terms of the suitability of the properties of prepared nanoadditive masterbatches for the process of antimicrobial nanocomposite PP fibre preparation.

2. Experimental

2.1. Materials

The following materials were used to prepare nanoadditive PP masterbatch samples (Table 1.):

- Powdered isotactic PP (LyondellBasell Company) with melt flow index (MFI) 10.2 g / 10 min.
- Inorganic nanoadditive: **A** – ultrafine precipitated calcium carbonate with mean particle size of 45 nm and a specific surface area of 120 m².g⁻¹ (Cales de Llierca, S.A.); **AMB-A** – ultrafine precipitated calcium carbonate with mean particle size of 45 nm and a specific surface area of 120 m².g⁻¹ modified by antimicrobial active ingredient (VÚTCH-CHEMITEX spol.sro).
- Dispersants: D1 – **mixture of glycols and aliphatic amines** (Clariant Corp);
D2 – stearic acid and poly ethylene glycol condensation product (Clariant Corp.).

Table 1. Composition of prepared PP masterbatches

Samples	PP		Nanoadditive		Dispersing system	
	Concentration [wt.%]	Type	Concentration [wt.%]	Type	Concentration [wt.%]	
PP	100.0	-	-	-	-	
I	86.0	A	10.0	D1 + D2	2.0 + 2.0	
II	86.0	A	10.0	D1	4.0	
III	86.0	AMB-A	10.0	D1 + D2	3.0 + 1.0	
IV	80.0	AMB-A	15.0	D1 + D2	3.0 + 2.0	

2.2. Preparation of PP masterbatches

PP masterbatches with a 10.0 wt.% nanoadditive concentration (I ; II ; III ; IV -- Table 1.) were prepared from the premix of powdered PP, nanoadditive, and dispersing system on a Werner-Pfleiderer ZDSK 28 twin-screw extruder with the diameter of 28 mm. The preparation process was performed at the constant spindle rotation speed of 250 min⁻¹ and a constant extrusion temperature of 220 ° C.

2.3. Methods

Rheological properties

Rheological properties were measured using a Göttfert RG20 capillary rheometer at temperatures of 230, 240 and 250 °C. A capillari with a circular diameter of L/D = 30/1 in the range of shear rates from 180 to 4500 s⁻¹ was used, with the masterbatch pre-heated over a period of 5 minutes. Based on various piston shifting rates and the measurement of the pressure gradient, uncorrected dependences of shear stress and viscosity on the shear rate for the evaluated masterbatches were generated to determine a flow consistency index (K) and a flow behaviour index (n), applying the Ostwald de Waele power law (Equation 1):

$$\tau = K \cdot D^n \quad (1)$$

where τ is shear stress and D is shear rate.

All masterbatches are polymer materials with a non-Newtonian behaviour. All measured rheological parameters were thus corrected using the Rabinowitsch correction [22].

An Arrhenius-type equation was used for the calculation of the flow activation energy of masterbatches (Equation 2):

$$\eta = A \cdot e^{E/RT} \quad (2)$$

where η represents absolute viscosity, R represents the gas constant, T represents absolute temperature and E represents flow activation energy. Viscosity was determined at three temperatures: 230, 240 and 250 °C, while the viscosity and flow activation energy of masterbatches were evaluated at shear rates of 500 s⁻¹ and 1000 s⁻¹.

Colour properties

The colour properties of drawn PP fibres with a fineness of 3.0 dtex and nanoadditive concentration of 0.1 – 0.5 wt.% were measured on a Hunterlab UltraScan device under the following conditions: lighting D65 – daylight with a temperature of 6500 K, observer 10°, color space CIELAB, CIELCh, Yxy. The following coloristic properties were evaluated:

L^* (CIELAB) D65 10° color gradient light to dark ,
 a^* (CIELAB) D65 10° - color gradient red to green,
 b^* (CIELAB) D65 10° - color gradient yellow to blue,
 WICIE – whiteness index,
 YIE-313/10 – yellowness index.

Processing properties

The MFI of masterbatches was evaluated using a Dynisco Kayness capillary rheo-viscometer according to Standard STN EN ISO 1133 Plastics: Determination of melt flow index and melt volume flow index of thermoplastic melts.

The parameter filterability was evaluated using a filtration single-screw extruder with a screw diameter of 25 mm and pore density of the filtration sieve of 16000 pores per cm². The filterability of the dispersion (F) is expressed as ratio of an increment of the pressure (Δp) on the filter to a weight unit of the filtrate (m) at the definite filtration conditions when:

$$F = \Delta p / m \quad (3)$$

Antimicrobial activity

Evaluation of the antimicrobial efficiency on the drawn modified PP fibres with a fineness of 3.0 dtex and nanoadditive concentration of 0.5 wt.% was performed according to AATCC 100:2015 method on Escherichia coli CCM bacterium.

3. Results and discussion

Rheological properties

The appropriate rheological behaviour of a masterbatch melt is an important precondition for its use in the preparation of fibres. The results obtained through our study of the effect of the types of inorganic nanoadditives A and AMB-A with the evaluated dispersing systems (Table 1) on the basic rheological characteristics of the melts of 10.0 wt.% PP masterbatches at temperatures of 230, 240 and 250 °C are presented in Tables 2 and 3.

Table 2. Viscosities (η) at shear rate (D) of PP and prepared PP masterbatches determined from flow curves corrected using the Rabinowitsch correction

Sample	η [Pas]					
	230 [°C]		240 [°C]		250 [°C]	
	$D = 500$ [s ⁻¹]	$D = 1000$ [s ⁻¹]	$D = 500$ [s ⁻¹]	$D = 1000$ [s ⁻¹]	$D = 500$ [s ⁻¹]	$D = 1000$ [s ⁻¹]
PP	177.8	116.4	169.9	112.5	157.1	104.9
I	123.9	79.5	118.3	75.7	107.0	69.2
II	145.5	91.1	132.3	83.7	120.1	76.2
III	133.6	73.9	124.7	67.6	117.2	62.1
IV	161.6	103.7	141.5	91.2	131.0	85.2

Table 3. Rheological parameters (K , n) and activation energies (E_A) for viscous flow of PP and prepared PP masterbatches determined from flow curves corrected by Rabinowitsch correction

Sample	230 [°C]		240 [°C]		250 [°C]		E_A [kJ.mol ⁻¹]	
	K	n	K	n	K	N	$D = 500$ [s ⁻¹]	$D = 1000$ [s ⁻¹]
PP	7924	0.389	6855	0.405	5884	0.417	13.5	11.4
I	7126	0.346	6008	0.361	5537	0.362	16,7	15,5
II	9695	0.324	8013	0.340	7092	0.344	20,6	16,8
III	6143	0.384	5355	0.395	4529	0.412	14,3	19,0
IV	8627	0.360	7231	0.367	6214	0.379	22,0	21,5

All prepared PP nanoadditives have rheological properties suitable for preparation of nanocomposite PP fibres. The most suitable of all is the premix III with the nanoadditive type AMB-A and dispersing system 3%D1 + 1%D2. Its viscosity is lower than that of PP and Newtonian power law model characteristics are similar to the additivated PP mass used in the preparation of PP fibres. Different rheological characteristics of sample IV melt are caused mainly by the increase in the concentration of AMB-A up to 15%. However, even with these characteristics, masterbatch IV is suitable for antimicrobial additivation of PP fibres.

Functional properties of PP masterbatch

Appropriate processing properties present the third important precondition for the application of PP nanoadditive in PP nanocomposite fibre preparation. The results of the processing properties of prepared PP premixes with inorganic nanoadditives A and AMB-A and dispersing systems used are presented in Table 4.

Table 4. Processing properties: melt flow index (MFI), viscosity (η), filterability (F) and associated variation coefficients (CVX) of prepared PP masterbatches (a) 230 °C/2.16 kg ($\tau = 19500$ Pa)

Sample	MFI [g/10 min] ^{a)}	CV _{MFI} [%]	η [Pa.s] ^{a)}	CV _{η} [%]	F [MPa.kg ⁻¹]
PP	10.2	2.2	797.2	2.1	-
I	13.8	2.6	604.9	2.6	92
II	15.4	2.7	557.0	2.7	157
III	11.4	2.3	728.5	2.3	94
IV	9.2	4.3	918.1	4.3	184

All prepared PP nanoadditive masterbatches have suitable rheological processing properties for the preparation of nanocomposite PP fibres. The low filterability of these masterbatches shows the high degree of dispersion of the nanoadditive in the PP matrix. Their use will have no negative effect on the technological stability of the fibre preparation process.

Colour properties

The influence of PP nanoadditive premixes on colour properties of additivated PP fibres is another important factor influencing their application in the preparation of PP nanocomposite fibres.

The values of colour properties and composition of PP fibres with the fineness of 3.0 dtex are presented in in Table 5.

Table 5. Composition and colour properties of pure PP and nanocomposite PP fibres

Nanoadditive		Dispersing system		L*	a*	b*	WICIE	YIE-313/10
Type	Concentration [wt.%]	Type	Concentration [wt.%]					
-	-	-	-	94.18	-0.32	-0.08	86.04	-0.41
A	0.10	D1+D2	0.02 + 0.02	93.54	-0.75	1.14	78.94	1.63
A	0.50	D1+D2	0.10 + 0.10	94.29	-2.02	5.95	58.61	9.66
A	0.10	D1	0.04	94.03	-0.44	1.54	78.28	2.64
A	0.50	D1	0.20	93.87	-0.76	3.66	68.15	6.42
AMB-A	0.10	D1+D2	0.03 + 0.01	93.77	-0.27	0.24	83.63	0.26
AMB-A	0.50	D1+D2	0.15 + 0.05	92.11	-0.06	1.53	73.83	2.97
AMB-A	0.10	D1+D2	0.03 + 0.02	94.53	-0.31	0.60	83.77	0.92
AMB-A	0.50	D1+D2	0.15 + 0.10	90.99	-0.66	1.82	69.87	3.09

In terms of colour properties, the premixes III and IV with the nanoadditive AMB-A and dispersing systems D1+D2 are the most suitable for preparation of nanocomposite PP fibres. Their colour properties are practically comparable to colour properties of pure PP fibres.

Antimicrobial activity of PP fibres

Antimicrobial activity is a major functional property in the application of PP nanoadditive premix in the process of nanocomposite AMB PP fibre preparation. The effect of inorganic nanoadditives A and AMB-A on antimicrobial activity of nanocomposite PP fibres with the fineness of 3.0 dtex and nanoadditive concentration of 0.5 wt.% is presented in the Table 6.

Table 6. Composition and antimicrobial activity of pure PP and nanocomposite PP fibres

Nanoadditive		Dispersing system		Antimicrobial activity (AMA) – determined bacterial reduction [%]
Type	Concentration [wt.%]	Type	Concentration [wt.%]	
-	-	-	-	None
A	0.50	D1 + D2	0.10 + 0.10	None
A	0.50	D1	0.20	None
AMB-A	0.50	D1 + D2	0.15 + 0.05	99.6
AMB-A	0.50	D1 + D2	0.15 + 0.10	99.3

The results in Table 6 show that pure PP fibres as well as nanocomposite PP fibres containing 0.5 wt.% of nanoadditive type A show no antimicrobial activity. On the contrary, nanocomposite PP fibres containing 0.5 wt.% of nanoadditive type AMB-A prepared using PP masterbatch III and IV show high antimicrobial activity with the bacterial reduction reaching 99%, which is a bactericidal activity.

4. CONCLUSIONS

Permanent AMB modification of PP fibres is achieved mainly by adding the main AMB additive to base PP during the spinning process. At the same time, the premix must have all the necessary rheological, processing and colour properties with antimicrobial activity. The results presented in this document show that all of the above stated preconditions were met with PP nanoadditive masterbatches III and IV in combination with the nanoadditive AMB-A (calcium carbonate modified by active antimicrobial ingredient) and dispersing systems D1+D2 (D1 – mixture of glycols and aliphatic amines; D2 – poly ethylene glycol condensation product). Based on these observations it can be stated that PP nanoadditive masterbatches III and IV are suitable for the preparation of antimicrobial nanocomposite PP fibres with bactericidal activity. To reach bacteriostatic level of antimicrobial activity, it is possible to decrease the concentration of antimicrobial additive AMB-A in PP fibres below the level of 0.5 wt.%.

ACKNOWLEDGEMENT

This work was supported by the Slovak Research and Development Agency under the contract No. APVV-15-0016.

References

1. An. (2017). *Global fiber production. Chemical Fibers International*, 67(4), 195-197.
2. Engelhardt, A. (2013). *Analysis of per capita fiber consumption. International Fiber Journal*, 27(5), 4-8.
3. An. (2013). *Man-made fiber production 2020. Chemical Fibers International*, 63(1), 20.
4. Purvis, C. (2010). *Challenges in the global man-made fibers market. Proceedings of 49th Dornbirn Man-Made Fibers Congress - Congress-Guide, Dornbirn, 2010*, 48.
5. De Schrijver, I., Eufinger, K., Van Neste, M., Ruys, L. (2009). *Nanotechnology in demanding textile applications, Proceedings of 48th Dornbirn Man-Made Fibers Congress - Congress-Guide, Dornbirn, 2009*, 63.
6. Sezen, M. (2009). *Nanotechnology and nanotextiles: technologies, markets, economics and future trends, Proceedings of 48th Dornbirn Man-Made Fibers Congress - Congress-Guide, Dornbirn, 2009*, 66.
7. Hongbin, L., Dan, S., Wang, Y., Feng, Ch. (2016). *Preparation and properties of silver-loaded chitosan-based antibacterial yarn. Chemical Fibers International*, 66(2), 84-85.

8. Cox, R., Mukherjee, A. (2016). *Antimicrobial Fibers – Technical Design and Performance Challenges*. *International Fiber Journal* 30(5), 29-31.
9. Gerhardt, A. (2016). *Antimicrobial Textiles – Optimizing for Performance, Safety and Efficacy*. *International Fiber Journal* 30(5), 14-19.
10. Espana, M. (2015). *New functional additive*. *Man-Made Fiber Year Book 2015*, 65, 73-75.
11. Greenfield, R.H. (2014). *Antimicrobial fabrics aim to help prevent healthcare associated infections*. *International Fiber Journal* 28(6), 14-17.
12. Kellie, G. (2013). *What does the nonwovens industry expect from the man-made fiber producers ?*, *Man-Made Fiber Year Book 2013*, 64, 71-75.
13. An. (2013). *New masterbatches for nonwovens*. *Man-Made Fiber Year Book 2013*, 64, 77.
14. An. (2013). *Hollow fiber with bacteriostatic properties*. *Chemical Fibers International*, 63(3), 132.
15. An. (2013). *Antimicrobial finishing of light-colored synthetic yarns and fibers*. *Chemical Fibers International*, 63(3), 136.
16. Henry, M. (2012). *Nanoscale silver – the next wave in smart textiles technologies*. *International fiber journal*, 26(6), 16-19.
17. A. Schulman [online] [accessed June 15, 2017]. Available on World Wide Web: <www.aschulman.com>.
18. Clariant [online] [accessed June 15, 2017]. Available on World Wide Web: <www.clariant.com/en/>.
19. BASF. *We create chemistry* [online] [accessed June 15, 2017]. Available on World Wide Web: <www.basf.com>.
20. Ciba Geigy. *Plastics* [online] [accessed June 15, 2017]. Available on World Wide Web: <<http://cibasc.com/plastics/>>.
21. Trovotech, *functional inorganic additives* [online] [accessed June 15, 2017]. Available on World Wide Web: <www.trovotech.com>.
22. Osswald, T. A., Rudolph, N. (2013). *Polymer rheology. Fundamentals and applications*. Carl Hanser (Munich), 198.

THE IMPACT OF STORAGE TIME ON THERMAL PROPERTIES OF PP/QA FIBERS

Mária Gavendová¹, Vladimíra Krmelová^{1*}, Tomáš Zatroch^{1,2}, Bibiana Bizubová^{1,2},
Michal Kleščík^{1,2}, Katarína Moricová¹

¹Faculty of Industrial Technologies, Trenčín University of Alexander Dubček, I. Krasku 491/30, 020 01 Púchov, Slovak Republic

²Chemosvit Fibrochem, a.s., Štúrova 101, 059 21 Svit, Slovak Republic

*corresponding author e-mail: vladimira.krmelova@fpt.tnuni.sk

Abstract:

Five samples of pre-oriented polypropylene (PP) fibers were prepared containing 0.5; 1; 1.5; 2 and 2.5 wt. % of organic pigment quinacridone (QA). Organic pigments commonly used for the coloration of PP fibers exhibit nucleating ability toward polypropylene crystallization. Pre-oriented PP/QA fibers were produced by melt spinning technique at lower take-up velocities as an intermediate for DTY (draw-textured yarn) or flat intermingled yarn mainly for textile applications. Pre-oriented PP/QA fibers exhibit change in morphology during storage time between spinning and drawing or draw-texturing. Differential scanning calorimetry (DSC) was used for evaluation of morphology of PP fibers. Change in crystallinity of PP/QA fibers depending on storage time was evaluated by melting enthalpy. The melting and crystallization temperatures as well as the crystallization enthalpy were evaluated, too. The measured values of the above mentioned properties were compared with parameters of non-modified PP fiber prepared under same technological conditions. The results show that different QA pigment content in PP fibers increased crystallization temperature by ~ 10 °C, but doesn't change crystallinity significantly in the concentration range used. Storage time of PP/QA fibers at laboratory conditions has not significant influence on their thermal properties in contrast PP/QA fibers tested immediately after manufacture. The basic mechanical properties of PP/QA fibers were presented, too.

Key words:

polypropylene fibers, pigments, thermal properties, mechanical properties, storage time

1. Introduction

Polypropylene is the most commonly used polyolefin polymer and comprises near about 8.5 % of all textile raw material produced worldwide. It is one of the rapidly growing synthetic fibers and fourth fastest growing synthetic fiber. In 2014 the global production for polypropylene fiber was around 6 million metric tons [1].

Historically, in the textile and fiber industry, polypropylene (PP) is commonly known to be used for bulk continuous filaments (BCF) for carpets and nonwovens for disposable diapers. However the low specific gravity and minuscule water absorption of PP appear to closely fit the needs of the apparel market. Indeed, various types of textured and flat PP fibers, much finer than above mentioned BCF, are currently used in wide range of functional sport garments such as apparel for hikers and mountaineers, apparel for winter sports, socks etc. Since the aliphatic/olefinic nature of PP does not allow the use of standard methods for surface dyeing of PP fibers which is necessary for their commercial attractiveness, PP is mixed with pigments prior to spinning [2].

It is expected that pigments in the fibers have a big influence on their structure. According to research pigments affect the structure of fibers on crystal and lamellar level [3, 4].

The structure of fibers is formed during solidification and crystallization of extruded polymer melt streams shortly after passing through the spinneret. At low take-up speeds applied tensile stress is low and crystallization is dominated by lower cooling rates results in monoclinic α crystals, the most common and stable crystalline form of PP. At take-up velocities used in industrial PP fiber production resulting tensile stress and increased cooling rates result in formation of mesophase, which is described as an intermediate between crystalline and amorphous phase with parallel helical polymer chains with large amount of disorder in lateral packing [5]. The complex crystalline β phase is formed only at specific conditions [6] or in case of fibers with the presence of β nucleating agents in the polymer melt extruded at appropriately selected spinning parameters [7].

This paper deals with evaluation of influence of different content of quinacridone (QA) on the thermal properties of PP/QA fibers in dependence on storage time. QA was primary used as a pigment, but is also known as very good nucleating agent for polypropylene. It was observed that in the presence of quinacridone in crystallization of PP a high amount of β -modification was achieved. Acting of pigments in PP fibers as nucleating agent provide a foreign surface and reduce the free energy of formation of a new polymer nucleus. Result of this is an increasing of crystallization temperature and enhancement of the crystallization rate [3]. The mechanical properties of prepared PP/QA fibers compared with parameters of reference PP fiber were evaluated, too.

2. Experimental

2.1. Materials

The following materials were used for preparation PP and PP/QA fibers:

Polypropylene (HT 2511) with melt flow index 25 g/10 min, in pellets form produced by Slovnaft a.s., Bratislava, Slovak Republic,

Polypropylene (Moplen HF 501N) with melt flow index 10 g/10 min, in powder form produced by Lyondellbasell, Tarragona, Spain,

Stantex S 6898: spinning oil produced by Pulcra Chemicals, Gerestried, Germany,

Quinacridone (Pigment Violet 19, figure 1) in powder form produced by Clariant, Basel, Switzerland,

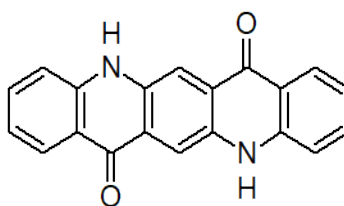


Figure 1. Molecular Structure of Quinacridone

Honeywell A-C® 6A: low density polyethylene (LDPE) homopolymer wax in a powder form used as dispersant produced by Honeywell, New Jersey, United States.

2.2. Fiber preparation

The PP pre-oriented fibers (POY) with different concentrations of QA (0.5; 1; 1.5; 2 and 2.5 wt. %) and a sample of non-dyed virgin PP POY as a reference for evaluation of influence of QA concentration were prepared in the company Chemosvit, Fibrochem a. s. (Svit, Slovakia) as intermediate products for further drawing and texturing operations. QA masterbatches were prepared using 12 % of polyethylene wax based dispersant (Honeywell A-C® 6A) and polypropylene (Moplen HF 501N) and

homogenized with subsequent peletization using a ZSK-25 extruder and peletizer (L/d=44). For each sample a mechanic mixture of masterbatch and granulated isotactic PP was prepared. Samples were spun using a laboratory scale spinning line with one spinneret. The speed of the metering pump was calibrated using pure PP to achieve final fineness of 140 dtex. Fineness of spun fibers was determined by determination of weight of 100 m of fiber wound by precise winder. The winding speed, spinning temperature, the temperature and flow of cooling air, speed of metering pump and flow of spin finish were kept constant and the melt pressure in the spinneret was monitored. A single spinneret with 50 orifices with diameter 0.35 mm was used. For testing purposes the PP/QA fibers were stored at laboratory conditions during 3 months.

Spinning conditions:

Spinneret temperature:	260 °C	Drawing speed:	1040 m/min
Number of orifices:	50	Metering pump speed:	7.80 rpm
Diameter of orifice:	0.35 mm	Cooling air temperature:	18 °C
Take-up speed:	1000 m/min	Cooling air velocity:	0.4 m/s

2.3. Methods used

The DSC studies were carried out using the TGA/DSC 2 (HT/1100) STARe System (Mettler Toledo) according to STN EN ISO 3146 [8]. The PP/QA samples were prepared by cutting to very small stripes of approximately 30 mg weight and pressed into ceramics crucibles of volume 150 µl. Subsequently they were heated to 250 °C at a rate of 10 °C/min in nitrogen atmosphere. Thus, a melting endotherm of sample with melting temperature (T_m) and melting enthalpy (ΔH_m) were obtained.

Then the sample was held at 250 °C for 5 min and cooled to temperature 30 °C at a cooling rate of 10 °C per minute and the crystallization exotherm with the crystallization temperature (T_c) and crystallization enthalpy (ΔH_c) were obtained [9].

In DSC, the crystallization characteristics are studied from the heat flows associated with corresponding transitions as a function of temperature. The crystallinity X_c [%] of the samples was calculated using following equation [10]:

$$X_c = \Delta H_m / \Delta H_m^+ \cdot 100$$

where ΔH_m is the melting enthalpy of the tested fiber, ΔH_m^+ is the extrapolated value of enthalpy corresponding to 100 % crystalline PP, which was obtained from literature as $\Delta H_m^+ = 198.11$ J/g [10]. The measuring was repeated every 14 days until 3 months.

The mechanical properties of PP and PP/QA samples were measured using Textechno Statimat CU tensile testing machine with a gauge length of 50 mm and deformation speed of 250 mm/min. The average of at least 10 individual measurements was used for each fiber. The mechanical characteristics (tenacity at break, elongation at break) were determined according to STN EN ISO 2062 [11].

3. Results and discussion

The selected results from DSC investigation are summarized in the tables 1–3. Table 1 summarizes the results from melting and crystallization process of PP/QA fibers and reference PP fiber immediately after manufacture, such as onset temperature (T_o), melting temperature (T_m), crystallization temperature (T_c) and crystallinity (X_c). The crystallinity of reference PP fiber was 40.52 %. The increasing content of QA in PP fibers resulted in the reduction of crystallinity and did not affect to the melting temperature (~ 170 °C). Figure 2 shows the DSC melting curves of reference PP and PP containing the quinacridone pigment (PP/QA). However, as seen on DSC crystallization

curves (figure 3), the exothermic peaks of PP/QA fibers are shifted to higher temperature in contrast of reference PP fiber. For reference PP fiber the crystallization starts at 120.43 °C. An exothermic peak representing the crystallization temperature occurs at 116.78 °C. For PP/QA fibers the peak occurs at higher crystallization temperatures of 125.56 – 127.46 °C. The increase of the T_c observed for quinacridone is very high and comparable with the increase of the T_c observed for effective nucleating agents [3]. However, differences in the crystallization temperature between fibers containing different concentrations of QA (0.5 – 2.5 wt. %) are insignificant. Therefore it is necessary to examine the interval 0.0 – 0.5 wt. % QA in PP fiber in the future. As the processes of spinning and draw texturing are carried out at different speeds, they cannot be made in one step continuous process and thus a period of storage of spun yarn before drawing and texturing is inevitable and change in quality during this time represents a disadvantage of the two step process [2, 12]. Pre-oriented PP/QA fibers exhibit change in morphology during storage, observation of which was the purpose of this research.

Table 1. Thermal properties of pre-oriented PP/QA fibers immediately after manufacture

Content of QA [wt. %]	Melting			Crystallization			Crystallinity X_c [%]
	T_o [°C]	T_m [°C]	ΔH_m [J.g ⁻¹]	T_o [°C]	T_c [°C]	ΔH_c [J.g ⁻¹]	
0.5	150.89	171.50	69.16	128.99	125.56	81.10	34.91
1.0	150.73	169.67	71.11	129.83	126.47	78.34	35.90
1.5	150.76	169.92	67.02	130.24	126.95	78.65	33.83
2.0	151.82	169.90	71.07	130.41	127.07	79.39	35.87
2.5	151.36	170.18	66.24	130.87	127.46	80.51	33.44
PP	152.03	170.48	80.27	120,43	116.78	80.21	40.52

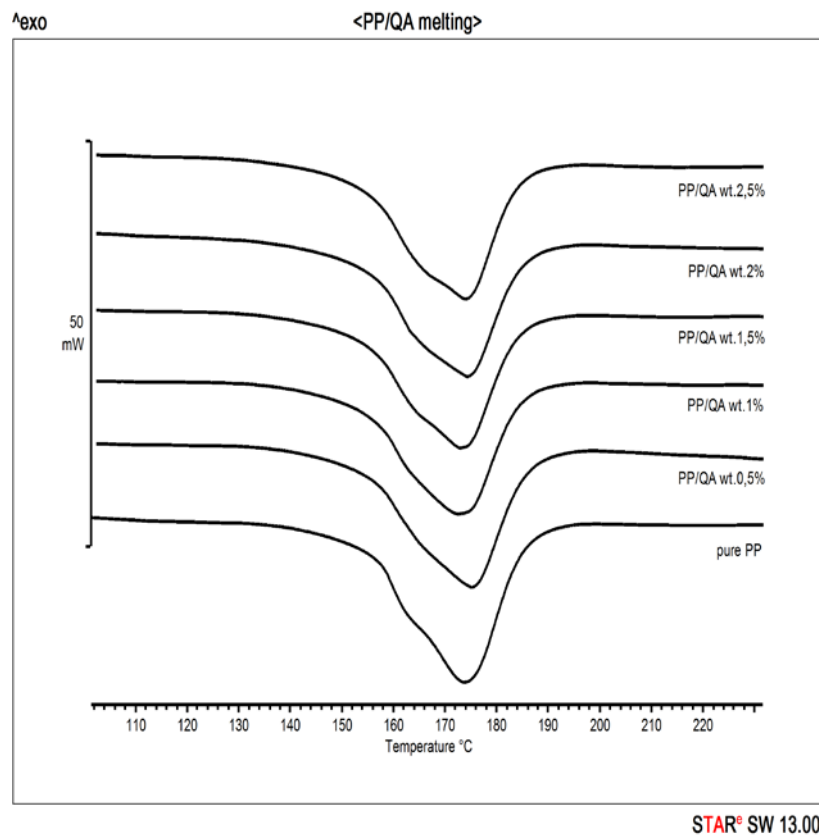


Figure 2. Melting curves of the PP/QA fibers and reference PP fiber

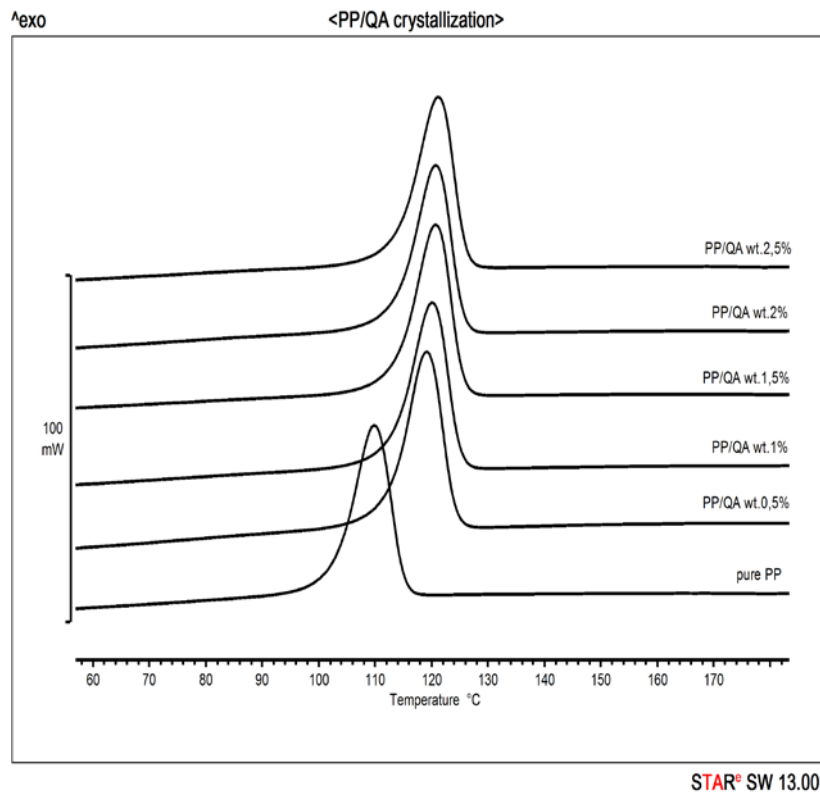


Figure 3. Crystallization curves of the PP/QA fibers and reference PP fiber

In table 2 there are DSC results of PP/QA fibers after 14 days of storage. The crystallinity of pre-oriented PP/QA fibers in contrast of reference PP fiber during storage time is presented in table 3. Changes in crystallinity of PP/QA fibers during storage in contrast PP/QA fibers tested immediately after manufacture were not significant. The crystallization temperature of PP/QA fibers was during storage approximately the same, or slightly increased. The crystallinity of reference PP fiber during storage time slightly decreased.

Preliminary research of PP/QA is complemented with mechanical properties evaluation.

Table 2. Thermal properties of pre-oriented PP/QA fibers after 14 days of storage

Content of QA [wt. %]	Melting			Crystallization			Crystallinity X_c [%]
	T_o [°C]	T_m [°C]	ΔH_m [J.g ⁻¹]	T_o [°C]	T_c [°C]	ΔH_c [J.g ⁻¹]	
0.5	151.11	170.80	71.39	129.19	125.83	82.88	36.03
1.0	153.62	170.65	70.22	129.84	126.52	85.89	35.44
1.5	150.66	171.82	65.34	130.01	126.53	78.52	32.98
2.0	150.86	171.36	69.71	130.38	126.88	81.56	35.19
2.5	150.89	170.78	67.44	130.58	127.29	80.41	34.04
PP	151.82	170.68	75.00	120.26	116.43	81.67	37.86

The results of effect of different QA pigment content on the basic mechanical properties of PP/QA fibers are presented in table 4. The addition of QA pigment in PP fibers resulted in the decrease in tenacity at break and elongation at break. Observed decrease in elongation at break is in paradox according to the fiber producer's experience, adding any filler to PP usually causes increase of elongation at break. Titanium dioxide and carbon black used as white respectively black pigment are a typical example.

Table 3. Crystallinity of pre-oriented PP/QA fibers during storage time

Content of QA [wt. %]	X_c [%] / storage time [days]						
	0	7	14	42	56	70	84
0.5	34.91	34.35	36.03	35.49	36.85	37.99	35.39
1.0	35.90	34.69	35.44	37.28	35.14	37.33	39.35
1.5	33.83	35.81	32.98	36.24	37.20	35.23	39.55
2.0	35.87	34.18	35.19	34.62	35.82	38.03	35.01
2.5	33.44	33.07	34.04	35.51	37.02	37.71	35.89
PP	40.52	38.24	37.86	38.60	39.43	36.22	-

Table 4. Mechanical properties of pre-oriented PP/QA fibers immediately after 7 days of storage

Content of QA [wt. %]	Tenacity at break [cN]	Elongation at break [%]
0.5	251.3 ± 17.2	282.9 ± 20.0
1.0	230.6 ± 13.6	287.8 ± 32.8
1.5	222.0 ± 9.0	285.2 ± 17.1
2.0	236.1 ± 3.7	310.4 ± 9.1
2.5	222.6 ± 12.4	259.4 ± 41.8
PP	313.5 ± 4.4	307.8 ± 34.0

4. CONCLUSIONS

In this work pre-oriented PP fibers with different content of quinacridone (QA) and reference PP fiber were prepared.

Effect of quinacridone content on the thermal properties of POY PP/QA fibers in dependence on storage time was studied. The mechanical properties of prepared PP/QA fibers were evaluated, too.

On the basis of the results obtained at the evaluation of thermal and mechanical properties of these fibers it can be stated shown, that:

The addition of QA pigment in PP fibers increased crystallization temperature by ~ 10 °C, which shows that it acts as nucleating agent. Differences in the crystallization temperature between PP fibers containing different concentrations of QA (0.5 – 2.5 wt. %) were insignificant. The interval 0.0 – 0.5 wt. % QA in PP fiber is necessary to examine in the future.

Storage time of PP/QA fibers has not significant influence on their thermal properties in contrast PP/QA fibers tested immediately after manufacture.

The addition of QA pigment in PP fibers resulted in the decrease in tenacity at break and elongation at break.

ACKNOWLEDGEMENTS

The contribution was supported by the Slovak grant agency VEGA 1/0589/17 and the project „Centrum pre testovanie kvality a diagnostiku materiálov“ ITMS code 26210120046 of the Operational Program Research and Development funded from European Fund of Regional Development.

References

1. *Polypropylene Fiber Market - Segmented By End Use Application And Geography - Trends And Forecasts 2016 – 2021*. (2016).
2. Moore, E. P. (1996). *Polypropylene Handbook: Polymerization, Characterization, Properties, Applications*. Munich: Carl Hanser Verlag. ISBN 978 3 446 18176 2
3. Broda, J. (2003). Nucleating Activity of the Quinacridone and Phthalocyanine Pigments in Polypropylene Crystallization. *Journal of Applied Polymer Science*, 90, 3957-3964.
4. Hricová, M., Marcinčin, A. (2004). Vplyv pigmentov na štruktúru a vlastnosti syntetických vlákien. III.časť. *Vlákná a textil*, 11(4), 140-146.
5. Broda, J. (2012). *Structure of Polypropylene Fibers Coloured with Organic Pigments*. Polypropylene. InTech. ISBN: 978-953-51-0636-4.
6. Leugering, H. J.& Kirsch, G. (1973). Effect of crystallization from oriented melts on crystalstructure of isotactic polypropylene. *Makromol. Chem.*, 33, Issue OCT, 17-23.
7. Yu, Y.; White, J.L. (2001). Comparison of structure development in quiescent crystallization, die extrusion and melt spinning of isotactic polypropylene and its compounds containing fillers and nucleating agents. *Polym.Eng.Sci.*, 41(7), 1292-1298.
8. STN EN ISO 3146 (1992). *Plastics. Determination of melting behavior (melting temperature or melting range) of semi-crystalline polymers*.
9. Steinmann, W., Walter, S., Beckers, M., Seide, G., Gries, T. (2013). *Thermal Analysis of Phase Transitions and Crystallization in Polymeric Fibers. Applications of Calorimetry in Wide Context*. (Elkordy, A. A. ed.).
10. Jambrich, M. (1987). *Štruktúra a vlastnosti vlákien*. Bratislava: SVŠT.
11. STN EN ISO 2062 (2009). *Textiles. Yarns from packages. Determination of single-and breaking force and elongation at break using constant rate of extension (CRE) tester*.
12. Hearle, J.W.S., Hollick, L., Wilson, D.K. (2000). *Yarn texturing technology*. Abington: Woodhead Publishing Ltd. ISBN 1 85573 575 X.

MODIFICATION OF PU- FOAM FOR IMPROVEMENT OF THERMAL COMFORT OF CAR SEAT

Funda Buyuk Mazari, Karel Adamek, Jakub Wiener, Adnan Mazari, Antonin Havelka

Department of Clothing, Technical University of Liberec, 46117 Liberec, Czech Republic
fundabuyuk@hotmail.com

Abstract

Seat is the one of the main aspects of the car to be considered for definition of the comfort of driving. This paper studied the Improvement of the (Poly Urethane) PU foams which is used for the cushion and the interlining part of the car seat. It is important to improve the PU foam because of their very poor permeability, which is not good for the thermal comfort of the driver. The theoretical prediction of the permeability is also important for new designs of the permeable PU foams. In this research the modeling of the air permeability of the PU foams also studied compared with the experimental results

Key words

Car seat, comfort, PU foam, heat transfer, air permeability

1. Introduction

An important aspect of vehicle comfort is the seat. Seats do not only have to have an attractive design for safety reasons, they must also have optimum comfort properties. In addition to ergonomic considerations of comfort, the climatic or thermophysiological comfort of the seat is important. This indicates whether the seat is able to support the thermoregulation of the body via heat and moisture transport. Scientific findings show that the performance of a driver over long distances significantly decreases if the car seats do not support posture and heat balance as required. This leads to exhaustion and loss of concentration,. It is also important for the health of the muscles and skin [1,5, 6].

Thermophysiological carseat comfort comprises the following four parameters [2]:

- i. The initial heat flow following the first contact with the seat. In other words; the sensation of warmth or cold in the first few minutes or even seconds after entering the car..
- ii. The dry heat flow on long journeys, i.e. the amount of body heat transferred by the seat.
- iii. The ability known as "breathability" to transfer any sweating away from the body. In so-called "normal sitting situations" there is no perceptible perspiration, but, nevertheless, the human body constantly releases moisture (so-called 'insensible perspiration'), which has to be taken away from the body
- iv. In the event of heavy perspiration (a car in the summer heat, stressful traffic situations) the ability to absorb perspiration without the seat feeling damp.

25% of human body is in contact with car seat and the car seat acts as an extra layer of the clothing thus the effecting parameter of the clothing comfort is the same for car seat thermal comfort as well [2,6]. Generally, car seats are composed of the following elements:

1. Metal structure.
2. Filling, cushion padding.
3. Seat cover:

One solution to reduce the degree of discomfort can be ventilation of the car seat. This can be the solution of both sense of high temperature and the high moisture. To be able to use the car with

ventilation systems it is important that the car seat should have the sufficient air permeability and should give the good distribution of the air [7-8].

2. Experimental Part

The experiment is performed with classical PU carseat cushion foam and PU perforated foams. Table 1 and the figure 1 below shows the details about the cushion foam materials.

Table 1. Properties for perforated PU foam used for the experiment

	Foam thickness mm	Number of holes	Hole diameter mm	Total area of foam sample mm ²	Area of holes mm ²	Area of solid foam mm ²
A	60	0	0	16505	0	16505
A1	60	7	10	16505	550	15955
A2	60	7	15	16505	1236	15268
A3	60	7	20	16505	2198	14307
B	85	0	0	16505	0	16505
B1	85	7	10	16505	550	15955
B2	85	7	15	16505	1236	15268
B3	85	7	20	16505	2198	14307



Figure 1. Real picture of the perforated foams

The foams are tested with upright cup method (ASTM E 96-66) for water vapour transmission. Testing is performed in a climate chamber with controlled condition to avoid condensation of moisture in the sample. The testing is performed for 3 hours and measurements are obtained after every 1 hour. The Air permeability of the samples are tested under different pressure difference by standard method ISO standard 9237. The results of airpermeability used for the simulation with software Fluent.

2.1. Perforation of foam using Laser technology

Fine holes are made through the PU-foams which are used as a part of car seat covers, by using Flexi-CO₂ laser device. Laser beams interact with fibres by local evaporation of material, thermal decomposition or changing the surface roughness. Samples obtained from company Adient, Czech Republic. Initially the basic properties like air permeability and water vapour permeability of specimen are tested using FX3300 and SDL-sweating guarded hot plate respectively.

The final product after perforation with LASER is shown in figure 2 and table 2 shows the properties of the sample.

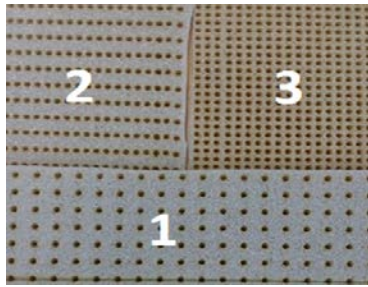


Figure 2. Thin PU foam with different density of perforation by LASER

Table 2. Holes dimension by Laser

Foam layers name	size of holes [mm]	Number of holes[n/cm ²]
0 (no holes)	0	0
1	2.5	4
2	2.5	6
3	2.5	9

3. Results and discussion

The results of water vapour transmission through the PU foams shows that the non-perforated foams A and B are almost impermeable to moisture and bigger size of the porosity is causing higher breathability of the foam, the foam A3 and B3 have the maximum air area (area of the holes) in the sample and shows a significant increase in the moisture permeability of the sample. A3 sample shows more permeability than the B3 which is due to the thickness difference of the sample and moisture permeability is dependent on the thickness of the sample.

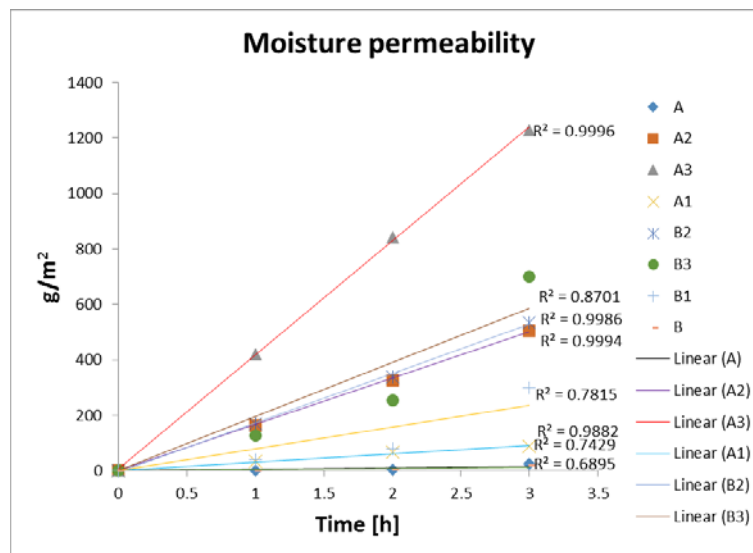


Figure 3. Water Vapour transmission through PU-foam

The air permeability is measured using machine SDLMO21S by standard ISO9237 shown in table 3.

Table 3. Permeability of perforated foam at different pressure differences

Pressure [pa]	Foam Layers permeability [mm/sec]			
	0	1	2	3
1	17	30	55	77.5
1.5	25	45	78	100
2	35	58	98	135
3	55	83	130	188

On the other hand the water vapor transmission is measured by standard Cup Method for the thinner PU foams which is perforated by laser and shows a direct linear relation between density of holes and the water vapour permeability as shown in figure 4.

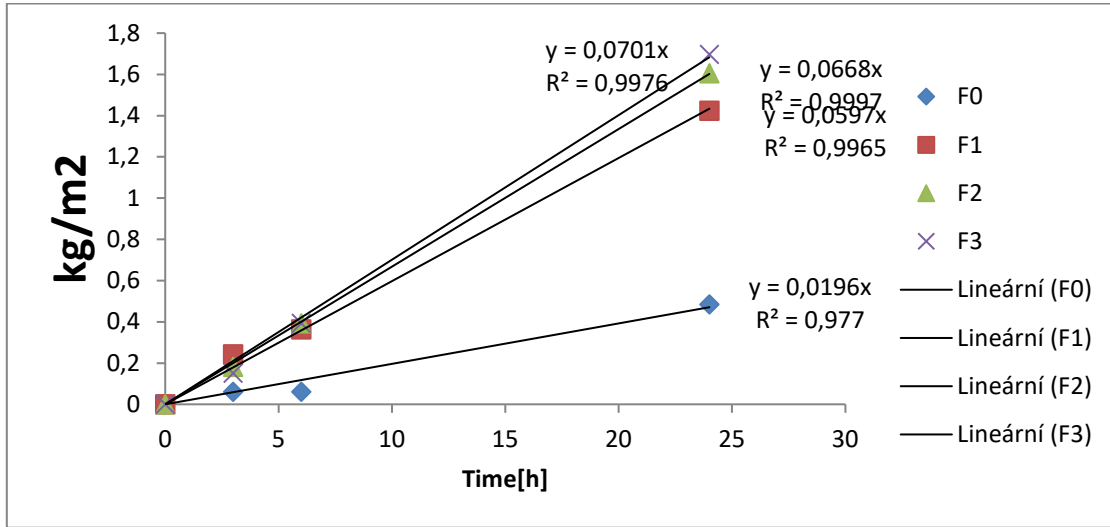


Figure 4 Effect of perforation on the water vapour permeability

3.1. Numerical simulation

Air permeability describes the rate of flow of a fluid through a porous material, and the mathematical expression is given by

$$q = Q / At \quad \text{Eq.1}$$

Where q is rate of flow (m/s), Q is volume of flow of fluid through the sample (m³), t is time (s) and A is the cross-sectional area (m²).

Textile material stand out as a unique class of porous media, which contain relatively high volume of air and very complex structure due to the random arrangement of fibres or pores. Air permeability is one of the most important properties of textile materials in many applications, Numerous researchers have worked on the air permeability of non-woven fabrics in both experiment [9,10,11] and analytical prediction [12,13,14]. Darcy derived an equation for calculating the air permeability based on hydraulic radius theory, which states that rate of flow is directly proportional to the pressure gradient causing the flow. The equation is as follows:

$$Q = A \cdot t \cdot (K_p \cdot \Delta P) / (\mu \cdot L) \quad \text{Eq.2}$$

Where Q is the rate of flow (m/s), k_p is the flow permeability coefficient (m²), Δp is the pressure gradient (pa), μ is the viscosity of the flow (pa·s), L is the thickness of sample (m), Q is the volume flowing in time (m³), A is the cross-section area (m²) where flow goes through, t is time (s).

The air flow and the water vapor permeability are the connected properties. This gives us the idea to theoretically analyses the flow of air through the textile layers and predict the performance of the car seat materials. For this research the software FLUENT is used for the theoretical analyses and the results are compared with the experimental results.

The permeability is defined as the volume flow V (m³/s) through the cross-section of the sample S (m²). So the permeability is identical with flow velocity through tested sample

$$w = V/S \text{ (m/s)}. \quad \text{Eq.3}$$

Thick PU cushion part of the car seat is used for this research. The classical foam and the foam with the perforation are used

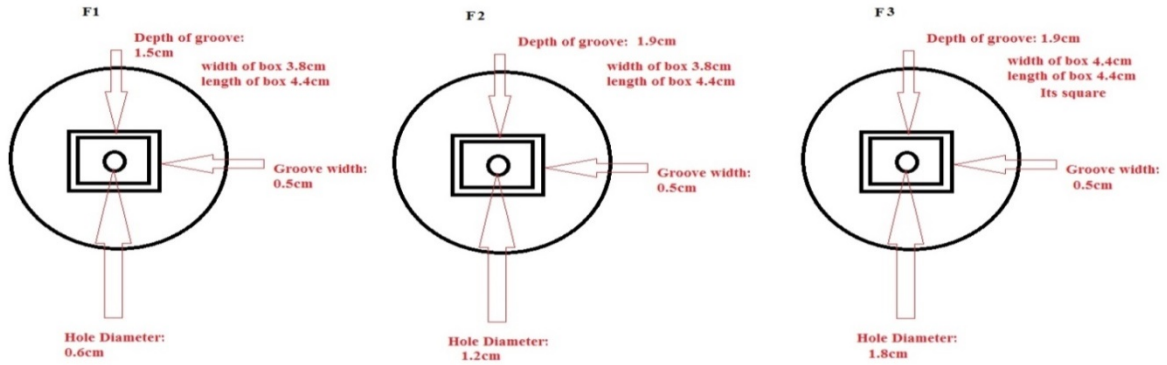


Figure 5. Description of real sample of PU-foam with holes

The Air permeability of the samples are tested under different pressure difference by standard method ISO standard 9237. Results are shown in figure 6. It is quite obvious that the PU-foam without holes is almost impermeable and the flow increases with the size of hole.

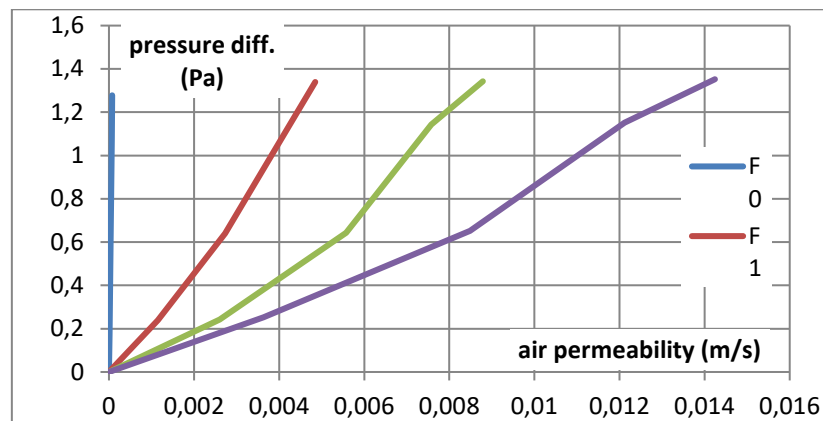


Figure 6. Air permeability at different pressure

Here is the method used for so-called „porous zone“, generally as the flow in 3-dimensional permeable volume (thick porous layer). Theoretical formulas [15] are analogous, so it is supposed to use the same procedure in 3D for homogenous permeability. Generally, the qualitative results (images of flow fields), are all right, but the quantitative results of simulations (m/s, kg/s etc.) are different from measured values. The permeability of the observed layer is given by its flow resistance. This resistance consists in general from the linear term, typical for instance for small velocities (so-called Darcy's law) and from the quadratic term, typical for flow around bodies or through channels (Weissbach's or Moody's law)

$$\Delta p = C_2 \cdot \rho / 2 \cdot t \cdot w^2 + \mu / \alpha \cdot t \cdot w \quad \text{Eq.4}$$

where

$w = V / S$ (m/s) flow velocity

V (m³/s) volume flow

S (m²) flow cross-section (here 20 cm²)

t (m) layer thickness

ρ (kg/m³) medium density (for atmospheric air 1,2 kg/m³)

μ (m²/s) viscosity (for air 1,806e-5)

α (m²), C_2 (1/m) unknown permeability parameters [15].

Two unknown permeability parameters α , C_2 , depending on the layer structure, can be determined from the experimental data.

$P_a = f(w/s)$ is substituted by quadratic function with very high correlation coefficient. Parameters of this substitution are used as follows:

Comparing the formula for pressure resistance as function of velocity

$$\Delta p = A \cdot w^2 + B \cdot w + C \quad \text{Eq. 5}$$

From Eq. 4 we can determine two unknown permeability parameters C_2 , α from

$$A = C_2 \cdot \rho / 2 \cdot t \quad \text{Eq. 6}$$

$$B = \mu / \alpha \cdot t, \quad \text{Eq. 7}$$

where A, B (and C, which should be equal zero) are parameters of the quadratic substitution.

For given values of

thickness	$t = 0,03 \text{ m}$,
air density	$\rho = 1,2 \text{ kg/m}^3$,
dynamic viscosity	$\mu = 1,806e-5 \text{ (Pa.s)}$

the permeability parameters are as follows

$$C_2 = 2 \cdot A / (\rho \cdot t)$$

$$\alpha = \mu \cdot t / B$$

Determined permeability parameters for F0 are

$$C_2 = 1,526e+09 \text{ (1/m)}, \quad 1/\alpha = 2,698e+10 \text{ (1/m}^2\text{)},$$

For testing purposes the foam F0 is used, only, foams F1, F2, F3 are not evaluated here, because the relevant models are created as foam body (permeability parameters of F0) with perforations and grooves.

The main results of the numerical simulation are shown in the table 3. Differences between flows of inlet and outlet are not important. Even if the holes area is 1,1% of the total area of sample, the main flow is going through holes and the flow through the foam material is less than 1% approximately. It could be stated that the foam is practically impermeable and used as compressible cushion.

Table 4. Inlet and outlet prediction of low

		area		mass flow		measured
		m ²	%	kg/s	%	kg/s.
inlet	foam	0.012858	78.2	0.92794e-6	0.3	
	grooves	0.003415	20.8	2.24480e-6	0.8	
	holes	0.000178	1.1	2.80000e-4	98.8	
	sum	0.016452		2.83300e-4		0.415e-4
outlet	foam	0.016273	98.9	2.07184e-6	0.7	
	holes	0.000178	1.1	2.81000e-4	99.2	
	sum	0.016451		2.83300e-4		0.415e-4

Next serial of flow fields presents main qualitative results. To get full details of individual flow fields different scales are used. The model is shown with different graphical representation.

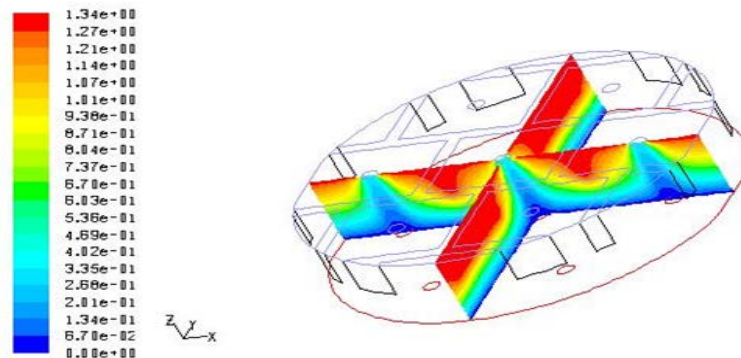


Figure 7. Pressure field – axial cross sections

Pressure is penetrating into blind/closed grooves, stopped at the groove bottom. In continuous holes the value is low due to conversion of the pressure into velocity.

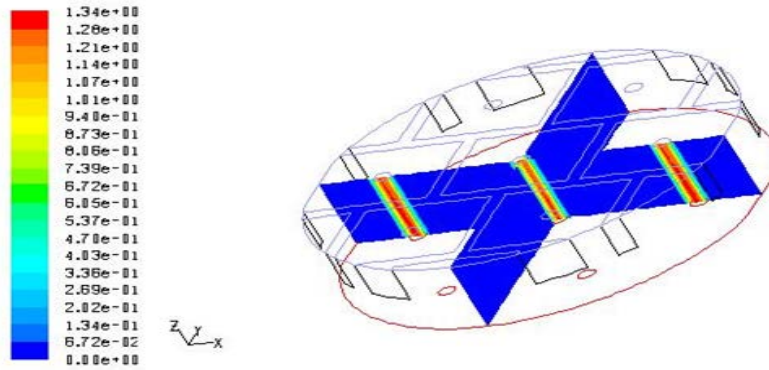


Figure 8. Velocity field – axial cross sections. full scale

The main flow is through holes, the flow through foam is extremely low.

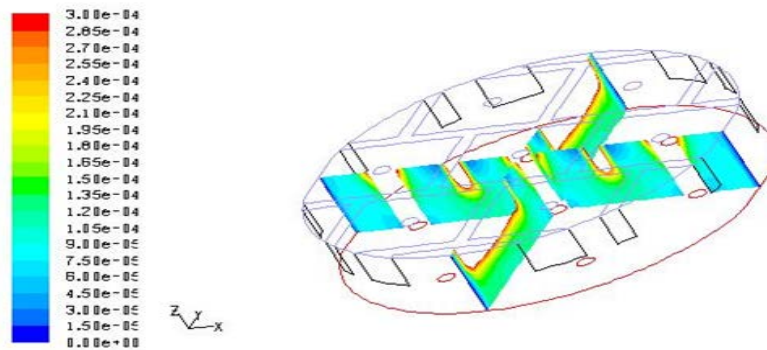


Figure 9. Axial cross sections. suppressed scale

Flow in grooves is stopped at the groove bottom and slightly is penetrating into foam volume. Simulation can explain details of flow in permeable volume.

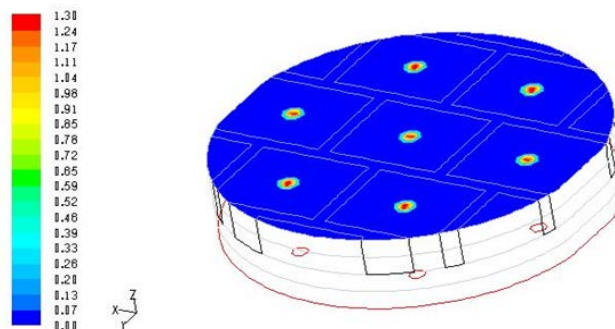


Figure 10. Velocity field at the inlet plane – full scale. Maximum in holes

The velocity field at the inlet plane is maximum in the holes.

3.2. Foam under load (pressed)

Hypothesis for this part of the model is that if the foam is pressed then the foam volume by 50% in the flow direction. The inner permeable cells are also pressed by 50% too, so eventually the permeability is also decreasing by 50% too. And more, it is supposed that geometry deformation is along the axis of deformation and there is no abnormal shape or buckling in cross directions.

For simple verification the model geometry remains the same. New parameters of permeability are determined as in the table 30 from the condition of 50% of measured flow.

Table 5. Permeability parameters for 50% flow (due to foam pressing)

	C2	α (m ²)	1/ α (1/m ²)
F0	1.111E+10	7.052E-12	1.418E+11

Results are summarized in the tab. 31 where original mass flows through foam and grooves is decreased by 28% and 27% respectively of original values. It means from 1% of the whole flow to 0.3% approximately. It has not any influence on the flow through holes, as it represents 99% of the whole flow and some small flow changes in foam and grooves does not have any influence.

Table 6. Prediction of flow under compression

		original		pressed	press/orig.
		kg/s	%	kg/s	%
inlet	foam	0.92794e-6	0.3	2.6134e-7	28.2
	grooves	2.24480e-6	0.8	6.0319e-7	26.7
	holes	2.80000e-4	98.8	2.8160e-4	100
	sum	2.83300e-4		2.8247e-4	99.7
outlet	foam	2.07184e-6	0.7	5.5473e-7	26.8
	holes	2.81000e-4	99.2	2.8190e-4	100
	sum	2.83300e-4		2.8247e-4	99.7

Two cases of full foams (F0, F1) were solved; differences between simulated and measured mass flows are 1%-5%, only. The detailed geometry gives good imagination about fine details of velocity and pressure field in the foam volume, the main flow is going through perforations.

On the other side, the simple model of “foam” presents the average flow, regardless of perforations and grooves. Therefore the correlation of measured and simulated mass flow is very good, but details of flow field inside the foam volume cannot be perceived.

Fig. shows 12 differences between mass flows in F0 and F1.

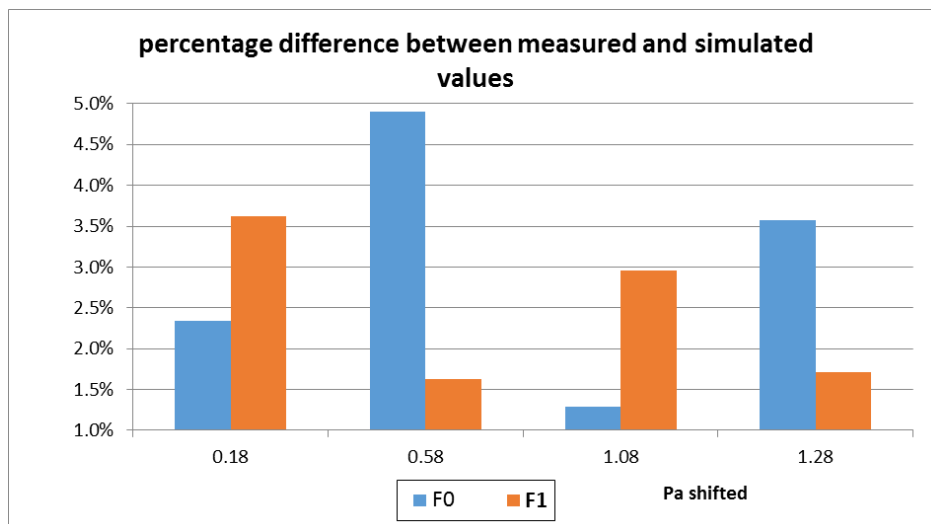


Figure 12. Difference between measured and simulated mass flows for foams F0 and F1

4. CONCLUSION

In conclusion from the experimental results it can be seen that the classical car seat materials contains many impermeable and sometimes as poor permeable parts. These layers are problem for the thermal comfort of the carseat. This definitely should be improved for the better comfort of the carseat. Experimental results shows that there is significant effect of the perforation for the permeability of the PU foam materials. And the simulation of the experimental data based on some theoretical model is important for the prediction of the results of different future design of PU foams

References

1. Umbach KH. *Physiologischer Sitzkomfort im Kfz'*, *Kettenwirk-Praxis*, 34 (2000a) pp.34–40.
2. Bartels, VT. *Physiologically optimized car seats*, in *Textile Advances in Automobile Industry*, Woodhead Publishing. 2008, pp.150-170. ISBN: 9781845693312
3. Jerkovic¹, I; Pallares, JM; Capdevila, X. *Study of the Abrasion Resistance in the Upholstery of Automobile Seats*, *AUTEX Research Journal*, 2010, Vol. 10, pp. 14-20.
4. Fung, W; Hardcastle, M. *Textiles in Automotive Engineering*, Woodhead Publishing Ltd., Cambridge, England,2001, ISBN: 1-58716-080-3
5. Umbach, KH. *'Parameters for the physiological comfort on car seats'*, 38th International Man-Made Fibres Congress, Dornbirn, Austria. 1999,
6. Martin W. Ferguson-Pell, *Seat Cushion Selection*, *Journal of Rehabilitation Research and Development Clinic Suppl.* 1990, Vol.2, pp.49-73.
7. Madsen, TL. *Thermal effects of ventilated car seats*, *International Journal of Industrial Ergonomics*,1994, Vol.13, pp. 253-258
8. Aniket, A; Gabhane, AV. *Waghmare, Design of Comfortable Advanced Ventilated Automotive Seat for Driver using CFD simulation*, *International Research Journal of Engineering and Technology*, 2016, Vol, 03 , pp. 1979-1985:
9. Kothari, VK. and Newton, A. *Air-Permeability of Nonwoven Fabrics*. *Journal of the Textile Institute*, 1974, Vol.65(10), pp. 525-531.
10. Mohammadi, M. and Banks-Lee, P. *Air permeability of multilayered nonwoven fabrics: Comparison of experimental and theoretical results*. *Textile Research Journal*, 2002. Vol.72(7), pp. 613-617.
11. Debnath, S. and Madhusoothanan, M. *Thermal resistance and air permeability of jute-polypropylene blended needle punched nonwoven*. *Indian Journal of Fibre & Textile Research*, 2011. Vol.36(2), pp. 122-131.
12. Kulichenko, AV. *Theoretical analysis, calculation, and prediction of the air permeability of textiles*. *Fibre Chemistry*, 2005. Vol. 37(5), pp. 371-380.
13. Mohammadi, M. and Lee, PB. *Air permeability of multilayer needle punched nonwoven fabrics: Theoretical method*. *Journal of Industrial Textiles*, 2002. Vol.32(1), pp. 45-57.
14. Song, WF and Yu, WD. *Fractal calculation of air permeability of nonwoven fabrics*. *Journal of the Textile Institute*, 2012, Vol. 103(8), pp. 817-826
15. Adámek, K. *Prodyšnost textilních vrstev*, XV. mezinár. konf. Aplik. exp. a numer. metod v mech. tekutin, ŽU Žilina, 2008
16. Snyckerski, M; Frontczak-Wasiak, I. *Influence of Furniture Covering Textiles on Moisture Transport in a Car Seat Upholstery Package*, *AUTEX Research Journal*, 2002, Vol. 2, No3, pp. 126-131

IMPACT OF HEAT ON RECOVERY EFFICIENCY OF CAR SEATS FABRICS

Viera Glombikova, Petra Komarkova, Kus Zdenek

Technical University of Liberec, Faculty of Textile Engineering, Department of Clothing Technology, Liberec, Czech Republic, Studentska 1402/2, +485353500, petra.komarkova@tul.cz

Abstract:

This paper deals with investigating performance of car seat fabrics in terms of their compression and recovery properties influenced by heat degradation. Polyurethane foam, nonwoven and 3D knitted spacer fabrics are commonly used as padding (in middle layer) in car seats cover. The current work presents an alternative approach to evaluate effectivity of car seat fabrics, namely behaviour of their middle layers before and after heat degradation which simulates hot summer condition. In summary, results show that 3D spacer is the most appropriate middle layer for car seat cover because of its recovery properties is very good at both before and after heat degradation (about 94 % from original thickness) on the contrary PU foam. The PU foam is very good at recovery behaviour under standard ambient conditions (temperature about 25°C) on the other hand PU foam recovery significantly decreases (about 40% against 3D spacer) after impact of high temperature.

Key words:

car seats cover, compression, recovery, heat degradation

1. Introduction

There are approximately 3-5 kg car seat cover fabrics used in each car [2]. Car seat covers are often composed of several layers of different materials, usually polyester fabric (or leather or synthetic leather) laminated to polyurethane foam (or 3D knitted spacer or nonwoven) backing by an adhesive. Each part of car seat cover brings different properties which affect both their durability and comfort in automotive seating. One group of researchers prefer polyethylene terephthalate (PET) fibres for automotive application (both for top and middle layers) due to their superior properties, like a high tenacity, abrasion, light, heat and chemical aging, UV resistance, dimensional stability, recyclability etc. [10, 6, 5, 4]. The others are in favour of modified PU foam (in middle layer) because of their excellent elasticity and very good recovery to compression [5]. Study on comparison of quality for different types of seat cover padding was carried out from aspects of physiological properties and relaxation behaviour after static and dynamic loading [9]. The result of this study showed that warp knitted spacer fabrics demonstrate better recovery to compression, better thermal properties and better breathability as compared to PU foam [9]. The other research found out that fabrics using monofilament as spacer yarn generally have higher compression resistance than multifilament yarns [10, 1]. Major car manufacturers evaluate degree of car seat durability, including relaxation behaviour after cyclic loading by special equipment, which uses the robot. This robot allows realistic simulation, of someone getting into and out of the seat (ingress/egress test), or of strong pulsation or vibration during driving [8]. The current study is focused on investigating performance of car seat fabrics in terms of their compression and recovery properties influenced by heat degradation which simulates hot summer condition.

2. Experimental

2.1. Materials

Tested materials were designed in order to understand the role of middle layer of textile sandwich car seats from point of view of their compression and relaxation behaviour. There were used different middle layers (polyurethane foam, nonwoven and 3D spacer) in the tested samples. Material in top layer was the same – PES woven fabric. Basic characteristics of all tested car seat fabrics are shown in Table 1. The Figure 1a) b) and c) show 3D structures of all tested middle layers by means of micro tomography system. Before being tested, the samples had been washed and conditioned for 24 hours. The measurement was carried out in an air-conditioned room under constant relative humidity of 65 % and the temperature of 21° C.

Table 1 Basic characteristic of the tested samples

Code	Structure	Raw material	Thickness [mm]	Weight [g/m ²]
<i>Top layer</i>				
	woven fabric, twill	100% PES, twill	0.7	203
<i>Middle layer</i>				
A	3D warp knitted spacer	100% PES	6.2	408
B	nonwoven	70% PES/30%wool	5.7	230
C	foam	100% PUR	4.1	247

Measurements of thickness were performed under 100 Pa.

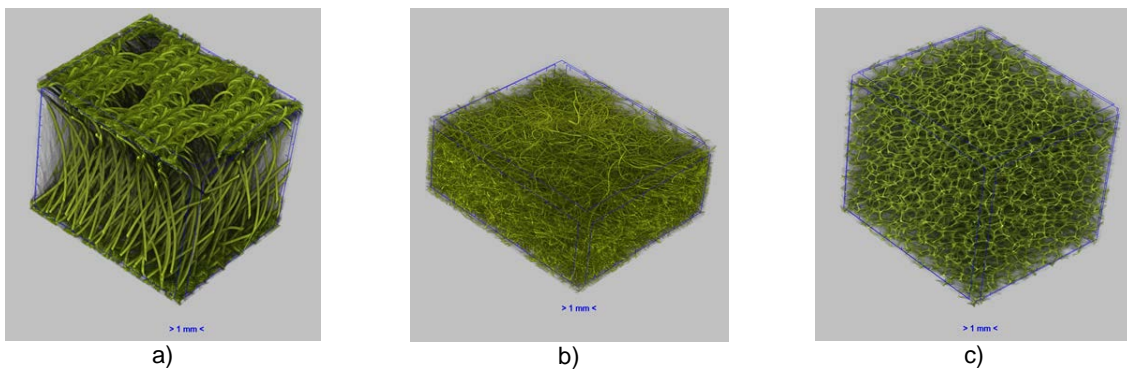


Figure 1 a) 3D spacer, b) nonwoven, c) foam

2.2. Methods

The compression and relaxation behaviour were investigated before and after degradation of tested samples in autoclave which simulates hot summer conditions. It is important to uncover how cyclic compressive loading combined with above mentioned degradation influence recovery of car seat cover for the lifetime period.

The results were compared and discussed in order to understand the real performance of tested materials. Final values (means) of all tested parameters correspond to five measurements on average. The coefficients of variation for all tests do not exceed 10 % and therefore not statistically significant.

Simulation of sample degradation by heat

Generally, the autoclave is a piece of equipment used for sterilizing various requirements in the lab by wet sterilization method. Car producer very often use this device for testing car seat fabric to simulate accelerated degradation by high temperature corresponds to hot summer conditions.

Principle autoclave is following. When water is heated in a closed container, saturated steam is produced under pressure. According to Boyle's Law, when volume of the steam is kept constant, the temperature is directly proportional to pressure. If the pressure is reduced, it boils at a lower

temperature. If the pressure rises, it boils at a greater temperature. The autoclave Sano LA-MCS was used for degradation of samples, see Figure 3. Applied conditions for degradation were: 120 °C during 20 hours.

Compression and relaxation behaviour

Repeated compression - recovery test was carried out by the device developed by Technical University of Liberec [3] as shown in Figure 2 Figure 1. This simple device consists of transparent Perspex cylinder (diameter of base is 14 cm) and pressure plate for set of required compression. Loading time was set to 24 hours and the pressure of static loading was 12 kPa. Value of pressure corresponds to maximum real loading of car seat during sitting of driver [7]. Relaxation behaviour given by the thickness recovery of samples was investigated after above mentioned compression test, when load was removed The measurement of recovery was carried out immediately, 10 min, 20 min, 40 min, 1 h, 2 h and 3h after test. The referred compression - recovery test was repeated 5 times for each sample. The thickness of tested samples was measured by compression tester SDL M 034A according to EN ISO 5084 both before and after loading (pressure 1000 Pa). The recovery R [%] were determined by means of equations (1), see below. Recovery is given as the degree which a sample mass recovered to its original height upon unloading.

$$R = \left(\frac{h_2}{h_1} \right) * 100 \quad [\%] \tag{1}$$

where h_1 is the original height of the samples, h_2 is the height of samples after removal of load.

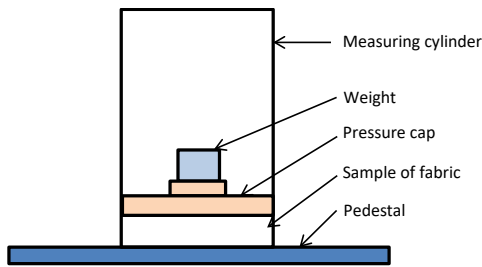


Figure 2 Schema of recovery measurement



Figure 3 SanoClave LA MCS

3. Results and discussion

The results of the recovery tests are presented in Figure 4 and Figure 5.

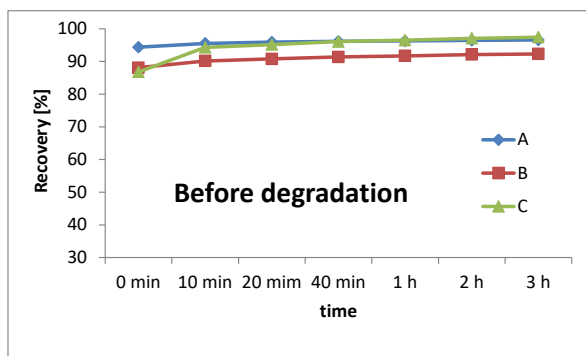


Figure 4 Recovery of tested samples before degradation

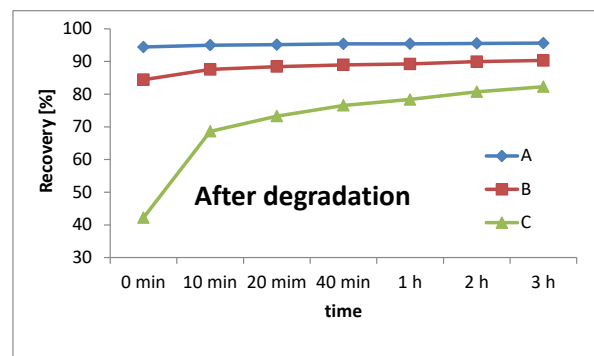


Figure 5 Recovery of tested samples after degradation

The results, as shown in Figures above, indicate that the difference between the groups was significant. The recovery before degradation of Group A (3D warp knitted spacer in middle layer) was

equal to recovery after degradation, i.e. 94,4% immediately 96,2% after 40 min and 96,6% after 3 hours. Group B (nonwoven) reports decrease of recovery after degradation about 2% than before degradation. The impact of degradation was most pronounced in Group C (foam) when recovery before degradation was 86,8% immediately, 96,1% after 40 min and 97,4% after 3 hours and recovery after degradation was 42,2%, 76,6% and 82,3%.

4. CONCLUSIONS

The results of this study are consistent with data obtained in other researches which studied using of 3D spacer in car seat cover. The most obvious finding to emerge from this study is that 3D spacer is the most appropriate middle layer for car seat cover in view of the fact that its recovery properties is very strong in both before and after heat degradation (about 94 % from original thickness) on the contrary PU foam. The PU foam is very good at recovery behaviour under standard ambient conditions (temperature about 25°C). On the other hand PU foam recovery significantly decreases (about 40% against 3D spacer) after impact of high temperature. PU foam is degraded by combination of hydrolysis and thermal oxidation, which causes shortening of the polymer chains. Further research could usefully explore compression and relaxation behaviour of tested materials using not static but dynamic loading. A further study might also focus on determining relaxation behaviour after lower degradation temperature than standardized 120°C.

ACKNOWLEDGEMENTS

This work was supported by the Ministry of Education, Youth and Sports of the Czech Republic and the European Union – European Structural and Investment Funds in the frames of Operational Programme Research, Development and Education – project Hybrid Materials for Hierarchical Structures (HyHi, Reg.No.CZ.02.1.01/0.0/0.0/16_019/0000843).

References

1. Chen, S., Long, H.R., 2014. Investigation on compression properties of polyurethane-based warp-knited spacer fabric composites for cushioning applications, Part II. Theoretical and experimental verification. *Industria Textila*, 65(6), 340-344.
2. Fung, W., Hardcastle, M., 2001. *Textiles in automotive engineering*. Woodhead Publishing limited Cambridge, England, UK, 384, ISBN: 9781855734937.
3. Glombikova, V., Apparatus for measuring compressibility of volume textile structures, national utility model application. 2013, Application number: 2013-27589, Registration number: 25543, Website:http://isdv.upv.cz/webap/webap.pts.det?xprim=1949313&lan=cs&s_majs=&s_puvo=%25Glomb%C3%ADkov%C3%A1%20viera&s_naze=&s_anot=
4. Glombikova, V., Komarkova, P., Havelka, A., Kolinova, M., 2018. Approach to evaluation of car seats fabrics performance. *Industria Textila*, 69(2), 96-103.
5. Jerkovic, I., Pallares, J. M., Capdevila, X., 2010. Study of the abrasion resistance in the upholstery of automobile seats. *Autex Research Journal*, 10(1), 14-20.
6. Koc, K. S., Mecit, D., Bozaci B., Ornek, M., Hockenberger, A., 2015. Effect of filament cross section on the performance of automotive upholstery fabric. *Journal of Industrial Textiles*, 46 (3), 1-15.
7. Mazari, F.B., Havelka, A., 2015. Pressure distribution of car seat at different angle of backrest. *Vlákna a textile*, (3-4), 33-39.
8. Stewart, R., O'Bannon, T., Müller, M., Beeh, F., 1999, *Creating the Next Generation Ingress/Egress Robot*. SAE Technical Paper 1999-01-0628, doi:10.4271/1999-01-0628.
9. Ye, X., Figueiro, R., Hu, H., Araujo, M., 2007. Application of warp - knitted spacer fabrics in car seats. *Journal of the Textile Institute*, 98(4), 337-343.
10. Yip, J., Ng, S.P., 2008. Study of three-dimensional spacer fabrics: Physical and mechanical properties. *Journal of materials processing technology*, 206(1-3), 359-364.

HEAT AND HUMIDITY TRANSFER IN SANDWICH TEXTILES FOR AUTOMOTIVE SEATS

Zuzana Drapáková¹, Vladimír Bajzík² and Luboš Hes²

¹ ŠKODA AUTO a. s., Technical development, tř. Václava Klementa 869, 29301 Mladá Boleslav, Czech Republic (Technical University of Liberec, Dept of Textile Evaluation, Studentská 2, 46117 Liberec, Czech Republic), e-mail: zuzkamail@gmail.com

² Technical University of Liberec, Dept of Textile Evaluation, Studentská 2, 46117 Liberec, Czech Republic, e-mail: vladimir.bajzik@tul.cz

Abstract:

The paper is about improving heat and humidity transfer coming from passenger through the car seat cover. A new composition of sandwich cover material for car seat has been developed to improve the comfort of the passenger seat. The replacement of polyurethane foam between the top design layer and the lower smooth layer, which serves to simple cover car seat, and the way these parts are joined to the sandwich is the fundamental change. A spacer knit has replaced polyurethane part of the sandwich. By doing this, the bottom layer is no longer needed; the material is sufficiently sliding for coating the car seat. The aim of the development of sandwich cover material was to improve its attributes by using existing design materials. It was not intended to develop or change the design material for another, the new one that would be more breathable and would have higher water vapor permeability. By measuring, we have found out which of the used design materials are the most suitable for the coating, which ones have the highest air and water vapor permeability and are therefore the most suitable for the new sandwich and car seat. The materials were tested on the Permetest and Textest FX3300 measuring devices. Changing the cover sandwich, increasing passenger comfort during summer months, was also meant to lead to the change in the development of new cover sandwich. The measurement shows, that thanks to this change the new car seat with the new cover material has a better permeability by 30% compared to the car seat with the concept of cover seat used so far. Complete seat measurement was carried out using a specially adjusted measuring head simulating the passenger position. The measured values in permeability of the car seat with standard seat cover was taken as 100% when compared to the new, for the better idea of the difference in functionality. The innovative coating material not only has better attributes when taking into consideration the driver's or passenger's comfort but is also better recyclable. Compared to the original state in which there is the polyurethane foam bonded between the two polyester materials by the upper and lower layer with flame lamination, in this case polyester spacer knit bonded by glue is used.

Key words:

sandwich seat cover materials, air-permeability, vapor-permeability, thermal-comfort

1. Introduction

Thermal comfort is important primarily for drivers in terms of focusing on driving. If the comfort isn't sufficient it may cause tiredness, sleepiness or irritation. Comfort is equally crucial for the rest of the passengers when it comes either to short term or long-term journeys. For this reason, emphasis should be placed on choosing the right material, on which passengers spend quite a bit of time seated.

Emphasis should be placed on the qualities of material, in this case the qualities of sandwich material and its ability to draw water vapor [1].

Presently car seats with heating are axiomatic part of the equipment of vehicles, which is ideal for winter season. Contrarily for the summer season active air-conditioned car seats are not a common matter. A more affordable option could be a passive air-conditioned seat, which would at least partially replace the missing and comfort-improving active air-conditioned car seat that is currently technologically and financially more demanding.

The functionality of the sandwich cloth assembly needs to be verified by measurement. Ideally, in a both objective and subjective way. Objectively using a permetest device that measures water vapor permeability and material breathability using the Textest 3300 device. The best way to do subjective measurement is to get as close as possible to the real situation, which in this case would be a road test on a car seat with an innovative coating.

2. Experimental

2.1. Measurement instruments

The measurement of materials was carried out on KHT TU Liberec on Permetest for measuring water vapor permeability and thermal resistance of textiles (Figure 1) [2] and TexTest FX3300 Air Permeability Tester III (Figure 2) for measuring air permeability [3].



Figure 1. Permetest



Figure2. Textest FX3300

2.2. Materials

The cover is made of sandwich material and consists of 3 parts (Figure 3):

1. The top part - design material - is made of polyester textile materials.
2. Medium part - filling, polyurethane foam in the central part with a height of 6-8 mm
3. Bottom - lining made of glove-knit polyester fabric for easy padding of the car seat.

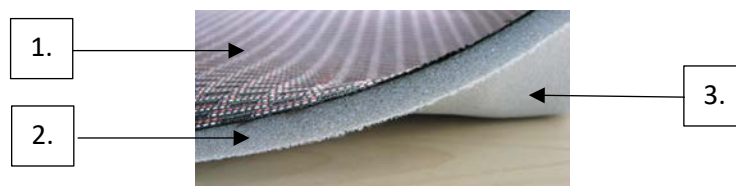


Figure 3. Sandwich material cover for car seats

Design material for the innovative car seat cover has been selected with existing coating materials. It was not desirable to create an entirely new material for both time and, above all, financial reasons. These materials must meet certain technical parameters according to the regulations. For example, abrasion resistance, tensile strength, bonding of layers, etc [4]. An important condition of materials is also a fulfilment of design requirements. For these and other reasons, design (top) materials for car seat coverings have been selected for further research.

For the middle part (layer), two materials were designed:

1. Reticulated foam (Figure 4) - foam material where the foam pores are opened by their controlled explosion in a closed box where the air is sucked out and oxygen and hydrogen supply a controlled reaction resulting in cracking of the contact bubble boundary. The pores remain open [5].
2. Distance knitting (Figure 5) - 3D knitted fabric made from 100% PES, which is made by joining two flats, independently created knitted fabrics with another dense monofilament thread set [6].



Figure 4. Reticulated foam

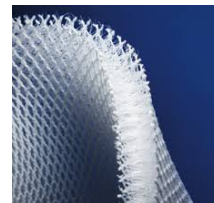


Figure 5. Distance knitted fabric

2.3. Methods

Three bonding options were selected for joining the sandwich layers:

1. sewing
2. bonding with powder glue
3. point bonding – hot melt

Based on the tests the permetest with added reference sample, 2 design materials with the best result of permeability and breathability were selected.

When it comes to the second part (middle) of the sandwich, the distance knitting has better qualities compared to the reticulated foam. Even if the reticulated foam has open pores, it is not sufficient for efficient vapor and air throughput. It no longer has the required stiffness. In addition, it is necessary to solve the lining for easy way to cover the car seat.

The third part was omitted due to the gliding qualities of the surface of the distance knitting. It is not necessary. The ease of coating was maintained without further modification or addition of the lining.

Based on these tests, the prototype of the cover for two car seats was made from the final samples:

1. design material with embossing
2. design material without any further final changes

The material of the sample number 2 had the best qualities, but the way of embossing had to be tuned so that the pattern was visible and the fibres of the distance knitting would not break, and it is also an extra operation, where you operate with heat and pressure to close other openings for the drainage of water vapours and air and thus the functionality of the whole sandwich decreases. However, not so much that the material of sample 2 is worse than sample material number 1, but it was our goal to test the subjective feeling of comfort on both materials - whether the embossing in conjunction with the distance knitting changed the perception of comfort. The material felt harder, stronger. The distance knitting is not so soft as the polyurethane foam, so the first time using it can be negatively evaluated, and it can also be negatively rated from a long-term ride test.


Figure 6. Serial sandwich of sample 2

Figure 7. Design material of sample 2 with distance knitting

Based on this information, two prototype car seats with other design material were built for subjective testing and also for the measurement of the permeability of the car seat (see Figure 6 and 7). The breathability of the whole car seat was measured by colleagues from the Department of Machine Parts and Mechanisms under the guidance of Mr. doc. Fliegel.

Higher breathability has been confirmed on the entire car seat by 30% compared to the current state. The comfort of the car seat has been accepted and positively evaluated as part of the subjective assessment for long-term road tests, including in the car seat with embossing.



The entire car seat has not been tested for the vapor permeability yet because an extra measuring device would have to be made for this measurement, which would be a further financial and time burden. Based on the measurement of the individual design materials for breathability and vapor permeability, the whole car seat for breathability and also based on a positive subjective assessment on long term road tests on hot summer days, it was decided that it is not necessary to measure the whole car seat for vapor permeability.

4. Results and discussion

Altogether, more than 50 samples of materials were measured. Approximately 8 lamination methods have been tested. Several samples of foam seat castings with an upgraded central part have been tested to improve comfort in the passive climate control of car seats and several prototype car seats have been built.

The table 1 shows the results of breathability and vapor permeability measurements of selected sandwich materials with PUR interlayer and PES lining, and the results of breathability and vapor permeability measurements of these selected materials, their design top part, interlayer with distance knitting, and a way of lamination for the building of prototype car seats of the sample 1 and sample 2.

Table 1. Serial samples of sandwich material with PUR foam

Sample of textile	Sandwich with PUR interlayer and lining				Sandwich with distance knitting			
	Air-permeability \bar{x} - Flow [l/m ² /s]	Vapor permeability		Air-permeability \bar{x} - Flow [l/m ² /s]	Vapor permeability		\bar{v} [%]	
		R_{et}	p [%] [Pa.m ² .W ⁻¹]		\bar{x}	v [%]		R_{et}
 Sample 1	128		10,3	9,2	229,3		18,8	5,2
			33,2	10,1			19,7	7,3
 Sample 2	280		7,7	19,0	510		13,5	17,2
			45,7	21,7			32,4	23,5

According to the results, the improvement of sandwich material in permeability and vapor permeability is evident [7].

Figure 8 shows the measurement of the overall breathability of the seat on three foam casting samples with an innovative sandwich coating and a comparison with the existing design of the car seat with standard foam casting and sandwich coating where the topcoat, PUR interlayer and lining are joined by flame lamination. Verification of breathability on the complete car seat showed an improvement of almost 30% compared to the standard car seat.

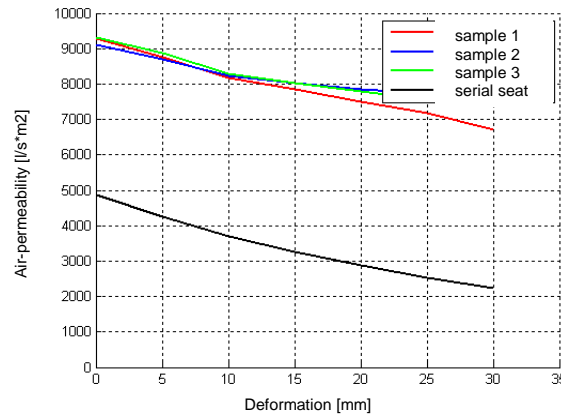


Figure 8. Measurement of the overall breathability of the seat on three foam samples with an innovative sandwich coating. Comparison with the existing car seat design

5. CONCLUSIONS

An objective evaluation of the innovated sandwich according to the measurement result shows a visible improvement in permeability and water vapor permeability. For material processing, the visual quality of the coating is also suitable for spot bonding lamination. Seating comfort is not negatively affected by this composition while maintaining at least 5 mm of the thickness of the distance knitting. Also, this cover concept does not affect other related seat components such as heating and SBR sensors.

In the subjective assessment of the car seat with an innovative sandwich cloth, the seat was positively evaluated in the sense of maintaining the existing comfort criteria and a visible improvement in thermal comfort. The passenger sweats less and the seat even contributes to comfort in the hot weather when driving longer.

ACKNOWLEDGEMENTS

Acknowledgements for support belong to KHT TU Liberec, ŠKODA AUTO A.S., Proseat and Fezko.

References

1. HES, L., SLUKA, P.: *Úvod do komfortu textilií*. Liberec: Technická univerzita v Liberci, 2005. ISBN 80-7083-956-0.
2. HES, L.: *Permetest*. Liberec: Sensora instruments & consulting, 2008. 1.
3. TEXTTEST AG; [online]. *Poslední revize 07. 08. 2008*, [cit. 2008-08-07]. Dostupné z: <<http://www.texttest.ch/en/FX3300-Lab-Air.html>>.

4. NOLIS, VW Konzernnorm. Konzernnorm VW50105. NOLIS nolis.wob.vw.vwg. [Online] VW, 7. 8 2010. [Citace: 15. 9 2012.] <http://nolis.wob.vw.vwg:15233/showprop/?id=651648&key=cbdmP26x1yHctM2Y4C0>.
5. JANDA P. Vlastnosti polyuretanový a retikulovaných pěn. [Dokument] Mladá Boleslav : PROSEAT, 2014. 1.
6. TYLEX LETOVICE: Distanční 3D úplety. <http://www.sindat.cz/>. [Online] SINDAT, 15. 5. 2012. [Citace 29. 10 2012]. <http://www.sindat.cz/technicke-pletene-textilie/en/dwn/distancni-3d-uplety.pdf>.
7. NOLIS, VW Konzernnorm. Textilien - Bestimmung der Luftdurchlässigkeit von textilen Flächengebilden (ISO 9237:1995). Burscheid : Konzernnorm Volkswagen, 1995. 1.

ABRASION AND ELECTRICAL RESISTANCE OF KEVLAR WITH PVD SURFACE TREATMENT

Mário Vančo¹, Jan Krmela^{1,2*}, Vladimíra Krmelová¹, Ludmila Balogová³, Artem Artyukhov⁴,
Františka Pešlová¹

¹Alexander Dubček University of Trenčín, Faculty of Industrial Technologies, I. Krasku 491/30, 020 01 Púchov, Slovak Republic

²University of Pardubice, Jan Perner Transport Faculty, Studentská 95, 532 10 Pardubice, Czech Republic

³VÚTCH-CHEMITEX, spol. s r.o., Rybníky 954, 011 68 Žilina, Slovak Republic

⁴Sumy State University, Processes and Equipment of Chemical and Petroleum-Refineries Department, Rym's'koho-Korsakova St, 2, Sumy, Ukraine

*corresponding author e-mail: jan.krmela@fpt.tnuni.sk, jan.krmela@upce.cz

Abstract:

In this contribution, the technical textile such as Kevlar aramid fabric with PVD surface treatment coating is studied experimentally. Kevlar fabric and PVD metal coated Kevlar fabric were tested on its abrasion resistance at test device Martindale type abrasion tester - C. & B. Tessile by standards STN EN 388 and STN EN 530. The samples were tested on a special woolen fabric and sandpaper. Next, the surface electrical resistance of Kevlar aramid fabric with PVD surface treatment coating was determined according to the standards STN EN 1149-1 and STN EN 1149-2.

Key words: Kevlar, PVD, coating, metal, abrasion resistance, electrical resistance

1. Introduction

This paper deals with the problem, which is in technical area devoted relatively little attention. This is an opportunity to apply the new PVD coating by metal [1] on technical textiles such as Kevlar aramid fabrics. Kevlar fabrics are extremely dense. Kevlar is made of para-aramid synthetic fiber. It has approximately five times higher strength than steel. Kevlar fiber has a high tensile strength – about 3 620 MPa and reaches a relative density of 1.44.

Kevlar fabric is an electrically non-conductive material. It has high electrical resistance values. We assumed that forming the Ti layer on the surface of the fabric could reduce the electrical resistance values and optionally, modify the fabric so that it is electrically conductive. To confirm or rebut this hypothesis, an electrical resistance test was performed on the fabric with PVD treatment and without modification.

Fiber achieves its strength thanks to crosslinking chemical chains. These intermolecular hydrogen bonds are formed by carboxyl groups of N H centers. Kevlar maintains its strength and resistance until to cryogenic temperatures (-196 °C). At higher temperatures, the tensile strength is reduced by about 10 – 20 %. At 160 °C, it loses 10 % of its strength after about 500 hours. At temperature of 260 °C, 50 % strength decrease occurs after 70 hours [1].

2. Experiments

Kevlar was selected as the material for the PVD surface treatment with metal coating (figure 1) and investigation of abrasion resistance and electrical resistance. Samples of fabrics have been coated by PVD technology using vacuum deposition on the coating device FLEXICOAT 850 [1]. The Ti coating was applied on a clean fabric of a thickness of 500 nm.



Figure 1. Kevlar with PVD surface treatment (left) and Kevlar without surface treatment (right)

The observed PVD metal coated Kevlar fabric had the followed parameters: fabric thickness 0.195 mm, surface weight of fabric 121 g·m⁻² and fabric density 621 kg·m⁻³.

PVD metal coated Kevlar fabric was tested on its abrasion resistance and electrical resistance. The tests were performed on the centre of investigation VÚTCH-CHEMITEX, spol. s r.o., Žilina, Slovak Republic.

2.1. Determination of abrasion resistance

Two standards were followed: STN EN 388 [2] and STN EN 530:2010 [3]. From the Kevlar fabric, 6 elementary samples of circular shape were cutted out with diameter approx. 45 mm. Their number was not higher due to lack of material, but obtaining initial information about the behavior of the materials under investigation can indicate that the number of samples is sufficient.

The samples were then fixed to the preparations and placed in a Martindale type abrasion tester - C. & B. Tessile (figure 2 left). The three samples were tested on a special woolen fabric that was normalized and intended for use as abrasive material. Another 3 samples were tested on 100 grain sandpaper.

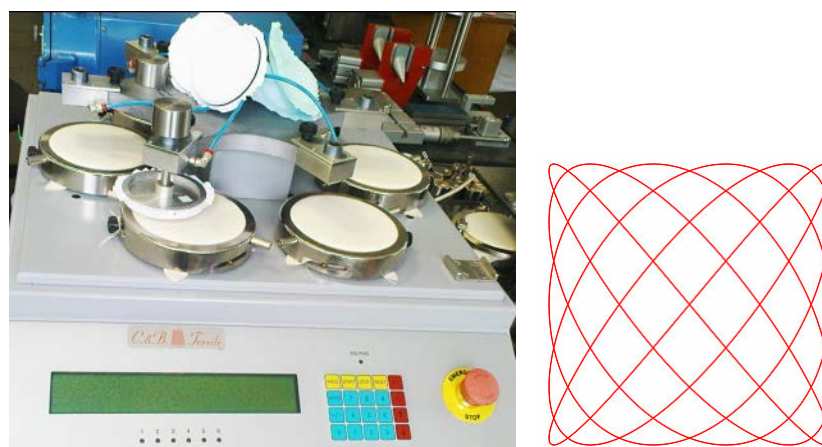


Figure 2. Martindale type abrasion tester - C. & B. Tessile (left) and specific patch of samples (right)

The samples were moved along a specific path on the abrasive material (see Figure 2 right). The samples were in constant motion and were continuously stressed in all directions in the plane. In this way, both the sample itself and the abrasion material were uniformly worn.

Test conditions were determined according to standard STN EN 388 [2] at temperature of 21 °C, relative humidity of 21 % and a sample load (nominal pressure) of 12 kPa.

2.2. Determination of electrical resistance

Surface electrical resistance of samples was determined according to the standard STN EN 1149-1 [4]. Also, the internal electrical resistance of the samples was determined according to the standard STN EN 1149-2 [5] on FISHER ELEKTRONIK Tera-Ohmmeter TO-3 device (figure 3). The device consisted of a measuring instrument and an air-conditioning chamber. In the chamber was placed a thermometer, a humectant and electrodes. The samples were conditioned in the above-mentioned chamber for 24 hours, at 23 °C and 21 % of relative humidity. The electrodes were in the form of metal cylinders with a diameter of 90 mm, so individual samples had to exceed this area to make the results relevant.



Figure 3. FISHER ELEKTRONIK Tera-Ohmmeter TO-3 device

Five measurements were made on each sample at five different locations. After placing the sample, the chamber was locked and after 15 s, the electrical resistance was measured. The electrical voltage of the device was set to 100 V with a tolerance of ± 5 V. All measurements were carried out in the humidity range of 20 to 30 %. The temperature in the chamber was constant.

3. Results and discussion

3.1. Abrasion resistance

Each elemental sample was evaluated by two independent observers. The figure 4 shows selected samples after tests as example. In table 1 are the mass before and after testing and also the mass lost of the samples that have been tested on the woolen fabric. In table 2 are the mass before and after testing and also the mass lost of the samples that have been tested on the sandpaper. The PVD surface treatment on Kevlar fabric was damaged after tests.

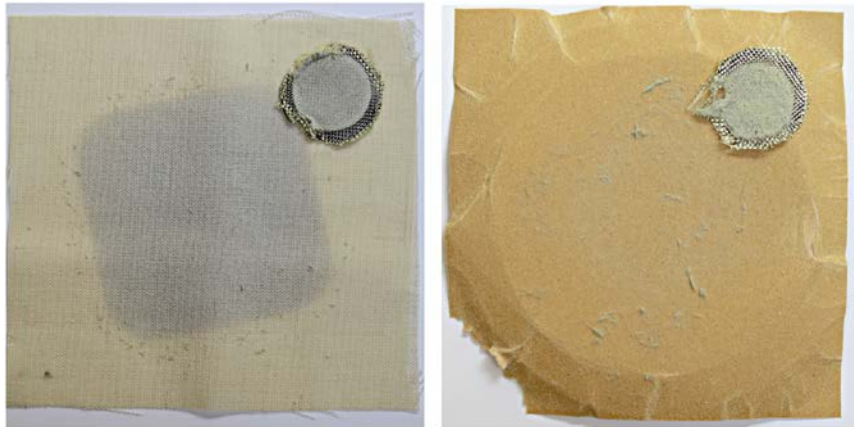


Figure 4. Sample after test on a special woolen fabric (left) and sample after test on 100 grain sandpaper (right)

Table 1. Results of samples that have been tested on the woolen fabric

Sample No.	Cycles interval (number of rubs) [-]	Mass of samples before testing [g]	Mass of samples after testing [g]	Mass loss [g]
1	2 001 – 3 000	0.1382	0.1251	0.0131
2	2 001 – 3 000	0.1550	0.1438	0.0112
3	6 001 – 8 000	0.1740	0.1503	0.0237

Table 2. Results of samples that have been tested on the sandpaper

Sample No.	Number of cycles (rubs) [-]	Mass of samples before testing [g]	Mass of samples after testing [g]	Mass loss [g]
4	50	0.1395	0.1372	0.0023
5	50	0.1968	0.1260	0.0108
6	24	0.1380	0.1369	0.0011

3.2. Electrical resistance

The table 3 shows the measurements of the surface electrical resistance measurement for the uncoated sample and for the PVD coated sample. The table 4 shows the measurements of the internal electrical resistance measurement for the uncoated sample and for the PVD coated sample.

From the obtained data, it can be stated that the PVD coating has influenced the surface electrical resistance by reducing it. PVD treatment has reduced the surface resistance value from the original 2560 Ω to 290 Ω . However, the surface of the sample did not become electrically conductive. This fact was attributed to the nature of the coating. Its thickness in μm is very low. The coating with its particles can not continuously join the single binding points of kevlar fabric. Therefore, despite the deposition of electrically conductive particles on the surface of the fabric, it did not become conductive, even though it dramatically reduced its electrical resistance. According to the following formula, it is possible to calculate the relative surface electrical resistance in Ω :

$$\rho = k \cdot R$$

where k is the geometric coefficient of the electrodes which has a value of 19.8. R is the measured value of surface electrical resistance in Ω .

Table 3. Surface electrical resistance measurement results

No. of measurement	Surface electrical resistance ($\Omega \cdot 10^9$)	
	Uncoated Kevlar sample	Coated Kevlar sample
1	618	313.7
2	3300	306.3
3	2260	341.0
4	3300	206.3
5	3300	284.9
Average	2560	290.4

Table 4. Internal electrical resistance measurement results

No. of measurement	Internal electrical resistance ($\Omega \cdot 10^9$)	
	Uncoated Kevlar sample	Coated Kevlar sample
1	522.7	499.2
2	514.6	508.2
3	453.0	718.2
4	611.9	572.8
5	417.0	471.6
Average	503.8	554.0

4. CONCLUSIONS

On basis of the results from the tests on woolen fabric, the average of loss of weight of all samples was 0.016 g. The average count of turns at which the sample was damaged was 4 167. The exposed surface of the samples was largely free of PVD metal coating. On basis of the results from the tests on sandpaper: the average count of turns at which the sample was damaged was 41. All samples showed low abrasion resistance by the tests on sandpaper.

When comparing the internal electrical resistance values, it can be stated that PVD did not change its values, even though the electrical resistance increased from the original approx. $504 \cdot 10^9 \Omega$ to $554 \cdot 10^9 \Omega$, what is an interesting change. A resistance drop was expected. The internal electrical resistance value of the fabric after PVD treatment has increased, although the change is negligible.

Relative surface electrical resistance values are shown in table 5. The value difference is about 8.8 times.

Table 5. Relative surface electrical resistance values

Relative surface electrical resistance (Ω)	
Uncoated Kevlar sample	Coated Kevlar sample
50 688.0	5 750.7

Kevlar with PVD surface treatment can be used for special applications but it is necessary next study and next standard tests.

ACKNOWLEDGEMENTS

The contribution was supported by the Cultural and Educational Grant Agency of the Slovak Republic KEGA 007TnUAD-4/2017 and the Slovak grant agency VEGA 1/0589/17.

References

1. Vančo, M., Krmela, J., Pešlová, F. (2016). The use of PVD coating on natural textile fibers. *Procedia Engineering*, 136, 341–345. DOI: 10.1016/j.proeng.2016.01.220.
2. Standard STN EN 388 (2017). *Ochranné rukavice proti mechanickým rizikám (Protective gloves against mechanical risks)*. (in Slovak).
3. Standard STN EN 530 (2010). *Odolnosť materiálu ochranných odevov proti oderu. Skúšobné metódy. (Abrasion resistance of protective clothing material. Test methods)*. (in Slovak).
4. Standard STN EN 1149-1 (2006). *Ochranné odevy. Elektrostatické vlastnosti. Časť 1: Skúšobná metóda na meranie povrchového odporu. (Protective clothing. Electrostatic properties. Part 1: Test method for measurement of surface resistivity)*. (in Slovak).
5. Standard STN EN 1149-2 (2000). *Ochranné odevy. Elektrostatické vlastnosti. Časť 2: Skúšobná metóda na meranie vnútorného elektrického odporu materiálu. (Protective clothing. Electrostatic properties. Part 2: Test method for measurement of the electrical resistance through a material (vertical resistance))*. (in Slovak).

PRODUCTION OF THERMO-REGULATING CARPET THROUGH PHASE CHANGE MATERIALS (PCMs) TECHNOLOGY

Azize Ince^{1,3*}, Sennur Alay Aksoy², Volkan Balci¹, Cem Gunesoglu³, Emine Cot¹, Sebnem Sozcu^{1,3}, M. Sakir Erboz¹

¹Kartal Halı Tekstil San. Tic. A.Ş., Şehitkamil, Gaziantep, Turkey, tel.: 090 342 357 01 00, fax: 090 342 357 0116

² Suleyman Demirel University, Faculty of Engineering, Textile Engineering Department, 32260 Isparta, Turkey, tel.: 090 246 2111187

³ Gaziantep University, Faculty of Engineering, Textile Engineering Department, 27310 Sehitkamil, Gaziantep, Turkey, tel.: 090 342 317 27 30, fax: 090 342 317 27 06

*azize.bical@hotmail.com

Abstract:

One of the important groups of smart textiles is the textiles that contained phase change materials (PCMs). There are many PCM applications in the biomedical, electronic, construction, automotive industry and textiles. PCMs are substances that absorb or release energy during phase change (from solid to liquid or liquid to solid). In this study thermo-regulating effect of micro-capsulated phase change materials (PCMs) on carpet comfort is investigated. Paraffins and PEG are applied to wilton type carpets to produce carpets those keep environment temperature for a long time at a range where human body feels comfortable. To achieve ideal comfort temperature, room temperature should be between 23-24 °C and floor temperature 23 - 25 °C. Different phase changing (paraffin and PEG) materials are used together to achieve cooling and heating effect and to keep temperature between ideal comfort temperatures. To prevent leakage of PCMs during melting of substance; a pretreatment such as microencapsulation is required. Complex coacervation method is used for encapsulation of PCMs.

Key words:

PCMs, complex coacervation, thermo-regulation, T-history, microencapsulation

1. Introduction

The main aim of rapidly developing science in many areas is to improve the comfort of human being. The world is gradually becoming more crowded with limited natural sources that force human-being to study on more effective use of these sources. Due to their high thermal energy storage capacity, phase changing materials are consumed in many areas as energy storage materials. While these materials absorb energy as they transform from solid to liquid; they release energy during liquid to solid transformation. As the environmental temperature rises up to the melting point of PCM, it absorbs and stores latent heat from the environment in the course of its melting. As the environmental temperature goes down, PCM releases the stored energy to environment during its solidification. Stored or released energy by PCM is used to prevent sudden temperature changes, to heat or cool the environment [1]. Including water, more than 500 PCMs are known and these materials differs from each other in their heat storage capacity and phase change temperatures. PCMs have different phase change temperatures above and below of comfort temperatures of human body and by selecting and

blending of them, it is possible to impart protection against discomfort. To achieve ideal comfort temperature, room temperature should be between 23-24 °C and floor temperature 23 - 25 °C.

Ghosh and Bhatkhande encapsulated PEG 600 by in-situ polymerization technique. Microcapsules were coated on % 100 cotton fabrics in a bath containing polyurethane as binder. The presence of PEG within microcapsules was confirmed by FTIR analysis. The energy storage capacity of encapsulated PEG was determined as 12.78 J/g [2].

Hawllader et al. [3] studied on encapsulation of paraffin wax by complex coacervation and spray drying methods. The effect of different parameters on PCM encapsulation efficiency, energy storage and release capacity is investigated. DSC analysis is showed that complex coacervation and spray drying methods have a thermal energy storage/release capacity of about 145–240 J/g.

Wang et al. published a study about impact of PCM on intelligent thermal-protective clothing. As the clothing assembly with and without PCM were compared, clothing assembly with PCM save around 30% of energy [4]. Alawadi [5] published a study on thermal analysis of a building brick containing PCM to reduce heat gain. Thermal analysis of bricks with cylindrical holes filled with PCM and different design parameters such as PCM quantity, type and location of PCM were investigated. According to experimental results, PCM incorporated brick reduced heat gain significantly and the amount of filled PCM showed a positive effect.

In this study different phase changing (paraffin and PEG) materials will be used together to achieve cooling and heating effect and to keep temperature between ideal comfort temperatures. Wilton type face to face carpet sample will be used for the application process. As a result of application thermo-regulating carpet will be produced. The encapsulation of PCMs has been developed to prevent migration of liquid core material within fibrous substrate and to decrease evaporation rates.

2. Experimental

2.1. Materials

The part of experimental work consist from encapsulation of PCMs with a natural polysaccharide and an animal protein by complex coacervation method, characterization of encapsulated PCMs, application of wilton type face to face carpets and investigation thermal behavior of treated carpet samples. Carpet samples that consist from acrylic/polyester pile yarns were produced in Kartal Hali.

To achieve ideal comfort temperatures room temperature should be between 23-24 °C and floor temperature 23 - 25 °C. In this process, n-hexadecane, n-eicosane, polyethylene glycol (PEG) 600, polyethylene glycol (PEG) 1000 were used together to achieve cooling and heating effect and to keep temperature between ideal comfort temperatures. PCMs for thermal energy storage are generally solid-liquid phase change materials and therefore they need encapsulation. Natural and biocompatible materials such as arabic-gum and gelatin were selected as the wall material of capsules. Gum arabic is a polysaccharide which is negatively charged above pH 2.2. Arabic gum and gelatin are oppositely charged polymers which were used to form complex structure. All pH adjustments were done with acetic acid. Tannic acid were used to storage of produced microcapsules. Span 20 and Glutaraldehyde (GA; 25% aqueous solution) was employed as cross-linking agent and surfactant respectively. An aqueous dispersion of a carboxylated styrene-butadiene copolymer was used at backside of carpet samples.

2.2. Methods

The mechanism of phase change is dynamic; therefore PCMs are continuously changing from solid to liquid or vice versa depending on environmental temperature. . The encapsulation of PCMs has been developed to prevent migration of liquid core material within fibrous substrate and decreasing evaporation rates. Microencapsulated PCMs consist of two parts; a polymer or inorganic shell and PCM as core material. Micro-encapsulation of PCMs was performed by complex coacervation method. There are two methods for coacervation; simple and complex. The only difference between these two

methods is phase separation step. Simple coacervation contains only one colloidal solute while complex coacervation involves two polymers charged oppositely (27).

Gelatin (cationic) and Arabic gum (anionic) polymer pairs are selected. Biodegradability property is the main reason to select these two polymers. As illustrated in the flow diagram of the complex coacervation method, microcapsules are added into tannic acid for 10 hours. If microencapsulated PCMs application to carpet takes place just after microencapsulation, this step can be eliminated. Figure 1 shows the process of complex coacervation method of PCMs.

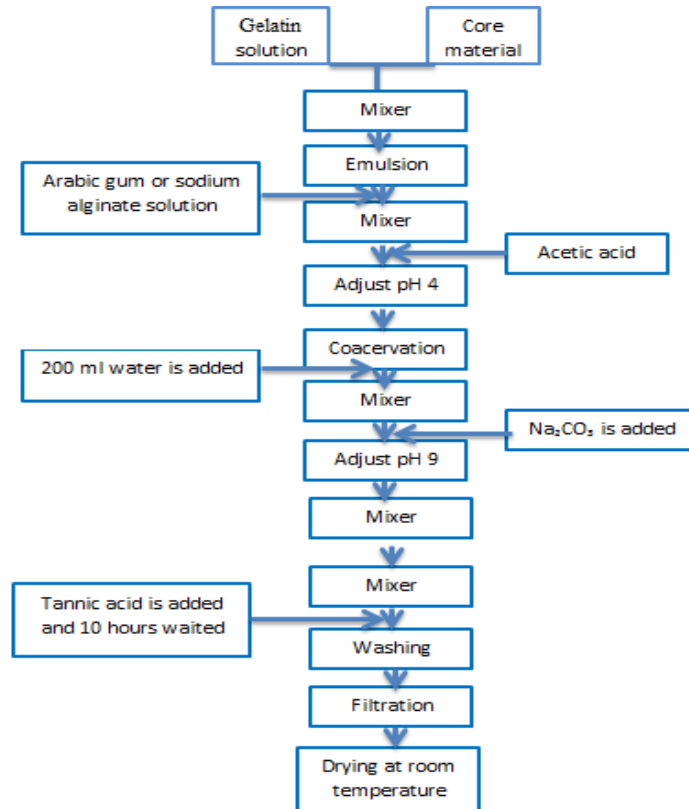


Figure 1. Flow diagram of complex coacervation encapsulation process

In the process, arabic gum and PCM was dispersed in distilled water and Spun 20 was added to this solution. The mixture was stirred at 3000 rpm for 30 min to generate a stable dispersion. Separately, gelatin solution was prepared by dissolving of it in distilled water and this solution was added drop by drop. Acetic acid was added to adjust pH 4-5 and stirred for 90 min. Coacervation between oppositely charged arabic gum and gelatin was started to deposit around PCM. Sodium carbonate (Na_2CO_3) was added in a dropwise mode to adjust pH 9. At this point, solution was diluted by adding distilled water and stirred for 30 min. Reaction medium was cooled to 5 °C and glutaraldehyde was added to harden of microcapsules. The microcapsules were treated with a 10% tannic acid solution. Complex coacervation process was completed by washings, filtering and drying of microcapsules at room temperature.

Microencapsulation process was carried out with different core materials. The detailed component of each sample is listed in Table 1.

Table1. Produced microencapsulated PCMs and their content

Sample	Shell materials	Core material
Sample I	Arabic Gum/Gelatin	n-eicosane
Sample II	Arabic Gum/Gelatin	n-hexadecane
Sample III	Arabic Gum/Gelatin	%80 n-eicosane - %20 PEG 1000
Sample IV	Arabic Gum/Gelatin	%80 hexadecane - %20 PEG 600

The spectroscopic analyses of microcapsules were performed by FTIR instrument. FTIR analysis was the important part to determine the presence of paraffin and PEG in the microcapsule structure.

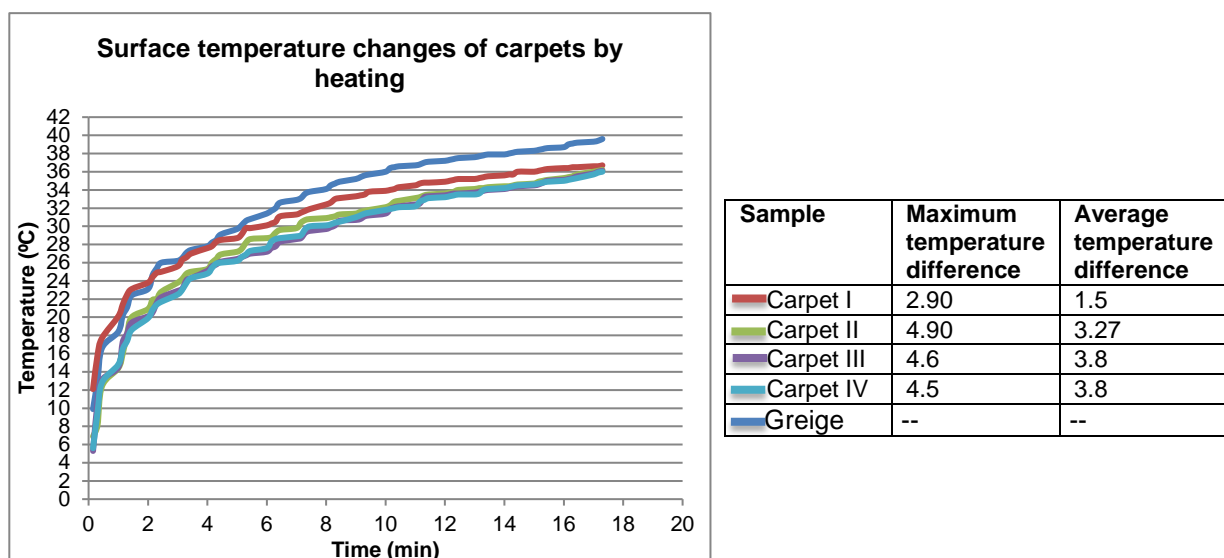
Application of microencapsulated PCMs to carpet samples was performed by mixing them into styrene butadiene latex. In the method, the mixture was stirred by ultrasonic mixture for 10 min at a power %40-50. This mixture was applied at backside of carpet by a simple brush.

The thermo-regulating effect of mic-PCMs will be investigated by T-History method. Test apparatus consists of a thermal camera, an insulated polyurethane box and a data logger. At the beginning of the test, mic-PCM applied carpet samples and untreated carpet sample are conditioned for 24 hours at 0 °C. The samples are placed into insulated box and the temperature of the air in the box is increased instantaneously up to 50 °C. The surface temperature of the sample carpet is recorded by data logger at every 30 s. Same procedure is applied for mic-PCM contained carpet samples and standard untreated carpet samples to compare the effect of PCMs on thermo-regulating.

3. Results and discussion

3.1. *T-History results of carpet samples*

To determine thermoregulating effect of PCMs, T-history measurement of treated samples and untreated sample was carried out. Temperature differences between PCM applied carpets and greige carpets are illustrated in Figure 2. Thermal camera results show that surface temperature of PCM applied carpets increase slower than standard carpet sample. The highest temperature difference observed between Carpet II and greige carpet at the beginning of test (4.90 °C). However the maximum average temperature difference observed for PEG applied samples.


Figure 2. Temperature differences between PCM treated carpet samples and greige carpet sample

As a general result, the warm up speed of PCM applied carpets slower than greige carpet. The surface temperature of the treated carpets lower than greige sample. This shows that PCM incorporated samples resist to heating and provide a cooling effect.

3.2. FTIR analysis results of microencapsulated PCMs

Figure 3 shows the FT-IR absorption spectra of Sample I, eicosane, arabic gum and gelatin. The absorption peaks at 2917 cm^{-1} and 2840 cm^{-1} are the C-H stretching in the IR spectrum of eicosane. These peaks can be observed in the spectra of Sample I at $2918\text{--}2849\text{ cm}^{-1}$ respectively. This approved the presence of eicosane in the microcapsules. Arabic gum was characteristic peak such as O-H stretching band centered at around 3400 cm^{-1} , C-H stretching and bending peak at 2922 cm^{-1} and C-O stretching peak around 1634 cm^{-1} . Gelatin shell of microcapsules was identified with the characteristic peaks: secondary amine stretch peaks (3440 cm^{-1}) and carbonyl stretch peaks between 1680 and 1630 cm^{-1} . The presence of acetal bonds between glutaraldehyde and OH groups of arabic gum/gelatin can be seen from the peaks at 1741 cm^{-1} . A new peak can be observed around 1655 cm^{-1} from IR spectra of sample I. This peak present the shift base C = N (imine) bound stretching vibration from glutaraldehyde and arabic gum reaction. All these information shows that the eicosane microcapsules were successfully formed.

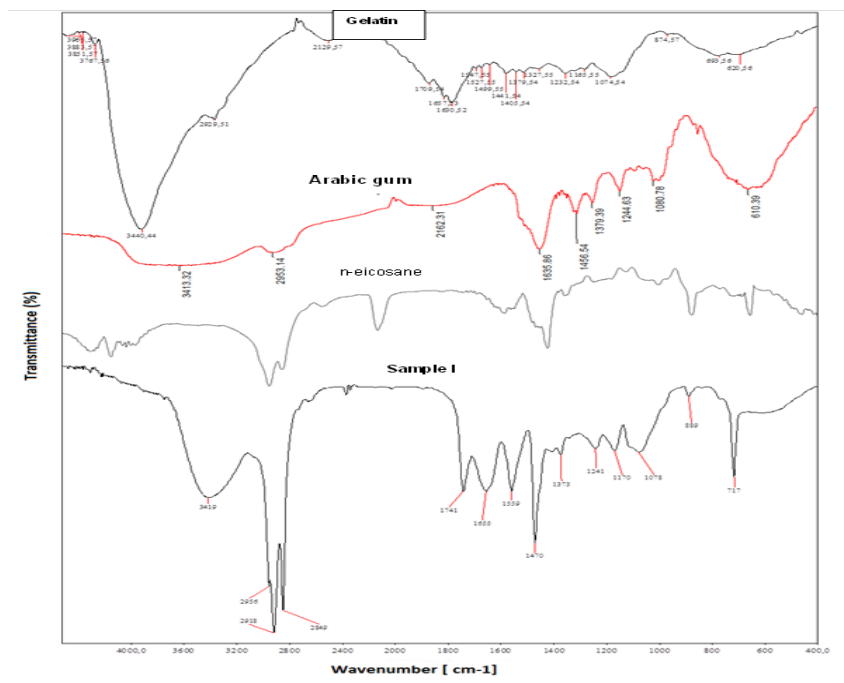


Figure 3. FT-IR absorption spectra of Sample I, eicosane, arabic gum and gelatin

Figure 4 shows the FT-IR absorption spectra of Sample II, hexadecane, arabic gum and gelatin. The two C-H stretching peaks at 2923 cm^{-1} and 2923 cm^{-1} in the IR spectra of n-hexadecane can be observed at sample II spectra at $2924\text{--}2854\text{ cm}^{-1}$ respectively. This is a proof of presence of n-hexadecane paraffin in the microcapsules. The presence of acetal bonds between cross linking agent (glutaraldehyde) and OH groups of arabic gum/gelatin can be seen from the peaks at 1742 cm^{-1} waveband. The peaks occurred at $3450\text{--}3423\text{ cm}^{-1}$ on spectrum of gelatin demonstrated the presence of secondary amine which is a characteristic peak for gelatin. IR spectrum of Sample II showed stretching vibrations peaks around 1654 cm^{-1} waveband. These peaks were caused by formation of C = N (imine) bound from glutaraldehyde and gelatin reaction. These results are the evidence of successful complex coacervation of microencapsulation of hexadecane.

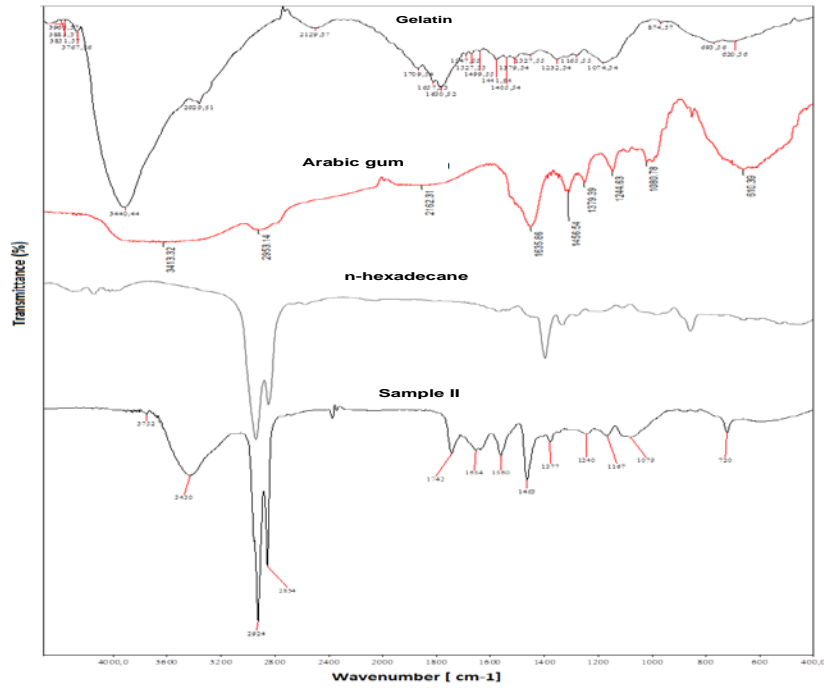


Figure 4. FT-IR absorption spectra of Sample II, hexadecane, arabic gum and gelatin

Figure 5 shows the FT-IR absorption spectra of Sample III, eicosane, PEG 1000, arabic gum and gelatin. The absorption peaks from eicosane spectra at 2917 and 2840 cm^{-1} for the C-H stretching can be seen on IR spectra of sample III at 2919-2851 cm^{-1} respectively. The characteristic peaks of PEG 1000 are the aliphatic C-H stretching vibrations at 2942-2804 cm^{-1} , aliphatic C-H stretching bending at 1457-1231 cm^{-1} and C-O stretching vibrations at 1100 cm^{-1} waveband. Similarly aliphatic C-H stretching bending at 1460-1241 cm^{-1} and C-O stretching vibrations at 1169 cm^{-1} can be seen from IR spectra of sample III. This is the evidence of presence of both eicosane and PEG 1000 in the structure of microcapsules. The presence of arabic gum and gelatin observed from acetal bonds which caused a peak around 1742 cm^{-1} .

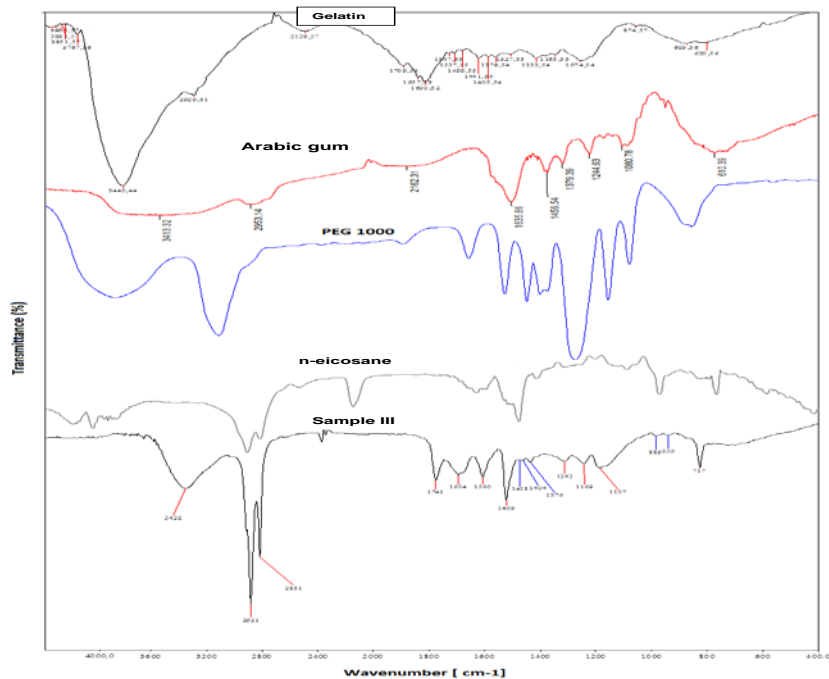


Figure 5. FT-IR absorption spectra of Sample III, eicosane, PEG 1000, arabic gum and gelatin

FTIR spectra of Sample IV, hexadecane, PEG 600, arabic gum and gelatin are shown in Figure 6. Similar to previous samples, two C-H stretching peaks at 2923 cm^{-1} and 2859 cm^{-1} in the IR spectra of n-hexadecane can be observed at sample IV spectra at $2924\text{--}2854\text{ cm}^{-1}$ respectively. PEG 600 spectra showed expected peaks at $2942\text{--}2804\text{ cm}^{-1}$, $1457\text{--}1231\text{ cm}^{-1}$ and 1100 cm^{-1} . These peaks are attributed to C-H stretching vibrations, aliphatic C-H bending vibrations and C-O stretching vibrations respectively. It is observed that C-O stretching vibrations at 1160 cm^{-1} and aliphatic C-H bending vibrations at $1460\text{--}1241\text{ cm}^{-1}$ in FT-IR spectrum of sample IV. These findings are proofs of core materials (PEG 600 and hexadecane) in the structure of microcapsules. The presence of arabic gum and gelatin observed from acetal bonds which caused a peak around 1741 cm^{-1} . The infrared spectrum of the gelatin has a characteristic band in the region of $3450\text{--}3423\text{ cm}^{-1}$. Again the peak around 1654 cm^{-1} showed the reaction between gelatin and glutaraldehyde. These informations indicate the formation of the gelatin-arabic gum wall material.

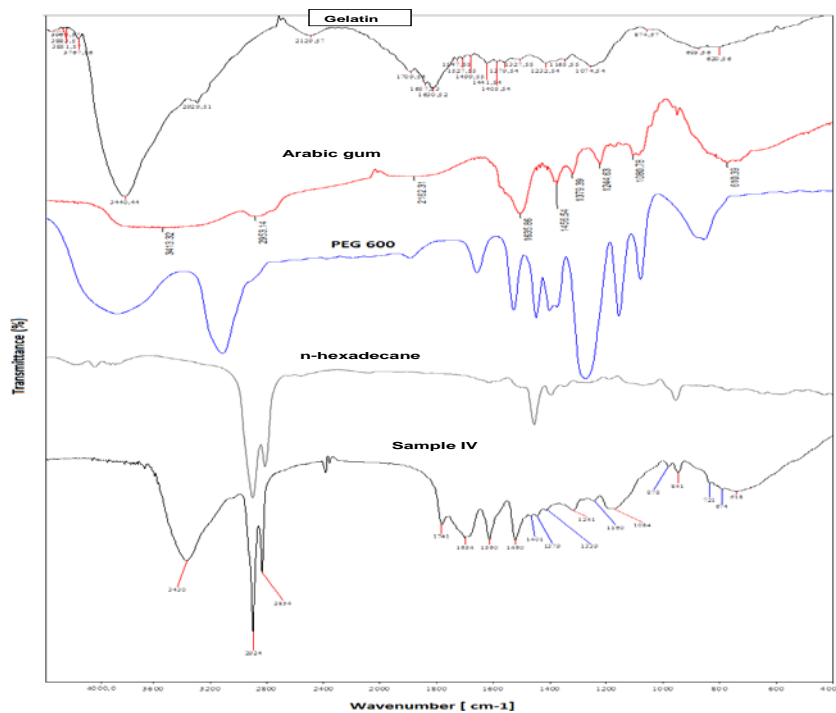


Figure 6. FT-IR absorption spectra of Sample IV, hexadecane, PEG 600, arabic gum and gelatin.

4. CONCLUSIONS

Developments in the field of smart and intelligent textiles draw attention steadily. Today with the rapid increasing of population, demand for energy became higher. Using PCMs for thermal energy storage systems became more popular due to their high latent heat storage capacity. This study shows that this latent heat can assist to keep ambient and floor temperatures within thermal comfort temperature ranges.

ACKNOWLEDGEMENTS

This study is funded by Scientific and Technological Research Council of Turkey (TUBİTAK) with the project number of 3170952.

References

1. S. Alay Aksoy and A. Kuru, «Telef Akrilik Elyaflardan IsıDüzenleme Özellikli YalıtımMalzemesi Üretimi,» Tesisat Mühendisliği, no. 144, 2014.
2. S. Ghosh and P. Bhatkhande, «Encapsulation of PCM for Thermo-Regulating Fabric Application,» *International Journal of Organic Chemistry*, vol: 2, pp. 366-370, 2012.
3. M. Hawlader, M. Uddin and M. M. Khin, «Microencapsulated PCM Thermal-Energy Storage System,» *Applied Energy*, vol 74, no. 1-2, 2003.
4. S. Wang, Y. Li, J. Hu, H. Tokura and Q. Song, «Effect of phase-change material on energy consumption of intelligent thermal-protective clothing,» *Polymer Testing*, vol 25, no. 5, pp. 580-587, August2006.
5. E. M. Alawadhi, «Thermal analysis of a building brick containing phase change material,» *Energy and Buildings*, vol 40, no. 3, 2008.
6. Jamekhorshid, S. Sadramelia and M. M.Farid, «A Review of Microencapsulation Methods of Phase Change Materials (Pcms) as a Thermal Energy Storage (TES) Medium,» *Renewable and Sustainable Energy Reviews*, vol: 31, pp. 531-542, March 2014.

A STUDY ON THE PERFORMANCE OF ANTI-MITE & ANTI-BACTERIAL TEXTILES FOR CLIENTS AT NURSING HOMES

Adnan Mazari¹, Antonin Havelka¹, Marcela Kolinova², Michal Martinka¹, Renata Nemcokova¹

¹ Department of Clothing, Faculty of Textile, Technical University of Liberec, 46117 Liberec, Czech Republic.

² The Institute for Nanomaterials, Advanced Technology and Innovation, Technical University of Liberec, 46117 Liberec, Czech Republic.

mazariadnanahmed@gmail.com

Abstract

The research is part of project "Meditex" which is related to improvement of clothing for the residence specially old people at the health facilities, social care centers, nursing homes and elderly, rehabilitation centers. Due to market demand and requirements at the care center, it is necessary to improve the functionality of the clothing. These clothing particularly focuses on client cloths, patient clothes, bedding and medical staff. In this research modified Poly propylene yarns made fabric with Anti-mite & Antibacterial finish are used to observe the thermo-physiological comfort properties, as in day care centers especially for the old clients the Mite is serious health issue. These finish fabric are usually uncomfortable and have rough feel. 6 different kinds of fabric are tested for anti-mite and for anti-bacterial and thermos-physiological comfort properties of the material. The materials show satisfactory results even after washing and can be used for making clothing or bedding material for the care centers.

Key words

Antimite, anti-bacterial, medical textile, performance clothing, nursing homes.

1. Introduction

House mites (house dust mites) are major problem for allergy in house hold, especially care centres. Unlike scabies mites do not burrow under skin and are actually not parasites but their major feed is human skin and commonly live in clothing and the bed linens.

House mites are directly associated with allergic rhinitis and asthma. There are many ways to remove these mites from environment but do not give effective results and also harmful to the nature. [1, 2].

Allergens from the house environment is a causal activity; however, the effectiveness of many available methods of elimination as well as the reduction of mite proliferation is still being analysed, but it remains controversial or it is denied [3 - 7]. The fabric finishes used for mattress and clothing is common application for the Anti-mite textile materials [7 - 12].

The goals of the project are to test textile fabric made from special finished yarn for Antimite and antibacterial application. The focus of the research initially is on the thermo physiological properties of the material as these chemical finishes negatively affect the comfort properties of the material.

Antimicrobial final treatment with effect

- Bactericidal destroys all bacteria,

- Bacteriostatic reduces bacterial growth.
They are distinguished

1. Germicidal treatments - with the effect of killing germs, the term used for the treatment limiting purulentness
2. Hygienic treatment - or disinfection treatment, eliminating pathogens of microorganisms by applications suitable means
3. Fungicidal treatments - limiting or destroying fungal growth
4. Reducing odors.

2. Experimental Part

The special modified Poly Propylene yarn (Antimite finish No.1799/16) made fabric were recommended by Parasitology institute at the Slovak Academy of Sciences in Kosice, Slovakia. Different PP yarn blend composition was used for this research work.

Three textile materials with standard Anti-mite finish are selected for this research. The composition and properties are shown in table below.

Table 1. Composition of materials

Number	Composition	Finish	Weight [g/m ²]
M1	90% POP10% elastan	Antimite	198.0
M2	70% POP 30% CO	Antimite	191.0
M3	18% POP/77% CO/5% elastan	Antimite	292.0
B1	61% Tencel/35% POP Ag/ 4% elastan	Anti bacterial	244
B2	48 Viloft/32% CO/20% POP Ag	Anti bacterial	189
B3	53% Trevira bioact./28% Viloft/19%CO	Anti bacterial	206

Following tests are carried out to observe the comfort and functional property of these materials.

1. Total hand value
2. Air permeability
3. Thermal resistance and water vapour permeability
4. Thermal effusivity

3. Results and discussion

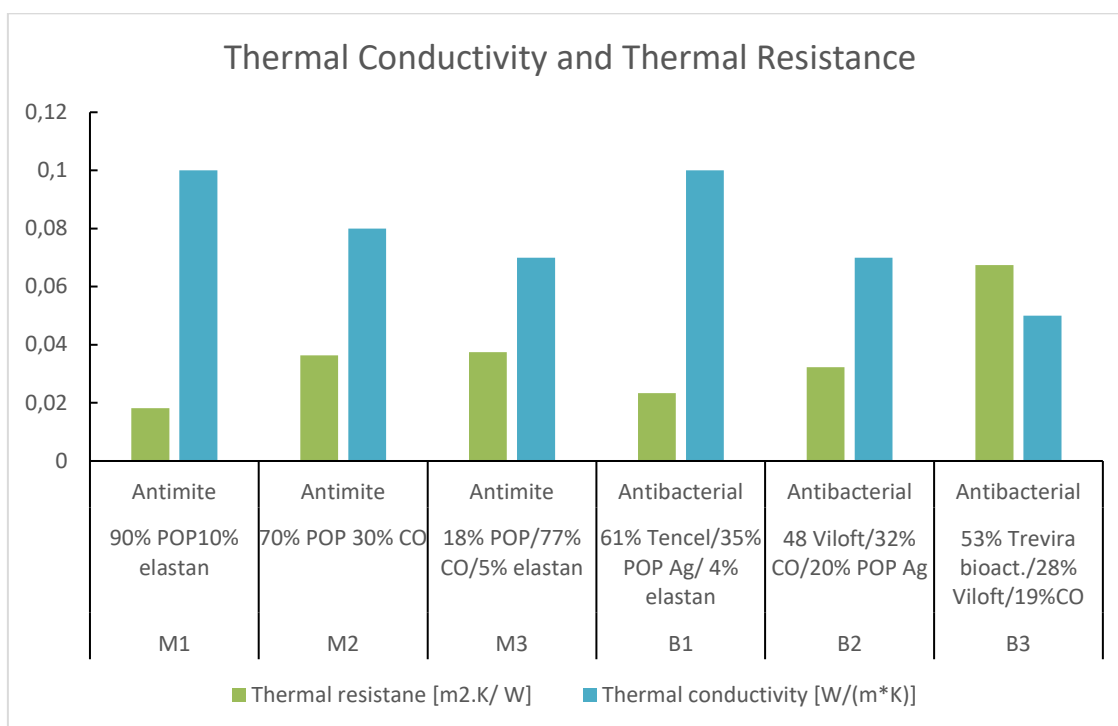
The samples are tested for multiple thermos physiological tests.

- 1- The total hand value is measured by Kawabata Evaluation System
- 2- The Air permeability is measured by device SDL M021S using CSN EN ISO 9237
- 3- Thermal resistance and water vapour resistance is measured using sweating guarded hotplate using ISO standard 11092
- 4- Thermal conductivity and Effusivity is measured by device C-THERM TCi using D7984-16

Table 2. Properties of the materials

Number	Composition	Finish	THV Feel	Air permeability [mm/s]	Thermal resistance [m ² .K/W]	Water vapour resistance [m ² .Pa/W]	Thermal conductivity [W/(m ² .K)]	Thermal absorptivity effusivity [W ² sm ⁻⁴ K ⁻²]
M1	90% POP10% elastan	Antimite	4.13	4.8	0.0182	4.0838	0.1	205
M2	70% POP 30% CO	Antimite	4.7	51	0.0363	4.5255	0.08	160
M3	18% POP/77% CO/5% elastan	Antimite	3.89	7.4	0.0375	5.5512	0.07	122
B1	61% Tencel/35% POP Ag/ 4% elastan	Antibacterial	4	8.2	0.0234	4.1738	0.1	208
B2	48 Viloft/32% CO/20% POP Ag	Antibacterial	5.71	32	0.0323	4.57	0.07	118
B3	53% Trevira bioact./28% Viloft/19%CO	Antibacterial	4.66	70	0.0674	6.6192	0.05	61

Thermal conductivity and thermal resistance of material is shown in figure 1.


Figure 1. Thermal property of the material

4. CONCLUSION

It can be concluded from our research that the Antimite and antibacterial textile materials have good total hand value and low thermal conductivity. Also the material has satisfactory air permeability. These factors are very important for comfort of textile clothing. It is also observed that the material has low water vapor resistance which makes it easy for the sweat and moisture from body to the environment. The high moisture and humidity in the microclimate is one of the significant reason which provides required conditions for the house mites to grow. The research work will continue in future regarding the performance of the material for Anti-mite ability and the effect of washing on life time of performance.

ACKNOWLEDGEMENT

Č.FV10098 Tul.č. 17766, MEDITEX - Výzkum a vývoj nových typů pokročilých textilních materiálů s vysokým potencionálem pro uplatnění ve speciálních textiliích určených pro zdravotní a následnou péči.

References

1. Buczyłko K. *Eliminacja alergenów w alergiina roztocze jest skuteczna i konieczna– kontra. Alergia Astma Immunol* 2004;9, pp. 27-30
2. Samoliński B. *Eliminacja alergenów walergii na roztocza jest skuteczna i konieczna– za. Alergia Astma Immunol.*2004; 9, pp. 23-5
3. Causer S.M., Lewis RD, Batek JM Sr,Ong K.H.; *Influence of wear, pile height,and cleaning method on removal of miteallergen from carpet. J Occup EnvironHyg.* 2004 Apr; 1(4), pp. 237-42.
4. Causer S., Shorter C., Sercombe J.;*Effect of floorcovering construction on FIBRES & TEXTILES in Eastern Europe 2008, Vol. 16, No. 4 (69) 125content and vertical distribution of housedust mite allergen, Der p I. J Occup EnvironHyg.* 2006 Apr; 3(4), pp. 161-8.
5. Gøtzsche PC, Johansen HK. *Housedust mite control measures for asthma:systematic review. Allergy.* 2008 Jun;63(6), pp. 646-59.
6. Gøtzsche P. C., Johansen H.K.; *Housedust mite control measures for asthma.Cochrane Database Syst Rev.* 2008 Apr16(2), CD001187
7. Senti G., Steinmann L.S., Fischer B.,et al.; *Antimicrobial silk clothing in thetreatment of atopic dermatitis provescomparable to topical corticosteroidtreatment. Dermatology.* 2006; 213(3),pp. 228-33.
8. Vojta P., Randels S., Stout J. et al.; *Effectsof physical interventions on house dustmite alergen levels In car pet, bed andupholstery dust In low-income, urban homes.*Environ Health 2001;109, pp. 815-9.
9. Colt J., Gunier R., Metayer C., et. al.;*Household vacuum cleaners vs the highvolumesurface sampler for collection ofcarpet dust samples in epidemiologicstudies of children. Environ Health* 2008;7, pp. 186-90.
10. Mason R.J.; *Fabrics for atopic dermatitis.Fam Health Care.* 2008; 18(2), pp. 63-5.11. Buczyłko K., Korzycka-Zaborowska B.,Michalak A.; *Wpływ złożonego preparatuakarycydu na poprawę objawów alergii naroztocza. Alergia Astma Immunol* 2008;13, pp. 42-52.
11. Ricci G., Patrizi A., Bellini F., et al.; *Use ofttextiles in atopic dermatitis: care of atopicdermatitis. Curr Probl Dermatol.* 2006;33, pp. 127-43.

HYDROPHOBIC AND ANTIBACTERIAL TREATMENT OF TEXTILES USING ORGANIC-INORGANIC HYBRID LAYERS PREPARED BY SOL-GEL

Vojtěch Miller¹, Hana Šourková², Irena Lovětinská Šlamborová¹, Petr Exnar¹, Jiří Škach³

¹Faculty of Science, Humanities and Education, Department of Chemistry, Technical University of Liberec, Studentska 2, 461 17 Liberec, Czech Republic. E-mail: vojtech2miller@gmail.com, irena.slamborova@tul.cz, petr.exnar@tul.cz - corresponding author

²The Institute for Nanomaterials, Advanced Technology and Innovation, Technical University of Liberec, Studentska 2, 461 17 Liberec, Czech Republic. E-mail: hana.sourkova@tul.cz

³Hernia Center, Regional Hospital of Liberec, Husova 357, 460 63 Liberec, Czech Republic. E-mail: jiri.skach@nemlib.cz

Abstract:

The sol-gel method allows the preparation of organic-inorganic layers with the possibility of adjusting the resulting properties to a relatively wide range. Potentially very interesting treatments are hydrophobic or antibacterial layers that can be applied to practically all types of textiles. Their main advantage is, in addition to their excellent adhesion to the fabric surface, their high resistance to both mechanical and chemical attack.

On non-polar textiles, the increase in layer adhesion is supported by surface plasma treatment. Resistance of layers on fabrics has been confirmed by functionality even after repeated washing.

Key words:

Sol-gel method, hydrophobicity, antibacterial layer, textile, organic-inorganic hybrid material, plasma treatment

1. Introduction

The sol-gel process is a chemical method for preparing nanolayers and is mainly used in the synthesis of the oxidic layers. Its utilization increases due to its universality and simplicity, without the need for expensive laboratory equipment for the vacuum processes. Other advantages include cleanliness and homogeneity of the final product.

The principle of the sol-gel process rests in the preparation of the sol – mainly from the alkoxides. Prepared sol is afterwards applied onto the surface of the substrate (by wetting, spraying, etc.). Evaporation of the remaining solvent and placing the sol in contact with the air humidity leads to an exponential increase in hydrolysis and rapid transformation of the sol into a gel and further to a xerogel. In the case of hybrid inorganic-organic materials, the final step is to polymerize the coating material either by the heat or by the UV light if there are any photo-initiators built into the nanolayer [1-3].

The research that includes the undertaken experiments in this paper targets the development of hydrophobic or antibacterial coating for the textile materials.

2. Experimental

2.1. Materials

Materials used

Pure cotton (further referred as Ba) and pure polyester (further referred as PE) were chosen for the first series of experiments that compares microbiological behavior of the textiles with antibacterial or hydrophobic (also antifouling) layers.

AMANDA (100% PE), CARLTON (100% Ba) and TAURUS (mixed Ba/PE 50/50) textiles were chosen for the second series of the experiments that deals with the optimization of the hydrophobic coating.

Monofilaments for the medical hernia nets Bard Mesh (polypropylene monofilament, further referred as PP monofilament), manufacturer C. R. Bard, Inc. and Parietex Hydrophobic 3-Dimensional Mesh (PE monofilament), manufacturer Covidien were chosen for the third series of the experiments that test possibilities of the treatment of the medical materials.

Preparation of sols and their application

All of the sols for the surface treatment of the tested textiles were prepared by the sol-gel method from 3-(trimethoxysilyl)propyl methacrylate and tetraethoxysilane in the isopropyl alcohol solvent by an acid catalysis.

The sol marked as AD30 was used for the antibacterial treatment – bounded cations of silver, copper and zinc were added to the basic composition and the acid catalysis was secured by adding a small amount of nitric acid. Composition of this sol and its preparation are protected by patents [4-6].

Hydrophobic treatments were applied by the sol AE10 and further by the sols from series AF (AF8-2, AF10-2 and AF12-2), all of them with added catalytic amount of a hydrochloric acid. As a hydrophobic agent in sols AE10, AF10-2 and AF12-2 was used trialkoxyalkylsilane with alkyl – hexadecyl in this case. The sols AE10 and AF10-2 were different only in the details of the preparation. The sol AF12-2 had enhanced volume of hexadecyl groups. The hexadecyl was substituted with a dodecyl in the sol AF8-2. The detailed process of synthesis of the hydrophobic sols is described in publication [7].

All of the layers are characterized by an excellent chemical resistance against all organic solvents and water solutions except highly concentrated alkali hydroxides and hydrofluoric acid. The thickness of the layers can be adjusted from 80 to 200 nm according to the dilution of the sols and the way of the application of the sol.

All of the samples of the textiles were cleaned by repeated soaking into the isopropyl alcohol or by a plasmatic treatment (in the case of the hernia nets) prior to the application of the sols. The application of the sols onto the surface of the tested textiles was done by foulard (pressure 5 bars, velocity of cylinders 3 m/min). The application of the sols onto the hernia nets was done by soaking the nets in the sol followed by pulling out – this process was chosen due to the structure of the material – knitwear. The application of the sols was followed by the heat polymerization, which was done in 85 °C/3 h (in the case of materials with PE or PP) or in 150 °C/2 h (in the case of pure Ba).

Plasmatic treatment of hernia nets

For enhancing adhesion of antibacterial layers onto the hernia nets and similar substrates it was necessary to treat the surface by plasma with a vacuum aperture by application of the oxygen plasma (device LA400, flow of oxygen 200 sccm with pressure 100 Pa, 10 s for PP monofilament, 60 s for PE monofilament) in the company SurfaceTreat Turnov. The adhesion of the applied layers especially onto the PP monofilament without this treatment was insufficient. There was also tested an atmospheric plasma treatment of the

surfaces but the results were inconvenient (worse adhesion of the layers with the low intensity, destruction of monofilaments with higher intensity).

2.2. Methods

Determining antibacterial properties

Following pathogenic bacterial strains from the Czech collection of microorganisms of Masaryk university Brno were used to test the antibacterial properties.

1. *Escherichia coli* (E.C.) - CCM 2024 (ATCC 9637), gramnegative bacteria (G-).
2. *Staphylococcus aureus* (S.A.) - CCM 2260 (ATCC 1260), grampositive bacteria (G+).

AATCC Test Method 147-2016 [8]

This method is qualitative, tentative and it should be done prior to the method AATCC 100-2012. The antibacterially treated sample is placed on the agar which is standardly applied with the bacterial inoculum in several lines. A modification of this method was used in this case where the bacterial inoculum was applied to the whole surface of the agar. After 24 hours of incubation there was rated grow of the bacteria under the tested sample as well as the inhibitory (halo) zone around the sample.

Specific conditions of the tests: There was cut a square sample of 18x18 mm (according to the norm). 1 ml of the bacterial inoculum with a concentration of 10⁵ CFU/ml was inoculated individually on a Petri dish with the blood agar. Tested sample was put in the middle of the dish and firmly pressed to the agar. The incubation took place in a thermostat with 37 °C for 24 hours. After the specified incubation there was the halo zone rated (its area) and the inhibition of bacteria under the sample (place of a sample).

AATCC Test Method 100-2012 [9]

This method is quantitative and there is rated a reduction factor which states the reduction (in percent) of the inoculated concentration of the bacteria due to the effect of the sample. The result is a number of survivor bacteria colonies (CFU) and from this number there is calculated inhibition degree (in %). It is always necessary to compare the treated sample with an untreated one (standard).

Specific conditions of the tests: There was cut a square sample of 18x18 mm which was placed into a sterile container. There was applied 100 µl of the respective bacterial strain with a concentration of 10⁵ CFU/ml. Incubation took place in the thermostat with 37 °C for 24 hours. After incubation there was added 10 ml of a physiological solution. After vortexing there was pipetted 1 ml and it was inoculated on the Petri dish with the blood agar (there were inoculated triplets from each sample). The result is a sum of number of colonies on all three dishes.

Determination of hydrophobicity

Krüss Drop Shape Analyser DSA30 device in Surface Treat Turnov was used to determine the wetting angles of water. The wetting angle was measured by measuring a small exactly-defined drops placed on the surface of the textile, with a defined volume of 3 µl. The results are calculated as the average of the 10 measurements with the corresponding standard deviation.

3. Results and discussion

3.1. Microbiological behavior of textiles with layers

The sol AD30 was used as an antibacterial treatment for the tested textiles (pure cotton Ba and pure polyester PE). Next to the antibacterial treatment based on the effect of cations Ag, Cu and Zn in the active layer there was also tried a treatment of the textiles with the hydrophobic sol AE10 where it was

assumed an antifouling effect will take place [10-11]. The antifouling effect restricts the adhesion and the number of bacteria and subsequent creation of the biofilm on the surface of the textile.

The details about the used sols and their application on the tested textile are mentioned in the paragraph 2.1. Testing of the antibacterial properties on the prepared samples of the textiles together with the untreated samples was done both by the qualitative AATCC Test Method 147-2016 and by the quantitative AATCC Test Method 100-2012. The results are summarized in tables 1 and 2.

Table 1. The results of the antibacterial testing of the textiles by the AATCC Test Method 147-2016.

Bacterial strain	Sample	Inhibition zone, inhibition
<i>Escherichia coli</i>	Ba - US	0 % inhibition zone, 0 % inhibition under the sample
	PE - US	0 % inhibition zone, 0 % inhibition under the sample
	Ba - AE10	0 % inhibition zone, 0 % inhibition under the sample
	PE - AE10	0 % inhibition zone, 0 % inhibition under the sample
	Ba - AD30	Inhibition zone d = 1.3 mm, 100 % inhibition under the sample
	PE - AD30	Inhibition zone d = 2.9 mm, 80 % inhibition under the sample
<i>Staphylococcus aureus</i>	Ba - US	0 % inhibition zone, 0 % inhibition under the sample
	PE - US	0 % inhibition zone, 0 % inhibition under the sample
	Ba - AE10	Inhibition zone d = 5.5 mm, 100 % inhibition under the sample
	PE - AE10	0 % inhibition zone, 0 % inhibition under the sample
	Ba - AD30	0 % inhibition zone, 100 % inhibition under the sample
	PE - AD30	Inhibition zone d = 5.5 mm, 100 % inhibition under the sample

US – untreated standard

Table 2. The results of the antibacterial testing of the textiles by the AATCC Test Method 100-2012.

Bacterial strain	Sample	Result	% inhibition
<i>Escherichia coli</i>	Ba - US	UQ	0 %
	PE - US	UQ	0 %
	Ba - AE10	28	100 %
	PE - AE10	300	99.9 %
	Ba - AD30	2	100 %
	PE - AD30	2	100 %
<i>Staphylococcus aureus</i>	Ba - US	UQ	0 %
	PE - US	450	Sample stops compact growth of test strain
	Ba - AE10	1	100 %
	PE - AE10	0	100 %
	Ba - AD30	2	100 %
	PE - AD30	0	100 %

US – untreated standard; UQ – unreadable quantity

According to the acquired results it is visible that the effects on the used bacterial strains differ in partial parameters. In both cases it can be said that the results are greatly positive.

The qualitative method with the hydrophobic treatment of AE10 with the bacterial strain *Escherichia coli* has not showed any inhibitory effect in any of the materials used. On the other hand, with the bacterial strain *Staphylococcus aureus* there has been noted an inhibition zone and 100% inhibition under the sample on the cotton sample. This means that the treatment on the cotton limits the adhesion and the grow of the bacteria *Staphylococcus aureus*. There has been no inhibitory effect noted on the polyester samples.

The quantitative method with the antibacterial treatment of AD30 showed the inhibition under the samples (that means the treatment stopped the growth of the bacteria under the material with a treatment) for both materials (Ba, PE) and there also appeared inhibition zones which indicates that the components of the final layer (cations Ag, Cu and Zn) partially release themselves into the surroundings and inhibit the bacterial strain.

The quantitative method proved excellent or very good inhibitory effect to all of the tested samples with layers. The number of cultivated bacterial colonies of *Escherichia coli* on the materials with the hydrophobic treatment AE10 has been larger than on the other treated samples. Nevertheless, even these results can be rated as good when compared with the standards.

The really important aspect is a stability of the antibacterial layer on the textile substrate which has been verified by repeated washing of cotton socks with the layer AD30. Still suitable antibacterial properties have been observed even after 50th washing by a standard washing cycle [2].

3.2. Hydrophobic treatment of textiles

The hydrophobic treatment of the textiles is interesting for a number of practical uses, mainly for outdoor finishes of sportswear and working cloth. Next to stopping the liquid water penetration, great penetration of water vapors and a long-term preservation of mechanical and utility properties of textiles it has also important ecological aspect. In contrary to a commonly used impregnations with the addition of fluorine compounds nor the tested sols nor the final layers contain any ecologically problematic components while keeping all the necessary requirements for the outdoor usage. Table 3 summarizes the results of test with three different test sols. As you can see in the results all of the textiles with the treatment have outstanding hydrophobic properties and there are basically no differences between the tested sols.

Table 3. The results of the water wetting angle measurement on the treated textiles (n = 10).

Textile	Sol	Water	
		Angle [°]	s _x [°]
AMANDA (PE)	US	Soaking	
AMANDA (PE)	AF8-2	124.5	4.0
AMANDA (PE)	AF9-2	125.8	2.5
AMANDA (PE)	AF12-2	126.3	2.6
CARLTON (Ba)	US	Soaking	
CARLTON (Ba)	AF8-2	122.8	5.3
CARLTON (Ba)	AF9-2	124.1	4.1
CARLTON (Ba)	AF12-2	124.0	3.2
TAURUS (Ba/PE)	US	Soaking	
TAURUS (Ba/PE)	AF8-2	135.3	4.1
TAURUS (Ba/PE)	AF9-2	132.5	3.0
TAURUS (Ba/PE)	AF12-2	135.1	4.6

s_x – standard deviation; US – untreated standard

3.3. Hernia nets

The hernia implants (nets) are used for a surgical solution of hernias which is a bag-like exit of a peritoneal cavity where part of the abdominal organs moves to. Although there is applied the latest knowledge and used modern materials in the surgical solution, one of the post-operative complication is an inflammation. In the material which are the hernia nets made of can occur so called hiding of the microorganisms from the effects of the immune system and persistence of inflammation or delay of break out in the range from several months to several years [12].

The most promising strategy in the present is the usage of an implant material with added antibacterial properties which stops the bacterial adhesion and creates a biofilm on its surface. The design of these resistant implants [13] is based on a modification of their surface by anti-adhesive substance, antimicrobial agents, antiseptic, antibiotic, metals or their ions or inhibitors of bacterial adherence coatings. These treatments should be nontoxic in the case of releasing controllably-degradable non-affecting original biomechanical properties of the material and non-obstructing integration of the implant to the organism.

Currently there are no hernia nets with the antimicrobial treatment which would meet all the requirements of the nontoxicity. Greatly promising treatment is the applied layer summarized below which contains ions of Ag, Cu, and Zn and very effectively stops growth of the pathogenic bacteria. The results of the testing in this work are summarized in table 4.

Table 4. The results of antibacterial testing of the hernia nets by the AATCC Test Method 147-2016.

Sample	<i>Escherichia coli</i>	<i>Staphylococcus aureus</i>
PP monofil - US	0 % inhibition under the sample	0 % inhibition under the sample
PE monofil - US	5 % inhibition under the sample	2 % inhibition under the sample
PP monofil - AD30	25 % inhibition under the sample	100 % inhibition under the sample
PE monofil - AD30	100 % inhibition under the sample, inhibition zone d = 2 mm	100 % inhibition under the sample, inhibition zone d = 1.5 mm

US – untreated standard

The applied antibacterial treatment to the surface of hernia implants enhanced their antibacterial effect in the comparison with the standards. Even the standard PE monofil proved inhibition under the sample for both the bacterial strains but after the application of the sol the inhibition improved and showed itself as inhibition zones with the material PE. This effect is, especially in the case of the hernia nets, requested because it will not only kill the bacteria in the application spot but also in the near surroundings and prevent creation of the inflammation which could appear as an after-effect of an operation.

4. CONCLUSIONS

The organic-inorganic hybrid layers based on 3-(trimethoxysilyl)propyl methacrylate and tetraethoxysilane prepared by the sol-gel method have great adhesion and long-term durability on the surface of the polar textiles. When the application to the non-polar textile is needed it is necessary to treat the surface of the textile with the low-pressure oxygen plasma.

Significant modification of the properties of the prepared layers can be achieved by adding the proper additions (nitrates of Ag, Cu and Zn for the antibacterial layers, trialkoxyalkylsilanes with alkyl with 12 to 16 carbons for the hydrophobic layers) to the basic composition of the sols.

By using the both standardized methods it was confirmed the antibacterial effectiveness of the layer AD30 on all of the tested textiles and the hernia nets. According to the achieved results it is noticeable that the effects on the used bacterial strains differ in partial parameters but in all of the cases, it can be said that the results are quite positive.

The really important aspect is a durability of the antibacterial layer on the textile substrate which has been verified by repeated washing of the cotton socks with the layer AD30. Still suitable antibacterial properties have been observed even after 50th washing by a standard washing cycle.

In the case of the hydrophobic layer AE10 there have been anticipated just a lesser antifouling effect during the antibacterial tests. The expectation has been confirmed. The qualitative method on the bacterial strain *Escherichia coli* did not show any inhibition effect on neither of the tested materials. On the other hand, the bacterial strain *Staphylococcus aureus* on the cotton showed the inhibition zone plus 100 % inhibition under the sample. That means the treatment on the cotton limits the adhesion and the grow of bacteria *Staphylococcus aureus*. There was no inhibitory effect observed on the polyester. The quantitative method on the other hand showed excellent or great inhibitory effect on all of the samples with the hydrophobic layers AE10. The number of the bacterial colonies of *Escherichia coli* on the materials with this treatment have been larger than on the other treated samples. Nevertheless, even these samples can be classified as great when compared with the untreated samples.

The measuring of the water wetting angles on the textiles with all of the types of hydrophobic treatments confirmed that all the textiles with treatment have excellent hydrophobic properties and among both the used sols and the textiles there were no real differences.

The antibacterial treatments of the textiles (both the classical and the hernia nets) are greatly perspective for a medical usage. This treatment causes antibacterial effect that leads to the death of tested bacteria. The hydrophobic treatment had significantly lower effectiveness during antibacterial tests. Still, for a number of usages in common life is it enough to stop adhesion and further bacterial growth (bacterial-static effect).

The hydrophobic treatment of the textiles is interesting for a number of practical uses, mainly for the outdoor finishes of sportswear and working cloth. In contrary to the commonly used impregnations with addition of fluorine compounds nor the tested sols nor the final layers contain any ecologically problematic components while keeping all the necessary requirements for the outdoor usage.

ACKNOWLEDGEMENTS

This publication was written at the Technical University of Liberec as part of the project TAČR TH02020145 "Hydrophobic UV-lacquers and nano-layers protecting substrates against bio-attack" and the SGS project no. 21176/11 by the Ministry of Education of the Czech Republic.

References

1. Zajícová, V., Exnar, P., Staňová, I. (2011). Properties of Hybrid Coatings Based on 3-trimethoxysilylpropyl methacrylate. *Ceramics – Silikáty*, 55(3), 221-227.
2. Šlamborová, I., Zajícová, V., Karpíšková, J., Exnar, P., Stibor, I. (2013). New Type of Protective Hybrid and Nanocomposite Hybrid Coatings Containing Silver and Copper with an Excellent Antibacterial Effect Especially Against MRSA. *Material Science and Engineering C*. 33(1), 265-273.
3. Exnar, P., Lovětinská-Šlamborová, I., Veverková, I., Danilová, I. (2015). Antimicrobial hybrid nanolayers prepared by sol-gel method. In: *NANOCON 2015, Conference Proceedings, Brno, Oct.14-16.2015. Ostrava: Tanger, 525-529. ISBN 978-80-87294-63-5.*
4. Šlamborová, I., Zajícová, V., Exnar, P. Antibacterial layer active against pathogenic bacteria, particularly against the MRSA bacterial strain, and the method of its production. CZ 303 250, 7.4.2011, 9.5.2012.
5. Šlamborová, I., Zajícová, V., Exnar, P., Stibor, I. Antibacterial layer active against pathogenic bacteria, particularly against the MRSA bacterial strain, and the method of its production. CZ 303 861, 23.5.2012, 18.4.2013; WO 2013174356, 28.11.2013; EP 2852630, 1.4.2015.
6. Lovětinská-Šlamborová, I., Zajícová, V., Exnar, P., Stibor, I. Antibacterial hybrid layer operating against pathogenic bacterial strains, particularly against the bacterial strain MRSA, and a method for its preparation. CZ 305 045, 28.8.2013, 25.2.2015; EP 2843019, 12.8.2014.
7. Miller, V., Bakalova, T., Exnar, P., Lovětinská Šlamborová, I., Louda, P. (2018). Mechanical resistance of hydrophobic inorganic-organic nanolayers with antifouling effect. *Manufacturing Technology*, in press.
8. AATCC Test Method 147-2016, Antibacterial Activity Assessment of Textile Materials: Parallel Streak Method.
9. AATCC Test Method 100-2012, Antibacterial Finishes on Textile Materials: Assessment of.
10. Yebra, D.M., Kiil, S., Dam-Johansen, K. (2004). Antifouling technology—past, present and future steps towards efficient and environmentally friendly antifouling coatings. *Progress in Organic Coatings*. 50(2), 75–104.
11. Nanoservice (2018). Antifouling-Nano DS. Retrieved September 5, 2018. Web site: <http://www.nanoservice.cz/Antifouling-lode/>.
12. Rastegarpour, A., Cheung, M., Vardhan, M., Ibrahim, M.M. et al. (2016). Surgical mesh for ventral incisional hernia repairs: Understanding mesh design. *Plastics Surgery*, 1, 41-50.
13. Mancino, A.T., Lalani, T. (2018). Wound infection following repair of abdominal wall hernia. Retrieved September 5, 2018. Web site: <https://www.uptodate.com/contents/wound-infection-following-repair-of-abdominal-wall-hernia/print>.

POLYMERIC NANOFIBERS PRODUCED BY NEEDLELESS ELECTROSPINNING

Evren Boyraz¹, Fatma Yalcinkaya²

¹Technical University of Liberec, Textile Faculty, Department of Material Engineering, Tel : +420 608 938 118 ,Studentska 1402/2, 46117, Czech Republic

²Technical University of Liberec, Centre for nanomaterials, Advanced Technology and Innovation, Department of Nanomaterials and Informatics, Studentska 1402/2, 46117, Czech Republic
E-mail: evrenboyraz@gmail.com

Abstract:

Nanotechnology is such technology which touches a raw nerve of the world with various application areas such as physics, chemistry, biology, information technologies, medicine, etc. Via nanotechnology, it is possible to create solutions which are vital to global warming, treatment of wastewater, artificial organs, etc.

The types of electrospinning are; basic needle electrospinning, melt electrospinning, gas-jacket electrospinning, bubble electrospinning, magneto electrospinning, conjugate electrospinning, co-axial electrospinning, needleless electrospinning and centrifugal electrospinning.

In this review, a comprehensive study about the preparation of polymeric solution for fabricating nanofibrous webs and the optimization process of needleless electrospinning system is provided. In addition to this, the future perspectives of produced nanofibers are also discussed.

Key words:

Nanotechnology, electrospinning, nanofibers, polymer

1. Introduction

Nanofibers have gained huge interesting driven by their unique and fascinating properties over their conventional fiber counterparts. Nanofibers compared to conventional fibers, with higher porosity, lower density, higher surface area to volume ratios and smaller pore size, offer an opportunity for use in a wide variety of applications including composite, filtration, protective clothing, composite materials, biomedical application (tissue engineering, scaffolds, bandages, and drug release systems), electronic applications, sensors, design of solar sails and flexible photocells. The research and development of nanofibers has gained much prominence in last decades. Fibers with a diameter range around 100-1000 nm are generally classified as nanofibers. There are several methods to fabricate nanofibers such as; drawing, template synthesis, island-in-the-sea, phase separation, self-assembly and electrospinning. Electrospinning process is one of the most successful methods among other methods for producing nanofibers and probably is the only process with the potential for mass production.

In recent decades, electrospinning has received a great deal of attention due to its versatility in the spinning of a wide variety of polymeric fibers, and its suitability in producing fibers with the fiber diameter on submicrometre or nanometre scales. Electrospinning technique allows the fabrication of a controllable continuous nanofiber webs made of synthetic polymers, of natural polymers, or of inorganic substances. This method was introduced more than 80 years ago [1, 2]. This method is an economical and simple method used in the preparation of polymer fibers. In general principle, high voltage is used to create an electric field between a droplet of polymer solution at the tip of a needle

and a collector plate. When the electrostatic force overcomes the surface tension of the polymeric solution, a Taylor's cone is formed and, continuous jet of polymer solution is ejected. During the solution movements towards to collector, the solvent evaporates and jet rapidly thins and dries. Randomly oriented, anisotropic fiber bundle is formed on the collector. The electrospinning system requires a detailed work on process and system parameters to form defect-free, homogenous, and smooth nanofibers.

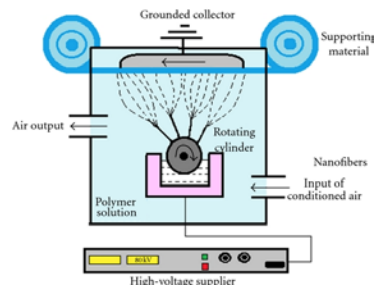


Figure 1. Schematic diagram of needle-free electrospinning system [3].

Recently, needle-free electrospinning system has been patented for the industrial scale production [4]. This method is known under the trade name Nanospider (Figure 1). Needle-free electrospinning is a viable route for the production of exceptionally continuous and uniform polymer nanofibers. Electrospinning is a combination of polymer science, electronics and fluid mechanics. Up to now, a fundamental mechanism of electrospinning is characterized only qualitatively. A thorough review on needle-free electrospinning technique is provided in the paper. The preparation of polymeric solution for fabricating nanofibrous webs, optimization of system and process parameters using various polymeric solution, and possible applications of nanofiber prepared by needle-free electrospinning system is discussed.

2. Nanofibers produced by Needleless electrospinning

Different polymers, such as poly(vinyl alcohol) (PVA) [5, 6], polyacrylonitrile [7], polyurethane [8], carbon nanotube/poly(vinyl alcohol) [9], and polyamic acid [10] have been used in rotating needleless electrospinning process. Based on that, the effect of solution concentration was reported on the electrospinning process. For example; when the concentration of polymer was low, the result was beaded fibers instead of uniform fibers. In another case, when the concentration of polymer was high, the stretching of the polymer into fine filaments was restricted because of high viscosity. However, there was a small effect of the polymer concentration variation on the fiber diameter when the polymer solution was successfully electrospun into uniform fibers.

The other parameters which effect the electrospinning process are; including solution conductivity and surface tension, applied voltage, collecting distance, ambient environment (e.g., temperature, gas environment, and humidity) and molecular weight.

For example; no fibers were electrospun when the molecular weight of PVA was lower than 67,000. The range of electrospun is from PVA was 80,000-150,000 [11]. The rotating speed of a spinneret is up to 200 rpm [6, 12]. It is depending on the spinning solution, spinneret dimension, and operating parameters. When the rotating speed was low, a thin solution layer is constituted on the spinneret surface. Otherwise, increasing the rotating speed generates a thicker solution layer. The processing of solution can be increased in this manner. But, when the rotating speed is too high, the solution could be thrown out from the fiber generator surface.

In order to provide continuance electrospinning, polyvinylpyrrolidone (PVP) solution was formed to the cone by a glass pipe in needleless electrospinning system [13] which used a rotary cone as a spinneret. The PVP solution was drawn down by gravity to the sites of fiber generating through the cone surface. It was found out that stable electrospinning was performed when a high voltage was applied to system and cone rotating speed was over 50 rpm, solution jets were generated from the

fiber generating sites. Moreover, the quality of fibers were the same and the production rate was 1000 times larger than conventional needle system.

The properties of solution (e.g., viscoelasticity and surface tension) is more important for downward electrospinning when the polymer solution is conveyed under the gravity than in the upward rotating electrospinning.

In needleless electrospinning system which was used a magnetic field to initiate the jet formation, the production rate of poly(ethylene oxide)(PEO) nanofibers was 12 times higher than multi-needle electrospinning.

In upward needleless electrospinning system which was using a stationary cylinder spinneret, the production rate of PEO nanofibers was 260 times larger than the production rate of conventional needle electrospinning(0.02 g/h). [14]

Consequently, it is very important the polymer type and solution properties on the system using organic solvent regarding the effect of electrospinning process and productivity.

3. Application of Nanofibers

In recent years, the value of needleless electrospinning increases in the electrospinning technology to produce nanofibers. Needleless electrospinning is a technology that nanofibers are directly spun from an open liquid surface.

The applications of nanofibers are; catalyst and enzyme carriers [15, 16] (chemical, reactions, enzyme for biological processes) , wound healing (antibacterial), reinforcements, electronic and optical nanodevices, protective clothing, energy generation and storage (supercapacitors, batteries, fuel cells, photovoltaic cells, separators, hydrogen-storage, piezoelectric power), microreactors, release control, tissue engineering scaffolds [17] (muscles, bones, cartilages, skins, blood vessels, neural tissues, others), environmental applications [18] (filtration (gas and liquid), desalination, noise reduction, adsorption (heavy metal ions and organic compounds), insect repellent/blocking) and sensors (physical applications, chemical applications, biological applications).

As industrial products, the most advanced and most used nanostructures are filtration, purification materials and components. These nanostructures can indeed specify efficiency of higher filtration and lower pressure than conventional air-filter. In addition, it is easy to clean, enabling customers to significantly extend the life of filters, thus reducing maintenance costs. Currently, water filters such as wastewater treatment and desalination, and energy storage as battery separators are potential products ready to market. On the other hand, another industry that draws attention is the new DuPont [19] battery charger (Energain), which improves performance and battery life by using nanomaterials for electrical vehicles.

4. CONCLUSIONS

Nanofibrous textiles have a numbers of possible applications in many field because of their unique characteristics including high specific surface area, high porosity, low density, and small pore size. For this reason, nanofiber has become a topic of great interest to researchers and engineers in recent years, and is now established as prioritized research area in many countries. The specific properties of materials such as high surface area to volume ration can be achieved by reduction of the size to the nano range. The preparation of nanofiber layers in industrial scale is quite challenge. In this review, a comprehensive review on the needle-free electrospinning system and their possible applications has been made. This paper shows the way toward a better understanding of the diverse application and importance of needle-free electrospinning for industrial scale.

ACKNOWLEDGEMENTS

This work was supported by the Ministry of Education, Youth and Sports of the Czech Republic and the European Union - European Structural and Investment Funds in the frames of Operational Programme Research, Development and Education - project Hybrid Materials for Hierarchical Structures (HyHi, Reg. No. CZ.02.1.01/0.0/0.0/16_019/0000843).

References

1. Formhals A. Process and apparatus for preparing artificial threads. US50028330A, United states.
2. Formhals A. Production of artificial fibres from fibre forming liquids. US2323025A.
3. Yener F, Jirsak O. Comparison between the Needle and Roller Electrospinning of Polyvinylbutyral. *J Nanomater* 2012; 2012: 1–6.
4. Jirsak O, Sanetnik F, Lukas D, et al. A Method of Nanofibers Production from a Polymer Solution Using Electrostatic Spinning and a Device for Carrying out the Method. WO/2005/024101, <https://patentscope.wipo.int/search/en/detail.jsf?docId=WO2005024101> (2005, accessed 6 September 2017).
5. X. Wang, H. Niu, T. Lin, and X. Wang, "Needleless electrospinning of nanofibers with a conical wire coil," *Polymer Engineering and Science*, vol. 49, no. 8, pp. 1582–1586, 2009.
6. H. Niu, T. Lin, and X. Wang, "Needleless electrospinning. I. A comparison of cylinder and disk nozzles," *Journal of Applied Polymer Science*, vol. 114, no. 6, pp. 3524–3530, 2009.
7. F. Cengiz, I. Krucinska, E. Gliscinska, M. Chrzanowski, and F. Goktepe, "Comparative analysis of various electrospinning methods of nanofibre formation," *Fibres & Textiles in Eastern Europe*, vol. 17, no. 1, pp. 13–19, 2009.
8. F. Cengiz and O. Jirsak, "The effect of salt on the roller electrospinning of polyurethane nanofibers," *Fibers and Polymers*, vol. 10, no. 2, pp. 177–184, 2009.
9. E. Kostakova, L. Meszaros, and J. Gregr, "Composite nanofibers produced by modified needleless electrospinning," *Materials Letters*, vol. 63, no. 28, pp. 2419–2422, 2009.
10. O. Jirsak, P. Sysel, F. Sanetnik, J. Hruza, and J. Chaloupek, "Polyamic acid nanofibers produced by needleless electrospinning," *Journal of Nanomaterials*, vol. 2010, Article ID 842831, 6 pages, 2010.
11. F. Cengiz, T. A. Dao, and O. Jirsak, "Influence of solution properties on the roller electrospinning of poly(vinyl alcohol)," *Polymer Engineering and Science*, vol. 50, no. 5, pp. 936–943, 2010.
12. F. Cengiz, I. Krucinska, E. Gliscinska, M. Chrzanowski, and F. Goktepe, "Comparative analysis of various electrospinning methods of nanofibre formation," *Fibres & Textiles in Eastern Europe*, vol. 17, no. 1, pp. 13–19, 2009.
13. O. Jirsak, F. Sanetnik, D. Lukas, V. Kotek, L. Martinova, and J. Chaloupek, "Process and apparatus for producing nanofibers from polymer solution electrostatic spinning," patent no.: EP1673493, CAN 142:393731, Technicka Univerzita v Liberci, Czech Republic, 2009.
14. D. Wu, X. Huang, X. Lai, D. Sun, and L. Lin, "High throughput tip-less electrospinning via a circular cylindrical electrode," *Journal of Nanoscience and Nanotechnology*, vol. 10, no. 7, pp. 4221–4226, 2010.
15. S. Kedem, J. Schmidt, Y. Paz, and Y. Cohen, "Composite polymer nanofibers with carbon nanotubes and titanium dioxide particles," *Langmuir*, vol. 21, no. 12, pp. 5600–5604, 2005.
16. H. Jia, G. Zhu, B. Vugrinovich, W. Kataphinan, D. H. Reneker, and P. Wang, "Enzyme-carrying polymeric nanofibers prepared via electrospinning for use as unique biocatalysts," *Biotechnology Progress*, vol. 18, no. 5, pp. 1027–1032, 2002.
17. Q. P. Pham, U. Sharma, and A. G. Mikos, "Electrospinning of polymeric nanofibers for tissue engineering applications: a review," *Tissue Engineering*, vol. 12, no. 5, pp. 1197–1211, 2006.
18. R. Gopal, S. Kaur, Z. Ma, C. Chan, S. Ramakrishna, and T. Matsuura, "Electrospun nanofibrous filtration membrane," *Journal of Membrane Science*, vol. 281, no. 1-2, pp. 581–586, 2006.
19. DuPont, DuPont Energain Separators for High Performance Lithium Ion Batteries, http://www2.dupont.com/Energy_Storage/en_US/products/products_energain.html (accessed July, 2012).

OUTPUTS FROM THE PROJECT ERASMUS+ KA107 AT FACULTY OF TEXTILE ENGINEERING

Pavla Těšinová

Technical University of Liberec, Faculty of Textile Engineering, Studentska 2, Liberec 461 15,
Czech Republic, pavla.tesinova@tul.cz, +420 48 535 3734

Abstract:

This paper deals with mobility numbers and topics of projects Erasmus+ KA107 in application period 2016-2018. During defined period it was realized mobility between FT TUL and non-European countries on behalf of successful application in countries China, Egypt, Thailand, USA, India, Japan and more. Applications involved mobility of students study and internships as well as teaching and training activities of staff.

Key words:

Erasmus+, Mobility of Students, Mobility of Staff, Programme Countries and Partner Countries

1. Introduction

Erasmus+ is the EU Programme in the fields of education, training, youth and sport in act by REGULATION (EU) No 1288/2013 OF THE EUROPEAN PARLIAMENT AND OF THE COUNCIL of 11 December 2013 establishing 'Erasmus+': the Union programme for education, training, youth and sport. Education, training, youth work and sport are chosen as a key to promote common European values, foster social integration, enhance intercultural understanding and a sense of belonging to a community, and to prevent violent radicalisation. The Erasmus+ Programme is designed to support Programme Countries' efforts to efficiently use the potential of Europe's talent and social assets in a lifelong learning perspective, linking support to formal, non-formal and informal learning throughout the education, training and youth fields. The Programme also enhances the opportunities for cooperation and mobility with Partner Countries, notably in the fields of higher education and youth. This investment in knowledge, skills and competences will benefit individuals, institutions, organisations and society as a whole by contributing to growth and ensuring equity, prosperity and social inclusion in Europe and beyond [1].

For over 25 years, Europe has funded the Erasmus programme, which has enabled over three million European students to spend part of their studies in another higher education institution in Europe. Erasmus+ now opens up these opportunities, allowing for mobility from and to other parts of the world. International mobility of students and staff is open to participants from higher education institutions established in Programme and Partner Countries. The application form however can only be filled out and submitted by a higher education institution from a Programme Country on behalf of the partners [2].

The Programme Country higher education institution needs to be holder of the Erasmus Charter for Higher Education (ECHE) and submits the application to its National Agency. The number of participants is for the total duration of the mobility project (e.g. 16 or 24 months). A project lasting 24 months does not prevent a higher education institution from applying for a new project every year.

Programme Countries are those countries participating fully in the Erasmus+ programme. To do so, they set up a National Agency and contribute financially to the programme. The 33 Programme Countries are: the 28 EU Member States, Iceland, Liechtenstein, Norway, the Former Yugoslav Republic of Macedonia and Turkey. Partner Countries are all the other countries in the world [2]. Projects in 2016 were not allowed for training mobility and it changed for year 2017 and further.

A mobility project consists of all the sets of mobility flows for which a higher education institution from a Programme Country requests funding in the application form. The applicant applies for all the sets of mobility flows with different Partner Countries under the same application. The selection of students - as well as the procedure for awarding them a grant - must be fair, transparent, coherent and documented, and shall be made available to all parties involved in the selection process. Possible selection criteria are the academic performance of the candidate, previous mobility experience, motivation, experience in the receiving country etc. In case of international credit mobility, the first criterion for selecting students must be academic merit, but with equivalent academic level, preference should be assigned to students from less advantaged socio-economic backgrounds [2]. If more faculties are willing to apply for the same country, it is necessary to cooperate in writing the application to be consistent as a complex still remaining exact description of each activity.

The mobility project must comprise one or more of the following activities [1,2]:

- **Student mobility for studies to/from Partner Countries;** the study period abroad must be part of the student's study programme to complete a degree at a short cycle, first cycle (Bachelor or equivalent), second cycle (Master or equivalent) and third or doctoral cycle. A study period abroad may include a traineeship period as well. Such a combination creates synergies between the academic and professional experience abroad and may be organized in different ways depending on the context: either one activity after the other or both at the same time. The combination follows the funding rules and minimum duration of study mobility.
- **Student mobility for traineeship to/from Partner Countries;** traineeships abroad at a workplace are supported during short cycle, first, second, third cycle studies.
- **Staff mobility for teaching to/from Partner Countries;** this activity allows HEI teaching staff or staff from enterprises to teach at a partner HEI abroad. Staff mobility for teaching can be in any subject area/academic discipline.
- **Staff mobility for training to/from Partner Countries;** this activity supports the professional development of HEI teaching and non-teaching staff in the form of training events abroad (excluding conferences) and job shadowing/observation periods/training at a partner HEI, or at another relevant organization abroad.

2. Applications for calls in 2016, 2017 and 2018

Despite application is given in university version for all faculties of TUL here will be discussed only one faculty as a segment. It was applied for mobility from/to Faculty of Textile Engineering to these Partner countries:

year 2016: 4 countries, Egypt, China, Thailand, USA. – all accepted, duration of project 2 years

year 2017: 2 countries, India, Japan – all accepted, duration of project 2 years

year 2018: 13 countries, Japan, Mauritius, New Zealand, Tunisia, Taiwan, Ukraine, USA, Kazakhstan, China, Thailand, Belarus, India, Israel - accepted Tunisia and Israel, duration of project 2 years.

Strategy for years 2016 and 2017 was to define couple of countries and finding out strength of application data in countries where prior cooperation is active and long with representative past. Because of acceptance of all countries for financial support in some budget at least, it was decided to increase number of countries for year 2018. All countries were recommended at least by one department of FT TUL with a contact person there. Application included countries with traditional cooperation on official bases but also quite fresh contacts on the personal experience only. It is necessary to say that the success was random and it was not defined by these two matters.

Year 2018 call for Erasmus+ KA107 was so overwhelmed in CR that only two countries was proved for granting. Revision of reviewer's comments did not shown fundamental problem in any country in the application. Even repeated application was not successful for countries like Thailand and China where in call 2016 was excellent outputs. Luckily, it does not stop cooperation based on stronger will then money on both sides.

3. Realized mobility numbers

It is important to mention average number of other mobility to see capacity of the faculty. In academic year 2017-18 was welcomed 41 students in Erasmus+ study/training mobility KA103 and also 41 students in other way of financing (self-payd or granted by home university another way). Towards the previous years just sum of mobility students: 2016-17 came 72 students, 2015-16 came 78 students, 2014-15 came 52 students. For more information, see source data from IS STAG of TUL and conference paper from 2016 year from Autex conference about successfulness of students coming from abroad to study at FT TUL [3].

Following description will include only countries with realized mobility only. Names of selected students and teachers are not stated because author do not have written permission for this exact publication though it is mentioned all necessary data for evaluation of the project so far realized.

3.1. Egypt

This mobility was applied in call 2016 and was accepted in full range. Mobility from Egypt to Liberec was predefined for one teacher for two months because teaching activity was expected in regular study courses KTT/TEX Textile Engineering for master study programme (registered 48 students in present form) and KTT/TTE Textile Technology for bachelor study programme (registered 7 students in present form). Mansoura University and National Research Centre proved the applicant who fulfilled mobility in beginning of year 2017. Together with teaching activities participant consulted doctoral students and research topics with faculty staff.

Table 1. Mobility within Egypt

Type of activity	Year of activity	Number of days total	Number of participants	Realised topics
Staff mobility for teaching to Liberec	2017	62	1	Textile engineering, material engineering, dyeing, printing and textile auxiliaries

3.2. Thailand

This mobility was applied in call 2016 for two universities in application, Rajamangala University of Technology Thanyaburi RMUTT and Rajamangala Universtiy of Technology Krungthep. The most of the mobility was fulfilled in 2017 and only university RMUTT was active in mobility. Number of applicants was higher in direction to Thailand. It was decided to divide number of mobility days to more staff members to be able to present more topics at the host university and to attract more students for coming to Liberec.

Students were studying on exact topics on the Department of Textile Evaluation, Department of Clothing Technology, Department of Textile Technology, Department of Material Engineering. Students satisfied with their level of knowledge and English level.

Teachers coming from Liberec to Thanyaburi were teaching on special lectures prepared specially for them with around 20-40 number of students depending on period they arrived. Courses last whole days with shearing of activities. Teachers coming from Thanyaburi to Liberec were teaching for doctoral students. Specially course of teacher experienced with project based learning was attended also by staff from FT TUL. Those teachers were included in the committee of doctoral forum of FT TUL with c. 30 participants in students. Committee evaluated all students' presentations and choose three the best.

Cooperation with Rajamangala University of Technology Thanyaburi is continuing also without Erasmus+ funding. Delegation of RMUTT president came to Liberec in December 2017 and two internship students attended for summer 2018. It was stated help in building of nanotechnology laboratory in RMUTT with cooperation of Department of Nonwovens and Nanofibrous Materials.

Table 2. Mobility within Thailand

Type of activity	Year of activity	Number of days total	Number of participants	Realised topics
Staff mobility for teaching to Liberec	2017	24	2	Production of nanofibers, nanotechnology, project based learning and case studies
Staff mobility for teaching from Liberec	2017	17	3	Clothing construction, car seats production, comfort properties evaluation, clothing comfort related to design work and comfort of sports clothing, somatotyping, study of body proportion, parametric clothing pattern construction, modelling of tight fit underwear in 3D software and analysis of the influence materials on the resulting 2D cutting parts, pattern cutting for lingerie, the metric pattern making method
Staff mobility for teaching from Liberec	2018	7	1	Electrostatic spinning, solubility, principles of polymer physics, application of nanofibrous materials in medical and technical applications
Student mobility for studies to Liberec	2017	360	4	Development and characterization of cement and geopolymers concrete composites, nanoindentation and nanoscratch testing, textile chemistry, application of CT tomography for the study of clothing materials



Figure 1. Group picture during course in RMUTT illustrating common number of students on courses



Figure 2. Teamwork during course in Thailand



Figure 3. Teamwork during course in Liberec

3.3. China

This mobility was applied in call 2016 for Wuhan Textile University, University of Science and Technology of China, Xi'an Polytechnic University and Zhejiang Sci-Tech University. Mobility was fulfilled with Zhejiang Sci-Tech University. The first mobility in 2016 helped to attract students for mobility to Liberec. Because of this begin of cooperation students mobility was possible to earn in one stage for all four possible in 2017. Students were good in English and skilled technically so they fit into study and research groups very well. Their final thesis were prepared on equipment and laboratory measurement on Department of Clothing Technology, Department of Material Engineering and Department of Textile Evaluation FT TUL.

Zhejiang Sci-Tech University became the main contact in China because of Erasmus+ mobility and project related with personal presence introduction there supported by Erasmus+ funding. One staff was supported twice because of his extraordinary relations with the host university.

All activities continue on the other basis of funding mostly sponsored by departments themselves or university support to student mobility. Nine more students came in summer 2018 for their internships to department of material engineering for their experiments on final theses.

Table 3. Mobility within China

Type of activity	Year of activity	Number of days total	Number of participants	Realised topics
Staff mobility for teaching from Liberec	2016	14	2	Development of electrically conductive and porous activated carbon web from acrylic fibrous wastes, ozone treatment of jute fibrous wastes for composite applications, preparation, characterization and applications of nanocellulose, nanotechnology, nanoscale phenomena, mechanical properties in nanoscale materials, carbon based nanomaterials, nanofibers, nanoparticles, nanocomposites
Staff mobility for teaching from Liberec	2018	27	3	Introduction to fabric design, structure property relation and non-conventional methods for evaluation, high performance fibrous materials, thermal and mechanical properties of high performance fibrous materials, nanoporous structures and their effect on heat phenomena, effect of hydrophobicity on microporous membranes, data treatment, linear and non-linear regression, design of experiments and consumer oriented design of textiles
Student mobility for studies to Liberec	2017	360	4	Sensorial comfort of textile materials - the Kawabata evaluation system (KES), bending rigidity, water-vapour permeability tests comparison, textile chemistry

3.4. USA

This mobility was applied in call 2016 and was concerned to the support of students because of expensive destination in USA and far travelling to the destination. All students realised part of their final thesis. Undergraduate students came from USA University of Alabama at Birmingham, where is strong cooperation with laboratory of Dr. Andrei Stanishevsky in nanotechnology. All topics were realised in this field. Doctoral students from Department of Nonwovens and Nanofibrous Materials FT TUL visited above mentioned university. Mobility both directions is not dependence on Erasmus+ but highly appreciated to allow increase in mobility numbers and prestigious status of students given by participation in Erasmus+ mobility programme. Cooperation will follow in the same numbers of mobility based on regular and continuous research topics together. Both departments are closely related in mentioned research areas.

Table 4. Mobility within USA

Type of activity	Year of activity	Number of days total	Number of participants	Realised topics
Student mobility for studies to Liberec	2018	180	2	Hybrid PVB/silica fibrous structures, Zirconia-based nanofibrous ceramics
Student mobility for studies from Liberec	2017	360	4	AC electrospinning, bioprinting, manufacturing of nanofibrous composites, centrifugal spinning

3.5. India

This mobility was applied in call 2017. Processing of Inter-institutional agreement lasts some time with IIT Delhi so arrival of students was realised in 2018 for summer period. Prolongation of visa process caused also necessity to split months for two arrivals. Three months uninterruptedly did not fit

properly into academic calendar of Indian students. Two months realisation was finished in summer and third month is planned for December 2018. Because students are working on their thesis in course DFT/ZST Foreign internship for 15 credits with one tutor at Department of Material Engineering, it is possible to realise this way.

Teacher's mobility from IIT Delhi is planned on winter period 2018 when this paper will be ready. It is prepared all documents prior arrival and just mobility is waiting to be fulfilled properly.

More students and staff can take advantage in mobility within IIT Delhi, Biju Patnaik University of Technology. Here is spare mobility for two students incoming, two outgoing and two teachers outgoing from Liberec for realisation in next period valid for call 2017.

Table 5. Mobility within India

Type of activity	Year of activity	Number of days total	Number of participants	Realised topics
Student mobility for studies to Liberec	2018	180	2	Textile engineering, material engineering, structure-property relation
Staff mobility for teaching to Liberec	2018	14	2	Fibrous filters for air filtration - fundamentals, manufacturing technologies, Internal structures, testing & characterization, material-structure-property relation, performance optimization, applications, progressive deformation of yarn structures, yarn fault detection using image and signal processing, 3D nonwoven structures

3.6. Japan

This mobility was applied in call 2017. The first participant contributed in mobility program is a student from Liberec to Shinshu University. Mobility is realised in summer-autumn period for his dissertation work experimental progress. Another two incoming students to Liberec will be welcomed until the project end from Shinshu University on the clothing topic preferably.

Table 6. Mobility within Japan

Type of activity	Year of activity	Number of days total	Number of participants	Realised topics
Student mobility for studies from Liberec	2018	90	1	Monitoring of the wearer with wearable electronics

4. CONCLUSIONS

FT TUL is experienced in mobility not only within Programme Countries but can manage quality exchange also with Partner Countries based on prior cooperation. It was already realised mobility in call 2016 and we are in progress in calls 2017, 2018. Continuation of mobility in academic year 2018-19 is expected to be fulfilled the rest of mobility in call 2017 with small overlap probably. Call 2018 was not enough successful though cooperation will continue. Tunisia and Israel will be destinations where we expect progress in relations with the help of Erasmus+ funding.

All mobility days/months were used significantly and responsibly fulfilled by all participants. Number of students is satisfactory and applicants exceeded funding possibilities. It display that capacity is still higher. Teachers were chosen according to their cooperation contacts and addressed very well courses of the host university.

Supported were not only participants above mentioned but also all people in contact with them, staff and students of both universities in cooperation action. Regional and international importance are high hand in hand with internationalisation at home. Local students were in contact with teachers at courses and with visiting students in labs and on courses. Students made experience with different teaching style and communication in English with foreigner accent. Staff learnt more about attracting students in different nation based on up to date teaching methods e.g. project learning method, activation of students by tools and experimental work management.

We can conclude that mobility was successful so far and continuation is under preparation process. Erasmus+ is a good tool for cooperation since well-known and respected brand which declare high level of participants and impact to institutions involved.



Figure 4. Publicity example, poster presentation of staff teaching mobility on International day TUL October 2017

ACKNOWLEDGEMENT

The project is financially supported by Erasmus+ KA107 č.2016-1-CZ01-KA107-023074, Erasmus+ KA107 č.2017-1-CZ01-KA107-034883, Erasmus+ KA107 č. 2018-1-CZ01-KA107-047257.

References

1. Erasmus+ Programme Guide Version 3 (2018): 10/08/2018 European Commission.
2. Erasmus+. International Credit Mobility. Frequently Asked Questions for Higher Education Institutions (HEIs). (2015) European Commission.
3. Tesinova, P., Ocheretna, L. Integration of Foreign Students into Textile Educational Courses – FT TUL Experience. Autex conference 2016. 1. ed. Slovenia (2016). Electronic version proceedings (8 pages). ISBN 978-961-6900-17-1.

ESTIMATION OF FOLDING AND LUMINANCE VALUES OF POLYPROPYLENE BCF YARNS USING ARTIFICIAL NEURAL NETWORK TECHNIQUE AND MODELING STUDY

Emre Yakut¹, Cem Güneşoğlu², Emine Çot³, Volkan Balcı³

¹Korkut Ata University, Department of Management Information Systems, 80000 Osmaniye, Turkey

²Gaziantep University, Department of Textile Engineering, 27000 Gaziantep, Turkey

³Kartal Carpets and Textile Company, Department of R&D, 27000 Gaziantep, Turkey Tel:

+903423470100 Fax: +903423570116 E-mail: emine.cot@sanathali.com

Abstract:

Polypropylene (PP) yarn commonly used in the production of machine carpets in the world is called BCF (Bulk Continuous Filament) and the production process consists of extrusion - cooling - lubrication - gravitation - texturizing - winding - twisting. It is a fact that PP yarn has a disadvantage in terms of softness and brightness compared to acrylic, polyamide and polyester used in the production of machine-made carpets. Twisting is also an effective parameter on the sense of softness that the yarn gives. Therefore, various R & D studies are carried out to determine the effect of production parameters on softness, crimp and brightness values of PP yarn and / or to determine the production parameters required for PP yarn production with the highest values.

In this study, it is aimed to develop an artificial neural network (ANN) algorithm which determines the crimp and brightness values of the heat set and freeze PP yarns by changing the BCF production parameters, the reverse engineering approach and the quantitative or categorical values of the production parameters for the yarn end with the target crimp and brightness values .

Key Words:

Artificial Neural Network, BCF, Polypropylene, Estimation, Crimp, Brightness.

1. Introduction

Synthetic yarns are widely used for the production of machine carpet in the world. Therefore, academic studies about the production and processing of synthetic fibers are increasing day by day. In recent years, polypropylene (PP) has led to its versatile and widely used in the carpet industry due to its low density, good processability, low cost, good elasticity, low melting point such as having superior properties [1].

Production processes of BCF yarn consist of extrusion-cooling-lubrication- drawing-texturized-winding and twisting. Raw material and masterbatch are mixed with certain ratio at dosing unit and filaments are passed through the spinneret holes in molten state. PP filaments are appropriately cooled and drawing process is carried out to product yarn in certain yarn count. Texturized (crimping) process is applied to yarn for bring needed bulkness and elasticity feature. Produced yarns are wound on the bobbins. Twisting and/or fixation processes are applied to BCF PP yarn that will be used as carpet yarn to take its final form.

As the BCF PP yarn passes through all these stages, the yarn number, cross-sectional area, number of filaments, extruder temperatures, godet temperatures and pressures are measured. Within the scope of this study, the effects of these parameter values on the brightness and twist of the yarn will be

determined. These determined parameter values will be used in the artificial neural network methodology to develop a model that predicts the effect of the yarn on the brightness and crimp properties.

Artificial neural networks are parallel and decentralized data processing structures that are inspired by the human brain. ANN have processing elements, interconnected by weighted connections, and each processing element has its own memory. In a typical ANN structure, the input layer gets the outer information and transmits the information (input) to one or more cells in the hidden layer without any change through the forward feed method. The hidden layer determines the match between input and output (weight function) by trial and error method (learning). In cases where the specified output values and the target output values are incompatible, the weighting functions are updated with error diffusion method. The general principle diagram of an artificial neural network model is given in Figure 1 below.

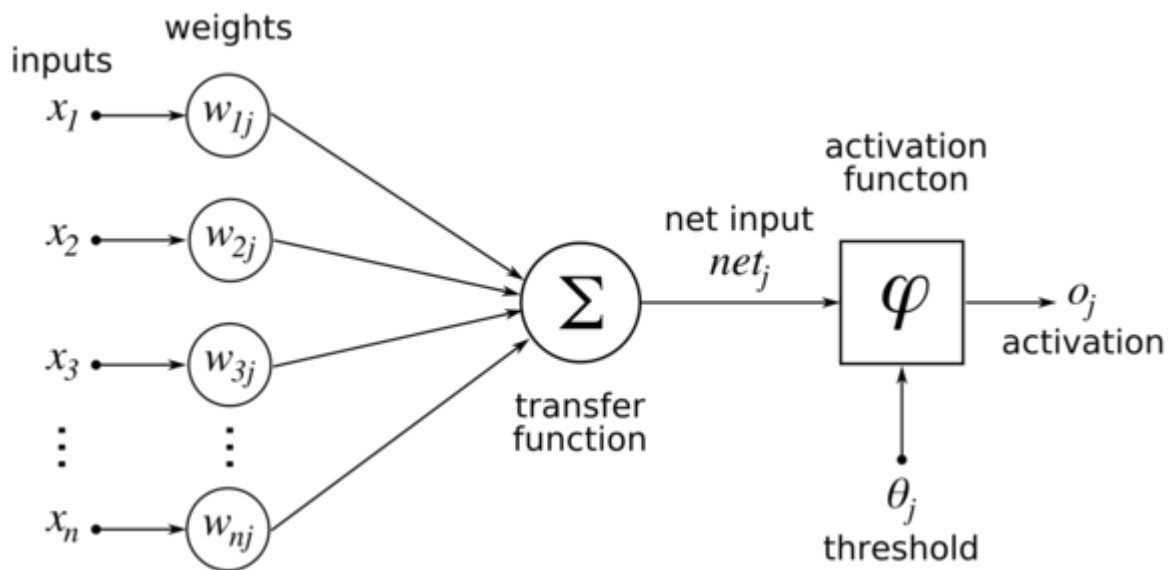


Figure 1. Artificial neural network model

2. Experimental

When consumer demands are evaluated in the carpet market, it seems that there is an increasing demand for softer, brighter and better resilience yarn and carpets to be produced from these yarns. In studies conducted for PP BCF yarns it is observed that changes in production parameters generally concern properties such as strength, elongation and compressibility.

Kebabci reported that the rate of change in the spinning speed of the BCF PP yarn production and the cross-sectional shape of the yarn have a significant effect on the yarn count, strength, breaking length and the amount of spin finish oil taken by yarn [1].

Sarkeshick at al. examined the changes that the heat set process brings to nature in BCF PP yarns. Heat set operation reduces tenacity, modulus, bending rigidity, crimp and tensile values while increases the linearly density of yarns. As a result of the changes at the end of the process, the resilience values of BCF PP yarns are improved and become more suitable for carpet pile yarn. The results of the heat set effect will be used to compare the results obtained with the ANN algorithm [2].

Dadgar is studied on the estimation of heat-set PP yarn properties by artificial neural network method, it has been shown that yarn twist, yarn count and process temperature are effective on the final yarn count, yarn tension, crimp and packaging factor [3].

Demiryürek reported that the properties of polyester / viscose blended open-end rotor yarn Artificial Neural Networks (ANN) for estimation of production before production and statistical models. In

conclusion, both ANN statistical models can be used for the prediction of yarn properties, however, the predictions of ANN gave more reliable results than statistical models [4].

2.1. Brightness and biological properties of BCF PP yarns

When consumer demands are evaluated, demands for softer, brighter and better resilience yarns and carpets to be produced from these yarns seem to be increasing day by day. The upgrading of the bending and compression module (increasing the softness) of the textile materials used in the carpet and the improvement of the resilience feature can be presented as a solution to the expectation in question. This viewpoint has led to various studies in order to improve the brightness, crimp, resilience and softness properties of PP BCF yarns.

BCF PP yarn of heat set, frieze or shaggy type is generally used as pile yarn in machine cases produced with wilton type face-to-face weaving technique. They affect the mechanical properties such as resilience, thickness, abrasion resistance, appearance preservation grade. Every stage of the production process has inputs that affect these properties. Their effects on yarn and carpet properties are made by collecting long-rolling production experiences and traditionally by trial and error. However, the abundance of data, the absence of a specific system for evaluation, and the lack of standards in determining production parameter values have led to a lack of industrial practice following BCF yarn production. In particular, BCF PP yarn production parameters such as curl and brightness, such as extremely high commercial value of yarn properties cannot be estimated, the production parameters are changed according to the finished yarn properties are carried out by changing the process. These preliminary studies in production cause time and cost loss. All these imperfections necessitate the passage of ANN study.

2.2. Artificial neural network method

In this paper, MATLAB18 will be used for creation ANN algorithm and as the ANN algorithm feed-forward, back propagation, momentum learning rate rule, sigmoid transfer function models will be applied. The constituted ANN models for each yarn property, the model with the smallest error rate will be chosen as the best successful model. With the obtained regression equations it enables to forecast the yarn properties by the constituted models. According to the optimum BCF production conditions heat set and frieze BCF yarns will be produced and will be used for pile yarn of the sample carpets. Then the mechanical properties of the sample carpets and the current production carpets will be compared. Also it can be possible to evaluate the effect of a new spinneret flat section design to brightness of yarn.

3. Results and discussion

In this study, the BCF PP production parameters of Kartal Carpet Company were used for the data. Firstly the drawing ratio, yarn number, filament number, fixed heat, cooling heat, frieze heat and etc. were used by Meta-analyze as the scope of this Project (Table 1).

Table 1. Parameter values of BCF PP yarn

DTex	PP	Number of Twist	Number of Filaments	Crimp Number	Extruder Exhausted Temperature (°C)	Cooling Temperature (°C)	Shooting Rate	Texture temperature (°C)	Texture Press (bar)
2600	25,9	145	255	4,74	238	19	3,2	160	7
2400	24,5	145	240	4,42	238	19	3,2	160	7
1750*2	24,5	170	160	5,67	238	18	3,3	155	7
2400*2	25,5	170	240	6,88	238	19	3,2	160	7
5000*2	24,5	140	255	9,52	238	19	3,2	160	7
2220	25,5	145	240	10,59	238	19	3,2	160	7

An analysis was made by MINITAB to determine the more effective parameters at the crimp value of heat set and frieze BCF yarns. As a result of this analysis the regression value is found 95.78% the effective five parameters are determined as number of twist, number of filaments, fixed heat, extruder exhausted temperature and drawing rate. Values was shown at table 2.

Table 2. MINITAB Results

Source	DF	Adj SS	Adj MS	F-Value	P-Value
Regression	8	1472,45	184,056	1178,20	0,000
PP	1	0,06	0,060	0,38	0,536
Number of Twist	1	79,87	79,867	511,25	0,000
Number of Filaments	1	5,63	5,629	36,03	0,000
Fixed Heat	1	5,46	5,465	34,98	0,000
Extruder Exhausted Temperature (°C)	1	39,71	39,710	254,20	0,000
Cooling Temperature (°C)	1	0,73	0,733	4,69	0,031
Fixed time (s)	1	0,91	0,911	5,83	0,016
Shooting Rate	1	17,96	17,956	114,94	0,000
Error	415	64,83	0,156		
Lack-of-Fit	57	15,74	0,276	2,01	0,000
Pure Error	358	49,09	0,137		
Total	423	1537,28			

Once the ANN input set was determined, the number of data variations was determined and samples were generated. The ANN module was operated until the optimal output result was achieved. MATLAB18 software from Mathworks and the accompanying Neural Network Toolbox were used in the design and operation of the network. A feedforward back-propagation artificial neural network having two intermediate layers is formed to estimate the model with five input variables and an output variable. In Figure 2, there were 5 processor elements that provide input variables to the network and input layer contains 1 processor element which has network output of the dependent variable. As a result of the experiments performed for the number of processor elements in the intermediate layers, it was decided to have 2 hidden layers and 10 neurons.

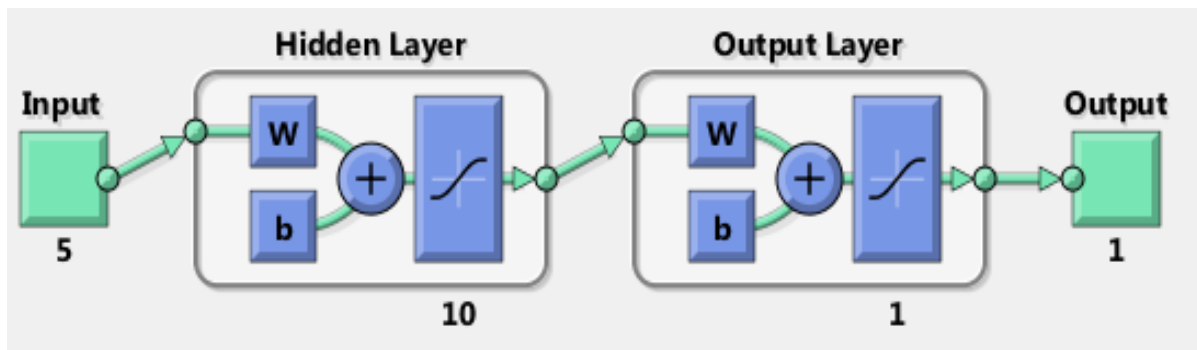


Figure 2. Artificial neural network architecture

The parameter values of the network was estimated based on the results of the experiment which gives the best error value. The selected parameter values of the network were shown in figure3. In addition, learning and momentum coefficients, according to the results of the test that gives the least error; 0.01 for momentum and 0.09 for momentum.

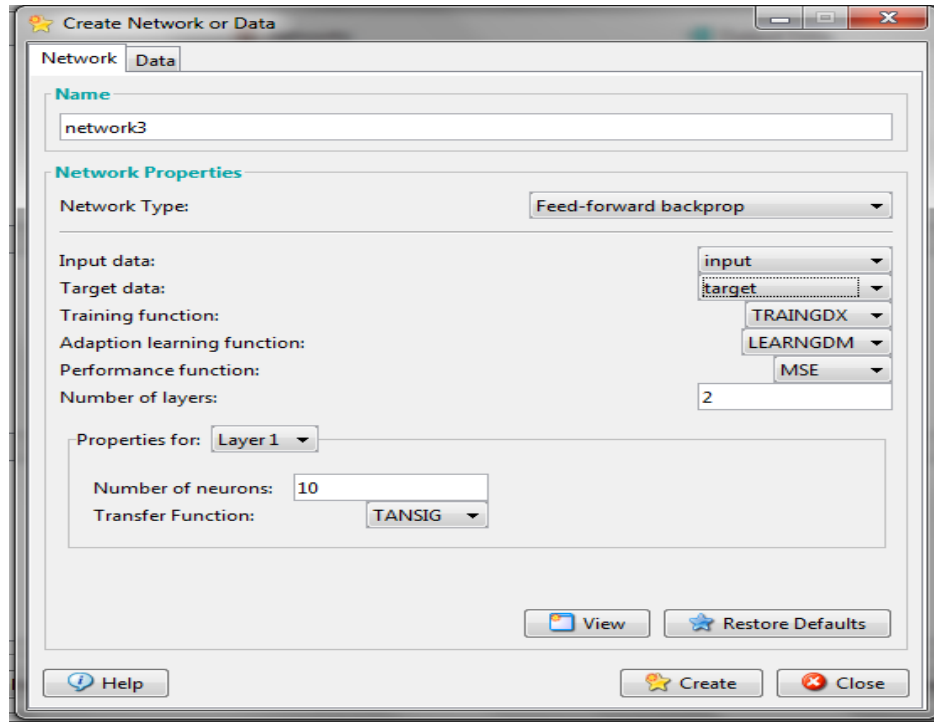


Figure 3. ANN parameters

After the creation of the model's architecture, the training process was started. At the beginning of the training process, the connection weights of the network are assigned randomly. 420 data was used as a training set for the training process. The remaining 150 data were separated as test data. As a result of the experiments, a minimum error has been obtained. Since the training process is completed with a very small error rate, when the actual values and the estimated values were shown in the same graph, the values were almost overlapping. This relationship was shown in Figure 4.

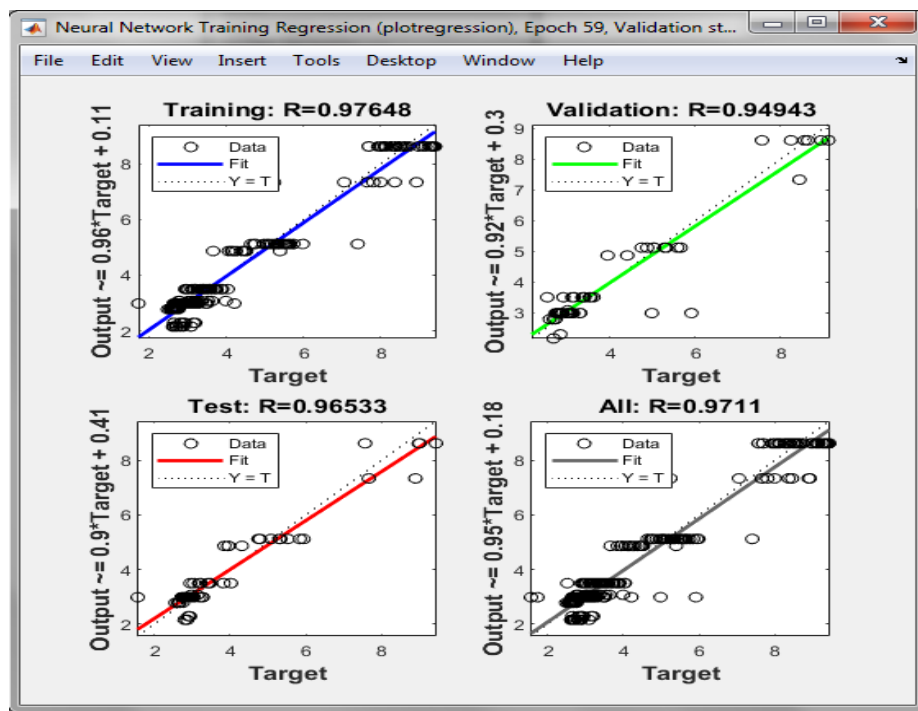


Figure 4: The regression results of ANN

Finally, the artificial neural network was asked to produce the result data for the 5 input variables that were not previously seen. The actual data and the results of the artificial neural network were shown in Table 3.

Table 3: Comparison of actual values with ANN output

Actual Values	Estimated Values	Difference	MSE Values
2,87	2,99	-0,12	0,02
4,31	4,31	0	0,00
5,13	5,31	-0,18	0,03
4,44	4,25	0,19	0,03
5,62	5,31	0,31	0,10
3,73	2,99	0,76	0,54
2,94	2,99	-0,05	0,00
3,74	2,99	0,75	0,56
3,84	3,42	0,42	0,18

As seen in Table 3, the artificial neural network is very close to the actual values and produced results consistent with the actual values.

4. CONCLUSIONS

In this study, as a result of the evaluation of ANN algorithm and categorical and numerical data, it is ensured that outputs are obtained quickly and production parameters are optimized. In the study, 2017 data were used as network learning data, and the data for the first three months of 2018 were used in the estimation of the network.

In the study, the criteria used in the current structure were taken into consideration and the criteria which were of greater importance over the results were selected through the MINITAB program.

Then, the determined parameters the feed nets which are the most widely used in the neural networks and which give successful results were selected and the resulting error was minimized.

Thus, it is ensured that the yarn production of the BCF yarn parameters is determined by estimating the crimp values before the yarn production.

In the continuation of the study, it will be ensured that the yarn brightness data is collected in sufficient level. Then, the data will be estimated in the ANN module.

References

1. Kebabcı M., (2015), *The Effect of Drawing Ratio and Cross-Sectional Shapes on the Properties of Polypropylene CF and BCF Yarns*, *Textile and Engineering*, 22: 100, 47-53.
2. Sarkeshick S., Tavanai H., Zarrebini M. and Morshed M., (2009) *An investigation on the effects of heat-setting process on the properties of polypropylene bulked continuous filament yarns*, *The Journal of The Textile Institute*, 100:2, 128-134, DOI: 10.1080/00405000701692429.
3. Dadgar M., Varkiyani S. and Merati A., (2015) *Comparison between artificial neural network and response surface methodology in the prediction of the parameters of heat set polypropylene yarns*, *The Journal of The Textile Institute*, 106:4, 417-430, DOI: 10.1080/00405000.2014.924656.
4. Demiryurek O., (2009), *Estimating polyester/viscousized open-end rotor yarn properties by setting artificial neural networks and statistical models*, *Scientific Research Projects of Cukurova University*, MMF.2005.D9.

MODELLING OF CONSTRUCTION OF WOVEN FABRIC

Brigita Kolčavová Sirková & Iva Mertová

Technical University of Liberec, Faculty of Textile Engineering, Department of Textile Technologies,
Liberec, Czech Republic brigita.kolcavova@tul.cz, iva.mertova@tul.cz

Abstract:

This paper is focused on modelling of woven fabric construction. Woven fabric construction is given by parameters of input yarns for all warp and weft (2D and 3D fabric) as well as fabric parameters: set of threads in warp and weft (number of ends/picks per one centimetres) and weave. Prediction of parameters of woven fabric construction in this article is created from definitions of individual pores in the mutual interlacing of two neighbouring threads in the warp and in the weft direction in repeat of weave or patter of woven fabric. All weaves for dobby and jacquard pattern is possible to create by the various combinations of four structural pores in repeat. For each pore it is possible to define the distance and subsequently the sett which correspond whit interlacing of repeat (pattern) of woven fabric.

Key words:

Woven fabric, structure, pore, models, interlacing, warp, weft, construction

1. Introduction

Woven fabric construction parameters define the individual parameters for production of all application of woven fabric for costumers. Many papers have been done in the past for definition and prediction of construction parameters of woven fabric. One main the theory of cloth setting focused on definition of construction of woven fabric was done by Brierley [1, 2]. The principle and his contribution is in square sett cloth based on: constant which varies according to kind of yarns and system of numbering, average counts of warp and weft yarns, average float, constant according to type of weave. The relation between the sett of threads and weaves are given by experimental work a large of series woven samples. The others contributions have been done in past are focused on describing the binding cell, mathematical expresion of the shape of the binding wave in cross-section in the fabric in the steady state [4-12]. Peirce model [3], Olofsson model [4], hyperbolic model, sine shape, parabolic model. These models are related to the plain weave. Model used Fourier series [5] are known as the most used models for plain and non-plaine weaves.

2. Definition of input parameters for modelling of construction of woven fabric

Construction parameters are based on geometric, strength and deformation ratio in the basic binding element in a plain weave and float part of non-plain weaves. Plain interlacing is formed only mutual crossing of warp and weft threads, thereby is limiting structure of woven fabric. All other weaves are looser weaves with specific float part. Float part is non-interlacing length of threads, where the position of float is given by the effect of woven fabric (warp and weft effect), see Figure 1. Study of basic element of the plain weave can be used for clarification and explanation of action during weaving and forming of

woven fabric in limited fabric structure of weaving. Construction parameters are possible to define on the basis of planar structure of woven fabric.

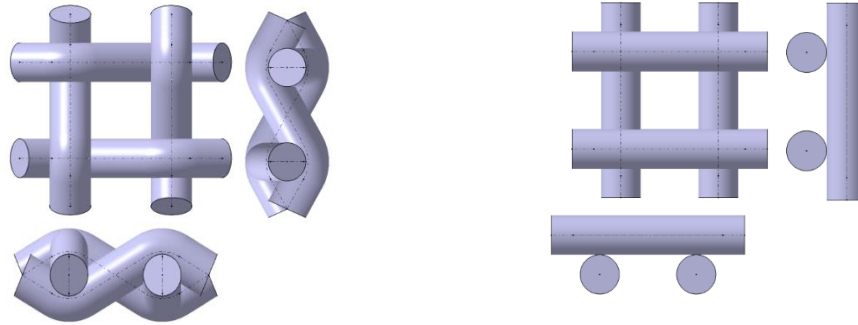


Figure 1. Illustration of woven fabric elements for plain weave (left side), float parts for non-plain weaves (right side)

The parameters of planar structure as geometric ratios (GE) in woven fabric are determined by the areas of one interlacing point, its dimension is given by distances $A \times B$. Warp and weft are in binding point defined by waviness having a height of binding wave $H_{1,2}$ by the shape of the binding wave as well as the resulting rake angle of binding waves [13]. Individual parameters of geometric ratios are possible to write as vector of geometric parameters GE , see equations (1).

$$GE = \left[\begin{array}{l} d_s = \frac{d_1 + d_2}{2} \\ A = \frac{1}{D_1} \\ B = \frac{1}{D_2} \\ H_1 = e_1 \cdot d_s \\ H_2 = e_2 \cdot d_s \\ e_2 = 1 - e_1 \\ \varphi = \arctg\left(\frac{dy}{dx}\right) \\ \psi = \arctg\left(\frac{dy}{dx}\right) \end{array} \right] \left(\begin{array}{l} d_s = \text{mean diameter of thread}; d_1 = \text{diameter of end} \\ d_2 = \text{diameter of pick} \\ A = \text{distance of ends}; D_1 = \text{density of ends} \\ B = \text{distance of picks}; D_2 = \text{density of picks} \\ H_1 = \text{height of binding wave of warp}; e_1 = \text{warp waviness} \\ H_2 = \text{height of binding wave of weft}; e_2 = \text{weft waviness} \\ \varphi = \text{angle of ends interlacing is given by shape of binding wave} \\ \psi = \text{angle of picks interlacing is given by shape of binding wave} \end{array} \right) \quad (1)$$

3. Definition of setting of woven fabric threads using the structural pore models of woven fabric weave

Weave in woven fabric are usually illustrates by patterns, which show the fabric design and way of interlacing. Patterns are usually drawn on squared paper as a sequence of dark and light pixels (show the position of the warp threads relative to the median plane of the fabric). Structural change in woven fabric formed by weave is based on definition of four basic pores - structural models in the weave repeat. In terms of structural pores are distinguished: Pore type 1 - full interlacing, Pore Type 2 - partial interlacing, Pore type 3 - doubling and Pore Type 4 - full float [13].

In the description of the planar geometry of woven fabric weave, besides writing of weave in pattern paper, it is possible to use a weave pattern depiction based on the matrix of structural pore models for twill and sateen basic weave (repeat size is 5 ends and picks), see Figure 2, 2b. The size of the matrix is based on the size of the pattern repeat. The number of warp threads in pattern repeat “no” determines the number of rows and the number of weft threads “nu” number of columns.

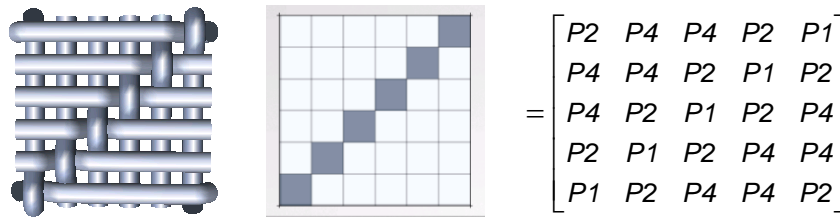


Figure 2. Matrix depiction of structural pore models of woven fabric for twill weave repeat with 5x5 threads

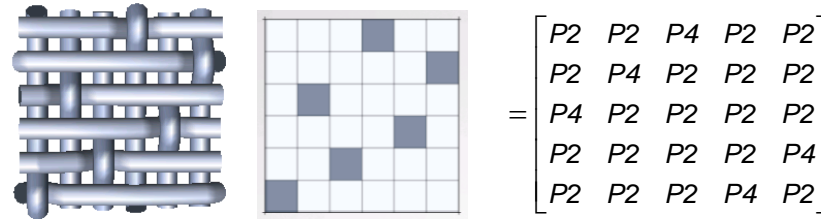


Figure 2b. Matrix depiction of structural pore models of woven fabric for sateen weave repeat with 5x5 threads

Definitions of individual pores is based on mutual interlacing of two neighbouring threads in the warp direction and in the weft direction. On the basis of these pores it is possible to create all structural binding solutions for dobby and jacquard fabrics too. Repeat of dobby weave, jacquard repeat of the pattern is based on the distribution of the individual pores in the area of pattern. The relative frequency of each RP1-4 pores in the area of the pattern (weave repeat) influences the behaviour of woven fabric during weaving as well as the resulting end-use and mechanical properties. Expression the relative frequency of each structural pores in the pattern repeat is given by equations (2).

$$RP1 = \frac{\sum P1}{n_o \cdot n_u} \quad RP2 = \frac{\sum P2}{n_o \cdot n_u} \quad RP3 = \frac{\sum P3}{n_o \cdot n_u} \quad RP4 = \frac{\sum P4}{n_o \cdot n_u} \quad (2)$$

For mathematical expression of sett of ends and picks in woven fabric is possible to use square sett of threads in woven fabric where the distance of threads is given by equation (3)

$$A = \frac{\left(\frac{100}{D_2} \cdot nu\right) \cdot \sqrt{4 \cdot (d_{str})^2 - (d_{str})^2}}{ppo \cdot \sqrt{4 \cdot (d_{str})^2 - (d_{str})^2} + d_2 \cdot (nu - ppo)} \quad B = \frac{\left(\frac{100}{D_1} \cdot no\right) \cdot \sqrt{4 \cdot (d_{str})^2 - (d_{str})^2}}{ppu \cdot \sqrt{4 \cdot (d_{str})^2 - (d_{str})^2} + d_1 \cdot (no - ppu)} \quad (3)$$

where A is distance of picks and B is distance of ends in woven fabric (expression of the distances are given for plain and non-plain weaves), d_{str} is mean diameter of threads (end and pick), d_1 , d_2 are diameter of end and pick, ppo , ppu are number of transition in warp and weft direction, no , nu are number of warp and weft threads in weave. Relationship of setting of woven fabric with weaves is given by definition of possible distances of threads in interlacing for individual pores. Pore P1 – is fully interlacing pores in weave, opposite pore is pore P4 – fully float pore, pore between P1 and P4 is pore P2 – it is pore which can react on length of float as well as on position of interlacing point in non-plain weaves, see Figure 3. Special pore P3 it is pore which can react only on direction interlacing change of identical position of threads in weaves (special case of rip and hopsac weaves – derived plain weaves), see Figure 3.

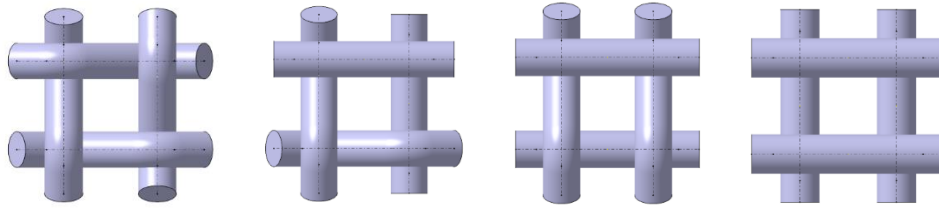


Figure 3. Woven fabric structural pores model from the left side P1, P2, P3, P4

For prediction of square setting of woven fabric it is possible to use the mathematical expression of mean distance of threads based on the sum of the partial distances of the threads in the individual pores, equation (5). The calculation of partial distances of threads are given by equation (6). In this case we will not express the P3 which has connection only for derived weaves. Prediction of square setting of woven fabric is given by equation (7).

$$\text{Mean distance of pores: } MDP_{1-4} = \frac{\sum P_{1-4}(\text{in one weft})}{n_o} \quad (5)$$

$$\text{Distance of pore: } P_1 = A(\text{for square sett } B \text{ is identical})$$

$$\text{Distance of pore: } P_2 = \frac{pp_{o,u} \cdot \sqrt{3} \cdot d_{str} + d_{str} \cdot (n_{o,u} - pp_{o,u})}{n_{o,u}} \quad (6)$$

$$\text{Distance of pore: } P_4 = d_{str}$$

$$\text{Square setting of woven fabric: } D_{\text{square fabric}} = \frac{1}{MDP_{1-4}} \quad (7)$$

P2	P4	P4	P4	P4	P4	P4	P4	P4	P2	P1
P4	P4	P4	P4	P4	P4	P4	P2	P1	P2	P2
P4	P4	P4	P4	P4	P4	P2	P1	P2	P4	P4
P4	P4	P4	P4	P4	P2	P1	P2	P4	P4	P4
P4	P4	P4	P4	P4	P2	P1	P2	P4	P4	P4
P4	P4	P4	P4	P4	A2	P4	P4	P4	P4	P4
P4	P4	P2	P1	P2	P4	P4	P4	P4	P4	P4
P4	P2	P1	P2	P4	P4	P4	P4	P4	P4	P4
P2	P1	P2	P4	P4	P4	P4	P4	P4	P4	P4
P1	P2	P4	P4	P4	P4	P4	P4	P4	P4	P2

Figure 4. Matrix depiction of structural pore models of woven fabric for twill weave repeat with 10x10 threads

For example here it is presentation of calculation of mean distance of threads for twill repeat (10x10), the calculation is given by equation (8). Composition of repeat of twill weave is given by pores P1, P2, P4. The float part represents her pore P4. Compactness of woven fabric represents pores P1 and P2. The calculation it is possible to apply for each basic weaves.

$$MDP_{1-4}(Twill10) = \frac{\sum (\text{distances of}) P_1 + 2 \cdot (P_2) + (P_4) \cdot 7}{10} \quad (8)$$

4. CONCLUSIONS

Construction of woven fabric is given by input parameters of yarns as well as parameters of woven fabric. Each yarn has own specific diameters which determine the number of threads in one layer of threads in limit sett position. Plain and non-plain interlacing it is possible to use for weaving of woven fabric. Increasing of crossing interlacing points decrease the setting of threads and opposite. Compactness of woven fabric are given by combination of parameters: crossing point in repeat, length of float and sett of threads. The float part is only one parts of interlacing which can increase the sett of threads, but it is necessary to include the composition of pores which define the whole weave repeat/pattern. Composition of structural pore models in weave repeat influence the calculation of sett of threads. For comparison the twill and sateen with repeat 5x5 threads. Twill has pores P1, P2, P4, the pore P1 in twill increase the compactness with smaller sett of threads in comparison with the same sateen which doesn't have pore P1 only pore P2, P4. Based on P2 it is possible to increase sett of threads based on smaller distance which this pores in structure of woven fabric has. The Brierley theory and his contribution to this problem focused on the square sett fabric include the parameter of float as weaves value obtained by the analyses of a large series of experiment. From his equations the formula doesn't have a limits but limit is given by the distance which is given as the reciprocal value of the yarn diameter.

ACKNOWLEDGEMENTS

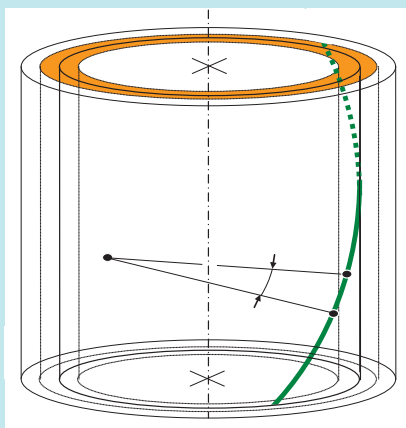
This work was supported by the Ministry of Education, Youth and Sports of the Czech Republic and the European Union - European Structural and Investment Funds in the frames of Operational Programme Research, Development and Education - project Hybrid Materials for Hierarchical Structures (HyHi, Reg. No. CZ.02.1.01/0.0/0.0/16_019/0000843).

References

1. Brierley S.: *Theory and Practice of Cloth Setting. The Textile Manuf.*, 1931, 58(3 – 4): pp. 4749, 130-132, 206-208,244-246..
2. Brierley, S.; "Cloth Setting reconsidered IV", *Textile Manufacturer*, 79, 1952, 533-537.
3. Peirce, F.T.: *The Geometry of Cloth Structure, Journal of Textile Institut*, Vol.28, 1937.
4. Olofsson B.; „A general model of a fabric as a geometric mechanical structure” *J. Textiles Isnt.* Nr11,55, pp. 541-557; 1964.
5. Sirková B.:*Study of the approximation of the individual models by a partial sum of Fourier series,* " *Vlakna a Textil*, vol. 7, no. 4, pp. 189-194, 2000.
6. Milašius V.: *Woven Fabric's Cross-Section: Problems, Theory, and Experimental Data, Fibres and Textiles in Eastern Europe* No 4(23)/98, pp. 48-50.
7. Nosek, S.: *The theory of weaving process, part I., Dům techniky ČSVTS*, 1988
8. Kolčavová Sirková, B., Mertová, I.: *Prediction of woven fabric properties using software protkatex,* *Autex Research Journal*, Volume: 13(1), Pages: 11-16, 2013
9. Nosek, S.: *The structure and geometry of the woven fabrics*, Liberec 1996
10. Backer, S.: *The relationship between the structural geometry of textile fabric and its physical properties, Part IV: Interstice geometry and air permeability, Textile Research Journal* 1951, Vol. 17 (10) 703-714
11. Lomov, S. V., G. Huysmans, and I. Verpoest: *Hierarchy of Textile Structures and Architecture of Fabric Geometric Models*, *Textile Research Journal*, Jun 2001; vol. 71
12. Barburski M., Masajtis J.; *Modelling of the Change in Structure of Woven Fabric under Mechanical Loading. FIBRES & TEXTILES in Eastern Europe, January/March 2009, Vol. 17, No. 1 (72) pp. 39-44.*
13. Kolčavová Sirková B., Mertová I.: *Woven fabric structural pore models analysis, Vlakna a Textil*, vol. 24, no. 1, pp. 15-24, 2017.

APPENDIX

Computational methodology for determination of yarn twist and diameter



Basic quantities and relations

Yarn: m ...mass, l ...length, D ...yarn **diameter**,
 Z ...yarn **twist**, $T = m/l$...yarn **count**

$$(T_{[\text{tex}]} = m_{[\text{g}]} / l_{[\text{km}]})$$

$\alpha = Z\sqrt{T}$...Koechlin's **twist coefficient**

$$(\alpha_{[m^{-1}ktex^{1/2}]} = Z_{[m^{-1}]} \sqrt{T_{[\text{tex}]} / 31.623 })$$

β_D ...**angle** of surface fibre
(at diameter D)

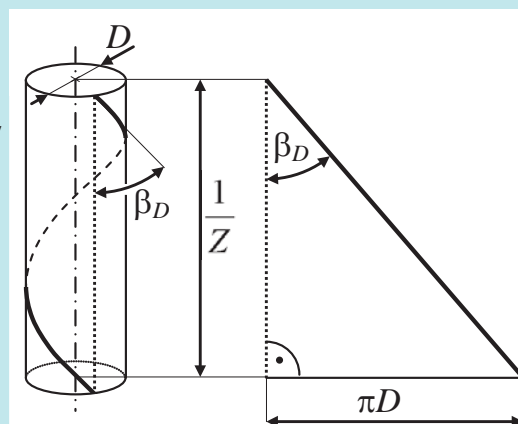
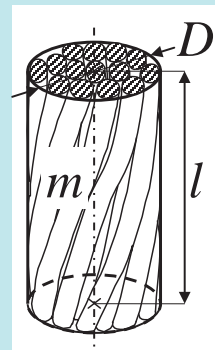
$\kappa = \pi D Z = \tan \beta_D$...**twist intensity**

$$(\kappa = \pi D_{[\text{mm}]} Z_{[m^{-1}]} / 1000 = \tan \beta_D)$$

β ...**general angle** (at radius r)

$$2\pi r Z = \tan \beta$$

$$(2\pi r_{[\text{mm}]} Z_{[m^{-1}]} / 1000 = \tan \beta)$$



V_c ...volume of yarn (with air), V ...fiber volume (without air),
 ρ ...fibers mass density, d ...equivalent fiber diameter

$$\mu = V/V_c = 4T/(\pi D^2 \rho) \dots \text{packing density of yarn}$$

$$\left(\mu = 4T_{[\text{tex}]} / \left(\pi D_{[\text{mm}]}^2 \rho_{[\text{kg m}^{-3}]} \right) \right)$$

It is valid from the last expression

$$D = \sqrt{4T/(\pi\mu\rho)} \quad , \quad D_{[\text{mm}]} = \sqrt{4T_{[\text{tex}]} / (\pi\mu\rho_{[\text{kg m}^{-3}]})}$$

Basic problem: What is the value of packing density?

$$t = (\pi d^2/4)\rho \dots \text{fiber fineness}, \quad (t_{[\text{tex}]} = (\pi d_{[\text{mm}]}^2/4)\rho_{[\text{kg m}^{-3}]})$$

$$\tau = T/t \dots \text{relative fineness of yarn} \quad (\tau = T_{[\text{tex}]} / t_{[\text{tex}]})$$

Note: τ is not the number n of fibers in yarn cross-section!
It is valid $\tau \geq n$ (e.g. $n/\tau \doteq 0.95$ for ring yarns).

Empirically: Different yarn **counts** T of staple yarns

- need different yarn **twists** Z and
- result in different yarn **diameters** D

(in consequence to mechanical behavior of fiber assembly)

There exist some **relations among these three quantities.**

Existing concepts

I) Pre-industrial age (from about 25000 years B.C.)

A set of useful relations was prepared according to **subjective feeling** of spinner for hand-spinning process.

IIa) Industrial spinning - easiest solution

(from 1828)

A series of useful relations was prepared according to **mathematical model** (semi-empirical model like **Koechlin**).

General assumption: We think yarns

- prepared from same fiber material,
- produced by using same technology,
- designated for the same (or analogical) end-use.

1. *special assumption:* Packing density μ is an increasing function of twist intensity κ **only**; $\mu = f(\kappa)$.

2. *special assumption:* Yarns are **geometrically similar**, i.e., twist intensity κ (angle β_D) of different yarns are same. (Remember that $\kappa = \tan \beta_D = \text{constant}$.)

Then, it is derived for yarns under consideration:

- $\mu, \kappa, \beta_D \dots$ **constants** - resulting from assumptions,

- $\alpha = \frac{\kappa \sqrt{\mu \rho}}{2\sqrt{\pi}}, \alpha_{[m^{-1} \text{ktex}^{1/2}]} = \frac{1000}{31.623} \frac{\kappa \sqrt{\mu \rho_{[\text{kg m}^{-3}]}}}{2\sqrt{\pi}} \dots$ **constant**,

- $D = K \sqrt{T}$, where $K = 2 / \sqrt{\pi \mu \rho}$,

$$D_{[\text{mm}]} = K_{[\text{mm tex}^{-1/2}]} \sqrt{T_{[\text{tex}]}} , K_{[\text{mm tex}^{-1/2}]} = 2 / \sqrt{\pi \mu \rho_{[\text{kg m}^{-3}]}} \dots$$
 constant

As it is **easy to calculate** yarn twist and diameter using these expressions, they are very frequently used in practice. However, based on our practical experience, they are **not found to be precise**. (Therefore, these relations were modified empirically by different researchers.)

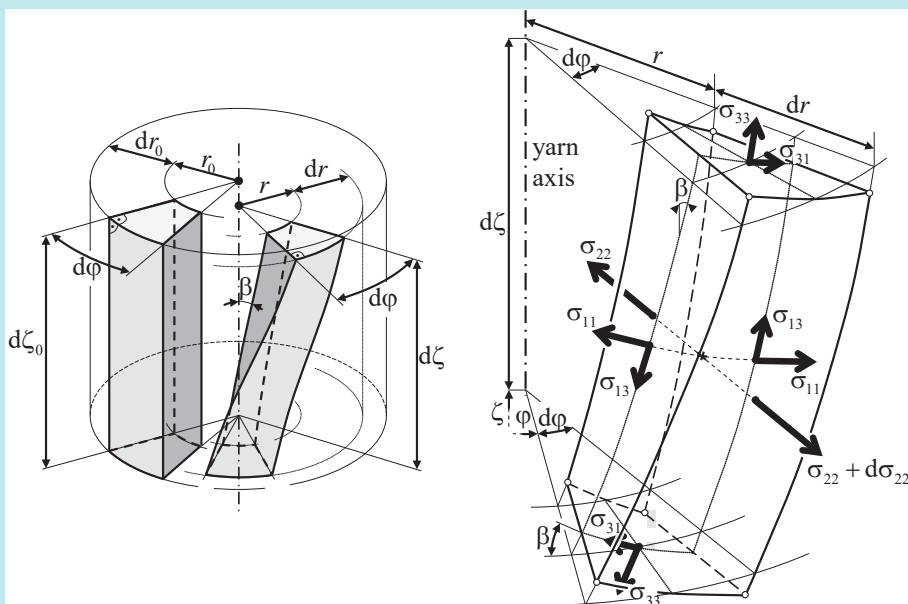
I Ib) A more exact model (20th century)

Useful relations could have been developed according to **model of continuum mechanics**.

Elements of fiber material in yarn:

Left – deformation of element by twisting.

Right – strains in deformed element



Solution – **diff. equation** of second order (see Ref. [1]):

$$\frac{d^2 r_0}{dr^2} = \frac{-1}{(1 + \varepsilon_2)^2} \left[\frac{\partial \sigma_{22}}{\partial \varepsilon_1} \frac{d\varepsilon_1}{dr} + \frac{\partial \sigma_{22}}{\partial \varepsilon_3} \frac{d\varepsilon_3}{dr} + \frac{\partial \sigma_{22}}{\partial \beta} \frac{d\beta}{dr} - \frac{\sigma_{22}}{r} + \frac{\sigma_{33}}{r} \sin^2 \beta + \frac{\sigma_{11}}{r} \cos^2 \beta + 2 \frac{\sigma_{13}}{r} \sin \beta \cos \beta \right], \text{ where}$$

$$\beta = \arctan(2\pi r Z), \quad \frac{d\beta}{dr} = \frac{\cos \beta \sin \beta}{r},$$

$$\varepsilon_1 = \frac{r}{r_0} \cos \beta - 1, \quad \frac{d\varepsilon_1}{dr} = \frac{1 + \varepsilon_1}{r} \left[\cos^2 \beta - \frac{1 + \varepsilon_1}{(1 + \varepsilon_2) \cos \beta} \right],$$

$$\varepsilon_2 = \frac{1}{dr_0/dr} - 1, \quad \frac{d\varepsilon_2}{dr} = -(1 + \varepsilon_2)^2 \frac{d^2 r_0}{dr^2},$$

$$\varepsilon_3 = \frac{d\zeta}{d\zeta_0} \frac{1}{\cos \beta} - 1, \quad \frac{d\varepsilon_3}{dr} = \frac{d\zeta}{d\zeta_0} \frac{\tan \beta \sin \beta}{r}.$$

Stresses:

$$\sigma_{11}, \sigma_{22}, \sigma_{33}, \sigma_{13}$$

Strains:

$$\varepsilon_1, \varepsilon_2, \varepsilon_3, \beta$$

Radii:

r_0 ...before twist
 r ...after twist

Axial lengths:

ζ_0 ...before twist
 ζ ...after twist

Boundary conditions: 1) If $r_0 = 0$ then $r = 0$

2) $\sigma_{22} = 0$ at yarn surface

Main required inputs:

- yarn twist Z , yarn count T ,
- change of axial length $d\zeta/d\zeta_0$ (related to yarn retraction and/or yarn axial tensioning),
- **law of deformation** of fiber assembly (stresses as functions of deformations, relation between stress & strain tensors)

Key properties estimated:

yarn **packing density** and yarn **diameter**; radial behaviors of stresses, deformations, and packing density; axial force on yarn; yarn retraction; stress-strain curve and torsional moment of yarn; etc.

However, unfortunately,

law of deformation of (anisotropic) fiber material in yarn **is not enough precisely known!**

Therefore, the solution of this differential equation still remains as an **open problem of research** in the area of yarn structure.

Semi-empirical model (our solution)

Assumption: Region of centripetal pressure is **very small**

- 1) near to yarn surface (small μ , small fiber-to-fiber friction, etc.),
- 2) near to yarn core (small angle β , i.e. fiber curvature).

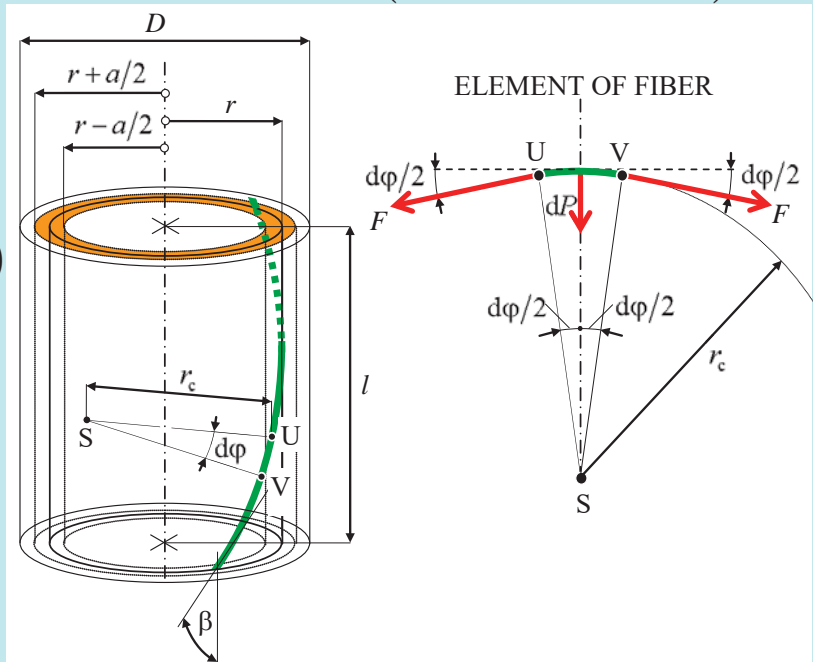
Significant centripetal pressure generates a

"compressing zone" somewhere "in-between" yarn core and yarn surface **only**.

Compressing zone (orange) on radii $(r - a/2, r + a/2)$

r ...mean radius,
 a ...thickness of zone,
 F ...tensile force
 in (green) fiber
 I was (geometrically)
 derived the pressure p developed
 in the compressing
 zone (Ref. [1])

$$p = C\sqrt{\mu} \frac{\alpha^2}{\rho\sqrt{\tau}}$$



C ...parameter of yarn relating to fibers and technology

Earlier, it was derived (from
 mechanics, using generalized
 Wyk's theory – Ref. [2])

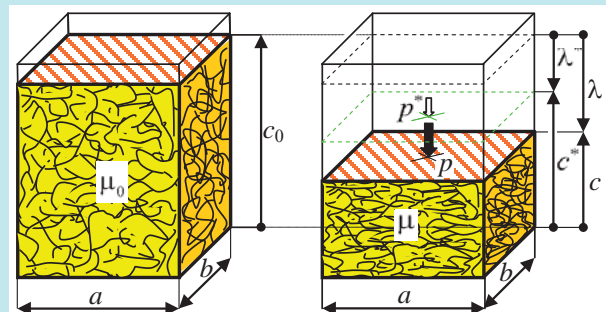
$$p = k_p b \frac{\mu^3}{\left[1 - (\mu/\mu_m)^{2+g}\right]^3}$$

$k_p b, g \doteq 1$...parameters of material,
 $\mu_m \doteq 0.9$...theoretical maximum packing density

Packing density (yarn diameter)

Comparing right-hand sides of last two equations we
 obtain the following expression

$$k_p b \frac{\mu^3}{\left[1 - (\mu/\mu_m)^{2+g}\right]^3} = C\sqrt{\mu} \frac{\alpha^2}{\rho\sqrt{\tau}}$$



Rearrangement – the first equation for packing density

$$\frac{\mu^{2.5}}{\left[1 - (\mu/\mu_m)^{2+g}\right]^3} = Q \left(Z T^{1/4} \right)^2, \quad \frac{\mu^{2.5}}{\left[1 - (\mu/\mu_m)^{2+g}\right]^3} = Q_{[m^2 \text{ tex}^{-1/2}]} \left(Z_{[m^{-1}]} T_{[\text{tex}]}^{1/4} \right)^2 \quad (a)$$

Common parameter

$Q_{[m^2 \text{ tex}^{-1/2}]}$
 related to
 - material
 - techno-
logy
Typical values:

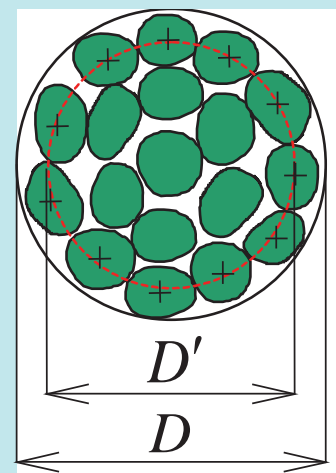
Values $Q [m^2 \cdot \text{tex}^{-1/2}]$; ($\mu_m = 0.9, g = 1$)				
Fibrous material		Spinning technology		
type	density ρ [$\text{kg} \cdot \text{m}^{-3}$]	combed	carded	OE, type BD
cotton	1520	$1.46 \cdot 10^{-7}$	$9.61 \cdot 10^{-8}$	$6.18 \cdot 10^{-8}$
viscose, cotton-type	1500	$4.12 \cdot 10^{-7}$		$1.76 \cdot 10^{-7}$
polyester, cotton-type	1360	$2.98 \cdot 10^{-7}$		$1.29 \cdot 10^{-7}$
wool	1310	$2.16 \cdot 10^{-7}$	$1.20 \cdot 10^{-7}$	$6.49 \cdot 10^{-8}$

Yarn twist

Schwarz constant $C_D = \frac{D'}{D} \doteq 1 - \sqrt{t_{[\text{tex}]} / T_{[\text{tex}]}}$

Modified 2. special Koechlin's assumption:
 Yarns are geometrically similar when angles β'_D (on the diameters D') of different yarns are same;

$$\tan \beta' = 2\pi (D'/2) Z = \pi D Z \frac{D'}{D} = \kappa C_D = \text{constant}$$



Rearrangement - the second form of equation (a):

$$\frac{\mu^{1.5}}{\left[1 - (\mu/\mu_m)^{2+g}\right]^3} = \frac{R}{\sqrt{T} \left(1 - \sqrt{t/T}\right)^2}, \quad \text{where } R = Q \frac{\tan^2 \beta' \rho}{4\pi} \quad (b)$$

or - by suitable dimensions -

$$\frac{\mu^{1.5}}{\left[1 - (\mu/\mu_m)^{2+g}\right]^3} = \frac{R_{[\text{tex}^{1/2}]}}{\sqrt{T_{[\text{tex}]}} \left(1 - \sqrt{t_{[\text{tex}]} / T_{[\text{tex}]}}\right)^2} \quad \text{(I)}$$

where $R_{[\text{tex}^{1/2}]} = Q_{[\text{m}^2 \text{tex}^{-1/2}]} 10^6 \frac{\tan^2 \beta' \rho_{[\text{kg m}^{-3}]}}{4\pi}$...parameter.

Finally, comparing equations (a) and (b) we obtain

$$\mu = \frac{Q}{R} Z^2 T \left(1 - \sqrt{t/T}\right)^2, \quad \mu = \frac{Q_{[\text{m}^2 \text{tex}^{-1/2}]}}{R_{[\text{tex}^{1/2}]}} Z_{[\text{m}^{-1}]}^2 T_{[\text{tex}]} \left(1 - \sqrt{t_{[\text{tex}]} / T_{[\text{tex}]}}\right)^2 \quad \text{(II)}$$

Let us think about two quite different yarn groups:

1. Same fiber material, same (or analogical) end-use, same technology, but **different yarn finenesses**;

Then: $\beta'_D = \text{constant}$ (modif. Koechlin's assumption),
 $R = Q \tan^2 \beta' \rho / (4\pi)$ - eq. (b) - is **constant**, too.

2. Same fiber material, same (or analogical) end-use, same yarn fineness, but **different type of technology**

Then: We need same level of compression, same fiber-to-fiber contacts, i.e. same packing density; so the left-

hand side of eq. (b) $\mu^{1.5} / \left[1 - (\mu/\mu_m)^{2+g}\right]^3 = \text{constant}$,

right-hand side of eq. (b) $R / \left[\sqrt{T} \left(1 - \sqrt{t/T}\right)^2\right] = \text{constant}$,

and so, the parameter R must be **constant** too.

Typical values for common yarns (weaving)

Generalized hypothesis:

$R_{[\text{tex}^{1/2}]}$
 is some **common parameter**, related to fiber material only.

Material	ρ [kg·m ⁻³]	R [tex ^{1/2}]
cotton - long staple	1520	2.145
cotton - medium staple	1520	2.500
viscose, cotton-type	1500	4.589
polyester, cotton-type	1360	3.563
wool	1310	2.341

Note: R resembles to generalized "twist coefficient".

How to calculate yarn diameter and yarn twist?

Inputs: fibre fineness t , fibre mass density ρ , yarn fineness T , maximum packing density $\mu_m = 0.9$, parameter $g = 1$, parameter Q (according to the fibre material and the spinning technology) and parameter R (according to the fiber material and the intended end-use)

Calculation – original model

1. **Packing density** - eq. (I)

$$\mu^{1.5} = \frac{R_{[\text{tex}^{1/2}]}}{\sqrt{T_{[\text{tex}]}} \left(1 - \sqrt{t_{[\text{tex}]} / T_{[\text{tex}]}}\right)^2}$$

(numerically or by table prepared in advance)

2. Yarn **diameter** $D_{[\text{mm}]} = \sqrt{4T_{[\text{tex}]} / (\pi \mu \rho_{[\text{kg m}^{-3}]})}$

3. Yarn **twist** – eq. (II)

$$\mu = \frac{Q_{[\text{m}^2 \text{tex}^{-1/2}]} Z_{[\text{m}^{-1}]}^2 T_{[\text{tex}]} \left(1 - \sqrt{t_{[\text{tex}]} / T_{[\text{tex}]}}\right)^2}{R_{[\text{tex}^{1/2}]}}$$

Calculation – approximation

Let us know more parameters of “middle yarn”: T^*, μ^*

“Helping” parameters:

$$A = 3 \frac{1 + (1 + g)(\mu^*/\mu_m)^{2+g}}{1 - (\mu^*/\mu_m)^{2+g}}, \quad B = \frac{1}{[1 - (\mu^*/\mu_m)^{2+g}]^3 (\mu^*)^{A-3}},$$

$$V = \frac{0.5 \sqrt{t_{[tex]}/T_{[tex]}^*}}{1 - \sqrt{t_{[tex]}/T_{[tex]}^*}}, \quad U_{[tex^{-V}]} = \frac{1 - \sqrt{t_{[tex]}/T_{[tex]}^*}}{(T_{[tex]}^*)^V}.$$

Twist exponent, and twist coefficient:

$$q = \frac{V(A-0.5)}{A-1.5} + \frac{A-1}{2(A-1.5)}, \quad \alpha_{q[m^{-1}tex^q]} = \frac{R_{[tex^{1/2}]}^{2(A-1.5)}}{Q_{[m^2 tex^{-1/2}]}^{1/2} U_{[tex^{-V}]}^{A-1.5} B^{2(A-1.5)}}$$

Then: Yarn twist: $Z_{[m^{-1}]} = \alpha_{q[m^{-1}tex^q]} / T_{[tex]}^q$,
packing density and diameter:

$$\mu = \left(\frac{Q_{[m^2 tex^{-1/2}]} }{B} \right)^{\frac{1}{A-0.5}} Z_{[m^{-1}]}^{A-0.5} T_{[tex]}^{\frac{1}{2A-1}}$$

$$D_{[mm]} = \sqrt{4T_{[tex]} / (\pi \mu \rho_{[kg m^{-3}]})}$$

Example – calculation:

Carded cotton yarns

T^* ...selected count of “middle” yarn
 μ^* ...packing density of “middle” yarn (calculated by original model)

Packing density:

warp $\mu = 0.012722 Z_{[m^{-1}]}^{0.49005} T_{[tex]}^{0.12251}$

knitted $\mu = 0.0088835 Z_{[m^{-1}]}^{0.53910} T_{[tex]}^{0.13477}$

Yarn twist:

warp $Z_{[m^{-1}]} = 5984.2 / T_{[tex]}^{0.63379}$

knitted $Z_{[m^{-1}]} = 5379.0 / T_{[tex]}^{0.64667}$

Common input parameters: $\mu_m = 0.9, g = 1,$
 $Q = 9.61 \cdot 10^{-8} m^2 tex^{-1/2}, \rho = 1520 kg m^{-3},$
 $t = 0.16 tex, “middle” yarn $T^* = 29.5 tex$.$

Quantity	Dimension	yarn	
		warp	knitted
R (input)	$tex^{1/2}$	2.500	2.000
μ^*	-	0.47760	0.44206
A	-	4.5812	4.2099
B	-	5.2283	3.9198
V	-	0.039750	0.039750
U	tex^{-V}	0.80975	0.80975
q	-	0.63379	0.64667
α_q	$m^{-1}tex^q$	5984.2	5379.0
Values of “middle” yarn:			
D^*	mm	0.22746	0.23643
Z^*	m^{-1}	700.57	602.85
$\alpha_{Koechlin}^*$	$m^{-1}ktex^{1/2}$	120.33	103.54

Example – comparison of packing density:

Carded cotton yarns

Experimentally:

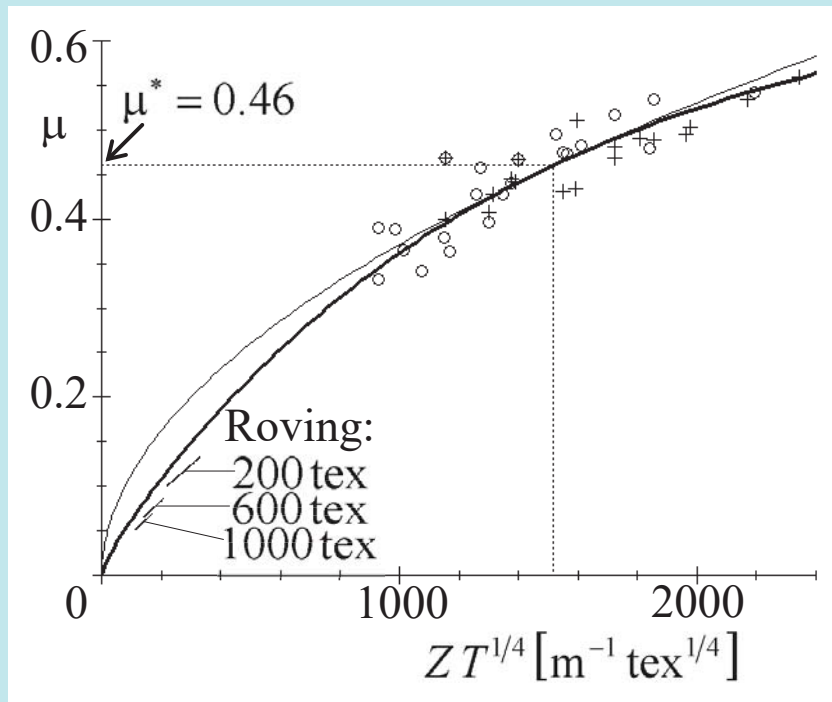
Points O, +
 (two sets of yarns)

Theoretical model:

Thick line

- original model, thin line

- approximation



Example – our calculation of twist coefficients:

Carded cotton yarns

Let us remind that:

Koechlin's type

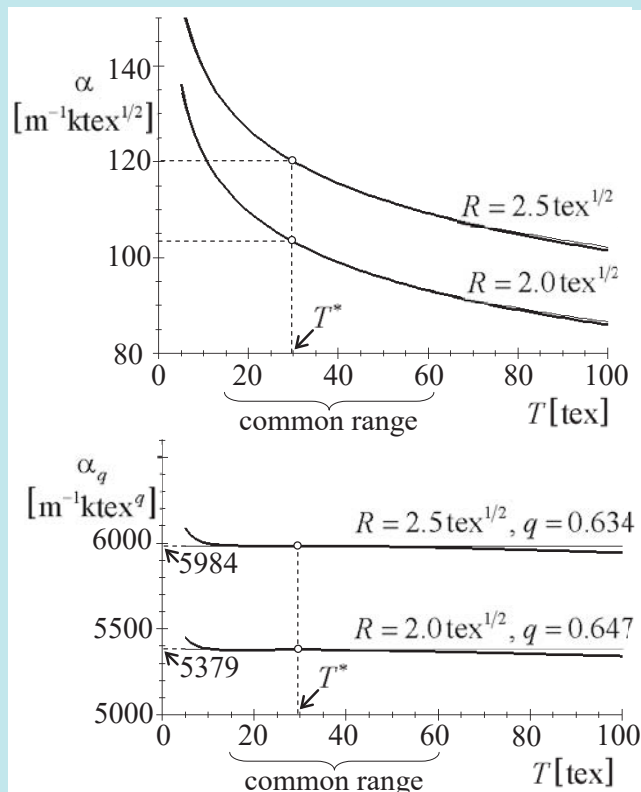
$$\alpha_{[m^{-1}ktex^{1/2}]} = Z_{[m^{-1}]} \sqrt{T_{[tex]}} / 31.623$$

Generalized type

$$\alpha_{q[m^{-1}tex^q]} = Z_{[m^{-1}]} T_{[tex]}^q$$

Note: Twist exponent q is near to Phrix's exponent $2/3$

Thick line - original model, thin line - approximation



Optimum yarn twist

σ_Y [N tex⁻¹]...yarn tenacity, σ_f [N tex⁻¹]...fiber tenacity

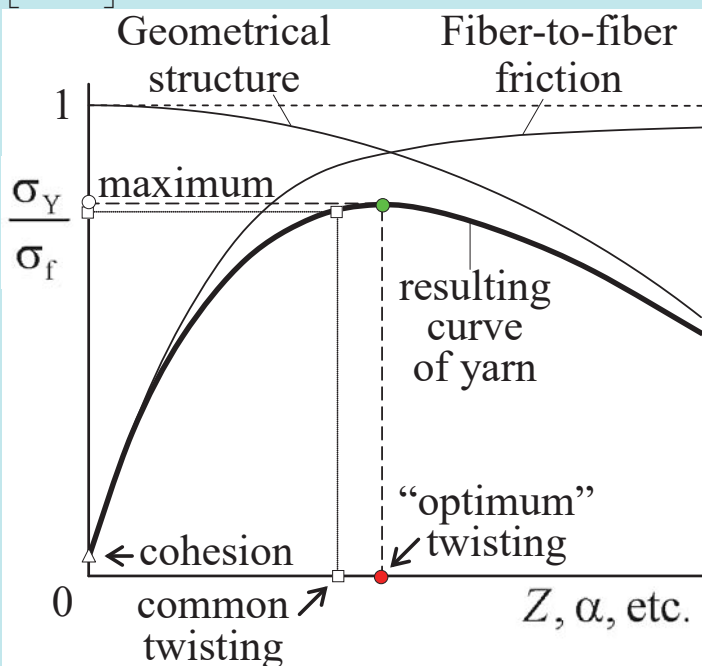
$\sigma_Y / \sigma_f \leq 1$..coefficient

of utilization of fiber strength by yarn

Optimum twist = twist at the maximum coefficient of utilization (*quantities have subscript 'o'*)

Two dominant influences:

1. **Geometry** of oblique fibers (*theoretically solvable, see Gegauff etc.*)
2. **Friction** among fibers (*unsolved problem!*)



Recommended values of α_o for carded cotton yarns

Points:

- ...Johansen 1930
- ×...Döttinger 1925

Empirical eqs. (dashed lines):

- M...Müller 1880
- S...Solovev 1951
- K...Korickij 1963

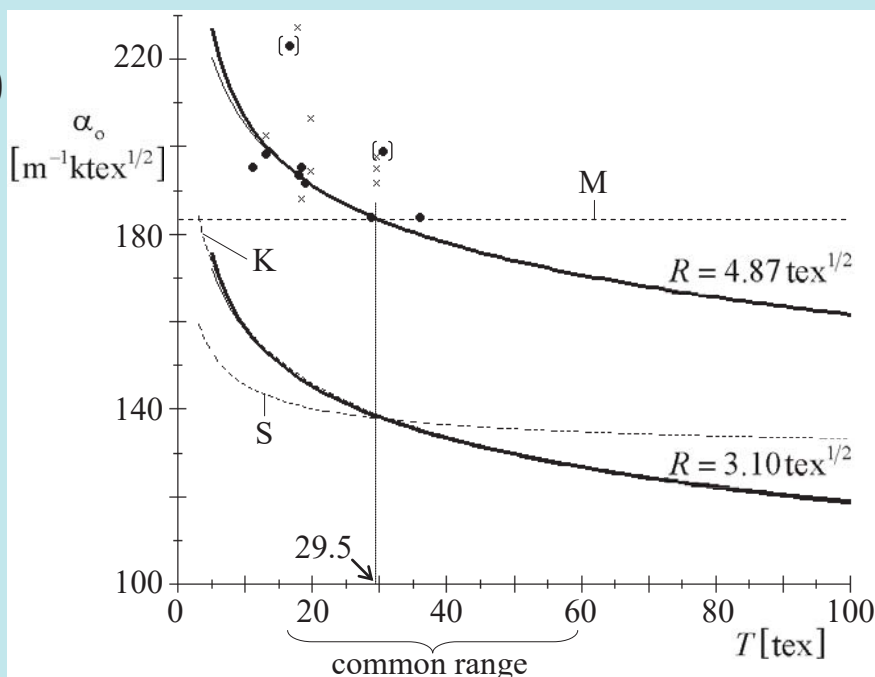
Our solving:

Full thick lines

...original model

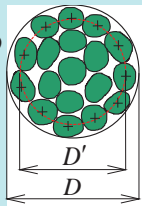
Full thin lines

...approximation



How to obtain optimum twist coefficient?

Angles β'_D
 (on the
 diameters D')



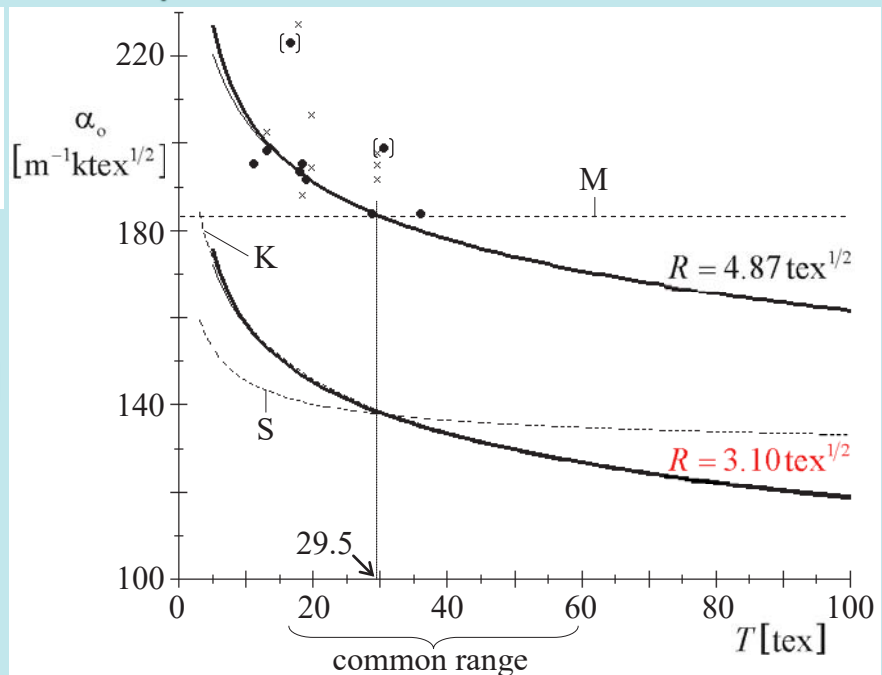
are same, i.e.
 parameter R_0 is
 constant for gi-
 ven fiber material
 (e.g. for carded
cotton yarns)

$$R_0 = 3.10 \text{ tex}^{1/2}$$

Note:

$$R_0 = 4.87 \text{ tex}^{1/2}$$

is too high for typical material and technology



Conclusion

1. Traditional model of yarn diameter and suitable twist (formulas like Koechlin) are easy but **not enough precise**.
2. Model using continuum mechanics could be relatively completed and precise but the most **important input** – law of deformation of fiber material – is **not enough fully known**.
3. Our (semi-empirical) model allowed us to **better understand** the principle of process of twisting and - consequently - determination of yarn **packing density, diameter, suitable yarn twist, and optimum yarn twist**. Approximated equations can be **easily applicable** to industrial praxis.
4. However, a complete solution is the work of **future research**.

Recommended books

for detailed study:

[1] Neckář, B. and Das, D., Theory of Structure and Mechanics of Yarns, Woodhead Publishing India Pvt. Ltd., New Delhi, 2018

[2] Neckář, B. and Das, D., Theory of Structure and Mechanics of Fibrous Assemblies, Woodhead Publishing India Pvt. Ltd., New Delhi, 2012

Thank you for your attention



Název/Title	22. konference STRUTEX (sborník) 22 nd conference STRUTEX (Proceedings)
Autor/Author	Kolektiv autorů/Team of Authors
Vydavatel/Publisher	Technická univerzita v Liberci Technical University of Liberec
Schváleno/Authorized	Rektorátem TU v Liberci dne 9. 10. 2018 čj. RE 44/18
Vyšlo/Date of issue	Prosinec / December 2018
Vydání/Edition	první/first
Tiskárna/Printed by	Vysokoškolský podnik Liberec, s.r.o., Studentská 1402/2, Liberec
Číslo publikace/Publication number	55-044-18

Tato publikace neprošla redakční ani jazykovou úpravou.

ISBN 978-80-7494-430-7



ISBN 978-80-7494-430-7